Ammonoïdes du Smithien (Trias inférieur) du Nord-Ouest du Guangxi (Chine du Sud) et modélisation biogéographique de la récupération biotique des ammonoïdes après l'extinction de masse Permien/Trias

Arnaud Brayard

Smithian (Early Triassic) Ammonoids from Northwestern Guangxi (South China) and Biogeographic Modelling of the Ammonoid Recovery after the Permian-Triassic Mass Extinction

---

Dissertation

zur

Erlangung der naturwissenschaftlichen Doktorwürde
(Dr. sc. nat.)

vorgelegt der

Mathematisch-naturwissenschaftlichen Fakultät

der Universität Zürich

Doppeldoktorat

Universität Zürich
-
Université Claude Bernard Lyon 1

von

Arnaud Brayard

von

Frankreich

Promotionskomitee

Prof. Dr. Hugo Bucher
(Leiter der Dissertation, Vertreter der Universität Zürich)
Dr. Gilles Escarguel
(Leiter der Dissertation, Vertreter der Universität Claude Bernard Lyon 1)
Prof. Dr. Øyvind Hammer
Prof. Pierre Hantzpergue
Prof. Dr. Peter Linder
Dr. Wolfgang Weitschat

Zürich, 2006

CONTENTS

Abstract:

The Permo-Triassic mass extinction (ca. 252 Ma) drastically affected the evolution of life, resulting in the decimation of more than 90% of marine species. Pre-crisis levels of marine ecosystem complexity were not reached until Middle Triassic time. Ammonoids (Cephalopoda) recovered much faster than other marine shelled invertebrates.

The Early Triassic is an appropriate period to study how climate and oceanic conditions influenced the recovery of marine organisms, especially in terms of taxonomic richness and paleobiogeography. Indeed, Early Triassic ammonoids represent an ideal case of an almost monophyletic clade evolving in a stable paleogeographical framework, which was largely influenced by other parameters such as sea surface temperature (SST), currents, water chemistry, etc.

First, in order to improve our understanding of the principal constraints controlling the dynamics of the ammonoid recovery, we constructed a "geophyletic model", in which SST and currents are the "forcing" parameters applied to the biogeographical dispersal of a randomly generated clade. Validation of the results of the "geophyletic model" was based on a comparison with the distribution patterns of present-day Atlantic foraminifers. Next, we applied the "geophyletic model" to Early Triassic paleogeography to simulate the spatial and temporal variations of ammonoid diversity during the recovery, in response to "forcing" parameters such as SST and currents. The model primarily demonstrates that the edification and shape of a marine latitudinal gradient of taxonomic richness is largely governed in a non-linear fashion by the shape and magnitude of the SST gradient.

Second, our simulation results were compared to the Early Triassic ammonoid record. Based on a refined global data set at the basin level, we investigate the paleobiogeographical global latitudinal and longitudinal diversity patterns in terms of climatic changes during the Early Triassic. During this period, the global first order trend in increasing ammonoid diversity was accompanied by a progressive change from cosmopolitan to latitudinally-restricted distributions. This change led to the emergence of a pronounced latitudinal diversity gradient during most of the Smithian and Spathian stages, which entails increased steepness of the SST gradient during the late Early Triassic. However, two brief episodes of ammonoid cosmopolitanism combined with low global diversity interrupted the first order increasing trend at the very beginning and very end of the Smithian. The analysis of endemicity indicates a rapid biogeographical maturing and structuring of faunas concomitant with the edification of the latitudinal diversity gradient. The distribution of taxa also reveals a pattern of latitudinal belts of faunal compositions across Panthalassa. Thus, Early Triassic ammonoid recovery in time and space is interpreted as having been largely controlled by the evolution of SST gradients.

The third part of this dissertation focuses on the taxonomy and biostratigraphic distribution of Smithian ammonoids from South China. With an equatorial paleoposition at the boundary between Tethys and Panthalassa, South China occupies a key position for the reconstruction of biogeographic patterns. A thorough bed by bed sampling provides for the first time a detailed stratigraphic

distribution of Smithian ammonoids in this area, which is by far the most complete succession in the Tethys. A new local zonation is established and correlated with other successions from mid- and high-paleolatitudes.

Keywords:

Ammonoids (Cephalopoda), Early Triassic recovery, Macroecology, Paleobiogeography, “geophyletic model”, Smithian, South China.

Zusammenfassung:

Das Perm/Trias-Massenaussterben vor ca. 252 Ma hatte tief greifende Auswirkungen auf die Evolution des Lebens. Über 90% der marinen Arten wurden ausgelöscht. Die marinen Ökosysteme erreichten ähnliche Komplexitätsgrade wie vor der Krise erst in der Mittleren Trias. Die Ammonoideen (Cephalopoda) jedoch erholten sich viel schneller als andere marine Schalen bildende Invertebraten.

Die Frühe Trias ist eine geeignete Zeitperiode für das Studium der Einflüsse von klimatischen und ozeanischen Bedingungen auf die Erholung mariner Organismen nach einem Massenaussterben, besonders in Bezug auf taxonomischen Reichtum und Paläobiogeographie. Die frühtriassischen Ammonoideen stellen den Idealfall eines fast monophylletischen Stammes dar, der sich in stabilen geologischen Rahmenbedingungen entwickelte und im Wesentlichen von anderen Parametern wie Oberflächentemperatur (Sea Surface Temperature, SST), Strömungen, Wasserchemie usw. beeinflusst wurde.

Um zu verstehen, welche die prinzipiellen Bedingungen sind, die die Dynamik der Ammonoideen-Erholung kontrollieren, haben wir als Erstes ein „geophyletisches Modell“ erarbeitet, in dem SST und Strömungen als bestimmende Faktoren auf die biogeographische Ausbreitung eines zufällig generierten Stammes angewandt werden. Die Resultate des „geophyletischen Modells“ wurden an Hand eines Vergleichs mit den Verbreitungsmustern rezenter Foraminiferen im Atlantischen Ozean bestätigt. Danach wandten wir das “geophylletische Modell” auf die frühtriassische Paläogeographie an, um die räumlichen und zeitlichen Variationen der Diversität der Ammonoideen während der Erholungsphase in Abhängigkeit von Parametern wie SST und Strömungen zu simulieren. Grundsätzlich betont das Modell, dass die Bildung und die Gestalt eines marinen breitenabhängigen Gradienten des taxonomischen Reichtums in erster Linie durch eine nicht-lineare Beziehung von der Gestalt und der Grösse des SST-Gradienten bestimmt werden.

Als zweiter Schritt wurden die Resultate der Simulation mit dem frühtriassischen Ammonoideenbeleg verglichen. Basierend auf einem verbesserten globalen Datensatz auf Becken-Niveau untersuchen wir die paläobiogeographischen globalen breiten- und längenabhängigen Diversitätsmuster in Bezug auf klimatische Veränderungen während der Frühen Trias. Während der Frühen Trias wurde der globale Trend erster Ordnung zunehmender Ammonoideen-Diversität von einem progressiven Wechsel von kosmopolitischen zu breitenabhängig begrenzten Verteilungen begleitet. Dies führte zur Entstehung eines deutlichen breitenabhängig Diversitätsgradienten während des grössten Teils der Stufen Smithian und Spathian, was eine erhöhte Steilheit des SST-Gradienten während der späten Frühen Trias bedingt. Allerdings wurde der zunehmende Trend erster Ordnung zu Beginn und am Ende des Smithian durch zwei kurze Episoden von Ammonoideen-Kosmopolitismus in Kombination mit tiefer globaler Diversität unterbrochen. Die Analyse von Endemismus zeigt rasche biogeographische Reifung und Strukturierung von Faunen an, die die Bildung des breitenabhängigen

Diversitätsgradienten begleiten. Die Verteilungen von Taxa zeigen auch ein Muster breitenabhängiger Faunengürtel über Panthalassa auf. Es wird daher angenommen, dass die frühtriassische Erholung der Ammonoideen in Zeit und Raum in erster Linie von der Entwicklung von SST-Gradienten bestimmt wurde.

Ein dritter Teil dieser Dissertation fokussiert auf die Taxonomie und Biostratigraphie von Ammonoideen des Smithian Südchinas. Mit einer äquatorialen Paläoposition an der Grenze zwischen der Tethys und Panthalassa hat Südchina eine Schlüsselposition für die Rekonstruktion biogeographischer Muster. Eine sorgfältige Schicht-für-Schicht-Beprobung ergab zum ersten Mal eine detaillierte stratigraphische Verteilung von Ammonoideen des Smithian in diesem Gebiet, die bei Weitem die vollständigste Abfolge in der Tethys darstellt. Eine neue lokale Zonierung wird vorgeschlagen und mit anderen Abfolgen von mittleren und hohen Paläobreiten korreliert.

Sclüsselwörter:

Ammonoideen (Cephalopoda), frühtriassische Erholung, Makroökologie, Paläobiogeographie, „geophyletisches Modell“, Smithian, Südchina.

ACKNOWLEDGEMENTS

This dissertation is the result of a research initiated five years ago at the university Claude Bernard of Lyon 1 (UCBL) by a Master thesis and next continued by a PhD thesis in “co-tutelle” between the Paläontologisches Institut und Museum der Universität Zürich (PIMUZ) and the UCBL. Thus, people to thank are numerous.

Firstly, in Switzerland, at PIMUZ, I would like to thank my PhD supervisor H. Bucher who offers me the opportunity to participate to this project with his enthusiasm, his scientific advices, his experience and his friendly support. Also at PIMUZ, I would like to thank C. Monnet who shared the same office than me and spent many exciting hours discussing with me. Next, I gratefully acknowledge:

- T. Galfetti and N. Goudemand (PIMUZ) who support me during the field in China, and because they are always enthusiastic for (scientific or not) debates. They especially gave me thoughtful feedbacks on my publications;
- S. Urdy (PIMUZ) who has tolerated my way of thinking during several years since our Master degree at UCBL;
- T. Brühwiler (PIMUZ), the latest participant to the project, who allowed me invading part of his desk with my specimens;
- P. Hochuli (PIMUZ) for its fruitful discussions and its productive collaboration;
- C. Klug (PIMUZ) for its vivacity and its openness on all (paleontological or not) subjects.

The PIMUZ’s staff is thanked for its huge work:

- M. Hebeisen, J. Huber and L. Pauli prepared most of the material from China;
- H. Lanz and R. Roth did all the photographic illustrations.

Secondly, in France, at UCBL, I would like to warmly thank my second PhD supervisor, G. Escarguel who welcomed me from biology to paleontology with a contagious enthusiasm. I would particularly thank its energy spending and its interest for all subjects concerning this project. He supports me since my Master degree without ever fail; I cannot begin to express my gratitude for all he done for me. Still at Lyon, I would like to thank all the PhD students from the labs. D. Barbe is also thanked for its help on the last draft of the manuscript. At Paris, I would like to thank F. Fluteau

(Institut de Physique du Globe de Paris) to its advices on Early Triassic climates and who kindly gives us the benefit of its latest paleogeographical maps.

I would like to thank J. Jenks (Salt Lake City) who kindly assisted us on the field in Idaho, to have lent comparative material, opened his house and provided a considerable work of English improvements of the monograph.

Great acknowledgements have to be done to all Chinese people who helped us in Guangxi.

感谢所有在我博士论文期间帮助和合作过的中国人。

I would particularly thank Kuang Guodun (Nanning) who provided his friendship, his judicious advices in the field, his patience. Thanks to him, we have also discovered China and its inhabitants.

I would like to thank my parents for their unwavering emotional and financial support during all these uncertain years. I would like to thank Emilie whose love and companionship played an immeasurable role in the success of this dissertation.

Finally, I am grateful to all of those not cited here but who helped me during this thesis on a friendly and/or scientific way.

Thanks to Ø. Hammer, P. Hantzpergue, P. Linder and W. Weitschat who have accepted to evaluate this thesis.

Last, I gratefully acknowledge financial support from the Swiss National Fund, and the Région Rhône-Alpes Eurodoc grant.

FOREWORD

Following the end-Permian mass extinction, the Early Triassic represents a time of major global changes. The transition between the Paleozoic and the Mesozoic faunas corresponds to two phases: the crisis and its recovery. Our knowledge of the first step: the mass extinction and its possible causes, is more developed and debated than the second step itself: the recovery. The latter implicates and groups together studies within many fields of the biology, ecology and of course paleontology. In this way, the complete understanding of the recovery requires advanced studies in global biodiversity, paleobiogeography and paleoecology. To complete this biotic approach, geochemical and radiochronological studies, for instance, are useful to precise the dynamics and the abiotic factors influencing the recovery.

1. General problematic and aims of this dissertation

Organisms that survived the Permian-Triassic mass extinction recovered at different paces. The starting point of this work stems from the mere empirical observation that among marine organisms, ammonoids (along with conodonts) were one of the earliest clades to recover and represent one of the marine dominant groups during the Early Triassic. Data compiled from the literature as well as newly obtained from field studies indicate that the ammonoid recovery was not a gradual process but was modulated by short-term ups and downs in diversity, suggesting that it was directly influenced by abiotic constraints such as climate and/or oceanic currents. Hence, reconstructing the dynamics and modalities of the Early Triassic ammonoid recovery, is the central theme of this work.

This dissertation is part of a multidisciplinary effort conducted at the Paleontological Institute and Museum of the University of Zurich where different aspects of the Early Triassic recovery are being investigated:

- 1: the reconstruction of spatial and temporal diversity patterns of Early Triassic ammonoids and their interpretation in terms of climate changes (A. Brayard);
- 2: the taxonomy and biostratigraphy of Smithian ammonoid faunas from the Nanpanjiang Basin (A. Brayard & H. Bucher);

- 3: the investigation of the Early Triassic oceanic and climatic changes by the means of points 1 and 2, and geochemical and palynological studies (T. Galfetti, P. Hochuli, H. Bucher);
- 4: the absolute age calibration of Triassic ammonoid faunas by means of radiometric dating of volcanic ashes (M. Ovtcharova, H. Bucher, A. Brayard, T. Galfetti).

In order to improve the knowledge of the ammonoid recovery, we selected a basin containing sections that would contribute to most of these aspects. Using the pioneer work of Chao (1950, 1959) on Early Triassic ammonoids as a starting point, preliminary surveys by Bucher in northwestern Guangxi (South China) revealed the under evaluated potential of this area. High-quality primary data (sampling of ammonoid sequences, volcanic ash layers, facies analysis, carbon isotopes, etc.) were acquired from this area. Simultaneously, a preliminary taxonomically consistent ammonoid data set including various other Early Triassic marine basins was constructed.

This thesis focuses on the diversity and biogeographical patterns of Early Triassic ammonoids and their interpretations. Emphasis is put on the relations between diversity changes in time and space, and controlling factors such as gradients of Sea Surface Temperature (SST) and oceanic circulation. The documented patterns are interpreted with the help of numerical simulations validated by an example drawn from present-day planktonic Foraminifera and SST gradient in the Atlantic Ocean.

2. Structure of the dissertation

This dissertation is organized to answer to different successive questions providing clues to the understanding of the Early Triassic ammonoid recovery:

Question 1 (Q_1): How spatial and temporal patterns of ammonoid diversity would have been influenced by Early Triassic changes in oceanography and climate?

Q_1 is answered by two articles published in *Palaeontologia Electronica* (Brayard et al. 2004) and the *Journal of Zoological Systematics and Evolutionary Research* (Brayard et al. 2005). These two chapters introduce a new 2D model based on a cellular-automaton approach in which SST and currents force the biogeographical dispersal of a randomly generated clade (a 2D “geophyletic” model). Conclusions of the model were validated on a present-day example: the Atlantic planktonic foraminifers, and then applied to the Early Triassic context. The approach used in this model allows us to discuss the edification of marine latitudinal diversity gradients with respect to SST gradients and oceanic currents.

Q_2: How did the global ammonoid diversity and endemicity patterns spatially and temporally change during the Early Triassic recovery?

This macroecological question is reported in a chapter which is published as an article in *Palaeogeography, Palaeoclimatology, Palaeoecology* (Brayard et al. in press). Among other things, we discuss the formation of a latitudinal gradient of ammonoid diversity concomitant with their diversification and the formation of marked SST gradient. The possibility of long-range ammonoid dispersal by the oceanic circulation is also discussed.

Q_3: What biogeographical indications can provide the comparison of faunal assemblages?

Q_3 is the purpose of a special chapter that is submitted as an article (Brayard et al. submitted). We quantitatively compare the similarity between ammonoid faunas during the entire Early Triassic by "classical" techniques (Cluster Analysis and Nonmetric Multidimensional Scaling) and a new approach ("*Bootstrapped Spanning Network*").

Q_4: Focusing on the Smithian stage, are field data from South China congruent with global data?

Until recently, qualitative and quantitative data from Tethyan equatorial Early Triassic ammonoid assemblages were few. Thus, the comprehension of global diversity patterns, especially between each side of the Panthalassa, was difficult to assess, thus preventing global climatic or paleoceanographic interpretations. This lack was partly filled by an intensive field work in South China, which is a key geographic area located under the Early Triassic equator and at the boundary between Tethyan and Panthalassic Oceans. These new data from South Chinese faunas represent ca. 4000 bed-rock sampled specimens from 7 sections.

These results are presented in a monographic treatment to be submitted to *Fossils & Strata* (Brayard & Bucher). Several genera and species are newly described and replaced in their stratigraphic position. In addition, a new and largely improved bed-rock controlled succession of Smithian ammonoids is presented for the northwestern Guangxi independently from the previous interpretations of Chao who applied the subdivision of Spath (1934). Empirical correlations are proposed with other mid- and high-paleolatitude successions.

Such systematic revision led to reconsider the phylogenetic position of some taxa, including potential survivors of the end-Permian crisis (i.e. *Proharpoceras*), a topic addressed in a paper to be submitted and not presented in this dissertation (Brayard et al. in prep).

Q_5: From the point of view of the dynamics of the ammonoid recovery, what supplementary information provide carbon isotope studies, radiometric ages and palynological studies?

These questions involve several collaborations corresponding to different articles co-authored by various members of the multidisciplinary project (Ovtcharova et al. 2006; Crasquin-Soleau et al. in

press; Galfetti et al. submitted; Hochuli et al. submitted). These articles are given in appendices, with the e Crasquin-Soleau et al. in press.

Old references cited in the foreword:

Chao, K., 1950. Some new ammonite genera of Lower Triassic from western Kwangsi. *Palaeontological Novitates*, **5**: 1-11.

Chao, K., 1959. Lower Triassic ammonoids from Western Kwangsi, China. *Palaeontologia Sinica. New Series B*, **9**. Science Press, Peking, 355 pp.

Spath, L.F. 1934. *The ammonoidea of the Trias, Catalogue of the fossil cephalopoda in the British Museum (Natural History), Part 4*. The Trustees of the British Museum, London, 521 pp.

Co-authored references of this thesis dissertation:

Brayard, A. and Bucher, H., to be submitted. Smithian (Early Triassic) ammonoid faunas from Northwestern Guangxi (South China): taxonomy and biochronology. *Fossils & Strata*.

Brayard, A., Bucher, H., Galfetti, T., Brühwiler, T., Jenks, J., Guodun, K. and Escarguel, G., in prep. The last Permian ammonoid survivor: *Proharpoceras* Chao.

Brayard, A., Bucher, H., Escarguel, G., Fluteau, F., Bourquin, S. and Galfetti, T., in press. The Early Triassic ammonoid recovery: paleoclimatic significance of diversity gradients. *Palaeogeography, Palaeoclimatology, Palaeoecology*.

Brayard, A., Escarguel, G. and Bucher, H., 2005. Latitudinal gradient of taxonomic richness: combined outcome of temperature and geographic mid-domains effects? *Journal of Zoological Systematics and Evolutionary Research*, **43**: 178-188.

Brayard, A., Escarguel, G. and Bucher, H., submitted. The biogeography of Early Triassic ammonoid faunas: clusters, gradients and networks. *Journal of Biogeography*.

Brayard, A., Héran, M.-A., Costeur, L. and Escarguel, G., 2004. Triassic and Cenozoic palaeobiogeography: two case studies in quantitative modelling using IDL. *Palaeontologia Electronica*, **7**: 22 pp.

Crasquin-Soleau, S., Galfetti, T., Bucher, H. and Brayard, A., in press: Early Triassic ostracods from northwestern Guangxi Province, South China. *Rivista Italiana di Paleontologia e Stratigrafia*, **112**.

Galfetti, T., Bucher, H., Brayard, A., Hochuli, P.A., Weissert, H., Guodun, K., Atudorei, V. and Guex, J., submitted. Late Early Triassic climate change: insights from carbonate carbon isotopes, sedimentary evolution and ammonoid paleobiogeography. *Palaeogeography, Palaeoclimatology, Palaeoecology*.

Hochuli, P., Galfetti, T., Brayard A., Bucher, H., Weissert, H. and Vigran, J.O., submitted: Stepwise biotic recovery from the Permian/Triassic boundary event related to climatic forcing. Evidence from palynology, ammonoids and stable isotopes. *Geology*.

Ovtcharova, M., Bucher, H., Schaltegger, U., Galfetti., T., Brayard, A. and Guex, J. 2006. New Early to Middle Triassic U-Pb ages from South China: calibration with ammonoid biochronozones and implications for the timing of the Triassic biotic recovery. *Earth and Planetary Science Letters*, **243**: 463-475.

INTRODUCTION TO CHAPTERS 1 AND 2
(Question 1)

1. Classical studies of past and present-day diversity patterns

Most diversity studies are based on taxonomic count because this measure is (i) the simplest to acquire, (ii) the more robust to sampling biases, and (iii) the less arbitrary in its definition and measurements.

The vast majority of studies of past and present-day global diversity (*sensu* taxonomic richness) patterns have demonstrated the existence of a Pole to Equator gradient, both on land and sea (e.g. Stehli et al. 1969; Williamson 1997; Gaston 2000). Other have shown, for instance, different large-scale patterns in longitude (e.g. Connolly et al. 2003), in altitude (e.g. Sanders 2002; Grytnes 2003; McCain 2004), in water depth (e.g. Rex 1981; Gray 1997; Rex et al. 1997; Pineda & Caswell 1998; Smith & Brown 2002), in endemism (e.g. Gaston 1994b), in range size (e.g. Gaston 1994a, 2003) or in size of organisms (e.g. Jablonski 1997; Kozlowski & Gawelczyk 2002; Roy et al. 2000, 2001, 2002). However, the processes explaining the edification of these large-scale patterns and especially the latitudinal diversity gradient are still object of debates, and the question is still if global major patterns can be satisfactorily explained or not. Evolutionary time is a dimension lacking in neontological studies, thus, a deep-time analysis as we present in the case of the Early Triassic ammonoids can greatly improve the knowledge on the edification of these large-scale patterns.

2. Classical explanations of distribution patterns and their tests by null models

Recently, factors invoked to control large-scale geographical patterns of biodiversity (*sensu* taxonomic richness) have been reviewed (e.g. Rhode 1992; Willig et al. 2003) and grouped in five main theoretical explanations: energy availability, habitat heterogeneity, evolutionary time (e.g. historical factors), area, and geometric constraints (Rahbek & Graves 2001; Whittaker et al. 2001). Yet, none already received a general consensus (e.g. Colwell et al. 2005; Hawkins et al. 2005; Zapata et al. 2005 for the debate concerning geometric constraints). Among these five classes, the geometric constraints hypothesis is particularly worthy of attention because of the probabilistic nature of its explanatory principle. In the absence of any deterministic environmental or historical gradients, the

formation of a latitudinal, longitudinal, altitudinal or depth gradient of taxonomic richness might be the direct and single consequence of the random spatial distribution and overlap of the ranges of taxa (Colwell & Hurtt 1994). This hypothesis is extremely simple and is extremely well adapted to serve as a null model as defined by Gotelli & Graves (1996):

"A null model is a pattern-generating model that is based on randomization of ecological data or random sampling from a known or imagined distribution. The null model is designed with respect to some ecological or evolutionary process of interest. Certain elements of the data are held constant, and others are allowed to vary stochastically to create new assemblage patterns. The randomization is designed to produce a pattern that would be expected in the absence of a particular mechanism."

Thus, theoretical patterns of species distribution generated by null models using geometric constraints can be compared with observed distribution patterns. In the case of marine organisms, under given observed SST and oceanic circulation conditions, differences between simulated and observed patterns would imply departure from the null hypothesis of random evolution as generated by the null model. For instance, such differences may result from non-random spatio-temporal fluctuations of speciation and extinction rates, as asserted by some evolutionary-time hypotheses (Pianka 1966; Rahbek & Graves 2001; Whittaker et al. 2001). Such differences could also result from non-random geographic dispersion of species, as directly or indirectly asserted by some energy availability, habitat heterogeneity and area hypotheses.

Such null model based on geometric constraints can be improved adding historical, phylogenetic and ecological factors controlling the migration, speciation and extinction, and distribution of taxa as suggested in the case of the "geophyletic model" of Brayard et al. (2004, 2005). For marine organisms, this improved null model comes to force the biogeographical dispersal of a randomly generated clade under specific SST and current conditions. Such model does not imply competition between species and, thus, supports some assertions of the "*Unified Neutral Theory of Biodiversity*" (*UNT*): a recent neutral theory suggested as governing community assembly evolution and stability (Bell 2001; Hubbell 2001; Webb et al. 2003), and differentiating itself from the classical theory of "*Niche Assembly*" (e.g. Hutchinson 1957; MacArthur 1970; Levin 1970; see Chase & Leibold 2003 for a recent review).

3. Which null model to use?

Null models based on a neutral approach of community assembly have many advantages compared to "*Niche Assembly*" models, notably in that they are easily interpretable (i.e. they use few parameters) and are well adapted to the description of trophic guilds (i.e. taxonomically related species occupying the same trophic level; Hubbell 2005). For instance, simple principles of the *UNT* are

surprisingly able to generate patterns with realistic parameter values such as distributions of relative abundances, species-area or abundance-range size relationships (e.g. Volkov et al. 2003).

Thus, taking into account the quality and quantity at hand, as well as the type of question we address in this thesis dissertation, the most tractable, relevant and useful null models are neutral models. Indeed, *"Niche assembly"* models would imply too many uncontrolled *ad hoc* hypotheses with too many parameters controlling the dynamics of the ammonoid recovery.

4. Test of the recovery of a clade after a mass extinction with a neutral and ecologically simple null model

The Early Triassic represents an appropriate period to study how climate and oceanic conditions influence the recovery of marine organisms after a mass extinction, especially in terms of taxonomic richness, paleobiogeography or endemism. Indeed, Early Triassic ammonoids represent an ideal case of a (quasi) monophyletic clade evolving in a stable geologic framework and thus only depending on the oceanic configuration (SST, currents, etc.; see Brayard et al. 2004, in press). Validation of results from the "geophyletic model" was obtained by a simulation of present-day distributions of planktonic Foraminifera within the Atlantic Ocean (Brayard et al. 2005). Next, we ran the "geophyletic model" within a numerical model of the Early Triassic paleogeography to simulate the diversification and distribution of diversity and the evolution of ammonoid species richness and biogeography after the Permo-Triassic mass extinction, in response to parameters such as SST, currents, and speciation and extinction rates (Brayard et al. 2004).

References:

Alonso, D. and McKane, A.J., 2004. Sampling Hubbell's neutral theory of biodiversity. *Ecology Letters*, **7**: 901-910.

Bell, G., 2001. Neutral macroecology. *Science*, **293**: 2413-2418.

Brayard, A., Bucher, H., Escarguel, G., Fluteau, F., Bourquin, S. and Galfetti, T., in press. The Early Triassic ammonoid recovery: paleoclimatic significance of diversity gradients. *Palaeogeography, Palaeoclimatology, Palaeoecology*.

Brayard, A., Escarguel, G. and Bucher, H., 2005. Latitudinal gradient of taxonomic richness: combined outcome of temperature and geographic mid-domains effects? *Journal of Zoological Systematics and Evolutionary Research*, **43**: 178-188.

Brayard, A., Héran, M.-A., Costeur, L. and Escarguel, G., 2004. Triassic and Cenozoic palaeobiogeography: two case studies in quantitative modelling using IDL. *Palaeontologia Electronica*, **7**: 22 pp.

Chase, J.M. and Leibold, M.A., 2003. *Ecological niches - Linking classical and contemporary approaches*. The University of Chicago Press, Chicago.

Colwell, R.K. and Hurtt, G.C., 1994. Nonbiological gradients in species richness and a spurious Rapoport effect. *The American Naturalist*, **144**: 570-595.

Colwell, R.K., Rahbek, C. and Gotelli, N.J., 2005. The mid-domain effect: there's a baby in the bathwater. *The American Naturalist*, **166**: E149-E154.

Connolly, S.R., Bellwood, D.R. and Hughes, T.P., 2003. Indo-Pacific biodiversity of coral reefs: deviations from a mid-domain model. *Ecology*, **84**: 2178-2190.

Gaston, K.J., 1994a. Measuring geographic range sizes. *Ecography*, **17**: 198-205.

Gaston, K.J., 1994b. *Rarity*. Chapman and Hall, London.

Gaston, K.J., 2000. Global patterns in biodiversity. *Nature*, **405**: 220-227.

Gaston, K.J., 2003. *The structure and dynamics of geographic ranges*. Oxford University Press, Oxford.

Gotelli, N.J. and Graves, G.R., 1996. *Null models in ecology*. Smithsonian Institution Press, Washington, 388pp.

Gray, S.J., 1997. Gradients in marine biodiversity. In: R.F.G. Ormond, J.D. Gage and M.V. Angel (Editors). *Marine biodiversity: patterns and processes*. Cambridge University Press, Cambridge, pp. 18-34.

Grytnes, J.A., 2003. Species-richness patterns of vascular plants along seven altitudinal transects in Norway. *Ecography*, **26**: 291-300.

Hawkins, B.A., Diniz-Filho, J.A.F. and Weis, A.E., 2005. The mid-domain effect and diversity gradients: is there anything to learn? *The American Naturalist*, **166**: E140-E143.

Hubbell, S.P., 2001. *The unified neutral theory of biodiversity and biogeography*. Princeton University Press, Princeton, NJ.

Hubbell, S.P., 2005. Neutral theory in community ecology and the hypothesis of functional equivalence. *Functional Ecology*, **19**: 166-172.

Hutchinson, G.E., 1957. Concluding remarks. *Cold Spring Harbour Symposium on Quantitative Biology*, **22**: 415-427.

Jablonski, D., 1997. Body-size evolution in Cretaceous molluscs and the status of Cope's rule. *Nature*, **385**: 250-252.

Kozlowski, J. and Gawelczyk, A.T., 2002. Why are species' body size distributions usually skewed to the right? *Functional Ecology*, **16**: 419-432.

Levin, S.A., 1970. Community equilibria and stability, and an extension of the competitive exclusion principle. *The American Naturalist*, **104**: 413-423.

MacArthur, R., 1970. Species packing and competitive equilibrium for many species. *Theoretical Population Biology*, **1**: 1-11.

McCain, C.M., 2004. The mid-domain effect applied to elevational gradients: species richness of small mammals in Costa Rica. *Journal of Biogeography*, **31**: 19-31.

Pianka, E.R., 1966. Latitudinal gradients in species diversity: a review of concepts. *The American Naturalist*, **100**: 33-46.

Pineda, J. and Caswell, H., 1998. Bathymetric species-diversity patterns and boundary constraints on vertical range distributions. *Deep-Sea Research II*, **45**: 83-101.

Rahbek, C. and Graves, G.R., 2001. Multiscale assessment of patterns of avian species richness. *Proceedings of the National Academy of Sciences of the United States of America*, **98**: 4534-4539.

Rex, M.A., 1981. Community structure in the deep-sea benthos. *Annual Review of Ecology and Systematics*, **12**: 331-353.

Rex, M.A., Etter, R.J. and Stuart, C.T., 1997. Large-scale patterns of species diversity in the deep-sea benthos. In: R.F.G. Ormond, J.D. Gage and M.V. Angel (Editors). *Marine biodiversity: patterns and processes*. Cambridge University Press, Cambridge, pp. 94-121.

Rohde, K., 1992. Latitudinal gradients in species diversity: the search for the primary cause. *Oikos*, **65**: 514-527.

Roy, K., Jablonski, D. and Martien, K.K., 2000. Invariant size-frequency distributions along a latitudianl gradient in marine bivalves. *Proceedings of the National Academy of Sciences of the United States of America*, **97**: 13150-13155.

Roy, K., Jablonski, D. and Valentine, J.W., 2001. Climate change, species range limits and body size in marine bivalves. *Ecology Letters*, **4**: 366-370.

Roy, K., Jablonski, D. and Valentine, J.W., 2002. Body size and invasion success in marine bivalves. *Ecology Letters*, **5**: 163-167.

Sanders, N.J., 2002. Elevational gradients in ant species richness: area, geometry, and Rapoport's rule. *Ecography*, **25**: 25-32.

Smith, K.F. and Brown, J.H., 2002. Patterns of diversity, depth range and body size among pelagic fishes along a gradient of depth. *Global Ecology and Biogeography*, **11**: 313-322.

Stehli, F.G., Douglas, R.G. and Newell, N.D., 1969. Generation and maintenance of gradients in taxonomic diversity. *Science*, **164**: 947-949.

Volkov, I., Banavar, J.R., Hubbell, S.P. and Maritan, A., 2003. Neutral theory and relative species abundance in ecology. *Nature*, **424**: 1035-1037.

Webb, C.O., Ackerly, D.D., McPeek, M.A. and Donoghue, M.J., 2003. Phylogenies and community ecology. *Annual Review of Ecology and Systematics*, **33**: 475-505.

Whitfield, J., 2002. Neutrality versus the niche. *Nature*, **417**: 480-481.

Whittaker, R.J., Willis, K.J. and Field, R., 2001. Scale and species richness: towards a general, hierarchical theory of species diversity. *Journal of Biogeography*, **28**: 453-470.

Williamson, M., 1997. Marine biodiversity in its global context. In: R.F.G. Ormond, J.D. Gage and M.V. Angel (Editors). *Marine biodiversity: patterns and processes*. Cambridge University Press, Cambridge, pp. 1-17.

Willig, M.R., Kaufman, D.M. and Stevens, R.D., 2003. Latitudinal gradients of biodiversity: pattern, process, scale, and synthesis. *Annual Review of Ecology and Systematics*, **34**: 273-309.

Zapata, F.A., Gaston, K.J. and Chown, S.L., 2005. The mid-domain effect revisited. *The American Naturalist*, **166**: E144-E148.

Accepted on 7 February 2005
JZS doi: 10.1111/j.1439-0469.2005.00311.178–188

[1]*Paläontologisches Institut und Museum der Universität Zürich, Karl-Schmid-Strasse 4, Zürich, Switzerland;* [2]*UMR-CNRS 5125, «Paléoenvironnements et Paléobiosphère», Université Claude Bernard Lyon 1, 2 rue Dubois, Villeurbanne Cedex, France*

Latitudinal gradient of taxonomic richness: combined outcome of temperature and geographic mid-domains effects?

A. Brayard[1,2], G. Escarguel[2] and H. Bucher[1]

Abstract

For several decades, the origin and ecological consequences of large-scale continental and marine Latitudinal Gradients of Taxonomic Richness (LGTR) have been intensively debated. Among the various hypotheses, it has been proposed that a LGTR is the by-product of a geographic mid-domain effect, i.e. the result of a random distribution of ranges of taxa between physical hard boundaries such as the continent/ocean interface. In order to more realistically evaluate the role of the mid-domain effect on the origin and evolution of the LGTR of marine planktonic organisms, we present a 2D model based on a cellular-automaton approach in which sea surface temperatures (SST) and currents are forced in the biogeographic dispersal of a randomly generated clade (a 2D 'geophyletic' model). Sensitivity experiments allow to evaluate the effects of currents, SST and the geographical origin of a clade on the formation and shape of a LGTR for planktonic organisms when coupled with a geographic mid-domain effect. Results are discussed in the light of the empirical LGTR of extant planktonic Foraminifera in the Atlantic Ocean. Independently of any other biotic or abiotic parameter, inclusive of the surface currents and origination/extinction absolute and relative rates, our simulations show that the coupling of the mid-domain effect with two critical parameters, namely the shape and intensity of the SST gradient and the geographic origin of a clade, produces realistic patterns of diversity when compared with the observed LGTR of extant atlantic planktonic foraminifera. The results illustrate a non-linear relation between a unimodal latitudinal SST gradient and a resulting bimodal LGTR characterized by a drop in species richness near the equator. This relation indicates that the SST gradient exerts a mid-domain effect on the LGTR. The latitudinal positions of the modal values of the LGTR are also found to be influenced by the geographic origin of the simulated clade.

Key words: Latitudinal gradient of taxonomic richness – probabilistic model – sea surface temperature – currents – mid-domain effect – Planktonic Foraminifera – Atlantic Ocean

Introduction

The latitudinal gradient of taxonomic richness (LGTR) is one of the most studied patterns of global biodiversity (e.g. Dobzhansky 1950; MacArthur 1965; Stehli et al. 1969; Currie and Paquin 1987; Gaston 2000; Hillebrand 2004). It is known to occur in a majority of taxonomic groups and is manifested in most cases as a decreasing number of taxa (species, genera or families) from low to high latitudes: tropical areas show higher taxonomic richness values than at the poles. The latitudinal diversity cline recognized on land and sea is classically described as unimodal with a taxonomic richness monotonically increasing from the pole to the equator (e.g. Pianka 1966; Gaston 2000). However, a second pattern has to be considered. It is often found in marine environments and consists of a bimodal gradient of taxonomic richness with two maxima centred near the Tropics of Cancer and Capricorn, separated by a drop of taxonomic richness near the equator (e.g. Rutherford et al. 1999). This bimodal pattern is usually interpreted as being a derivative from a primarily unimodal richness gradient.

Classical explanations

Although many ecologists, biogeographers and biologists have discussed the ecological and evolutionary mechanisms at the origin of LGTR (see Rohde 1992 and Willig et al. 2003 for a review of the different classical factors), hypotheses explaining the spatial structure and temporal variability of the distribution of taxonomic richness on Earth are still contentious (e.g. Clarke 1992; Chown and Gaston 2000).

Indeed, about 30 possible explanations have been proposed to explain the origin of the LGTR. Most of them imply empirical, direct or indirect relationships between taxonomic richness and climatic gradients. These involve, e.g. potential evapotranspiration (Currie and Paquin 1987), temperature (Turner et al. 1987), productivity (Kaspari et al. 2000), which are all grouped within the energy-hypothesis (Currie 1991). Other explanations imply evolutionary and dispersal rates (e.g. Pianka 1966; Graham et al. 1996; Wilson 1998). Some of the determinants of the formation of the LGTR can also involve parameters such as area, predation and competition levels, or biotic spatial heterogeneity. It has been shown that the majority of these hypotheses cannot be used for the purpose of a general or unique explanation; moreover, most of them contain various degrees of circularity or are not supported by sufficient evidence (Rohde 1992). Considered separately, each of these appears insufficient to fully explain the existence of the LGTR as observed on land and sea. Furthermore, most of these hypotheses do not take into account the phylogenetic time dimension, i.e. the deep-time scale at which species originate, evolve, and become extinct.

The mid-domain effect

Biodiversity and geometric constraints

Recently, all of these hypotheses were reduced to five main explanations grouped in the following classes: energy availability, habitat heterogeneity, evolutionary time, area, and geometric constraints (Rahbek and Graves 2001; Whittaker et al. 2001). Among these five classes, the geometric constraints hypothesis is particularly worthy of attention because of the probabilistic nature of its explanatory principle. In the absence of any deterministic environmental or historical gradients, the formation of a latitudinal, longitudinal, altitudinal or depth gradient of taxonomic richness might be the

direct and single consequence of the random spatial distribution and overlap of the ranges of taxa. Under these conditions, the random placement (in one or two dimensions) of species geographic ranges on a bounded domain (e.g. sea, continent, island, mountain) never generates a uniform spatial distribution, but always produces a peak of taxonomic richness near the centre of the area: the 'mid-domain effect' (Colwell and Hurtt 1994; Ney-Nifle and Mangel 1999; Colwell and Lees 2000; Jetz and Rahbek 2001; Grytnes and Vetaas 2002; McCain 2003, 2004; Colwell et al. 2004). Following this hypothesis, the latitudinal, longitudinal, altitudinal or bathymetric positions of the species ranges directly determine the shape of the taxonomic gradient.

Evaluation of the mid-domain effect in biogeographic patterns

Earlier 1D simulations with geometrically constraining boundaries (Colwell and Hurtt 1994; Colwell and Lees 2000) showed that a LGTR can be the simple geometric by-product (the mid-domain effect result) of the random distribution of taxa ranges between 'hard' boundaries (e.g. coast lines), and that a LGTR does not necessarily require any biotic and/or abiotic deterministic explanation. This result can be applied to any living organism and any particular biogeographic setting. An LGTR emerges even if no deterministic environmental gradient is applied in the simulation. By producing a mid-domain effect, this null geometric model suggests that an observed LGTR can simply be the result of chance: between two fixed boundaries, randomly distributed ranges always give rise to a peak or a plateau of taxonomic richness (Lees et al. 1999; Jetz and Rahbek 2001). Thus, the random location of ranges between fixed geographic boundaries may generate distributions of taxonomic richness comparable with empirical distributions.

Several of the documented past or present taxonomic richness gradients present, at first approximation in both hemispheres, a parabolic-shape with a maximum value at middle or low latitudes (McCoy and Connor 1980; Turner 1981; France 1992; Angel 1993; Crow 1993; Brown and Lomolino 1998; Willig and Lyons 1998; Crame 2000, 2001, 2002; Culver and Buzas 2000; Sax 2001; Ellison 2002; Connolly et al. 2003; Shen and Shi 2004), intermediate altitudes (Rahbek 1995, 1997; Fleishman et al. 1998; Kessler 2001; Lomolino 2001; Grytnes and Vetaas 2002; Sanders 2002; Grytnes 2003; Bhattarai et al. 2004; McCain 2004) or intermediate marine depths (Rex 1981; Paterson and Lambshead 1995; Pineda and Caswell 1998; Smith and Brown 2002). For instance, the distribution of many Madagascan insect species and the resulting, dome-shaped LGTR with a modal value at mid-latitudes and elevations, are less in agreement with climatic variables than with the prediction of the geometric mid-domain model (Lees et al. 1999). It has also been documented that species richness of ant communities peaks at mid-elevations, suggesting that the mid-domain effect could also have an important part in the development of altitudinal gradients (Sanders 2002; McCain 2004).

Nevertheless, the geometric model has generally a poor explanatory power, especially when applied to 2D cases and has been heavily criticized (Bokma et al. 2001; Koleff and Gaston 2001; Hawkins and Diniz-Filho 2002; Laurie and Silander 2002; Valle de Britto Rangel and Diniz-Filho 2003; Zapata et al. 2003; see Colwell et al. 2004 for a discussion of the concept and applications of the mid-domain effect). Possible errors in sampling or interpolation of the number of taxa can also explain some of the discrepancies between the output of geometric models and observed LGTR (e.g. Colwell and Hurtt 1994; Rahbek 1995; Grytnes and Vetaas 2002). Problems inherent to the construction of the geometric models can also arise as most of the previous tests of geometric null models versus observed data did not factor in an environmental or historical component. This addition may adjust the output of geometric models and observed LGTR. For instance, it is often considered that the dispersion limits of a taxon could be deterministically controlled in low latitudes/altitudes by the increase of severe biotic conditions like competition or predation (Kaufman 1995; Brown et al. 1996; Sax 2001). Furthermore, it is generally suggested that severe abiotic conditions at high latitudes/altitudes (e.g. frequent climatic variations and/or extremely low-temperatures) could induce natural boundaries for the ranges of many organisms. Consequently, geometric models with a random placement of the ranges of species should be combined with environmental parameters in order to more realistically predict observed LGTR.

In order to better understand the consequences of the omission of the environmental gradients and the phylogenetic time dimension in the construction of geometric models, we introduce here a more general, cellular automaton-type, 2D geometric model based on a step-by-step simulation and constrained biogeographic dispersal of a random phylogeny – a 'geophyletic' model. Results of the simulations are illustrated in the particular biogeographic, thermal and ocean currents configuration of the present-day North and South Atlantic. They are discussed in the light of the well-documented present latitudinal gradient of species richness of planktonic Foraminifera (Hemleben et al. 1989; Hilbrecht 1996; Arnold and Parker 1999; Rutherford et al. 1999). Our approach evaluates the effects of currents, sea surface temperatures (SST), speciation and extinction rates, as well as species thermal dependence on the formation and shape of a species richness gradient for planktonic organisms. We also discuss the respective influence of these parameters in combination with a possible geographic mid-domain effect. This work is a first step toward the biogeographic modelling and evaluation of climatic influences in the recovery of marine organisms after mass extinctions (Brayard et al. 2004).

Materials and Methods

The studied bounded geographic area

The model is based on three 120×120 matrices representing the Atlantic Ocean and its bordering continents (North and South America, Europe and Africa). Each cell represents one square degree between 100°W and 20°E (continent boundaries), and 60°N and 60°S (latitudinal proxies of the weakening of the SST gradient). The three matrices are: (1) The biogeographic matrix, where the presence or absence of each simulated taxon (hereafter, species) in each sea cell is recorded (as we focus on planktonic organisms, continental cells are obviously 'non-colonisable'). (2) The sea surface temperatures matrix (data from the National Oceanic and Atmospheric Administration, Fig. 1a). (3) The sea surface currents (SSC) matrix, with directions and intensities based on the present Atlantic surface currents (data from Pickard and Emery 1990; Fig. 1b). Because the map represents a non-iso-surface, a correction-factor (varying with latitude) is applied so that the amount of displacement of each species during one time iteration is kept latitude-independent.

General concept of the 'geophyletic' model

Our algorithm consists of a step-by-step generation of a random clade (i.e. a monophyletic assemblage of taxa, using a simple standard

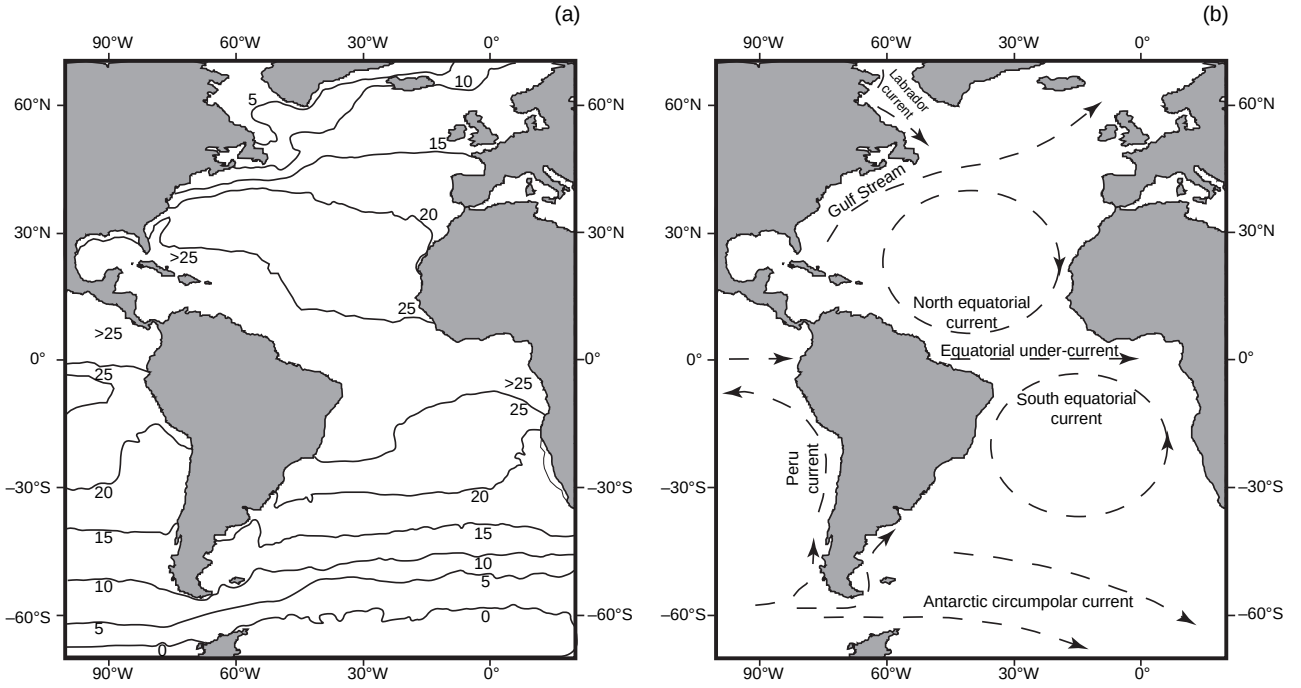

Fig. 1. Atlantic Ocean (a) SST (data from the National Oceanic and Atmospheric Administration) and (b) generalized surface circulation (data from Pickard and Emery 1990)

Markovian procedure) and its geographic dispersion (*sensu* Rosen 1992 and Cecca 2002) under the direct control of the SST and SSC matrices. It stands in contrast with the classic 'MBL' algorithm (Raup et al. 1973; Raup and Gould 1974; Gould et al. 1977; Raup 1977; Stanley et al. 1981) in that it simultaneously controls the growth of the random clade at the local (i.e. cell) level and at the global level. The local geographic control on the evolutionary dynamic of the clade generates ecologically more realistic null models of phylogenesis and community assembly evolution (Hubbell 2001; Webb et al. 2003). Actually, our 'geophyletic' model can be described as being globally time-homogeneous in that species origination and extinction probabilities are statistically constant at the global clade level. It is also locally time-inhomogeneous in that local extinction probability is kept species richness-dependent in order to avoid ecologically unrealistic overcrowding of species in local communities. Our model thus combines characteristics of the two main options of the MBL model ('Damped-Equilibrium' and 'Freely Floating') described by Gould et al. (1977; see Raup 1985).

Inheritance rule of the thermal ranges between mother and daughter species is set as follows: the thermal range of the daughter species must include the temperature of the cell where speciation occurred (extrinsic, physical constraint; Fig. 2). Consequently, the thermal ranges of a mother and a daughter species at least partly intersect (intrinsic, phylogenetic constraint). The effects of this partial constraint imposed on the random evolution of the species thermal range throughout speciation events compare with the Markovian Drift Coefficient used by MacLeod (2002). It is worth noting that in no way is this inheritance process a type of selection controlling the simulation, the thermal range of the daughter species being free to assume many values of the ancestral thermal range. The choice to add this constraint to the model is supported by the observed latitudinal overlap in distributions of closely related planktonic foraminifera (de Vargas et al. 2001).

The amplitude of each thermal range can be either fixed or randomly chosen from 5°C to 15°C to cover the vast majority of observed distributions of planktonic organisms. Uniform or non-uniform probability functions can be selected for the sorting of thermal ranges. For instance, higher probabilities of random sorting were chosen and assigned to the thermal ranges comprised between 10 and 15 °C in order to more realistically reflect observed distributions of planktonic Foraminifera. Indeed, most planktonic Foraminifera are restricted to

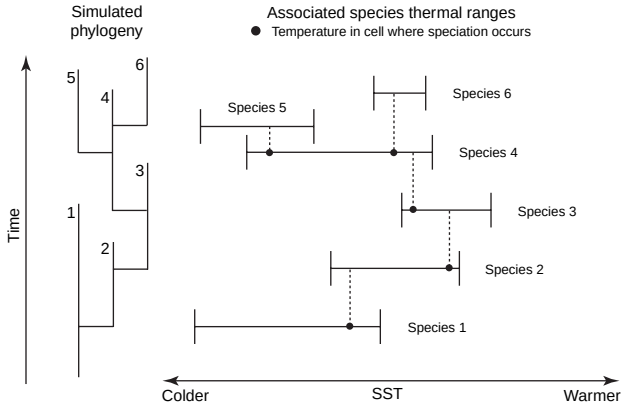

Fig. 2. Illustration of the inheritance rule of the thermal ranges between mother and daughter species

portions of the SST gradient such as the tropics, the temperate or the high latitudes, each of these portions spanning temperature ranges of about 10–15°C (Hemleben et al. 1989; Arnold and Parker 1999). This choice of thermal ranges is also in agreement with the temperatures of foraminifer cultures (Bijma et al. 1990).

The amplitude of each thermal range is converted to a 2D geographic range located between 60°N and 60°S. A simulated species can have its geographic range overlapping part of the northern and/or southern hemisphere, or covering the equatorial region. Geometric spatial constraints operate between continent boundaries and the approximate limit of weakening of the SST gradient (near 60°N and 60°S in the Atlantic Ocean). Thus, a geometrical mid-domain effect is expected within this bounded domain, with a near-equatorial peak of diversity. During the simulations, each simulated species can move independently from others (ecological associations of species are deliberately ignored in order to generate the 'geophyletic' null model), under the limiting controls of SST and SSC matrices.

Procedure steps of the algorithm

Each time-iteration of the algorithm can be divided into five steps, where the controlling parameters of the simulation are tested consecutively for each filled cell of the biogeographic matrix (Fig. 3). (1) Speciation: a new species can originate in any cell filled by the mother-species, given a probability of speciation inversely correlated with the number of neighbouring cells occupied by the mother-species. Changes in speciation rates during the simulation are allowed. (2) Species displacement: a species occurring in a cell can move into any other randomly chosen adjacent cell, provided that it is not already present in that new cell and that the temperature of the new cell is compatible with its own thermal range. The SSC matrix directly controls the probability distribution for each cell and each species. The probability of dispersion can be adjusted to correspond to the intensity of the surface currents (accelerating or slowing down the propagation of the species). Consequently, each species is let free to colonize part or all of the geographic area compatible with its thermal range. (3) Extinction: two cases with distinct associated probabilities, 'local' and 'complete' extinctions, are distinguished and treated separately. The disappearance of a given species in one cell ('local' extinction) does not affect the neighbouring cells occupied by the same species. In the case of a 'complete' extinction, all the cells filled by the species are simultaneously emptied. As for the speciation rates, both 'local' and 'complete' extinction rates can be modified during the simulation. (4) Diversity threshold of cells (i.e. carrying capacity): in order to avoid ecologically unrealistic accumulations of species in cells, 'local' extinctions are randomly generated (i.e. the probability of 'local' extinction is deterministically increased) in cells where the number of species is greater than a given threshold saturation value. This threshold determines the number of species supported by the environment. The default value is arbitrarily fixed at 30 species, a value based on the observed maximum association of co-existing species of Atlantic planktonic Foraminifera (Rutherford et al. 1999). (5) Finally, the species richness is calculated for each cell of the biogeographic matrix as the sum of co-occurring species. Even if these four first steps are successively executed for each filled cell at each time iteration, the speciation, extinction and displacement events may not necessarily occur, thus making the changes in species richness of a given cell independent from those of other cells.

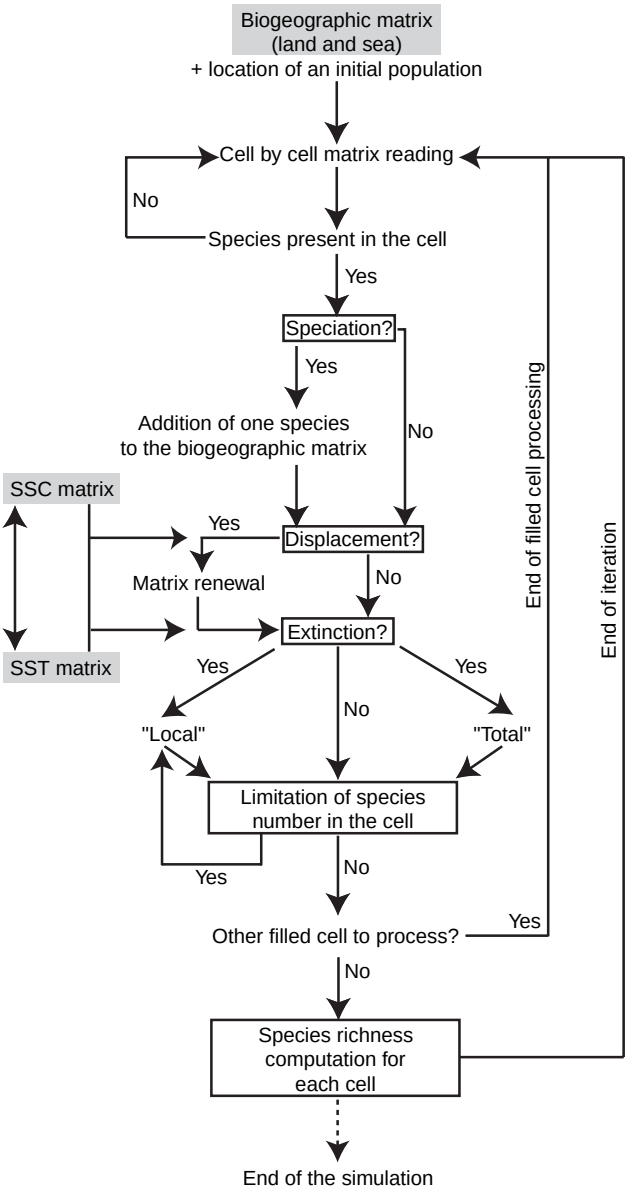

Fig. 3. Flow chart of the 2D 'geophyletic' model. See text for details about the different tests and procedures contained in each step

Therefore, running our 'geophyletic' model for several hundreds of iterations (depending on the selected speciation and extinction rates) allows us to construct theoretical patterns of species richness distribution under the SST and SSC-constrained hypothesis of random evolution and geographic dispersal. Such theoretical patterns of species distribution can thus be compared with observed distribution patterns. Under given observed SST and SSC conditions, differences between simulated and observed patterns would imply departure from the null hypothesis of random evolution as generated by the model. For instance, such differences may result from non-random spatio-temporal fluctuations of speciation and extinction rates, as asserted by some 'evolutionary-time' hypotheses (Pianka 1966; Rahbek and Graves 2001; Whittaker et al. 2001). Such differences could also result from non-random geographic dispersion of species, as directly or indirectly asserted by some 'energy availability', 'habitat heterogeneity' and 'area' families hypotheses.

Results

Patterns of latitudinal species richness

We ran our 'geophyletic' model, constrained by modern Atlantic SST and SSC conditions, using the following speciation and extinction probability values: allopatric speciation $= 5 \times 10^{-6}$, parapatric speciation $= 2 \times 10^{-6}$, sympatric speciation $= 1 \times 10^{-6}$, 'local' extinction $= 1 \times 10^{-2}$, and 'total' extinction $= 1 \times 10^{-4}$ (it must be here again stressed that speciation and 'local' extinction are controlled at the local, one square degree cell level). With such parameter values, the simulations reached a stable dynamic equilibrium after *c.* 1000 iterations. The results presented and discussed hereafter were obtained from 1200 iterations; several independent simulations (initiated with distinct, randomly chosen uniform pseudo-random number generator seeds) yielded very similar patterns of diversity indicating that the model had reached equilibrium.

Given the assumption of an inter-tropical geographic origin of the clade, we simulated the distribution of species richness and its corresponding LGTR for planktonic organisms (Fig. 4, to be compared with Fig. 5a). Contrary to the classic expectation of monotonically increasing species richness from the pole to the equator (unimodal LGTR from pole-to-pole), the simulated distributions and gradients clearly show two peaks of maximum species richness centred near the Tropics of Cancer and Capricorn, separated by a marked drop around the equator (bimodal LGTR).

The shape of the LGTR observed for extant Foraminifera is very similar to that simulated by the 'geophyletic' model,

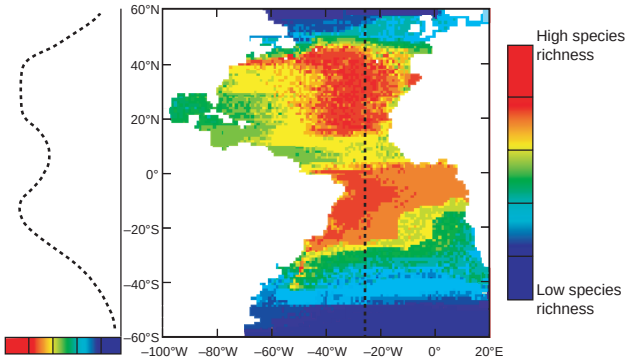

Fig. 4. Pattern of distribution of planktonic species richness and associated LGTR simulated with present-day SST and SSC data, randomly generated 10–15°C thermal ranges, a low latitude last common ancestor and no latitudinal gradients of origination and extinction rates (see text for details)

with a marked drop of species richness near the equator and highest diversities occurring at the same tropical latitudes (~15° to 30° in each hemisphere). Our results are close to the pattern predicted by Rutherford et al. (1999; Fig. 5b) on the single basis of the observed polynomial relation between SST and species richness. Even if our results correctly reproduce, both qualitatively and quantitatively, the observed diversity pattern of Atlantic planktonic Foraminifera at a global scale, some minor differences between the simulated and observed diversity patterns exist, notably on the longitudinal location of the maxima of species richness. In the southern hemisphere, the maxima of species richness are shifted toward the west in our simulations. Another discrepancy is the absence of a diversity peak within the Caribbean Sea.

Influential parameters

In order to test the stability and reproducibility of the results, we performed sensitivity experiments by successively varying the parameters controlling the simulations.

The sea surface temperature latitudinal gradient

We first examined the impact of the unimodal pole-to-pole latitudinal gradient of SST on the simulation results. Its intensity has a strong influence on the simulated LGTR: the steeper the SST gradient, the more bimodal the shape of the LGTR. Consequently, the simulated LGTR is unimodaly centred on the equator only for very weak SST gradients. Our simulations, therefore, suggest that the SST gradient is a crucial physical parameter controlling the emergence and shape of the LGTR.

In most of our simulations, the non-linear relation between the simulated bimodal LGTR and SST values is best fit with a third-order polynomial (associated determination coefficient R^2 comprised between 0.85 and 0.95), which allows a faithful description of the simulated decreasing richness centred on the equator (Fig. 6). Graphical investigation of the simulated SST/LGTR relationship for various sets of controlling parameters suggests that the inferred third-order polynomial distribution can satisfactorily be divided into three distinct linear segments, which can be isolated by linear Piecewise Analysis (Neter et al. 1990; Toms and Lesperance 2003). For simulations based on the present Atlantic thermal conditions, and independent of the values of other parameters, SST values display two remarkably stable slope changes in the SST/LGTR relation. The first slope change is situated at *c*. 10°C and the second is found at *c*. 22–24°C. The first middle/high-latitudes segment is always associated with low values of species richness and corresponds to a low or nil increase of species richness with temperature. The second middle/low-latitudes segment corresponds to a marked increase of species richness with

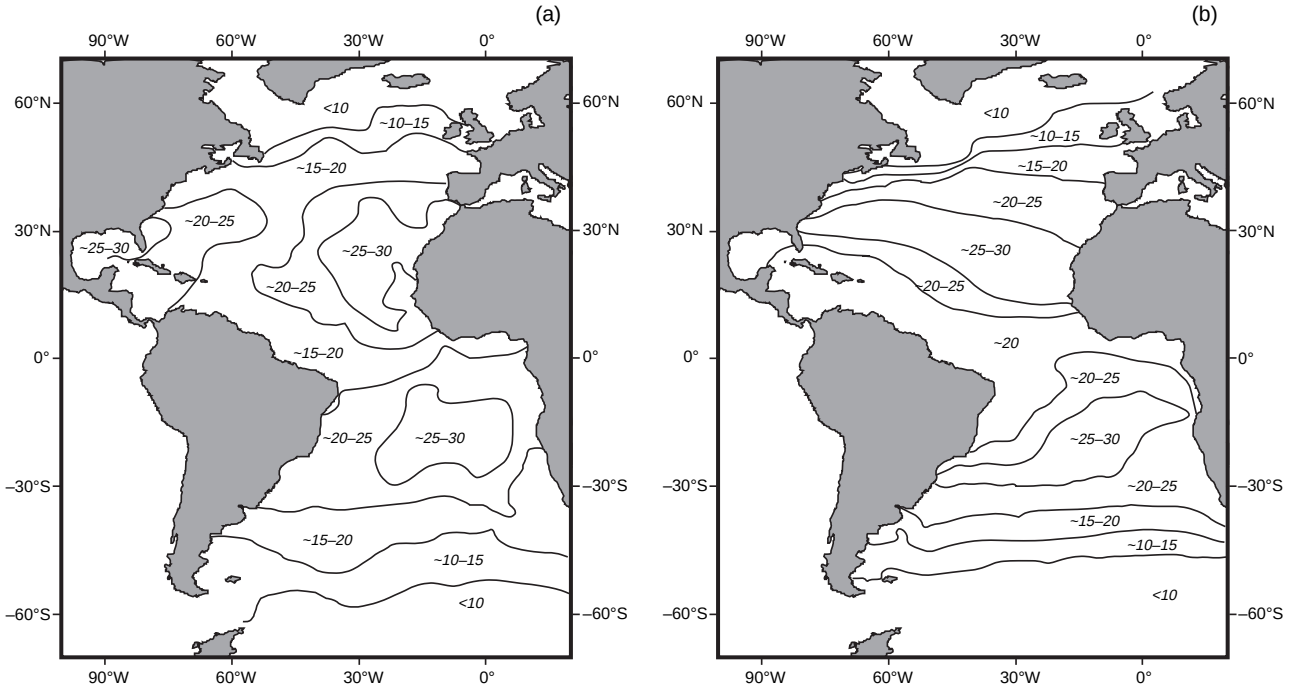

Fig. 5. Present-day (a) and predicted (b) planktonic foraminiferal diversity in the Atlantic (adapted from Rutherford et al. 1999)

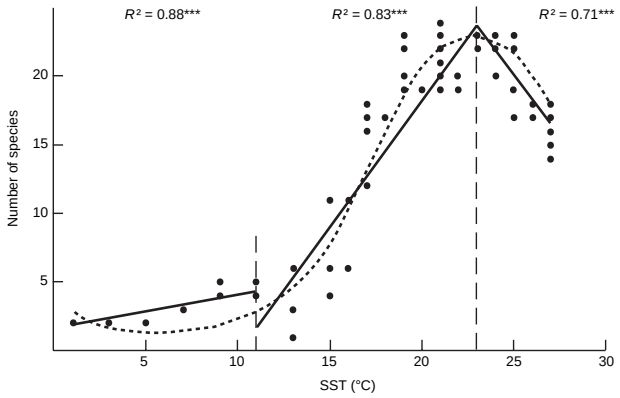

Fig. 6. Third-order polynomial and Piecewise analysis of the SST-LGTR relation corresponding to Fig. 4

temperature. The third segment (inter-tropical latitudes) corresponds to a significant decrease of species richness with temperature. The location of the thermal breakdown around 22–24°C is also observed by Rutherford et al. (1999: Fig. 3). The breakdown at *c*. 10°C is also documented in empirical data but is less pronounced. This convergence between the observed and simulated SST/LGTR relationship suggests that our 'geophyletic' model generates realistic patterns of diversity.

Amplitude of the thermal ranges of the simulated species
This biological parameter does not affect the bimodal structure of the simulated LGTR but strongly controls its shape. For a given set of simulation parameters yielding a bimodal LGTR, randomly generated broad thermal ranges yield a relatively flattened, but always bimodal LGTR, while narrow thermal ranges yield a relatively steep bimodal LGTR with modal values slightly closer to the equator.

Intensities of the SSC
Although SSC have a strong influence on the timing and local modalities of the dispersion of simulated species, they have no influence on the shape and magnitude of the simulated LGTR. Even in the extreme and unrealistic case where no SSC are imposed in the model, a bimodal LGTR centred on the Tropics of Cancer and Capricorn persists.

Geographic origin of the simulated clade
The geographic origin of the clade has an unexpected effect on the simulated LGTR: the lower the latitude of origination of a clade, the closer the two modal values of the simulated bimodal LGTR. A simulated bimodal LGTR centred on the Tropics of Cancer and Capricorn will result from a tropical last common ancestor. A simulated bimodal LGTR with modes placed at higher latitudes will be generated by a mid- or high-latitudes last common ancestor. This result does not appear to be an artefact illustrating non-equilibrated simulation outputs: it was observed for numerous independent runs of various lengths and corresponds to the steady state of the model. Instead, it is most likely to be the direct consequence of the partial inheritance of the thermal range imposed by speciation events as defined in the model (Fig. 2).

Speciation and extinction rates
Although the extinction and speciation probabilities obviously control the dynamics of the simulation (i.e. the number of iterations required for the model to reach a dynamic equilibrium steady state), their absolute or relative values do not affect the shape of the simulated diversity pattern. Moreover, gradual or abrupt changes of these rates during the simulation do not really modify the results at the global geographic scale. Finally, gradients of origination and extinction rates varying with latitudes have absolutely no effects on the shape and magnitude of the simulated LGTR.

Maximal diversity threshold
All other things being equal, changing the value of the empirical diversity threshold changes the amplitude of the LGTR but does not affect its unimodal or bimodal structure nor the latitudinal location of the modes.

Discussion

Latitudinal gradient of taxonomic richness and sea surface temperature

Although the LGTR is frequently documented in empirical data, it is most often modelled with a simple or multiple linear regression (e.g. Kaufman and Willig 1998; Stevens 2004). This usually leads to consider that observed past and present marine as well as terrestrial LGTRs are unimodal gradients centred near the equator. In this context, the frequently observed drop of species richness around the equator is masked by the search for a linear relation between latitude and taxonomic richness, and thus often interpreted as the consequence of some sampling or analytical artefact (e.g. Crame 2002). It consequently remains generally poorly understood, if not completely ignored.

While linear regression and correlation methods are useful if the LGTR has a unimodal shape, they obviously fail to model a bimodal LGTR as it is actually observed for planktonic Foraminifera (Rutherford et al. 1999) and most of the present and past LGTRs (McCoy and Connor 1980; Brown and Lomolino 1998; Kaufman and Willig 1998; Crame 2000, 2001, 2002; Culver and Buzas 2000; Sax 2001; Grytnes and Vetaas 2002). The fact that a bimodal LGTR is documented – even if not always recognized – for marine taxa as varied as Foraminifera (Rutherford et al. 1999), bivalves (Crame 2000, 2001, 2002), brachiopods (Shen and Shi 2004), bryozoans (Clarke and Lidgard 2000), prosobranch gastropods (Roy et al. 1998), crayfish (France 1992), fish (Angel 1993) or seaweed (Bolton 1994), as well as for terrestrial taxa amphibians, reptiles, birds or mammals (McCoy and Connor 1980; Currie 1991; Sax 2001), strongly suggests that this pattern is not an artefact and is controlled by a parameter common to all of these cases. The results of our simulations suggest that this central, primary parameter is likely to be the latitudinal temperature gradient.

All other things being equal, and regardless of the latitudinal location of maximal taxonomic richness values, the general bimodal structure of the LGTR generated by our 2D 'geophyletic' model appears to be mostly controlled by a single parameter: the shape and magnitude of the SST gradient. The third-order polynomial relation between LGTR and SST values, and the inter-tropical decrease of species richness in particular, can be explained as the direct consequence of the overlap of thermal ranges (a thermal mid-domain effect) of species constrained by a non-uniform SST gradient. When constrained by a steep and sigmoid-like SST

gradient such as that of the present-day (Fig. 7a), the latitudinal projection of randomly distributed thermal ranges always generates a LGTR with modal values located at intermediate latitudes (Fig. 7c). For the same distribution of thermal ranges, reduced steepness of the SST gradient (Fig. 7b) leads to a weakened LGTR (Fig. 7d). Consequently, our model suggests that the global shape of a given LGTR can be interpreted as a simple geometric (mid-domain) effect produced by, and modulated by, the shape and magnitude of the SST gradient.

Our simulations indicate that under present-day Atlantic conditions, simulated clades always generate two peaks of species richness at the latitudes of the Tropics of Cancer and Capricorn while a single modal value should be expected near the equator as a result of the single geographic mid-domain effect. Superimposition of the SST gradient on the simple geographic mid-domain effect splits the expected unimodal LGTR into two roughly symmetric species richness gradients peaking at intermediate latitudes, between maximum and minimum SST values (Fig. 7). This result leads to consider each hemisphere as a bounded thermal domain where the principle of the mid-domain effect effectively applies. The observed bimodal LGTR can thus be interpreted as resulting from the combination of two distinct geometric mid-domain effects: geographic and thermal.

Geographic origin of the first simulated species

In addition to the shape and magnitude of the SST gradient, the geographic location of the first simulated species appears to be important in controlling the location of the LGTR modes. This evolutionary parameter corresponds to an intrinsic phylogenetic control of the biogeographic development of the simulated clade; it by no means implies latitudinally differentiated extinction and/or speciation rates, but simply corresponds to the origination area of the simulated taxonomic group. This effect is very likely to result from the partial inheritance of the thermal range of the mother species during each simulated speciation event. During the simulated history of a clade, some of the new species may thus progressively diffuse away from the thermal range of their common ancestor (Fig. 2).

From this point of view, it appears that a way to obtain a simulated LGTR similar to the one observed for present Atlantic planktonic Foraminifera (and many other taxonomic groups) requires a steep SST gradient and a biogeographic dispersal from middle to low latitudes. This interpretation is consistent with the oversimplified theory that characterizes the tropics as a 'cradle' and the poles as a 'museum' (Crame 1992, 2001; Chown and Gaston 2000). Conversely, simulations of clades originating at middle to high latitudes always produce LGTR modal values at middle to high latitudes. Although less frequently documented, such high latitudinal modal values are known for Phocidae (Stevens 1989; Proches 2001), some pelagic seabirds (Proches 2001), some bivalves (Crame 2002; Valdovinos et al. 2003), and prosobranchs (Valdovinos et al. 2003).

The latitudinal gradient of Atlantic planktonic Foraminifera

In the case of present-day Atlantic foraminifera, observed and modelled distributions and gradients indicate that species richness clearly decreases with the highest temperatures. This is confirmed by a significant third-order polynomial covariation between species richness and SST values (Rutherford et al. 1999). This bimodal pattern was first interpreted as the consequence of mixed water assemblages near the equatorial convergence between the North and South Atlantic gyres (Rutherford et al. 1999; Clarke and Lidgard 2000). A second hypothesis suggesting that the equatorial SST values are too high to maintain the physiological functioning of foraminifera, has also been proposed by Rutherford et al. (1999). However, as noted by these authors and Bijma et al. (1990), this explanation is not entirely convincing as many foraminifera were bred and reproduced with relatively good success at temperatures higher than the maximum SST values observed in the Atlantic Ocean (*c.* 30°C).

The similarities observed between the LGTR simulated by our 2D 'geophyletic' model and most observed distributions and gradients of species richness (especially for foraminifera (Rutherford et al. 1999; Fig. 5) suggest that, in a given geographic context, a realistic LGTR can be simulated by controlling only two primary drivers: the shape and magnitude of the SST gradient and the geographic origin of the

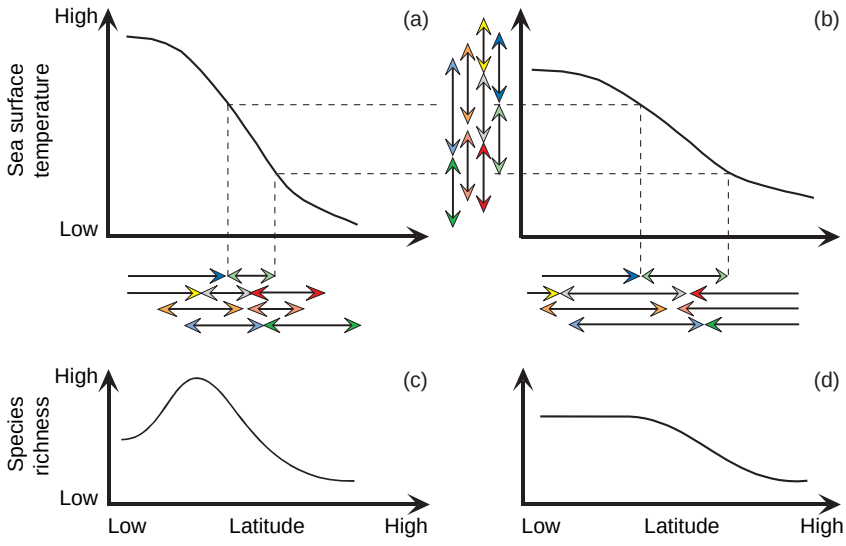

Fig 7. Illustration of the causal effect of the magnitude of the SST gradient on the shape and magnitude of the resulting LGTR. The latitudinal projection (horizontal arrows) of a given random distribution of thermal ranges (vertical arrows) on a steep (a) or weakened (b) SST gradient leads to a steep bimodal (c) or weakened unimodal (d) LGTR, respectively. The different colours of arrows correspond to different species

evolutionary history of the clade. The persistence of bimodal gradient in simulations where oceanic currents are suppressed, suggests that the inter-tropical drop of species richness may not result from mixed water assemblages in the convergence zone between the North and South Atlantic gyres. Similarly, the fact that the simulated gradient is unaffected by the values and degree of latitudinal differentiation of speciation and/or extinction rates indicates that no such hypothesis is necessary to generate observed LGTR (*fide* Sax 2001; Hille Ris Lambers et al. 2002; Bromham and Cardillo 2003; *contra* Rohde 1992; Jablonski 1993; Arnold and Parker 1999; Chown and Gaston 2000; Buzas et al. 2002; Crame 2002). Simulated changes in the thermal ranges of species also indicate that the difference of frequency between widespread species having a broad latitudinal range linked to a large (e.g. 15°C) temperature range and restricted species having a narrow latitudinal range linked to a small (e.g. 5°C) temperature range does not eliminate the bimodal structure of the LGTR, but strongly influences its shape by either decreasing or increasing its steepness.

Historical explanation of the drop in present-day equatorial foraminiferal diversity involves the effect of the successive glaciation episodes during Plio-Quaternary times. Such episodes directly controlled the biogeographic distributions of foraminifera and other pelagic organisms by shrinking or expending their geographic ranges (e.g. Lazarus et al. 1995; Wilson 1998; Kandiano et al. 2004). However, alternations between the present-day SST gradient (inter-glacial conditions) and a steeper and colder SST gradient (glacial conditions) during the simulation do not modify the bimodal structure of the LGTR. Therefore, along with other explanations such as differential evolutionary rate or the current effect, this historical hypothesis does not appear to be a fundamental factor in the making of a bimodal LGTR.

Other classically invoked factors not taken into account in our simulations, such as energy availability, productivity, seasonality or geographic area (Rohde 1992), all strongly directly or indirectly covary with latitude. These factors also do not appear necessary for generating a realistic, large-scale bimodal LGTR, although their relative influences remain to be tested with the same type of simulations. This of course does not imply that all of these factors do not participate at local or regional levels (e.g. in generating regions of maximum or minimum richnesses such the Amazon Basin or the Caribbean islands), but it plays down their respective roles as primary causes or limiting factors for the global shape of the large scale LGTR. For instance, the longitudinal discrepancies between the observed and simulated patterns of diversity are certainly because of the effects of these numerous additional factors.

Conclusion

The 2D 'geophyletic' model presented in this paper allows realistic simulations of the modern distribution of species richness and bimodal gradient for present Atlantic planktonic Foraminifera. It emphasizes a simple relationship between the observed latitudinal SST gradient and LGTR (Fig. 7). Extending this result to numerous other marine taxonomic groups that also present a bimodal LGTR allows us to hypothesize that a large-scale marine LGTR is a double geometric by-product of the geographic context and of the latitudinal SST gradient combined with the dispersal history of the clade. To a first order, our simulation model suggests that classically invoked biotic or abiotic parameters such as SSC, differential evolutionary rates, ecological associations (Rahbek and Graves 2001; Whittaker et al. 2001) are unnecessary to simulate bimodal large-scale LGTRs. Nevertheless, as all LGTR include local or regional variations and exceptions, such second order parameters are obviously required to explain the finer structure of the pattern of taxonomic richness. In this context, it seems logically difficult to consider only one biotic (e.g. physiologic) or abiotic (physical environment) parameter as the single deterministic cause in the development of marine LGTRs. Thus, other proposed factors underlying a LGTR should be tested with similar models to see if similar patterns emerge. Moreover, similar models should ideally be constructed with different clades to test if thermal range, dispersion ability, diversity threshold or other parameters help to modulate the formation and evolution of bimodal diversity pattern. To complement this, a third dimension (e.g. depth of marine species) should be added: in the special case of Foraminifera, the role of depth (also related to the thermal gradient) has been identified in speciation processes (e.g. Schneider and Kennett 1999). Subsequently, a 3D model, while computationally much more time-consuming, could greatly improve and refine the resulting simulated diversity pattern.

In the absence of other constraints, the results of null models based on the mid-domain effect may not always yield realistic results (e.g. Koleff and Gaston 2001; Hawkins and Diniz-Filho 2002; Valle de Britto Rangel and Diniz-Filho 2003; Zapata et al. 2003). However, when used in combination with climatic and evolutionary constraints, this type of probabilistic model can reproduce the essential patterns of LGTR. In turn, the better characterization of the non-linear relation between a given SST gradient, and the corresponding global structure of a large scale LGTR, enables prediction of the relative changes in the shape, magnitude and evolution of past SST gradients for well-documented fossil LGTRs (Brayard et al. 2004).

Acknowledgements

We thank S. Legendre (UMR-CNRS 5125, Lyon) and P. Linder (University of Zürich) for stimulating comments on an earlier draft version and two anonymous reviewers for insightful remarks on a first version of this paper. Three JZSER reviewers, F. Cecca, R.K. Colwell and N. MacLeod, provided constructive critics which helped us to improve the manuscript. M. Williams (British Antarctic Survey) and S. Gilder (Institut de Physique du Globe, Paris) kindly improved the English spelling. This work was supported by the Swiss NSF project 2100-068061.02 (A.B. and H.B.), the program CNRS/INSU-Eclipse, project 00-10 (A.B. and G.E.), and a Rhône-Alpes-Eurodoc grant (A.B.).

Résumé

Gradients latitudinaux de richesse taxonomique: résultat combiné des effets de milieu de domaine géographique et thermique?

Depuis plusieurs décennies, l'origine et l'interprétation écologique des Gradients Latitudinaux de Richesse Taxonomique (LGTR) marins ou continentaux, ont été intensivement débattues. Parmi de nombreuses hypothèses, il a été proposé qu'un LGTR puisse être le sous-produit d'un effet de milieu de domaine géographique, i.e. le résultat d'une distribution aléatoire des répartitions des taxa entre deux limites physiques telles que l'interface continent/océan. Afin d'évaluer plus efficacement le rôle de cet effet sur l'origine et l'évolution des LGTR des organismes planctoniques marins, nous proposons un modèle 2D basé sur une approche de type automate cellulaire dans laquelle les

températures des eaux de surface (SST) et les courants régulent la dispersion biogéographique d'une phylogénie générée aléatoirement (un modèle «géophylétique»). Ce modèle permet d'évaluer les effets des courants, des SST et de la dépendance thermique des espèces sur la mise en place et la forme d'un LGTR impliquant des organismes planctoniques. Il permet aussi de discuter des influences respectives de ces paramètres quand ils sont superposés à l'effet de milieu de domaine géographique. Les résultats sont discutés à partir du LGTR empirique des foraminifères planctoniques atlantiques actuels. Indépendamment de tout autre paramètre biotique ou abiotique, y compris les courants ainsi que les taux relatifs et absolus d'apparition et d'extinction, les simulations font apparaître que le couplage de l'effet de milieu de domaine à deux contraintes principales, la forme et l'intensité du gradient de SST ainsi que la localisation géographique de l'origine du clade, produit des représentations réalistes de la diversité comparées au LGTR observé pour les foraminifères planctoniques actuels de l'océan atlantique. Nos résultats indiquent une relation non-linéaire entre la structure globale d'un gradient unimodal de SST et le LGTR bimodal correspondant, montrant une baisse de richesse spécifique au niveau de l'équateur. Cette relation suggère que le gradient de SST exerce un effet de milieu de domaine thermique sur le LGTR. Les positions latitudinales des modes du LGTR sont aussi influencées par le lieu d'origine du clade simulé.

References

Angel, M. V., 1993: Biodiversity of the pelagic Ocean. Conserv. Biol. **7,** 760–772.

Arnold, A. J.; Parker, W. C., 1999: Biogeography of planktonic Foraminifera. In: Gupta, B. S. K. (ed.), Modern Foraminifera. Dordrecht: Kluwer Academic Publishers, 103–122.

Bhattarai, K. R.; Vetaas, O. R.; Grytnes, J. A., 2004: Fern species richness along a central Himalayan elevational gradient, Nepal. J. Biogeogr. **31,** 389–400.

Bijma, J.; Faber, W. W., Jr; Hemleben, C., 1990: Temperature and salinity limits for growth and survival of some planktonic foraminifers in laboratory cultures. J. Foramin. Res. **20,** 95–116.

Bokma, F.; Bokma, J.; Monkkonen, M., 2001: Random processes and geographic species richness patterns: why so few species in the north? Ecography **24,** 43–49.

Bolton, J. J., 1994: Global seaweed diversity: patterns and anomalies. Bot. Mar. **37,** 241–245.

Brayard, A.; Héran, M.-A.; Costeur, L.; Escarguel, G., 2004: Quantitative paleobiogeographic modelling using IDL®: Triassic and Cenozoic applications. Palaeontol. Elec. **7,** 22.

Bromham, L.; Cardillo, M., 2003: Testing the link between the latitudinal gradient in species richness and rates of molecular evolution. J. Evolution. Biol. **16,** 200–207.

Brown, J. H.; Lomolino, M. V., 1998: Biogeography. Sunderland: Sinauer Associates, Inc.

Brown, J. H.; Stevens, G. C.; Kaufman, D. M., 1996: The geographic range: size, shape, boundaries, and internal structure. Ann. Rev. Ecol. Syst. **27,** 597–623.

Buzas, M. A.; Collins, L. S.; Culver, S. J., 2002: Latitudinal difference in biodiversity caused by higher tropical rate of increase. Proc. Natl Acad. Sci. U.S.A. **99,** 7841–7843.

Cecca, F., 2002: Palaeobiogeography of Marine Fossil Invertebrates – Concepts and Methods. London and New York: Taylor and Francis.

Chown, S. L.; Gaston, K. J., 2000: Areas, cradles and museums: the latitudinal gradient in species richness. Trends Ecol. Evol. **15,** 311–315.

Clarke, A., 1992: Is there a latitudinal diversity cline in the sea? Trends Ecol. Evol. **7,** 286–287.

Clarke, A.; Lidgard, S., 2000: Spatial patterns of diversity in the sea: bryozoan species richness in the North Atlantic. J. Anim. Ecol. **69,** 799–814.

Colwell, R. K.; Hurtt, G. C., 1994: Nonbiological gradients in species richness and a spurious Rapoport effect. Am. Nat. **144,** 570–595.

Colwell, R. K.; Lees, D. C., 2000: The mid-domain effect: geometric constraints on the geography of species richness. Trends Ecol. Evol. **15,** 70–76.

Colwell, R. K.; Rahbek, C.; Gotelli, N. J., 2004: The mid-domain effect and species richness patterns: what have we learned so far? Am. Nat. **163,** E1–E23.

Connolly, S. R.; Bellwood, D. R.; Hughes, T. P., 2003: Indo-Pacific biodiversity of coral reefs: deviations from a mid-domain model. Ecology **84,** 2178–2190.

Crame, J. A., 1992: Evolutionary history of the polar region. Hist. Biol. **6,** 37–60.

Crame, J. A., 2000: Evolution of taxonomic diversity gradients in the marine realm: evidence from the composition of recent bivalve faunas. Paleobiology **26,** 198–215.

Crame, J. A., 2001: Taxonomic diversity gradients through geological time. Divers. Distrib. **7,** 175–189.

Crame, J. A., 2002: Evolution of taxonomic diversity gradients in the marine realm: a comparison of Late Jurassic and Recent bivalve faunas. Paleobiology **28,** 184–207.

Crow, G. E., 1993: Species diversity in aquatic angiosperms: latitudinal patterns. Aquat. Bot. **44,** 229–258.

Culver, S. J.; Buzas, M. A., 2000: Global latitudinal species diversity gradient in deep-sea benthic foraminifera. Deep-Sea Res. I **47,** 259–275.

Currie, D., 1991: Energy and large-scale patterns of animal- and plant-species richness. Am. Nat. **137,** 27–49.

Currie, D.; Paquin, V., 1987: Large-scale biogeographic patterns of species richness of trees. Nature **329,** 326–327.

Dobzhansky, T., 1950: Evolution in the tropics. Am. Sci. **38,** 209–221.

Ellison, A. M., 2002: Macroecology of mangroves: large-scale patterns and processes in tropical coastal forests. Trees-Stuct. Funct. **16,** 181–194.

Fleishman, E.; Austin, G. T.; Weiss, A. D., 1998: An empirical test of Rapoport's rule: elevational gradients in montane butterfly communities. Ecology **79,** 2482–2493.

France, R., 1992: The North American latitudinal gradient in species richness and geographic range of freshwater crayfish and amphipods. Am. Nat. **139,** 342–354.

Gaston, K. J., 2000: Global patterns in biodiversity. Nature **405,** 220–227.

Gould, S. J.; Raup, D. M.; Sepkoski, J. J., Jr; Schopf, T. J. M.; Simberloff, D. S., 1977: The shape of evolution: a comparison of real and random clades. Paleobiology **3,** 23–40.

Graham, R. W.; Lindelius, E. L.; Graham, M. A.; Schroeder, E. K.; Toomey, R. S.; Anderson, E.; Barnosky, A. D.; Burns, J. A.; Churcher, C. S.; Grayson, D. K.; Guthrie, R. D.; Harington, C. R.; Jefferson, G. T.; Martin, L. D.; McDonald, H. G.; Morlan, R. E.; Semken, H. A.; Webb, S. D.; Werdelin, L.; Wilson, M. C., 1996: Spatial response of mammals to Late Quaternary environmental fluctuations. Science **272,** 1601–1606.

Grytnes, J. A., 2003: Species-richness patterns of vascular plants along seven altitudinal transects in Norway. Ecography **26,** 291–300.

Grytnes, J. A.; Vetaas, O. R., 2002: Species richness and altitude: a comparison between null models and interpolated plant species richness along the Himalayan altitudinal gradient, Nepal. Am. Nat. **159,** 294–304.

Hawkins, B. A.; Diniz-Filho, J. A. F., 2002: The mid-domain effect cannot explain the diversity gradient of Neartic birds. Global Ecol. Biogeogr. **11,** 419–426.

Hemleben, C.; Spindler, M.; Anderson, O. R., 1989: Modern Planktonic Foraminifera. Berlin: Springer Verlag.

Hilbrecht, H., 1996: Extant planktic foraminifera and the physical environment in the Atlantic and the Indian Oceans. Mitt. Geol. Inst. Eidgen., Tech. Hochsch. Univ. Zürich, Neue Folge. **300,** 1–93.

Hille Ris Lambers, J.; Clark, J. S.; Beckage, B., 2002: Density-dependent mortality and the latitudinal gradient in species diversity. Nature **417,** 732–735.

Hillebrand, H., 2004: On the generality of the latitudinal diversity gradient. Am. Nat. **163,** 192–211.

Hubbell, S. P., 2001: The Unified Neutral Theory of Biodiversity and Biogeography. Princeton, NJ: Princeton University Press.

Jablonski, D., 1993: The tropics as a source of evolutionary novelty through geological time. Nature **364,** 142–144.

Jetz, W.; Rahbek, C., 2001: Geometric constraints explain much of the species richness pattern in African birds. Proc. Natl Acad. Sci. U.S.A. **98,** 5661–5666.

Kandiano, E. S.; Bauch, H. A.; Müller, A., 2004: Sea surface temperature variability in the North Atlantic during the last two glacial-interglacial cycles: comparison of faunal, oxygen isotopic, and Mg/Ca-derived records. Palaeogeogr. Palaeoclim. Palaeoecol. **204,** 145–164.

Kaspari, M.; O'Donnell, S.; Kercher, J. R., 2000: Energy, density, and constraints to species richness: ant assemblages along a productivity gradient. Am. Nat. **155,** 280–293.

Kaufman, D. M., 1995: Diversity of New World mammals: universality of the latitudinal gradients of species and bauplans. J. Mammal. **76,** 322–334.

Kaufman, D. M.; Willig, M. R., 1998: Latitudinal patterns of mammalian species richness in the New World: the effects of sampling method and faunal group. J. Biogeogr. **25,** 795–805.

Kessler, M., 2001: Patterns of diversity and range size of selected plant groups along an elevational transect in the Bolivian Andes. Biodivers. Conserv. **10,** 1897–1921.

Koleff, P.; Gaston, K. J., 2001: Latitudinal gradients in diversity: real patterns and random models. Ecography **24,** 341–351.

Laurie, H.; Silander, J. A. J., 2002: Geometric constraints and spatial pattern of species richness: critique of range-based null models. Divers. Distrib. **8,** 351–364.

Lazarus, D.; Hilbrecht, H.; Spencer-Cervato, C.; Thierstein, H., 1995: Sympatric speciation and phyletic change in *Globorotalia truncatulinoides*. Paleobiology **21,** 28–51.

Lees, D. C.; Kremen, C.; Andriamampianina, L., 1999: A null model for species richness gradients: bounded range overlap of butterflies and other rainforest endemics in Madagascar. Biol. J. Linn. Soc. **67,** 529–584.

Lomolino, M. V., 2001: Elevation gradients of species-density: historical and propective views. Global Ecol. Biogeogr. **10,** 3–13.

MacArthur, R. H., 1965: Patterns of species diversity. Biol. Rev. **40,** 510–533.

MacLeod, N., 2002: Testing evolutionary hypotheses with adaptive landscapes: use of random phylogenetic-morphological simulation studies. Math. Geol. **6,** 45–55.

McCain, C. M., 2003: North American desert rodents: a test of the mid-domain effect in species richness. J. Mammal **84,** 967–980.

McCain, C. M., 2004: The mid-domain effect applied to elevational gradients: species richness of small mammals in Costa Rica. J. Biogeogr. **31,** 19–31.

McCoy, E. D.; Connor, E. F., 1980: Latitudinal gradients in the species diversity of North American mammals. Evolution **34,** 193–203.

Neter, J.; Wasserman, W.; Kutner, M. H., 1990: Applied Linear Statistical Models. Homewood-Boston: Irwin Inc.

Ney-Nifle, M.; Mangel, M., 1999. Species-area curves based on geographic range and occupancy. J. Theor. Biol. **196,** 327–342.

Paterson, G. L. J.; Lambshead, P. J. D., 1995: Bathymetric patterns of polychaete diversity in the Rockall Trough, northeast Atlantic. Deep-Sea Res. I **42,** 1199–1214.

Pianka, E. R., 1966: Latitudinal gradients in species diversity: a review of concepts. Am. Nat. **100,** 33–46.

Pickard, G. L.; Emery, W. J., 1990: Descriptive Physical Oceanography: An Introduction. Oxford: Pergamon Press.

Pineda, J.; Caswell, H., 1998: Bathymetric species-diversity patterns and boundary constraints on vertical range distributions. Deep-Sea Res. II **45,** 83–101.

Proches, S., 2001: Back to the sea: secondary marine organisms from a biogeographic perspective. Biol. J. Linn. Soc. **74,** 197–203.

Rahbek, C., 1995: The elevational gradient of species richness: a uniform pattern? Ecography **18,** 200–205.

Rahbek, C., 1997: The relationship among area, elevation, and regional species richness in neotropical birds. Am. Nat. **149,** 875–902.

Rahbek, C.; Graves, G. R., 2001: Multiscale assessment of patterns of avian species richness. Proc. Natl Acad. Sci. U.S.A. **98,** 4534–4539.

Raup, D. M., 1977: Stochastic models in evolutionary palaeontology. In: Hallam, A. (ed.), Patterns of Evolution, as Illustrated by the Fossil Record. Developments in Palaeontology and Stratigraphy. Amsterdam: Elsevier, 59–78.

Raup, D. M., 1985: Mathematical models of cladogenesis. Paleobiology **11,** 42–52.

Raup, D. M.; Gould, S. J., 1974: Stochastic simulation and evolution of morphology – towards a nomothetic paleontology. Syst. Zool. **23,** 305–322.

Raup, D. M.; Gould, S. J.; Schopf, T. J. M.; Simberloff, D. S., 1973: Stochastic models of phylogeny and the evolution of diversity. J. Geol. **81,** 525–542.

Rex, M. A., 1981: Community structure in the deep-sea benthos. Ann. Rev. Ecol. Syst. **12,** 331–353.

Rohde, K., 1992: Latitudinal gradients in species diversity: the search for the primary cause. Oikos **65,** 514–527.

Rosen, B. R., 1992: Empiricism and the biogeographic black box: concepts and methods in marine palaeobiogeography. Palaeogeogr. Palaeoclim. Palaeoecol. **92,** 171–205.

Roy, K.; Jablonski, D.; Valentine, J. W.; Rosenberg, G., 1998. Marine latitudinal diversity gradients: test of causal hypotheses. Proc. Natl Acad. Sci. U.S.A. **95,** 3699–3702.

Rutherford, S.; D'Hondt, S.; Prell, W., 1999: Environmental controls on the geographic distribution of zooplankton diversity. Nature **400,** 749–753.

Sanders, N. J., 2002: Elevational gradients in ant species richness: area, geometry, and Rapoport's rule. Ecography **25,** 25–32.

Sax, D. F., 2001: Latitudinal gradients and paleogeographic ranges of exotic species: implications for biogeography. J. Biogeogr. **28,** 139–150.

Schneider, C. E.; Kennett, J. P., 1999: Segregation and speciation in the Neogene planktonic foraminiferal clade *Globoconella*. Paleobiology **25,** 383–395.

Shen, S.-Z.; Shi, G. R., 2004: Capitanian (Late Guadalupian, Permian) global brachiopod palaeobiogeography and latitudinal diversity pattern. Palaeogeogr. Palaeoclim. Palaeoecol. **208,** 235–262.

Smith, K. F.; Brown, J. H., 2002: Patterns of diversity, depth range and body size among pelagic fishes along a gradient of depth. Global Ecol. Biogeogr. **11,** 313–322.

Stanley, S. M.; Signor, III, P. W.; Lidgard, S.; Karr, A. F., 1981: Natural clades differ from 'random' clades: simulations and analyses. Paleobiology **7,** 115–127.

Stehli, F. G.; Douglas, R. G.; Newell, N. D., 1969: Generation and maintenance of gradients in taxonomic diversity. Science **164,** 947–949.

Stevens, G. C., 1989: The latitudinal gradient in geographic range: how so many species coexist in the Tropics. Am. Nat. **133,** 240–256.

Stevens, R. D., 2004: Untangling latitudinal richness gradients at higher taxonomic levels: familial perspectives on the diversity of New World bat communities. J. Biogeogr. **31,** 665–674.

Toms, J. D.; Lesperance, M. L., 2003: Piecewise regression: a tool for identifying ecological thresholds. Ecology **84,** 2034–2041.

Turner, J. T., 1981: Latitudinal patterns of calanoid and cyclopoid copepod diversity in estuarine waters of eastern North America. J. Biogeogr. **8,** 369–382.

Turner, J. R. G.; Gatehouse, C. M.; Corey, C. A., 1987: Does solar energy control organic diversity? Butterflies, moths and the British climate. Oikos **48,** 195–205.

Valdovinos, C.; Navarrete, S. A.; Marquet, P. A., 2003: Mollusk species diversity in the Southeastern Pacific: why are there more species towards the pole? Ecography **26,** 139–144.

Valle de Britto Rangel, T. F. L.; Diniz-Filho, J. A. F., 2003: Spatial patterns in species richness and the geometric constraint simulation model: a global analysis of mid-domain effect in Falconiformes. Acta Oecol. **24,** 203–207.

de Vargas, C.; Renaud, S.; Hilbrecht, H.; Pawlowski, J., 2001: Pleistocene adaptive radiation in Globorotalia truncatulinoides: genetic, morphologic, and environmental evidence. Paleobiology **27,** 104–125.

Webb, C. O.; Ackerly, D. D.; McPeek, M. A.; Donoghue, M. J., 2003: Phylogenies and community ecology. Annu. Rev. Ecol. Syst. **33,** 475–505.

Whittaker, R. J.; Willis, K. J.; Field, R., 2001: Scale and species richness: towards a general, hierarchical theory of species diversity. J. Biogeogr. **28,** 453–470.

Willig, M. R.; Lyons, S. K., 1998: An analytical model of latitudinal gradients of species richness with an empirical test for marsupials and bats in the New World. Oikos **81,** 93–98.

Willig, M. R.; Kaufman, D. M.; Stevens, R. D., 2003: Latitudinal gradients of biodiversity: pattern, process, scale, and synthesis. Ann. Rev. Ecol. Syst. **34,** 273–309.

Wilson, G. D. F., 1998: Historical influences on deep-sea isopod diversity in the Alantic Ocean. Deep-Sea Res. II **45,** 279–301.

Zapata, F. A.; Gaston, K. J.; Chown, S. L., 2003: Mid-domain models of species richness gradients: assumptions, methods and evidence. J. Anim. Ecol. **72,** 677–690.

Authors' addresses: Arnaud Brayard, Paläontologisches Institut und Museum der Universität Zürich, Karl-Schmid-Strasse 4, CH-8006 Zürich, Switzerland; and UMR-CNRS 5125, «Paléoenvironnements et Paléobiosphère», Université Claude Bernard Lyon 1, 2 rue Dubois, F-69622 Villeurbanne Cedex, France. E-mail: arnaud.brayard@univ-lyon1.fr (for correspondence); Gilles Escarguel, UMR-CNRS 5125, «Paléoenvironnements et Paléobiosphère», Université Claude Bernard Lyon 1, 2 rue Dubois, F-69622 Villeurbanne Cedex, France; Hugo Bucher, Paläontologisches Institut und Museum der Universität Zürich, Karl-Schmid-Strasse 4, CH-8006 Zürich, Switzerland.

Palaeontologia Electronica
http://palaeo-electronica.org

TRIASSIC AND CENOZOIC PALAEOBIOGEOGRAPHY: TWO CASE STUDIES IN QUANTITATIVE MODELLING USING IDL®

Arnaud Brayard, Marie-Anne Héran, Loïc Costeur, and Gilles Escarguel

ABSTRACT

This work presents two examples of palaeobiogeographic reconstruction using the Interactive Data Language® (IDL). Although this meta-language is devoted to geoscientists and offers an array of easily usable tools, few palaeontologists actually use it. Our purpose is to illustrate how the IDL can be used to generate clear and direct visualizations of simulation results and interpolation methods for personal Geographic Information Systems (GIS).

The first example is a paleogeographic simulation of the biodiversity evolution of planktonic species (and especially ammonoids) in the Early Triassic. Principal results of this global scale simulation are that the formation of a marine latitudinal gradient of species richness depends on the shape and magnitude of the Sea Surface Temperature (SST) gradient, and the geographic location of the group's ancestor. Thus, the recovery pattern of Early Triassic ammonoids species richness can be simulated and explained by a general increasing trend in steepness of the SST gradient.

The second example describes a custom-designed GIS for large European Neogene continental mammals. Species richness and ecomorphologic parameters are interpolated, monitored in several ways, and discussed. Comparisons with the present-day distribution of large European mammals are also drawn and allow us to recognize that a broad North/South aridity gradient already existed by the Late Miocene with more open environments in Southern Europe.

Arnaud Brayard. Paläontologisches Institut und Museum der Universität Zürich, Karl-Schmid Strasse 4, CH-8006 Zürich, Switzerland and UMR-5125 CNRS, Paléoenvironnements et Paléobiosphère, Université Claude Bernard Lyon 1, 2 rue Dubois, F-69622 Villeurbanne Cedex, France
Arnaud.Brayard@univ-lyon1.fr
Marie-Anne Héran. UMR-5125 CNRS, Paléoenvironnements et Paléobiosphère, Université Claude Bernard Lyon 1, 2 rue Dubois, F-69622 Villeurbanne Cedex, France. marie-anne.heran@univ-lyon1.fr
Loïc Costeur. UMR-5125 CNRS, Paléoenvironnements et Paléobiosphère, Université Claude Bernard Lyon 1, 2 rue Dubois, F-69622 Villeurbanne Cedex, France. loic.costeur@univ-lyon1.fr
Gilles Escarguel. UMR-5125 CNRS, Paléoenvironnements et Paléobiosphère, Université Claude Bernard Lyon 1, 2 rue Dubois, F-69622 Villeurbanne Cedex, France. gilles.escarguel@univ-lyon1.fr

KEY WORDS: palaeobiogeography; numerical modelling; species richness; interpolations; Early Triassic; Neogene; interactive data language
PE Article Number: 7.2.6A

Submission: 5 May 2004 Acceptance: 2 November 2004

INTRODUCTION

The field naturalist vision is being increasingly abandoned in palaeontology, favouring desktop study ahead of fieldwork and leading to virtual palaeoworlds. Even though the numerical dimension may alienate scientists and disconnect them from the actual parameters of their problems, the use of numerical simulations can allow the testing of hypotheses that depend on multiple variables that putatively control the dynamic evolution of a system (Cleland 2001). Moreover, quantitative visualization offers illustrations or animations that may convey ideas more effectively. This paper investigates how powerful Interactive Data Language® (IDL) tools can be used to interactively visualize, analyse, and discuss results from large palaeontological data sets.

This work presents two examples of palaeobiogeographic reconstructions, one Triassic and one Cenozoic, using the IDL programming environment. We begin by examining the Triassic example, a general 2D palaeobiogeographic model based on the constrained spreading of random phylogenies (Brayard 2002). Simulations are carried out in the biogeographic, thermal, and ocean current setting of the Early Triassic. Modelled and present-day Pacific Ocean Sea Surface Temperatures (SST) and Sea Surface Currents (SSC) are applied to discuss the recovery and distribution of planktonic species following the Permo-Triassic crisis. In the second part, we focus on IDL's Geographic Information Systems (GIS) facilities that can be used to plot mammal diversity and ecomorphologic data on Neogene palaeogeographic maps.

Both models are written with IDL 5.2 and run on Windows 98 and XP, Unix/Linux, and MacOS systems. IDL represents a complete computing and programming system for interactive analysis and visualization of data sets (Marschallinger 2001). IDL is a programming meta-language implemented in ENVI (Environment for Visualizing Images®) by Research Systems Inc. This meta-language is especially dedicated to numerical analysis and 2D/3D image processing. Several pre-packaged graphic modules are able to interact with each other, giving IDL a major advantage in time required for application development compared with other, more popular languages like FORTRAN or C. Yet IDL keeps its compatibility with standard programming languages through specialized functions.

IDL allows the user to create custom procedures, functions, or applications using simple matrix representation without using explicit loop structures to process matrix data, further reducing development time. IDL also allows the creation of graphic user interfaces. Results can be viewed immediately after processing using many pre-packaged graphic tools. All IDL functions, additional functions, and examples can be downloaded on the Research Systems Inc. homepage (http://www.rsinc.com). An open-source clone (PyDL) of IDL is also developed in Python for Linux.

In geosciences, this language has been used primarily for satellite image analysis and 2D/3D object modelling in applications such as the spatiotemporal analysis of basin history. The use of IDL in palaeontology is still rare and usually limited to the reconstruction and analysis of fossil morphology (Marschallinger 2001). In this work, IDL is used as a tool for calculating and visualizing palaeobiogeographic maps. The palaeobiological implications of this study will not be discussed in great detail; rather we concentrate on the construction of the two models and the benefits of IDL.

EXAMPLE 1: A 2-D EVOLUTIONARY/DISPERSAL PALAEOBIOGEOGRAPHIC RECONSTRUCTION OF EARLY TRIASSIC AMMONOIDS

Overview of the Geological and Palaeogeographic Context

Early Triassic palaeogeography is relatively simple, largely because continents were joined together in a single block known as Pangea. Pangea was surrounded by a wide ocean (Panthalassa) and partially bisected by the Tethys Sea (Elmi and Babin 1996). The Triassic was followed by the largest mass extinction ever at the Permo-Triassic boundary. During this crisis, more than

90% of marine species disappeared (Raup and Sepkoski 1982). The reef fauna was severely affected and during this period trilobites became extinct (Erwin 1993, 1994). The Early Triassic appears to have been marked by poorly diversified faunal communities, composed of mobile species and a high percentage of predators (Erwin 1998, 2001). The Permo-Triassic crisis is considered to be the Phanerozoic's most drastic reorganisation of ecosystems and animal diversity.

By the Late Permian latitudinal temperature gradients were steep, but, in the late Upper Permian and in the earliest Triassic (Griesbachian), latitudinal temperature gradients were warmer and weaker from the pole to the equator. This change can be inferred from both the fossil record and climatic simulations (Hotinski et al. 2001, Kidder and Worsley 2004). The evolution of the latitudinal temperature gradient during the rest of the Early Triassic (Dienerian, Smithian, and Spathian) is still poorly understood (Kidder and Worsley 2004). However, the recovery of marine and terrestrial organisms following the crisis was reached by the Spathian/Anisian boundary (Erwin and Pan 1996), indicating that the latitudinal temperature gradient probably shifted by that time, with colder temperatures at high latitudes.

Ammonoids were the most prominent marine group during the earliest Triassic (Kummel 1973; Tozer 1973), when they were cosmopolitan with few species. The situation changed through quick diversification and organisation into latitudinal gradients of species richness (Dagys 1988). The greatest biogeographic differentiation of ammonoid faunas was observed in the Spathian with high endemism in boreal ammonoids (Dagys 1997). There were no important palaeogeographic events during the Early Triassic, which makes it an appropriate period to study the climatic influence on the biodiversity of ammonoids or other marine organisms possessing at least one planktonic or pseudo-planktonic living stage. We used a numerical model of the Early Triassic palaeogeography, to simulate the redistribution of biodiversity and the evolution of planktonic or pseudo-planktonic organisms, in response to parameters such as SST, SSC, and speciation and extinction rates.

Algorithm

The probabilistic model presented below uses two physical environmental factors (SST and SSC) to control geographic displacements, speciation events, and extinction of planktonic species (Brayard 2002). We used an algorithm based on the idea of cellular automata. These automata are divided in modules interacting with each other via action or reaction loops. Depending on local conditions, numerical objects (e.g., cells, sand particles) can interact and self-organize, creating spatial and temporal patterns (Wootton 2001).

The program was designed in three parts (Figure 1). The main module built the Early Triassic palaeogeography from a digitized version of a published reconstruction (Smith et al. 1994, from 60° North and 60° South and from 180° West to 180° East, Figure 2). The geographic space is represented as an X * Y matrix corresponding to the longitudinal (X) and latitudinal (Y) subdivisions in which each grid-cell represents a quadrate of 360/X° by 120/Y°. Land is coded as 1 and sea as 0. The system also handled the biogeographic distribution of n simulated species whose presence (coded as number 1) or absence (coded as number 0) are saved in a matrix with dimensions X * Y * n, where n is the number of species.

The second module applied a latitudinal gradient of SST to the X * Y * n biogeographic matrix, which constrains geographic displacements, speciation events, and local extinctions for each simulated species based on a fixed or random thermal range for that species. Because the shape, intensity, and evolution of the SST gradient through the Early Triassic are actually unknown, we constructed a number of hypothetical SST gradients using the present-day Pacific gradient as a starting point (data from the National Oceanic and Atmospheric Administration http://polar.wwb.noaa.gov). Even if the Panthalassic Ocean was significantly wider than the modern Pacific, the choice of the Pacific SST gradient as a model is justified by the global geographic similarity between the two.

The third module managed the distribution, direction, and intensity of oceanic currents. The module is activated every time a species displacement on the biogeographic grid is called for. We also derived the Early Triassic current configuration from the present-day Pacific as represented in the current data published by Pickard and Emery (1990). The matrix of currents was constructed by choosing a single direction of current (among eight possible directions) for each cell. Each direction was coded by a number from one to eight. Zero is equivalent to the lack of a current and therefore equal probability of displacement in any directions (Figure 3). Current intensity was represented using discrete probabilities of displacements – the higher the probability in one direction, the higher the strength of the current (Figure 3). Use of continuous probabilities (e.g., calculated from equations of diffusion and advection) would make the displacements more realistic; nevertheless, it would involve

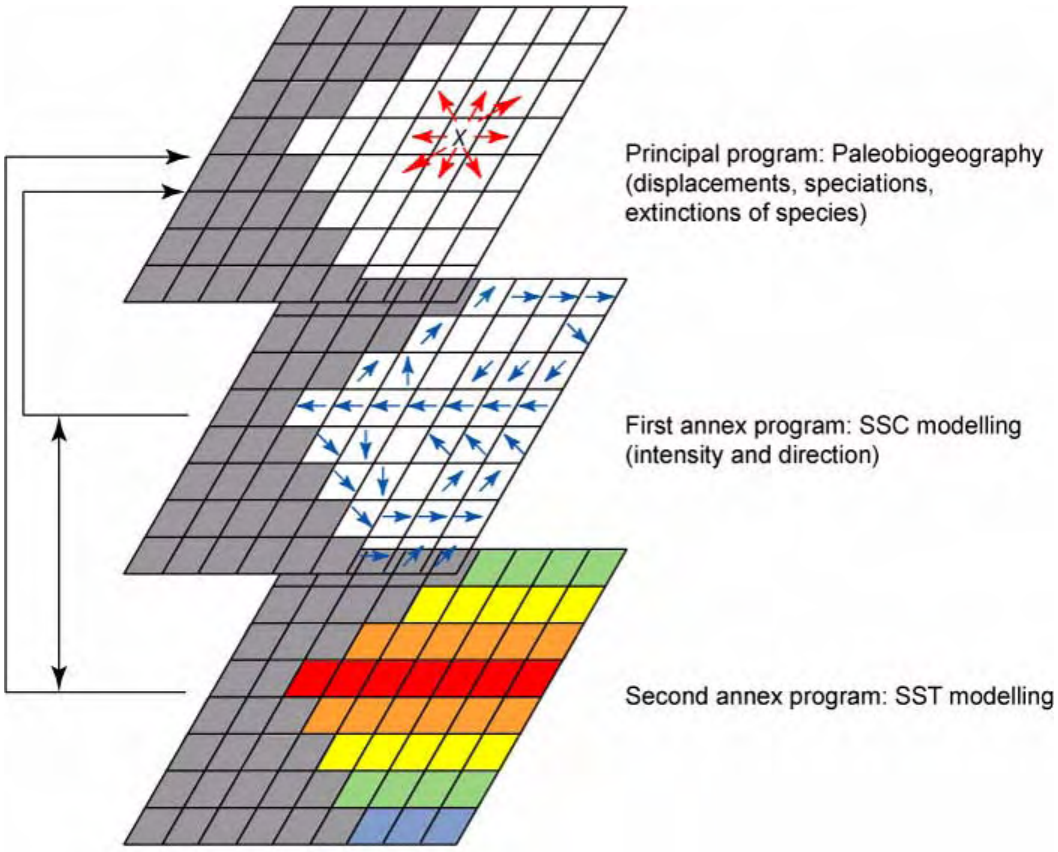

Figure 1. Simplified algorithm decomposed in three principle parts.

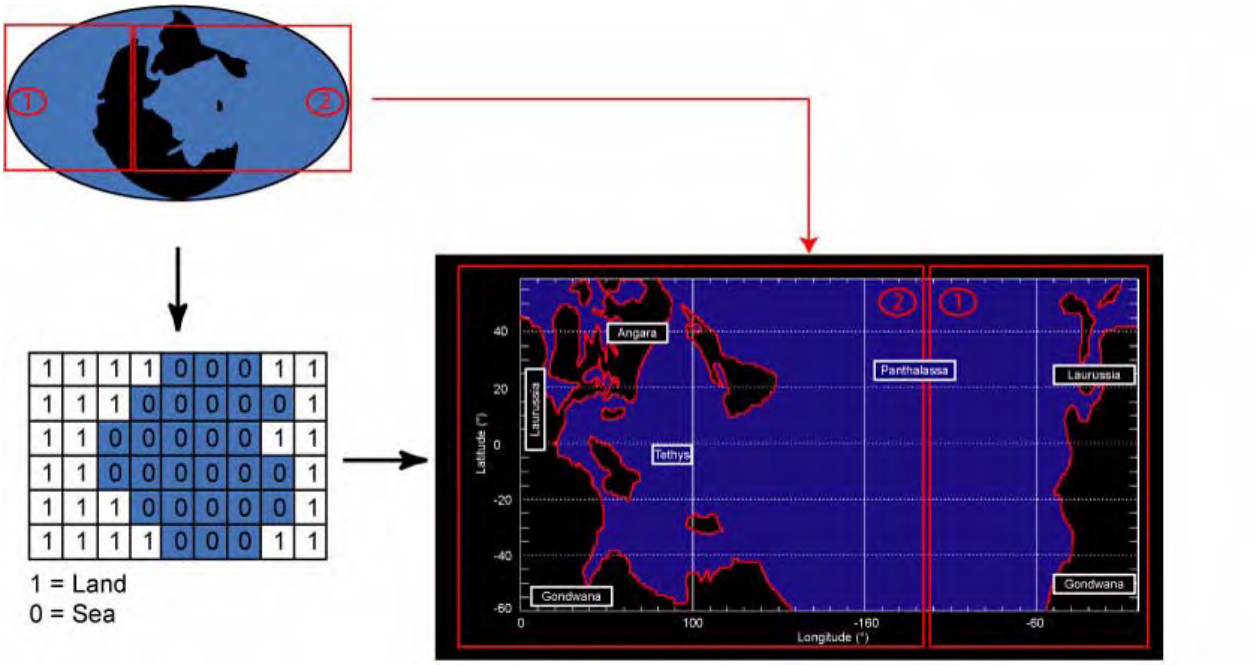

Figure 2. Construction of the Early Triassic palaeogeographic map based on Smith et al. (1994).

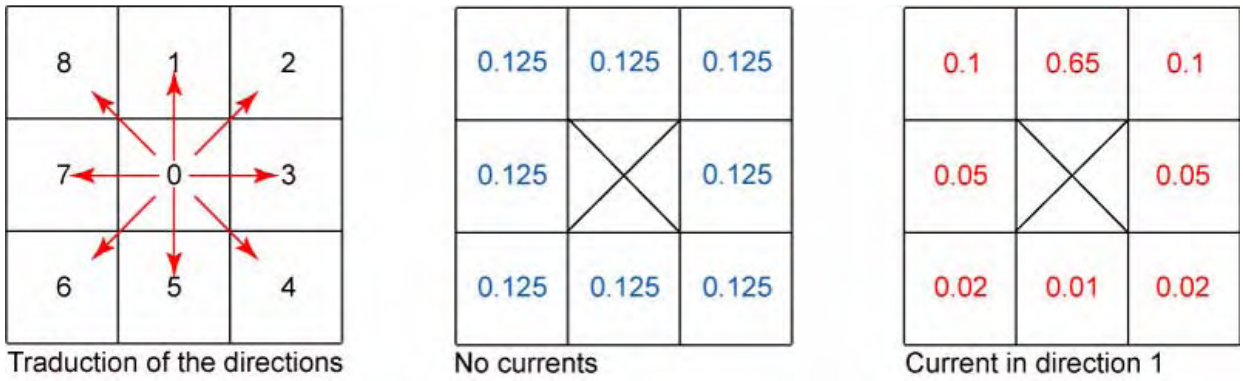

Figure 3. Probabilities of displacements for a simulation without currents and another with a current in the direction 1.

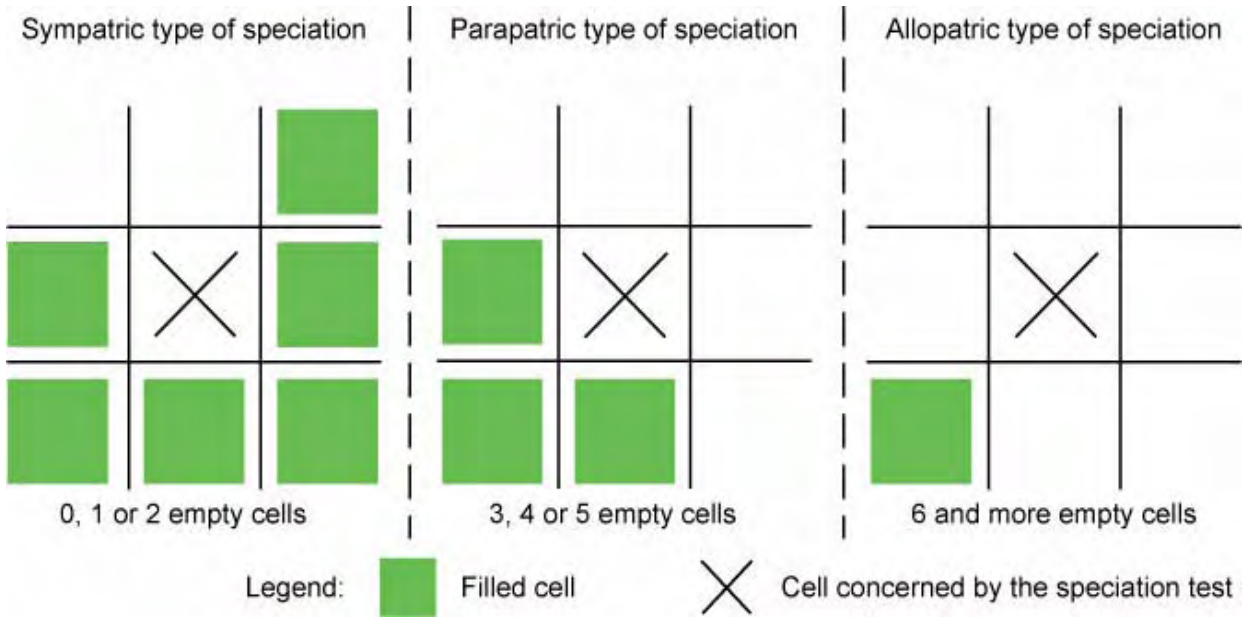

Figure 4. Quantification process of the geographic isolation of a simulated species and corresponding speciation type.

serious complications in computation without affecting the broader-scale simulation results.

The algorithm of the program can be divided in five successive steps where our parameters are successively tested:

1. Speciation: Given a fixed probability of speciation, a new species can be created in a cell occupied by its "parent-species." Three types of speciation events were distinguished: sympatric, parapatric, and allopatric, each with its own probability of occurrence. The type of speciation depended on the number and location of adjacent filled cells (Figure 4). Speciation probability and number of surrounding filled cells were inversely correlated. A species was added (cladogenesis) to the biogeographic matrix in the form of a supplementary layer by extending the n-dimension (Figure 5).
2. Displacement: A species occupying a cell can move to surrounding cells only if those cells are not already filled with the same species, and only if displacements in that direction are allowed by the superimposed oceanic currents. The module managed displacements in four successive steps in which first current direction, then intensity, then species displacement direction, and finally displacement success were determined (Figure 6).
3. Extinction: Two cases were distinguished: "local" and "complete" extinction, each having its own probability of occurrence. A species extinction in a filled cell ("local" extinction) did not affect the neighbouring cell filled with this species. In the case of a "complete" extinc-

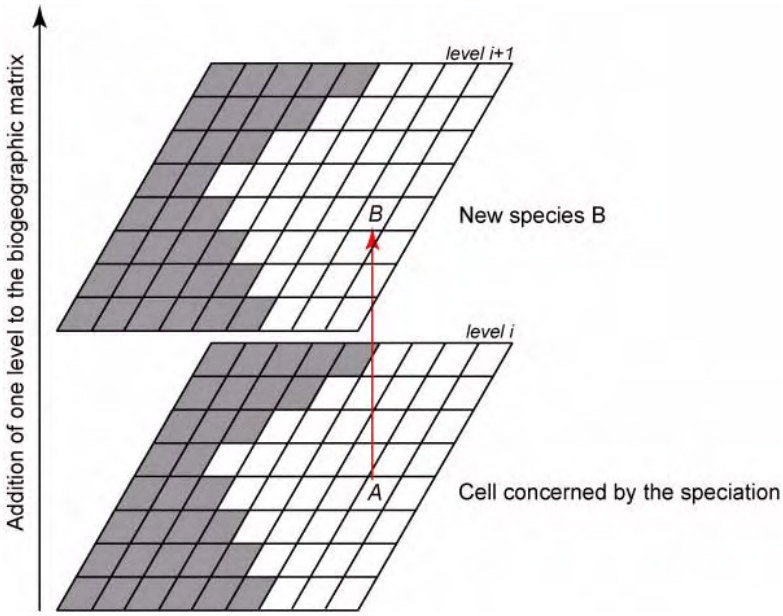

Figure 5. Illustration of a speciation event.

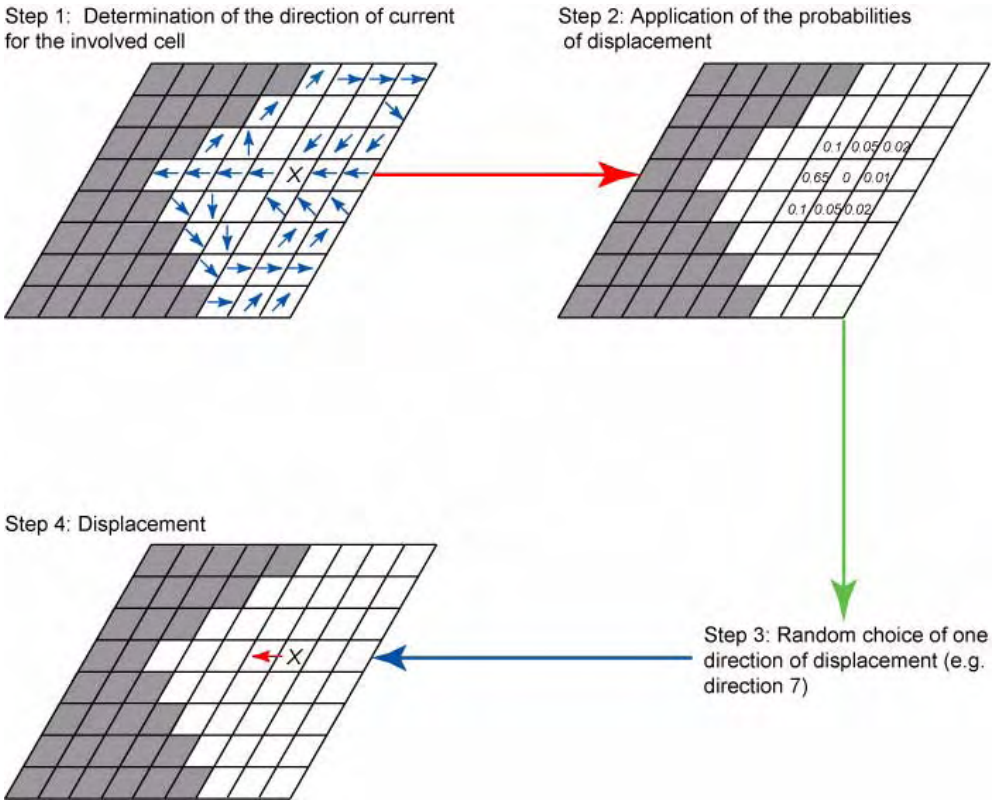

Figure 6. Illustration of how current displacement is modelled.

tion, all cells filled with the same species are simultaneously emptied.

4. Diversity check: The program checked for cells whose diversity threshold has been reached to avoid an ecologically unrealistic accumulation of species (Figure 7).
5. Species richness monitoring: Finally, the program calculated the species richness for each cell as the sum of co-occurring species.

Even if these five steps are successively executed for each cell and time iteration, speciation, extinction, and displacement events do not neces-

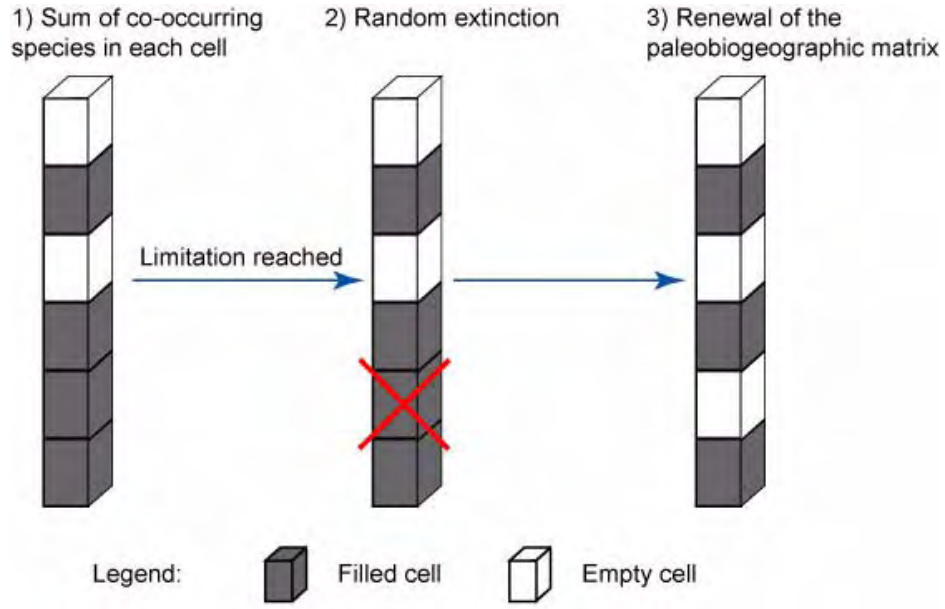

Figure 7. Limitation of the species richness in one cell given a threshold of co-occurring species.

sarily occur. As a result, the evolutionary rate of each cell is independent from cell to cell.

Results

Running our model for several hundred iterations (depending on the SST gradient and the selected speciation and extinction rates) allows us to construct theoretical patterns of species richness distribution under SST and SSC constraints. These theoretical patterns can be compared to the real ones observed in Early Triassic ammonoids.

Simulation Running without Currents and with a Weak SST Gradient. As a benchmark, we ran a simulation with no SSC and only a weak SST gradient, implying a weak or nil latitudinal and/or longitudinal bias in the geographic distribution of the simulated species. The results represent a random and thus statistically homogeneous distribution of the simulated species (Figure 8): simulated species are logically not organized along a diversity gradient. This example may correspond to the wide palaeogeographic distribution of the first earliest Triassic invertebrate marine species (like the two surviving ammonoid genera *Otoceras* or *Ophiceras*, *Lingula* for brachiopods or *Claria* for bivalves; Kummel 1973, Erwin and Pan 1996). This null model suggests that the SST gradient strongly influences the emergence and the general structure of a latitudinal gradient of species richness (LGSR).

Impacts of Currents on the Simulation. In order to visualize the impact of currents, we can apply them fully, partially, or not at all. If we impose no diffusion and only transport in the direction of the current, the species is destined to stay in the oceanic gyres for many iterations, but if we allow both diffusion and transport in the direction of the current, species are distributed along the principal currents, as well as in intermediate zones (Figure 9.1-4). Our simulations indicate that currents have a strong influence only over the timing (especially on the dispersal throughout the Panthalassa) and local patterns of dispersion of the simulated species. They have no influence on the shape and magnitude of the simulated LGSR on a global scale. If we remove currents from the simulation, the general shape and magnitude of the LGSR is conserved. Mixed water assemblages driven by currents do not seem to be the preponderant factor for explaining patterns of low species diversity in some convergence zones (e.g., equatorial, contra Casey 1989; Rutherford et al. 1999; Kiessling 2002).

Simulations with the Present-Day SST Gradient. If we apply the present-day SST gradient to the model, we might expect a LGSR similar to the classical view of species richness increasing monotonically and regularly from the poles to the equator. This pattern has been recognized in terrestrial and marine environments and for faunas and floras from all geological time periods (Stehli et al. 1969; Schopf 1970; Rex et al. 1993; Gaston 2000; Crame 2002; see also Rhodes 1992 for a review of hypotheses about the formation of latitudinal gradients in species richness).

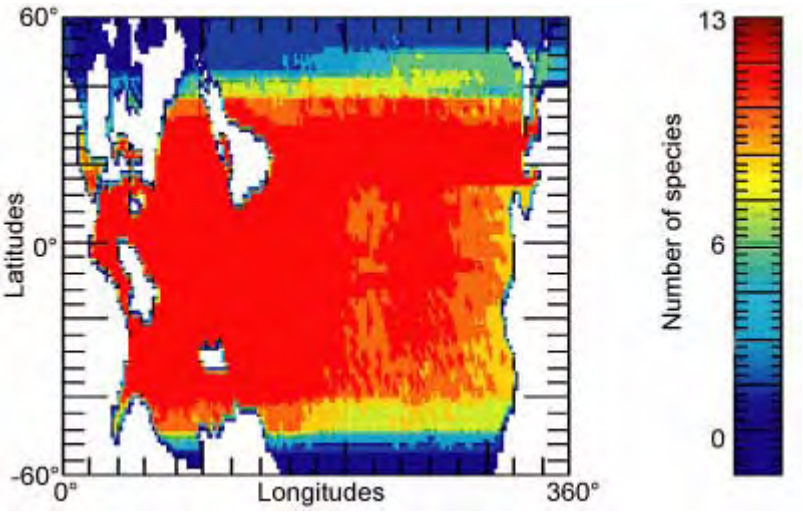

Figure 8. Visualization of the simulation results with a weak SST gradient and no SSC.

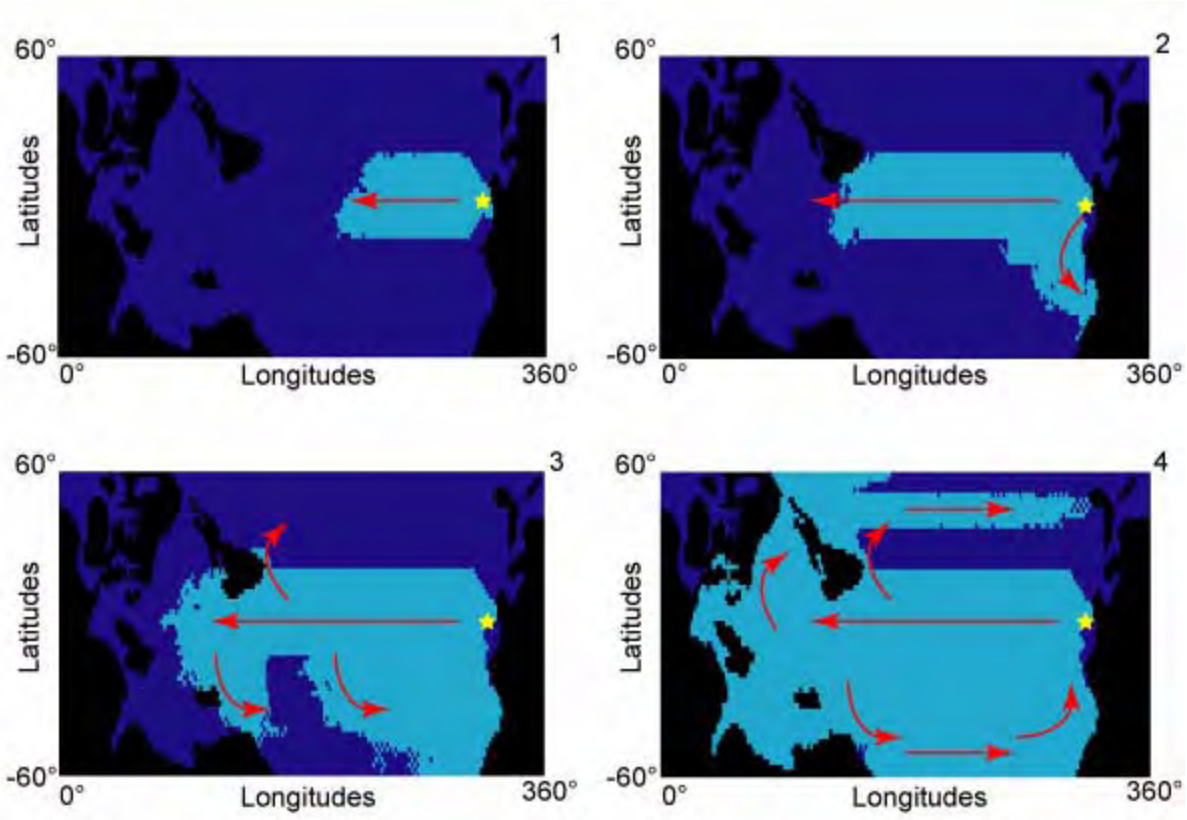

Figure 9. Example of a simulated species not sensitive to temperatures, spreading from the West coast of Pangea throughout the Panthalassic Ocean. The yellow star indicates the position of the species origination.

However, our results suggest a quite different pattern with a slight decrease in species richness near the equator (Figure 10.1). In fact, most of the simulations found maximal species richnesses close to the Tropics of Cancer and Capricorn. This pattern results from the geometric overlap of the species distributions as influenced by the shape and intensity of the SST gradient (Figure 11). This by-product of superimposed thermal ranges has been described in the modern setting as the “mid-domain effect” (Colwell and Hurtt 1994, Colwell and Lees, 2000, Colwell et al. 2004). This principle suggests that observed LGSR may simply be the result of chance. In situations with two fixed boundaries, randomly distributed ranges never generate a uniform spatial distribution but always

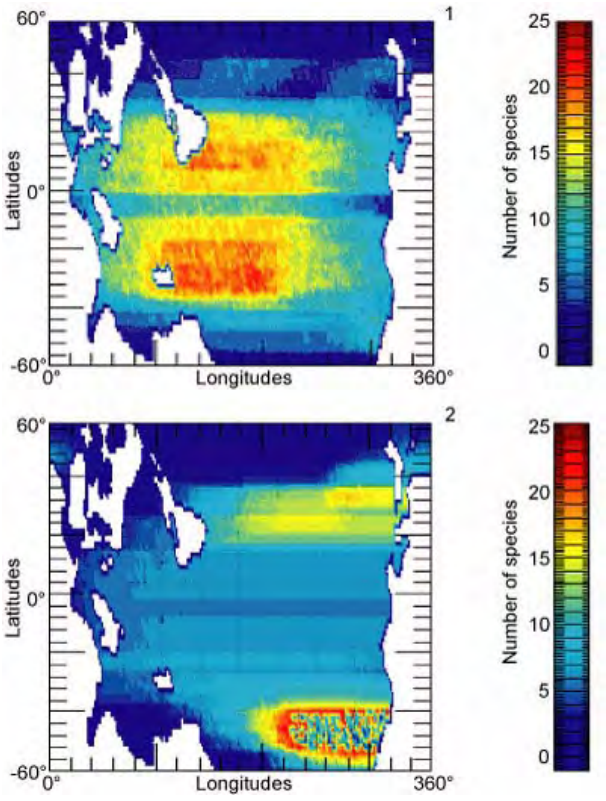

Figure 10. Visualization of the simulation results 1) with a present-day SST gradient 2) with a present-day SST gradient and first simulated species originated in middle/high latitudes (50°N).

give rise to a peak or a plateau of species richness. In the absence of any environmental or historical gradients, the formation of an LGSR may be solely the consequence of the spatial distribution of the thermal ranges of species as controlled by the SST gradient. If we change the SST gradient, the LGSR also changes (Figure 8). If a change takes place in the thermal ranges of species or in the position of the ancestral species, the LGSR is immediately affected (example in Figure 10.2).

Our simulation thus indicates that the formation of a gradient of taxonomic richness for marine organisms with at least one planktonic or pseudoplanktonic stage can be partially, if not completely due to: 1) the superimposition of species thermal ranges according to the geometry of the SST gradient; 2) the evolutionary history of the taxa (latitudinal position of the lineage origination); and 3) the characteristic parameters of individual species affecting the local species distribution.

Simulation of a Changing SST Gradient Applied to the Early Triassic. The SST gradient can be changed at any given iteration of a simulation. When a simulation starts with the present-day SST gradient and then a weak SST gradient is applied, the species distribution becomes homogenized and cosmopolitan. Species whose thermal range excludes them from the coldest temperatures disappear. When we change the SST gradi-

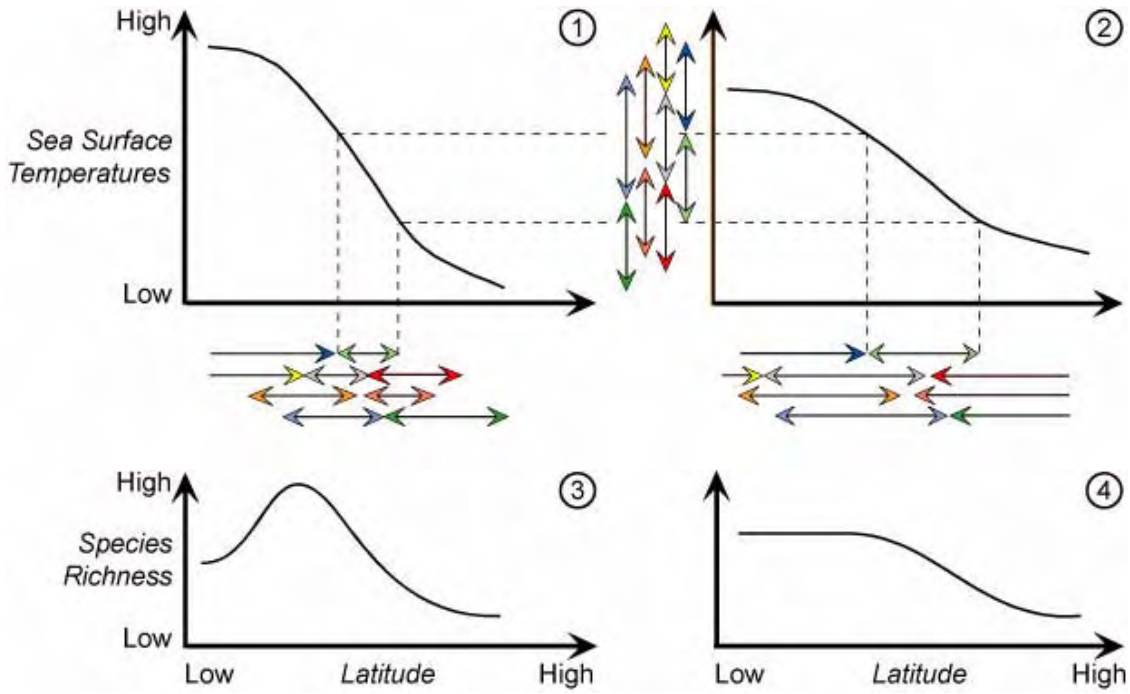

Figure 11. Illustration of the causal effect of the magnitude of the SST gradient on the shape and magnitude of the resulting LGSR. The latitudinal projection (horizontal arrows) of a given random distribution of thermal ranges (vertical arrows) on a steep (1) or weakened (2) SST gradient leads to a steep bimodal (3) or weakened unimodal (4) LGSR, respectively.

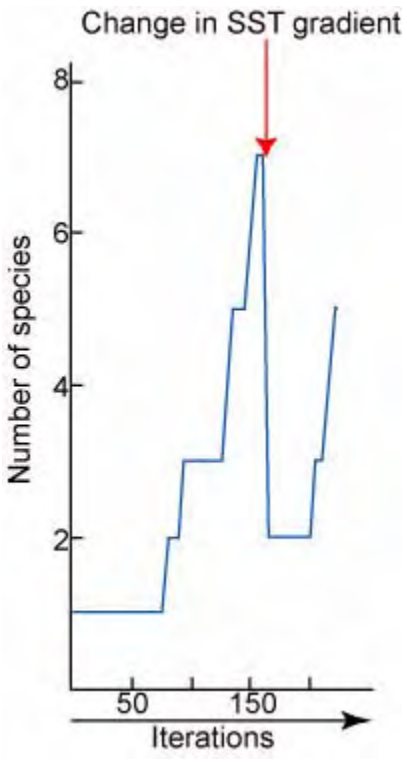

Figure 12. Illustration of the drop in species richness when an abrupt increase of the SST gradient occurs.

ent to be warmer and weaker, only tropical species survive after which they colonize higher latitudes. However, with a colder, weaker SST gradient, only high latitudes species survive and progressively invade low latitudes. If we proceed in reverse, setting a weak SST gradient at the start and abruptly changing it to a very steep one, we obtain a drop in the total species richness (Figure 12).

All thermal variations yield disruptions in species richness. On a global scale, this type of simulation can easily represent climatic changes in time and space and their consequences on the distribution of species on Earth. Changes of the SST gradient during the simulation evoke changes that reproduce observed diversity curves. For example, in Figure 13 we identified a sequence of changes to the SST gradient that can be hypothesized to have occurred during the Early Triassic. The SST parameters of the program were iteratively constrained to produce a species richness curve that maximally corresponds to the real diversity curve. The beginning of the simulation corresponds to the weak and warm pole-to-equator SST gradient of the Permo-Triassic boundary. Principal observations are: 1) a lowering of the SST gradient corresponds to a decreasing of endemism; 2) a steepening of the SST gradient leads to an increase of latitudinally restricted taxa.

The recovery of ammonoids after the Permo-Triassic extinction was not a continuous increase in species richness (Figure 13) or of the steepness of the LGSR, but was a sequence of increases and decreases. These fluctuations also differed latitudinally. In spite of their geographic complexity, our simulation indicates that the fluctuations of species richness can easily be modelled with simple changes in the SST gradient, which strongly sug-

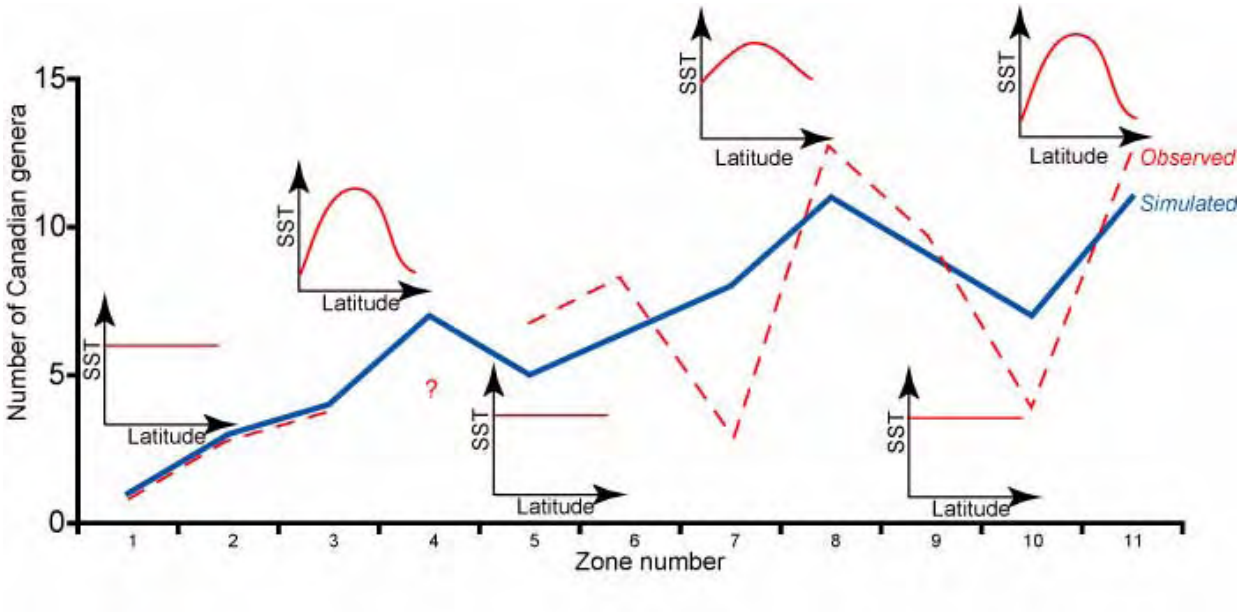

Figure 13. Evolution of the Canadian ammonoid generic richness (middle palaeolatitudes) during the Early Triassic (based on Tozer [1994] and unpublished data) and possible corresponding evolution of the SST gradient as suggested by our simulation results. Zone numbers correspond to the Canadian ammonoid zonation by Tozer (1994).

gests that such SST gradient directly influences the marine species richness and its distribution on Earth.

It appears that the formation of global-scale marine LGSR may be due to the shape and magnitude of the SST gradient, and to the location of the ancestral species. Even if it seems problematic to invoke only a single biotic (e.g., physiologic) and/or abiotic (physical environment) factor, the origin of the latitudinal species richness gradient can be the simple geometric by-product of the geographic overlap of thermally constrained species ranges. Through our model, IDL improved the visual understanding of the consequences of a changing climate on the distribution of species. IDL is completely adapted to run and visualize biogeographic models with an evolutionary time dimension.

EXAMPLE 2: BIODIVERSITY AND PALAEOENVIRONMENTAL INTERPOLATED BIOGEOGRAPHIC MAPS OF EUROPEAN NEOGENE LARGE LAND MAMMAL FAUNAS

The following example shows how the Interactive Data Language can be used to model biodiversity and ecomorphologic proxies in the European Neogene geographic context.

The European continental Neogene has yielded hundreds of localities containing mammal remains. This important collection of data is now being used to study the evolution of biodiversity (Fortelius et al. 1996, Costeur et al. in press) and palaeoecology of the mammalian communities (Fortelius et al. 1996, Van Dam and Weltje 1999, Fortelius et al. 2002, Jernvall and Fortelius 2002). The different studies cited above have brought to light different large scale or regional patterns linked to climatic and/or geographic evolution in large or small mammal faunas. Our purpose here was twofold. First, we investigated the large mammal species geographic distribution in relation to the Neogene palaeogeography. Second, we used ecomorphologic parameters to characterize large mammal communities on a taxon-free (Damuth 1992) ecological basis in order to infer past environments.

Palaeogeographic maps of the Neogene have been suggested (Rögl 1999, Meulenkamp and Sissingh 2003) but few biodiversity and/or palaeoecological studies have attempted to represent classical analysis results on maps. The IDL metalanguage and its representation facilities offer the opportunity to investigate biogeographic and environmental patterns resulting from the analysis of mammalian communities with direct visualizations onto palaeogeographic maps.

Data

Two different datasets were used. The first was a collection of extant European large mammals (data from Legendre 1989 and unpublished, and Héran unpublished), which was be used to test IDL interpolation functions. Comparisons of the results with recent studies on the distribution of land mammals (Baquero and Telleria 2001) provided information on the reliability of the IDL tool.

The second dataset was a compilation of 100 Tortonian European localities that have yielded large fossil mammals (Costeur unpublished). Their presence/absence as well as different ecomorphologic parameters (e.g., hypsodonty, tooth crown height) were recorded and evaluated. We used these to produce palaeobiogeographic maps of the distribution of species richness and of environmental proxies such as humidity/aridity. Palinspastic palaeogeographic backgrounds were built from published maps (Rögl 1999, Meulenkamp and Sissingh 2003), and their settings will be explained in the next section. Spatiotemporal coordinates for each locality were amalgamated from their ages and present-day latitude and longitude.

Algorithm

The algorithm used here was simpler than in the simulation of Triassic species richness. The algorithm was built in three steps.

Step One: Data Acquisition.

1. Palaeogeographic maps were generated as before using Tortonian and Recent maps of Europe and North Africa. The first step was to load the map into a corresponding 60 x 100 binary matrix (zero for oceanic areas, one for continental areas; see Figure 2 for an overview of the process). Each map covered the area between 30° North to 59.5° North and 10° West to 39.5° East. Each cell of the matrix thus represented an area of 0.5° x 0.5° corresponding to a mean surface of ca. 2200 km.
2. Faunal data: Locality characteristics (palaeogeographic coordinates and values to be interpolated) were read by the program from a text file provided by the user.

Step Two: Interpolation.

Our program offers two interpolation methods from among those included in the IDL library: Delaunay triangulation and Thin Plate Spline (TPS; Yu 2001). Sugihara and Inagaki (1995) described the Delaunay triangulation method. We will not dis-

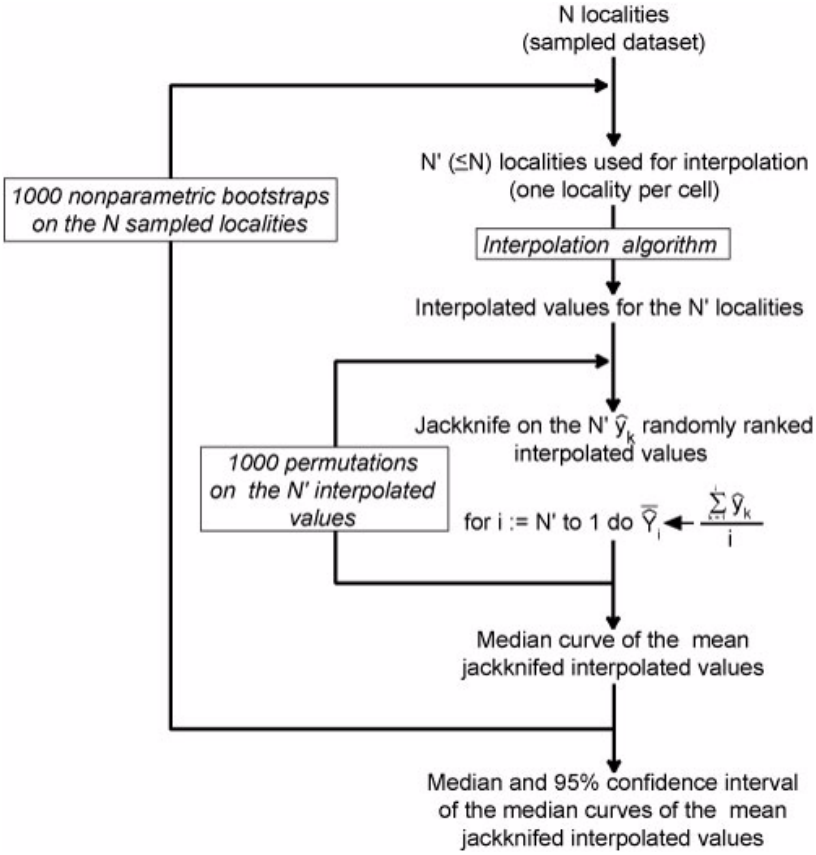

Figure 14. Flowchart illustrating the three nested levels of the "quality" test algorithm for an interpolation method.

cuss the mathematical foundations of these techniques here, but the basis for this interpolation method is to construct connected triangles between the data points and use them to determine unknown values by calculating a regression between their vertices. Thin Plate Splines apply a tight surface using a smooth bivariate function that takes the data points into account and assumes a minimum curvature of the surface (Monnet et al. 2003).

Other interpolation methods exist, including the popular Kriging-Cokriging method (Boer et al. 2001). Even though the Kriging algorithm is implemented as a routine in IDL, we did not use it because of the high subjectivity needed to choose the parameters that best fit the variogram, and because it is a computationally difficult method that requires an extensive practical experience compared to TPS and Delaunay triangulation.

TPS and Delaunay triangulation interpolate on a gridded geographic matrix so locality data provided by the user were placed in a matrix of the same dimensions as the palaeogeographic one (i.e., within cells of 0.5° x 0.5°). If more than one locality falls into the same cell, which is often the case with coarse resolution, several choices are proffered. Depending on the needs of the investigation, the minimum, maximum, mean, or median value of the parameter can be computed. The interpolation is then conducted on the matrix generated from the computed values. The computation does not distinguish coastal boundaries; a "continent" filter is later applied for visualization.

Step Three: Output.

A twofold sub-routine allows the validity of the results to be tested:

1. We first evaluated the "quality" of the interpolation results; for example, testing whether the dataset is large enough to yield a stable mean interpolated value regardless of the spatial distribution of the samples. To do this, we performed an analysis similar to a standard rarefaction procedure in which the relationship between the size of the set localities and the mean interpolated value was assessed. An algorithm involving three nested levels was applied (Figure 14):
   - The innermost level is a jackknife applied on the N' interpolated values associated with the sampled cells (N' ≤ N sampled localities because several sampled localities can be located in the same geographic cell). The resulting curve is made of N' mean interpolated values; it depends on the (arbitrary) order by which the N' inter-

polated values were successively removed.

- The second level was a random permutation of the N' interpolated values to randomize the removal order of the jackknife, which results in a median jackknifed curve which is independent of the removal order of the interpolated values, but still depends on the N sampled values;.
- The third level is a nonparametric bootstrap (random re-sampling with replacement) applied on the N sampled localities in order to estimate the median and confidence interval associated with the mean interpolated value parameter. The resulting relationship (and its associated bootstrapped confidence interval) between the number of localities and the mean interpolated value strongly depends on the shape of the distribution of the interpolated variable, and thus illustrates an important statistical characteristic of the interpolation method that was used.

2. We then tested the reliability of the TPS-interpolated values by computing the correlation coefficient between observed and predicted values (Monnet et al. 2003). This second test is obviously meaningless in the case of the Delaunay triangulation as the interpolated values for the sampled localities are the observed ones by definition of the method.

Results

We tested the reliability of the IDL tool on the present-day distribution of large European mammal species richness. We interpolated species richness across Europe from 151 evenly distributed sampling points using Delaunay triangulation and TPS (Figure 15).

Species richness is highest in Central Europe and decreases toward coastal areas as already demonstrated by Baquero and Telleria (2001). Those authors indicated that this pattern is consistent with a peninsular effect and decreasing land areas toward the borders as well as with the environmental parameters that prevail on the study area and the historical factors that affected Europe during the Quaternary. Both interpolation methods produced this same general pattern.

We then investigated the link between present-day environmental variables and the distribution of species throughout Europe by means of direct comparisons between plots of morphologic characters related to the animals' ecology and plots of diverse environmental variables. Such comparisons for present-day faunas would serve as a basis for relating large Neogene mammals to their environment.

Each species was assigned to a dental crown height class: brachydont (1), mesodont (2), or hypsodont (3) when their teeth possessed low, intermediate, or high crowns, respectively (Fortelius et al. 2002). Each dental crown height class characterizes a particular type of diet, from one dominated by non-abrasive plants (mostly found in rather closed and humid environments) to one dominated by highly abrasive plants (mostly found in open and arid environments; Fortelius and Solounias 2000). Mean dental crown height was calculated across species for each locality. Figure 16 shows Delaunay triangulation and TPS interpolations of the present-day mean dental crown height values, and Figures 17 and 18 present the quality of the interpolation methods (note that the bootstrapped median jackknifed curves are shorter than the observed one due to random re-sampling of the same sampled localities reducing the number N' of geographic cells involved in the interpolation). For both methods the bootstrap median of the median jackknifed mean interpolated values, and their associated 95% confidence intervals were remarkably constant, even for small-sized datasets. The negative bias that appeared with small-sized datasets (N' < 15 localities) is the logical consequence of the strongly right-skewed distribution of the mean hypsodonty values of the sampled localities. It is worth noting that the bootstrapped 95% confidence intervals estimated for the TPS method were wider than for the Delaunay triangulation method illustrating the greater sensitivity of the TPS algorithm to spatial heterogeneity of data.

Figure 16 depicts a broad North/South gradient with a few areas of higher tooth crown height in eastern Spain, southern France, Switzerland, and northeastern Italy. If we directly compare this map to the present-day precipitation and temperature interpolated maps (Delaunay Triangulation, Figure 19), we can associate the latitudinal differentiation with lower precipitation and higher temperature in the south, which is itself associated with more arid and open environments, thus explaining the hypsodonty maximum in that region. A multiple correlation analysis with temperature and precipitation as independent variables and hypsodonty as the dependent variable indicated a significant association: Pearson r = 0.522, bootstrapped (n = 10000) 99% Confidence Interval: 0.22 – 0.72; Mantel's t 0.0001 (n = 10000, H0 = no multi-linear association).

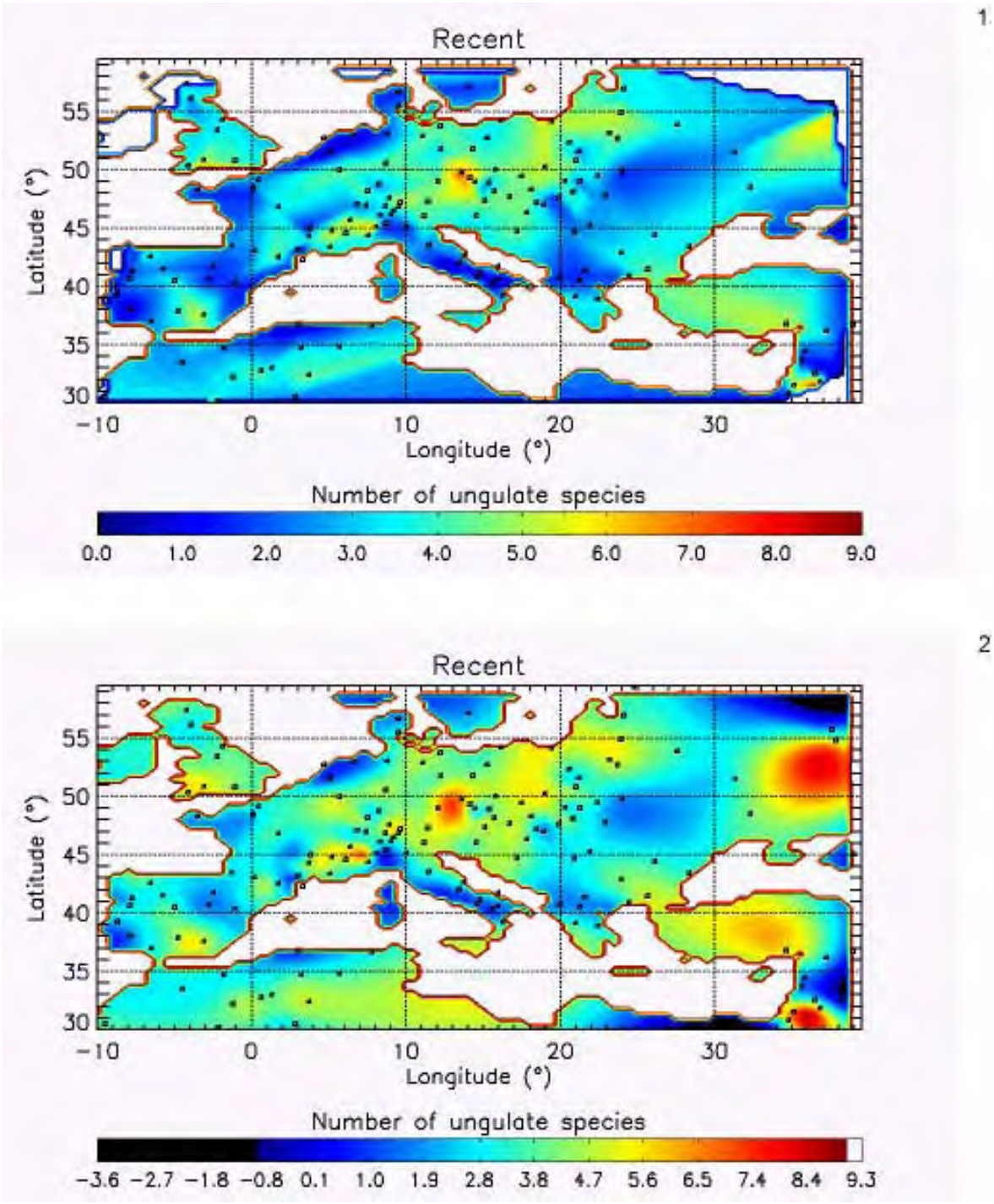

Figure 15. Present-day species richness of ungulates in Europe: 1) Delaunay triangulation interpolation, 2) TPS interpolation. Faunal locations are shown by open squares.

Once the link between climatic parameters and ecomorphologic parameters such as mean hypsodonty has been characterized, it is possible to use that relationship to interpolate a similar map for fossil data. Here we present an example for the large Tortonian mammals (the other Neogene continental stages have also been investigated in the same way). Figure 20 shows the hypsodonty pattern for 100 Tortonian sites distributed throughout Europe. We plotted the results onto a palaeogeographic map drawn from Rögl (1999) using palaeocoordinates calculated from present-day coordinates, as well as stratigraphic and geographic positions. Figures 21 and 22 show the quality of fit

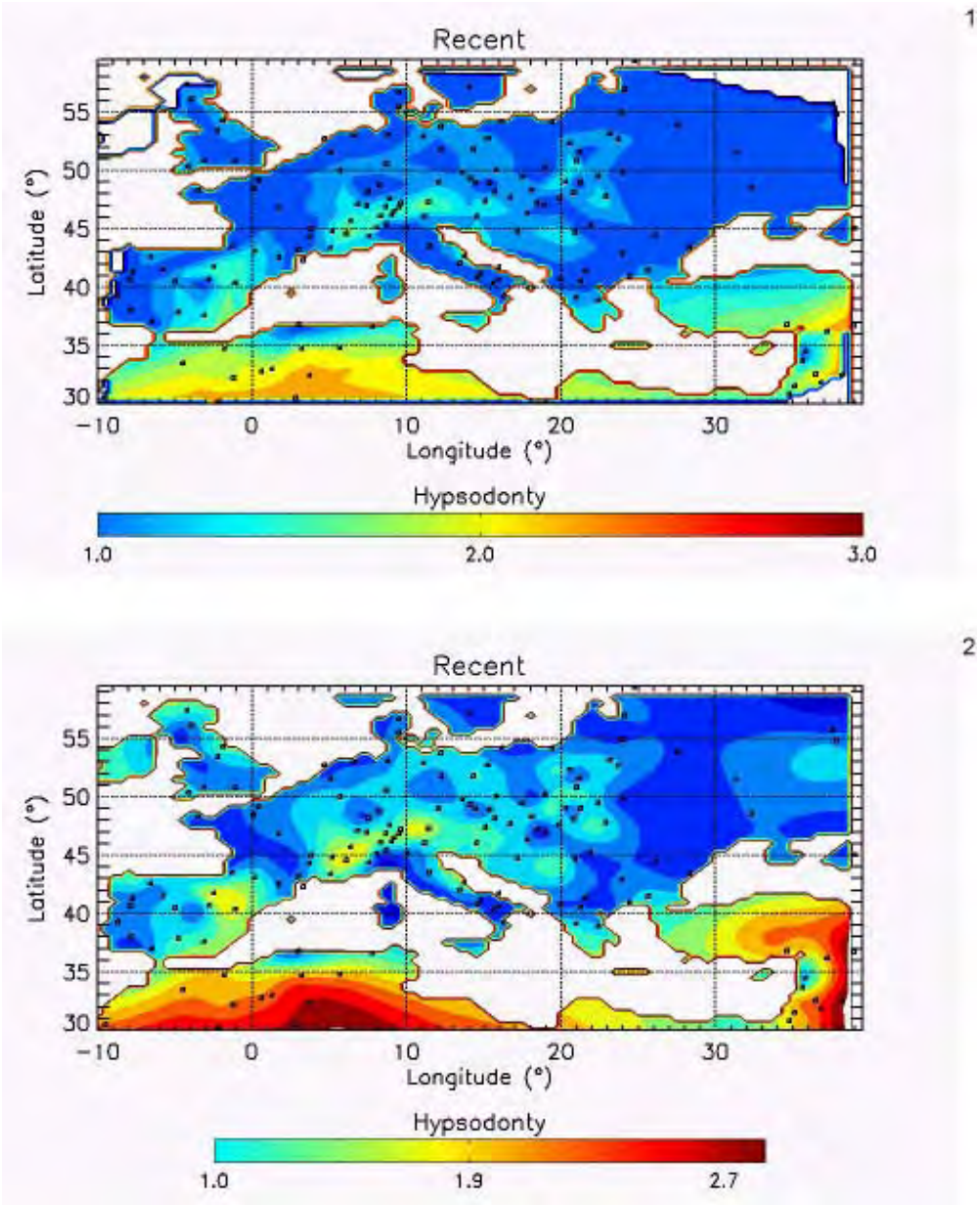

Figure 16. Present-day distribution of ungulates hypsodonty: 1) Delaunay triangulation interpolation, 2) TPS interpolation. Fauna locations are shown by open squares.

for Delaunay and TPS-interpolated data. As for the present-day data, the bootstrap median of the median jackknifed mean interpolated values and its associated 95% confidence interval were independent of the size of the analyzed dataset. Here the low skewness of the hypsodonty distribution makes the two interpolation methods immune to very small-sized dataset bias. As already mentioned, the TPS method showed a wider bootstrapped 95% confidence interval than the Delaunay method due to its greater sensitivity to spatial heterogeneity. Indeed, the fact that the bootstrapped median jackknifed curves were uniformly shifted upwards for the TPS-interpolated Tortonian dataset indicates that this parameter is critical. Thus the TPS-interpolated values should be interpreted very cautiously.

The Tortonian hypsodonty pattern broadly shows a North/South gradient with the highest values being mainly concentrated in the Iberian Peninsula and in the Greek-Iranian block (Bonis et al. 1992). The central-eastern European localities (eastern France, Germany, Switzerland, Austria, and Romania) have lower mean values of tooth crown height. Note that the sharp decrease observed towards the northern boundary is an

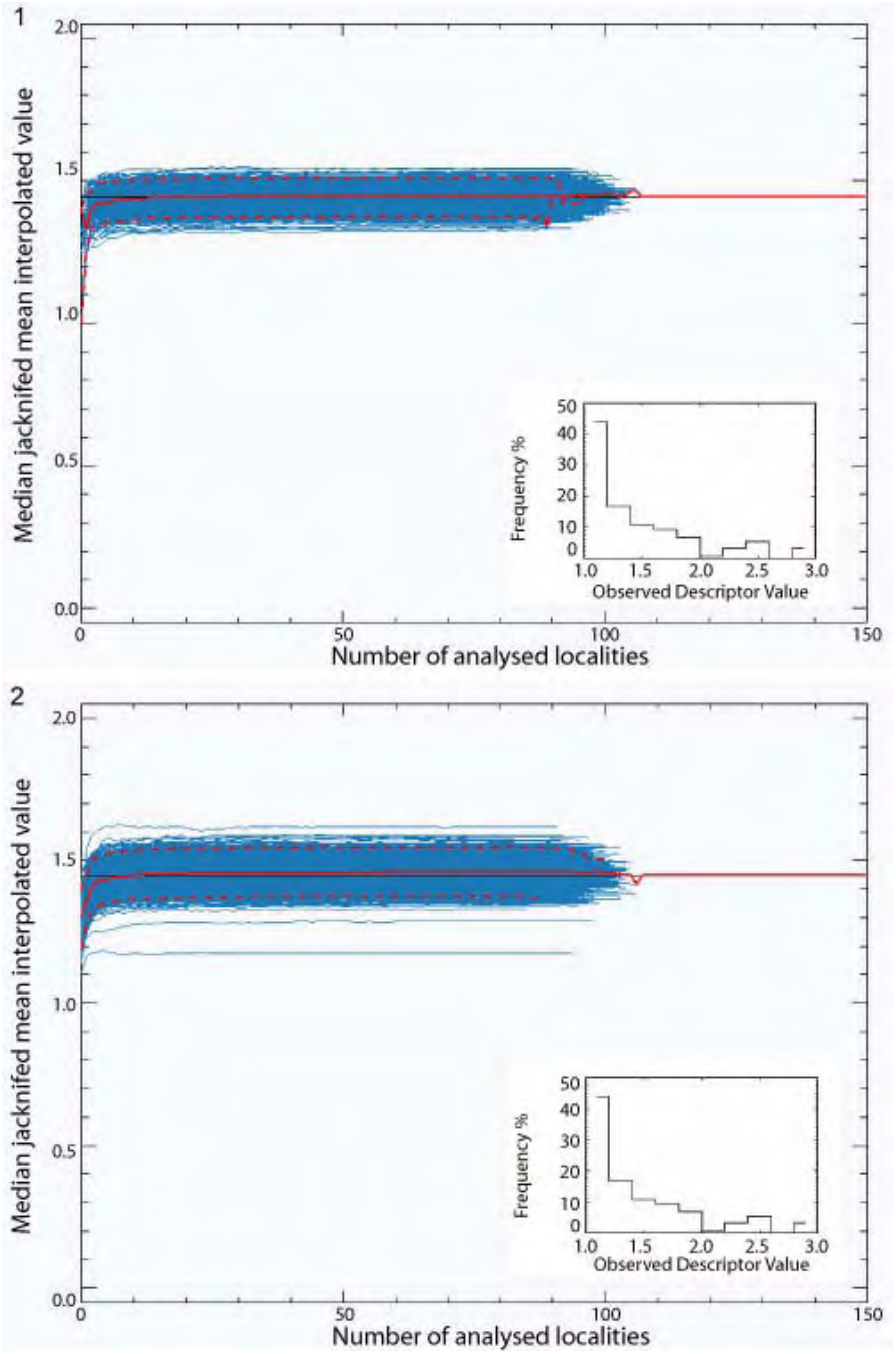

Figure 17. Test of the "quality" of 1) Delaunay triangulation and 2) TPS interpolations of present-day ungulates hypsodonty in Europe (see figure 14 and text for details).

artefact of the interpolation method (an edge effect) due to a lack of data in high latitudes.

Here, IDL allowed us, through its interpolation methods and visualization facilities, to infer the species richness distribution and the tooth crown height biogeographic patterns of European large mammals. The present-day distribution of species richness produced by the IDL interpolation tool was consistent with previous works (Baquero and Telleria 2001). Regarding ecomorphologic analyses, hypsodonty was largely related to two climatic parameters (precipitation and temperature) and closely followed a North/South climatic gradient, where the more arid and open environments were to the South. Based on these results, we computed the same ecomorphologic parameter for Tortonian large mammals localities and found out that the North/South broad gradient already existed by late Miocene time.

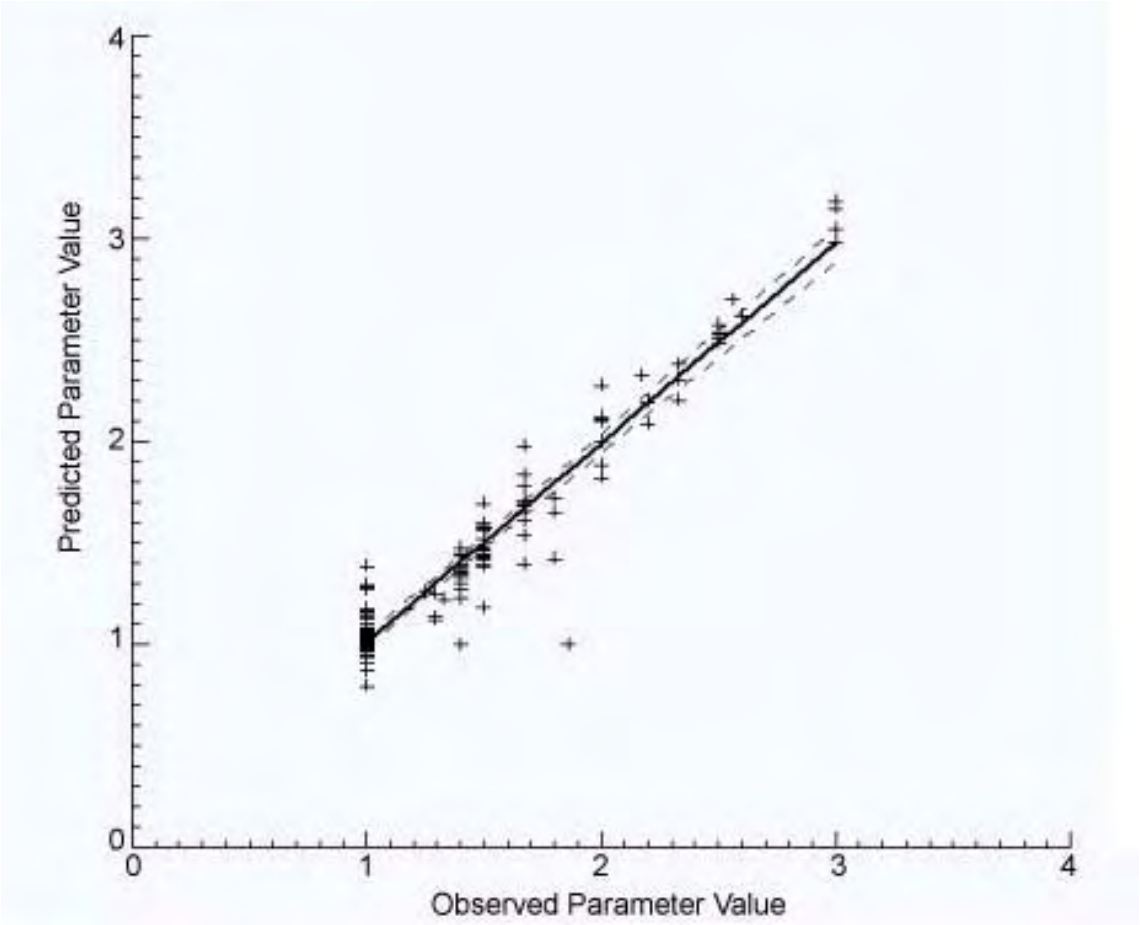

Figure 18. Observed versus TPS-interpolated values; Pearson r = 0.967, bootstrapped (n = 10000) 99% Confidence Interval: 0.93 – 0.99; Mantel's t 0.0001 (n = 10000, H0 = no linear association).

Our fossil map resolution suffers from the low number of localities (100) relative to the large geographic scale taken into account (the whole European continent), as well as from the absence of high latitudes localities due to glacial removal of Miocene continental sediments from northern Europe. Apart from these limitations and the previously discussed problem of spatial heterogeneity, the interpolation methods used in the Tortonian example, especially Delaunay triangulation, seem to produce reliable results.

CONCLUSIONS

We employed IDL to simulate the biodiversity evolution of planktonic species in the Early Triassic and to model biodiversity indices and ecomorphologic parameters for large European Neogene continental mammals.

IDL's flexibility allowed us to generate clear and straightforward visualizations of our results through its large array of pre-packaged routines. Multiple graphic output windows permitted a direct comparison of complementary results such as the effect of SST and currents on the distribution of Early Triassic ammonoid biodiversity. The creation of customized GIS is facilitated by IDL, and the parameters involved in spatial interpolation of data can easily be monitored in several ways (e.g., spacing of grid points for triangulation and TPS, range of values to be interpolated, interpolated data smoothing, spherical gridding for triangulation). The program routines are easily modified by users for their own purposes.

We used IDL version 5.2, which does not provide all 2-D interpolation methods, limiting the type of data that can be analysed, but it complements more specialized software such as Arcview©, which offers more interpolations but is less capable of importing palaeogeographic maps. In addition, the latest version of IDL (6.0) offers a more convivial user interface as well as improved options, including several additional interpolation methods, further animation possibilities, 3-D reconstruction and auto-executable programs. Thus, with a minimum knowledge of computer programming, this

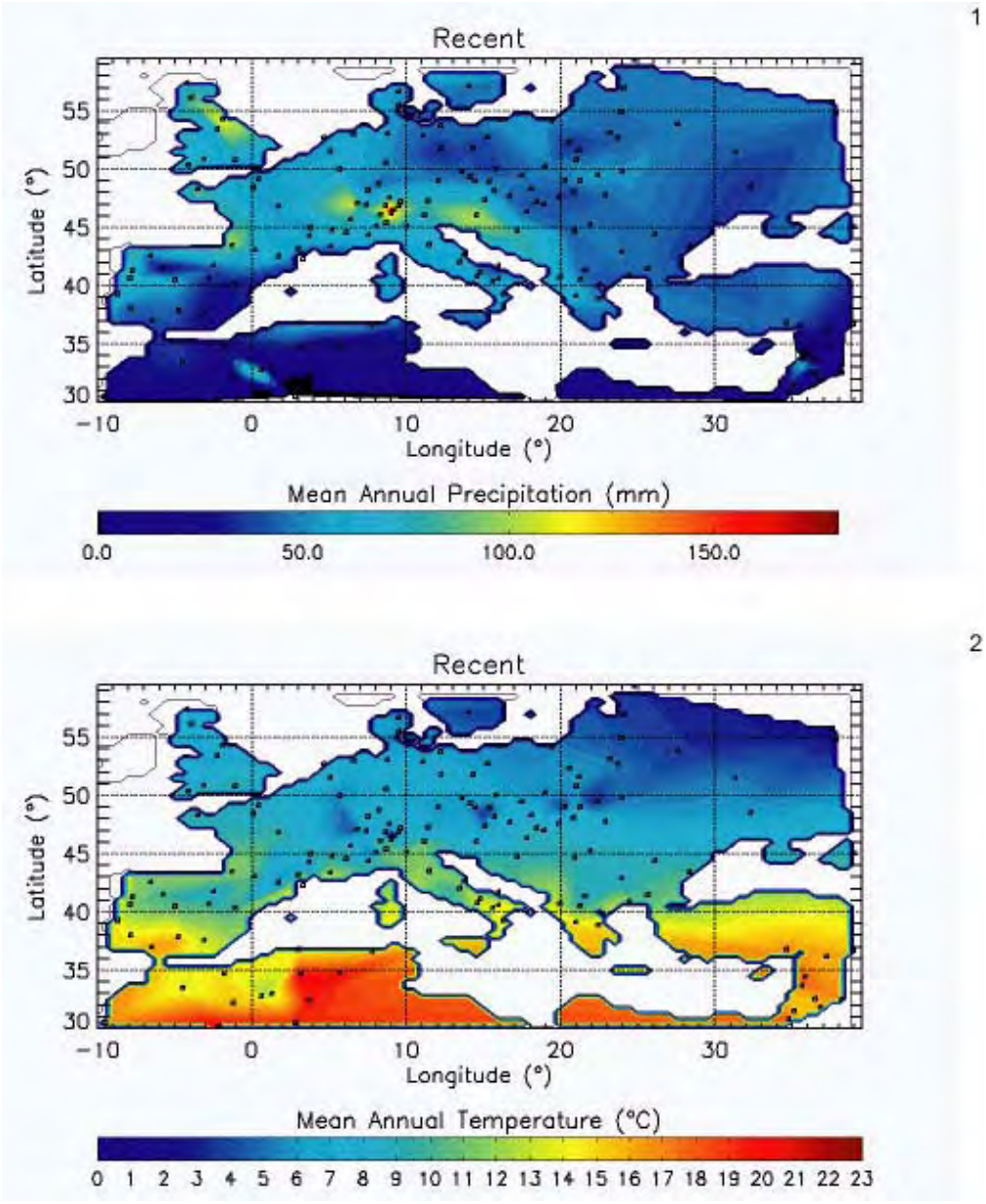

Figure 19. Delaunay triangulated maps for present-day 1) mean annual precipitation, and 2) mean annual temperature. Localities used are shown by open squares; climatic data from LocClim 1.0.

undervalued meta-language offers an array of easily usable tools for a large proportion of palaeontologists.

ACKNOWLEDGMENTS

This work was supported by the Swiss National Fund, project 2100-068061.02 (A.B), the program CNRS/INSU-Eclipse, project 00-10 (A.B and G.E), and a Region Rhône-Alpes-Eurodoc grant (A.B). We thank B. Vrielynck (Université Paris VI) for calculating Neogene locality palaeocoordinates and P. Allemand (Université Claude Bernard Lyon1) for his help on spatial interpolation. T. Galfetti and C. Klug (PIM Zürich) are thanked for the Italian and German abstracts. This manuscript benefited from the generous effort and the corrections of A. Mason and P.D. Polly. We are grateful to two anonymous reviewers for their constructive comments.

REFERENCES

Baquero, R., and Telleria, J.L. 2001. Species richness, rarity and endemicity of European mammals: a biogeographical approach. *Biodiversity and Conservation,* 10:29-44.

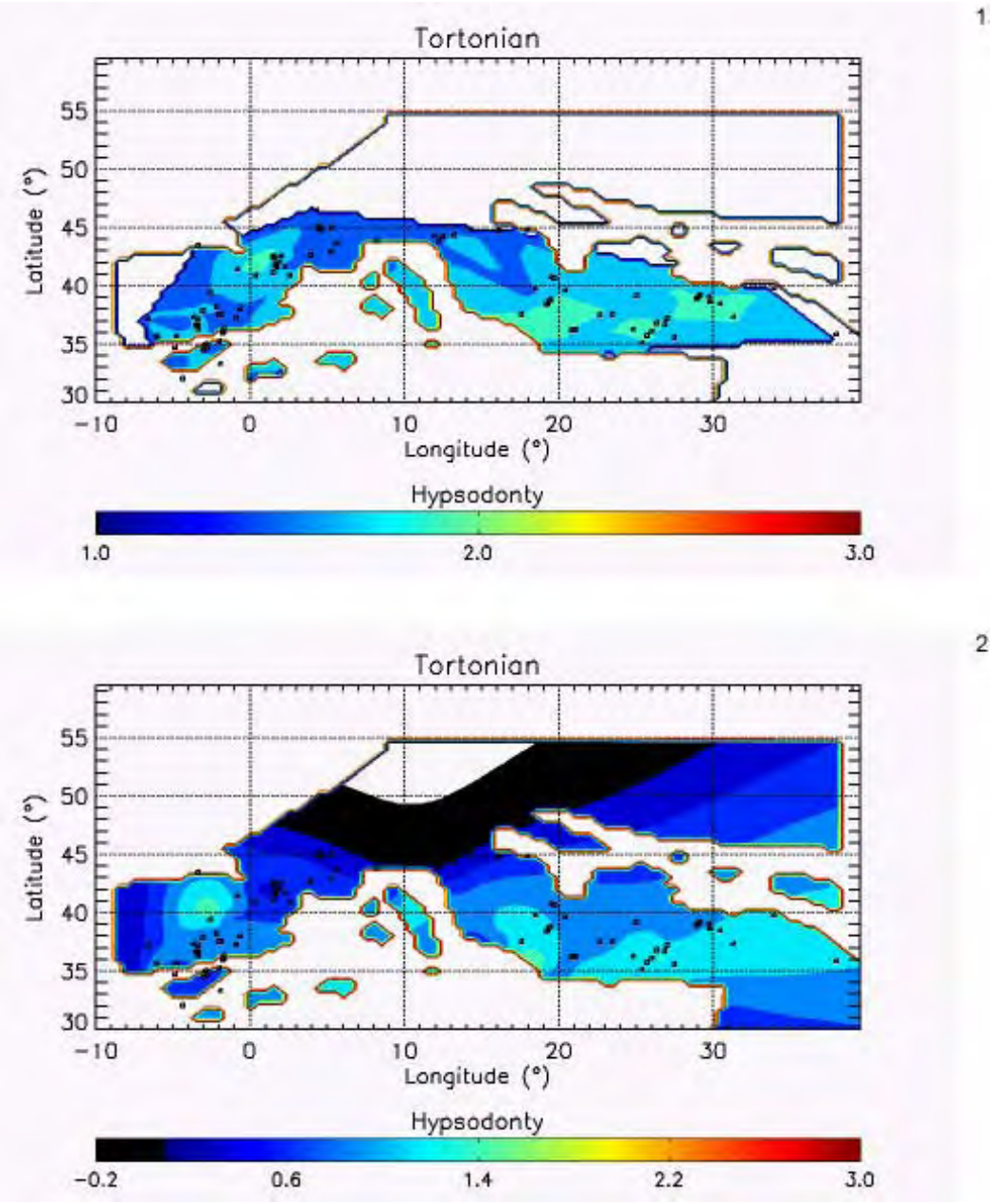

Figure 20. Hypsodonty pattern for 100 European Tortonian sites: 1) Delaunay triangulation interpolation, 2) TPS interpolation. Faunal locations are shown by open squares.

Boer, E.P., de Beurs, K.M., and Hartkamp, A.D. 2001. Kriging and thin plate splines for mapping climate variables. *International Journal of Applied Earth Observation and Geoinformation,* 3:146-154.

Bonis, D.L., Bouvrain, G., Geraads, D., and Koufos, G.D. 1992. Diversity and paleoecology of Greek late Miocene mammalian faunas. *Palaeogeography, Palaeoclimatology, Palaeoecology,* 91:99-121.

Brayard, A. 2002. *Modélisation de l'impact des contraintes climatiques sur la restauration de la biodiversité (sensu Richesse Spécifique) après une crise d'extinction majeure.* Unpublished MSc. Thesis, University Claude Bernard Lyon 1, France.

Casey, R.E. 1989. Model of modern polycystine radiolarian shallow-water zoogeography. *Palaeogeography, Palaeoclimatology, Palaeoecology,* 74:15-22.

Cleland, C.E. 2001. Historical science, experimental science, and the scientific method. *Geology,* 29:987-990.

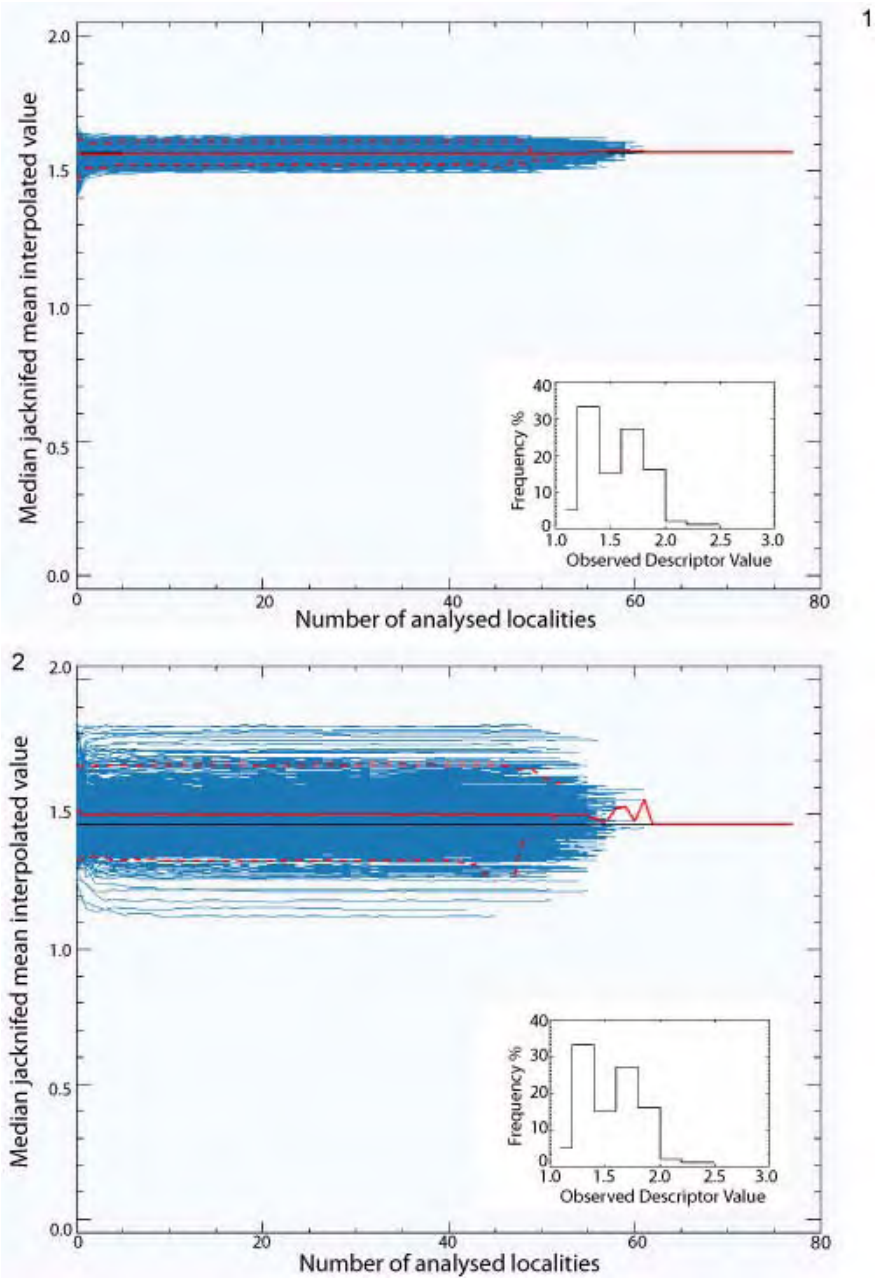

Figure 21. Test of the "quality" of 1) Delaunay triangulation and 2) TPS interpolations of Tortonian ungulates hypsodonty in Europe (see Figure 14 and text for details).

Colwell, R.K., and Hurtt, G.C. 1994. Nonbiological gradients in species richness and a spurious Rapoport effect. *The American Naturalist,* 144:570-595.

Colwell, R.K., and Lees, D.C. 2000. The mid-domain effect: geometric constraints on the geography of species richness. *Trends in Ecology and Evolution,* 15:70-76.

Colwell, R.K., Rahbek, C., and Gotelli, N.J. 2004. The mid-domain effect and species richness patterns: what have we learned so far? *The American Naturalist,* 163:E1-E23.

Costeur, L., Legendre, S., and Escarguel, G. In press. European large mammals palaeobiogeography and biodiversity from the Early Miocene to the Mid-Pliocene. Palaeogeographic and climatic impacts. *Revue de Paléobiologie, Volume Spécial 9*.

Crame, J.A. 2002. Evolution of taxonomic diversity gradients in the marine realm: a comparison of Late Jurassic and Recent bivalve faunas. *Paleobiology,* 28:184-207.

Dagys, A.S. 1988. Major features of the geographic differentiation of Triassic ammonoids, p. 341-349. In Wiedmann, J., and Kullmann, J. (eds.), *Cephalopods - Present and Past*. Schweizerbart'sche Verlagsbuchhandlung, Stuttgart.

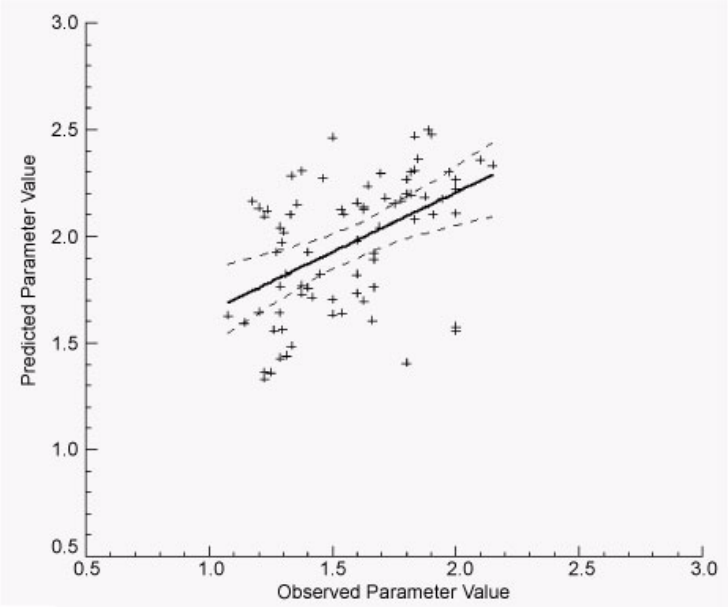

Figure 22. Observed versus TPS-interpolated values; Pearson r = 0.493, bootstrapped (n = 10000) 99% Confidence Interval: 0.21 – 0.70; Mantel's t 0.0001 (n = 10000, H0 = no linear association).

Dagys, A.S. 1997. A new Late Olenekian (Triassic) ammonoid of low paleolatitude affinity from Arctic Asia (Eastern Taimyr). *Paläontologische Zeitschrift,* 71:217-220.

Damuth, J. 1992. Taxon-free characterization of animal communities, p. 183-203. In Behrensmeyer, A.K. et al. (eds.), *Terrestrial Ecosystems through Time.* University of Chicago Press, Chicago.

Elmi, S., and Babin, C. 1996. *Histoire de la Terre.* Masson, Paris.

Erwin, D.H. 1993. *The Great Phanerozoic Crisis: Life and Death in the Permian*, Columbia University Press, New York.

Erwin, D.H. 1994. The Permo-Triassic extinction. *Nature,* 367:231-235.

Erwin, D.H. 1998. The end and the beginning: recoveries from mass extinctions. *Trends in Ecology and Evolution,* 13:344-349.

Erwin, D.H. 2001. Lessons from the past: biotic recoveries from mass extinctions. *Proceedings of the National Academy of Sciences of the United States of America,* 98:5399-5403.

Erwin, D.H., and Pan, H.-Z. 1996. Recoveries and radiations: gastropods after the Permo-Triassic mass extinction, p. 223-229. In Hart, M.B. (ed.), *Biotic Recovery from Mass Extinction Events*. Geological Society Special Publication, Plymouth.

Fortelius, M., Eronen, J., Jernvall, J., Liu, L., Pushkina, D., Rinne, J., Tesakov, A., Vislobokova, I., Zhang, Z., and Zhou, L. 2002. Fossil mammals resolve regional patterns of Eurasian climate change over 20 million years. *Evolutionary Ecology Research,* 4:1005-1016.

Fortelius, M., and Solounias, N. 2000. Functional characterization of ungulate molars using the abrasion-attrition wear gradient: a new method for reconstructing paleodiets. *American Museum Novitates,* 3301:1-36.

Fortelius, M., Werdelin, L., Andrews, P., Bernor, R.L., Gentry, A., Humphrey, L., Mittman, H.-W., and Viratana, S. 1996. Provinciality, diversity, turnover, and paleoecology in land mammals faunas of the later Miocene of Western Eurasia, p. 414-448. In Bernor, R.L., Fahlbush, V., and Mittman, H.-W. (eds.), *The Evolution of Western Eurasian Neogene Mammals Faunas.* Columbia University Press, New York.

Gaston, K.J. 2000. Global patterns in biodiversity. *Nature,* 405:220-227.

Hotinski, R.M., Bice, K.L., Kump, L.R., Najjar, R.G., and Arthur, M.A. 2001. Ocean stagnation and end-Permian anoxia. *Geology,* 29:7-10.

Jernvall, J., and Fortelius, M. 2002. Common mammals drive the evolutionary increase of hypsodonty in the Neogene. *Nature,* 417:538-540.

Kidder, D.L., and Worsley, T.R. 2004. Causes and consequences of extreme Permo-Triassic warming to globally equable climate and relation to Permo-Triassic extinction and recovery. *Palaeogeography, Palaeoclimatology, Palaeoecology,* 203:207-237.

Kiessling, W. 2002. Radiolarian diversity patterns in the latest Jurassic-earliest Cretaceous. *Palaeogeography, Palaeoclimatology, Palaeoecology,* 187:179-206.

Kummel, B. 1973. Aspects of the Lower Triassic (Scythian) stage, p. 557-571. In Logan, A., and Hills, L.V. (eds.), *The Permian and the Triassic Systems and Their Mutual Boundary*. Canadian Society of Petroleum Geologists, Calgary.

Legendre, S. 1989. Les communautés de mammifères du Paléogène (Eocène supérieur et Oligocène) d'Europe occidentale: structure, milieux et évolution. *Müncher Geowissenschaftliche Abhandlungen (A),* 16:1-110.

LocClim1.0 2002. Environment and natural resources working paper 9 (CD-ROM). Supplied by the Food and Agriculture Organization of the United Nations.

Marschallinger, R. 2001. Three-dimensional reconstruction and visualization of geological materials with IDL - examples and source code. *Computers and Geosciences,* 27:419-426.

Meulenkamp, J.E., and Sissingh, W. 2003. Tertiary palaeogeography and tectonostratigraphic evolution of the northern and southern Peri-Tethys platforms and the intermediate domains of the African-Eurasian convergent plate boundary zone. *Palaeogeography, Palaeoclimatology, Palaeoecology,* 196:209-228.

Monnet, C., Bouchet, S., and Thiry-Bastien, P. 2003. ISOPAQ, a MATLAB program for stratigraphic and isopach mapping: example application to the French Bajocian (Jurassic) sediments. *Computers and Geosciences,* 29:1101-1110.

Pickard, G.L., and Emery, W.J. 1990. *Descriptive Physical Oceanography: An Introduction.* Pergamon Press, Oxford.

Raup, D.M., and Sepkoski, J.J. 1982. Mass extinctions in the marine fossil record. *Science,* 215:1501-1503.

Rex, M.A., Stuart, C.T., Hessler, R.R., Allen, J.A., Sanders, H.L., and Wilson, G.D.F. 1993. Global-scale latitudinal patterns of species diversity in the deep-sea benthos. *Nature,* 365:636-639.

Rögl, F. 1999. Mediterranean and Paratethys paleogeography during the Oligocene and Miocene, p. 8-22. In Agusti, J., Rook, L., and Andrews, P. (eds.), *Hominoid Evolution and Climatic Change in Europe. Volume 1. The Evolution of Neogene Terrestrial Ecosystem in Europe.* Cambridge University Press, Cambridge.

Rhodes, K. 1992. Latitudinal gradients in species diversity: the search for the primary cause. *Oikos,* 65:514-527.

Rutherford, S., D'Hondt, S., and Prell, W. 1999. Environmental controls on the geographic distribution of zooplankton diversity. *Nature,* 400:749-753.

Schopf, T.J.M. 1970. Taxonomic diversity gradients of ectoprocts and bivalves and their geologic implications. *Geological Society of America Bulletin,* 81:3765-3768.

Smith, A.G., Smith, D.G., and Funnell, B.M. 1994. *Atlas of Mesozoic and Cenozoic Coastlines.* Cambridge University Press, Cambridge.

Stehli, F.G., Douglas, R.G., and Newell, N.D. 1969. Generation and maintenance of gradients in taxonomic diversity. *Science,* 164:947-949.

Sugihara, K. and Inagaki, H., 1995. Why is the 3D Delaunay triangulation difficult to construct? *Information Processing Letters,* 54: 275-280.

Tozer, E.T. 1973. The earliest marine Triassic rocks: their definition, ammonoid fauna, distribution and relationship to underlying formations, p. 549-556. In Logan, A., and Hills, L.V. (eds.), *Permian and Triassic Systems and their Mutual Boundary.* Canadian Society of Petroleum Geologists, Calgary.

Tozer, E.T. 1994. Canadian Triassic ammonoid faunas. *Geologic Survey of Canada Bulletin,* 467:1-663.

Van Dam, J., and Weltje, G.J. 1999. Reconstruction of the Late Miocene climate of Spain using rodent palaeocommunity successions: an application of end-member modelling. *Palaeogeography, Palaeoclimatology, Palaeoecology,* 151:267-305.

Wootton, T.J. 2001. Local interactions predict large-scale pattern in empirically derived cellular automata. *Nature,* 413:841-844.

Yu, Z.W. 2001. Surface interpolation from irregularly distributed points using surface splines, from Fortran program. *Computers and Geosciences,* 27:877-882.

CONCLUSIONS TO CHAPTERS 1 AND 2
(Question 1)

1. Conclusions relative to the Early Triassic recovery and the formation of diversity gradients

The "geophyletic model" allows realistic simulations of the present-day latitudinal gradient of diversity of Atlantic planktonic foraminifers and also of the past patterns of recovery and distribution of Early Triassic ammonoids. The model emphasizes that:

- the formation of a marine latitudinal gradient of taxonomic richness depends to a first order on the shape and magnitude of the SST gradient. The taxonomic richness and the SST gradient are linked by a simple, positive relationship: the steeper the SST gradient, the steeper the diversity gradient;
- in the case of a very steep SST gradient (i.e. the present-day one), the SST/diversity relationship becomes non-monotonous: the diversity gradient usually presents a bimodal shape with two maxima located near the Tropics of Cancer and Capricorn and a drop of diversity between them;
- other invoked biotic and abiotic parameters such as the oceanic circulation, differential evolutionary rates and ecological associations are not necessary to simulate such gradient of diversity;
- the geographical origin of the clade determines the latitudinal positions of the modal values of a latitudinal gradient of diversity;
- accepting this first order causal relationship between the SST and diversity gradients, allows the prediction of changes in the shape and magnitude of past SST gradients from well-documented fossil diversity gradients such as for Early Triassic ammonoids.

2. Perspectives from the "geophyletic model"

The "geophyletic model" essentially highlights that the edification of a diversity gradient can be explained by the combined action of a geographic mid-domain effect (MDE) and a thermal MDE. Yet, results based on MDE are often criticized because they do not always produce realistic patterns of

biodiversity (e.g. Hawkins & Diniz-Filho 2002; Laurie & Silander 2002; Rangel & Diniz-Filho 2003, 2005; Hawkins et al. 2005; Zapata et al. 2005). The "geophyletic model" is the first one to demonstrate that MDE models, when coupled with phylogenetic (e.g. evolutionary) and environmental (e.g. climatic) constraints, can produce realistic large-scale diversity patterns. This type of combination between MDE, phylogeny and environmental gradient(s) appears as a promising line of research for MDE models and their validation. Indeed, several workers (e.g. Davies et al. 2005; Smith et al. 2005) start to integer these parameters to their own models.

References:

Hawkins, B.A. and Diniz-Filho, J.A.F., 2002. The mid-domain effect cannot explain the diversity gradient of Neartic birds. *Global Ecology and Biogeography*, **11**: 419-426.

Hawkins, B.A., Diniz-Filho, J.A.F. and Weis, A.E., 2005. The mid-domain effect and diversity gradients: is there anything to learn? *The American Naturalist*, **166**: E140-E143.

Laurie, H. and Silander, J.A.J., 2002. Geometric constraints and spatial pattern of species richness: critique of range-based null models. *Diversity and Distributions*, **8**: 351-364.

Rangel, T.F.L.V.B. and Diniz-Filho, J.A.F., 2003. Spatial patterns in species richness and the geometric constraint simulation model: a global analysis of mid-domain effect in Falconiformes. *Acta Oecologica*, **24**: 203-207.

Rangel, T.F.L.V.B. and Diniz-Filho, J.A.F., 2005. Neutral community dynamics, the mid-domain effect and spatial patterns in species richness. *Ecology Letters*, **8**: 783-790.

Smith, S.A., Stephens, P.R. and Wiens, J.J., 2005. Replicate patterns of species richness, historical biogeography, and phylogeny in Holartic treefrogs. *Evolution*, **59**: 2433-2450.

Zapata, F.A., Gaston, K.J. and Chown, S.L., 2005. The mid-domain effect revisited. *The American Naturalist*, **166**: E144-E148.

INTRODUCTION TO CHAPTERS 3 AND 4
(Questions 2 and 3)

Chapters 3 and 4 are both based on a taxonomically homogeneous data set standardised at the basin-level, spanning all the Early Triassic. Our analyses depart from previous published macroecological studies on past diversity patterns. Indeed, we use a meaningful level of spatial resolution (i.e. the basin level) allowing realistic reconstructions of large-scale biogeographical patterns. The first chapter directly focuses on the observed large-scale taxonomic diversity and endemicity patterns observed for the Early Triassic ammonoids. These observed patterns are directly compared to the results obtained from the application of the "geophyletic model" to the Early Triassic context. In the second chapter, the biogeographical structure of faunal assemblages during the Early Triassic is explored by means of "classical" analyses such as Cluster Analysis and Nonmetric Multidimensional Scaling but also by a new approach interpreting inter-faunal similarities as networks.

All these approaches are complementary and provide different insights on the spatial and temporal dynamics of the ammonoid recovery.

The second part of the chapter 4 is not directly linked to the Early Triassic ammonoids, but is devoted to the construction of a Geographical Information System (GIS) for Cenozoic mammals, based on the same programming language used in the "geophyletic" model.

Available online at www.sciencedirect.com
SCIENCE DIRECT®
ELSEVIER
PALAEO
Palaeogeography, Palaeoclimatology, Palaeoecology xx (2006) xxx–xxx
www.elsevier.com/locate/palaeo

The Early Triassic ammonoid recovery: Paleoclimatic significance of diversity gradients

Arnaud Brayard [a,b,*], Hugo Bucher [a], Gilles Escarguel [b], Frédéric Fluteau [c], Sylvie Bourquin [d], Thomas Galfetti [a]

[a] *Paläontologisches Institut und Museum der Universität Zürich, Karl-Schmid Strasse 4, CH-8006 Zürich, Switzerland*
[b] *UMR-CNRS 5125, "Paléoenvironnements et Paléobiosphère", Université Claude Bernard Lyon 1, 2 rue Dubois, F-69622 Villeurbanne Cedex, France*
[c] *Laboratoire de Paléomagnétisme, Institut de Physique du Globe de Paris, 4 place Jussieu, F-75252 Paris Cedex 05, France*
[d] *Geosciences Rennes, UMR-CNRS 6118, Université de Rennes 1, Campus de Beaulieu, Bat. 15, F-35042 Rennes Cedex, France*

Received 15 September 2005; received in revised form 7 February 2006; accepted 16 February 2006

Abstract

Ammonoids recovered much faster than other marine shelly invertebrates after the end-Permian mass extinction. Based on a refined global data set at the basin level, we investigate the paleobiogeographical global latitudinal and longitudinal diversity patterns in terms of climatic changes during the Early Triassic. Such analysis differs from already published qualitative or quantitative studies in that it estimates faunal patterns and endemicity at an ecologically meaningful level of spatial resolution, i.e. at the basin level. During the Early Triassic, the global first order trend in increasing ammonoid diversity was accompanied by a progressive change from cosmopolitan to latitudinally-restricted distributions. This led to the emergence of a clear latitudinal diversity gradient during most of the Smithian and Spathian stages, which entails increased steepness of the Sea Surface Temperature gradient during the late Early Triassic. However, two brief episodes of ammonoid cosmopolitanism combined with low global diversity interrupted the first order increasing trend at the very beginning of the Smithian and at its very end. The longitudinal analysis of Smithian distributions indicates a westward decrease of diversity within the Tethys, which faded away during the Spathian. Analysis of endemicity indicates a rapid biogeographical maturing and structuring of faunas concomitant with the edification of the latitudinal diversity gradient.

Keywords: Early Triassic; Ammonoids; Paleobiogeography; Generic richness; Sea surface temperature; Recovery

1. Introduction

The Permo-Triassic mass extinction drastically affected the evolution of Life with the disappearance of typical end-Paleozoic communities. The level of diversity has never been so reduced since the Cambrian with an estimated loss greater than 90% of marine species (e.g. Raup, 1979). The recovery of marine and terrestrial ecosystems was very slow compared to other mass extinctions (e.g. Erwin, 1998) and is considered to be globally ended in the Anisian (Middle Triassic). The delay in the onset of the recovery is an intriguing aspect of the Permo-Triassic mass extinction which may be due

* Corresponding author. Paläontologisches Institut und Museum der Universität Zürich, Karl-Schmid Strasse 4, CH-8006 Zürich, Switzerland. Tel.: +41 1 634 26 98; fax: +41 1 634 49 23.
E-mail address: arnaud.brayard@univ-lyon1.fr (A. Brayard).

0031-0182/$ - see front matter © 2006 Elsevier B.V. All rights reserved.
doi:10.1016/j.palaeo.2006.02.003

to the persistence of harsh and unfavourable climatic and/or oceanographic conditions (e.g. global warming, anoxia, stratified waters…).

During the survival phase of the Early Triassic, the first marine inhabitants were very particular and composed of generalist, cosmopolitan and opportunist organisms (e.g. *Lingula* for the brachiopods; *Claraia* for the bivalves) with simple communities and low diversity (Kummel, 1973b; Erwin, 1990, 1994). Even if many clades did not completely recover until the Spathian or the Anisian times (e.g. corals [Stanley, 2003], foraminifers [Tong and Shi, 2000] or radiolarians [Racki, 1999; Yao and Kuwahara, 2000; Hori et al., 2003]), some rare diversified post-extinction faunas demonstrate that marine invertebrates did found some refuges (e.g. Oman, see Krystyn et al., 2003; Twitchett et al., 2004). However, the dominant pattern is that poorly diversified and small-sized benthonic shelly faunas predominated during the Early Triassic and most of the Anisian (e.g. Fraiser and Bottjer, 2004; Fraiser et al., 2005).

The low diversity and cosmopolitan assemblages of generalist organisms until the end of Early Triassic or beginning of the Middle Triassic suggest that environmental conditions were unfavourable during the survival phase and changed during the recovery phase. Climatic simulations also indicate that the beginning of the Early Triassic should be globally and uniformly warm (e.g. Hotinski et al., 2001; Kidder and Worsley, 2004; Péron et al., 2005).

At least one exception has to be noted in the differential recovery of marine organisms: ammonoids quickly rediversified during the Early Triassic and became the most prominent part of the marine faunas during this time interval, where they became extremely widespread and abundant (Kummel, 1957, 1973a,b). Their greatest geographical differentiation was first reached during the Spathian (Kummel, 1973b; Dagys, 1988, 1997).

In this paper we investigate the global paleobiogeographical distribution of ammonoids and its relation with diversity. Patterns of distribution and diversity are discussed in terms of climatic changes during the Early Triassic.

2. Geological and paleontological settings

2.1. Position of land masses and seas

Gondwana, Laurussia and Angara were grouped in the Pangean supercontinent during the end of Permian (Elmi and Babin, 1996). The Pangea edification ended with the Ouralian orogenesis resulting from the collision between Angara and Laurussia (e.g. Smethurst et al., 1998). Later on, Gondwana slowly began to break up. The sea/land repartition was dominated by a very large oceanic domain, the Panthalassa which represented approximately 90% of the end-Permian Ocean, and a smaller ocean covering the last ~10%, the Tethys, which formed a West–East encroachment in the Pangea. The Tethys was centred on the Equator and connected to the East with the Panthalassa.

With the progressive end-Permian opening of the Neotethys, several oceanic plates (e.g. Cimmerian and Cathaysian microcontinents) shifted northward across the Tethys (e.g. Ricou, 1994; Stampfli and Borel, 2002). All these Gondwanian fragments or "transit plates" as coined by Ricou (1994) accreted to Laurasia during the Triassic (Kazmin, 1991; Besse et al., 1998). Numerous back-arc basins opened with the Northward subduction of the Paleotethys all along the southern Eurasian margin, from Austria to China (Stampfli and Borel, 2002).

During the Early Triassic, several terranes travelled through the Panthalassa and were accreted to the western margin of Pangea (see Tozer, 1982; Nichols and Silberling, 1979; Belasky and Runnegar, 1994; Belasky, 1996; Belasky et al., 2002 for Chulitna, eastern Klamath, Stikinia, Wrangellia terranes of North America) or to the eastern margin of the Pangea (e.g. Adams et al., 2002 and Kojima, 1989 for New Zealand and Japan terranes, respectively). Although many terranes were travelling across oceans, major continents and oceans remained stable during the Early Triassic, thus providing a reliable geographical frame for extracting short-term biogeographical patterns of ammonoids (Fig. 1).

2.2. Stratigraphy and timescale

The Early Triassic is commonly subdivided into two (Induan and Olenekian), three (Griesbachian, Nammalian and Spathian: see Guex, 1978) or four stages (Griesbachian, Dienerian, Smithian and Spathian: see Tozer, 1967). These subdivisions are always subject to debates (e.g. Kozur, 2003) but the Sub-Commission on Triassic Stratigraphy decided to adopt the two-fold subdivision in 1992. Yet, Induan and Olenekian are not accepted by all Triassic workers. The two-fold subdivision system was defined by Kiparisova and Popov (1956) in two different realms: Tethyan and Boreal. The Induan has its type-locality in the Salt Ranges (Tethyan realm) whereas the Olenekian is derived from the Olenek River in Siberia (Boreal realm). Because the ammonoid turnover at the Induan/Olenekian boundary

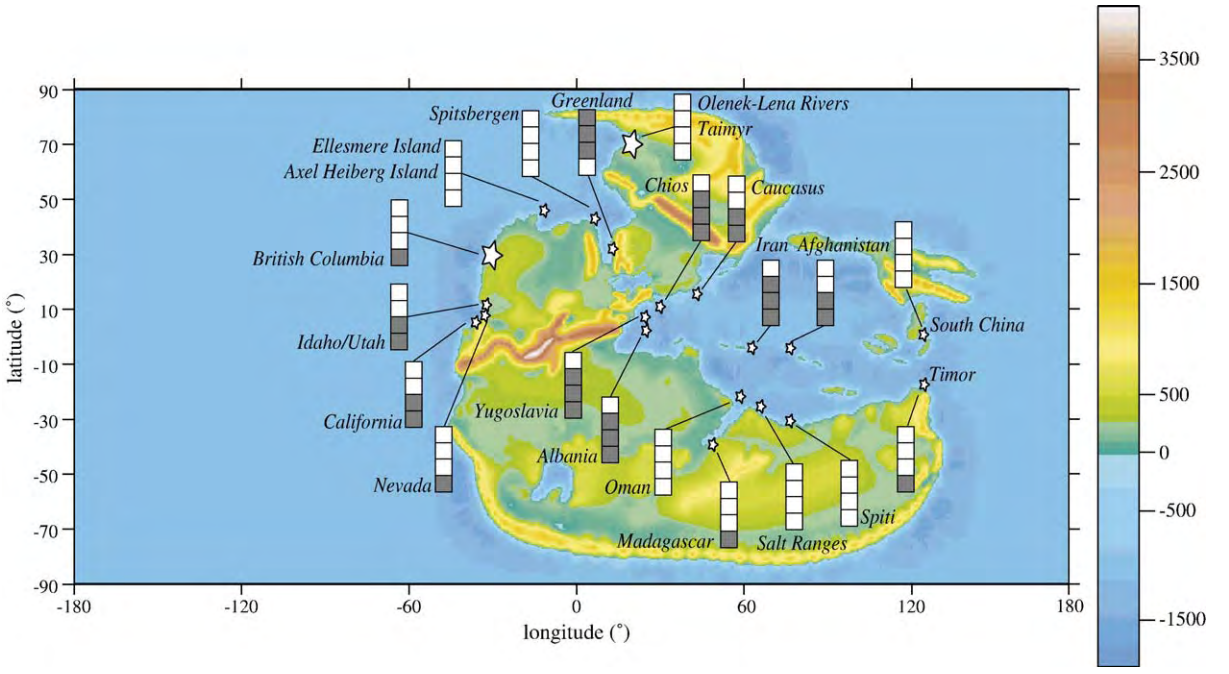

Fig. 1. Paleogeographic map of the Smithian and Spathian (modified from Péron et al., 2005) with the paleoposition of the studied basins and localities. Size of the stars indicates only the relative size of the sampling area. Small bars indicate the temporal distribution of specimens found in the studied station (from base to top: 1st square: Griesbachian, 2nd: Dienerian, 3rd: Smithian, 4th: Spathian; a grey square indicates an absence of specimens from the stage and a white square indicates presence of specimens from this stage). Right color scale bar corresponds to the altitude and bathymetry (in meters).

is comparatively minor with respect to other Early Triassic events (e.g. Smithian/Spathian boundary), correlating the Induan/Olenekian boundary across the Boreal and Tethyan realms is far from clear. Hence, in this work we use the four stage subdivision defined by Tozer (1967), whose boundaries are well-defined in terms of ammonoids (Fig. 2). Moreover, the duration of the Spathian has now been demonstrated to be of ca. 3

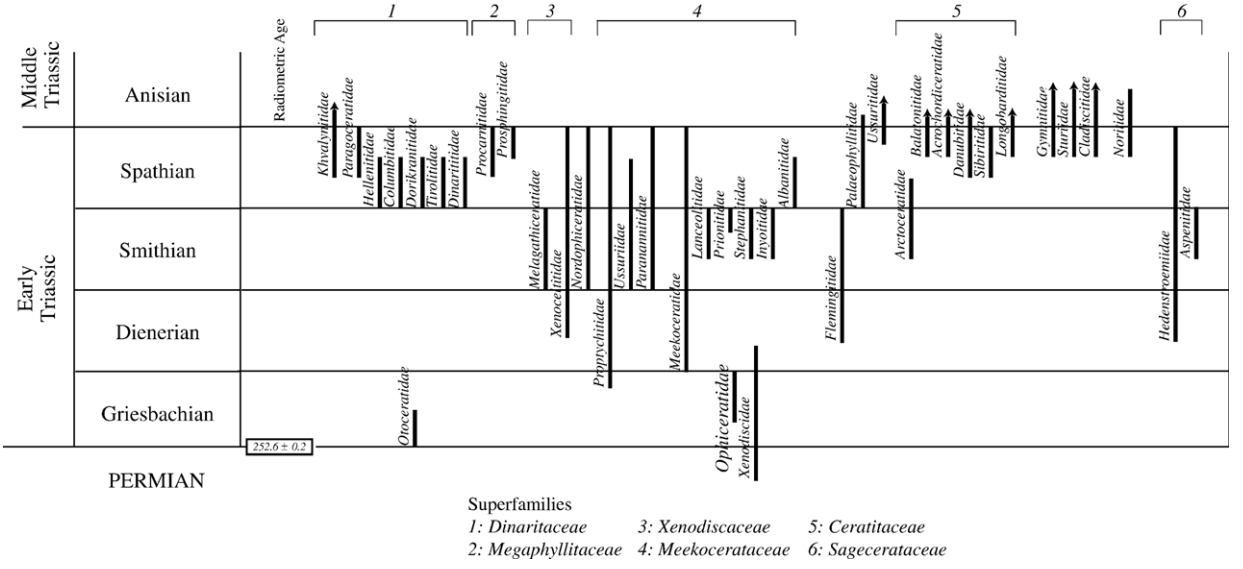

Fig. 2. Chronostratigraphic subdivisions of the Early Triassic (radiometric age by Mundil et al., 2004) and temporal distribution of the ammonoid families (modified after Tozer, 1981a,b, 1994).

myr, which amount to at least half of the duration of the Early Triassic (see Ovtcharova et al., 2006 and hereafter).

2.3. The ammonoid recovery

Ammonoids recovered and diversified faster than most other marine clades during the Early Triassic (Kummel, 1957, 1973a,b; Fig. 2). Only conodonts possibly recovered at a more or less comparable rate (e.g. Tozer in Hallam, 1996).

Otoceras, a characteristic early Griesbachian genus, was the last derivative of the Permian family Araxoceratidae. This genus only had a short existence during the earliest Triassic (Griesbachian), without further known descendents (Tozer, 1973). All other Triassic ceratitids are usually considered to derive from the Permian Xenodiscidae family, with *Ophiceras* as a bridging taxon between Xenodiscidae and Early Triassic families (Kummel, 1973a,b; Wiedmann, 1973; Kennedy, 1977; Tozer, 1981a). Hence, patterns of diversification and distribution of most if not all Early Triassic ammonoids are likely to reflect those of a monophyletic clade derived from xenodiscids such as *Ophiceras*. *Otoceras* and *Ophiceras* co-occurred during the earliest Triassic, yet *Ophiceras* was the most widespread genus.

Tethyan ammonoid faunas were generally more diverse than Boreal or Panthalassic faunas (e.g. Tozer, 1981b). A first low diversity phase spanned the Griesbachian and Dienerian. Then diversity globally increased until it dropped down again around the Smithian/Spathian boundary (Fig. 3). Boreal ammonoids were generally less diverse, with a variable endemism, and their greatest geographical differentiation was reached during the Spathian (Kummel, 1973b; Dagys, 1997). Although less severe than the Smithian/Spathian boundary event, another significant and global drop of generic richness occurred around the Spathian/Anisian boundary (Bucher, 1989).

3. Data set and method

3.1. Studied localities and ammonoid genera

The diversity and distribution patterns of ammonoids were analyzed from a data set including about twenty Tethyan and Panthalassic basins (Table 1, Fig. 1). Some of the basins were defined as early as the end of the 19th century (e.g. Spiti, Timor). The ammonoid data was compiled from published and unpublished systematic, biostratigraphical or paleobiogeographical contributions (ongoing work of Brayard–Bucher and Bucher–Guex for the Smithian and Spathian stages, respectively). Despite the fact that some of the Early Triassic ammonoid zones can be recognized at a world-wide scale, achieving global correlations at the zone level for the entire Early Triassic still requires further work. Hence, time resolution was essentially limited to the stage level in the present analysis.

We processed all the available data at the generic level in order to avoid the important taxonomic bias still pervading the species-level. Although species counts are theoretically more objective than genus richness,

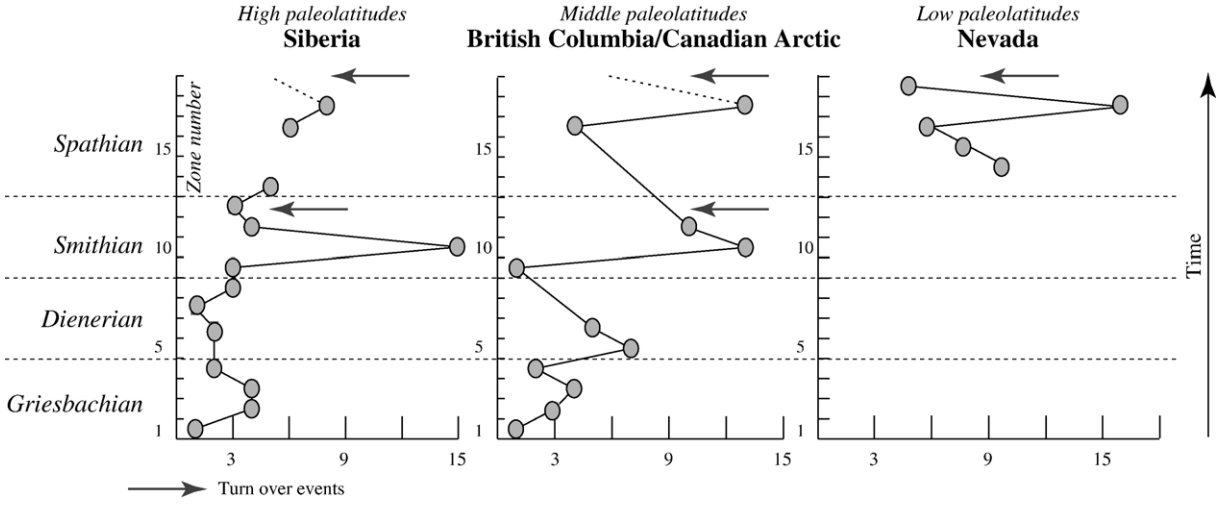

Fig. 3. Evolution of the ammonoid generic richness during the Early Triassic for low, middle and high latitudes (correlations and data for high and middle paleolatitudes after Dagys, 1999; Dagys and Ermakova, 1988, 1990, 1996; Tozer, 1994; for Nevada, data is unpublished).

Table 1
Sources for fossil data

Localities	Data					
Madagascar	Collignon, 1933–1934	Bando, 1977				
Albania	Arthaber, 1908	Arthaber, 1911	Germani, 1997			
Caucasus	Popov, 1962	Shevyrev, 1968	Shevyrev, 1995			
Yugoslavia	Petrovic and Mihajlovic, 1935	Krystyn, 1974	Posenato, 1992			
Chios	Renz and Renz, 1947	Renz and Renz, 1948	Gaetani et al., 1992	Mertmann and Jacobshagen, 2003		
Spiti and Qinghai/ Xizang Tibet	Diener, 1897	Krafft, 1900	Krafft and Diener, 1909	Kummel, 1970b		
	Wang and He, 1981	He et al., 1986	Waterhouse and Gupta, 1985	Wu, 1983		
Salt Ranges and Kashmir	Waagen, 1895	Kummel and Teichert, 1966	Kummel, 1966	Kummel, 1970a	Kummel and Teichert, 1970	Guex, 1978
	Diener, 1913	Bando, 1981	Nakazawa, 1981			
Oman	Tozer and Calon, 1990	Blendinger, 1995	Krystyn et al., 2003	Unpublished data		
Iran	Tozer, 1972					
Afghanistan	Kummel, 1968a	Kummel and Erben, 1968	Collignon, 1973			
Timor	Wanner, 1913	Welter, 1922	Kummel, 1968b	Nakazawa and Bando, 1968		
Guangxi and South China	Hsu, 1937 Wang, 1984	Chao, 1950 Wang, 1985	Chao, 1959 Unpublished data	Wang and He, 1980	Guo, 1982	
California Nevada Idaho/Utah	Hyatt and Smith, 1905	Smith, 1932	Kummel and Steele, 1962 Mathews, 1929	Silberling and Wallace, 1969 Kummel, 1957	Unpublished data	
British Columbia	Tozer, 1963	Tozer, 1965	Tozer, 1967	Tozer, 1994		
Greenland	Spath, 1930	Spath, 1935	Trümpy, 1969			
Spitsbergen	Frebold, 1929	Frebold, 1930	Kummel, 1961	Tozer and Parker, 1968	Korchinskaya, 1972	Weitschat and Lehmann, 1978
	Korchinskaya, 1982	Korchinskaya, 1983	Korchinskaya and Vavilov, 1987	Weitschat and Dagys, 1989	Mørk et al., 1999	Unpublished data
Ellesmere/Axel Heidberg Islands	Tozer, 1965	Tozer, 1967	Tozer, 1994			
Olenek/Lena River and Okhotsk/Kolyma lands	Popov, 1961	Popov, 1968	Dagys and Ermakova, 1988 Sp	Dagys and Ermakova, 1990 Sm	Dagys, 1999	Ermakova, 2001
	Dagys and Ermakova, 1996	Ermakova, 1999	Zakharov, 2002a			
General	Mojsisovics, 1886	Noetling, 1905	Diener, 1912	Spath, 1934	Kummel, 1969	Zakharov, 1971

References are given in Appendix A.

ammonoid genera are evidently more stable and conservative entities. The database contains a total of 185 genera (11 genera in the Griesbachian, 22 in the Dienerian, 61 in the Smithian, 93 in the Spathian). Taxonomy at the genus-level is based on the classification of Tozer (1981a, 1994), emended with some recently described genera. Greatest care was taken to make a consistent use of generic names. Only a few occurrences reported in the literature still lack adequate illustrations that would confirm the generic assignments, but these are unlikely to seriously modify the global patterns in diversification and distribution.

Paleolatitude measurements were taken from the published literature or interpolated from a new Early Triassic map (Péron et al., 2005). This map is a synthesis of different published reconstructions and takes into account the latest and most reliable data (see Péron et al., 2005). When a basin encompasses several localities, an average latitude and longitude was taken into account. Most of the available data are distributed within the

northern hemisphere, only a few Early Triassic localities being known from the southern hemisphere (e.g. Allison and Briggs, 1993) other than those from the Tethyan encroachment. In this study, we have excluded data from allochtonous terranes whose latitudinal and longitudinal positions are too poorly constrained (e.g. the Chulitna terrane for the Smithian). Hence, the exclusion of some terranes removes some endemic genera from the data set (e.g. *Paleokazachstanites* or *Burijites* from Primorye).

3.2. Reconstructions of paleogeographical ranges, generic richness, and computational analysis

In order to assess the effects of preservation and/or sampling biases, we devised a two-level analysis of the compiled data set: (i) "real presence" where only observed occurrences are taken into account, and (ii) "real + virtual presences" where the distribution of each genus was reconstructed by taking into account its most extreme latitudinal and longitudinal occurrences. The genus was considered as "virtually" present in all basins included in this reconstructed biogeographical domain (Fig. 4). This approach would theoretically conflict with bipolar distributions. However, as data other than Tethyan are missing in the southern Early Triassic hemisphere, it does not artificially expand the latitudinal distributions of actual bipolar genera. The final generic presence/absence matrix is presented in the Table 2A–D. GIS-based approaches can also be used to reconstruct past paleobiogeographical ranges (e.g. Rode and Lieberman, 2004). However, the relatively simple Early Triassic paleogeography does not make it necessary to use such methods and occurrences can be directly plotted on the paleogeographical map.

Based on this data set, we carried out an analysis of the generic richness as a function of paleolatitude in order to test the classical "energy hypothesis" of the edification of a latitudinal diversity gradient (Rohde, 1992). At the same time, we also considered the relationship between generic richness and longitude. On the basis of the observed occurrences ("real presences"), bootstrapped 95% Confidence Intervals for latitudinal and longitudinal gradients were estimated for each basin assemblage by random resampling with replacement within the set of "virtually present + absent" genera.

In addition, we generated a generic Occurrence Ratio Profile (ORP) for each stage by computing for each genus the percentage of basins where it is actually or actually and virtually present. We consider such percentage as a proxy for the generic endemicity. Then, the frequency distribution of the *n* Occurrence Ratios corresponding to the *n* genera recorded in the data set is graphed as a ten-class histogram with a 10% binsize. The bootstrapped Confidence Intervals associated to the observed frequencies are estimated by constructing and analysing several (10,000 in this work) presence/absence pseudo-matrices generated by random resampling with

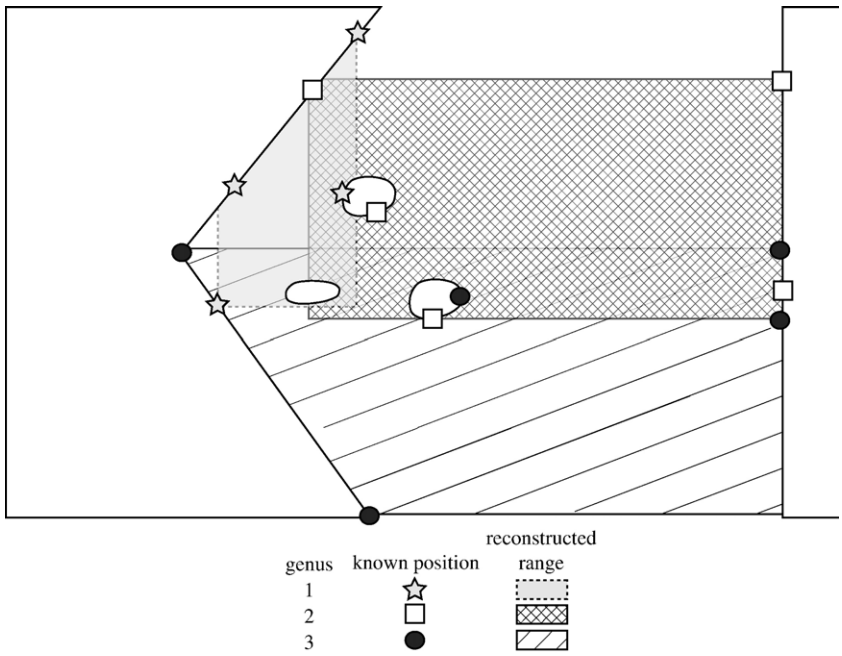

Fig. 4. Schematic range reconstructions of the ammonoid genera.

replacement of taxa. Then, the observed profiles were compared to their respective null distribution models as generated by random reshuffling of taxa occurrences among localities (this permutation model corresponds to the third method of permutation of a taxon × locality occurrence matrix as discussed by Legendre et al., 1997). This method of permutation generates the null hypothesis that for each basin, a fixed number of genera (preserved by the permutation model and corresponding to a first order to a fixed number of ecological niches) randomly colonize the basin through a lottery where the exact identity of each genus does not matter. Hence, this null hypothesis implicitly assumes that the geographical location and physical and environmental characteristics of the basin do not control the detailed taxonomic composition of its generic assemblage, but only control its generic richness, i.e. its number of colonisable "niches".

Such basin level based analysis departs from already published qualitative or quantitative studies (e.g. Dagys, 1988; McGowan, 2005) in that it estimates faunal endemicity at an ecologically meaningful level of spatial resolution. Indeed, taxonomic assemblages recorded within basins, i.e. areas ranging in most cases between surface scales of 10^4 to 10^6 km^2, correspond to a first order to metacommunities, i.e. "sets of local communities that are linked by dispersal of multiple interacting species" (see Leibold et al., 2004). The variations of taxonomic composition at this regional scale of γ diversity (Whittaker, 1977) are known to be independent from local processes controlling α diversity but strongly depend on historical and biogeographical constraints (e.g. origination, extinction and migration rates; Brown, 1995; Rosenzweig, 1995; Gaston and Blackburn, 2000; Lieberman, 2000; Hillebrand and Blenckner, 2002) as well as on global physiographic and environmental conditions (Arita and Rodríguez, 2004). This makes the regional metacommunity level an ecologically meaningful level of functional organization with its own dynamic and own interaction rules partly emerging from local community integration. Moreover, the metacommunity level is also partly determined by globally controlled physical and historical parameters (Ricklefs, 1987, 2004; Leibold et al., 2004).

4. Results

4.1. Griesbachian

During Griesbachian time, no latitudinal or longitudinal generic richness gradient can be recognized (Figs. 5A, 6A). The bootstrapped Confidence Intervals associated with these generic richness transects suggest that this feature is not an artefact generated by the meagre amount of Griesbachian data. The ammonoid fauna appears very cosmopolitan and homogeneous (Figs. 7A and 8A), as illustrated by the respective distributions of *Ophiceras*, *Hypophiceras* or *Otoceras*. The rest of the Griesbachian genera are preferentially found in middle or high-latitude basins (e.g. *Tompophiceras*), but the comparatively scarce data from the Early Triassic southern hemisphere prevents further in-depth comparisons.

4.2. Dienerian

A weak latitudinal diversity gradient emerges and marks the onset of a change in the paleogeographical distribution of ammonoids (Fig. 5B). A weak longitudinal diversity gradient cannot be excluded in the Tethys (Fig. 6B). Many genera are longitudinally distributed across the entire Panthalassa, thus indicating the onset of a latitudinal zonation (e.g. *Pleurogyronites*, *Ambites*, *Pleurambites*). Hence, a weak endemism emerges during the Dienerian (Figs. 7B and 8B). It involves genera confined to northern Siberia or to the southern border of the Tethys (e.g. *Eovavilovites*, *Tompoproptychites*, *Collignonites*).

4.3. Smithian

A clear unimodal latitudinal diversity gradient first emerges during the Smithian (Fig. 5C), whereas the longitudinal analysis of Smithian distributions suggests a flat gradient across the Panthalassa and a marked westward decrease of the diversity gradient within the Tethys (Fig. 6C). This longitudinal gradient in the Tethys suggests that different factors influenced the modes of distribution and dispersal of ammonoids between the Tethys and the Panthalassa. Some genera such as *Aspenites*, *Lanceolites*, *Inyoites* or *Owenites*, which are essentially restricted to the intertropical belt, indicate strong longitudinal similarities between the Tethyan and the tropical eastern Panthalassic basins (California, Nevada, Idaho).

At the complete stage level, the generic assemblages become more and more endemic (Figs. 7C and 8C), even if some successive distinct biogeographical configurations can be distinguished. At the very beginning of the Smithian the widespread and very abundant genus *Hedenstroemia* indicates a short phase of high cosmopolitanism. For the following phase, the Tethyan and Equatorial basins include more endemic genera than the high-latitude ones. This illustrates an intensification of

Table 2

A. Griesbachian occurrences

	Hypophiceras	*Metophiceras*	*Tompophiceras*	*Otoceras*	*Wordieoceras*	*Discophiceras*	*Ophiceras*	*Vishnuites*	*Bukkenites*	*?Anotoceras*	*Aldanoceras*
Spiti	**1**	**1**	0	**1**	0	0	**1**	**1**	0	**1**	0
Salt Ranges	**1**	1	0	0	0	0	1	1	0	1	0
Oman	0	0	0	0	0	**1**	**1**	0	**1**	**1**	0
Guangxi	**1**	**1**	**1**	**1**	0	1	**1**	1	1	0	0
Greenland	**1**	**1**	**1**	0	**1**	**1**	**1**	**1**	**1**	0	0
Spitsbergen	**1**	1	**1**	**1**	1	1	**1**	**1**	1	0	0
Ellesmere	**1**	1	**1**	**1**	**1**	**1**	**1**	**1**	**1**	0	0
Olenek	**1**	**1**	**1**	**1**	**1**	0	**1**	0	0	0	**1**

B. Dienerian occurrences

	Xenodiscoides	*Gyrophiceras*	*Kashmirites*	*Sakhaitoides*	*Eoptychites*	*Dunedinites*	*Koninckites*	*Vavilovites*	*Eovavilovites*	*Tompaproptychites*	*Proptychites*	*Kingites*	*Paranorites*	*Heilongites*	*Collignonites*	*Meekophiceras*	*Pleurogyronites*	*Ambites*	*Pleurambites*	*Gyronites*	*Prionolobus*	*Flemingites*	*Pseudosageceras*
Madagascar	0	0	0	0	0	0	0	0	0	0	0	0	0	0	**1**	0	0	0	0	0	**1**	**1**	**1**
Spiti	0	0	**1**	0	0	0	**1**	0	0	0	**1**	**1**	0	0	0	**1**	**1**	**1**	0	0	**1**	**1**	**1**
Salt Ranges	**1**	**1**	**1**	0	**1**	0	**1**	0	0	0	**1**	**1**	**1**	**1**	0	0	0	**1**	**1**	**1**	**1**	1	**1**
Oman	0	0	0	0	0	0	0	0	0	0	0	0	0	0	0	0	0	**1**	0	0	1	1	1
Timor	1	0	**1**	0	0	0	1	0	0	0	1	1	0	1	0	1	1	1	1	0	**1**	**1**	**1**
Guangxi	1	0	1	0	0	0	**1**	0	0	0	**1**	1	**1**	1	0	1	1	1	1	0	**1**	**1**	**1**
Nevada	1	0	1	0	0	0	1	0	0	0	1	1	0	1	0	1	1	**1**	1	0	1	1	1
Canada	**1**	0	**1**	0	0	**1**	**1**	**1**	0	0	**1**	1	0	1	0	**1**	**1**	**1**	**1**	0	**1**	**1**	1
Spitsbergen	0	0	**1**	0	0	0	0	**1**	0	0	0	0	0	0	0	0	0	0	0	0	0	0	1
Ellesmere	0	0	**1**	0	0	0	0	**1**	0	0	**1**	**1**	0	**1**	0	**1**	0	**1**	0	0	0	0	**1**
Olenek	0	0	0	**1**	0	0	0	**1**	**1**	**1**	0	0	0	0	0	0	0	0	0	0	0	0	**1**

C. Smithian occurrences

	Kashmirites	*Keloceras*	*Sakhaites*	*Pseudocelites*	*Prefflorianites*	*Eukashmirites*	*Hanielites*	*Glyptophiceras*	*Xenocelites*	*Subvishnuites*	*Melagathiceras*	*Juvenites*	*Thermalites*	*Proharpoceras*	*Lepiskites*	*Clypeoceras*	*Clypeoceratoides*	*Pseudaspidites*	*Paraspidites*	*Lingyunites*	*Wyomingites*	*Anaflemingites*	*Meekoceras*	*Gyronites*	*Prionolobus*	*Flemingites*	*Euflemingites*	*Anaxenaspis*	*Pseudoflemingites*	*Subflemingites*	*Arctoceras*
Madagascar	0	0	0	0	0	0	0	0	0	0	0	0	0	0	0	**1**	0	0	0	0	0	0	0	0	**1**	**1**	0	0	0	0	0
Spiti	**1**	0	0	**1**	0	0	0	0	**1**	0	0	0	0	0	0	**1**	0	**1**	0	0	0	0	0	0	**1**	**1**	0	0	0	0	0
Salt Ranges	**1**	0	0	**1**	0	**1**	0	**1**	**1**	0	0	**1**	0	0	0	**1**	0	0	**1**	0	0	0	**1**	0	**1**	1	0	0	0	0	**1**
Oman	0	0	0	**1**	0	0	0	0	0	0	0	0	0	**1**	0	1	0	0	0	0	**1**	0	**1**	0	1	**1**	**1**	0	0	0	0
Timor	**1**	0	0	**1**	0	**1**	**1**	0	1	**1**	0	1	0	0	0	0	0	1	0	0	1	0	1	0	**1**	**1**	**1**	0	**1**	**1**	1
Afghanistan	1	0	0	**1**	0	0	0	0	1	**1**	0	**1**	0	1	0	**1**	0	1	0	0	**1**	0	**1**	0	0	**1**	1	0	0	0	**1**
Guangxi	1	0	0	0	**1**	0	0	0	1	1	0	**1**	0	**1**	0	**1**	0	**1**	0	**1**	1	0	**1**	0	0	**1**	**1**	0	0	0	**1**
California	1	0	0	0	**1**	0	0	0	1	0	0	1	0	0	0	0	0	**1**	0	0	1	0	**1**	0	0	1	1	0	0	0	**1**
Nevada	1	0	0	0	0	0	0	0	1	0	0	**1**	0	0	0	0	0	**1**	0	0	1	**1**	**1**	0	0	1	**1**	0	0	0	**1**
Idaho	1	0	0	0	0	0	0	0	1	0	**1**	**1**	**1**	0	0	0	0	**1**	0	0	**1**	**1**	**1**	0	0	1	**1**	0	0	0	1
Caucasus	0	0	0	0	**1**	0	0	0	0	**1**	0	1	0	0	0	0	0	0	0	0	**1**	0	**1**	0	0	0	0	0	0	0	0
Canada	**1**	0	0	0	0	0	0	0	**1**	0	1	1	1	0	0	0	0	0	0	0	**1**	0	**1**	**1**	0	**1**	**1**	**1**	0	0	**1**
Spitsbergen	**1**	0	0	0	0	0	0	0	**1**	0	1	0	0	0	0	0	0	0	0	0	0	0	0	0	0	0	**1**	1	0	0	**1**
Ellesmere	**1**	0	0	0	0	0	0	0	**1**	0	**1**	**1**	**1**	0	0	0	0	0	0	0	0	0	1	0	0	0	**1**	**1**	0	0	**1**
Olenek	0	**1**	**1**	0	0	0	0	0	**1**	0	**1**	0	0	0	**1**	0	**1**	0	0	0	0	0	0	0	0	0	0	**1**	0	0	**1**

	Submeekoceras	*Ussuria*	*Metussuria*	*Parussuria*	*Oxyussuria*	*Platussuria*	*Anasibirites*	*Garfeyites*	*Hemiprionites*	*Prionites*	*Wasatchites*	*Parastephanites*	*Anawasachites*	*Arctoprionites*	*Stephanites*	*Invoites*	*Lanceolites*	*Elkoceras*	*Paranannites*	*Owenites*	*Metinyoites*	*Clypites*	*Cordillerites*	*Tellerites*	*Hedenstroemia*	*Pseudosageceras*	*Mesohedenstroemia*	*Aspenites*	*Hemiaspenites*	*Pseudaspenites*
Madagascar	0	0	0	0	0	0	0	0	0	0	0	0	0	0	0	0	0	0	0	0	0	0	0	**1**	**1**	**1**	0	0	0	0
Spiti	0	0	0	0	0	0	**1**	0	**1**	**1**	**1**	0	0	0	0	0	0	0	0	0	0	0	0	**1**	**1**	**1**	0	**1**	0	0
Salt Ranges	0	0	0	0	0	0	**1**	0	**1**	**1**	**1**	**1**	0	0	**1**	0	0	0	0	0	0	**1**	0	0	**1**	**1**	0	1	0	0
Oman	**1**	**1**	0	0	0	0	**1**	0	0	0	0	0	0	0	0	**1**	0	0	**1**	**1**	0	0	0	0	**1**	**1**	0	**1**	0	**1**
Timor	**1**	**1**	0	0	0	0	**1**	0	**1**	**1**	0	0	0	0	1	1	0	0	1	**1**	**1**	0	0	0	**1**	**1**	0	**1**	0	**1**
Afghanistan	**1**	1	0	0	0	0	**1**	0	**1**	1	**1**	0	0	0	1	1	0	0	**1**	**1**	0	0	0	0	1	**1**	0	1	0	1
Guangxi	1	**1**	**1**	0	0	**1**	**1**	0	1	1	1	0	0	0	1	**1**	**1**	0	**1**	**1**	0	0	**1**	0	**1**	**1**	**1**	**1**	0	**1**

Table 2 (*continued*)

	Submeekoceras	*Ussuria*	*Metussuria*	*Parussuria*	*Oxyussuria*	*Platussuria*	*Anasibirites*	*Gurleyites*	*Hemiprionites*	*Prionites*	*Wasachites*	*Parastephanites*	*Anawasachites*	*Arctoprionites*	*Stephanites*	*Inyoites*	*Lanceolites*	*Elkoceras*	*Paranannites*	*Owenites*	*Metinyoites*	*Clypites*	*Cordillerites*	*Tellerites*	*Hedenstroemia*	*Pseudosageceras*	*Mesohedenstroemia*	*Aspenites*	*Hemiaspenites*	*Pseudaspenites*
California	1	0	**1**	**1**	0	0	1	0	1	1	1	0	0	0	**1**	**1**	**1**	0	1	**1**	0	0	1	0	1	**1**	0	**1**	0	0
Nevada	1	0	1	**1**	0	0	**1**	0	1	1	**1**	0	0	0	0	1	**1**	**1**	**1**	**1**	0	0	1	0	1	**1**	0	**1**	**1**	0
Idaho	**1**	0	**1**	0	0	0	**1**	**1**	**1**	1	**1**	0	0	0	0	**1**	**1**	**1**	**1**	**1**	0	0	**1**	0	1	**1**	0	**1**	**1**	0
Caucasus	0	0	0	**1**	0	0	0	0	0	0	0	0	0	0	0	**1**	**1**	0	0	**1**	0	0	0	0	0	**1**	0	0	0	0
Canada	0	0	0	0	**1**	0	**1**	0	**1**	**1**	**1**	0	**1**	**1**	0	0	0	0	1	0	0	0	**1**	0	1	**1**	0	0	0	0
Spitsbergen	0	0	0	0	0	0	**1**	0	**1**	0	**1**	0	0	**1**	0	0	0	0	1	0	0	0	0	**1**	1	**1**	0	0	0	0
Ellesmere	0	0	0	0	0	0	0	0	**1**	**1**	**1**	0	**1**	**1**	0	0	0	0	1	0	0	0	0	0	**1**	**1**	0	0	0	0
Olenek	0	0	0	0	0	0	0	0	0	0	**1**	0	0	0	0	0	0	0	0	0	0	0	0	0	**1**	**1**	0	0	0	0

D. Spathian occurences

	?Xenodiscoides	*Sulioticeras*	*Hemilecanites*	*Paranoritoides*	*Proptychitoides*	*Evenites*	*Koninckitoides*	*Arctomeekoceras*	*Boreomeekoceras*	*Neomeekoceras*	*Pseudosvalbardiceras*	*Bajarunia*	*Nordophiceras*	*Boreoceras*	*Pseudokymatites*	*Subinyoites*	*Iscalitoides*	*Chiotites*	*Chioceras*	*Protropites*	*Zenoites*	*Vickohlerites*	*Popovites*	*Albanites*	*Byrrangoceras*	*Hyrcanites*	*Kiparisovites*	*Tozericeras*	*Pseudosageceras*	*Cordillerites*	*Metasageceras*	*Beatites*
Madagascar	0	0	0	0	0	0	0	0	0	0	0	0	0	0	0	0	0	0	0	0	0	0	0	0	0	0	0	0	**1**	0	0	0
Spiti	0	0	0	0	0	0	0	0	0	0	0	0	0	0	0	**1**	0	0	0	0	0	0	0	0	0	0	0	0	**1**	0	0	0
Salt Ranges	0	0	0	**1**	0	0	0	0	0	0	0	0	0	0	0	0	0	0	0	0	0	0	0	0	0	0	0	**1**	**1**	0	0	0
Oman	0	0	0	0	0	0	0	0	0	0	0	0	0	0	0	0	0	0	0	0	0	0	0	0	0	0	0	0	**1**	0	0	0
Timor	0	0	0	0	**1**	0	0	0	0	0	0	0	0	0	0	0	0	0	0	0	0	**1**	0	**1**	0	0	0	0	**1**	0	0	0
Afghanistan	0	0	0	0	1	0	0	0	0	0	0	0	0	0	0	0	**1**	0	0	0	0	**1**	0	1	0	0	0	0	**1**	0	0	0
Iran	0	0	0	0	**1**	0	0	0	0	0	0	0	0	0	0	0	**1**	0	0	0	0	1	0	**1**	0	0	0	0	1	0	0	0
Guangxi	0	1	0	0	**1**	0	0	0	0	0	0	0	0	0	0	0	**1**	0	0	0	0	1	0	1	0	0	0	0	**1**	**1**	0	0
Albania	0	**1**	0	0	**1**	0	0	0	0	0	0	0	0	0	0	0	**1**	0	0	**1**	0	0	0	**1**	0	0	0	0	0	**1**	0	**1**
California	**1**	1	1	0	1	0	0	0	0	0	0	0	0	0	0	0	1	0	0	0	0	0	0	0	0	0	0	0	**1**	1	0	0
Yugoslavia	0	**1**	**1**	0	0	0	0	0	0	0	0	0	0	0	**1**	0	0	0	0	0	0	0	0	0	0	0	0	0	0	0	0	0
Nevada	0	1	**1**	0	**1**	0	0	0	0	0	0	0	0	0	0	0	**1**	0	0	0	0	0	0	0	0	0	0	0	**1**	**1**	0	0
Idaho	0	1	0	0	**1**	0	0	0	0	**1**	0	0	**1**	0	0	0	**1**	0	0	0	0	0	0	0	0	0	0	0	**1**	1	0	0
Chios	0	**1**	**1**	0	**1**	0	0	0	0	0	0	0	0	0	0	0	**1**	**1**	**1**	0	**1**	**1**	0	**1**	0	0	0	0	**1**	1	**1**	0
Caucasus	0	1	0	0	0	0	0	0	0	0	0	0	0	0	0	0	**1**	0	0	0	1	0	**1**	0	0	**1**	**1**	0	1	1	0	0
Canada	0	**1**	0	0	0	0	0	0	0	1	0	0	1	0	0	0	**1**	0	0	0	1	0	1	0	0	0	0	0	**1**	1	0	0
Spitsbergen	0	0	0	0	0	0	0	0	0	0	**1**	0	0	0	0	0	0	0	0	0	1	0	1	0	0	0	0	0	1	0	0	0
Ellesmere	0	0	0	0	0	0	0	**1**	0	**1**	0	0	1	0	0	0	0	0	0	0	**1**	0	1	0	0	0	0	0	**1**	0	0	0
Olenek	0	0	0	0	0	**1**	**1**	**1**	**1**	0	**1**	**1**	**1**	**1**	0	0	0	0	0	0	0	0	0	0	1	0	0	0	**1**	0	0	0

	Dinarites	*Pseudodinarites*	*Dagnoceras*	*Stacheites*	*Balkanites*	*Tirolites*	*Diaplococeras*	*Dorikranites*	*Columbites*	*?Tirolites*	*Procolumbites*	*Pleurocolumbites*	*?Ceratites*	*Hellenites*	*Pallasites*	*Pseudoharpoceras*	*Paragoceras*	*Epicelites*	*Epicelitioides*	*Subcolumbites*	*Fengshanites*	*Prenkites*	*Tunglanites*	*Khvalynites*	*Metadagnoceras*	*Metahedenstroemia*	*Procarnites*	*Doaboceras*	*Neopopanoceras*	*Digitophyllites*	*Procarnitoides*	*Prosphingites*
Madagascar	0	0	0	0	0	0	0	0	0	0	0	0	0	0	0	0	0	0	0	0	0	0	0	0	0	0	0	0	0	0	0	0
Spiti	0	0	0	0	0	**1**	0	0	0	0	0	0	0	0	0	0	0	0	0	0	0	0	0	0	0	0	0	0	0	0	0	0
Salt Ranges	0	0	0	**1**	0	**1**	0	0	**1**	0	0	0	0	0	0	**1**	0	0	**1**	0	0	0	0	0	0	**1**	0	0	0	0	0	0
Oman	0	0	0	1	0	1	0	0	1	0	0	0	0	0	0	0	0	0	**1**	0	0	0	0	0	0	**1**	0	0	0	0	0	0
Timor	0	0	**1**	1	0	1	0	0	1	0	0	0	0	0	0	0	**1**	0	0	**1**	0	0	0	0	**1**	0	**1**	0	0	0	0	0
Afghanistan	0	0	1	1	0	1	0	0	1	0	0	0	0	0	0	0	1	0	0	1	**1**	1	0	0	1	0	**1**	**1**	0	0	0	0
Iran	0	0	**1**	**1**	0	**1**	0	0	**1**	0	0	0	0	0	0	0	**1**	0	**1**	**1**	1	**1**	0	0	**1**	0	**1**	0	0	0	0	0
Guangxi	0	0	**1**	1	0	1	0	0	1	0	0	0	0	**1**	0	0	**1**	0	0	1	**1**	**1**	**1**	0	1	0	**1**	0	0	**1**	0	0
Albania	0	0	**1**	1	0	**1**	0	0	0	0	0	0	0	**1**	0	0	**1**	**1**	0	**1**	**1**	**1**	**1**	0	**1**	**1**	**1**	0	0	0	0	0
California	0	0	0	1	0	1	0	0	1	0	0	0	0	0	0	0	1	0	0	1	1	0	0	0	**1**	0	1	0	**1**	0	0	0
Yugoslavia	**1**	**1**	0	**1**	**1**	**1**	**1**	0	0	0	0	0	0	0	0	0	0	0	0	0	0	0	0	0	0	0	0	0	0	0	0	0
Nevada	0	0	0	**1**	0	1	0	0	1	0	0	0	0	0	0	0	**1**	0	0	**1**	**1**	0	0	0	**1**	0	1	0	0	0	0	0
Idaho	0	0	0	**1**	0	**1**	0	0	**1**	**1**	**1**	0	**1**	0	0	0	0	0	0	0	0	0	0	0	1	0	1	0	0	0	0	0
Chios	**1**	1	**1**	**1**	0	1	0	0	**1**	0	0	0	0	**1**	**1**	0	**1**	**1**	0	**1**	**1**	**1**	**1**	0	**1**	0	**1**	0	0	0	0	0
Caucasus	**1**	**1**	0	**1**	0	**1**	0	1	0	0	**1**	0	0	**1**	0	0	0	0	0	0	0	0	0	**1**	1	0	**1**	0	0	0	0	0
Canada	0	0	0	0	0	**1**	0	0	0	0	0	0	0	0	0	0	0	0	0	0	0	0	0	0	0	**1**	0	**1**	0	0	0	**1**
Spitsbergen	0	0	0	0	0	0	0	0	0	0	0	0	0	0	0	0	0	0	0	0	0	0	0	0	0	0	0	0	0	0	0	0
Ellesmere	0	0	0	0	0	0	0	0	0	0	0	0	0	0	0	0	0	0	0	0	0	0	0	0	0	0	0	0	0	0	0	**1**
Olenek	0	0	0	0	0	0	0	0	0	0	0	0	0	0	0	0	0	0	0	0	0	0	0	0	0	0	0	0	0	**1**	**1**	

(continued on next page)

the geographical differentiation despite the fact that some cosmopolitan genera still do persist (e.g. *Arctoceras*, *Flemingites*, *Pseudosageceras*). Finally, this pattern of biogeographical distribution is markedly altered during the very end of the Smithian (*Anasibirites* Zone and its high-latitude correlative, the *Anawasachites tardus*

Table 2 (*continued*)

	Sibirites	*Parasibirites*	*Tjurpites*	*Kazakhstanites*	*Olenikites*	*Svalbardiceras*	*Keyserlingtes*	*Olenekoceras*	*Monacanthites*	*Prohungarites*	*?Middlemissites*	*Qilianshanites*	*Dalmatites*	*?Prohungarites*	*?Hungarites yatesi*	*Eodanubites*	*Preflorianitoides*	*Proacrochordiceras*	*?Acrochordiceras*	*Eoacrochordicereas*	*Eogymnites*	*Ziyunites*	*Procladiscites*	*Paleophyllites*	*Eophyllites*	*Mangyshlakites*	*Meropella*	*Leiophyllites*	*Ussurites*
Madagascar	0	0	0	0	0	0	0	0	0	0	0	0	0	0	0	0	0	0	0	0	0	0	0	0	0	0	0	0	0
Spiti	0	0	0	0	0	0	**1**	0	0	0	**1**	0	0	0	0	0	0	0	0	0	0	0	**1**	0	0	0	0	**1**	0
Salt Ranges	0	0	0	**1**	0	0	0	0	0	**1**	0	0	0	0	0	0	0	0	0	0	0	0	1	0	0	0	0	1	0
Oman	0	0	0	1	0	0	0	0	0	0	0	0	0	0	0	0	0	0	0	0	0	0	1	0	0	0	0	1	0
Timor	0	0	0	0	0	0	**1**	0	0	**1**	0	0	0	0	0	0	0	0	0	0	0	0	0	**1**	0	0	0	**1**	0
Afghanistan	0	0	0	0	0	0	1	0	0	1	0	0	0	0	0	0	0	0	0	0	0	0	1	1	**1**	0	0	1	0
Iran	0	0	0	**1**	0	0	0	0	0	0	0	0	0	0	0	0	0	0	0	0	0	0	1	1	**1**	0	0	**1**	0
Guangxi	0	0	0	0	0	0	1	0	0	1	0	**1**	0	0	**1**	**1**	**1**	0	0	**1**	0	**1**	**1**	1	0	0	0	**1**	0
Albania	0	0	0	0	0	0	0	0	0	0	0	0	0	0	0	0	0	0	0	0	**1**	0	**1**	0	**1**	0	0	0	0
California	0	0	0	0	0	0	**1**	0	0	1	0	0	1	0	**1**	0	0	0	0	0	0	0	0	0	0	0	0	1	0
Yugoslavia	0	0	0	0	0	0	0	0	0	0	0	0	**1**	0	0	0	0	0	0	0	0	0	**1**	0	0	0	0	0	0
Nevada	0	0	0	0	0	0	1	0	0	**1**	0	0	1	**1**	**1**	0	0	0	**1**	0	0	0	0	0	0	0	0	1	0
Idaho	0	0	0	0	0	0	1	0	0	**1**	0	0	**1**	**1**	0	0	0	0	**1**	0	0	0	0	0	0	0	0	0	0
Chios	0	0	0	0	0	0	0	0	0	0	0	0	0	0	0	0	0	0	0	**1**	0	**1**	**1**	**1**	0	**1**	**1**	0	0
Caucasus	0	0	**1**	**1**	0	0	0	0	0	0	0	0	0	0	0	0	0	0	0	0	0	0	0	0	0	**1**	0	**1**	0
Canada	0	0	0	0	0	**1**	**1**	0	**1**	1	0	0	0	0	0	0	0	0	0	0	0	0	0	0	0	0	0	**1**	**1**
Spitsbergen	0	0	0	0	0	**1**	**1**	0	**1**	**1**	0	0	0	0	0	0	0	**1**	0	0	0	0	0	0	0	0	0	1	**1**
Ellesmere	0	0	0	0	**1**	**1**	**1**	0	0	0	0	0	0	0	0	0	0	0	0	0	0	0	0	0	0	0	0	**1**	**1**
Olenek	**1**	**1**	0	0	**1**	0	**1**	**1**	0	0	0	0	0	0	0	0	0	0	0	0	0	0	0	0	0	0	0	0	**1**

Bold numbers indicate real presences.
Normal numbers indicate interpolated presences. See Appendix 1 for references.

Zone), with a severe drop in diversity (Figs. 3 and 5D) accompanied by a return to essentially cosmopolitan distributions as shown by *Xenoceltites* and Prionitids (Fig. 9).

4.4. Spathian

An even steeper latitudinal gradient finally characterizes Spathian times (Fig. 5E). However, it differs from the Smithian one in being asymmetrically bimodal instead of unimodal, with two maxima separated by ca. 20° in latitude, thus delineating a marked peri-Equatorial decrease. A special attribute of this gradient is the increase of generic richness in the Boreal realm. Unlike the latitudinal gradient, the longitudinal differentiation previously observed between the Panthalassa and the Tethys fades away (Fig. 6D). This suggests that the primary environmental factors controlling the spatial distribution of the ammonoids may become identical again in the two oceanic realms. At the entire stage level, the generic endemicity reached its maximum value (Figs. 7D and 8D). Few genera such as the long-ranging genus *Pseudosageceras* do actually display a cosmopolitan distribution.

4.5. Interpolated generic richness maps

The generic richness for the Smithian and Spathian basins can be interpolated to visualize preliminary diversity contours (Fig. 10A, B). For this purpose, we used the simple Delaunay triangulation as implemented in the Isopaq software (Monnet et al., 2003a). This method of interpolation is well suited here because the values interpolated for sampled basins are the observed ones by definition and only intervening values are interpolated. This method avoids the over or underestimation effect often observed with more complex interpolation methods such as the Thin Plate Splines or Kriging. In the case of the Smithian and Spathian, the number of basins is still too small for a reliable interpretation of a worldwide interpolation (Brayard et al., 2004). Yet, these contours allow first order estimates of the diversity pattern evolution. The Smithian interpolated map clearly highlights the latitudinal and longitudinal diversity gradients. The Spathian interpolated map illustrates the complexity of the distribution of ammonoid genera and indicates the existence of a western Tethyan diversity hot-spot including a high proportion of endemic genera (e.g. *Diaplococeras*, *Meropella*, *Protropites*, *Pseudokymatites*).

5. Discussion

5.1. End-Permian versus Early Triassic climates: data and models

After the Carboniferous–Permian glaciation, the Late Paleozoic marine biogeographical provinces were well differentiated, with a pronounced provincialism (e.g. Bambach, 1990; Nie et al., 1990; Shen and Shi, 2004) suggesting a steep latitudinal temperature gradient, possibly coupled with an intensive thermo-haline

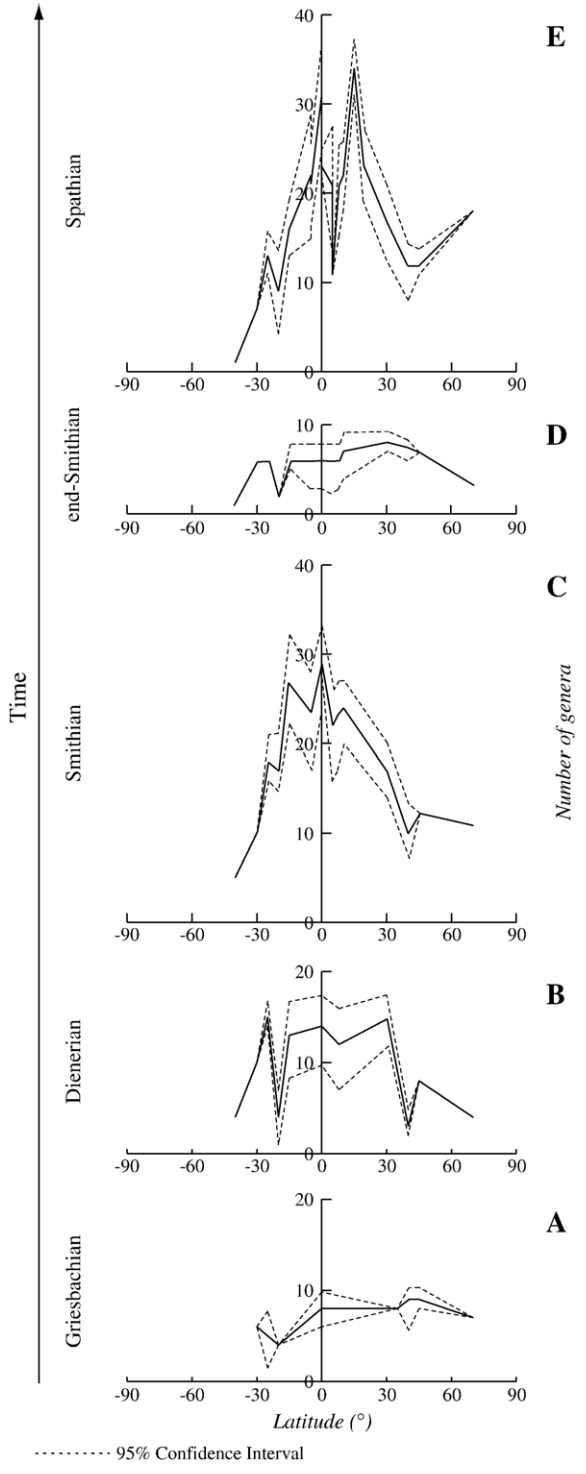

Fig. 5. Latitudinal diversity patterns during the A) Griesbachian, B) Dienerian, C) Smithian, D) end-Smithian, E) Spathian.

oceanic circulation (e.g. Beauchamp and Baud, 2002). Floras and climate-sensitive sedimentary rocks also indicate a relatively marked latitudinal temperature gradient showing the complete spectrum of temperature biomes (Rees, 2002; Gibbs et al., 2002; Rees et al., 2002).

Moreover, climatic models of the end-Permian indicate a steep temperature gradient coupled with a high seasonal variability (e.g. Crowley et al., 1987, 1989;

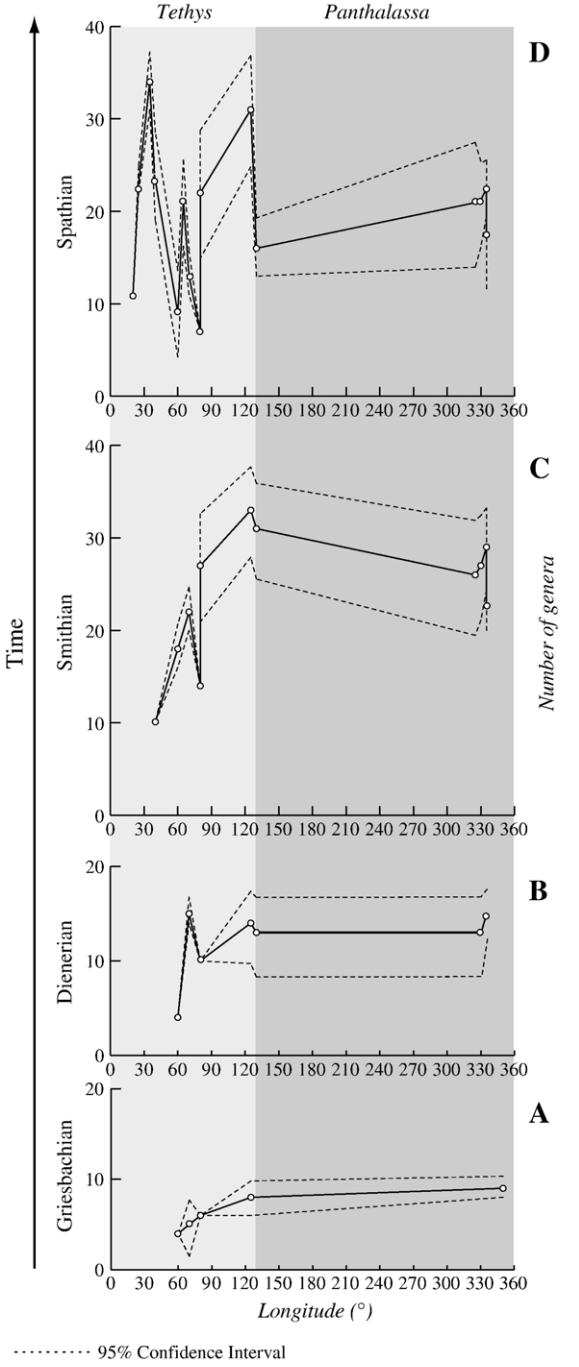

Fig. 6. Longitudinal diversity patterns for intertropical basins (30°N–30°S) during the A) Griesbachian, B) Dienerian, C) Smithian, D) Spathian.

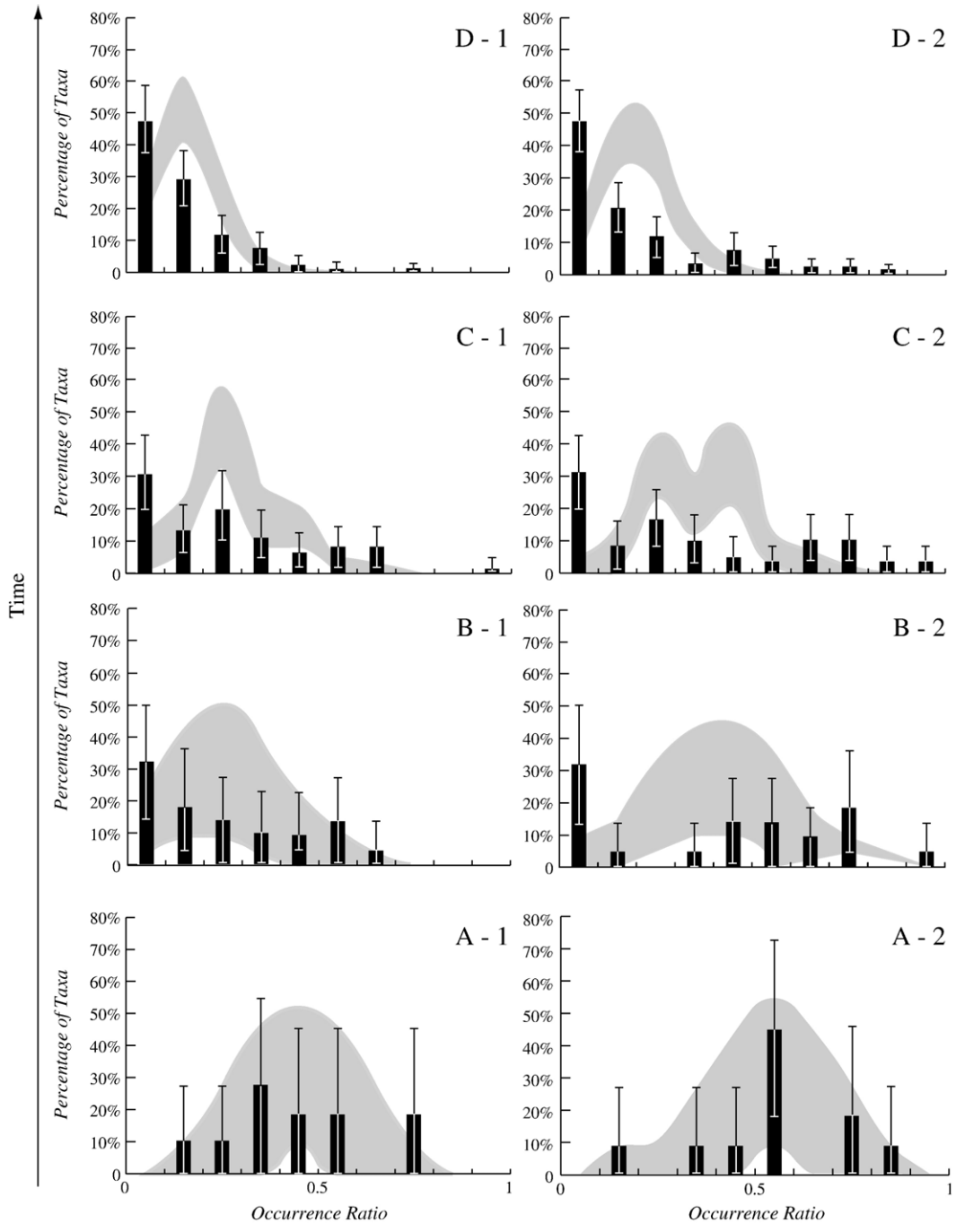

Fig. 7. Generic Occurrence Ratio Profiles for Early Triassic ammonoids. A) Griesbachian, B) Dienerian, C) Smithian, D) Spathian; 1) ORP computed from observed genera only, 2) ORP computed from observed and interpolated genera. Bootstrapped 95% Confidence Intervals associated to the observed Occurrence Ratios (error bars on the histogram) estimated with 10,000 iterations; 95% ORP null distribution (shaded area) estimated with 10,000 iterations under a lottery permutation model (see text for details).

Kutzbach and Gallimore, 1989; Kutzbach and Ziegler, 1993; Fluteau et al., 2001). During the end of the Permian and the beginning of the Early Triassic, simulated temperature gradients suggest warm waters in high latitudes (Kutzbach et al., 1990). Recent computer simulation by Hotinski et al. (2001; see Hotinski et al., 2002; Zhang et al., 2003 for a discussion) adopts this scenario, assuming a latitudinal

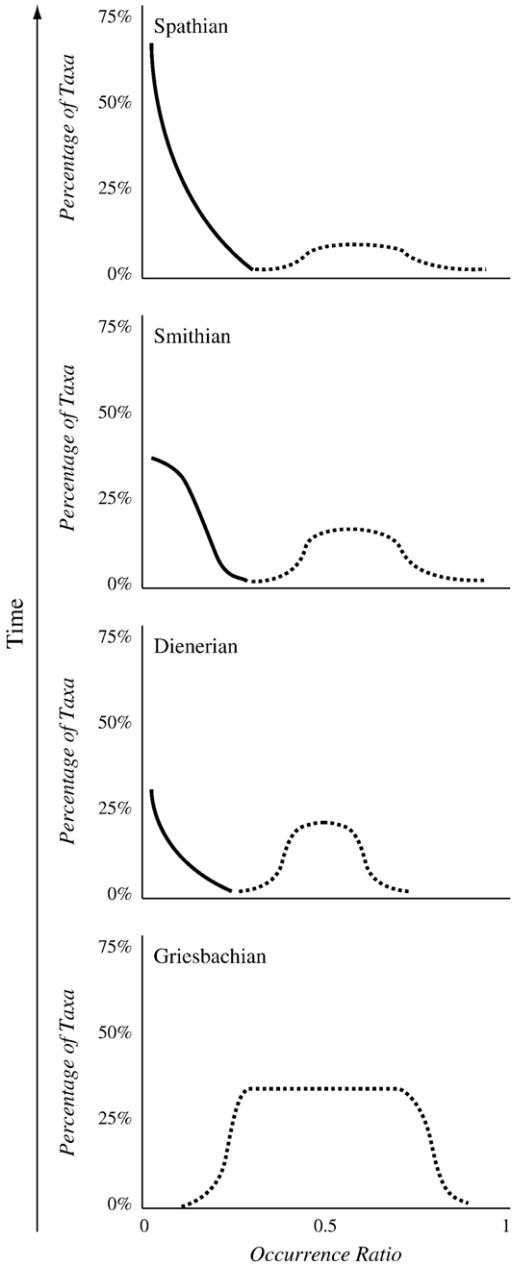

Fig. 8. Simplified generic ORP (Fig. 7) evidencing the Early Triassic trend toward increasing endemicity and decreasing cosmopolitanism. Based on the ORP shapes, genera are empirically divided in two groups: endemic (ER < ca. 1/4; continuous line) and cosmopolitan (OR > ca. 1/4; dotted line).

sea surface temperature (SST) gradient of only 16 °C (with polar temperature of 12 °C). Such a weak SST gradient may have slowed down the deep oceanic circulation and ultimately lead to anoxia which has been put forward as a possible cause of the Permo-Triassic mass extinction and the delayed recovery (e.g. Wignall and Hallam, 1992; Wignall and Twitchett, 1996, 2002; Isozaki, 1997; Kato et al., 2002; Twitchett et al., 2004). Recent hypothetical and simplified climatic scenario for the end-Permian and the beginning of the Early Triassic assumed a restricted oceanic-surface circulation and a weaker latitudinal temperature gradient (e.g. Kidder and Worsley, 2004).

The characteristically Equatorial symmetrical position of Pangea during the Late Permian also affects the Tethyan climatic conditions by creating a "megamonsoon" around the Tethys (e.g. simulations by Kutzbach and Gallimore, 1989; Parrish, 1995; Fluteau et al., 2001). In response, interior climates of Pangea should be drier with an increase of seasonal rainfalls along the circum-Tethyan coasts. However, the only Early Triassic climatic simulation available to date (Péron et al., 2005) indicates the disappearance of the "megamonsoon" possibly due to the northward drift of Gondwana.

Some paleontological and geological data support the simulation results, for instance:

- ice caps are absent from the very end-Permian, indicating that the latitudinal temperature gradient is less steep than the present-day one;
- some Spitsbergen rocks indicate that some warm-water algae migrated from low to high-latitudes by the Early Triassic (Wignall et al., 1998);
- the demise of biogenic cherts during the Late Permian indicates that Pangean coasts were bathed by cold currents before the mass extinction but not during the recovery interval, suggesting a complete or partial stop of the thermo-haline oceanic circulation during this period (Beauchamp and Baud, 2002);
- the Early Triassic biomes are also less distinct, with warm temperate floras extending to high latitudes (Rees, 2002). Temperate biomes migrate poleward during the Permo-Triassic boundary indicating a global warming trend (Ziegler et al., 1993). Coal forming plants are replaced by plants adapted to drier conditions (Rees, 2002);
- the loss of the Late Permian provinciality and the cosmopolitan distribution of many species in the marine realm are the predominant trait and also suggests a high warming trend during the earliest Triassic (Kummel, 1973b; Bambach, 1990).

All cited paleontological data and the unique Early Triassic computer simulation (Péron et al., 2005) lead to the general statement that the latitudinal temperature gradient was probably weak during the earliest Triassic, as a result of a global warming. The end-Permian mass extinction recovery is generally considered to have lasted until

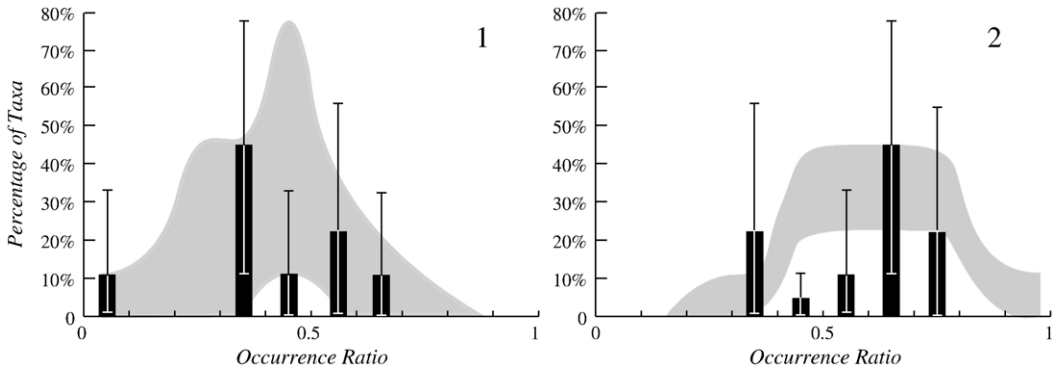

Fig. 9. Generic Occurrence Ratio Profiles for end-Smithian ammonoids (see Fig. 7 for legend). 1) ORP computed from observed genera only, 2) ORP computed from observed and interpolated genera. These ORP illustrate a short faunal event which markedly affected the biogeographical structuring of ammonoids by strongly decreasing the global level of endemicity (compare with Fig. 7C). Comparisons with the associated latitudinal gradient pattern (Fig. 5D) suggest that this event is of climatic origin (see text for details).

the end-Spathian or the Early Anisian, but ammonoid diversity recovered much earlier than many other marine clades. How does this differential recovery relate or reflect climatic changes during the Early Triassic?

5.2. Modes of life, distribution and dispersion

Many of the present-day marine organisms such as bivalves, brachiopods or gastropods possess at least one

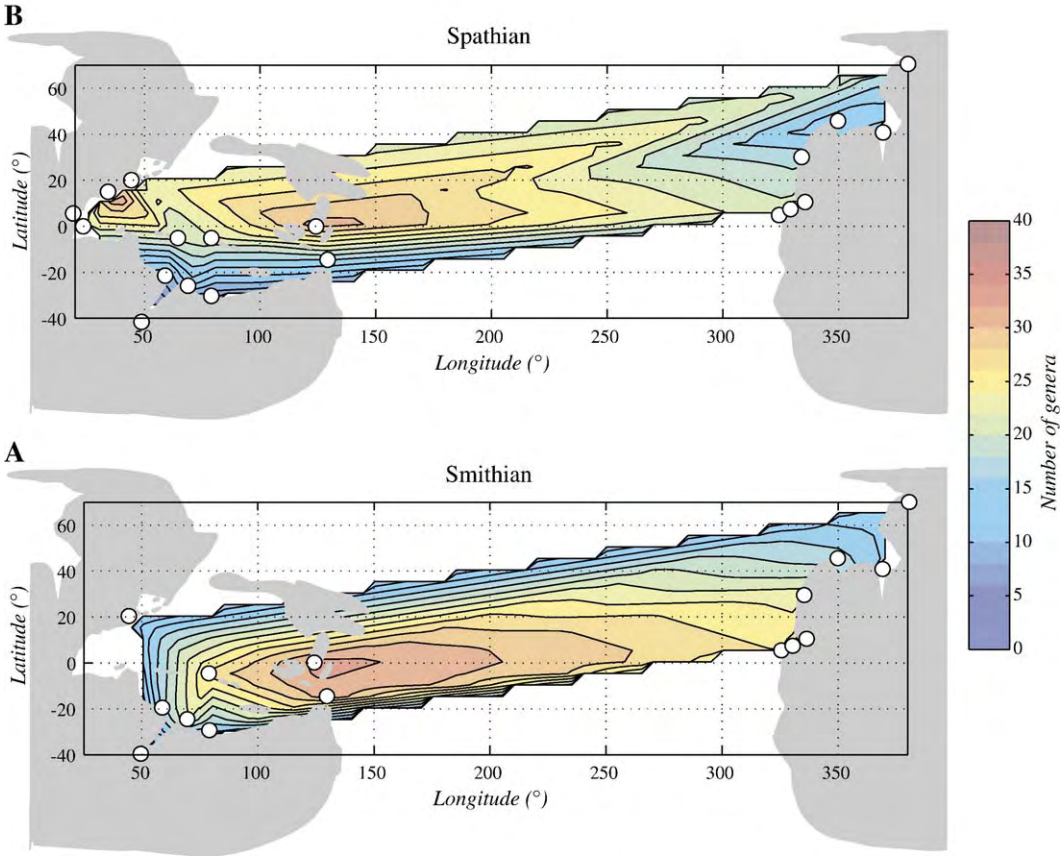

Fig. 10. Preliminary diversity contours for the A) Smithian, B) Spathian. Interpolation was realized using the software Isopaq© (Monnet et al., 2003a) and the Delaunay Triangulation method.

juvenile planktonic stage allowing their passive dispersal by ocean currents along coastlines of continents and across ocean basins (e.g. Scheltema, 1968, 1979, 1986). The exact mode of dispersal of ammonoids is unknown but the comparison with present-day coleoids (the best candidate as an ammonoid sister group; Boletzky, 2004) strongly suggests that they had also a juvenile planktonic phase (e.g. Tozer, 1982; Tanabe et al., 1993). An active long-distance migration of the adult form has to be brushed aside due to their morphology (e.g. Jacobs, 1992; Jacobs and Chamberlain, 1996), and because broad and deep oceanic basins such as the Panthalassa may have represented severe biogeographical barriers. A second possibility is the dispersal by rafting. Without evidence supporting that juveniles or egg capsules of ammonoids were able to attach to floating objects, this mode of transport can only be considered as minor.

Furthermore, the Spathian ammonoid latitudinal diversity gradient evidenced in this work (Fig. 5E) presents an asymmetrically bimodal shape centred on the thermal Equator. Such gradient closely mimics the present-day bimodal latitudinal gradients of taxonomic richness as observed for organisms possessing at least one planktonic stage (see Section 5.3.2.). This typical pattern reinforces the hypothesis of a juvenile planktonic phase for ammonoids as observed in many groups of their phylum (coleoids, bivalves). A passive dispersal mode during early growth stages appears to be a necessary explanation with respect to the observed distributions and very long distance crossing within paleolatitudinal belts. The ammonoid distributions observed during the Smithian and Spathian stages show that several genera are only encountered within narrow latitudinal bands. This point is well illustrated by *Aspenites*, *Lanceolites*, *Pseudaspidites*, *Hanielites* (Smithian), *Tirolites*, *Fengshanites*, *Hellenites*, *Columbites*, *Proptychoides* (Spathian) which are confined to the Equatorial belt. Such zonal distributions indicate that a wide ocean such as the Panthalassa is not an obstacle to ammonoid dispersion and strongly suggest that SST could be a preponderant controlling parameter, even when compared to sea-level fluctuations. Indeed, ammonoid distribution and dispersion are often considered to be linked to sea-level changes or the opening of oceanic corridors (e.g. Enay, 1980; Hallam, 1989; Hantzpergue, 1995; O'Dogherty et al., 2000), but the deterministic causal relationship between sea-level changes and diversity appear complex to determine (e.g. Macchioni and Cecca, 2002). Time intervals characterized by reduced epicontinental seas such as the Early Triassic are likely to favour temperature as the prime controlling factor as opposed to time intervals characterized by vast epicontinental seas and paleogeographical fragmentation (e.g. Cretaceous).

It is also worth noting that the Early Triassic Panthalassa was straddled with terranes (Tozer, 1982) which could also enhance the capacity of long-distance dispersal of ammonoids (the Panthalassa covered more than 20,000 km in width). Hence, even if a precise location of the centres of speciation and diversification is always difficult — if not impossible — to attest, the following biogeographical scenario emerges from available evidence on ammonoid diversity and distribution.

From the Dienerian on, the intensification of the SST gradient and winds surely increases possible North and South Equatorial currents (in comparison to the present-day Pacific Ocean configuration, see Pickard and Emery, 1990). In this case, every Panthalassic terrane can be considered as a stepping-island facilitating a westward dispersal of ammonoids. On the one hand, the West coasts of Pangea may act as a centre of dispersion in the direction of the Tethys across the Panthalassa, the Tethys being a receptacle of migration but also a cradle for new endemic genera (especially during the Spathian). On the other hand, the existence of a potential Equatorial Countercurrent (although deeper and involving a smaller water volume than the North and South Equatorial current) may also make it possible for some genera to migrate eastward across the Panthalassa, as already proposed by Newton (1988) in her theory of pantropic distribution.

5.3. Diversity patterns

5.3.1. Latitudinal gradient of diversity: the classical pattern

The latitudinal gradient of diversity is one of the most studied patterns of both past and present-day global biodiversity (e.g. Dobzhansky, 1950; Stehli et al., 1969; Currie and Paquin, 1987; Rosenzweig, 1995; Roy et al., 1998; Gaston, 2000; Rex et al., 2000; Cecca et al., 2005). It is known to occur in the majority of taxonomic groups and is manifested by a decreasing number of taxa (in most cases, species, genera or families) from low to high latitudes. The latitudinal diversity cline is usually described as unimodal with a taxonomic richness monotonically increasing from the Pole to the Equator, and centred near the Equator (e.g. Pianka, 1966; Gaston, 2000). Yet, a second pattern often interpreted as a particular derivative of the unimodal cline must be considered. It consists of a bimodal gradient of taxonomic richness with two maxima centred near the Tropics of Cancer and Capricorn and a drop of

taxonomic richness near the Equator (e.g. Rutherford et al., 1999; Kiessling, 2002; Shen and Shi, 2004; Worm et al., 2005; Dolan et al., 2006). This Equatorial low is frequently observed for extant and past marine organisms.

The ecological and evolutionary mechanisms explaining the spatial structure and temporal variability of latitudinal gradients of diversity are still contentious (see Rohde, 1992 for a review of the different classical factors). About thirty possible explanations have been proposed to explain the origin of the latitudinal gradients of diversity. Most of them imply empirically derived, direct or indirect relationships between taxonomic richness and climatic gradients and can be regrouped within the energy-hypothesis (Currie, 1991). The climate and especially the temperature are known to influence directly the dispersal and the distribution of species (see Brayard et al., 2004, 2005). Other explanations can involve evolutionary and dispersal rates (e.g. Pianka, 1966) or parameters such as predation or competition levels. Nevertheless, the majority of these last hypotheses cannot be used for the purpose of a general or unique explanation. Moreover, most of them contain various degrees of circularity or are not supported by sufficient evidence (Rohde, 1992).

5.3.2. Temporal variability of the latitudinal diversity gradient

Considering the stable and relatively simple Early Triassic paleogeography, SST is likely to have been the major first order parameter controlling the distribution of ammonoids. Based on this hypothesis, the absence of a latitudinal diversity gradient, the global low diversity, and the high cosmopolitanism observed during the Griesbachian (Figs. 5A, 6A, 7A) are compatible with a flat SST gradient, possibly implying a weak oceanic surface-circulation. At this time, dispersion of genera was certainly slow and ended into uniform distributions.

The first latitudinal differentiation occurred during the Dienerian (Fig. 5B), which correlatively suggests the onset of a contrasted SST gradient. This early phase ended with the beginning of the Smithian (*Hedenstroemia hedenstroemi* Zone of the Canadian Arctic and Siberia). This time interval is characterized by an impoverished and cosmopolitan fauna, suggesting a brief return to a poorly contrasted SST gradient. Increasing trend in latitudinal gradient of taxonomic richness quickly resumed during Mid-Smithian times (*Meekoceras gracilitatis* Zone of the Nevada and its approximate higher latitude correlative, the *Euflemingites romunderi* Zone) until it was again severely interrupted during the latest Smithian time (*A. tardus* Zone of the Canadian Arctic and Siberia and its low latitude correlative, the *A. pluriformis* Zone). The latest Smithian diversity dropdown was also accompanied by marked cosmopolitan distributions (e.g. *Xenoceltites*, prionitids), which again suggests a major and brief climatic event leading to an almost flat SST gradient (as modelled by Brayard et al., 2004, 2005). Extremely contrasted diversity gradients resumed shortly after the Smithian/Spathian boundary and persisted during the entire Spathian. The Smithian/Spathian boundary also corresponds to the biggest evolutionary turnover of ammonoids throughout the entire Early Triassic (see Fig. 2). Latitudinal biogeographical differentiation (Figs. 7D and 8D) and global diversity values (Fig. 5E) peaked during the Spathian. A global transgression at the beginning of this stage may also have contributed to the rise of the global diversity of ammonoids. However, whatever its amplitude, sea-level only cannot account for the observed pronounced latitudinal distributions. Again, the preponderant controlling parameter seems to have been a contrasted SST gradient.

The clearly bimodal Spathian gradient of latitudinal diversity differs from the classically recognized unimodal one (e.g. Stehli et al., 1969; Gaston, 2000), but closely mimics the extant or fossil gradients observed for foraminifers, radiolarians, brachiopods or predator fishes (e.g. Rutherford et al., 1999; Kiessling, 2002; Shen and Shi, 2004; Worm et al., 2005, respectively). In the literature, this type of diversity gradients is explained by many hypotheses: (i) possible mesothermal waters in low-latitudes; (ii) less habitable areas (Shen and Shi, 2004); (iii) Equatorial water mixing-assemblages; (iv) Equatorial current effect or (v) extreme Equatorial temperatures (Rutherford et al., 1999). Yet, another possible explanation to this drop of generic richness near the Equator is the influence of geometric constraints on the distribution of organisms (Colwell et al., 2004). These constraints act by combining a geographic mid-domain effect with a thermal mid-domain effect to engender the Equatorial drop of diversity (Brayard et al., 2005). The geographic mid-domain effect generates the first order increasing of taxonomic richness from high to low latitudes, and then the thermal mid-domain effect divides it in two hemispheric gradients peaking near the Tropics. This hypothesis applies very well to marine organisms, notably those possessing at least one planktonic stage, and illustrates the overall importance of SST on the differentiation and distribution of ammonoids. From this point of view, the intertropical drop of generic richness has nothing to do with differential extinction of tropical forms (e.g. due to a sudden cooling event) but is the

direct consequence of the geographic constraints imposed by the SST on living organisms.

The relative important amount of Early Spathian genera in the Boreal domain is an intriguing point. A relative isolation of the Boreal seas, promoting speciation of endemic taxa appears as a possible explanation.

5.3.3. Longitudinal gradient: what cause?

Although interrupted by several episodes of cosmopolitanism, the progressive emergence of a steep latitudinal gradient of generic richness is the first order biogeographical trend observed during the recovery of Early Triassic ammonoids. Yet, another interesting biogeographical pattern of Early Triassic ammonoids is the existence of a longitudinal gradient within the Tethys during Smithian times.

Contrary to the latitudinal diversity gradient which is linked to the SST gradient, a longitudinal diversity gradient cannot be directly explained by the SSTs because the solar energy supply does not vary significantly with longitudes. Present-day longitudinal gradients (e.g. best exemplified by corals) are generally explained by the eastward deepening of the mean SST and thermocline, with the added difficulty of larvae having to cross the Pacific without a sufficient number of stepping islands (Belasky, 1996).

Concerning the Early Triassic ammonoids, the existence of a longitudinal gradient seems to have been possible within the Tethys during the Smithian and to lesser degree during the Dienerian. The number of terranes within the Tethys was sufficient to allow the westward ammonoid dispersion. Nevertheless, a limiting factor may have been the absence or a sluggish surface circulation within the Tethys.

In some distant Tethyan sections (e.g. Spiti on the northern Gondwanian margin and Guangxi in the South China Block), an abrupt facies change is recorded at the Smithian/Spathian boundary. It is manifested by a drastic reduction of the clastic input (dryer conditions) and the end of anoxic water–sediment interface (strengthening of the oceanic circulation and stronger ventilation; Galfetti et al., 2004). This paleoceanographic change is compatible with the rise of highly contrasted SST gradient as inferred from ammonoids. It is also congruent with a Spathian sea-level change, which may have led to additional opportunities for biogeographical partitioning and speciation of ammonoids. These marked changes in facies and biodiversity may have resulted from modifications of the Tethyan circulation. From the Spathian on, the Tethyan oceanic circulation may have intensified and true latitudinal temperature belts established. The end of anoxia around the Smithian/Spathian boundary on several Tethyan outer platforms (Galfetti et al., 2004) could be the sign of an intense SST gradient (strong oceanic circulation and ventilation) or an indication of the end of the relative isolation between Panthalassic and Tethyan water masses. However, this hypothesis is still difficult to verify and requires further investigations.

Another hypothesis explaining the longitudinal gradient in the Tethys can also be derived from a geometric mid-domain effect generated by the global narrow triangular shape of the Tethyan encroachment (Colwell et al., 2004; Brayard et al., 2004). Yet, this hypothesis does not explain why all ammonoid genera do not latitudinally colonize the western part of the Tethys and is somewhat in contradiction with the fact that endemic genera are confined to the easternmost part of the Tethys.

This last point could be the combined outcome of the lack of western Tethyan basins and a potential less efficient sampling in this part of the Tethys. Our present-day knowledge is not sufficient to completely rule out this hypothesis.

5.3.4. Evolution of the generic occurrence ratio profile

Another, complementary way to look at the evolution of the biogeographical structuring of the Early Triassic ammonoid faunas relies on the computation and statistical analysis of Occurrence Ratio Profiles as proxies for the structure and dynamic of the global taxonomic endemicity level through Early Triassic times (Figs. 7 and 8). Distinct situations characterize each stage and evidence a global trend starting from a cosmopolitan configuration (Griesbachian) to a marked endemic configuration (Spathian). When compared to the ORP null distributions under a lottery model of random "niche" colonization (permutation model 3 in Legendre et al., 1997; see Section 3.2.), this trend appears to be the consequence of an increasingly heterogeneous biogeographical structuring of faunas. In practice, this evolution is expressed by a significantly higher than predicted percentage of very sparsely distributed (OR < ca. 0.1) as well as highly widespread (OR > ca. 0.5) genera, compensated by a significantly lower than predicted percentage of "intermediate" genera (OR between ca. 0.1 and 0.5). Hence, based on the selected null model, the biogeographical global configuration appears to be initially random (neither under nor over-"distributed") and then more and more non-random throughout the Early Triassic. Such biogeographical maturing is fully coherent with respect to the emergence and increasing steepness of the latitudinal SST gradient as suggested by the latitudinal

diversity gradient (Fig. 5) and by the interpolated generic richness maps (Fig. 10). Moreover, when latitudinal diversity gradient flattened again during the latest Smithian, the biogeographical distribution of genera becomes random again, as evidenced by the ORP (Fig. 9).

5.4. Phases of recovery

Cosmopolitan faunas at the beginning of the Griesbachian are likely to correspond to a short survival interval sensu Kauffman and Erwin (1995) with generalist and opportunistic genera. For ammonoids, this phase seems extremely reduced and ends before the Dienerian. The Dienerian stage marks the real start of the recovery interval with several new genera branching off from the *Ophiceras* stock. The Early Triassic radiation of ammonoids was largely shaped by the evolution of the SST gradient and its fluctuations. The ammonoid recovery was completed in the middle Spathian.

The formation of a pronounced latitudinal diversity gradient from the Smithian on also indicates that the rates of recovery were probably not homogeneous in time and space (contra McGowan, 2005). The latest radiometric ages obtained from South China indicate a total duration of the Early Triassic ca. 5 myr and a possible duration of the Spathian of ca. 3 myr, i.e. more than half the entire Early Triassic (Ovtcharova et al., 2006). Thus, the four Early Triassic stages are of extremely uneven duration, making the two fold subdivision of the Early Triassic even more inadequate. Hence, we believe that Early Triassic paleobiogeographical studies should preferably be based on the four stage subdivision which provides better time constraints. This new calibration also clearly illustrates the very high tempo of the ammonoid recovery during the Griesbachian, Dienerian and Smithian.

5.5. Climatic significance

The current understanding of the extremely warm climates of the Early Triassic (e.g. Hotinski et al., 2001; Kidder and Worsley, 2004) should be refined and adjusted in the light of the ammonoid paleobiogeography. They are apparently the first marine invertebrates to fully recover. They clearly indicate rapid changes in their distributions and diversity patterns which are highly suggestive of climatic modifications. These sudden faunal biogeographical changes are more easily explained in terms of climatic changes than eustatic changes alone.

As in the simple model of Kidder and Worsley (2004), the Griesbachian appears as a stage of extreme warm and uniform climate. The same model for the Dienerian/Smithian suggests a more intense but always warm climatic gradient. For these stages, ammonoids also indicate an intensification of the SST gradient but with brief reversed phases during the earliest and the latest Smithian. The Griesbachian hothouse climate and the weakly pronounced Dienerian SST gradient may have led to a weak oceanic circulation and a prolonged Early Triassic anoxia (e.g. Wignall and Twitchett, 1996, 2002). So, if the duration of anoxic bottom waters on the platforms may have influenced the timing of recovery of benthic organisms (e.g. Fraiser and Bottjer, 2005), it did not influence that of epipelagic organisms such as ammonoids. However, the edification of a clear bimodal latitudinal diversity gradient for Spathian ammonoids and the end of anoxia on outer platforms are both compatible with a steeper SST gradient. A new normal oceanic circulation was able to re-oxygenate oceanic waters during the Spathian.

6. Conclusions

The recovery in time and space of Early Triassic ammonoids was largely shaped by the latitudinal SST gradient and its short-term fluctuations. Previous suggested correlations between diversity and sea-level (e.g. Hallam and Wignall, 1999) or anoxia (e.g. Wignall and Hallam, 1992) should be considered more as indirect causes or supplementary mechanisms. Other causal relationships proposed between the Permian–Triassic mass extinction and trap volcanism (e.g. Bowring et al., 1998; Reichow et al., 2002; Mundil et al., 2004) or hydrate gas release (e.g. Morante, 1996; de Wit et al., 2002; Dickens, 2003) have to be seriously taken into account due to their multiple feedbacks on climates and especially in the cause of long-trend warming.

In this context, we show that the global recovery of Early Triassic ammonoids proceeded together with the emergence of a latitudinal gradient of generic richness. This first order global increasing trend in ammonoid diversity was interrupted by two short-term events characterized by diversity downs combined with cosmopolitan distributions. The most dramatic of these events occurred at the very end of the Smithian and ended with a major evolutionary turnover at the Smithian/Spathian boundary. This sequence of global biogeographical patterns strongly suggest that an increase of the steepness of the SST gradient is the general climatic trend for the Early Triassic (Fig. 11)

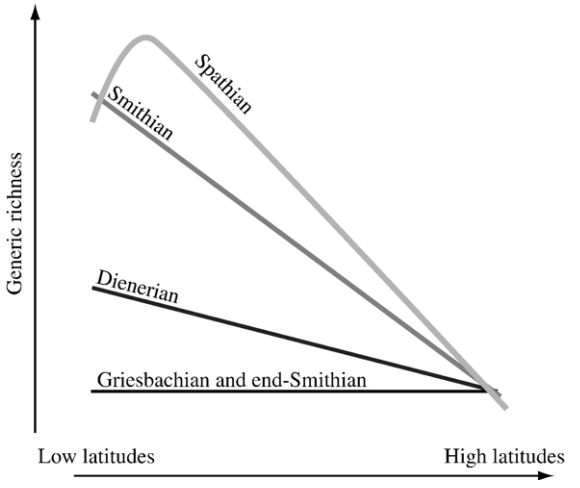

Fig. 11. Schematic evolution of the latitudinal gradient of ammonoid generic richness corresponding to the variations of the SST gradient during the Early Triassic.

with brief interruptions characterized by weak SST gradient (or more uniform climate) as suggested by short-lived and low-diversity cosmopolitan faunas.

Moreover, patterns of generic distributions seem to have been influenced by oceanic currents, especially within the Tropics where the ammonoid dispersal across the Panthalassa is clearly observed.

From another point of view, this study underlines the remarkable ability of ammonoids to recover very quickly from the Permo-Triassic mass extinction. Indeed, global diversity levels equal to or greater than pre-crisis ones were reached ca. 3 to 4 myr after the Permo-Triassic crisis, which involve extremely high origination rates at all infra-ordinal levels. Such unusual reactivity strongly calls for further paleoecological investigations, especially with regard to the nature of Early Triassic oceanic primary producers that enabled the precocious evolutionary rebound of the ammonoids. It also highlights that ammonoids were comparatively less affected by anoxic conditions on outer platforms (see Monnet et al., 2003b for the Cenomanian–Turonian anoxic event) than most other marine invertebrates.

Acknowledgements

This work was supported by the Swiss NSF project 2100-068061.02 (A.B and H.B) and a Rhône-Alpes-Eurodoc grant (A.B). G. Stringer kindly improved the English spelling. B.S. Lieberman provided insightful remarks and constructive critics which helped us to improve the manuscript.

Appendix A. Supplementary data

Supplementary data associated with this article can be found, in the online version, at doi:10.1016/j.palaeo.2006.02.003.

References

Adams, C.J., Barley, M.E., Maas, R., Doyle, M.G., 2002. Provenance of Permian–Triassic volcaniclastic sedimentary terranes in New Zealand: evidence from their radiogenic isotope characteristics and detrital mineral age patterns. New Zealand Journal of Geology and Geophysics 45, 221–242.

Allison, P.A., Briggs, D.E.G., 1993. Paleolatitudinal sampling bias, Phanerozoic species diversity, and the end-Permian extinction. Geology 21, 65–68.

Arita, H.T., Rodríguez, P., 2004. Local–regional relationships and the geographical distribution of species. Global Ecology and Biogeography 13, 15–21.

Bambach, R.K., 1990. Late Paleozoic provinciality in the marine realm. In: McKerrow, W.S., Scotese, C.R. (Eds.), Palaeozoic Palaeogeography and Biogeography. Geological Society Memoir, vol. 12, pp. 307–323.

Beauchamp, B., Baud, A., 2002. Growth and demise of Permian biogenic chert along northwest Pangea: evidence for end-Permian collapse of thermohaline circulation. Palaeogeography, Palaeoclimatology, Palaeoecology 184, 37–63.

Belasky, P., 1996. Biogeography of Indo-Pacific larger foraminifera and scleractinian corals: a probabilistic approach to estimating taxonomic diversity, faunal similarity, and sampling bias. Palaeogeography, Palaeoclimatology, Palaeoecology 122, 119–141.

Belasky, P., Runnegar, B., 1994. Permian longitudes of Wrangellia, Stikinia, and Eastern Klamath terranes based on coral biogeography. Geology 22, 1095–1098.

Belasky, P., Stevens, C.H., Hanger, R.A., 2002. Early Permian location of western North American terranes based on brachiopod, fusulinid, and coral biogeography. Palaeogeography, Palaeoclimatology, Palaeoecology 179, 245–266.

Besse, J., Torcq, F., Gallet, Y., Ricou, L.E., Krystyn, L., Saidi, A., 1998. Late Permian to Late Triassic palaeomagnetic data from Iran: constraints on the migration of the Iranian block through the Tethyan Ocean and initial destruction of Pangaea. Geophysical Journal International 135, 77–92.

Boletzky, S.v., 2004. "Nude ammonoids": a challenge to cephalopod phylogeny. Geobios 37, 117–118.

Bowring, S.A., Erwin, D.H., Jin, Y.G., Martin, M.W., Davidek, K., Wang, W., 1998. U/Pb zircon geochronology and tempo of the end-Permian mass extinction. Science 280, 1039–1045.

Brayard, A., Héran, M.-A., Costeur, L., Escarguel, G., 2004. Triassic and Cenozoic palaeobiogeography: two case studies in quantitative modelling using IDL. Palaeontologia Electronica 7. 22 pp.

Brayard, A., Escarguel, G., Bucher, H., 2005. Latitudinal gradient of taxonomic richness: combined outcome of temperature and geographic mid-domains effects? Journal of Zoological Systematics and Evolutionary Research 43, 178–188.

Brown, J.H., 1995. Macroecology. University of Chicago Press, Chicago.

Bucher, H., 1989. Lower Anisian ammonoids from the northern Humboldt Range (northwestern Nevada, USA) and their bearing upon the Lower–Middle Triassic boundary. Eclogae Geologicae Helvetiae 82, 945–1002.

Cecca, F., Vrielynck, B., Lavoyer, T., Gaget, H., 2005. Changes in the ammonite taxonomical diversity gradient during the Late Jurassic–Early Cretaceous. Journal of Biogeography 32, 535–547.

Colwell, R.K., Rahbek, C., Gotelli, N.J., 2004. The mid-domain effect and species richness patterns: what have we learned so far? The American Naturalist 163, E1–E23.

Crowley, T.J., Mengel, J.G., Short, D.A., 1987. Gondwanaland's seasonal cycle. Nature 329, 803–807.

Crowley, T.J., Hyde, W.T., Short, D.A., 1989. Seasonal cycle variations on the supercontinent of Pangaea. Geology 17, 457–460.

Currie, D., 1991. Energy and large-scale patterns of animal- and plant-species richness. American Naturalist 137, 27–49.

Currie, D., Paquin, V., 1987. Large-scale biogeographical patterns of species richness of trees. Nature 329, 326–327.

Dagys, A., 1988. Major features of the geographic differentiation of Triassic ammonoids. In: Wiedmann, J., Kullmann, J. (Eds.), Cephalopods — Present and Past. Schweizerbart'sche Verlagsbuchhandlung, Stuttgart, pp. 341–349.

Dagys, A., 1997. A new Late Olenekian (Triassic) ammonoid of low paleolatitude affinity from Arctic Asia (Eastern Taimyr). Paläontologische Zeitschrift 71, 217–220.

de Wit, M.J., Ghosh, J.G., De Villiers, S., Rakotosolofo, N., Alexander, J., Tripathi, A., Looy, C.V., 2002. Multiple organic carbon isotope reversals across the Permo-Triassic boundary of terrestrial Gondwana sequences: clues to extinction patterns and delayed ecosystem recovery. The Journal of Geology 110, 227–240.

Dickens, G.R., 2003. Rethinking the global carbon cycle with a large, dynamic and microbially mediated gas hydrate capacitor. Earth and Planetary Science Letters 213, 169–183.

Dobzhansky, T., 1950. Evolution in the tropics. American Scientist 38, 209–221.

Dolan, J.R., Lemée, R., Gasparini, S., Mousseau, L., Heyndrickx, C., 2006. Probing diversity in the plankton: using patterns in Tintinnids (planktonic marine ciliates) to identify mechanisms. Hydrobiologia 555, 143–157.

Elmi, S., Babin, C., 1996. Histoire de la Terre. Masson, Paris.

Enay, R., 1980. Paléobiogéographie et Ammonites jurassiques: "rythmes fauniques" et variations du niveau marin; voies d'échanges, migrations et domaines biogéographiques. Mémoire Hors-Série - Société Géologique de France 10, 261–281.

Erwin, D.H., 1990. End-Permian. In: Briggs, D.E.G., Crowther, P.R. (Eds.), Palaeobiology: A Synthesis. Blackwell Science, Oxford, pp. 187–193.

Erwin, D.H., 1994. The Permo-Triassic extinction. Nature 367, 231–235.

Erwin, D.H., 1998. The end and the beginning: recoveries from mass extinctions. Trends in Ecology and Evolution 13, 344–349.

Fluteau, F., Besse, J., Broutin, J., Ramstein, G., 2001. The Late Permian climate. What can be inferred from climate modelling concerning Pangea scenarios and Hercynian range altitude? Palaeogeography, Palaeoclimatology, Palaeoecology 167, 39–71.

Fraiser, M.L., Bottjer, D.J., 2004. The non-actualistic Early Triassic gastropod fauna: a case study of the Lower Triassic Sinbad limestone member. Palaios 19, 259–275.

Fraiser, M.L., Bottjer, D.J., 2005. Restructuring of benthic level-bottom shallow marine communities due to prolonged environmental stress during the aftermath of the end-Permian mass extinction. C. R. Palevol 4, 583–591.

Fraiser, M.L., Twitchett, R.J., Bottjer, D.J., 2005. Unique microgastropod biofacies in the Early Triassic: indicator of long-term biotic stress and the pattern of biotic recovery after the end-Permian mass extinction. C. R. Palevol 4, 543–552.

Galfetti, T., Bucher, H., Brayard, A., Weissert, H., Guex, J., Atudorei, V., Hochuli, P., 2004. Early Triassic sedimentary evolution, carbonate carbon isotope changes and ammonoid recovery: records from southern China block and the northern Indian margin. 2nd Swiss Geoscience Meeting. Lausanne, Switzerland.

Gaston, K.J., 2000. Global patterns in biodiversity. Nature 405, 220–227.

Gaston, K.J., Blackburn, T.M., 2000. Pattern and Process in Macroecology. Blackwell Science, Oxford.

Gibbs, M.T., Rees, P.M., Kutzbach, J.E., Ziegler, A.M., Behling, P.J., Rowley, D.B., 2002. Simulations of Permian climate and comparisons with climate-sensitive sediments. The Journal of Geology 110, 33–55.

Guex, J., 1978. Le Trias inférieur des Salt Ranges (Pakistan): problémes biochronologiques. Eclogae Geologicae Helvetiae 71, 105–141.

Hallam, A., 1989. The case for sea-level change as a dominant causal factor in mass extinction of marine invertebrates. Philosophical Transactions of the Royal Society of London 325, 437–455.

Hallam, A., 1996. Major bio-events in the Triassic and Jurassic. In: Walliser, O.H. (Ed.), Global Events and Event Stratigraphy in the Phanerozoic: Results of the International Interdisciplinary Cooperation in the IGCP-Project 216 "Global Biological Events in Earth History". Springer-Verlag, Berlin, pp. 265–283.

Hallam, A., Wignall, P.B., 1999. Mass extinctions and sea-level changes. Earth Science Reviews 48, 217–250.

Hantzpergue, P., 1995. Faunal trends and sea-level changes: biogeographic patterns of kimmeridgian ammonites on the western European shelf. Geologische Rundschau 84, 245–254.

Hillebrand, H., Blenckner, T., 2002. Regional and local impact on species diversity — from pattern to processes. Oecologia 132, 479–491.

Hori, R.S., Campbell, H.J., Grant-Mackie, J.A., 2003. Triassic radiolaria from Kaka Point structural belt, Otago, New Zealand. Journal of the Royal Society of New Zealand 33, 39–55.

Hotinski, R.M., Bice, K.L., Kump, L.R., Najiar, R.G., Arthur, M.A., 2001. Ocean stagnation and end-Permian anoxia. Geology 29, 7–10.

Hotinski, R.M., Kump, L.R., Bice, K.L., 2002. Comment on "Could the Late Permian deep ocean have been anoxic?" by R. Zhang et al. Paleoceanography 17, 1052.

Isozaki, Y., 1997. Permo-Triassic boundary superanoxia and stratified superocean: records from the lost deep sea. Science 276, 235–238.

Jacobs, D.K., 1992. Shape, drag, and power in ammonoid swimming. Paleobiology 18, 203–220.

Jacobs, D.K., Chamberlain Jr., J.A., 1996. Buoyancy and hydrodynamics in ammonoids. In: Landman, N., Tanabe, K., Davis, R.A. (Eds.), Ammonoid Paleobiology. Topics in Geobiology. Plenum Press, New York, pp. 169–224.

Kato, Y., Nakao, K., Isozaki, Y., 2002. Geochemistry of Late Permian to Early Triassic pelagic cherts from southwest Japan: implications for an oceanic redox change. Chemical Geology 182, 15–34.

Kauffman, E.G., Erwin, D.H., 1995. Surviving mass extinctions. Geotimes 40, 14–17.

Kazmin, V.G., 1991. Collision and rifting in the Tethys Ocean: geodynamic implications. Tectonophysics 196, 371–384.

Kennedy, W.J., 1977. Ammonite evolution. In: Hallam, A. (Ed.), Patterns of Evolution as Illustrated by the Fossil Record. Developments in Paleontology and Stratigraphy. Elsevier, Amsterdam, pp. 251–304.

Kidder, D.L., Worsley, T.R., 2004. Causes and consequences of extreme Permo-Triassic warming to globally equable climate and relation to Permo-Triassic extinction and recovery. Palaeogeography, Palaeoclimatology, Palaeoecology 203, 207–237.

Kiessling, W., 2002. Radiolarian diversity patterns in the latest Jurassic–earliest Cretaceous. Palaeogeography, Palaeoclimatology, Palaeoecology 187, 179–206.

Kiparisova, L.D., Popov, Y.D., 1956. Subdivision of the lower series of the Triassic System into stages. Transactions of the Academy of Sciences of the USSR. Nauka 109, 842–845 (in Russian).

Kojima, S., 1989. Mesozoic terrane accretion in northeast China, Sikhote–Alin and Japan regions. Palaeogeography, Palaeoclimatology, Palaeoecology 69, 213–232.

Kozur, H.W., 2003. Integrated ammonoid, conodont, radiolarian zonation of the Triassic and some remarks to stage/substage subdivision and the numeric age of the Triassic stages. Albertiana 28, 57–74.

Krystyn, L., Richoz, S., Baud, A., Twitchett, R.J., 2003. A unique Permian–Triassic boundary section from the Neotethyan Hawasina basin, central Oman mountains. Palaeogeography, Palaeoclimatology, Palaeoecology 191, 329–344.

Kummel, B., 1957. Paleoecology of Lower Triassic formations of southeastern Idaho and adjacent areas. Geological Society of America, Memoir 67, 437–468.

Kummel, B., 1973a. Aspects of the Lower Triassic (Scythian) stage. In: Logan, A., Hills, L.V. (Eds.), The Permian and the Triassic Systems and their Mutual Boundary. Canadian Society of Petroleum Geologists, Calgary, pp. 557–571.

Kummel, B., 1973b. Lower Triassic (Scythian) molluscs. In: Hallam, A. (Ed.), Atlas of Paleobiogeography. Elsevier, Amsterdam, pp. 225–233.

Kutzbach, J.E., Gallimore, R.G., 1989. Pangaean climates: megamansoons of the megacontinent. Journal of Geophysical Research 94, 3341–3357.

Kutzbach, J.E., Ziegler, A.M., 1993. Simulation of Late Permian climate and biomes with an atmosphere–ocean model: comparisons with observations. Philosophical Transactions of the Royal Society of London. Series B, Biological Sciences 341, 327–340.

Kutzbach, J.E., Guetter, P.J., Washington, W.M., 1990. Simulated circulation of an idealized ocean for Pangaean time. Paleoceanography 5, 299–317.

Legendre, P., Galzin, R., Harmelin-Vivien, M.L., 1997. Relating behavior to habitat: solutions to the fourth-corner problem. Ecology 78, 547–562.

Leibold, M.A., Holyoak, M., Mouquet, N., Amarasekare, P., Chase, J.M., Hoopes, M.F., Holt, R.D., Shurin, J.B., Law, R., Tilman, D., Loreau, M., Gonzalez, A., 2004. The metacommunity concept: a framework for multi-scale community ecology. Ecology Letters 7, 601–613.

Lieberman, B.S., 2000. Paleobiogeography: Using Fossils to Study Global Change, Plate Tectonics, and Evolution. Plenum Press/Kluwer Academic Publishers, New York.

Macchioni, F., Cecca, F., 2002. Biodiversity and biogeography of Middle–Late Liassic ammonoids: implications for the Early Toarcian mass extinction. Geobios. Memoire Special 24, 165–175.

McGowan, A.J., 2005. Ammonoid recovery from the Late Permian mass extinction. C. R. Palevol 4, 517–530.

Monnet, C., Bouchet, S., Thiry-Bastien, P., 2003a. ISOPAQ, a MATLAB program for stratigraphic and isopach mapping: example application to the French Bajocian (Jurassic) sediments. Computers & Geosciences 29, 1101–1110.

Monnet, C., Bucher, H., Escarguel, G., Guex, J., 2003b. Cenomanian (early Late Cretaceous) ammonoid faunas of western Europe: Part II. Diversity patterns and the end-Cenomanian anoxic event. Eclogae Geologicae Helveticae 96, 381–398.

Morante, R., 1996. Permian and Early Triassic isotopic records of carbon and strontium in Australia and a scenario of events about the Permian–Triassic boundary. Historical Biology 11, 289–310.

Mundil, R., Ludwig, K.R., Metcalfe, I., Renne, P.R., 2004. Age and timing of the Permian mass extinctions: U/Pb dating of closed-systems zircons. Science 305, 1760–1763.

Newton, C.R., 1988. Significance of "Tethyan" fossils in the American Cordillera. Science 242, 385–391.

Nichols, K.M., Silberling, N.J., 1979. Early Triassic (Smithian) ammonites of Paleoequatorial affinity from the Chulitna terrane, south-central Alaska. Geological Survey Professional Paper 1121-B, B1–B5.

Nie, S., Rowley, D.B., Ziegler, A.M., 1990. Constraints on the locations of Asian microcontinents in Palaeo–Tethys during the Late Palaeozoic. In: McKerrow, W.S., Scotese, C.R. (Eds.), Palaeozoic Palaeogeography and Biogeography. Geological Society Memoir, London, pp. 397–409.

O'Dogherty, L., Sandoval, J., Vera, J.A., 2000. Ammonite faunal turnover tracing sea-level changes during the Jurassic (Betic Cordillera, southern Spain). Journal of the Geological Society (London) 157, 723–736.

Ovtcharova, M., Bucher, H., Schaltegger, U., Galfetti, T., Brayard, A., Guex, J., 2006. New Early to Middle Triassic U–Pb ages from South China: calibration with ammonoid biochronozones and implications for the timing of the Triassic biotic recovery. Earth and Planetary Science Letters 243, 463–475.

Parrish, J.T., 1995. Geologic evidence of Permian climate. In: Scholle, P.A., Peryt, T.M., Ulmer-Scholle, D.S. (Eds.), The Permian of Northern Pangea. Springer–Verlag, Berlin, pp. 53–61.

Péron, S., Bourquin, S., Fluteau, F., Guillocheau, F., 2005. Paleoenvironment reconstructions and climate simulations of the Early Triassic: impact of the water and sediment supply on the preservation of fluvial systems. Geodinamica Acta 18, 431–446.

Pianka, E.R., 1966. Latitudinal gradients in species diversity: a review of concepts. American Naturalist 100, 33–46.

Pickard, G.L., Emery, W.J., 1990. Descriptive Physical Oceanography: An Introduction. Pergamon Press, Oxford.

Racki, G., 1999. Silica-secreting biota and mass extinctions: survival patterns and processes. Palaeogeography, Palaeoclimatology, Palaeoecology 154, 107–132.

Raup, D.M., 1979. Size of the Permo-Triassic bottleneck and its evolutionary implications. Science 206, 217–218.

Rees, P.M., 2002. Land-plant diversity and the end-Permian mass extinction. Geology 30, 827–830.

Rees, P.M., Ziegler, A.M., Gibbs, M.T., Kutzbach, J.E., Behling, P.J., Rowley, D.B., 2002. Permian phytogeographic patterns and climate data/model comparisons. The Journal of Geology 110, 1–31.

Reichow, M.K., Saunders, A.D., White, R.V., Pringle, M.S., Al'Mukhamedov, A.I., Medvedev, A.I., Kirda, N.P., 2002. $^{40}Ar/^{39}Ar$ dates from the West Siberian basin: Siberian flood basalt province doubled. Science 296, 1846–1849.

Rex, M.A., Stuart, C.T., Coyne, G., 2000. Latitudinal gradients of species richness in the deep-sea benthos of the North Atlantic. Proceedings of the National Academy of Sciences of USA 97, pp. 4082–4085.

Ricklefs, R.E., 1987. Community diversity: relative roles of local and regional processes. Science 235, 167–171.

Ricklefs, R.E., 2004. A comprehensive framework for global patterns in biodiversity. Ecology Letters 7, 1–15.

Ricou, L.E., 1994. Tethys reconstructed: plates, continental fragments and their boundaries since 260 Ma from Central America to Southeastern Asia. Geodinamica Acta 7, 169–218.

Rode, A., Lieberman, B.S., 2004. Using GIS to study the biogeography of the Late Devonian biodiversity crisis. Palaeogeography, Palaeoclimatology, Palaeoecology 211, 345–359.

Rohde, K., 1992. Latitudinal gradients in species diversity: the search for the primary cause. Oikos 65, 514–527.

Rosenzweig, M.L., 1995. Species Diversity in Space and Time. Cambridge University Press, Cambridge.

Roy, K., Jablonski, D., Valentine, J.W., Rosenberg, G., 1998. Marine latitudinal diversity gradients: tests of causal hypotheses. Proceedings of the National Academy of Sciences of USA 95, pp. 3699–3702.

Rutherford, S., D'Hondt, S., Prell, W., 1999. Environmental controls on the geographic distribution of zooplankton diversity. Nature 400, 749–753.

Scheltema, R.S., 1968. Dispersal of larvae by Equatorial ocean currents and its importance to the zoogeography of shoal-water tropical species. Nature 217, 1159–1162.

Scheltema, R.S., 1979. Dispersal of pelagic larvae and the zoogeography of Tertiary marine benthic gastropods. In: Gray, J., Boucot, A.J. (Eds.), Historical Biogeography, Plate Tectonics, and the Changing Environment. Oregon State University Press, Corvallis, pp. 391–397.

Scheltema, R.S., 1986. On dispersal and planktonic larvae of benthic invertebrates: an eclectic overview and summary of problems. Bulletin of Marine Science 39, 290–322.

Shen, S.-Z., Shi, G.R., 2004. Capitanian (Late Guadalupian, Permian) global brachiopod palaeobiogeography and latitudinal diversity pattern. Palaeogeography, Palaeoclimatology, Palaeoecology 208, 235–262.

Smethurst, M.A., Khramov, A.N., Torsvisk, T.H., 1998. The Neoproterozoic and Paleozoic palaeomagnetic data for the Siberian Plateform: from Rodinia to Pangea. Earth-Science Reviews 43, 1–24.

Stampfli, G., Borel, G.D., 2002. A plate tectonic model for the Paleozoic and Mesozoic constrained by dynamic plate boundaries and restored synthetic oceanic isochrons. Earth and Planetary Science Letters 196, 17–33.

Stanley, G.D.J., 2003. The evolution of modern corals and their early history. Earth-Science Reviews 60, 195–225.

Stehli, F.G., Douglas, R.G., Newell, N.D., 1969. Generation and maintenance of gradients in taxonomic diversity. Science 164, 947–949.

Tanabe, K., Landman, N.H., Mapes, R.H., Faulkner, C.J., 1993. Analysis of a carboniferous embryonic ammonoid assemblage — implications for ammonoid embryology. Lethaia 215–224.

Tong, J., Shi, G.R., 2000. Evolution of the Permian and Triassic foraminifera in south China. In: Yin, H., Dickins, J.M., Shi, G.R., Tong, J. (Eds.), Permian–Triassic Evolution of Tethys and Western Circum-pacific. Developements in Palaeontology and Stratigraphy. Elsevier, Amsterdam, pp. 291–307.

Tozer, E.T., 1967. A standard for Triassic time. Geologic Survey of Canada Bulletin 156, 1–141.

Tozer, E.T., 1973. The earliest marine Triassic rocks: their definition, ammonoid fauna, distribution and relationship to underlying formations. In: Logan, A., Hills, L.V. (Eds.), Permian and Triassic Systems and their Mutual Boundary. Canadian Society of Petroleum Geologists, Calgary, pp. 549–556.

Tozer, E.T., 1981a. Triassic ammonoidea: classification, evolution and relationship with Permian and Jurassic forms. In: House, M.R., Senior, J.R. (Eds.), The Ammonoidea. The Systematics Association, London, pp. 65–100.

Tozer, E.T., 1981b. Triassic ammonoidea: geographic and stratigraphic distribution. In: House, M.R., Senior, J.R. (Eds.), The Ammonoidea. The Systematics association, London, pp. 397–431.

Tozer, E.T., 1982. Marine Triassic faunas of North America: their significance for assessing plate and terrane movements. Geologische Rundschau 71, 1077–1104.

Tozer, E.T., 1994. Canadian Triassic ammonoid faunas. Geologic Survey of Canada Bulletin 467, 1–663.

Twitchett, R.J., Krystyn, L., Baud, A., Wheeley, J.R., Richoz, S., 2004. Rapid marine recovery after the end-Permian mass-extinction event in the absence of marine anoxia. Geology 32, 805–808.

Whittaker, R.H., 1977. Evolution of species diversity in land communities. In: Hecht, M.K., Steere, W.C., Wallace, B. (Eds.), Evolutionary Biology. Plenum Press, New York, pp. 1–67.

Wiedmann, J., 1973. Ammonoid (r)evolution at the Permian–Triassic boundary. In: Logan, A., Hills, L.V. (Eds.), The Permian and Triassic Systems and their Mutual Boundary. Canadian Society of Petroleum Geologists, Calgary, pp. 513–521.

Wignall, P.B., Hallam, A., 1992. Anoxia as a cause of the Permian/Triassic mass extinction: facies evidence from northern Italy and the western United States. Palaeogeography, Palaeoclimatology, Palaeoecology 93, 21–46.

Wignall, P.B., Twitchett, R.J., 1996. Oceanic anoxia and the end Permian mass extinction. Science 272, 1155–1158.

Wignall, P.B., Twitchett, R.J., 2002. Extent, duration, and nature of the Permian–Triassic superanoxic event. Geological Society of America Special Paper 356, 395–413.

Wignall, P.B., Morante, R., Newton, R., 1998. The Permo-Triassic transition in Spitsbergen: $\delta^{13}C_{org}$ chemostratigraphy, Fe and S geochemistry, facies, fauna and trace fossils. Geological Magazine 135, 47–62.

Worm, B., Sandow, M., Oschlies, A., Lotze, H.K., Myers, R.A., 2005. Global patterns of predator diversity in the open oceans. Science 309, 1365–1369.

Yao, A., Kuwahara, K., 2000. Permian and Triassic radiolarians from the southern Guizhou Province, China. Journal of Geosciences, Osaka City University 43, 1–19.

Zhang, R., Follows, M.J., Marshall, J., 2003. Reply to comment by Roberta M. Hotinsky, Lee R. Kump, and Karen L. Bice on "Could the Late Permian deep ocean have been anoxic?". Paleoceanography 18, 1095.

Ziegler, A.M., Parrish, J.M., Yao, J., Gyllenhaal, E.D., Rowley, D.B., Parrish, J.T., Nie, S., Bekker, A., Hulver, M.L., 1993. Early Mesozoic phytogeography and climate. Philosophical Transactions of the Royal Society of London. Series B, Biological Sciences 341, 297–305.

Appendix 1: references for Table 1

Arthaber, G.v., 1908. Ueber die Entdeckung von Untertrias in Albanien und ihre faunistiche Bewertung. Mitteilungen der Geologischen Gesellschaft in Wien 1, 245-289.

Arthaber, G.v., 1911. Die Trias von Albanien. Beiträge zur Paläontologie und Geologie 24, 169-276.

Bando, Y., 1977. On some Lower Triassic ammonoids from Ankilokaza, Madagascar. Bulletin of the National Science Museum, Series C (Geology) 3, 133-141.

Bando, Y., 1981. Lower Triassic ammonoids from Guryul Ravine and the Spur three kilometres north of Burus. In: Nakazawa, K., and Kapoor, H.R. (Eds.), The Upper Permian and Lower Triassic faunas of Kashmir. Palaeontologia Indica, New series, pp. 137-171.

Blendinger, W., 1995. Lower Triassic to Lower Jurassic cephalopod limestones of the Oman Mountains. Neues Jahrbuch für Geologie und Paläontologie, Mh 10, 577-593.

Chao, K., 1950. Some new ammonite genera of Lower Triassic from western Kwangsi. Palaeontological Novitates 5, 1-11.

Chao, K., 1959. Lower Triassic ammonoids from Western Kwangsi, China. Palaeontologia Sinica. New Series B, 9. Science Press, Beijing.

Collignon, M., 1933-1934. Paléontologie de Madagascar XX - Les céphalopodes du Trias inférieur. Annales de Paléontologie 12-13, 151-162 & 1-43.

Collignon, M., 1973. Ammonites du Trias inférieur et moyen d'Afghanistan. Annales de Paléontologie 59, 127-163.

Dagys, A., 1999. Evolution of the family Sibiritidae and detailed biostratigraphy of the Siberian Upper Olenekian (Triassic). In: Olóriz, F., and Rodriguez-Tovar, F. J. (Eds.), Advancing Research on Living and Fossil Cephalopods. Academic/Plenum Publishers, New York, pp. 109-123.

Dagys, A., Ermakova, S.P., 1988. Boreal Late Olenekian ammonoids. Transactions of the Academy of Sciences of the USSR, Nauka, Moskow (in Russian, with English abstr.).

Dagys, A., Ermakova, S.P., 1990. Early Olenekian ammonoids of Siberia. Transactions of the Academy of Sciences of the USSR, Nauka, Moskow (in Russian, with English abstr.).

Dagys, A., Ermakova, S.P., 1996. Induan (Triassic) ammonoids from North-Eastern Asia. Revue de Paléobiologie 15, 401-447.

Diener, C., 1897. The cephalopoda of the Lower Trias. Palaeontologia Indica, Series XV, Himalayan fossils 2, 1-181.

Diener, C., 1912. The Trias of the Himalayas. Memoirs of the Geological Survey of India 36, 1-176.

Diener, C., 1913. Triassic faunae of Kashmir. Palaeontologia Indica 5, 1-133.

Ermakova, S.P., 1999. *Sakhaitoides*, a new Early Triassic ammonoid genus. Paleontological Journal 33, 610-613.

Ermakova, S.P., 2001. Description and taxonomy of a new Early Triassic genus *Eovavilovites* (Ammonoidea, Ceratitida). Paleontological Journal 35, 259-261.

Frebold, H., 1929. Untersuchungen über die fauna, die stratigraphie und paläogeographie der Trias Spitzbergens. Skrifter om Svalbard og Ishavet 26, 1-66.

Frebold, H., 1930. Die altersstellung des fischhorizontes, des grippianiveaus und des unteren saurierhorizontes in Spitzbergen. Skrifter om Svalbard og Ishavet 28, 1-36.

Gaetani, M., Jacobshagen, V., Nicora, A., Kauffmann, G., Tselepidis, V., Fantini Sestini, N., Mertmann, D., Skourtsis-Coroneou, V., 1992. The Early-Middle Triassic boundary at Chios. Rivista Italiana de Paleontologia e Stratigraphia 98, 181-204.

Germani, D., 1997. New data on ammonoids and biostratigraphy of the classical Spathian Kçira sections (Lower Triassic, Albania). Rivista Italiana de Paleontologia e stratigraphia 103, 267-292.

Guex, J., 1978. Le Trias inférieur des Salt Ranges (Pakistan): problèmes biochronologiques. Eclogae Geologicae Helvetiae 71, 105-141.

Guo, P.-X., 1982. On the occurrence of late Lower Triassic ammonoids from Anhui and Jiangsu. Acta Palaeontologica Sinica 21, 560-568 (in Chinese, with English abstr.).

He, G., Wang, Y.-G., Chen, G.-L., 1986. Early and Middle Triassic cephalopods of Mt. Burhan Budai, Central Qinhai. In: Carboniferous and Triassic strata and fossils from the southern slope of Mt. Burhan Budai, Qinhai, Nanking, pp. 171-274 (in Chinese, with English abstr.).

Hsü, T.-Y., 1937. Contribution to the marine Lower Triassic fauna of Southern China. Bulletin of the Geological Society of China 16, 303-347.

Hyatt, A., Smith, J.P., 1905. The Triassic cephalopod genera of America. USGS Professional Paper 40, 1-394.

Korchinskaya, M.V., 1972. Biostratigraphy of Triassic deposits of Svalbard. Bulletin of Canadian Petroleum Geology 20, 742-749.

Korchinskaya, M.V., 1982. Explanatory note on the biostratigraphic scheme of the Mesozoic (Trias) of Spitsbergen. USSR Ministry of Geology, PGO Sevmorgeologia (in Russian).

Korchinskaya, M.V., 1983. New ceratitids from the Upper Olenek sediments of Spitsbergen. Paleontological Journal 3, 109-112 (in Russian).

Korchinskaya, M.V., Vavilov, M.N., 1987. Early Induan ammonoids from Spitsbergen. In: Zakharov, Y.D., Onoprienko, Y.I. (Eds.), Problems of the Permian and Triassic biostratigraphy of East USSR. Far-Eastern Scientific Centre, USSR Academy of Science, Vladivostok, pp. 64-72 (in Russian).

Krafft, A.v., 1900. Stratigraphical notes on the Mesozoic rocks of Spiti. In: Griesbach, C.L. (Eds.), General report on the work carried on by the Geological Survey of India for the period from the 1st april 1899 to the 31st march 1900. Office of the Superintendent, Government Printing, India, Calcutta, pp. 199-229.

Krafft, A.v., Diener, C., 1909. Lower Triassic cephalopoda from Spiti, Malla Johar, and Byans. Palaeontologia Indica 6, 1-186.

Krystyn, L., 1974. Die *Tirolites*-Fauna (Ammonoidea) der untertriassischen Werfener Schichten Europas und ihre stratigraphische Bedeutung. Oesterreichische Akademie der Wissenschaften, Mathematisch - Naturwissenschaftliche Klasse, Abteiling I 193, 29-50.

Krystyn, L., Richoz, S., Baud, A., Twitchett, R.J., 2003. A unique Permian-Triassic boundary section from the Neotethyan Hawasina basin, Central Oman Mountains. Palaeogeography, Palaeoclimatology, Palaeoecology 191, 329-344.

Kummel, B., 1957. Paleoecology of Lower Triassic formations of southeastern Idaho and adjacent areas. Geological Society of America Memoir 67, 437-468.

Kummel, B., 1961. The Spitsbergen arctoceratids. Bulletin of the Museum of Comparative Zoology 123, 499-532.

Kummel, B., 1966. The Lower Triassic formations of the Salt Range and Trans-Indus Ranges, West Pakistan. Bulletin of the Museum of Comparative Zoology 134, 361-429.

Kummel, B., 1968a. Additinal Scythian ammonoids from Afghanistan. Bulletin of the Museum of Comparative Zoology 136, 483-503.

Kummel, B., 1968b. Scythian ammonoids from Timor. Breviora, Museum of Comparative Zoology 283, 1-21.

Kummel, B., 1969. Ammonoids of the Late Scythian. Bulletin of the Museum of Comparative Zoology 137, 1-701.

Kummel, B., 1970a. Ammonoids from the Kathwai Member, Mianwali Formation, Salt Range, West Pakistan. In: Kummel, B., Teichert, C. (Eds.), Stratigraphic boundary problems: Permian and Triassic of West Pakistan. The University Press of Kansas, University of Kansas - Departement of Geology Special Publication 4, Lawrence, pp. 177-192.

Kummel, B., 1970b. Lower Triassic (Scythian) ammonoids from Nepal. Breviora, Museum of Comparative Zoology 345, 1-21.

Kummel, B., Erben, H.K., 1968. Lower and Middle Triassic cephalopods from Afghanistan. Palaeontographica 129, 95-148.

Kummel, B., Steele, G., 1962. Ammonites from the *Meekoceras gracilitatus* zone at Crittenden Spring, Elko County, Nevada. Journal of Paleontology 36, 638-703.

Kummel, B., Teichert, C., 1966. Relations between the Permian and Triassic formations in the Salt range and Trans-Indus ranges, West pakistan. Neues Jahrbuch für Geologie und Paläontologie, Abh. 125, 297-333.

Kummel, B., Teichert, C., 1970. Stratigraphy and paleontology of the Permian-Triassic boundary beds, Salt Range and Trans-Indus Ranges, West Pakistan. In: Kummel, B., Teichert, C. (Eds.), Stratigraphic boudary problems: Permian and Triassic of West Pakistan. The University Press of Kansas - Departement of Geology Special Publication 4, Lawrence, pp. 1-110.

Mathews, A.A.L., 1929. The Lower Triassic cephalopod fauna of the Fort Douglas area, Utah. Walker Museum Memoirs 1, 1-46.

Mertmann, D., Jacobshagen, V., 2003. Upper Olenekian (Spathian) ammonoids from Chios (Lower Triassic, Greece): Taxonomy and stratigraphic position. Rivista Italiana de Paleontologia e stratigraphia 109, 417-447.

Mojsisovics, E., 1886. Arktische Triasfaunen. Mémoires de l'Académie Impériale des Sciences de St-Pétersbourg, VIIe série 33, 1-159.

Mørk, A., Elvebakk, G., Forsberg, A.W., Hounslow, M.W., Nakrem, H.A., Vigran, J.O., Weitschat, W., 1999. The type section of the Vikinghøgda Formation: a new Lower Triassic unit in central eastern Svalbard. Polar Research 18, 51-82.

Nakazawa, K., 1981. Analysis of Late Permian and Early Triassic faunas of Kashmir. Palaeontologia Indica 469, 191-204.

Nakazawa, K., Bando, Y., 1968. Lower and Middle Triassic ammonites from Portuguese Timor (palaeontological study of Portuguese Timor, 4) 34, 83-114.

Noetling, F., 1905. Die asiatische Trias. In: Frech, F. (Ed.), Lethaea geognostica. Verlag der E. Schweizerbart'schen Verlagsbuchhandlung (E. Nägele), Stuttgart, pp. 107-221.

Petrovic, K.V., Mihajlovic, D., 1935. La faune des céphalopodes trouvée dans le Trias inférieur en Monténégro (Yougoslavie) ses caractéristiques et son importance. Annales Géologiques de la Péninsule Balkanique 12, 253-259.

Popov, Y., 1961. Triassic ammonoids of northeastern USSR. Transactions, Scientific Research Institute for the Geology of the Arctic (NIIGA), 79, 1-179 (in Russian).

Popov, Y., 1962. Some Early Triassic ammonoids of northern Caucasus. Transactions of the Academy of Sciences of the USSR 127, 176-184 (in Russian).

Popov, Y., 1968. Early Triassic ammonoids from *Prohungarites similis* zone in northern Yakutia. Paleontological Journal 3, 134-137 (in Russian).

Posenato, R., 1992. *Tirolites* (Ammonoidea) from the Dolomites, Bakony and Dalmatia: taxonomy and biostratigraphy. Eclogae Geologicae Helvetiae 85, 893-929.

Renz, C., Renz, O., 1947. Übersicht über eine untertriadische Ammonitenfauna von der Insel Chios (Griechenland). Verhandlungen der Naturforschenden Gesellschaft in Basel 63, 58-79.

Renz, C., Renz, O., 1948. Eine untertriadische Ammonitenfauna von der griechischen Insel Chios. Schweizerische Palaeontologische Abhandlungen 66, 3-98.

Shevyrev, A.A., 1968. Triassic ammonoidea from the southern part of the USSR. Transactions of the Palaeontological Institute, 119. Nauka, Moscow (in Russian).

Shevyrev, A.A., 1995. Triassic ammonites of northwestern Caucasus. Transactions of the Palaeontological Institute 264, 1-174 (in Russian).

Silberling, N.J., Wallace, R.E., 1969. Stratigraphy of the Star Peak Group (Triassic) and overlying Lower Mesozoic rocks Humboldt Range, Nevada. Geologic Survey Professional Paper 592, 1-50.

Smith, J.P., 1932. Lower Triassic ammonoids of North America. USGS Professional Paper 167, 1-199.

Spath, L.F., 1930. The Eotriassic invertebrate fauna of east Greenland. Saertryk af Meddelelser øm Grønland 83, 1-90.

Spath, L.F., 1934. The ammonoidea of the Trias. Catalogue of the fossil cephalopoda in the British Museum (Natural History). The Trustees of the British Museum, London.

Spath, L.F., 1935. Additions to the Eo-Triassic invertebrate fauna of East Greenland. Meddelelser øm Grønland 98, 1-115.

Tozer, E.T., 1963. Lower Triassic ammonoids from Tuchodi Lakes and Halfway River areas, northeastern British Columbia. Geological Survey of Canada Bulletin 96, 1-30.

Tozer, E.T., 1965. Latest Lower Triassic ammonoids from Ellesmere Island and northeastern British Columbia. Geological Survey of Canada Bulletin 123, 1-45.

Tozer, E.T., 1967. A standard for Triassic time. Geologic Survey of Canada Bulletin 156, 1-141.

Tozer, E.T., 1972. Triassic ammonoids and *Daonella* from the Nakhlak Group, Anarak Region, Central Iran. Geological Survey of Iran, Report 28, 29-39.

Tozer, E.T., 1994. Canadian Triassic ammonoid faunas. Geologic Survey of Canada Bulletin 467, 1-663.

Tozer, E.T., Calon, T.J., 1990. Triassic ammonoids from Jabal Safra and Wadi Alwa, Oman, and their significance. In: Robertson, A.H.F., Searle, M.P., Ries, A.C. (Eds.), The Geology and Tectonics of the Oman Region. Geological Society Special Publication, pp. 203-211.

Tozer, E.T., Parker, J.R., 1968. Notes on the Triassic biostratigraphy of Svalbard. Geological Magazine 105, 526-542.

Trümpy, R., 1969. Lower Triassic ammonites from Jameson Land (East Greenland). Meddelelser øm Grønland 168, 78-116.

Waagen, W., 1895. Salt-Range fossils. Vol 2: Fossils from the ceratite formation. Palaeontologia Indica 13, 1-323.

Wang, Y.-G., 1984. Earliest Triassic ammonoid faunas from Jiangsu and Zhejiang and their bearing on the definition of Permo-Triassic boundary. Acta Palaeontologica Sinica 23, 257-269 (in Chinese, with English abstr.).

Wang, Y.-G., 1985. Remarks on the Scythian-Anisian boundary. Rivista Italiana de Paleontologia e stratigraphia 90, 515-544.

Wang, Y.-G., He, G., 1980. Triassic ammonoid sequence of China. Rivista Italiana de Paleontologia 85, 1207-1220.

Wang, Y.-G., He, G., 1981. Some Triassic ammonoids from Xizang., p. 283-313, Palaeontology of Xizang. Book 3. Series of the Scientific expedition to the Qinghai-Xizang plateau (in Chinese).

Wanner, J., 1913. Geologie von Timor. Geologische Rundschau 4, 136-153.

Waterhouse, J.B., Gupta, V.J., 1985. *Cyclolobus* and *Otoceras* from Spiti, Northwest india. Contribution to Himalayan Geology 3, 219-224.

Weitschat, W., Dagys, A., 1989. Triassic biostratigraphy of Svalbard and a comparison with NE-Siberia. Mitteilungen aus dem Geologischen - Paläontologisches Institut - Universität Hamburg 68, 179-213.

Weitschat, W., Lehmann, U., 1978. Biostratigraphy of the uppermost part of the Smithian stage (Lower Triassic) at the Botneheia, W-Spitsbergen. Mitteilungen aus dem Geologischen - Paläontologisches Institut - Universität Hamburg 48, 85-100.

Welter, O.A., 1922. Die ammoniten der Unteren trias von Timor. E. Schweizerbart'sche Verlagsbuchhandlung (Erwin Nägele), Stuttgart.

Wu, S., 1983. Ammonoids. In: Yang, Z., Yin, H., Xu, G., Wu, S., He, Y., Liu, G., Yin, J. (Eds.), Triassic of the South Qilian mountains. Geological Publishing House, Peking, pp. 179-184.

Zakharov, Y.D., 1971. Lower Triassic ammonoid *Otoceras* from the Boreal Province. Paleontological Journal 3, 324-333.

Zakharov, Y.D., 2002. Ammonoid succession of Setorym River (Verkhoyansk Area) and problem of Permian-Triassic Boundary in Boreal Realm. Journal of China University of Geosciences 13, 107-123.

Article type: Original article

THE BIOGEOGRAPHY OF EARLY TRIASSIC AMMONOID FAUNAS: CLUSTERS, GRADIENTS, AND NETWORKS

Arnaud BRAYARD[1,2,*], **Gilles ESCARGUEL**[2,*] **& Hugo BUCHER**[1]

1 - Paläontologisches Institut und Museum der Universität Zürich, Karl-Schmid Strasse 4, CH-8006 Zürich, Switzerland.

2 - UMR-CNRS 5125, « Paléoenvironnements et Paléobiosphère », Université Claude Bernard Lyon 1, 2 rue Dubois, F-69622 Villeurbanne Cedex, France.

* - order is alphabetical: both authors contributed equally to this work.

Corresponding author: Arnaud BRAYARD, Paläontologisches Institut und Museum der Universität Zürich, Karl-Schmid Strasse 4, CH-8006 Zürich, Switzerland.

Phone number: +41 (0) 1 634 26 98

Fax number: +41 (0) 1 634 49 23

arnaud.brayard@univ-lyon1.fr

Submitted to *Journal of Biogeography*

Manuscript information: Number of text pages: 20

Number of figures: 8

Number of tables: 1

Total number of characters: ca. 48200

Running title: Quantitative biogeography of Early Triassic ammonoids

ABSTRACT

1. Aim:

To quantitatively investigate the spatial and temporal biogeographical relationships of the recovery of ammonoid faunas after the end-Permian mass extinction using three complementary numerical approaches among which is a new, non-hierarchical clustering strategy.

2. Location:

The faunal data set consists of a taxonomically homogenised compilation of the spatial and temporal occurrences of ammonoid genera within 20 Early Triassic Tethyan and Panthalassic sites ranging from 40°S and 70°N in paleolatitudes.

3. Methods:

In addition to hierarchical Cluster Analysis (CA) and Nonmetric Multidimensional Scaling (NMDS), we introduce here a third, new numerical approach allowing the visualisation of a nonmetric inter-assemblages similarity structure as a connected network constructed without inferring additional internal nodes. The resulting network, which we call a "*Bootstrapped Spanning Network*" (BSN), allows the simultaneous identification of partially or totally nested as well as gradational linear or reticulated biogeographical structures.

4. Results:

The identified inter-localities relationships indicate that the very beginning of the Early Triassic (Griesbachian) corresponds to a very simple biogeographical context, representing a time of great cosmopolitanism for ammonoids. This context shifts rapidly to a more complex configuration indicative of a more endemic and latitudinally-restricted distribution of the ammonoids during the late Early Triassic (Smithian and Spathian).

5. Main conclusions:

From a biogeographical point of view, our results illustrate a very rapid (less than ca. 2 myr) Early Triassic recovery of the ammonoid faunas, in contrast to many other marine organisms. This recovery is linked with a marked increase in the overall biogeographical heterogeneity, and parallels the edification of a latitudinal gradient of taxonomic richness, which may be essentially controlled by the progressive intensification of the gradient of Sea Surface Temperature.

From a methodological point of view, we show that a BSN is a simple, intuitively legible picture of the nested as well as gradational taxonomic similarity relationships, hence providing a good synthesis (and additional insights) between CA and NMDS results. Moreover, it eliminates major flaws of CA and NMDS techniques, notably it does not require the taxonomic space, within which inter-

assemblage similarities are calculated, to be a topological metric space where the notions of “neighbourhood” and “small distance” are equivalent.

6. Keywords:

Ammonoids, Early Triassic recovery, Biogeography, Cluster Analysis, Nonmetric Multidimensional Scaling, Bootstrapped Spanning Network

INTRODUCTION

In many aspects, the Early Triassic represents a major episode of Earth history, especially concerning the still debated dynamics and modalities of the biological diversity recovery after the end-Permian mass extinction. Whereas the cause(s) of the Mother of all mass extinctions are being investigated since several decades (see Erwin *et al.*, 2002; Benton & Twitchett 2003; Erwin 2006, for recent reviews), interest in the post-crisis recovery time is much more recent (e.g. Chen *et al.*, 2005; Fraiser *et al.*, 2005; Twitchett & Oji 2005).

Previous studies concerning the ammonoid recovery during the Early Triassic demonstrate a rapid diversification when compared with many other marine organisms. This diversification is concomitant with the formation of a latitudinal gradient of diversity (Brayard *et al.*, 2004, in press). The study of generic endemism and richness also indicates that the Early Triassic is the time of a rapid global restructuring of ammonoid faunas. However, little is still known concerning the detailed biogeographical relationships and their evolution throughout Early Triassic times.

The results presented and discussed in this paper are based on the numerical analysis of four biogeographical data sets (Brayard *et al.*, in press) covering both Tethyan and Panthalassic realms and correspond to the four, well defined successive Early Triassic stages as used by ammonoid workers (e.g. Tozer 1967): Griesbachian (11 genera × 8 localities), Dienerian (23 genera × 11 localities), Smithian (61 genera × 15 localities) and Spathian (93 genera × 19 localities). Parallel to the use of classical Cluster Analysis (CA) and Nonmetric Multidimensional Scaling (NMDS) (e.g. Field *et al.*, 1982; Legendre & Legendre 1998), we introduce a new, non-hierarchical clustering strategy in order to investigate these spatial and temporal relationships. Our approach relies on the construction of a "Bootstrapped Spanning Network" (BSN), i.e. a connected network deduced from a Minimum Spanning Network by simultaneously minimizing the number of edges and maximizing the overall product of the bootstrap Confidence Intervals of the remaining edges. The merits and flaws of each method are briefly discussed, and BSN is shown to provide insights which cannot be easily recovered from CA and NMDS results.

GEOLOGICAL AND PALEONTOLOGICAL SETTINGS

Position of land masses and seas

The Early Triassic paleogeographical configuration is relatively simple with a single super-continent stretching from Pole-to-Pole: the Pangea, surrounded by a wide Ocean, the Panthalassa (Elmi & Babin 1996; **Fig. 1**). A westward encroachment of the Pangea continent was formed by a smaller ocean: the Tethys, essentially located between 30°N and 30°S. During the Early Triassic, the Tethys and the

Panthalassa included several shifting oceanic plates (e.g. Cimmerian and Cathaysian microcontinents; Chulitna, eastern Klamath, Stikinia, Wrangellia terranes; Japan and New Zealand; see Nichols & Silberling 1979; Tozer 1982; Kojima 1989; Ricou 1994; Adams *et al.*, 2002; Belasky *et al.*, 2002; Stampfli & Borel 2002). However, the major continents remained stable during the Early Triassic, providing a reliable geographical framework from which biogeographical signals from marine faunas can be extracted.

Timescale

In this work, we use the four stage subdivision (Griesbachian, Dienerian, Smithian and Spathian; **Fig. 2**) as established by Tozer (1967), whose boundaries are well defined in terms of ammonoids for all latitudes and in both Tethyan and Panthalassic Oceans. Hence, we do not follow the decision of the Sub-commission on Triassic Stratigraphy in adopting a two-fold subdivision for the Early Triassic, with the Induan and Olenekian stages. Indeed, this subdivision is not accepted by all Triassic workers because it was defined in 1956 by Kiparisova & Popov in two different, geographically different realms: Tethyan (low-paleolatitudes) and Boreal (high-paleolatitudes). Thus, the correlation of the Induan/Olenekian boundary across these realms is still problematic. Moreover, ammonoid and conodont turnovers appear less important at this boundary in comparison with other Early Triassic events (e.g. Smithian/Spathian boundary; Orchard 2005; Brayard *et al.*, in press).

The ammonoid recovery

After the end-Permian mass extinction, the ammonoid recovery was much faster than most other clades, contending with that of the conodonts for the most rapid diversification (e.g. Kummel 1973a, 1973b; Orchard 2005). Only two ceratitid genera survived the mass extinction: *Otoceras* and *Ophiceras*. *Otoceras* was the last derivative of the Permian Araxoceratidae and only had a short existence in the Early Triassic (Griesbachian). All other Mesozoic ammonoids are usually considered to derive from the Permian family Xenodiscidae, *Ophiceras* being a bridging taxon (e.g. Tozer 1981).
After an initial short phase of low diversity spanning the Griesbachian and Dienerian, the diversity increased until it dropped dramatically at the very end of the Smithian (Brayard *et al.*, in press). Evidence for a global sea-level change coinciding with this event is still wanting, but it nevertheless correlates with a major perturbation of the carbon cycle (Galfetti *et al.*, submitted) and a marked increase of the xerophytic components of the boreal vegetation (Hochuli *et al.*, submitted). The maximum latitudinal differentiation of ammonoid faunas was thus reached during the Spathian, with the formation of a steep latitudinal diversity gradient (Dagys 1988; Brayard *et al.*, in press). Although of lesser intensity than the end-Smithian event, a second important drop in diversity occurred around

the Spathian/Anisian boundary (i.e. the Early/Middle Triassic boundary). Thus, the recovery pattern of ammonoid diversity was not monotonous and gradual but underwent a succession of ups and downs.
The Early Triassic represents a time of formation and intensification of a latitudinal gradient of taxonomic richness which is best explained by the edification and intensification of a latitudinal gradient of Sea Surface Temperature. Parallel to this latitudinal structuring, a global partitioning of faunas consisting of a significant increase of endemic taxa is evidenced by means of Occurrence Ratio Profile Analysis (Brayard *et al.*, 2004, 2005, in press).

DATA SET AND METHOD

Nature of the data

The faunal data set consists of a taxonomically homogenised compilation of the occurrences of 185 genera in 20 sites within known Early Triassic ammonoid assemblages (Brayard *et al.*, in press; **Fig. 1**). The use of the genus level allows the control of most of the systematic bias, which essentially resides at the species level but still enables the extraction of detailed paleobiogeographical structures and faunal signals (e.g. Shen & Shi 2000). A site may represent a fauna or a succession of faunas from a unique, extensively sampled section, or a composite record of several local assemblages from the same sedimentary basin ranging in most cases between surface scales of 10^4 to 10^6 km^2.
Faunas belonging to terranes with uncertain or unknown paleopositions (e.g. South Kitakami of Japan, South Primorye) are not included in this study. This leads to the exclusion of some extremely rare genera from the data set (e.g. *Durvilleoceras* from New Zealand or *Burijites* from South Primorye). Homogenisation of the taxonomy follows the classification of Tozer (1981) emended with some recently described genera or revised systematic positions (e.g. Tozer 1994; Shevyrev 1995; Brayard *et al.*, in press; Brayard in progress). The time subdivisions correspond to the Griesbachian, Dienerian, Smithian and Spathian.

Classical Q-mode clustering and ordination analyses

Following the protocol of Field *et al.* (1982), we first performed a two-fold Q-mode analysis of the four biogeographical data sets (one set per time subdivision) involving hierarchical Cluster Analysis (CA) and Nonmetric Multidimensional Scaling (NMDS). As these two approaches are based on distinct assumptions both about the nature of the similarity structure to be extracted, and on different analytical ways to achieve it (see next section), a comparison and combination of their results strongly reinforces the confidence in the identified biogeographical structures (*e.g.* Sneath & Sokal 1973; Field *et al.*, 1982; Legendre & Legendre 1998). Both CA and NMDS analyses are based on the preliminary computation of a symmetrical matrix of dissimilarity. We used the *non-metric coefficient* of Watson *et*

al. (1966; noted D_{13} by Legendre & Legendre 1998: 286), *i.e.* the 1-complement of the *Dice's* (1945) or *Sørensen's* (1948) *coefficient* of similarity (noted S_8 by Legendre & Legendre 1998: 256):

$$D_{i,j} = \frac{E_i + E_j}{N_i + N_j} = 1 - \frac{2 \times C_{i,j}}{N_i + N_j} = 1 - S_{i,j},$$

where E_i and E_j are the number of genera observed only in assemblages *i* and *j*, respectively, N_i and N_j are the total number of genera in assemblages *i* and *j*, respectively, and $C_{i,j}$ is the number of genera shared by assemblages *i* and *j*. This coefficient corresponds, for binary data, to the *percentage difference* (Odum 1950) or *Bray & Curtis'* (1957) *coefficient*. We preferred this semimetric coefficient to other metric and perhaps more classical ones (e.g. the *Simpson's* and *Jaccard's coefficient*) for the double weight given to shared presences, and thus relative under-weighting of absence as an indication of faunal differences. As already emphasised by Legendre & Legendre (1998: 256), such relative over-weighting of double presences is an appealing property due to the always ambiguous meaning of absence, which does not necessarily reflect *real* differences between the compared taxonomic assemblages.

Firstly, hierarchical Cluster Analysis was performed on the square root of the dissimilarity matrix in order to achieve metricity and euclideanarity (Gower & Legendre 1986). Then, we constructed the corresponding dendrogram using the UPGMA (Unweighted arithmetic average clustering; Rohlf 1963; Clifford & Stephenson 1975) method of clustering as available in the NEIGHBOR program of the PHYLIP package, version 3.65 (Felsenstein 2005). For each analysed data set, we performed an internal validation of the resulting classification by computing Confidence Intervals on the observed clusters using nonparametric bootstrap based on 9999 pseudo-samples generated with the BIO-BOOT software (Escarguel, 2005). Only clusters with a bootstrap proportion ≥50% were finally retained for discussion of the biogeographical signal.

Secondly, we performed a Nonmetric Multidimensional Scaling (NMDS; Shepard 1962a, b, 1966; Kruskal 1964a, b; Mead 1992) of the raw (untransformed) dissimilarity matrix. Since NMDS (i) does not require the analysed dissimilarity matrix to be a metric, and (ii) is unaffected by monotonic transformation such as the square root transformation, CA and NMDS results can be directly compared to one another. We used NMDS as implemented in the PAST software, version 1.34 (Hammer *et al.*, 2001), based on the 'purely nonmetric' algorithm developed by Tagushi & Oono (unpublished, 2005). The ordination of assemblages was achieved in a two-dimensional coordinate system based on the least-squares objective function:

$$f = \sqrt{\sum_{i,j} \left(o_{i,j} - \hat{o}_{i,j} \right)^2}$$

where $o_{i,j}$ is the rank of the observed dissimilarity between taxonomic assemblages *i* and *j*, and $\hat{o}_{i,j}$ is the fitted rank of this biogeographical couple in the reduced ordinated space (Hammer, pers. com.

2005). Multiple runs were performed for each data set in order to maximize the chance of capturing the global minimum of the objective function.

Comparison, advantages and disadvantages of CA and NMDS methods

The fundamental difference between these two similarity-based approaches is that CA focuses on the nested taxonomic relationships between assemblages and is therefore unable to identify any gradational signal (which corresponds to an additive but not ultrametric structuring of the observed dissimilarity matrix), whereas NMDS aims at extracting intergradational information in a reduced space and is of little or no use in identifying hierarchical structures. Indeed, as already emphasised by Legendre & Legendre (1998: 482), "ordinations in reduced space may misrepresent the structure by projecting together clusters of objects which are distinct in higher dimensions". Hence, as any biogeographical pattern combines hierarchical and gradational structuring of the taxonomic assemblages, both approaches are useful and provide complementary information about the compositional resemblance of the studied assemblages.

On the one hand, despite its mathematical simplicity and the rather intuitive reading of dendrograms, CA shows several disadvantages when applied to biological data sets (e.g. Field *et al.*, 1982; Legendre & Legendre 1998; Escarguel 2005). The main problem is that, by its very nature and whatever the employed algorithm, a hierarchical Cluster Analysis will extract an ultrametric structure from any observed dissimilarity matrix, even if no such structure is present in the observed data (see appendix *in* Lapointe & Legendre 1992). Hence, a dendrogram tends to overemphasize discontinuities and thus may force a gradational series into several discrete groups that actually do not exist. Finally, the cophenetic matrix corresponding to a dendrogram may be a poor structural reflection of the observed dissimilarity matrix. In addition, in the context of biogeographical analyses, two points are particularly worthy of attention:

- contrary to, e.g. phylogenetic trees, the internal nodes of a biogeographical dendrogram do not have any necessary functional and/or historical meaning, making them difficult to interpret from a strict biological point of view;
- taxonomic assemblages may have intrinsically reticulated relationships. By construction, such reticulations cannot be recovered by CA.

On the other hand, NMDS shows a great ability to recover even spatially complex (e.g. circular, star-shaped, etc.) gradients from a semimetric signal in a reduced, usually one to three-dimensional space. In spite of its flexibility and ability to handle missing data, NMDS suffers from computational difficulties linked to (i) the arbitrary choice of an objective function to be minimized, and (ii) the failure of the iterative algorithm in converging toward the global minimum of this function. This second point can usually be solved by repeated analysis from different, randomly chosen starting

points. Although not always necessary (depending on the geometry of the objective function), it may become prohibitively time-consuming when handling large data sets.

The "Bootstrapped Spanning Network" method

In addition to these different disadvantages of the CA and NMDS methods, we note that, when applied to taxonomic incidence or abundance data, both suffer from a fundamental flaw due to phylogenetical, biogeographical and ecological constraints controlling the spatial distribution and abundance of taxa. As a consequence of such historical and functional constraints, the taxonomic similarity between assemblages, in whatever way it is estimated, does not evolve in a homogeneous topological metric space where the notions of "neighbourhood" and "small distance" are equivalent. Strictly speaking, this situation, which is rather classical when working with spatialised discrete data, makes topological methods such as CA and NMDS mathematically inadequate, and strongly calls for alternate, pretopological approaches of structural analysis (e.g. Largeron & Bonnevay 2002).

For all of these reasons, we introduce here a simple and intuitive method to visualise a nonmetric inter-assemblages similarity structure as a connected network (potentially allowing for cycles) constructed without inferring additional internal nodes. The resulting network, which we called a "*Bootstrapped Spanning Network*", allows the simultaneous identification of partially or totally nested as well as gradational biogeographical structures. Even if not formally embedded in pretopological theory (e.g. Čech 1966), this method has an obvious strong affinity with the concepts of pseudoclosure and pretopological space defined as a collection of minimal closed subsets, where "neighbourhood" and "small distance" are not equivalent characteristics of a couple of objects.

The construction of a "*Bootstrapped Spanning Network*" (BSN) involves a three-step straightforward procedure (**Fig. 3**) with:

(i) the preliminary computation of the undirected Minimum Spanning Network (MSN; i.e. the shortest connected network *sensu* Prim 1957; see Bandelt *et al.*, 1999) associated to the observed dissimilarity matrix;

(ii) the estimation, for each edge of the observed MSN, of its associated bootstrap Confidence Interval. This estimation is achieved by repeated computation of the dissimilarity matrix and corresponding MSN for pseudo-samples randomly generated by nonparametric bootstrap of the observed data set;

(iii) the removing, starting from the weakest (lowest bootstrap C.I.) to the strongest observed edge, of the observed MSN edges in order to simultaneously:
- minimise the number of edges of the MSN ($\geq N$-1 where N is the number of compared assemblages);
- maximise the overall product of the bootstrap Confidence Intervals associated to the remaining edges.

The procedure ends when the removing of any remaining edge makes the network not connected, or stops increasing the overall product of the bootstrap C.I. When several edges or sets of edges (i.e., edges linked to a same node) share the same bootstrap C.I.-value, the sets are randomly ordered, and then the edges are removed in a random order within each set; if a "disconnecting edge" belongs to such a set of tied edges, a "conservative" decision is taken and none of them are eliminated.

Thus, the resulting BSN can be viewed as the *simplest connected network best supported by the available data* in order to describe the more or less complex, reticulated, nested and/or gradational similarity relationships between the compared assemblages. It is worth noting that, even if starting from a Minimum Spanning Network, the resulting BSN is not "minimal" in the sense that the observed edge lengths are not considered in the removing procedure. On the one hand, by connecting vertices without inferring additional internal nodes, the BSN method is particularly well suited to biogeographical analysis, as it does not require any post hoc hypothesis about the existence of potentially meaningless (as "historically non-functional") biogeographical entities. On the other hand, the statistical backgrounds of this technique make it immune to a major flaw of the Minimum Spanning Tree clustering techniques, namely that MST algorithms tend to become non-convergent when the observed pairwise dissimilarities decrease relatively to their associated error.

Finally, the resulting inter-assemblage relationships can be easily visualised and interpreted by drawing the BSN on a (paleo)geographic map where the studied taxonomic assemblages are spatially located, e.g. using the PAJEK software (Batagelj & Mrvar 2005). The density and orientation of the BSN edges on such a map give direct qualitative indications about the biogeographical clusters and/or gradients underlying the analysed data set. In addition, three complementary summary statistics can easily be computed in order to synthesise the geometric characteristics of the BSN:

- the Density Coefficient (DC), i.e. the ratio between the inferred and maximum ($\frac{N(N-1)}{2}$, corresponding to a complete network) number of edges;
- the Mean Degree of a Node (MND), i.e. the mean number of incident edges on each node of the BSN;
- the Mean Shortest Path Length (MSPL), i.e. the mean of the minimal numbers of edges in the walk between two nodes.

In the context of biogeographical analysis, DC can be considered as a rough proxy of the mean degree of cosmopolitanism of the analysed taxa: the higher the DC, the more taxonomically homogeneous the compared assemblages. MND and MSPL are representative of the intensity of the taxonomic neighbourliness between assemblages, and can thus be viewed as two complementary indices of structural complexity of the BSN.

RESULTS

Griesbachian (Fig. 4)

Bootstrapped CA yields a weakly supported hierarchy with only four clusters showing CI-values > 50%, two of them being very close to the 50% threshold-value (**Fig. 4A**). Hence, only two southern Tethyan localities (Spiti and Salt Ranges; group Gr1) appear biogeographically well distinct from all the others. With the exception of the geographically close localities of Ellesmere and Spitsbergen, no supported biogeographical hierarchy can be emerges for the remaining localities.

The NMDS map displays two principal close groups of localities (**Fig. 4B**): the group Gr1 as already illustrated by CA and a second group made up of the other localities except Oman.

Hence, NMDS emphasizes the strong biogeographical difference of the latter when compared to the other localities, a feature not evidenced by CA. However, such difference could be due, at least partially, to a relative lack of sampling of this still poorly known Tethyan Ammonoid fauna.

The BSN shows a main group of closely related localities made of Ellesmere, Spitsbergen, Greenland and South China, even if the two latter are not directly linked to one another (**Fig. 4C**). The geographical position of Greenland in a “cul-de-sac” can explain this situation.

Gr1 and the Olenek are closely linked to this main group whereas Oman appears extremely isolated (as already indicated by NMDS) and barely connected to the network with a very weak link. The Density Coefficient (DC) as well as the Mean Shortest Path Length (MSPL) and the Mean Node’s Degree (MND) all indicate a high degree of ammonoid cosmopolitanism during this stage (**Tabl. 1**).

Consequently, CA and NMDS suggest that Griesbachian ammonoids do not display any global geographical or latitudinal hierarchical or gradational structuring. Nevertheless, with the noticeable exception of the still poorly known Oman fauna, the BSN indicates a weak geographical structuring of the data around a Panthalassic biogeographical node, information not detected by CA and NMDS. This overall configuration illustrates the widespread distribution of Griesbachian genera throughout the Tethyan and Panthalassic oceans, as already suggested by endemicity analysis (Brayard *et al.*, in press).

Dienerian (Fig. 5)

The bootstrapped CA (**Fig. 5A**) allows the individualization of three main clusters with geographical significance: Di1, including intertropical localities; Di2, corresponding to the Boreal realm (Spitsbergen and Olenek); and Di3, containing African-Gondawanan sites (Oman and Madagascar). In spite of its geographical proximity with Di1 and Di2, Ellesmere is not clustered to one of these two groups but is intercalated between the three main clusters.

The NMDS analysis (**Fig. 5B**) returns a similar biogeographical structuring and allows a more precise biogeographical location of Ellesmere between Di1 and Di2 groups.

The BSN (**Fig. 5C**) provides an essentially similar pattern and allows some complementary insights. Ellesmere is geographically correctly intercalated between British Columbia (Di1) and Spitsbergen (Di2). The Di1 group is made of five highly connected localities (British Columbia, Nevada, Guangxi, Timor, Spiti) plus the Salt Ranges which is only connected to Guangxi. Thus, the BSN reflects strong affinities within intertropical sites even if they are distributed on both sides of the Panthalassa. This noticeable intensification of fauna relationships is reflected in the three synthetic descriptive parameters (**Table 1**). Di3 connects itself to Di1 via the Spiti.

Hence, the three approaches indicate a weak Dienerian biogeographical global structuring corresponding to the differentiation of two "extreme" provinces (Boreal and African) from a main intertropical cluster. This is particularly evident for the eastern side of Panthalassa (Di3) where sites are latitudinally connected. This latitudinal differentiation is concomitant to the appearance of the first latitudinal diversity gradient of ammonoids (Brayard *et al.*, in press).

Smithian (Fig. 6)

The bootstrapped CA (**Fig. 6A**) identifies three well supported clusters: Sm1, corresponding to northeastern Panthalassic localities (Olenek, Spitsbergen, Ellesmere, British Columbia); Sm2 including three, geographically close equatorial localities from eastern Panthalassa (Idaho, Nevada, California); and Sm3, grouping two well diversified South Tethyan localities (Salt Ranges and Spiti). All other Tethyan localities display unresolved relationships with these three clusters.

The NMDS (**Fig. 6B**) recovers the Sm2 and Sm3 groups. The eastern Panthalassa localities (Sm1) are plotted close to three equatorial Tethyan localities (South China, Timor, Afghanistan), defining here a low-latitudes group not identified by CA. The Madagascar, Oman and Caucasus localities are relatively poorly sampled. Their positions on the NMDS map do not evidence any clear biogeographical relationships with the other studied localities.

The BSN (**Fig. 6C**) allows the recovery of the structures evidenced by CA and NMDS (Sm1, Sm3, the equatorial group including Sm2) and gives more precision about the three remaining Tethyan localities. As it could be expected on geographical evidences, Madagascar is linked to Sm3. Oman is strongly connected to the equatorial group. Caucasus shows the weakest link of the network with an eastern Panthalassic locality (California). This preferential biogeographical link could reflect a relative disconnection of the oceanic circulation in the western part of the Panthalassa, probably due to the geographical location of land masses in the eastern Tethys (e.g., North and South China).

Considered together, the three approaches thus evidence a clear latitudinalisation of the biogeographical structuring with a northward eastern Panthalassic gradient and a southward Tethyan gradient, both departing from a trans-oceanic equatorial main group of localities. This biogeographical

latitudinal structuring of faunal relationships closely paralelizes the marked latitudinal diversity gradient and higher level of endemicity evidenced at this time (Brayard *et al.*, in press; **Table 1**).

Spathian (Fig. 7)

The CA (**Fig. 7A**) allows the characterisation of four well supported clusters: northeastern Panthalassic localities (Sp1), equatorial Panthalassic localities (Sp2), equatorial Tethyan localities (Sp3) and a southern Tethyan group (Sp4) including Salt Ranges and Oman but not Spiti and Madagascar. Four Tethyan localities display unresolved relationships with these four clusters. Within the Sp3 group, Albania and Chios show strong relationships due to several shared endemic taxa (e.g. *Chiotites*, *Chioceras*, *Beatites*).

The NMDS (**Fig. 7B**) shows a V-shaped gradational structuring where the four main clusters recognized by the CA are well individualized. In addition, it suggests a grouping of Panthalassic and Tethyan localities (Sp2 and Sp3). Caucasus is intercalated between low-latitudes of North equatorial Tethyan and Panthalassic localities, whereas Spiti and Madagascar fall at the Tethyan extremity of the gradient.

The BSN (**Fig. 7C**) synthesises all this information and provides further details. Caucasus is strongly connected to Chios. Eastern Panthalassic and central Tethyan localities are highly linked. Yugoslavia shows a weakly supported link with equatorial Panthalassic localities.

Even if not strictly identical, the Spathian biogeographical context thus appears very close to the Smithian one, with a marked Panthalassic and Tethyan latitudinal structuring and a strong trans-oceanic equatorial connection. Remarkably, this configuration corresponds to the marked latitudinal diversity gradient and high global level of endemism evidenced at this time (Brayard *et al.*, in press; **Table 1**).

DISCUSSION AND CONCLUSION

Evolutionary biogeography of Early Triassic ammonoids

The three types of analysis used in this work outline an insightful biogeographical evolutionary scheme fully consistent with previous results. Firstly, this evolution runs parallel to the edification and steepening of a latitudinal gradient of taxonomic richness, which has been suggested to be essentially controlled by the progressive intensification of the gradient of Sea Surface Temperature, thus contracting the latitudinal ranges of taxa (Brayard *et al.*, 2004, 2005, in press). This correlation is particularly well illustrated by the “Bootstrapped Spanning Networks”, which clearly show a narrowing of the latitudinal distribution of ammonoid faunas sharing strong trans-oceanic faunal

similarities (**Fig. 8**). This result supports the hypothesis of the existence of a planktonic phase for ammonoids that enabled them to passively cross the Panthalassic Ocean by current transport (Brayard *et al.*, in press). Secondly, this evolution is perfectly congruent with the observed significant increase of the overall level of taxonomic endemicity (Brayard *et al.*, in press).

Hence, departing from a simple, neither hierarchical nor gradational cosmopolitan post-crisis configuration during Griesbachian times, our data evidence an increasingly mature biogeographical structuring of the ammonoid faunas. At the end of the analyzed time series, the Spathian appears as the time of maximum latitudinal biogeographical differentiation, including several low-latitude centers of diversity corresponding, for this period, to areas of endemicity (e.g., Chios, South China; Brayard *et al.*, in press). This full picture of the post-Permo/Triassic crisis ammonoid settlement of the Panthalassic and Tethyan oceans markedly departs from previous ones, which described these faunas as spatially and temporally globally homogeneous throughout the Early Triassic (Dagys 1988, McGowan 2005). When combined with new numerical ages data indicating that the Spathian times represent ca. 3 my., i.e., more than half of the entire Early Triassic (Ovtcharova *et al.*, 2006), our results illustrate a very rapid (less than ca. 2 myr; see **Fig. 2**) post-crisis recovery of the ammonoid faunas in contrast to many other marine organisms (e.g., brachiopods, bivalves; see Chen *et al.*, 2005). Interestingly, this feature strongly echoes independent views about the fallacy of an alleged delay in the post-crisis recovery dynamics as the spurious consequence of the incompleteness of the fossil record (Lu *et al.*, 2006). Early Triassic faunas and floras are still poorly known, and our data could well indicate that the delayed recovery after the end-Permian mass extinction (e.g., Payne *et al.*, 2004) is the actual result of a global preservation bias and sampling artifact, generating Signor-Lipps and Jaanusson effects. Hence, parallel to the necessary methodological and theoretical considerations about the very nature of the fossil record and the way to mathematically correct it for the various potential biases and artifacts which affect it, long-term field and paleontological work are also necessary in order to qualitatively and quantitatively increase the amount of data to be handled. In the case of the Early Triassic ammonoids, such systematical work demonstrates the previously unexpected rapidity of the post-crisis recovery; we wager that more work will confirm this result for several other groups.

The “Bootstrapped Spanning Network”: a new tool for quantitative biogeography

The biogeographical results presented and discussed in this work come from two classical complementary approaches complemented by a new one: the “Bootstrapped Spanning Network” (BSN) method. In short, a BSN can be defined as the simplest connected network best supported by the available data. As such, it can be viewed as the minimal biogeographical hypothesis required in order to explain, based on the available data, the taxonomic interdependencies observed between the studied assemblages. We show here that a BSN is a simple, intuitively legible picture of the nested as well as

gradational taxonomic similarity relationships, hence providing a good synthesis (and additional insights) between Cluster Analysis and Nonmetric Multidimensional Scaling outputs. Moreover, it eliminates the four major flaws of CA and NMDS techniques as discussed above:

- no additional (internal) nodes are added, ensuring the full network only consists of functionally and historically meaningful entities – the studied taxonomic assemblages;
- gradational, nested and reticulated aspects of biogeographical relationships are fully preserved and simultaneously recovered without creating any artifactual structure not supported by the data;
- the BSN can be easily and directly displayed onto a (paleo)geographical framework (**Fig. 8**), preserving it from the arbitrariness of CA and NMDS graphical outputs;
- contrary to CA and NMDS, the BSN does not require the taxonomic space, where the systematic assemblages are described and compared, to be a topology.

Finally, all these appealing properties, which remain to be more deeply investigated from a pretopological theory point of view, make the BSN method a good alternative to classical cluster and spatial multivariate techniques in order to unravel the often complex relationships linking taxonomic assemblages through space and time.

Acknowledgements:

This work was supported by the Swiss NSF project 200020-105090/1 (A.B and H.B), and a Rhône-Alpes-Eurodoc grant (A.B). The computer programs (written in IDL®-language) used in the computations of this work are available on request from the second author (gilles.escarguel@univ-lyon1.fr). G. Stringer kindly improved the English version.

References:

Adams, C.J., Barley, M.E., Maas, R. & Doyle, M.G. (2002) Provenance of Permian-Triassic volcaniclastic sedimentary terranes in New Zealand: evidence from their radiogenic isotope characteristics and detrital mineral age patterns. *New Zealand Journal of Geology and Geophysics*, **45**, 221-242.

Bandelt, H.-J., Forster, P. & Röhl, A. (1999) Median-joining networks for inferring intraspecific phylogenies. *Molecular Biology and Evolution*, **16**, 37-48.

Batagelj, V. & Mrvar, A. (2005) PAJEK (Program for Analysis and Visualization of Large Network) version 1.07. Distributed by the authors. University of Ljubljana. http://vlado.fmf.uni-lj.si/pub/networks/pajek/

Belasky, P., Stevens, C.H. & Hanger, R.A. (2002) Early Permian location of western North American terranes based on brachiopod, fusulinid, and coral biogeography. *Palaeogeography, Palaeoclimatology, Palaeoecology*, **179**, 245-266.

Benton, M.J. & Twitchett, R.J. (2003) How to kill (almost) all life: the end-Permian extinction event. *Trends in Ecology and Evolution*, **18**, 358-365.

Bray, J.R. & Curtis, J.T. (1957) An ordination of the upland forest communities of southern Wisconsin. *Ecological Monographs*, **27**, 325-349.

Brayard, A., Bucher, H., Escarguel, G., Fluteau, F., Bourquin, S. & Galfetti, T. (in press) The Early Triassic ammonoid recovery: paleoclimatic significance of diversity gradients. *Palaeogeography, Palaeoclimatology, Palaeoecology*.

Brayard, A., Escarguel, G. & Bucher, H. (2005) Latitudinal gradient of taxonomic richness: combined outcome of temperature and geographic mid-domains effects? *Journal of Zoological Systematics and Evolutionary Research*, **43**, 178-188.

Brayard, A., Héran, M.-A., Costeur, L. & Escarguel, G. (2004) Triassic and Cenozoic palaeobiogeography: two case studies in quantitative modelling using IDL. *Palaeontologia Electronica*, **7**, 22p.

Čech, E. (1966) *Topological spaces*. Wiley, London.

Chen, Z.-Q., Kaiho, K. & George, A.D. (2005) Survival strategies of brachiopod faunas from the end-Permian mass extinction. *Palaeogeography, Palaeoclimatology, Palaeoecology*, **224**, 232-269.

Clifford, H.T. & Stephenson, W. (1975) *An introduction to numerical classification*. Academic Press, New York.

Dagys, A.S. (1988) Major features of the geographic differentiation of Triassic ammonoids. *Cephalopods - Present and past* (ed. by J. Wiedmann and J. Kullmann), pp. 341-349. Schweizerbart'sche Verlagsbuchhandlung, Stuttgart.

Dice, L.R. (1945) Measures of the amount of ecologic association between species. *Ecology*, **26**, 297-302.

Elmi, S. & Babin, C. (1996) *Histoire de la Terre*. Masson, Paris.

Erwin, D.H. (2006) *Extinction - How Life on Earth nearly ended 250 million years ago*. Princeton University Press, Princeton.

Erwin, D.H., Bowring, S.A. & Jin, Y.G. (2002) End-Permian mass extinctions: a review. *Geological Society of America Special Paper*, **356**, 363-383.

Escarguel, G. (2005) Mathematics and the lifeway of Mesopithecus. *International Journal of Primatology*, **26**, 801-823.

Felsenstein, J. (2005) PHYLIP (Phylogeny Inference Package) version 3.6. Distributed by the author. Department of Genome Sciences, University of Washington, Seattle.

Field, J.G., Clarke, K.R. & Warwick, R.M. (1982) A practical strategy for analysing multispecies distribution patterns. *Marine Ecology Progress Series*, **8**, 37-52.

Fraiser, M., Twitchett, R.J. & Bottjer, D.J. (2005) Unique microgastropod biofacies in the Early Triassic: indicator of long-term biotic stress and the pattern of biotic recovery after the end-Permian mass extinction. *C.R. Palevol*, **4**, 475-484.

Galfetti, T., Bucher, H., Brayard, A., Hochuli, P.A., Weissert, H., Guodun, K., Atudorei, V. & Guex, J. (submitted) Late Early Triassic climate change: insights from carbonate carbon isotopes, sedimentary evolution and ammonoid paleobiogeography. *Palaeogeography, Palaeoclimatology, Palaeoecology*.

Gower, J.C. & Legendre, P. (1986) Metric and Euclidean properties of dissimilarity coefficients. *Journal of Classification*, **3**, 5-48.

Hammer, Ø., Harper, D.A.T. & Ryan, P.D. (2001) PAST: Paleontological Statistics Software Package for Education and Data Analysis. *Palaeontologia Electronica*, **4**, 9pp.

Hochuli, P.A., Galfetti, T., Brayard, A., Bucher, H., Weissert, H. & Vigran, J.O. (submitted) The Smithian/Spathian boundary event: a major climatic turnover following the end-Permian biotic crisis. Evidence from palynology, ammonoids and stable isotopes. *Geology*.

Kiparisova, L.D. & Popov, Y.D. (1956) Subdivision of the lower series of the Triassic System into stages. Doklady Akademia Nauk SSSR, **109**, 842-845 (in Russian).

Kojima, S. (1989) Mesozoic terrane accretion in Northeast China, Sikhote-Alin and Japan regions. *Palaeogeography, Palaeoclimatology, Palaeoecology*, **69**, 213-232.

Kruskal, J.B. (1964a) Multidimensional scaling by optimizing goodness of fit to a nonmetric hypothesis. *Psychometrica*, **29**, 1-27.

Kruskal, J.B. (1964b) Nonmetric dimensional scaling: a numerical method. *Psychometrica*, **29**, 115-129.

Kummel, B. (1973a) Aspects of the Lower Triassic (Scythian) stage. *The Permian and the Triassic systems and their mutual boundary* (ed. by A. Logan and L.V. Hills), pp. 557-571. Canadian Society of Petroleum Geologists, Calgary.

Kummel, B. (1973b) Lower Triassic (Scythian) molluscs. *Atlas of Paleobiogeography* (ed. by A. Hallam), pp. 225-233. Elsevier, Amsterdam.

Lapointe, F.-J. & Legendre, P. (1992) A statistical framework to test the consensus among additive trees (cladograms). *Systematic Biology*, **41**, 158-171.

Largeron, C. & Bonnevay, S. (2002) A pretopological approach for structural analysis. *Information Sciences*, **144**, 169-185.

Legendre, P. & Legendre, L. (1998) *Numerical ecology*. Elsevier, Amsterdam.

Lu, P.J., Yogo, M. & Marshall, C.R. (2006) Phanerozoic marine biodiversity dynamics in light of the incompleteness of the fossil record. *Proceedings of the National Academy of Sciences of the United States of America*, **103**, 2736-2739.

McGowan, A.J. (2005) Ammonoid recovery from the Late Permian mass extinction. *C. R. Palevol*, **4**, 517-530.

Mead, A. (1992) Review of the development of Multidimensional Scaling Methods. *Statistician*, **41**, 27-39.

Mundil, R., Ludwig, K.R., Metcalfe, I. & Renne, P.R. (2004) Age and timing of the Permian mass extinctions: U/Pb dating of closed-systems zircons. *Science*, **305**, 1760-1763.

Nichols, K.M. & Silberling, N.J. (1979) Early Triassic (Smithian) ammonites of Paleoequatorial affinity from the Chulitna terrane, South-central Alaska. *Geological Survey Professional Paper*, **1121-B**, B1-B5.

Odum, E.P. (1950) Bird populations of the Highlands (North Carolina) plateau in relation to plant succession and avian invasion. *Ecology*, **31**, 587-605.

Orchard, M.J. (2005) On the explosive radiation of Lower Triassic conodonts: a new multielement perspective. Triassic chronostratigraphy and biotic recovery, Chaohu, China. *Albertiana*, **33**, p.65.

Ovtcharova, M., Bucher, H., Schaltegger, U., Galfetti, T., Brayard, A. & Guex, J. (2006) New New Early to Middle Triassic U-Pb ages from South China: calibration with ammonoid biochronozones and implications for the timing of the Triassic biotic recovery. *Earth and Planetary Science Letters*, **243**, 463-475.

Payne, J.L., Lehrmann, D.J., Wei, J., Orchard, M.J., Schrag, D.P. & Knoll, A.H. (2004) Large perturbations of the carbon cycle during recovery from the end-Permian extinction. *Science*, **305**, 506-509.

Péron, S., Bourquin, S., Fluteau, F. & Guillocheau, F. (2005) Paleoenvironment reconstructions and climate simulations of the Early Triassic: impact of the water and sediment supply on the preservation of fluvial systems. *Geodinamica Acta*, **18**, 431-446.

Prim, R.C. (1957) Shortest connection networks and some generalizations. *Bell System Technical Journal*, **36**, 1389-1401.

Ricou, L.E. (1994) Tethys reconstructed: plates, continental fragments and their boundaries since 260 Ma from Central America to South-eastern Asia. *Geodinamica Acta*, **7**, 169-218.

Rohlf, F. (1963) Classification of *Aedes* by numerical taxonomic methods (Diptera: Culicidae). *Annual Review of the Entomological Society of America*, **56**, 798-804.

Shen, S. & Shi, G.R. (2000) Wuchiapingian (early Lopingian, Permian) global brachiopod palaeobiogeography: a quantitative approach. *Palaeogeography, Palaeoclimatology, Palaeoecology*, **162**, 299-318.

Shepard, R.N. (1962a) Analysis of proximities: multidimensional scaling with an unknown distance function. I. *Psychometrica*, **27**, 125-140.

Shepard, R.N., (1962b) The analysis of proximities: multidimensional scaling with an unknown distance function. II. *Psychometrica*, **27**, 219-246.

Shepard, R.N. (1966) Metric structures in ordinal data. *Journal of Mathematical Psychology*, **3**, 287-315.

Shevyrev, A.A. (1995) Triassic ammonites of northwestern Caucasus. *Transactions of the Palaeontological Institute*, **264**, 1-174 (in Russian).

Sneath, P.H.A. & Sokal, R.R. (1973) *Numerical taxonomy - The principles and practice of numerical classification*. W.H. Freeman, San Fransico.

Sørensen, T. (1948) A method of establishing groups of equal amplitude in plant sociology based on similarity of species content and its application to analysis of the vegetation on Danish commons. *Biologiske Skrifter Det Kongelige Danske Videnskabernes Selskab*, **5**, 1-34.

Stampfli, G. & Borel, G.D. (2002) A plate tectonic model for the Paleozoic and Mesozoic constrained by dynamic plate boundaries and restored synthetic oceanic isochrons. *Earth and Planetary Sciences Letters*, **196**, 17-33.

Tagushi, Y.-H. & Oono, Y. (2005) Relational patterns of gene expression via non-metric multidimensional scaling analysis. *Bioinformatics*, **21**, 730-740.

Tagushi, Y.-H. & Oono, Y. (unpublished) Novel non-metric MDS algorithm with confidence level test [Available at: http://granular.com/MDS/src/paper.pdf].

Tozer, E.T. (1967) A standard for Triassic time. *Geologic Survey of Canada Bulletin*, **156**, pp.141.

Tozer, E.T. (1981) Triassic ammonoidea: classification, evolution and relationship with Permian and Jurassic forms. *The ammonoidea* (ed. by M.R. House and J.R. Senior), pp. 65-100. The Systematics association, London.

Tozer, E.T. (1982) Marine Triassic faunas of North America: their significance for assessing plate and terrane movements. *Geologische Rundschau*, **71**, 1077-1104.

Tozer, E.T. (1994) Canadian Triassic ammonoid faunas. *Geologic Survey of Canada Bulletin*, **467**, pp.663.

Twitchett, R.J. & Oji, T. (2005) Early Triassic recovery of echinoderms. *C.R. Palevol*, **4**, 463-474.

Watson, L., Williams, W.T. & Lance, G.N. (1966) Angiosperm taxonomy: a comparative study of some novel numerical techniques. *Journal of the Linnean Society of London (Botany)*, **59**, 491-501.

Biosketches:

Arnaud Brayard is a PhD student in paleontology. His main research topic is the paleobiogeography and diversity of early Triassic ammonoids, with emphasis on interactions between climatic changes and large-scale biodiversity patterns in time and space.

Gilles Escarguel is a paleomammalogist whose research interests are focused on quantitative paleobiogeography, and statistical investigations of biodiversity changes through geological time.

Hugo Bucher is a paleobiologist focusing on the evolution and paleobiography of Mesozoic ammonoids, with emphasis on interactions between major abiotic changes, large-scale biodiversity patterns in time and space, and morphological evolutionary responses.

Figure captions:

Fig. 1: Paleogeographical map of the Early Triassic (modified from Péron *et al.*, 2005) with the paleoposition of the studied basins and localities. Cartouches' filled cells indicate the temporal distribution of samples in the studied localities (from base to top: 1st cell: Griesbachian, 2nd: Dienerian, 3rd: Smithian, 4th: Spathian).

Fig. 2: Chronostratigraphic subdivisions of the Early Triassic (radiometric ages from Mundil *et al.*, 2004 and Ovtcharova *et al.*, 2006).

Fig. 3: Flow chart illustrating the main steps of the "*Bootstrapped Spanning Network*" method.

Fig. 4: Biogeographical structuring of the Griesbachian dataset. A) UPGMA majority-rule consensus tree (bootstrap Confidence Intervals estimated with 10000 iterations); B) Nonmetric Multidimensional Scaling map; C) "Bootstrapped Spanning Network": numbers indicate the bootstrap Confidence Intervals for each edge (100% when not reported).

Fig. 5: Biogeographical structuring of the Dienerian dataset. See fig. 4 for details.

Fig. 6: Biogeographical structuring of the Smithian dataset. See fig. 4 for details.

Fig. 7: Biogeographical structuring of the Spathian dataset. See fig. 4 for details.

Fig. 8: Evolution of the ammonoid biogeographical provinces during the Early Triassic, illustrating the narrowing of the latitudinal distribution of ammonoid faunas sharing strong trans-oceanic faunal similarities (subequatorial shaded area; map modified from Péron *et al.*, 2005).

Table:

	Density Coefficient	*Mean Shortest Path Lenght*	*Mean Node's Degree*
Griesbachian	32.14	2.21	2.25
Dienerian	25.45	2.78	2.55
Smithian	15.23	3.7	2.13
Spathian	14.62	3.54	2.63

Table 1: Complementary coefficients of the BSN analysis

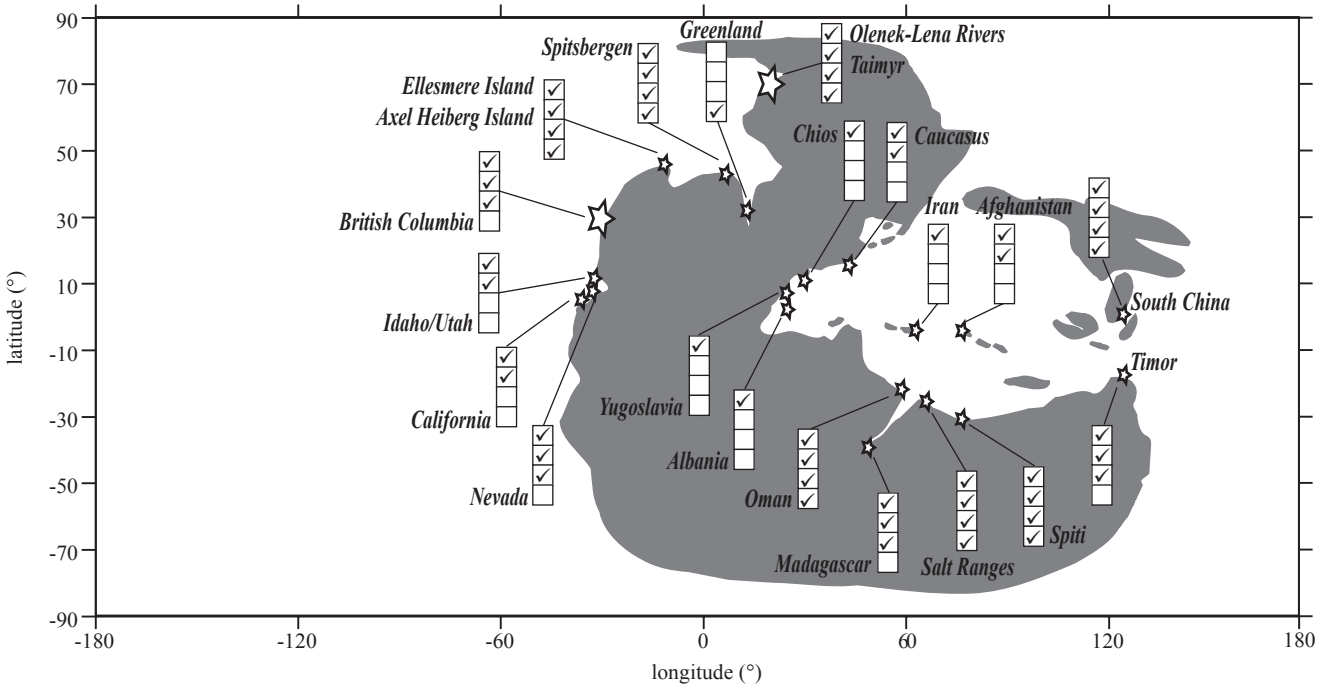

Fig. 1. Brayard et al.

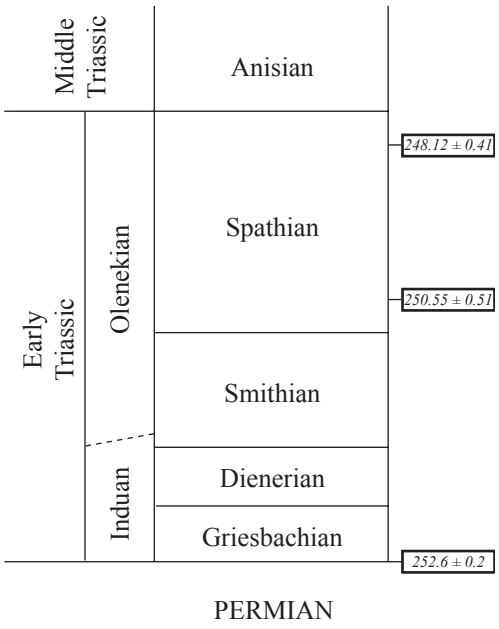

Fig. 2. Brayard et al.

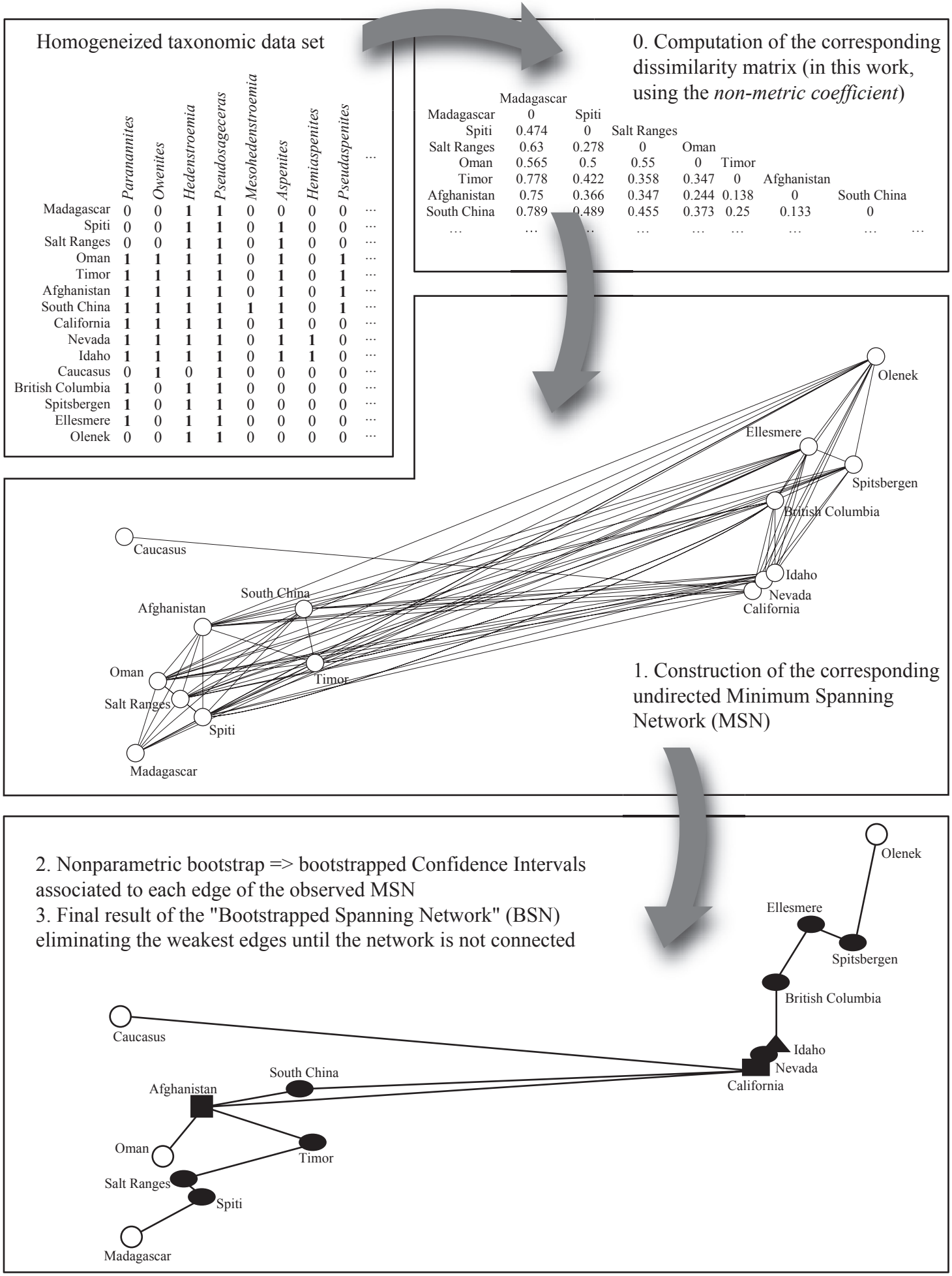

Fig. 3. Brayard et al.

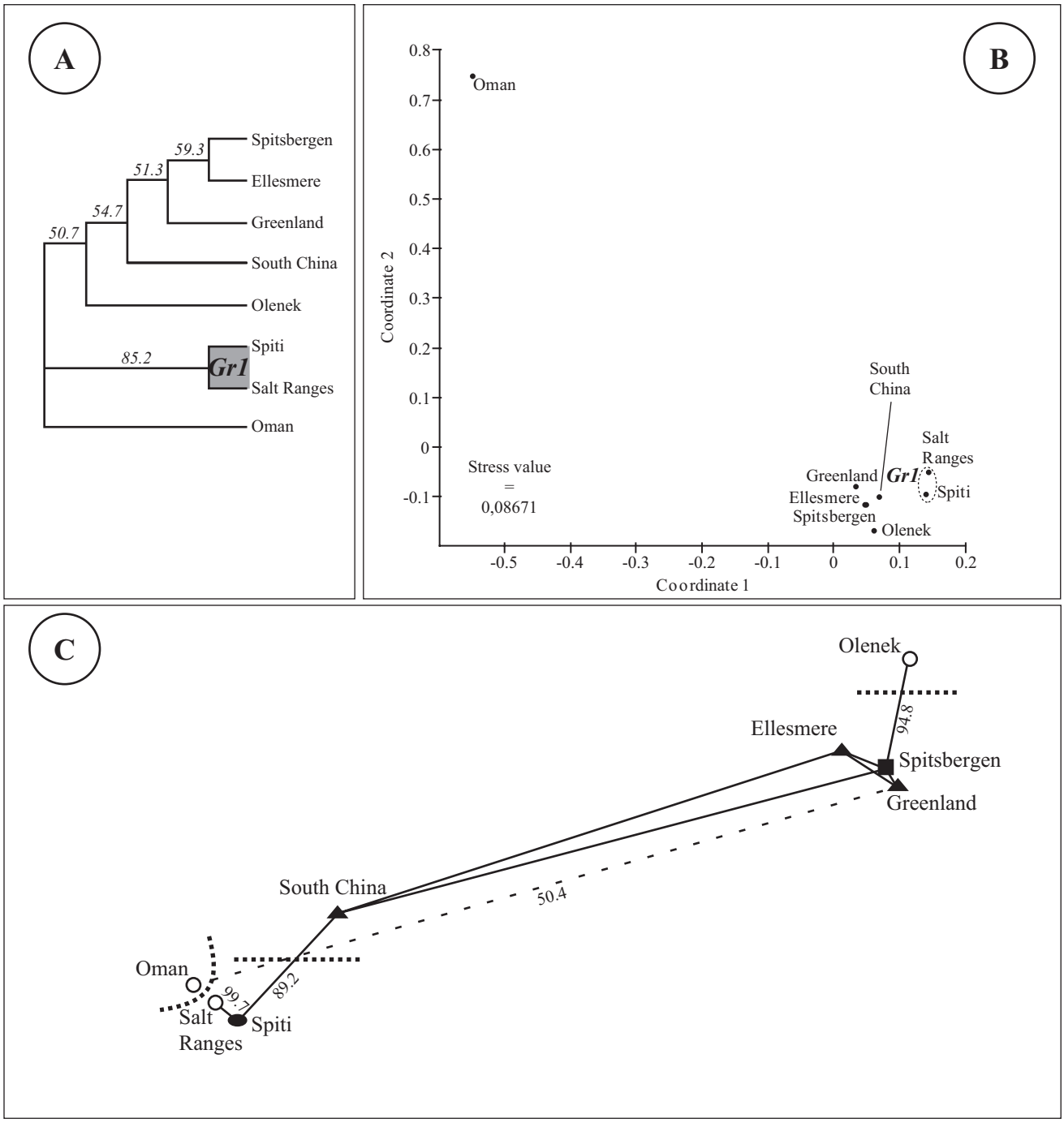

Fig. 4. Brayard et al.

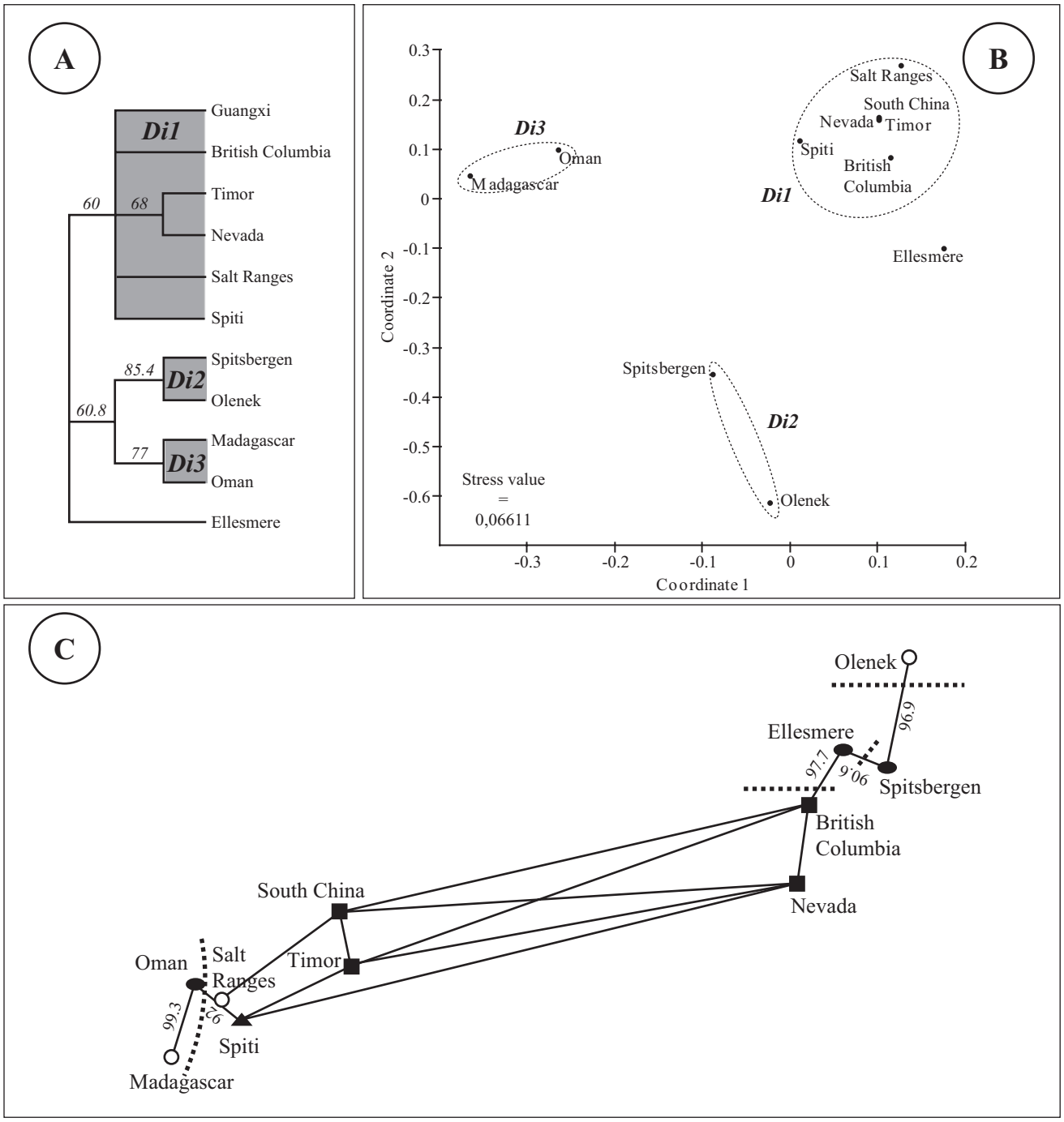

Fig. 5. Brayard et al.

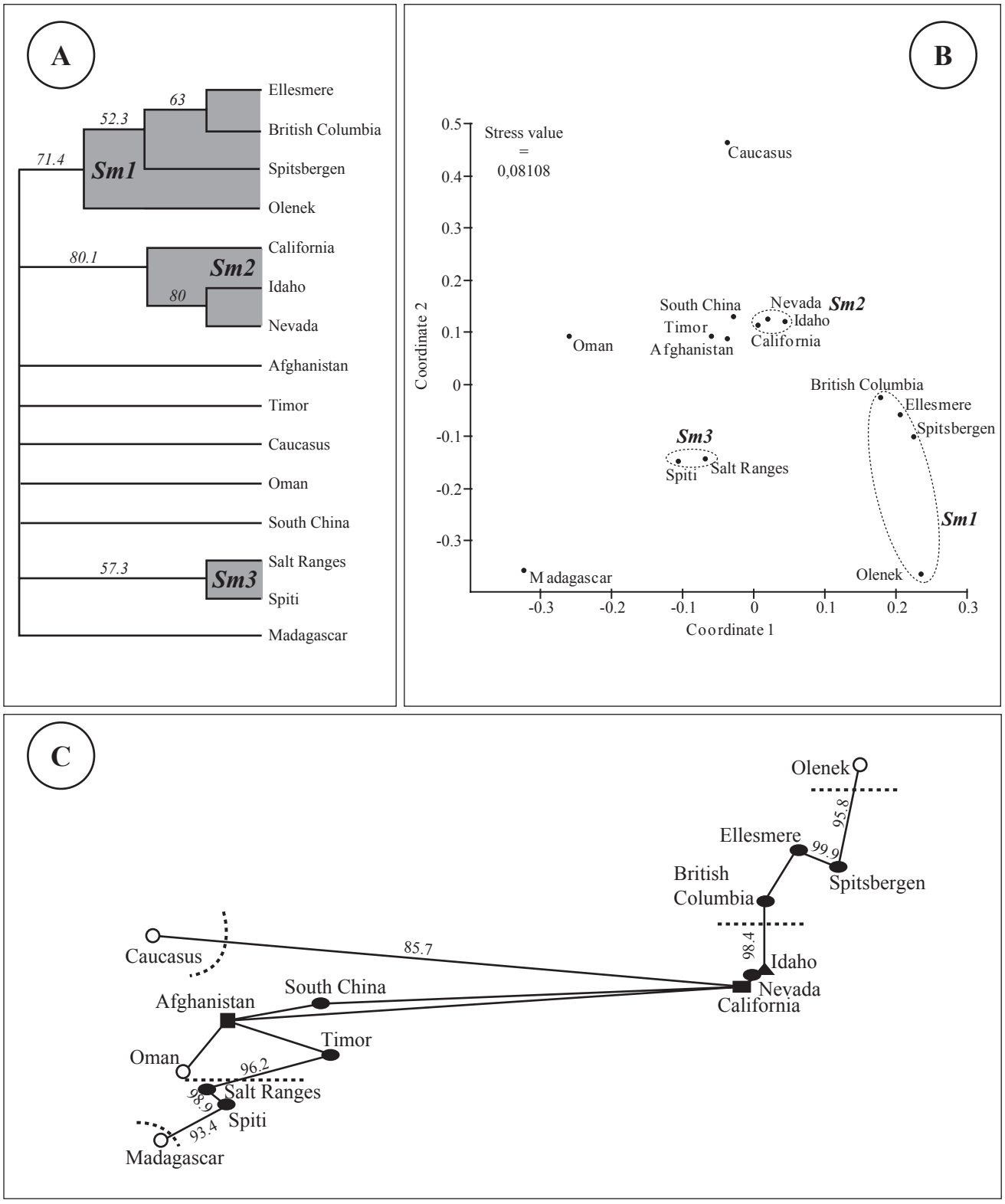

Fig. 6. Brayard et al.

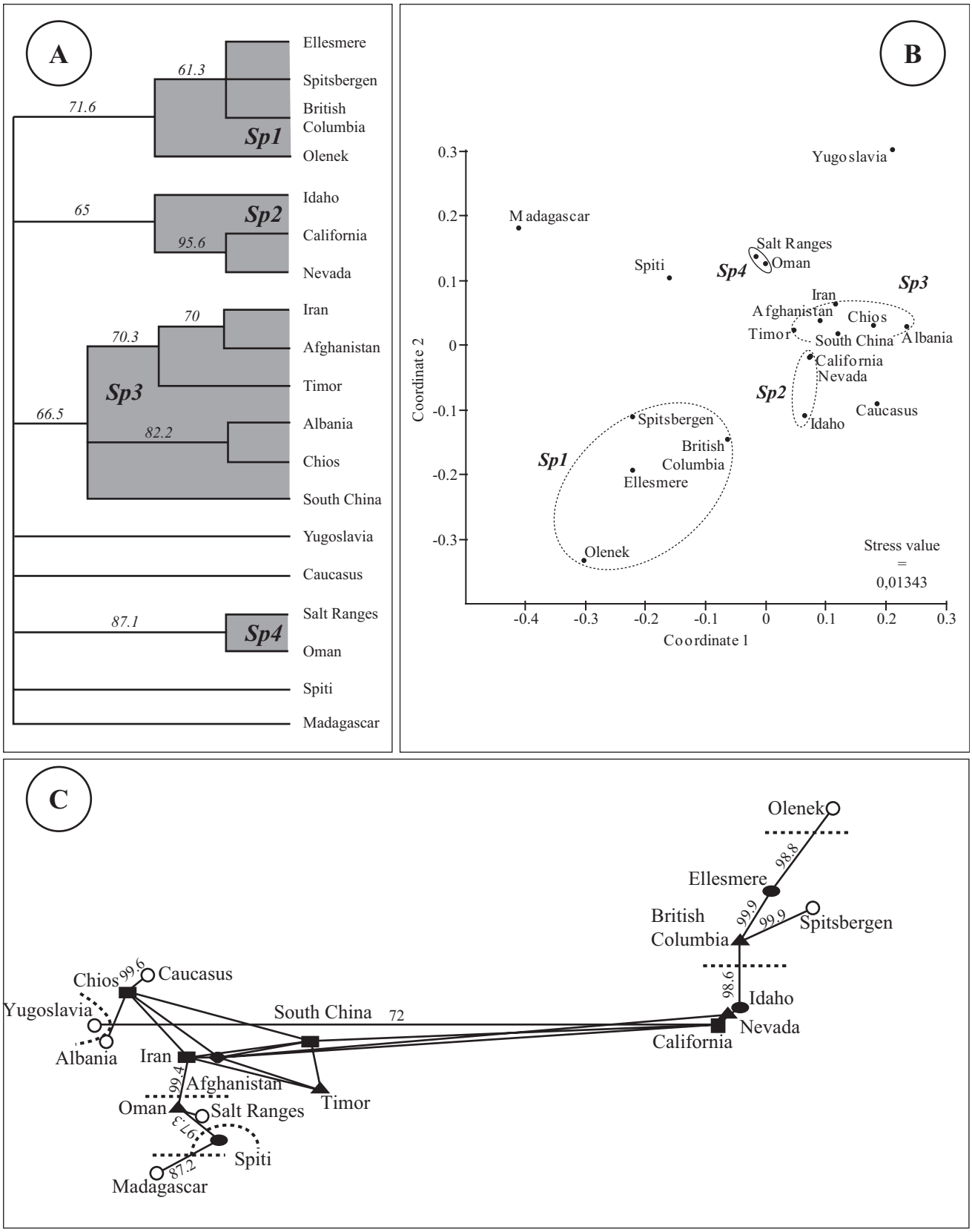

Fig. 7. Brayard et al.

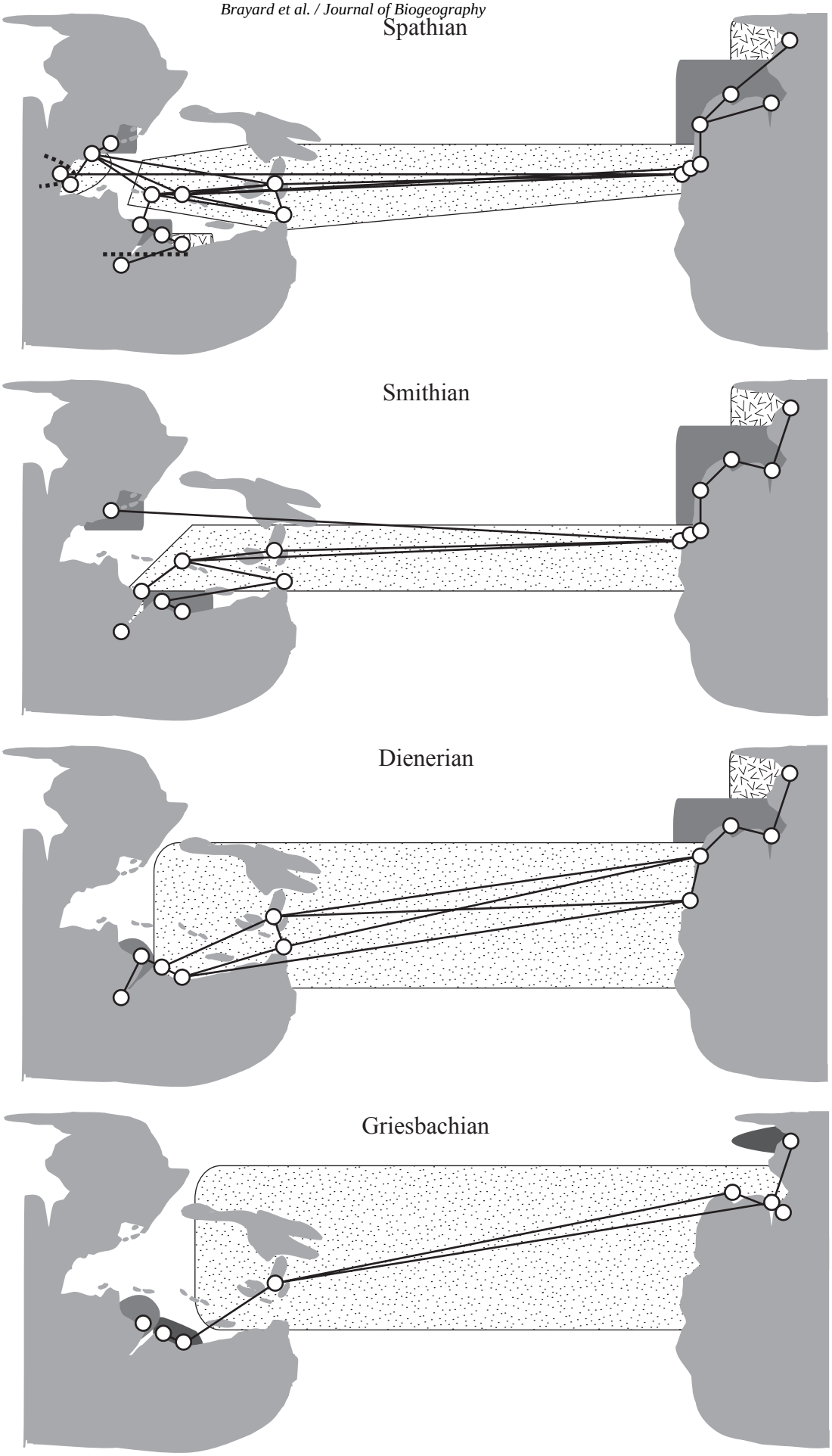

Fig. 8. Brayard et al.

INTRODUCTION TO CHAPTER 5
(Question 4)

The homogenised data set presented in this thesis dissertation is accompanied by the monographic description of newly documented Smithian ammonoid faunas from the northwestern Guangxi (South China), based on a populational and statistical approach. These faunas revealed the existence of 14 new genera and 34 new species, and allow the construction of a high-resolution ammonoid succession for Tethyan equatorial faunas.

SMITHIAN (EARLY TRIASSIC) AMMONOID FAUNAS FROM NORTHWESTERN GUANGXI (SOUTH CHINA): TAXONOMY AND BIOCHRONOLOGY

Arnaud BRAYARD[1, 2] **& Hugo BUCHER**[1]

1 - Paläontologisches Institut und Museum der Universität Zürich, Karl-Schmid Strasse 4, CH-8006 Zürich, Switzerland.

2 - UMR-CNRS 5125, « Paléoenvironnements et Paléobiosphère », Université Claude Bernard Lyon 1, 2 rue Dubois, F-69622 Villeurbanne Cedex, France.

Corresponding author: Arnaud BRAYARD, Paläontologisches Institut und Museum der Universität Zürich, Karl-Schmid Strasse 4, CH-8006 Zürich, Switzerland.

Phone number: +41 (0) 44 634 26 98

Fax number: +41 (0) 44 634 49 23

arnaud.brayard@univ-lyon1.fr

Submitted to *Fossils & Strata*

Manuscript information: Number of text pages: 126

Number of figures: 67

Number of tables: 1

Number of plates: 45

Total number of characters: ca. 185 000

Abstract:

Intensive sampling of the Luolou Formation in northwestern Guangxi (South China) leads to the recognition of several new ammonoid faunas of Smithian age and to the construction of a new biostratigraphical zonation for the Smithian paleoequatorial region. These faunas significantly enlarge the scope of the Smithian stage, and the new zonal scheme facilitates correlation with other mid- and high-paleolatitude faunal sucessions (i.e. British Columbia and Siberia). In ascending order, the new biostratigraphic sequence comprises the "*Hedenstroemia hedenstroemi* beds", the "*Kashmirites densistriatus* beds", the "*Flemingites rursiradiatus* beds", the "*Owenites koeneni* beds", and the "*Anasibirites multiformis* beds". Thus, the Smithian of this paleoequatorial region now includes a newly introduced lowermost subdivision that is approximatively correlative with the *H. hedenstroemi* Zone of British Columbia and Siberia. Likewise, the newly introduced uppermost subdivision is equivalent to the *Anawasatchites tardus* Zone of British Columbia and Siberia.

Fourteen new genera (*Sinoceltites*, *Weitschaticeras*, *Hebeisenites*, *Jinyaceras*, *Xiaoqiaoceras*, *Nanningites*, *Wailiceras*, *Leyeceras*, *Urdyceras*, *Galfettites*, *Guangxiceras*, *Larenites*, *Guodunites*, *Procurvoceratites*) and 34 new species (*Hanielites gracilus*, *H. angulus*, *Xenoceltites variocostatus*, *X. pauciradiatus*, *Sinoceltites admirabilis*, *Weitschaticeras concavum*, *Hebeisenites varians*, *H. evolutus*, *H. compressus*, *Jinyaceras bellum*, *Juvenites procurvus*, *Paranorites jenksi*, *Xiaoqiaoceras involutus*, *Wailiceras aemulus*, *Leyeceras rothi*, *Urdyceras insolitus*, *Galfettites simplicitatis*, *Pseudoflemingites goudemandi*, *Guangxiceras inflata*, *Anaflemingites hochulii*, *Arctoceras strigatus*, *Anasibirites evolutus*, *Hemiprionites klugi*, *Inyoites krystyni*, *Paranannites ovum*, *P. globosus*, *P. dubius*, *Hedenstroemia augusta*, *Cordillerites antrum*, *Pseudaspenites evolutus*, *Guodunites monneti*, *Procurvoceratites pygmaeus*, *P. ampliatus*, *P. subtabulatus*) are described.

Key words:

Ammonoids, Smithian, Early Triassic, northwestern Guangxi, South China, Luolou Fm.

1. Introduction

The marine Permo-Triassic boundary record is well preserved in South China and has attracted the attention of many scientists ever since the Meishan section was chosen as the GSSP (Yin *et al.* 1996, 2001). Moreover, Early Triassic marine sedimentary formations are also abundant in the Guangxi and Guizhou provinces of South China. The pioneer contributions of Chao (1950, 1959) first documented the occurrence of rich Early Triassic ammonoid faunas in northwestern Guangxi. Chao (op. cit.) directly integrated his data within the "Flemingitan" and "Owenitan" subdivisions of the biostratigraphic scheme of Spath (1934), thus overlooking any potential improvements. Since Chao's works, few papers have been published on the Early Triassic ammonoids of South China, and none of them has reassessed the Smithian ammonoid succession from northwestern Guangxi.

In order to better understand the dynamics of the biotic recovery following the Permo-Triassic mass extinction, Early Triassic paleobiogeographical and diversity studies now receive more and more attention (e.g. Brayard *et al.* 2004, in press; Fraiser *et al.* 2005; Twitchett & Oji 2005). From this perspective, the South Chinese record is of prime importance. Indeed, marine Early Triassic paleoequatorial sections are few (see Brayard *et al.* in press), thus emphasising the importance of the abundant ammonoid data from South China. Furthermore, the widely accepted paleoequatorial position of the South China Block (SCB) during the Early Triassic makes it a key biogeographical reference, since the majority of recent works dealing with Early Triassic ammonoids come from either from mid or high paleolatitudal settings (e.g. Tozer 1994; Dagys & Ermakova 1990).

Our investigations in northwestern Guangxi have led to the discovery of several new Early Triassic faunas. In this paper we focus on the taxonomy and biostratigraphy of Smithian ammonoid faunas, as well as their implication for low paleolatitude diversity and biochronology. Global correlations across latitudes and between both sides of Panthalassa are also discussed, as are the new paleobiogeographical and phylogenetic implications.

2. Geological framework

2.1. General context

Southwestern Asia is a complex collage of orogenic belts and successive accretions of Gondawana-derived continental blocks (Boulin 1991). China is tectonically complex and

composed of several blocks that traveled throughout the Tethys during the Permian and Triassic (Enkin *et al.* 1992). Southwestern China is located at the junction of the Chinese, Southeast Asian, and Indian plates, as well as the Tibetan block (Fan 1978), but the kinematic and temporal frame of their amalgamation is not well understood (Gilder *et al.* 1995). The South China Block (SCB) and North China Block (NCB), were located in the low-latitudes of the eastern Tethys during the Early Triassic. Paleomagnetic data indicate that the SCB was situated near the Equator (Gilder *et al.* 1995).

2.2. Triassic deposits in South China

Marine Triassic sediments, represented by carbonate platforms and deep-water facies, are widespread in the South China Block and other neighbouring blocks. They are especially well developed and exposed in Tibet, Qinghai, Yunnan, Guizhou, Guangxi and Sichuan (e.g. Hsü 1940, 1943; Chao 1959; and Wang *et al.* 1981). Generally, in the SCB, the Early Triassic and Anisian are represented by marine deposits, while the Upper Triassic is composed of continental sediments (Tong & Yin 2002).

Marine deposits in northwestern Guangxi belong to the Youjiang sedimentary province, which was part of the SCB during Early Triassic time. Sedimentary deposits in this province, which is also known as the “Nanpanjiang Basin”, consist of clastic and carbonate rocks deposited in a deep-water basin with a few smaller, isolated carbonate platforms distributed within Guangxi and Guizhou provinces (e.g. Lehrmann *et al.* 2003). The basin is bordered on the north and west by the large Yangtze carbonate platform, and Early Triassic deposits are generally distributed along the northern and western edges of this platform.

2.3. The Luolou Formation

The Luolou Fm., which represents an important portion of the Early Triassic outer platform facies in southern Guizhou and northwestern Guangxi, was first made known by Chao (1950, 1959). Its lower part mainly consists of dark, thin limestone beds alternating with dark shales, whereas its upper part is composed of massive, grey, nodular limestone. Overlying the Luolou Fm. is the +1,000 meter thick Baifeng Fm. of Anisian age, which consists mainly of clastic turbidites. This influx of terrigeneous material suggests a generalized drowning of the basin at that time, and thus, a concomitant modification in directions or rates of convergence between the South and North China blocks (Gilder *et al.* 1995).

2.4. Sections from northwestern Guangxi

All studied sections are located in northwestern Guangxi (**Fig. 1**). The Luolou Fm. is located on the periphery of the Carboniferous-Permian karstic massives, which is often in fault contact with middle Triassic siliciclatics. Classical sections such as Tsoteng, sampled by Chao (1950, 1959), were resampled in order to obtain a precise, detailed record, since bed-by-bed sampling was not systematically utilized for the original collections. The type section near Luolou is now poorly exposed and therefore, was not resampled. With the exception of Tsoteng, all sampled sections (**Figs. 2** to **9**, Table 1) yielding numerous fossiliferous layers were first correlated by means of lithological or marker beds (e.g. the 3 m thick limestone band containing the "*Flemingites rursiradiatus* beds"), which then facilitated the construction of a synthetic range chart for ammonoid faunas (**Fig. 10**).

The Smithian lithological succession is very similar within the Jinya and Leye areas and can be easily summarized. Dark shales alternating with thin, laminated micritic limestone beds (e.g. **Fig. 3**, and see Galfetti *et al.* submitted for details) characterize the lower portion of the Smithian. These recessive rocks are usually only partly exposed and ammonoids are relatively rare. It is for this reason that the exact position of the Dienerian/Smithian boundary has not yet been precisely established. These lowermost beds are overlain by a conspicuous, ca. 3m thick, grey, thin-bedded limestone unit. This unit contains the "*Flemingites rursiradiatus* beds", and it represents an important lithological marker found in all sections. This marker is overlain by the "*Owenites koeneni* beds", which consist of dark, laminated micritic limestone beds intercalated within dark shales. Overlying these beds are reddish-weathering, dark carbonate silts, which contain the *"Anasibirites multiformis* beds*"*. The uppermost few meters consist of black shales containing small-sized, early diagenetic limestone nodules yielding a few plant remains and typical *Xenoceltites* of latest Smithian age. Finally, the Smithian/Spathian boundary is characterized by an abrupt change to carbonate deposition. Contrasting with those of the Leye and Jinya areas, rocks of Smithian age in the Tsoteng area are almost exclusively composed of limestone.

3. Biostratigraphy

3.1. General subdivisions

Although several different schemes have been proposed for stage subdivision of the Early Triassic, near unanimous agreement on any particular scheme remains somewhat elusive. The Early Triassic is commonly divided into two, three or four stages as follows: two stages (Induan and Olenekian; the Olenekian encompassing the Smithian and the Spathian); three stages (Griesbachian, Nammalian and Spathian); or four stages (Griesbachian, Dienerian, Smithian and Spathian). In this paper we utilize the four stage subdivision proposed by Tozer (1967), whose boundaries are well-defined in terms of ammonoids.

3.2. Chinese subdivisions

A Chinese commission proposed its own two-fold subdivision for the Early Triassic, based initially on lithological differences (Tong *et al.* 2001; Tong & Yin 2002). Recently, the Chaohu section (Anhui Province, eastern China) was proposed as a GSSP candidate for the Induan/Olenekian boundary (IOB), with placement based on: i) the FAD of the conodont *Neospathodus waageni* and ii) below the FAD of the Smithian ammonoids *Flemingites* and *Euflemingites* (Tong *et al.* 2004). In the Tethyan areas, the association of the ammonoids *Flemingites* and *Euflemingites* is classically recognized as the lowermost fauna of the Smithian stage. Yet, these two flemingitids do not represent the oldest Smithian fauna. Therefore, the lowermost ammonoid faunas of the Smithian are not accounted for in the Chinese proposal. Hence, the lowest zone of the Smithian in the mid- and high-paleolatitudes (i.e. the *Hedenstroemia hedenstroemi* Zone of British Columbia and Siberia; **Fig. 11**, see Tozer 1994 and Ermakova 2002, respectively) could not be easily correlated with localities in the equatorial paleolatitudes.

Focusing only on the Smithian, the previous South Chinese subdivisions (e.g. Tong & Yin 2002) are no more precise, since they were essentially based on the work of Chao (1959). The original subdivisions of Chao (1959), e.g. “Flemingitan” and “Owenitan”, are based on the scheme established by Spath (1934). Although the application of Spath’s subdivisions to the ammonoid succession of the Luolou Fm. is correct in a global sense, it can be further refined. Tentative refinements by Chinese workers (see Tong & Yin 2002) were unfortunately based neither on a

systematic revision of the data provided by Chao, nor detailed bed-by-bed sampling. The succession of Smithian ammonoids from Chaohu is reported to include *Flemingites-Euflemingites* Zone and the *Anasibirites* Zone (Tong *et al.* 2004). Very poor preservation may probably explain unusual associations such as *Owenites* or *Juvenites* with together prionitids (*Anasibirites* and *Wasatchites*), or the co-occurence of *Anasibirites* with *Isculitoides*, the latter being typically restricted to the late Spathian.

This study presents for the first time the actual distribution, based on bed-by-bed sampling, of Smithian ammonoids of the Luolou Formation. The zonation presented in this paper is partially new and greatly expands the number of successive paleoequatorial ammonoid faunas (**Fig. 11**). No formal zone names are introduced here and we prefer to use the term "beds" to describe the local faunal sequence. Ultimately, testing the validity and lateral reproducibility of formal zones should await biochronological analysis of data from other basins in conjunction with a fully standardized taxonomy.

3.2.1. "*Hedenstroemia hedenstroemi* beds"

These beds, characterized by the unique occurrence of *Hedenstroemia hedenstroemi*, represent the oldest known Smithian ammonoid fauna in the Luolou Fm. This fauna correlates with the *H. hedenstroemi* Zone of mid- and high-paleolatitudes (e.g. British Columbia and Siberia respectively, see Tozer 1994 and Ermakova 2002). However, the scarcity of Dienerian ammonoids makes it difficult to accurately place the Dienerian-Smithian boundary in the Luolou Fm.

3.2.2. "*Kashmirites densistriatus* beds"

Typically, these beds occur just below the "*Flemingites rursiradiatus* beds" in a sequence of thin limestone beds and small-sized nodules. This subdivision, representing a distinctive faunal association, coincides with the first occurrence of *Kashmirites densistriatus*, which is associated with such diagnostic genera as *Wailiceras*, *Sinoceltites* or *Cordillerites*. Furthermore, the last occurrence of *Paranorites* and *Gyronites* is also recorded in these beds. An exact correlative of this unique fauna does not exist within mid- and high-paleolatitude basins. It has not yet been established whether the "*Kashmirites densistriatus* beds" is approximately equivalent to the upper part of the *H. hedenstroemi* Zone and the lower part of the *Euflemingites romunderi* Zone of mid-paleolatitude sequences, or the lower part of the *Lepiskites kolymensis* Zone of the high-paleolatitude record.

3.2.3. "*Flemingites rursiradiatus* beds"

This subdivision is extremely well documented and contains the most abundant, diverse fauna of the Smithian within the Luolou Fm. Among the most common genera are: *Flemingites*, *Pseudaspidites*, *Submeekoceras*, *Pseudaspenites* and *Mesohedenstroemia*. It is at least partly correlative with the *E. romunderi* Zone from British Columbia (Tozer 1994) and the *L. kolymensis* Zone from Siberia (Ermakova 2002).

3.2.4. "*Owenites koeneni* beds"

Although these beds include different successive faunas, *Owenites koeneni* is common to each of these. The succession is clearly displayed in Jinya and consists of the following horizons in ascending order:

- "*Ussuria* horizon": characterized by the co-occurrence of *Ussuria kwangsiana*, *Metussuria* sp. indet. and *Parussuria compressa*.
- "*Hanielites* horizon": characterized by the simultaneous, but restricted presence of *Hanielites elegans*, *Proharpoceras carinatitabulatus*, and *Paranannites ovum* n. sp. This subdivision is best documented in Yuping. It is usually restricted to a single bed in both Yuping and Jinya areas.
- "*Inyoites* horizon": characterized by the co-occurrence of *Inyoites krystyni* n. sp. and *Pseudoflemingites goudemandi* n. sp.

With the exception of the long ranging and broadly distributed *Pseudosageceras*, the "*Owenites koeneni* beds" have no common species or genus with the in mid- or high-paleolatitude record, thus preventing recognition of exact correlatives. Indeed, the "*Owenites koeneni* beds" are composed of genera typically restricted to the intertropical belt.

3.2.5. "*Anasibirites multiformis* beds"

Diagnostic species occurring in this uppermost subdivision include *Anasibirites multiformis* and *Xenoceltites pauciradiatus* n. sp. This poorly diversified fauna correlates with the *Anawasatchites tardus* Zone of British Columbia (Tozer 1994) and Siberia (Ermakova 2002).

4. Systematics

All systematic descriptions follow the classification established by Tozer (1981, 1994). Biometric analyses follow the procedure of Monnet & Bucher (2005).

4.1. Intraspecific variability: the population approach

Ammonoid species usually exhibit a continuous intraspecific variation ranging from involute, compressed and weakly ornamented variants to more evolute, depressed variants with coarser ornamentation. Within a single species, the frequency of these variants displays a typical normal distribution. This type of variation was coined “First Buckman’s Law of Covariation” by Westermann (1966) and has been well illustrated and discussed by e.g. Dagys & Weitschat (1993), Dagys *et al.* (1999), and Hammer & Bucher (2005).

Generally, robust variants present the most informative characters. Morphologies of smooth and compressed variants are less-well discernible and tend to converge across closely allied species or genera, thus making identification difficult. Thus, recognition of intraspecific variation is a crucial step for species identification. The statistical population approach usually has not been applied to Early Triassic ammonoids, with a few exceptions (e.g. Kummel & Steele 1962; Dagys & Ermakova 1988).

Interestingly, the morphological disparity of Smithian ammonoids seems to be restricted to a small number of morphological “themes”. For example, the convergence of shell shapes is a frequent morphological phenomenon among Smithian ammonoids. The vast majority of shells lack marked ornamentation or are tabulate. Furthermore, the same type of ornamentation is repeated between different families. For instance, an extremely involute and oxycone shape is found in many genera such as: *Hedenstroemia*, *Pseudosageceras* and *Cordillerites*. In the same way, many phylogenetically unrelated genera such as *Flemingites*, *Arctoceras* or *Dieneroceras* may be strigated. In most extreme cases, the suture line must be relied upon to provide key characters at the family level.

4.2. Measurements and statistical tests

The quantitative morphological range of each species is expressed utilizing the four classic geometrical parameters of the ammonoid shell: diameter (D), whorl height (H), whorl width (W) and umbilical diameter (U). However, whorl width measurement is often hindered by corrosion or dissolution of the upward side of the shell.

The three parameters (H, W and U) are plotted in absolute values as well as in relation to diameter (H/D, W/D, and U/D). If a species is represented by at least 30 specimens, the normality of each parameter is graphically assessed by means of a probability plot (Monnet & Bucher, 2005) and statistically tested by mean of a Lilliefors (1967) test. The Lilliefors test is a non-parametric

"closeness of fit" test of normality based on a correction of the Kolmogorov-Smirnov test for a sample with unspecified mean and variance (Lilliefors 1967). It evaluates the null hypothesis that the investigated data have a normal distribution with unspecified mean and variance, whereas the alternative hypothesis is that the investigated data do not have a normal distribution. The result of the test is indicated in the legend of the calculated normal curve associated with the measurements. A "Normal" label indicates that the test cannot reject the null hypothesis of normality (at a confidence level of 95%), while "Not normal" indicates that the hypothesis of a normal distribution is rejected (at a type-I error rate <5%). The normal probability plot presents a graphical test of normality. If the data conform to a normal distribution, the plot will be linear. Other probability density functions will generate departure from a linear plot.

Some species are also quantitatively compared by means of box and mean plots (Monnet & Bucher 2005). The box plot displays the 25^{th}, 50^{th} (median) and 75^{th} percentiles of the range of measures covered by 99% of the specimens from a normally distributed sample. Outliers represent specimens not falling within the normal distribution. Furthermore, the mean plot displays the mean and its associated 95% Confidence Interval. Box and mean plots also allow for the graphical comparison of H, W and U for different species.

4.3. Allometry

Previous graphs and statistical tests focus on the analysis of single parameters, which reflect phenotypic differences. The growth trajectory of H, W and U (isometry or allometry) are also studied in order to detect and quantify possible heterochronic processes, or changes in size-based allometries of the geometry of the shell dimensional parameters.

Isometric growth implies that the parameter of interest has a constant ratio as a function of D, i.e. follows a linear equation. In contrast, allometric growth implies departure from linearity. To test the type of growth of each parameter, its values are fitted both by a linear and exponential equation by means of the reduced major axis fitting method (see Monnet & Bucher 2005). The resulting fitted curves are then tested by means of the coefficient of determination, the dispersion of residuals, and the Z-statistic associated with the allometric exponent. A better fit is obtained if the correlation coefficient tends towards one and the residuals tend to be closely scattered around the line. The Z-statistic tests the null hypothesis that the allometric exponent is equal to one (i.e. isometric growth). In this study, allometry results are displayed as a graph representing the allometric or isometric growth trajectory of H, W and U.

4.4. Systematic descriptions

Repository of figured and measured specimens is abbreviated PIMUZ (Paläontologisches Institut und Museum der Universität Zurich). Locality numbers are reported on the measured sections (**Figs. 2 to 9**).

Class Cephalopoda Cuvier, 1797

Subclass Ammonoidea Zittel, 1884

Order Ceratitida Hyatt, 1884

Superfamily Xenodiscaceae Frech, 1902

Family **Xenoceltitidae** Spath, 1930

Kashmirites Diener, 1913

Type species: *Celtites armatus* - Waagen, 1895, p. 75, pl. 7, figs. 1a-b, 7a-c

Kashmirites armatus (Waagen, 1895)

Pl. 2, Figs.1-10

		1895	*Celtites armatus* - Waagen, p. 75, pl. 7, figs. 1a-b, 7a-c
?	p	1895	*Celtites subrectangularis* - Waagen, p. 73, pl. 7, figs. 6a-c
		1922	*Kashmirites subrobustus* - Welter, p. 121, pl. 9, figs. 13-15
?		2004	*Flemingites* sp. - Tong *et al.*, p. 200, pl. 2, fig. 11, text-fig. 8

Occurrence:

Jin4, 21, 24, 30; FSB1/2; WFB; Sha2; "*Flemingites rursiradiatus* beds".

Description:

Moderately evolute, thick platycone with a subtabulate to tabulate (for robust variant) venter, a rounded to subangular (for robust variant) ventral shoulder and nearly parallel to slightly convex flanks,forming a subquadratic whorl section. Umbilicus with moderately high, perpendicular wall and rounded shoulders. Ornamentation consists of distant, conspicuous ribs arising on umbilical shoulder and fading away on ventral shoulder. Ribs generally prominent near mid-flank, sometimes creating appearance of tubercules on inner whorls. On some specimens, fine radial

growth lines are visible on venter. Suture line ceratitic and simple with high ventral saddle and smaller umbilical saddle.

Measurements:
See **Fig. 12**.

Discussion:
This species is characterized by a wide range of intraspecific variability. Robust variants have a thick quadratic section and subangular ventral shoulders. Suture line illustrated for *Flemingites* sp. by Tong *et al.* (2004) is clearly distinct from that of Flemingitidae, but resembles that of *Kashmirites*.

Kashmirites densistriatus Welter, 1922

Pl. 3, Figs.1-4

		1922	*Kashmirites densistriatus* - Welter, p. 123, pl. 10, figs. 9-16
		1922	*Kashmirites evolutus* - Welter, p. 124, pl. 10, figs. 1-5
		1973	*Anakashmirites evolutus* - Collignon, p. 145, pl. 5, fig. 11
		1973	*Anakashmirites densistriatus* - Collignon, p. 145, pl. 5, fig. 4
		1973	*Anakashmirites oyensi* - Collignon, p. 146, pl. 5, figs. 9-10
v	?	1978	*Eukashmirites* aff. *E. densistriatus* - Guex, pl. 1, fig. 6; pl. 7, figs. 1-4, 12; pl. 8, figs. 2, 5

Occurrence:
Jin64, 67; FW8; "*Kashmirites densistriatus* beds".

Description:
Very evolute, serpenticonic shell, with a broadly arched venter, rounded ventrolateral shoulders, and generally flat, parallel flanks, but slightly convex for thinner specimens. Umbilicus with moderately high, perpendicular wall and subangular shoulders. Variocostate ornamentation with more or less dense, pronounced ribs arising on umbilical shoulder, becoming weakly forward projected before ending abruptly on ventral shoulder. Suture line ceratitic with high ventral and lateral saddle. Umbilical saddle clearly smaller. Suture line of robust variants can be slightly stretched.

Measurements:

See **Fig. 13**.

Discussion:

K. densistriatus could conceivably represent a compressed and finely ribbed variant of *K. evolutus* (see Welter 1922). However, available material is not abundant enough to demonstrate continuous intraspecific variation between these two morphs. *K. densistriatus* is easily distinguished from *K. armatus* by its more evolute coiling, smaller whorl width, and finer ribbing (see **Fig. 20**). This species is used as an index for the "*Kashmirites densistriatus* beds".

Preflorianites Spath, 1930

Type species: *Danubites strongi* - Hyatt & Smith, 1905, p. 165, pl. 9, figs. 4-10

Preflorianites* cf. *P. radians Chao, 1959

Pl. 3, Figs. 5-11

1959 *Preflorianites radians* - Chao, p. 196, pl. 3, figs. 6-8

1968 *Preflorianites* cf. *P. radians* - Zakharov, p. 137, pl. 27, figs. 5-6

Occurrence:

Jin4, 10, 13, 15, 23, 24, 28, 29, 30, 51; FSB1/2; "*Flemingites rursiradiatus* beds".

Description:

Evolute, moderately compressed shell with a narrowly rounded to subangular venter (may vary from angular to subtabulate), rounded ventral shoulders, and parallel to slightly convex flanks. Umbilicus moderately high with perpendicular wall and rounded shoulders. Ornamentation consists of more or less dense, straight, radial ribs arising on umbilical shoulders and fading away low on ventral shoulders. Some very thin, radial, growth lines visible, especially on more compressed specimens. Venter completely smooth. Suture line ceratitic with serrated lobes, and ventral lobe more elongated than others.

Measurements:

See **Fig. 14**.

Discussion:

This species essentially differs from *P. strongi* (Hyatt & Smith) by its subtabulate venter, and from *P. toulai* (Smith, 1932) by its more evolute coiling.

Pseudoceltites Hyatt, 1900

Type species: *Celtites multiplicatus* - Waagen, 1895, p. 78, pl. 7, figs. 2a-c

Pseudoceltites angustecostatus Welter, 1922

Pl. 4, Figs. 1-7

	1922	*Xenodiscus angustecostatus* - Welter, p. 110, pl. 4, figs. 14-17
?	1922	*Xenodiscus oyensi* - Welter, p. 111, pl. 5, figs. 1, 2, 17
	1968	*Anakashmirites angustecostatus* - Kummel & Erben, p. 128, pl. 19, figs. 1-8
	1973	*Anakashmirites angustecostatus* - Collignon, p. 144, pl. 5, figs. 7-8
v ?	1978	*Eukashmirites angustecostatus* - Guex, pl. 7, fig. 4

Occurrence:

Jin12; T5; "*Owenites koeneni* beds".

Description:

Slightly evolute, moderately compressed shell with a circular to broadly rounded venter, rounded ventral shoulders and convex flanks. Umbilicus with high, perpendicular wall and rounded shoulders. Ornamentation consists of dense, radial ribs arising on umbilical shoulder and ending high on ventral shoulders. Radial growth lines clearly visible, especially on ventral shoulder where ribs disappear. Suture line ceratitic with broad saddles, typical of Xenoceltitidae.

Measurements:

See **Fig. 15**.

Discussion:

The morphology of this species is similar to *P.* cf. *P. radians*, but it is slightly more evolute, has a more quadratic whorl section and more pronounced ribs, as well as visible growth lines (see **Fig.**

20). Its ribs are denser and more conspicuous than those of *Preflorianites*. *P. angustecostatus* is also found associated with *Owenites* in Timor and Afghanistan.

Hanielites Welter, 1922

Type species: *Hanielites elegans* - Welter, 1922, p. 145, pl. 14, figs. 7-11

Hanielites elegans Welter, 1922

Pl. 5, Figs. 1-5

	1922	*Hanielites elegans* - Welter, p. 145, pl. 14, figs. 7-11
	1934	*Hanielites elegans* - Spath, p. 243, figs. 82a-d
v	1959	*Hanielites evolutus* - Chao, p. 280, pl. 37, figs. 8-12, text-fig. 36b
v	1959	*Hanielites elegans* var. *involutus* - Chao, p. 281, pl. 37, figs. 4-6, text-fig. 36a
v	1959	*Hanielites rotulus* - Chao, p. 281, pl. 37, figs. 12-15
v	1959	*Owenites kwangsiensis* - Chao, pl. 22, figs. 1, 2, 5, 6

Occurrence:

Jin45; Yu1; "*Owenites koeneni* beds".

Description:

Small, slightly involute, somewhat thick platycone with a subangular to angular venter (sometimes bearing a delicate keel), rounded ventral shoulders, and flat, parallel flanks forming a generally quadratic whorl section. Shallow umbilicus with low, perpendicular wall and slightly rounded shoulders. Ornamentation is variocostate, varying from sinusoidal radiating plications to distinct ribs arising on umbilical shoulders, becoming forward projected low on ventral shoulder, and then crossing venter in a weak manner. Ribs become stronger approaching ventral shoulders and broken on ventral shoulders. Suture line ceratitic with broad lateral lobe.

Measurements:

See **Fig. 16**.

Discussion:

This species is characteristic of the lowermost "*Owenites koeneni* beds" and is often found associated with *Proharpoceras*.

Hanielites carinatitabulatus Chao, 1959

Pl. 5, Figs. 9a-c

v 1959 *Hanielites carinatitabulatus* - Chao, p. 282, pl. 37, figs. 1-3, text-fig. 36c

Occurrence:

Jin45; Yu1; "*Owenites koeneni* beds".

Description:

Moderately involute, thick platycone with a subtabulate to broadly rounded venter (bearing delicate keel), rounded ventral shoulders and flat to slightly convex flanks forming a robust, quadratic whorl section. Umbilical wall higher than *H. elegans*, but with oblique slope and rounded shoulders. Ornamentation consists of very distinct, prorsiradiate ribs arising on umbilical shoulder, developing great intensity on ventral shoulder, becoming strongly forward projected and rapidly disappearing near keel. No thin plications are visible. Ribs form weak tuberculation on inner whorls. Suture line ceratitic with saddles decreasing in size from venter to umbilicus.

Measurements:

See **Fig. 16** and **appendix 1**.

Discussion:

This species is rare and is represented by a single specimen in Chao's collection and by only two specimens in our own material. *H. carinatitabulatus* differs from *H. elegans* by its more prominent ribs, absence of thin plications, its more involute coiling, and its deeper, narrower umbilicus.

***Hanielites gracilus* n. sp.**

Pl. 5, Figs. 6-8

Occurrence:

Jin10, 45; "*Owenites koeneni* beds".

Diagnosis:

Hanielites with a moderately involute, laterally compressed shell, a keeled, angular venter, and dense, but weak plications and prorsiradiate ribs.

Holotype:
PIMUZ 25834, Loc. Jin45, Jinya, "*Owenites koeneni* beds", Smithian.

Etymology:
Species name refers to the alternation of small, thin ribs and plications.

Description:
Moderately involute, compressed shell with an angular venter bearing a distinctive keel, rounded ventral shoulders, and parallel flanks forming a subrectangular whorl section. Ornamentation consists of an alternation of thin prorsiradiate plications and ribs arising on flank above umbilical shoulder, then projecting forward onto venter and terminating near keel. Suture line ceratitic with broad, markedly indented lateral lobe. A small auxiliary series is also present.

Measurements:
See **Fig. 16** and **appendix 1**.

Discussion:
This species is quite rare, but is easily distinguished from *H. elegans* by its more involute coiling, more angular ventral shoulders and its denser, more conspicuous alternation of ribs and plications. It also differs from *H. carinatitabulatus* by the presence of thin plications and a shallower umbilicus.

***Hanielites angulus* n. sp.**

Pl. 5, Figs. 10a-d

Occurrence:
Yu1; "*Owenites koeneni* beds".

Diagnosis:
Laterally compressed *Hanielites* with a subangular to narrowly rounded venter, rounded ventral shoulders, and weak, forward projecting, biconcave ribs disappearing near the venter.

Holotype:
PIMUZ 25836, Loc. Yu1, Yuping, "*Owenites koeneni* beds", Smithian.

Etymology:
Species name refers to the angular shape of the venter.

Description:
Moderately involute, compressed platycone with a subangular to narrowly rounded venter (without keel), rounded ventral shoulders and parallel flanks. Umbilicus with low, perpendicular wall and rounded shoulders. Ornamentation consists of slightly prorsiradiate, biconcave ribs, thin and weak at umbilical shoulder, stronger on flank, disappearing on ventral shoulder. Suture line unknown.

Measurements:
See **Fig. 16** and **appendix 1**.

Discussion:
This new species is represented by a single specimen. It is tentatively assigned to *Hanielites* because of its distinct morphology, but its peculiar ornamentation appears to be quite uncommon. However, the erection of a new genus cannot be justified on the basis of this single, fragmentary specimen.

Xenoceltites Spath, 1930

Type species: *Xenoceltites subevolutus* = *Xenodiscus* cf. *X. comptoni* (non Diener) - Frebold, 1930, pl. 3, figs. 1-3

***Xenoceltites variocostatus* n. sp.**

Pl. 6, Figs. 1-14; Pl. 7, Figs. 1-6

? 1895 *Dinarites coronatus* - Waagen, p. 27, pl. 7, figs. 9-10

Occurrence:

Jin33, 90, 91, 101, 105, 106; FW7, 12; NW13; Yu5, 6; "*Anasibirites multiformis* beds".

Diagnosis:
Evolute *Xenoceltites* with extremely variocostate ribbing on inner whorls.

Holotype:
PIMUZ 25838, Loc. NW13, Waili, "*Anasibirites multiformis* beds", Smithian.

Etymology:
Species name refers to its variocostate ribbing.

Description:
Slightly evolute, compressed platycone with rounded venter, rounded ventral shoulders, and slightly convex flanks, becoming gently convergent at a point low on ventral shoulder. Whorl section compressed in juvenile stages, becoming ovoid at maturity. Umbilicus wide, with moderately deep, oblique wall and rounded shoulders. For most juvenile specimens, ornamentation consists of conspicuous, sinuous, prorsiradiate ribs arising on umbilical shoulder, becoming strongly forward projected at ventral shoulders, and crossing venter with distinctive adoral curve. On some juvenile specimens, this strong forward projection and adoral curve imparts a somewhat crenulated appearance to the venter. These large, distinctive ribs gradually lose strength and eventually disappear in later stages. Growth lines are also visible and may be pronounced, particularly on adult whorls. Suture line ceratitic, typical of Xenoceltitidae, with broad ventral saddle and very small umbilical saddle.

Measurements:
See **Fig. 17**. Whorl height and width as well as umbilical diameter exhibit significant allometric growth. Height tends to increase more rapidly than diameter for larger specimens.

Discussion:
Spath (1934) distinguished three species within the genus *Xenoceltites*: *X. subevolutus*, *X. spitsbergensis* and *X. gregoryi.* These species essentially differ from each other according to their umbilical diameter and costation. The ornamentation on the new Chinese specimens invites comparison with *X. spitsbergensis* (e.g. bulges, ribs with a strong forward projection, and thin growth lines), but *X. spitsbergensis* has a more serpenticonic coiling. *Xenoceltites subevolutus*

seems to have about the same degree of involution as our specimens, but its ornamentation is less conspicuous and its whorl section is more compressed (see Weitschat & Lehmann 1978). The measurements of *X. matheri* (Dagys & Ermakova 1990) are extremely close to our species, but it differs by its very weak ornamentation. Regardless of the motivation of various authors in differentiating between species, they are all morphologically similar and display wide ranges of intraspecific variation.

***Xenoceltites pauciradiatus* n. sp.**

Pl. 7, Figs. 7-9

Occurrence:

Jin33; Yu5; 6; "*Anasibirites multiformis* beds".

Diagnosis:

Thick whorled *Xenoceltites* with moderately involute coiling. Variocostate ribbing restricted to the inner whorls.

Holotype:

PIMUZ 25858, Loc. Jin33, Jinya, "*Anasibirites multiformis* beds", Smithian.

Etymology:

Species name refers to its weak ornamentation.

Description:

Moderately involute, compressed platycone with a highly arched venter, rounded ventral shoulders, and convex flanks with maximum curvature near umbilical shoulder. Umbilicus with moderately high, obliquely sloped wall and rounded shoulders. For juvenile specimens, ornamentation consists of very thin straight ribs which appear as weak tubercules on inner whorls. Ornamentation on mature specimens consists only of fine, dense growth lines. Suture line unknown.

Measurements:

See **Fig. 18**.

Discussion:

X. pauciradiatus n. sp. differs from *X. variocostatus* n. sp. by its more involute coiling, its greater whorl height in relation to diameter and its very weak ornamentation on adult specimens. Unfortunately, we did not find a sufficient number of specimens to statistically justify the erection of a new species. However, its phenotypic differences are hopefully characteristic.

Xenoceltitidae gen. indet.

Pl. 8, Figs. 8a-d

Occurrence:

Yu22; "*Anasibirites multiformis* beds".

Description:

Evolute, compressed shell with a low rounded to subtabulate venter, rounded ventral shoulders and slightly convex flanks. Character of umbilicus difficult to determine on fragmentary specimen, but umbilical depth appears moderate with perpendicular wall and rounded shoulders. Ornamentation on body chamber consists only of very thin growth lines and distant plications. Suture line ceratitic with three broad saddles.

Discussion:

The overall shape of this single specimen, its evolute coiling and suture line indicate that it probably belongs to Xenoceltitidae. It apparently differs from *X. variocostatus* and *X. pauciradiatus* by its more evolute coiling.

***Sinoceltites* n. gen.**

Type species: *Sinoceltites admirabilis* n. gen., n. sp.

Composition of the genus:

Type species only.

Diagnosis:

Small sized, moderately evolute xenoceltitid with rounded whorl section and forward projected ribs that cross the venter. Mature body chamber with growth striae only.

Etymology:
Genus name refers to China.

Occurrence:
"*Kashmirites densistriatus* beds".

Discussion:
This genus, with its rounded whorl shape and distinctive ribs that cross the venter, differs from all other xenoceltitids, which generally are more evolute and laterally compressed.

***Sinoceltites admirabilis* n. gen, n. sp.**

Pl. 8, Figs. 1-6

Diagnosis:
As for the genus.

Holotype:
PIMUZ 25861, Loc. Jin61, Waili, "*Kashmirites densistriatus* beds", Smithian.

Etymology:
From the Latin, meaning admirable.

Occurrence:
Jin61, 64; "*Kashmirites densistriatus* beds".

Description:
Moderately evolute, slightly compressed shell with a broadly arched venter, rounded ventral shoulders, and nearly parallel flanks. Umbilicus with moderately high, oblique wall and rounded shoulders. Ornamentation consists of convex growth lines and prorsiradiate ribs that weaken on the ventral shoulder before crossing the venter. Suture line unknown, all specimens completely recrystallized.

Measurements:

See **Fig. 19**.

Discussion:
This species is morphologically close to *Juvenites*? *tenuicostatus* (Dagys & Ermakova 1990), but it is thinner and more evolute. It differs from other xenoceltitids by its overall shape and smaller adult size, and by its ribs that tend to weaken near the ventral shoulder, but still cross the venter. However, its measurements exhibit the same overall percentages for height, width and diameter (see **Fig. 20**).

***Weitschaticeras* n. gen.**

Type species: *Weitschaticeras concavum* n. gen., n. sp.

Composition of the genus:
Type species only.

Diagnosis:
Laterally compressed, serpenticonic Xenoceltitidae with a tabulate venter and variable concave ribs.

Etymology:
Named after W. Weitschat.

Occurrence:
"*Owenites koeneni* beds".

Discussion:
This new genus is easily distinguished by its conspicuous concave ribs, and its tabulate venter, which is relatively rare among the Xenoceltitidae.

***Weitschaticeras concavum* n. gen., n. sp.**

Pl. 8, Figs. 9a-d

Diagnosis:

As for the genus.

Holotype:
PIMUZ 25869, Loc. Jin27, Jinya, "*Owenites koeneni* beds", Smithian.

Etymology:
Species name refers to the characteristic concave ribs.

Occurrence:
Jin27; "*Owenites koeneni* beds".

Description:
Evolute serpenticone, with a tabulate venter, rounded ventral shoulders and parallel flanks. Shallow umbilicus with low, oblique wall and rounded shoulders. Ornamentation consists of variable, but distinct concave ribs that cross venter. Suture line ceratitic, typical for Xenoceltitidae, with broad lateral saddle.

Measurements:
See **appendix 1**.

Family **Melagathiceratidae** Tozer, 1971

***Hebeisenites* n. gen.**

Type species: *Kashmirites varians* - Chao, 1959, p. 277, pl. 36, figs. 1-6, 13; pl. 37, figs. 18-19, 26-28

Composition of the genus:
Three species: *Kashmirites varians* Chao (1959), *Hebeisenites evolutus* n. gen., n. sp., and *Hebeisenites compressus* n. gen., n. sp.

Diagnosis:
Laterally compressed Melagathiceratidae with moderate to very evolute coiling, a laterally compressed whorl section, variable constrictions and a ceratitic suture line.

Etymology:
Named after M. Hebeisen.

Occurrence:
"*Flemingites rursiradiatus* beds" and "*Owenites koeneni* beds".

Discussion:
This new genus has a ceratitic suture line and its whorl section is completely different than the more globular *Thermalites*, and *Juvenites* type species: *J. kraffti*. Thus, a new genus is erected based principally on its more compressed whorl section and ceratitic suture line.

***Hebeisenites varians* (Chao, 1959) n. gen.**

Pl. 9, Figs. 1-11

	1959	*Kashmirites varians* - Chao, p. 277, pl. 36, figs. 1-6, 13; pl. 37, figs. 18-19, 26-28
?	1959	*Kashmirites prosiradiatus* - Chao, p. 278, pl. 36, fig. 7; pl. 37, figs. 29-31
?	1959	*Pseudoceltites contractus* - Chao, p. 275, pl. 36, fig. 8
?	1959	*Pseudoceltites ellepticus* - Chao, p. 277, pl. 36, figs. 9-12, 14-15, 30
?	1959	*Pseudoceltites kwangsianus* - Chao, p. 276, pl. 36, figs. 16-17

? p 1994 *Thermalites needhami* - Tozer, p. 54, pl. 22, figs. 5a-c only

Occurrence:

Jin4, 11, 13, 23, 24, 28, 29, 30, 51; Sha1; T6, T50; "*Flemingites rursiradiatus* beds". Jin10; "*Owenites koeneni* beds".

Description:

Moderately evolute, small, compressed platycone with a subtabulate to rounded venter, subangular to abruptly rounded ventral shoulders, and parallel flanks gradually convergent to ventral shoulder, forming subrectangular to subquadratic whorl section. Shallow umbilicus with low, perpendicular wall and rounded shoulders. Ornamentation is characteristic for the species and consists of several different, but distinct constrictions that may be prorsiradiate and/or rursiradiate. Also, body chamber of mature specimens may exhibit small plications. These constrictions and plications cross the venter, but generally weaken before doing so. This species exhibits a very wide range of intraspecific variation with respect to height, width and ornamentation. Suture line weakly ceratitic and very simple, consisting of high ventral saddle and unique small, but wide lateral saddle.

Measurements:

See **Fig. 21**. Whorl height exhibits isometric growth, whereas width and umbilical diameter display allometric growth. The umbilicus tends to become proportionally more open as diameter increases.

Discussion:

Initially, this species was placed within the genus *Kashmirites* by Chao (1959). However, its very simple suture line and ornamentation consisting of distinct constrictions justify its assignment to the Melagathiceratidae. This genus represents an extreme variant of the family with its conspicuous lateral compression and moderately evolute coiling. The suture line initially illustrated by Chao appears to be quite peculiar and may be the result of excessive grinding.

Tozer (1994) illustrated a possible variant of *Thermalites needhami*, which is very much similar to *H. varians*, but he did not make a definitive assignment regarding the specimen, since its suture was not visible. Furthermore, this variant appears to be quite different from other specimens he assigned to this species (see pl. 22, figs. 6a-b). Therefore, it probably should be assigned to *H. varians*.

***Hebeisenites evolutus* n. sp.**

Pl. 9, Figs. 12-17

Diagnosis:

Hebeisenites with very evolute coiling, an arched venter and deep constrictions.

Holotype:

PIMUZ 25886, Loc. Jin10, Jinya, "*Flemingites rursiradiatus* beds", Smithian.

Etymology:

The species name refers to its evolute coiling.

Occurrence:

Jin28, 29, 30; "*Flemingites rursiradiatus* beds". Jin10; "*Owenites koeneni* beds".

Description:

Very evolute, moderately compressed, nearly serpenticonic shell with an arched venter, rounded ventral shoulders, and gently convex flanks. Umbilicus with perpendicular, moderately high wall and rounded shoulders. Ornamentation characteristic of Melagathiceratidae with deep, variable constrictions. Suture line possesses two different sized saddles, and appears to be goniatitic, but this may be due to excessive preparation, or the denticulations, if present, may be very few and very small.

Measurements:

See **Fig. 22**.

Discussion:

This species can be distinguished from *H. varians* by its more evolute coiling (**Fig. 24**) and deeper constrictions.

***Hebeisenites compressus* n. gen., n. sp.**

Pl. 9, Figs. 18-25

Diagnosis:

Evolute, very compressed small sized *Hebeisenites* with a tabulate venter, constrictions and a very simple suture line.

Holotype:

PIMUZ 25888, Loc. Jin30, Jinya, "*Flemingites rursiradiatus* beds", Smithian.

Etymology:

Refers to its extreme lateral compression.

Occurrence:

Jin23, 28, 29, 30; "*Flemingites rursiradiatus* beds".

Description:

Evolute, very compressed, small shell with a tabulate to subtabulate venter, nearly angular ventral shoulders, and slightly convex flanks. Shallow umbilicus with oblique, low wall and rounded shoulders. Ornamentation consists of distinctive sinuous constrictions and plications. Suture line very simple, with large lateral saddle and two large lobes. Lobes not well defined, but may be ceratitic.

Measurements:

See **Fig. 23**.

Discussion:

This species can be distinguished from *H. varians* and *H. evolutus* by its evolute coiling, its more compressed shell, and its tabulate to subtabulate venter **(Fig. 24)**.

***Jinyaceras* n. gen.**

Type species: *Jinyaceras bellum* n. gen., n. sp.

Composition of the genus:

Type species only.

Diagnosis:

Laterally compressed Melagathiceratidae with moderately evolute coiling, weakly convergent flanks, and variable, prorsiradiate constrictions.

Etymology:

Genus name refers to the small town of Jinya (Guangxi, South China).

Occurrence:

"*Flemingites rursiradiatus* beds" and "*Owenites koeneni* beds".

Discussion:

Jinyaceras is distinguished from *Hebeisenites* by its more involute coiling, its more broadly arched venter, and its thicker whorls; from *Juvenites* by its more compressed shape.

***Jinyaceras bellum* n. gen., n. sp.**

Pl. 10, Figs. 1-19

Diagnosis:

As for the genus.

Holotype:

PIMUZ 25894, Loc. Jin28, Jinya, "*Flemingites rursiradiatus* beds", Smithian.

Etymology:

From the Latin for "handsome".

Occurrence:

Jin4, 11, 13, 23, 26, 28, 30, 41; FW2, 3, 4, 5; Sha1; T6, T50; "*Flemingites rursiradiatus* beds". Jin10; "*Owenites koeneni* beds".

Description:

Moderately evolute, subglobular shell with a broadly arched to nearly circular venter, rounded ventral shoulders and flanks varying from convex to broadly convergent from umbilical shoulder to circular venter. Umbilicus with moderately high, perpendicular wall and subangular shoulders.

Umbilical width varies with amount of lateral compression. Ornamentation consists of variable, but distant prorsiradiate constrictions, which form very small, compact plications on body chamber of mature specimens. Constrictions nearly disappear on venter. Suture line simple and ceratitic, with a high and wide ventral saddle and smaller lateral saddle.

Measurements:

See **Fig. 25**. Whorl height is characterized by allometric growth, while umbilical diameter exhibits isometric growth. Whorl height increases proportionally as diameter increases.

Discussion:

This species can be distinguished from *Hebeisenites varians* by its obviously more involute coiling and its conspicuously projected ornamentation. It is closely allied to *Juvenites septentrionalis* Smith (1932) by its similar ornamentation, but the latter's juvenile whorls are more involute. The suture line of juvenitids is also different (i.e. goniatitic).

Juvenites Smith, 1927

Type species: *Juvenites kraffti* - Smith, 1927, p. 23, pl. 21, figs. 1-10

Juvenites* cf. *J. kraffti Smith, 1927

Pl. 10, Figs. 20-23

1927 *Juvenites kraffti* - Smith, p. 23, pl. 21, figs. 1-10

1932 *Juvenites kraffti* - Smith, p. 109, pl. 21, figs. 1-10

Occurrence:

Jin23, 30, 51; "*Flemingites rursiradiatus* beds".

Description:

Slightly evolute, subglobular *Juvenites* with an arched venter and a more or less depressed whorl section. Umbilicus with perpendicular, relatively high wall and rounded shoulders. Ornamentation consists of distant, forward projected constrictions. Suture line unknown for our specimens.

Measurements:

See **appendix 1**.

Discussion:

This species is distinguished by its very depressed whorl section and its somewhat more evolute coiling, but its scarcity prevents us from utilizing statistics to assign our specimens to *J. kraffti*.

***Juvenites procurvus* n. sp.**

Pl. 22, Figs. 6-12

? 1959 *Juvenites septentrionalis* - Chao, p. 289, pl. 25, figs. 6-10

Diagnosis:

Juvenites with dense, but distinct, straight constrictions projected toward the aperture.

Holotype:

PIMUZ 26010, Loc. T11, Tsoteng, "*Owenites koeneni* beds", Smithian.

Etymology:

Species name refers to its forward projected constrictions.

Occurrence:

Jin18, 27, 45; T5, 11, 12; Yu3; "*Owenites koeneni* beds".

Description:

Moderately involute, globular shell with an arched venter and flanks convergent from umbilical shoulders to rounded venter (without distinct ventral shoulders). Umbilicus with a high, nearly perpendicular wall and somewhat abruptly rounded shoulders. Ornamentation consists of dense, straight, forward projected constrictions, becoming denser on mature body chamber. Constrictions appear more prominent near umbilicus. Suture line ceratitic with two broad saddles and a weakly indented lateral lobe.

Measurements:

See **Fig. 26**.

Discussion:

This species is easily distinguished from other juvenitids by its straight, strongly forward, projected constrictions, which are denser on its body chamber than are those of *J. septentrionalis.* During preparation of the suture line, a weak indentation of the lateral lobe was revealed. Tozer (1981) divided the Melagathiceratidae according to the suture line (ceratitic or goniatitic). Many of the Melagathiceratidae illustrated in this study exhibit ceratitic suture lines, thus, contradicting Tozer's interpretation. Therefore, it is safe to assume that many genera of this family probably do not have a goniatitic suture line. However, *J. procurvus* is characterized by its globular shape and distinct constrictions, which are diagnostic of *Juvenites*.

Superfamily Meekocerataceae Waagen, 1895

Family **Proptychitidae** Waagen, 1895

Paranorites Waagen, 1895

Type species: *Paranorites ambiensis* - Waagen, 1895, p. 158

***Paranorites jenksi* n. sp.**

Pl. 10, Figs. 24-26

? 1959 *Paranorites ellipticus* - Chao, p. 217, pl. 10, figs. 9-10, text-fig. 16a

Diagnosis:
Evolute proptychitid with slightly convex flanks, a subtabulate venter and sinuous plications near the umbilicus.

Holotype:
PIMUZ 25917, Loc. Jin67, Waili, "*Kashmirites densistriatus* beds", Smithian.

Etymology:
Named after J. Jenks.

Occurrence:
Jin66, 67; "*Kashmirites densistriatus* beds".

Description:
Slightly involute, compressed platycone with a subtabulate venter, rounded ventral shoulders on mature specimens (slightly angular for juveniles), and nearly parallel flanks with weak curvature at mid-flank. Umbilicus with high, overhanging wall and narrowly rounded shoulders. Ornamentation consists of very thin growth lines and distant plications arising near umbilicus and disappearing on upper flanks. These plications are especially visible on juvenile specimens. Ceratitic suture line typical of proptychitids with elongated, leaning saddles and indented lobes as well as a complex auxiliary series.

Measurements:

See **appendix 1**.

Discussion:

This species is very similar in shape to *Paranorites ambiensis* Waagen (1895), but it clearly differs by its less complex suture line, which is actually closer to that of *Koninckites*.

Pseudaspidites Spath, 1934

Type species: *Aspidites muthianus* - Krafft & Diener, 1909, p. 59, pl. 6, fig. 5; pl. 15, figs. 1-2

Pseudaspidites muthianus (Krafft & Diener, 1909)

Pl. 11, Figs. 1-10; Pl. 12, Figs. 1-4

	1932	*Clypeoceras muthianum* - Smith, p. 64, pl. 27, figs. 1-7
p	1932	*Ussuria waageni* - Smith, pl. 21, figs. 34-36 only
	1934	*Pseudaspidites muthianus* - Spath, p. 164
v	1959	*Pseudaspidites lolouensis* - Chao, p. 229, pl. 13, figs. 17-21, text-figs. 20a, 21a
v	1959	*Pseudaspidites kwangsianus* - Chao, p. 230, pl. 12, figs. 6-8, text-fig. 21d
v	1959	*Pseudaspidites simplex* - Chao, p. 231, pl. 13, figs. 6-13; pl. 45, figs. 5-7, text-fig. 20b, 21b
v	1959	*Pseudaspidites stenosellatus* - Chao, p. 231, pl. 13, figs. 4-5; pl.45, fig.8, text-fig. 21c
v	1959	*Pseudaspidites aberrans* - Chao, p. 232, pl. 13, figs. 14-15, text-fig. 20d
v	1959	*Pseudaspidites longisellatus* - Chao, p. 232, pl. 13, figs. 1-3, text-fig. 20c
?	1959	*Proptychites pakungensis* - Chao, p. 236, pl. 18, figs. 1-2
v	1959	*Proptychites hemialis* var. *involutus* - Chao, p. 237, pl. 15, figs. 13-16, text-fig. 24d
?	1959	*Proptychites markhami* - Chao, p. 239, pl. 15, figs. 3-5, text-fig. 23c
v	1959	*Proptychites angusellatus* - Chao, p. 240, pl. 15, figs. 1-2
v	1959	*Proptychites sinensis* - Chao, p. 240, pl. 16, figs. 5-6; pl. 17, figs. 14-16, text-fig. 22c
v	1959	*Proptychites latilobatus* - Chao, p. 243, pl. 16, figs. 1-2; pl. 19, figs. 4-5
v	1959	*Proptychites abnormalis* - Chao, p. 243, pl. 16, figs. 3-4
v	1959	*Clypeoceras lenticulare* - Chao, p. 225, pl. 12, figs. 3-5, text-fig. 19b
v	1959	*Clypeoceras tsotengense* - Chao, p. 225, pl. 12, figs. 1-2
?	1959	*Clypeoceras kwangiense* - Chao, p. 226, pl. 17, figs. 1-2, text-fig. 19a
v	1959	*Ussuriceras* sp. indet. - Chao, p. 247, pl. 19, fig. 1

v 1959 *Pseudohedenstroemia magna* - Chao, p. 265, pl. 41, figs. 13-16; pl. 45, figs. 1-2, text-fig. 32b

1962 *Pseudaspidites muthianus* - Kummel & Steele, p. 673

Occurrence:

Jin4, 11, 13, 15, 21, 23, 24, 28, 29, 30, 51; FSB1/2; WFB; FW2, 3, 4, 5; Sha1, 2; T6, T50; "*Flemingites rursiradiatus* beds". Jin10; "*Owenites koeneni* beds".

Description:

Very involute, compressed platycone with a subtabulate venter for mature specimens (rounded for juveniles), abruptly rounded to slightly angular ventral shoulders, and flat to slightly convex flanks. Narrow umbilicus, with high, perpendicular, wall and distinctive, abruptly rounded shoulder, similar to Arctoceratidae. Although most specimens are smooth with no discernable ornamentation, a few bear distant, straight or flexuous ribs. Umbilical bullae are present on only two specimens. When well preserved, suture line exhibits distinctly phylloid saddles and well individualized auxiliary lobe. Saddles tend to be curved adorally. If preparation is insufficient or preservation is poor, suture line can appear more or less complex (e.g. loss of the curved saddles, see **pl. 11, figs. 1d and 7e-10**).

Measurements:

See **Fig. 27**. Whorl height and umbilical diameter exhibit allometric growth. Estimated diameter of largest specimen exceeds 20 cm.

Discussion:

Preservation quality as well as laboratory preparation methods can directly affect the overall shape of these particular specimens, thus making it possible to confuse their identity with certain other genera, e.g. the Arctoceratidae. Likewise, the quality of preservation of this particular type of suture line can alter its appearance in such a manner that it could easily be mistaken as being representative of numerous different families ranging from the Ussuriidae to the Hedenstroemiidae.

P. wheeleri Kummel & Steele (1962) essentially differs from *P. muthianus* by its suture line, which exhibits a greater individualization of the denticulations of the lobes. This difference may not be valid, and *P. wheeleri* may actually be a variant of *P. muthianus*. This hypothesis must be confirmed by sufficient measurements of *P. wheeleri*. Similarly, if other specimens with

umbilical bullae are found, their morphological range must be determined to confirm whether the form is a variant.

***Pseudaspidites* sp. indet.**

Pl. 12, Figs. 6a-d

Occurrence:
Jin27; "*Owenites koeneni* beds".

Description:
Morphologically similar to *P. muthianus*, but laterally compressed with nearly parallel flanks. Suture line similar to that of *P. muthianus*.

Measurements:
See **appendix 1**.

Discussion:
Since *Pseudaspitidites* sp. indet. is represented by only one specimen, it cannot be assigned to *P. muthianus* with any degree of certainty.

***Xiaoqiaoceras* n. gen.**

Type species: *Xiaoqiaoceras involutus* n. gen, n. sp.

Composition of the genus:
Type species only.

Diagnosis:
Proptychitid with extremely involute coiling and a relatively simple suture line.

Etymology:
Named after Wan Xiaqiao (Beijing).

Occurrence:

"*Flemingites rursiradiatus* beds".

Discussion:
The morphology of this genus is typical of proptychitids, except for its extremely involute coiling (occluded umbilicus). Compared to other proptychitid genera, its simplified suture line differentiates this genus within the family.

***Xiaoqiaoceras involutus* n. gen., n. sp.**

Pl. 13, Figs. 12-16

Diagnosis:
As for the genus.

Holotype:
PIMUZ 25948, Loc. Jin4, Jinya, "*Flemingites rursiradiatus* beds", Smithian.

Etymology:
Species name refers to its involute coiling.

Occurrence:
Jin4, 23, 30, 51; "*Flemingites rursiradiatus* beds".

Description:
Extremely involute shell, with a subtabulate to rounded venter, rounded ventral shoulders, and slightly convex flanks. Umbilicus occluded, but rapid increase in whorl width forms distinctly rounded umbilical shoulders. Ornamentation consists only of very thin growth lines. Suture line is simplified compared to other proptychitids with small saddles, and with broadly denticulated lobes. Lateral lobe is broad, trifid and deeply indented. An auxiliary series is present but less complex than, for instance *P. muthianus*.

Measurements:
See **Fig. 28**.

Discussion:

This species can be distinguished from other proptychitids by its extremely involute coiling and its peculiar, simplified suture line. However, as with all proptychitids, the suture line exhibits an obvious auxiliary series. This characteristic suture line may be a consequence of its extremely involute coiling and morphology.

Lingyunites Chao, 1950

Type species: *Lingyunites discoides* - Chao, 1950, p. 2, pl. 1, fig. 1

Lingyunites discoides Chao, 1950

Pl. 13, Figs.1-8

1950 *Lingyunites discoides* - Chao, p. 2, pl. 1, figs. 1a-b, text-fig. 1

1959 *Lingyunites discoides* - Chao, p. 223, pl. 11, figs. 12-16, text-fig. 18

Occurrence:

Jin4, 13, 15, 23, 28, 29, 30, 41, 51; "*Flemingites rursiradiatus* beds". Jin10; "*Owenites koeneni* beds".

Description:

Very involute, discoidal shell, with a subtabulate to tabulate venter, abruptly rounded to slightly angular ventral shoulders, and nearly flat flanks with maximum curvature at mid-flank. Umbilicus very narrow, with moderately high, perpendicular wall and narrowly rounded shoulders. Ornamentation generally consists of very weak plications on flank near umbilicus, but a few small specimens exhibit sinuous plications across entire flank. Suture line ceratitic with three principal saddles and an individualized auxiliary series. Lateral saddle is turned toward the umbilicus and resembles suture line of *Pseudaspidites*.

Measurements:

See **Fig. 29**.

Discussion:

This species can easily be confused with small specimens of *Mesohedenstroemia kwangsiana* due to its subtabulate venter. Furthermore, if the suture line is not well preserved, it can exhibit a

similar, complex appearance. This genus, with its very involute coiling, is closely related to *Clypeoceras*, differing only by its subtabulate to tabulate venter. Measurements reported by Chao (1959) correspond to ours, but the whorl width of Chao's specimens appears to be somewhat wider.

***Nanningites* n. gen.**

Type species: *Nanningites tientungense* n. gen.

Composition of the genus:
Type species only.

Diagnosis:
Proptychitid with extremely involute coiling, a distinctive bicarinate venter and very angular ventral shoulders.

Etymology:
Genus name refers to the city of Nanning (Guangxi).

Occurrence:
"*Flemingites rursiradiatus* beds".

Discussion:
The ornamentation of *Nanningites* closely resembles that of *Lingyunites discoides* Chao (1950), but *N. tientungense* is clearly distinguished by its distinctive bicarinate venter and its nearly closed umbilicus.

Nanningites tientungense (Chao, 1959) **n. gen.**

Pl. 13, Figs. 9-11

?	1909	*Aspidites spitiensis* - Krafft & Diener, p. 54, pl. 16, figs. 3-8
	1959	*Clypeoceras tientungense* - Chao, p. 228, pl. 17, figs. 7-9
	1959	*Clypeoceras ensanuforme* - Chao, p. 227, pl. 17, figs. 10-13, 16

Occurrence:
Jin23, 29, 30; Sha1; T6, T50; "*Flemingites rursiradiatus* beds".

Description:
Extremely involute, discoidal shell with a generally tabulate venter (bicarinate on some specimens), a nearly closed umbilicus, angular ventral shoulders, and weakly convex flanks. Umbilicus extremely narrow, with oblique, moderately high wall and abruptly rounded shoulder. Ornamentation consists of sinuous, forward projected plications, becoming more prominent on outer whorls. Fine growth lines parallel to plications occasionally visible. Ceratitic suture line appears less complex than that of *Lingyunites discoides*, but since it is not well preserved, considerable doubt exists regarding systematic affinities of this species.

Measurements:
See **appendix 1**.

***Wailiceras* n. gen.**

Type species: *Wailiceras aemulus* n. gen, n. sp.

Composition of the genus:
Type species only.

Diagnosis:
Smooth proptychitid with very involute**,** egressive coiling, and a tabulate venter.

Etymology:
The genus name refers to the Waili village (Guangxi, South China).

Occurrence:
"*Kashmirites densistriatus* beds".

Discussion:
This genus exhibits strong affinities with Dienerian proptychitids such as *Koninckites*, but it also has its own distinctive characteristics, e.g. egressive coiling, a tabulate venter and a perpendicular

umbilical wall. It also invites comparison with younger proptychitids such as *Pseudaspidites*, and thus, may represent a transitional morphology between Dienerian and Smithian proptychitids. The suture line has a well individualized auxiliary series, which indicates a close relationship with proptychitids rather with meekoceratids.

***Wailiceras aemulus* n. gen., n. sp.**

Pl. 14, Figs. 1-9

? 1909 *Meekoceras infrequens* - Krafft & Diener, p. 44, pl. 30, figs. 7a-d

Diagnosis:
As for the genus.

Holotype:
PIMUZ 25953, Loc. Jin61, Jinya, "*Kashmirites densistriatus* beds", Smithian.

Etymology:
Name from the Latin, meaning "imitating", and referring to its resemblance to the genus *Meekoceras*.

Occurrence:
Jin61, 64, 65, 67, 68; FW8; "*Kashmirites densistriatus* beds".

Description:
Very involute, compressed, discoidal shell with a tabulate venter, very angular ventral shoulders, and slightly convex flanks having maximum curvature at mid-flank. Shell exhibits egressive coiling. Umbilicus relatively narrow, with high, perpendicular wall and abruptly rounded shoulders. Specimens are generally smooth, but larger sizes may exhibit very weak plications parallel to growth lines. Thin, weak, forward projected ribs are rarely seen on very small specimens. Ceratitic suture line, with well developed auxiliary series, is typical of proptychitids.

Measurements:
See **Fig. 30**.

Discussion:

This species displays similarities with *Lingyunites discoides* Chao (1950) such as a discoidal whorl section, a tabulate venter, and a similar suture line. However, measurements reported by Chao are different from ours.

Wailiceras aemelus shows strong affinities with *Meekoceras infrequens* Krafft & Diener (1909). Both apparently share very close shell shape. Their stratigraphic positions are compatible, and *M. infrequens* resembles a proptychitid more than a meekoceratid. The illustration of *M. infrequens* by Krafft & Diener (1909) is ambiguous, especially the rounded section of the last whorl. *W. aemulus* differs from *M. infrequens* by the presence of plications and a tabulate venter on the last whorl section. Since we have several specimens from Guangxi and a precise stratigraphic position for *W. aemulus*, it is preferable to create a species separate from *M. infrequens*.

***Leyeceras* n. gen.**

Type species: *Leyeceras rothi* n. gen, n. sp.

Composition of the genus:

Type species only.

Diagnosis:

Proptychitid with moderately evolute coiling, a subtabulate venter and thin lirae.

Etymology:

Genus name refers to the Leye city (Guangxi, South China).

Occurrence:

"*Owenites koeneni* beds".

Discussion:

This proptychitid exhibits very close affinities with *Koninckites radiatus* Waagen (1895). In fact, *K. radiatus* probably can be included within the variation of *L. rothi*, and since it does not agree well with the type species of *Koninckites*, we suggest it may actually be a synonym of *L. rothi*.

***Leyeceras rothi* n. gen., n. sp.**

Pl. 15, Figs. 1-3

? 1895 *Koninckites radiatus* - Waagen, p. 273, pl. 32, figs. 2a-c

Diagnosis:
As for the genus.

Holotype:
PIMUZ 25964, Loc. Jin43, Jinya, "*Owenites koeneni* beds", Smithian.

Etymology:
Named after R. Roth (Zurich).

Occurrence:
Jin12, 27, 43, 45; "*Owenites koeneni* beds".

Description:
Moderately evolute shell with slightly convex flanks, a subtabulate venter, rounded ventral shoulders, and umbilicus with perpendicular, moderately high wall and rounded shoulders. Ornamentation consists of very weak, distant plications as well as radial lirae on flanks. Suture line typical of proptychitids with three principal elements slanted toward umbilicus. Although suture line on our specimen is not well preserved, it apparently has an indented ventral saddle.

Measurements:
See **appendix 1**.

Discussion:
In contrast to the illustrated specimen of *Koninckites radiatus* (see Waagen 1895, pl. 32, fig. 2a-c), our species may exhibit a suture line with less numerous elements at a comparable diameter.

***Urdyceras* n. gen.**

Type species: *Urdyceras insolitus* n. gen, n. sp.

Composition of the genus:
Type species only.

Diagnosis:
Proptychitid with slightly involute coiling, a very tabulate venter and radial, distant folds.

Etymology:
Named for S. Urdy (Zurich).

Occurrence:
"*Flemingites rursiradiatus* beds".

Discussion:
This genus is similar in some features to *Meekoceras rota* (Waagen, 1895), *Proptychites undatus* (Waagen, 1895) and *Proptychites plicatus* (Waagen, 1895). However, *P. undatus* and *P. plicatus* do not have a tabulate venter, and *M. rota* exhibits phylloid saddles.

***Urdyceras insolitus* n. gen., n. sp.**

Pl. 15, Figs. 4a-d

Diagnosis:
As the genus diagnosis.

Holotype:
PIMUZ 25965, Loc. Jin30, Jinya, "*Flemingites rursiradiatus* beds", Smithian

Etymology:
From the Latin meaning "uncommon".

Occurrence:

Jin30; "*Flemingites rursiradiatus* beds".

Description:
Slightly involute shell with slightly convex flanks, a tabulate venter, angular ventral shoulders, and umbilicus with moderately high, perpendicular wall and rounded shoulders. Ornamentation consists of distant radial folds and fine growth lines. Suture line ceratitic with long, deeply indented lateral lobe, without auxiliary series. Lateral saddle gently inclined toward umbilicus.

Measurements:
See **appendix 1**.

***Proptychitidae* gen. indet.**

Pl. 12, Figs. 5a-d

Occurrence:
Jin30; "*Flemingites rursiradiatus* beds".

Description:
Involute shell with a tabulate venter, rounded ventral shoulders, and convex flanks with maximum lateral curvature at mid-flank. Narrow umbilicus with moderately high, perpendicular wall and rounded shoulders. Ornamentation consists only of straight folds. Suture line peculiar with some similarity to proptychitids, particularly *Pseudaspidites*. Lobes appear less indented, but umbilical lobe seems to be curved. An auxiliary series is present, but is less divided. Most striking difference is absence of a ventral saddle. Although it may be present at larger diameters, our single specimen is not sufficiently well preserved to detect its presence.

Measurements:
See **appendix 1**.

Discussion:
With respect to shape and a portion of its suture line, our specimen exhibits some affinities with Proptychitidae. However, without additional specimens, we cannot assign it with any confidence to a specific genus.

Family **Meekoceratidae** Waagen, 1895

Gyronites Waagen, 1895

Type species: *Gyronites frequens* – Waagen, 1895, p. 292, pl. 37, figs. 1-4

Gyronites* cf. *G. superior Waagen, 1895

Pl. 16, Figs. 1-3

1895 *Gyronites superior* - Waagen, p. 294, pl. 37, figs. 6a, b

Occurrence:

Jin61, 66, 68; "*Kashmirites densistriatus* beds".

Description:

Moderately evolute, very compressed shell with a tabulate venter, slightly angular ventral shoulders on adult specimens (very angular for juveniles), and convex flanks with maximum curvature at mid-flank. Mid-flank position of change in curvature is somewhat prominent, creating a very weak longitudinal ridge on flanks. Moderately wide, shallow umbilicus with very low, perpendicular wall and rounded shoulders. Ornamentation consists only of strongly forward projected, fine, sinuous growth lines. Suture line typical for *Gyronites* with three elongated saddles, a deep umbilical lobe and a simple auxiliary series.

Measurements:

See **Fig. 31**.

Discussion:

As noted by Waagen (1895), it is difficult to distinguish different species of *Gyronites* from the type species. Following the conclusions of Waagen, *G. superior* is differentiated by its slightly more involute coiling (see Waagen, 1895, pl. 37, fig. 1a and 6a) and its significantly more compressed whorl section. The flanks of *G. frequens* also appear to be more rounded. Our specimens are referable to *G. superior* even though small differences exist in the degree of lateral compression. To our knowledge, the material here attributed to *Gyronites superior* represents the youngest occurrence of this genus.

Family **Dieneroceratidae** Spath, 1952

Dieneroceras Spath, 1934

Type species: *Ophiceras dieneri* - Hyatt & Smith, 1905, p. 118, pl. 8, figs. 16-29

Dieneroceras tientungense Chao, 1959

Pl. 16, Figs. 5-12

v	1959	*Dieneroceras tientungense* - Chao, p. 192, pl. 2, figs. 5-6, 8-10, 29
v	1959	*Dieneroceras*? *vermiforme* - Chao, p. 192, pl. 2, figs. 14-16, 28, text-fig. 7b
v	1959	*Dieneroceras ovale* - Chao, p. 192, pl. 2, figs. 11-13, text-fig. 7a

Occurrence:

Jin4, 13, 23, 24, 28, 29, 30, 41, 43, 45, 51; Yu2, 3; "*Flemingites rursiradiatus* beds". Jin10; "*Owenites koeneni* beds".

Description:

Very evolute serpenticone exhibiting significant variation in whorl section, ranging from nearly ovoid with flat, parallel flanks and subtabulate venter, to gently rounded with slightly convex flanks and broadly arched venter. Ventral shoulders generally rounded. Very wide, fairly shallow umbilicus with moderately low, perpendicular wall and rounded shoulders. Ornamentation generally consists of very delicate strigation near venter, as well as a few weak folds and minor constrictions, especially on mature specimens. Suture line ceratitic, typical of family with two high ventral and lateral saddles and smaller umbilical saddle. Lobes are narrow.

Measurements:

See **Fig. 32**. Whorl height is characterized by allometric growth, while umbilical diameter displays isometric growth.

Discussion:

Some confusion surrounds this genus because it includes several species exhibiting a simple morphology, but with quite different rates of volution (*e.g. D. spathi* Kummel & Steele and *D. knechti* (Hyatt & Smith)), and it also has been assumed to be a very long-ranging genus, first

appearing in the Smithian and surviving until the Lower Spathian (Dagys & Konstantinov 1984). Furthermore, it has been synonymized with *Wyomingites* (Tozer 1981), thus creating confusion with regard to its classification. In addition, considerable disagreement exists with respect to its familial designation (*e.g.* Flemingitidae for Spath 1934 and Smith 1932; Dienerocerati dae for Kummel 1952; Meekoceratidae for Tozer 1981).

Its rate of coiling and ornamentation (especially the strigation) closely mimic the Flemingitidae and suggest possible links with this family. Yet, its suture line is simpler and quite different. Based on its morphology, it is difficult to understand the justification for assigning it to a different family, and especially the Meekoceratidae.

Spathian species attributed to this genus have different ornamentation (*e.g.* tubercules: *D. tuberculatum* Dagys & Konstantinov) and often, a more complex suture line (*D. demokidovi* Dagys & Konstantinov). Their assignment to *Dienerocerasremains doubtful.*

Wyomingites Hyatt, 1900

Type species: *Meekoceras aplanatum* – White, 1879, p. 112

Wyomingites aplanatus (White, 1879)

Pl. 17, Figs. 1-3

	1879	*Meekoceras aplanatum* - White, p. 112
	1880	*Meekoceras aplanatum* - White, p. 112, pl. 31, figs. 1a, b, d
	1895	*Xenaspis*? *aplanata* - Waagen, p. 290
	1900	*Wyomingites aplanatus* - Hyatt, p. 556
	1902	*Ophiceras aplanatum* - Frech, p. 631, fig. e
	1905	*Meekoceras aplanatum* - Hyatt & Smith, p. 146, pl. 11, figs. 1-14; pl. 64, figs. 17-22; pl. 77, figs. 1-2
	1932	*Flemingites aplanatus* - Smith, p. 51, pl. 11, figs. 1-14; pl. 22, figs. 1-23; pl. 39, figs. 1-2; pl. 64, figs. 17-32
	1962	*Wyomingites* cf. *W. aplanatus* - Kummel & Steele, p. 696, pl. 99, figs. 3-4
?	1979	*Wyomingites aplanatus* - Nichols & Silberling, pl. 1, figs. 19-21

Occurrence:

Jin13, 28, 30, 41; "*Flemingites rursiradiatus* beds".

Description:

Very evolute, laterally compressed shell with a subrectangular whorl section, a tabulate venter, rounded ventral shoulders, and nearly parallel flanks. Moderately wide umbilicus with low, perpendicular wall and rounded shoulders. Ornamentation consists of conspicuous strigation (as in *Flemingites*) and highly variable, dense to distant wavy ribs, varying also in strength. Ribs may be replaced by small plications at maturity. Suture line ceratitic, simple and structurally similar to *Dieneroceras*.

Measurements:

See **Fig. 33**.

Discussion:

The strigate ornamentation of this genus can easily cause it to be confused with flemingitids, and yet, its suture line is similar to that of *Dieneroceras*. Tozer (1981) synonymized *Dieneroceras* with *Wyomingites*, which he then placed within the Meekoceratidae. However, their respective morphology and suture line are similar enough to justify placing these two genera in a specific family: the Dieneroceratidae. Compared to *W. scapulatus* Tozer (1994), *W. aplanatus* is more evolute and displays more prominent strigation as well as more variable ribbing. This genus apparently exhibits highly variable ornamental strength.

Family **Flemingitidae** Hyatt, 1900

Flemingites Waagen, 1892

Type species: *Ceratites flemingianus* - de Koninck, 1863, p. 10, pl. 7, fig. 1

Flemingites flemingianus (de Koninck, 1863)

Pl. 18, Figs. 1-5

	1863	*Ceratites flemingianus* - de Koninck, p. 10, pl. 7, fig. 1
	1895	*Flemingites flemingianus* - Waagen, p. 199, pl. 12, fig. 1; pl. 13, fig. 1; pl. 14, fig. 1
	1933	*Flemingites flemingi* - Collignon, p. 25, pl. 5, fig. 1
v	1959	*Flemingites ellipticus* - Chao, p. 206, pl. 4, figs. 5-7, 10-12, text-fig. 12a

Occurrence:

Jin4, 15, 28, 30; FW4/5, FW2, 3, 4, 5; T6, T50; "*Flemingites rursiradiatus* beds".

Description:

Evolute shell exhibiting a subcircular to subquadratic whorl section with a broadly rounded to circular venter and slightly convex flanks, gently converging toward venter. Umbilicus moderately wide with high, perpendicular wall and broadly rounded shoulders. Ornamentation consists of noticeable radial or slightly rursiradiate ribs, as well as very conspicuous, dense strigation covering entire shell at all growth stages larger than ~1 cm in diameter. Suture line ceratitic with well indented lobes and nearly phylloid saddles.

Measurements:

See **Fig. 34**.

Discussion:

Flemingites compressus Waagen (1895), from the Salt Range, with its more ovoid whorl section may represent a variant of the type species. The suture line of *F. flemingianus* is apparently highly variable.

Flemingites rursiradiatus Chao, 1959

Pl. 19, Figs. 1-7; Pl. 20, Figs. 1-3

?	p	1933	*Flemingites griesbachi* - Collignon, p. 28, pl. 6, figs. 2, 2a only
	v	1959	*Flemingites rursiradiatus* - Chao, p. 205, pl. 6, figs. 1-5, 8-10, text-figs. 13a-b

Occurrence:

Jin4, 13, 21, 23, 24, 28, 29, 30, 41; FSB1/2; WFB; FW2, 3, 4, 5; Sha1, 2; "*Flemingites rursiradiatus* beds".

Description:

Laterally compressed serpenticone with a subtabulate to tabulate venter, rounded ventral shoulders, and subrectangular whorl section for robust specimens, and a narrower, tabulate venter with subangular ventral shoulders on more compressed specimens. Flanks parallel near umbilicus, then gradually converge to the venter. Fairly wide umbilicus with moderately high, perpendicular wall and rounded shoulders. Ornamentation consists of strigation on flanks and variable strength, conspicuous rursiradiate ribs, arising on umbilical shoulder, usually becoming very faint on ventral shoulder, then crossing venter in manner ranging from barely perceptible to highly conspicuous. These ribs may become straight to slightly concave on adult specimens, and the intensity of more robust ribs can create "polygonal coiling" effect as they cross the venter. Suture line ceratitic with rounded (but not completely phylloid) lateral saddle.

Measurements:

See **Fig. 35.** Whorl height and umbilical diameter exhibit isometric growth.

Discussion:

This species differs from other flemingitids by its conspicuous rursiradiate ribs on the inner whorls, which disappear on the venter. Apparently, this species exhibits an extremely wide range of intraspecific variation and the loss of rursiradiate ribs on some adult specimens raises the possibility that many of the larger specimens (e.g. several of Diener's Himalaya specimens) originally assigned to different species may, in fact, belong to *F. rursiradiatus*.

Flemingites radiatus Waagen, 1895

Pl. 20, Figs. 4-6

	1895	*Flemingites radiatus* - Waagen, p. 197, pl. 11, figs. 1a-b
?	1933	*Flemingites radiatus* - Collignon, p. 172, pl. 5, figs. 2-3
	1934	*Flemingites radiatus* - Spath, p. 111, fig. 28

Occurrence:

Jin4, 28, 30; FSB1/2; T6, T50; "*Flemingites rursiradiatus* beds".

Description:

Moderately evolute, laterally compressed shell with a rectangular whorl section, parallel flanks, a broadly arched to subtabulate venter and rounded ventral shoulders. Umbilicus wide with moderately high, perpendicular wall and rounded shoulders. Ornamentation consists of forward projected, weak ribs and weak strigation on flanks. Suture line ceratitic and similar to *Flemingites rursiradiatus*.

Measurements:

See **Fig. 36**.

Discussion:

F. radiatus is characterized by its conspicuous rectangular section, and its coiling is more involute than *F. rursiradiatus*. This species can be confused with *Wyomingites aplanatus* since they both have laterally compressed shells with (sub)rectangular whorl sections and similar strigate ornamentation. The much weaker plications and the less rectangular whorl section of *F. radiatus* provide means of distinction with *W. aplanatus*.

***Flemingites* sp. indet.**

Pl. 20, Figs. 7a-c

Occurrence:

Jin67; "*Kashmirites densistriatus* beds".

Description:

Evolute, laterally compressed shell with slightly convex flanks, gradually convergent from umbilical shoulder, an extremely thin, tabulate venter, and angular ventral shoulders. Umbilicus fairly wide with moderately high, oblique wall and rounded shoulders. Ornamentation consists of extremely weak plications on inner whorls and sinuous, convex ribs on outer whorls. Sinuous growth lines parallel to the ribs also visible on outer whorls. A portion of flank near venter exhibits conspicuous, typical strigate ornamentation. Suture line unknown.

Discussion:
This single specimen probably represents a new species and can be distinguished from other *Flemingites* by its lateral compression and absence of ornamentation on its inner whorls. However, it is preferable not to erect a new species based on such a very fragmentary specimen. *Flemingites* sp. indet. is the lowest occurring species of *Flemingites* in all studied sections.

***Galfettites* n. gen.**

Type species: *Galfettites simplicitatis* n. gen., n. sp.

Composition of the genus:
Type species only.

Diagnosis:
Laterally compressed Flemingitidae with smooth, flat, parallel flanks and a very narrowly curved venter.

Etymology:
Named after T. Galfetti (Zurich).

Occurrence:
"*Owenites koeneni* beds".

Discussion:
This genus is clearly distinguished from *Flemingites* and *Euflemingites* by its absence of strigation, and from *Anaxenaspis* and *Pseudoflemingites* by its absence of ribs or plications.

Furthermore, *Galfettites* is the only genus within Flemingitidae that exhibits flat, parallel flanks on adult whorls.

***Galfettites simplicitatis* n. gen., n. sp.**

Pl. 21, Figs. 1-2

Diagnosis:
As for the genus.

Holotype:
PIMUZ 26002, Loc. Jin27, Jinya, "*Owenites koeneni* beds", Smithian.

Etymology:
From the Latin, meaning simplicity in reference to the absence of marked ornamentation.

Occurrence:
Jin27, 45; "*Owenites koeneni* beds".

Description:
Very evolute, very compressed shell with a very narrowly curved to subtabulate venter, abruptly rounded ventral shoulders, and flat, parallel flanks for about two thirds of flank, then gradually convergent to venter. Umbilicus wide, with high, nearly perpendicular wall and rounded shoulders. Available specimens do not exhibit any ornamentation. Suture line ceratitic, typical of Flemingitidae, with phylloid saddle only present in umbilical part. Auxiliary series is well developed.

Measurements:
See **Fig. 37**.

Discussion:
Galfettites simplicitatis n. gen., n. sp. is easily distinguished from other Flemingitidae by its peculiar whorl section and its absence of ornamentation.

Pseudoflemingites Spath, 1930

Type species: *Ophiceras nopscanum* - Welter, 1922, p. 104, pl. 4, figs. 4-5 only

***Pseudoflemingites goudemandi* n. sp.**

Pl. 22, Figs. 1-5

Diagnosis:

Serpenticonic *Pseudoflemingites* with very weak ribbing on juvenile whorls, and a high, ovoid whorl section, without strigation.

Holotype:

PIMUZ 26004, Loc. Jin99, Jinya, "*Owenites koeneni* beds", Smithian.

Etymology:

Named for N. Goudemand (Zurich).

Occurrence:

Jin12, 99; NW1; T11; Yu3; "*Owenites koeneni* beds".

Description:

Very evolute, compressed serpenticone with a low rounded venter, rounded ventral shoulders, and more or less convex flanks forming a highly variable whorl section ranging from suboval to subrectangular (robust specimens). Umbilicus with moderately high, perpendicular wall and rounded shoulders. Ornamentation consists only of extremely weak, disparate folds on juvenile stages. No strigation observed. Suture line typical for Flemingitidae with three nearly phylloid saddles, broad indented lobes and poorly defined, small auxiliary series.

Measurements:

See **Fig. 38**.

Discussion:

Although this species does not exhibit ribbing typical of the type species, its mode of coiling, absence of strigation and simple suture line justify its assignment to *Pseudoflemingites*.

Anaxenaspis Kiparisova, 1956

Type species: *Xenaspis orientalis* - Diener, 1895, p. 42, pl. 3, fig. 3

?*Anaxenaspis* sp. indet.

Pl. 23, Figs. 1a-b

Occurrence:
Jin45; "*Owenites koeneni* beds".

Description:
Evolute, compressed shell with a subtabulate venter, rounded ventral shoulders, convex flanks, and wide umbilicus with moderately high, gently sloping wall and rounded shoulders. Ornamentation consists of dense, forward projected ribs, especially visible on inner whorls. Suture line unknown.

Measurements:
See **appendix 1**.

Discussion:
The assignment of this specimen to *Anaxenaspis* is uncertain, and is based only on its similar morphology with Flemingitidae and the absence of strigation.

***Guangxiceras* n. gen.**

Type species: *Guangxiceras inflata* n. gen., n. sp.

Composition of the genus:
Type species only.

Diagnosis:
Flemingitidae with weak bullae on the inner whorls and very weak folds on the outer whorls. Inner whorls are inflated in contrast to the more compressed outer whorls.

Etymology:
Genus name refers to the Guangxi province (South China).

Occurrence:
"*Owenites koeneni* beds".

Discussion:
This genus is clearly distinguished from other Flemingitidae, and especially *Anaxenaspis* and *Pseudoflemingites*, by the weak nodes present on its inner whorls. It also differs by its inflated inner whorls, which are in contrast with its more compressed outer whorls. The suture line agrees in plan with that of Flemingitidae, but displays a compressed umbilical saddle.

***Guangxiceras inflata* n. gen., n. sp.**

Pl. 23, Figs. 2a-e

Diagnosis:
As for the genus.

Holotype:
PIMUZ 26016, Loc. Jin27, Jinya, "*Owenites koeneni* beds", Smithian.

Etymology:
Species name refers to the morphology of the inner whorls.

Occurrence:
Jin27; "*Owenites koeneni* beds".

Description:
Laterally compressed shell with nearly parallel flanks on outer whorls and significantly inflated flanks on inner whorls. Inner whorls exhibit serpenticonic coiling, whereas outer whorl is only moderately evolute with respect to next inner whorl. Outer whorl exhibits a subtabulate venter and rounded ventral shoulders. Umbilicus very wide, with moderately high, oblique wall (higher on inner whorls), and rounded shoulders. Ornamentation consists only of weak bullae and folds

on inner whorls and very weak folds on outer whorls. Suture line ceratitic with very elongated saddles. Lateral lobe deeply indented and umbilical saddle laterally compressed. Umbilical and lateral saddles slanted slightly toward umbilicus.

Measurements:
See **appendix 1**.

Anaflemingites Kummel & Steele, 1962

Type species: *Anaflemingites silberlingi* - Kummel & Steele, 1962, p. 667, pl. 102, fig. 10, text-fig. 7a

***Anaflemingites hochulii* n. sp.**

Pl. 24, Figs. 3-6

Diagnosis:
Anaflemingites with highly variable morphology and ornamentation throughout ontogeny. Sinuous growth lines and weak ventrolateral strigation are present on juvenile whorls, while mature specimens exhibit only gentle, fold-type ribs.

Holotype:
PIMUZ 26020, Loc. Jin45, Jinya, "*Owenites koeneni* beds", Smithian.

Etymology:
Named for P.A. Hochuli (Zurich).

Occurrence:
Jin42, 45; Yu2; "*Owenites koeneni* beds".

Description:
Moderately evolute, laterally compressed shell with a subtabulate venter, abruptly rounded ventral shoulders on juvenile whorls, more gently rounded on larger specimens, and convex flanks exhibiting maximum lateral curvature at mid-flank on juvenile whorls, and more compressed, nearly parallel flanks on mature specimens. Umbilicus wide, with low, nearly

perpendicular wall and rounded shoulders. Ornamentation on juvenile whorls consists of variable, sinuous growth lines and weak folds, as well as very weak strigation near venter. Our larger specimens mainly exhibit only conspicuous radial folds. Suture line ceratitic with well indented lobes and narrow saddles.

Measurements:
See **Fig. 39**.

Discussion:
Upon comparison of our specimens with the holotype of *A. silberlingi* Kummel & Steele (1962), we find significant differences that fully justify the erection of a new species. Indeed, strigation appears to be present on the entire flank of the holotype, and not just near the venter as with our specimens. Furthermore, the folds and growth lines exhibited by *A. hochulii* n. sp. are much more conspicuous. The lobes of the suture line illustrated by Kummel & Steele (1962) also appear narrower than for *A. hochulii* n. sp. The distinct morphology of this genus and the presence of strigation have led us to include it within the Flemingitidae, and not the Meekoceratidae as suggested by Tozer (1981) based only on its suture line.
Anaflemingites differs from *Flemingites* by its weaker folds and strigation, from *Galfettites* and *Guangxiceras* by the presence of a strigation.

Family **Arctoceratidae** Arthaber, 1911

Arctoceras Hyatt, 1900

Type species: *Ceratites polaris* - Mojsisovics, 1886, p. 31, pl. 7, figs. 1a, b

***Arctoceras strigatus* n. sp.**

Pl. 25, Figs. 1-2

Diagnosis:

Moderately involute *Arctoceras* without umbilical tuberculation, but with obvious strigation on the entire flank, and two very weak, longitudinal ridges on flank.

Holotype:

PIMUZ 26023, Loc. Jin15, Jinya, "*Owenites koeneni* beds", Smithian.

Etymology:

Named for its conspicuous strigation.

Occurrence:

Jin15; FSB1/2; "*Owenites koeneni* beds".

Description:

Moderately involute, somewhat thick platycone with a subtabulate to broadly rounded venter, rounded ventral shoulders, and weakly convex flanks convergent to venter. Deep umbilicus with very high, perpendicular wall and abruptly rounded shoulders without tuberculation. Ornamentation consists of very noticeable strigation on flanks, becoming weaker on venter, as well as distant, weak, radial straight folds on lower and mid-flanks. Barely visible (see Plate 25, Fig. 2c) on flanks are two, very weak, longitudinal ridges located at about one third and two thirds of the distance across the flank. Suture line ceratitic, typical for Arctoceratidae, with deeply indented lobes and small auxiliary series. Umbilical and lateral saddles slightly slanted toward umbilicus.

Measurements:

See **appendix 1**.

Discussion:

This species differs primarily from *A. tuberculatum* (Smith) by its absence of umbilical tuberculation, but *A. tuberculatum* exhibits a somewhat weaker strigation, and its ribs are more sinuous and even more distant (see Kummel 1961). It is also distinguishable from *A. blomstrandi* (Lindström) by its less involute coiling, its subtabulate to broadly rounded venter and its more pronounced strigation and ribs. We believe that it may be necessary to revise the definition of *A. blomstrandi* in light of some of the conspicuous differences in ornamentation on specimens illustrated by Kummel (1961). Interestingly, the strigation of *A. strigatus* is more pronounced on the flanks than on the venter.

***Arctoceras* sp. indet.**

Pl. 27, Figs. 4a-c

Occurrence:

FW4/5; "*Flemingites rursiradiatus* beds".

Description:

Moderately involute, laterally compressed, high whorled platycone with nearly parallel flanks, a subtabulate venter, rounded ventral shoulders, and deep umbilicus with very high, flat, slightly oblique wall and abruptly rounded shoulders. Ornamentation consists of distant, weakly convex ribs, more prominent at mid-flank. No strigation visible. This species is represented only by a fragmentary body chamber. Suture line unknown. Estimated maximum diameter: greater than 15 cm.

Discussion:

This species differs from *A. tuberculatum* (Smith 1932) by its lack of umbilical tuberculation and strigation, and from *A. strigatus* n. sp. by its absence of strigation. *A. blomstrandi* (Lindström 1865) is slightly more involute.

Submeekoceras Spath, 1934

Type species: *Meekoceras mushbachanum* - White, 1879, p. 113

Submeekoceras mushbachanum (White, 1879)

Pl. 17, Fig. 4; Pl. 26, Figs. 1-9

	1879	*Submeekoceras mushbachanum* - White, p. 113
	1880	*Submeekoceras mushbachanum* - White, p. 114, pl. 32, figs. 1a-d
	1902	*Prionolobus mushbachanum* - Frech, p. 631, fig. c
	1904	*Submeekoceras mushbachanum* - Smith, p. 376, pl. 41, figs. 1-3; pl. 43, figs. 1-2
	1905	*Meekoceras (Koninckites) mushbachanum* - Hyatt & Smith, p. 149, pl. 15, figs. 1-9; pl. 16, figs. 1-3; pl. 18, figs. 1-7; pl. 70, figs. 8-10
	1914	*Submeekoceras mushbachanum* - Smith, p. 77, pl. 72, figs. 1-2; pl. 73, figs. 1-6; pl. 74, figs. 1-23
	1915	*Submeekoceras mushbachanum* - Diener, p. 193
non	1922	*Meekoceras mushbachanum* - Welter, p. 126
	1932	*Meekoceras (Koninckites) mushbachanum* - Smith, p. 61, pl. 15, figs. 1-9; pl. 16, figs. 1-3 pl. 18, figs. 1-7; pl. 38, fig. 1; pl. 59, figs. 17-21; pl. 70, figs. 8-10; pl. 74, figs. 1-23; pl. 75, figs. 1-6; pl. 76, figs. 1-3
	1932	*Meekoceras (Koninckites) mushbachanum* var. *corrugatum* - Smith, p. 61, pl. 38, fig. 1
	1932	*Meekoceras (Koninckites) evansi* - Smith, p. 60, pl. 35, figs. 1-3; pl. 36, figs. 1-18
	1934	*Submeekoceras mushbachanum* - Spath, p. 255, fig. 87
v	1959	*Paranorites ovalis* - Chao, p. 217, pl. 9, figs. 16-19, text-fig. 16b
?	1959	*Prionolobus ophionus* var. *involutus* - Chao, p. 201, pl. 9, figs. 11-15, text-fig. 11b
v	1959	*Prionolobus hsüyüchieni* - Chao, p. 202, pl. 9, figs. 9-10, text-fig. 11c
?	1959	*Meekoceras (Submeekoceras) tientungense* - Chao, p. 317, pl. 14, figs. 6-7, text-fig. 45b
v	1959	*Meekoceras (Submeekoceras) subquadratum* - Chao, p. 317, pl. 14, figs. 1-5; pl. 39, figs. 8-9, text-fig. 45c
v	1959	*Meekoceras densistriatum* - Chao, p. 310, pl. 38, figs. 1-3, 19, text-fig. 43b
v	1959	*Meekoceras yukiangense* - Chao, p. 311, pl. 39, figs. 1-7, text-fig. 44a
v	1959	*Meekoceras kaohwaiense* - Chao, p. 311, pl. 40, figs. 16-18, text-fig. 44b
v	1959	*Meekoceras pulchriforme* - Chao, p. 313, pl. 40, figs. 14-15, text-fig. 44c
?	1959	*Meekoceras jolinkense* - Chao, p. 314, pl. 14, figs. 12-15
v	1959	*Meekoceras lativentrosum* - Chao, p. 309, pl. 38, figs. 15-18, text-fig. 43a
v	1959	*Proptychites latumbilicutus* - Chao, p. 234, pl. 19, figs. 2-3, text-fig. 22a
?	1959	*Proptychites kaoyunlingensis* - Chao, p. 234, pl. 16, figs. 7-8, text-fig. 22b
p	1968	*Arctoceras mushbachanum* - Kummel & Erben, p. 131, pl. 21, fig. 1 only

Occurrence:

Jin4, 11, 13, 22, 23, 24, 26, 28, 29, 30, 41, 51; FSB1/2; WFB; FW4/5; Sha1; T6, T50; "*Flemingites rursiradiatus* beds". Jin10, 27; "*Owenites koeneni* beds".

Description:

Slightly evolute, somewhat compressed platycone with flat, parallel flanks, a broadly rounded to subtabulate venter and rounded ventral shoulders. Deep umbilicus with very high, flat, perpendicular wall and abruptly rounded shoulders. Ornamentation consists of sinuous growth lines on all specimens, and weak, but noticeable fold-type ribs similar to *Arctoceras*, on a few specimens. Although strigation is not visible on our specimens, it may be present on another specimen of this genus from South China.

The morphology of juvenile specimens is similar to *Arctoceras tuberculatum*, but without umbilical tubercles. Mature specimens are more evolute and somewhat more laterally compressed. Suture line ceratitic with three principal saddles and an auxiliary series. As already noticed by Kummel & Erben (1968, p. 133), an examination of numerous specimens reveals considerable variation in the suture lines. This variation is also true for the genus *Arctoceras*. However, the lateral lobe of *Arctoceras* is always more deeply indented. The auxiliary series and saddles become longer with ontogenetic growth.

Measurements:

See **Fig. 40**. Whorl height, width and umbilical diameter exhibit isometric growth. Estimated largest diameter exceeding 15 cm.

Discussion:

This species clearly belongs to the Arctoceratidae. However, with the exception of a few species such as *A. tuberculatum*, differentiation between species can be difficult for juvenile members of the family. The specimen illustrated by Kummel & Erben (1968, pl. 21, fig. 2) is too involute to be referred to as *S. mushbachanum*.

Family **Ussuridae** Spath, 1930

Ussuria Diener, 1895

Type species: *Ussuria schamarae* - Diener, 1895, p. 26, pl. 3, figs. 4a-c, 5a-c

Ussuria kwangsiana Chao, 1959

Pl. 27, Figs. 1-3

	1959	*Ussuria kwangsiana* - Chao, p. 258, pl. 31, figs. 8-10, text-fig. 30a
?	1959	*Ussuria pakungiana* - Chao, p. 258, pl. 31, figs. 1-3, text-figs. 30c, d
?	1959	*Ussuria longilobata* - Chao, p. 259, pl. 31, figs. 4-7, text-fig. 30b

Occurrence:

Jin27, 45; "*Owenites koeneni* beds".

Description:

Extremely involute, compressed oxycone with a very narrowly curved venter, becoming somewhat acute on larger specimens, a rapidly expanding whorl height, and convex flanks with maximum thickness near the umbilicus. Umbilicus nearly occluded, but deep with high, almost perpendicular wall and abruptly rounded shoulders. Ornamentation consists only of very weak plications and very fine radial growth lines. Suture line sub-ammonitic, typical of genus. Ventral lobe deeply indented, all saddles are monophylloid and narrower than lobes. Simple auxiliary series not completely preserved, but is visible.

Measurements:

See **Fig. 41**.

Discussion:

This species is more laterally compressed than the type species *U. schamarae*. *Ussuria* superficially resembles *Pseudosageceras*. However, the bicarinate venter and the suture line of *Pseudosageceras* are highly distinctive.

Metussuria (Hyatt & Smith), 1905

Type species: *Ussuria waageni* - Hyatt & Smith, 1905, p. 90, pl. 65, figs. 1-5; pl. 66, figs. 1-12; pl. 67, figs. 1-2; pl. 85, figs. 1-8

***Metussuria* sp. indet.**

Pl. 25, Figs. 3-8

Occurrence:

Jin27; "*Owenites koeneni* beds".

Description:

Very involute, very compressed oxycone with a narrowly rounded venter (more or less subtabulate for juveniles) and convex flanks with maximum lateral curvature near umbilicus, gradually convergent to venter. Umbilicus nearly occluded with low, oblique wall and rounded shoulders. Ornamentation consists only of weak folds and thin, radial growth lines. Suture line with diphylloid saddles and deeply indented lobes, and a complex auxiliary series.

Measurements:

See **Fig. 41**. Estimated largest diameter exceeding 20 cm.

Discussion:

The morphology and measurements of *Metussuria* sp. indet. are very close to those of *U. kwangsiana*, but it can be distinguished by its more complex suture line, its slightly more compressed whorl section, and its somewhat shallower umbilicus. *Metussuria* sp. indet. is more compressed than the type species, and it is difficult to definitely assign it to *M. spathi* Chao (1959), since the illustrations given by Chao are insufficient.

Metussuria differs from *Parussuria* Spath (1934) by the absence of strigation.

Parussuria Spath, 1934

Type species: *Ussuria compressa* - Hyatt & Smith, 1905, p. 89, pl. 3, figs. 6-11

Parussuria compressa (Hyatt & Smith, 1905)

Pl. 13, Fig. 17

	1905	*Ussuria compressa* - Hyatt & Smith, p. 89, pl. 3, figs. 6-11
	1932	*Sturia compressa* - Smith, p. 93, pl. 3, figs. 6-11
?	1932	*Sturia woodini* - Smith, p. 94, pl. 51, figs. 5-6
	1934	*Parussuria compressa* - Spath, p. 213, figs. 66c, d
	1962	*Parussuria compressa* - Kummel & Steele, p. 690, pl. 99, fig. 23; pl. 102, fig. 11
?	1968	*Parussuria semenovi* - Zakharov, p. 59, pl.5, fig. 4
	1995	*Parussuria compressa* - Shevyrev, p. 37, pl. 4, fig. 6, text-fig. 16

Occurrence:

Jin27; "*Owenites koeneni* beds".

Description:

Very involute, compressed oxycone with a narrowly rounded venter and slightly convex flanks with maximum lateral curvature near umbilicus, gradually converging to venter. Umbilicus nearly occluded, with moderately high, oblique wall and rounded shoulders. Ornamentation consists of thin, radial growth lines, and weak strigation, which is characteristic of this species. Suture line unknown due to fragmentary preservation of only specimen.

Discussion:

This genus is very similar to *Ussuria* and *Metussuria*, but differs by its more indented, complex suture line, and most importantly by its strigation. *P. latilobata*, assigned to the Ussuridae by Chao (1959), is questionable because it was found in the Spathian, which supposedly does not include Ussuridae. Furthermore, the suture line of *P. latilobata* appears to be either poorly preserved, or it has been excessively ground away during preparation. All measurements of *Ussuria*, *Metussuria* and *Parussuria* are quite close, thus indicating the probability of very strong phylogenetic affinities. This similarity also suggests that it can be very difficult to distinguish between species of the family, unless the suture line and/or subtle ornamentation (e.g. strigation) is preserved.

Family **Prionitidae** Hyatt, 1900

Anasibirites Mojsisovics, 1896

Type species: *Sibirites kingianus* - Waagen, 1895, p. 108, pl. 8, figs. 1a-c, 2a-c

Anasibirites multiformis Welter, 1922

Pl. 28, Figs. 1-6

?	p	1895	*Sibirites tenuistriatus* - Waagen, p. 138, pl. 9, figs. 2a-b
	p	1922	*Anasibirites multiformis* - Welter, p. 138, pl. 15, figs. 12-13, 23-24; pl. 16, figs. 6-19
?		1929	*Anasibirites welleri* - Mathews, p. 14, pl. 2, figs. 17-19
?		1929	*Anasibirites emmonsi* - Mathews, p. 14, pl. 2, figs. 20-26

Occurrence:

Jin16, 48, 100, 101; FW6; NW12; "*Anasibirites multiformis* beds".

Description:

Moderately evolute, compressed platycone with a subtabulate to tabulate venter, angular to subangular ventral shoulders, and slightly convex flanks with maximum thickness near umbilicus for juveniles and mid-flank for mature specimens. Moderately deep umbilicus with oblique wall and rounded shoulders. Upon comparison of various species of *Anasibirites*, it becomes readily apparent that it must be redefined according to its characteristic, but highly variable ornamentation (see discussion):

- very few distinct ribs:
- dense, concave and thick striae: exhibited by all developmental stages, strongly forward projected, crossing venter without significant deviation.

In contrast with other *Anasibirites* species, its ribs are not pronounced and they do not alternate with weak ribs and growth lines. Ceratitic suture line is typical of prionitids.

Measurements:

See **Fig. 42**.

Discussion:

It is extremely difficult to distinguish various species of *Anasibirites* from each other due to their similarity in suture lines and extreme variability of ornamentation, as well as a lack of measurements for previously illustrated species. Quite often, different workers (e.g. Kummel & Erben 1968) concluded that all previously described species should be placed within the synonymy of a single species related to the type species: *A. kingianus*. However, a comprehensive study of the various types of ornamentation and umbilical characteristics suggests the existence of at least four main species:

- *A. kingianus* (Waagen, 1895): Distinguishing characteristics include an obviously arched venter and ornamentation consisting of an alternation of sinuous, weak and strong, forward projecting ribs. Ribs strongly attenuated on adult specimens.
- *A. pluriformis* (Guex 1978): with a tabulate to subtabulate venter, a perpendicular umbilical wall, and ornamentation consisting of weak and/or distinct ribs forming umbilical and ventral tuberculations on some robust specimens. Ribs are more radial.
- *A. multiformis* (Welter 1922; redefined here): with a tabulate to subtabulate venter and identical ornamentation on all developmental stages (dense, concave, forward projected growth lines with very few distinct ribs).
- *A. evolutus* n. sp.: It exhibits forward projected growth lines, and a regular alternation of concave, weak and strong ribs, as well as more evolute coiling at small sizes. In contrast to *A. pluriformis*, robust variants do not exhibit umbilical tubercules. This alternation of ribbing strength is somewhat attenuated on adult specimens, thus making it even more difficult to distinguish it from other species.

Unfortunately, the lack of measurements for many previously described species precludes a definitive validation of this new proposal.

Discussion:

A. multiformis displays a very strong resemblance to *Sibirites tenuistriatus* (Waagen, 1895), and may, in fact, be a synonym of this species. The various species attributed to *Anasibirites* by Chao (1959) do not correspond to this genus, with the exception of *A. multiformis* var. *alternatus*. *A. multiformis* represents a simplified “theme” of ornamentation within the genus *Anasibirites*.

***Anasibirites evolutus* n. sp.**

Pl. 28, Figs. 7-9

?	p	1922	*Anasibirites multiformis* - Welter, p. 138, pl. 15, figs. 9-11, 14-16, 19-20, 25-27
?		1929	*Anasibirites alternatus* - Mathews, p. 23, pl. 4, figs. 22-23
?		1929	*Anasibirites romeri* - Mathews, p. 23, pl. 4, figs. 24-25
?		1929	*Anasibirites gibsoni* - Mathews, p. 29, pl. 5, figs. 4-5
?		1959	*Anasibirites multiformis* var. *alternatus* - Chao, p. 328, pl. 40, fig. 11
?		1964	*Anasibirites pacificus* - Bando, p. 73, pl. 3, figs. 5-7; pl. 5, figs. 8, 11, 13, 14; pl. 6, figs. 8, 9, 11
?		1964	*Anasibirites ehimensis* - Bando, p. 74, pl. 3, fig. 12
?	p	1968	*Anasibirites nevolini* - Zakharov, p. 131, pl. 25, fig. 5

Diagnosis:

Anasibirites exhibiting more evolute coiling at smaller stages, and regular alternation of concave ribs with striae.

Holotype:

PIMUZ 26051, Loc. FW6, Waili, "*Anasibirites multiformis* beds", Smithian.

Etymology:

The name refers to its more evolute coiling at smaller sizes.

Occurrence:

Jin16, 48; FW6; "*Anasibirites multiformis* beds".

Description:

Moderately evolute, compressed platycone with a tabulate to subtabulate venter, sub-angular to abruptly rounded ventral shoulders, and slightly convex flanks with maximum curvature near umbilicus. Umbilicus with moderately high, oblique wall and rounded shoulders Ornamentation consisting of a regular alternation of forward projected, concave weak/ strong ribs and growth lines. Stronger ribs do not form umbilical and ventral tubercules. Ornamentation somewhat attenuated on adult specimens. Suture line identical to other species of *Anasibirites*.

Measurements:

See **Fig. 43**.

Discussion:

Coiling more evolute for juvenile specimens than *A. multiformis*. Although this species is not abundant, it is distinctive as evidenced by the measurements of involution.

Hemiprionites Spath, 1929

Type species: *Goniodiscus typus* - Waagen, 1895, p. 129, pl. 9, figs. 7-10

Hemiprionites* cf. *H. butleri (Mathews, 1929)

Pl. 29, Figs. 1-7

1929 *Goniodiscus butleri* - Mathews, p. 35, pl. 6, figs. 18-21

Occurrence:

Jin16, 48; FW6; "*Anasibirites multiformis* beds".

Description:

Involute, compressed shell with a tabulate venter on juvenile whorls, a tabulate or bicarinate venter on mature specimens, angular ventral shoulders, and convex flanks with maximum lateral curvature at mid-flank. Umbilicus extremely narrow at juvenile stages, becoming more open, with noticeable egression at adult stages. On adult specimens, umbilicus has high, gently inclined wall and rounded shoulders. Ornamentation on inner whorls similar to *Anasibirites* and exhibits growth lines crossing the venter. On adult stages, growth lines are more visible, and some develop into weak folds. Suture line ceratitic, similar to *H. typus* with three broad saddles and a small auxiliary series.

Measurements:

See **Fig. 44**.

Discussion:

H. butleri differs from the type species of the genus by its more involute coiling, its greater whorl height and its bicarinate venter on some specimens. Its coiling is significantly more involute than *Anasibirites*. Other species described by Mathews in 1929, with the exception of *H. walcotti*, can be grouped together as variant of the type species. This genus, as is true for all prionitids, displays a great morphological variation. Chinese specimens are morphologically close to *H. butleri,* but it is not possible to firmly assign them to this species, given the lack of a sufficient number of measured American specimens.

***Hemiprionites klugi* n. sp.**

Pl. 30, Figs. 1-4

Diagnosis:
Extremely involute *Hemiprionites* throughout ontogeny, displaying an ovoid whorl section and egressive coiling on adult stages.

Holotype:
PIMUZ 26062, Loc. FW6, Waili, "*Anasibirites multiformis* beds", Smithian.

Etymology:
Named for C. Klug (Zurich).

Occurrence:
Jin16; FW6; "*Anasibirites multiformis* beds".

Description:
Very involute throughout ontogeny, with slight egressive coiling on mature specimens. Compressed shell with an ovoid whorl section, a tabulate venter (thiner than *H.* cf. *H. butleri),* rounded ventral and umbilical shoulders, and convex flanks with maximum curvature at mid-flank. Umbilicus with high, perpendicular wall. No visible ornamentation. Suture line differs from type species, but retains same number of elements. Auxiliary series shorter than for type species.

Measurements:
See **Fig. 45**.

Discussion:

H. klugi n. sp. differs from *H.* cf. *H. butleri* by its ovoid whorl section, its thiner venter and its peculiar suture line. The suture line of *H. klugi* n. sp. may be similar to some species of *Wasatchites*. *H. walcotti* Mathews (1929) is similar to our Chinese specimens, but the lack of measurements prevents comparison with *H. klugi* n. sp. Furthermore, the suture line of *H. walcotti* is more similar to the type species than to *H. klugi* n. sp.

Family **Inyoitidae** Spath, 1934

Inyoites Hyatt & Smith, 1905

Type species: *Inyoites oweni* - Hyatt & Smith, 1905, p.134, pl. 6, figs. 1-16; pl. 69, figs. 1-9; pl. 78, figs. 1-8

***Inyoites krystyni* n. sp.**

Pl. 31, Figs. 1-4; Pl. 32, Figs. 1-2

?	1959	*Subvishnuites tientungensis* - Chao, p. 210, pl. 7, figs. 17-18
?	1959	*Subvishnuites* sp. indet. - Chao, p. 210, pl. 44, figs. 9-10

Occurrence:
Jin12, 99; Yu3; "*Owenites koeneni* beds".

Diagnosis:
Large-sized and very evolute *Inyoites* with a conspicuous, lanceolate venter and very weak, rursiradiate folds.

Holotype:
PIMUZ 26067, Loc. Yu3, Yuping, "*Owenites koeneni* beds", Smithian.

Etymology:
Named for L. Krystyn (Vienna).

Description:
Very evolute, compressed shell with a lanceolate venter and a conspicuous keel (present only when outer shell is preserved), rounded ventral shoulders, and parallel flanks. Umbilicus very wide, with moderately high, oblique wall and rounded shoulders. Ornamentation composed of dense, rursiradiate folds on inner whorls, becoming weaker on mature specimens. Suture line ceratitic with indented lobes and three large saddles on adult specimens.

Measurements:

See **Fig. 46**.

Discussion:

I. krystyni n. sp. can be essentially distinguished from other *Inyoites* species by its large size, its more evolute coiling, and its weaker ornamentation.

Subvishnuites Spath, 1930

Type species: *Vishnuites sp.*, Welter, 1922, p. 137, pl. 13, figs. 3-5

Subvishnuites stokesi (Kummel & Steele, 1962)

Pl. 29, Figs. 8a-d

	1962	*Inyoites stokesi* - Kummel & Steele, p. 672, pl. 99, figs. 19-22
?	1973	*Inyoites stokesi* - Collignon, p. 137, pl. 1, figs. 10, 10a

Occurrence:

Jin12; "*Owenites koeneni* beds".

Description:

Compressed serpenticone with a very angular venter, a wide, fairly shallow umbilicus with rounded shoulders, and slightly concave flanks converging towards venter. Thin, rursiradiate folds most prominent on the dorsal half of whorl, but disappear toward venter. Suture line saddles rounded and indented with an auxiliary series composed of small denticulations.

Measurements:

See **appendix 1**.

Discussion:

S. stokesi is also found in the "*Meekoceras* beds" of California, Nevada, Utah and Idaho. This species was first assigned to *Inyoites*, but it differs from *I. oweni* Hyatt & Smith (1905) by its lack of a hollow keel and its angular venter. Since its general shape is closer to the genus *Subvishnuites* Spath (1930), it is preferable to assign this species to *Subvishnuites*.

Subvishnuites was tentatively placed within the Xenoceltidae by Tozer (1981). However, it has much more in common with the Inyoitidae (e.g. its angular venter), and is not compatible with the morphologically simple Xenoceltidae.

Family **Lanceolitidae** Spath, 1934

Type species: *Lanceolites compactus* - Hyatt & Smith, 1905, p. 113, pl. 4, figs. 4-10 ; pl. 5, figs. 7-9; pl. 78, figs. 9-11

Lanceolites compactus Hyatt & Smith, 1905

Pl. 30, Figs. 5a-c

	1905	*Lanceolites compactus* - Hyatt & Smith, p. 113, pl. 4, figs. 4-10 ; pl. 5, figs. 7-9; pl. 78, figs. 9-11
	1932	*Lanceolites compactus* - Smith, p. 90, pl. 4, figs. 4-10; pl. 5, figs. 7-9; pl. 21, figs. 21-23; pl. 28, figs. 17-20; pl. 40, figs. 9-11; pl. 60, fig. 10
	1962	*Lanceolites compactus* - Kummel & Steele, p. 692, pl. 102, figs. 6-9
?	1979	*Lanceolites compactus* - Nichols & Silberling, pl. 2, figs. 39-43
	1984	*Lanceolites bicarinatus* - Vu Khuc, p. 85, pl. 7, figs. 2a-b, text-fig. H18
	1995	*Lanceolites compactus* - Shevyrev, p. 39, pl. 2, figs. 1-2

Occurrence:

Jin12; T5; "*Owenites koeneni* beds".

Description:

Extremely involute, discoidal shell with a narrow, concave, bicarinate venter and slightly convex flanks, more convergent on outer half of whorl. Umbilicus is occluded and shell exhibits a rapidly expanding whorl width. No visible ornamentation on our specimens. Suture line, although poorly preserved on our specimens, is typical of that of the genus with its single, broad and indented lateral lobe.

Measurements:

See **Fig. 47**.

Discussion:

This species can be distinguished from *L. bicarinatus* by its greater whorl width.

Lanceolites bicarinatus Smith, 1932

Pl. 30, Figs. 6a-d

	1932	*Lanceolites bicarinatus* - Smith, p. 90, pl. 55, figs. 1-13
v	1959	*Lanceolites orientalis* - Chao, p. 263, pl. 41, figs. 5-9
	1995	*Lanceolites bicarinatus* - Shevyrev, p. 40, pl. 4, fig. 3

Occurrence:

Jin12, 45; Yu7; "*Owenites koeneni* beds".

Description:

Extremely involute, very compressed, discoidal shell with a lenticular whorl section, a concave, bicarinate venter, angular ventral shoulders, and convex flanks with maximum lateral curvature one third of distance across flank from umbilicus. Umbilicus occluded, with rapidly expanding whorl width, totally embracing penultimate volution. No ornamentation observed. Suture line very peculiar, but typical of genus with very broad, deeply indented lobe followed by several auxiliary elements. All saddles are narrow.

Measurements:

See **Fig. 47**.

Discussion:

The morphology of the specimen illustrated by Chao (1959) is very similar, but its suture line is quite different. This may be the result of excessive grinding during laboratory preparation. *L. bicarinatus* essentially differs from the type species by its distinctive, bicarinate venter.

Family **Paranannitidae** Spath, 1934

Paranannites Hyatt & Smith, 1905

Type species: *Paranannites aspenensis* - Hyatt & Smith, 1905, p. 81, pl. 8, figs. 1-15
pl. 73, figs. 1-30

Paranannites* aff. *P. aspenensis Hyatt & Smith, 1905
Pl. 33, Figs. 1-10

	1905	*Paranannites aspenensis* - Hyatt & Smith, p. 81, pl. 8, figs. 1-15; pl. 73, figs. 1-30
	1932	*Paranannites aspenensis* - Smith, p. 98, pl. 8, figs. 1-15; pl. 73, figs. 1-30
	1932	*Paranannites columbianus* - Smith, p. 99, pl. 32, figs. 11-25
	1932	*Paranannites compressus* - Smith, p. 98, pl. 31, figs. 19-21
	1932	*Paranannites pertenuis* - Smith, p. 98, pl. 31, figs. 13-15
	1933	*Paranannites cottreaui* - Collignon, p. 58, pl. 8, figs. 5a-b
	1934	*Paranannites aspenensis* - Spath, p. 190, pl. 14, figs. 6a-c, text-figs. 57a-h
	1957	*Paranannites aspenensis* - Kummel in Arkell *et al.*, p. L138, figs. 172-7a-c
v	1959	*Paranannites aspenensis* - Chao, p. 284, pl. 24, figs. 11, 12
v	1959	*Paranannites* cf. *P. aspenensis* - Chao, p. 284, pl. 24, figs. 1-7
v	1959	*Paranannites ptychoides* - Chao, p. 284, pl. 24, figs. 8-10, text-figs. 37a
	1962	*Paranannites aspenensis* - Kummel & Steele, p. 676, pl. 100, figs. 14-17
?	1966	*Paranannites aspenensis* - Hada, p. 112, pl. 4, figs. 5a-b
	1968	*Paranannites aspenensis* - Kummel & Erben, p. 124, pl. 19, figs. 16-23
	1979	*Paranannites aspenensis* - Nichols & Silberling, pl. 2, figs. 1-10

Occurrence:
Jin4, 13, 23, 28, 29, 30; FW2, 3, 4, 5; "*Flemingites rursiradiatus* beds". Jin10; "*Owenites koeneni* beds".

Description:
Globose, involute, slightly compressed paranannitid with an arched venter, rounded ventral and umbilical shoulders, and parallel flanks near umbilicus, then gradually convergent to venter. Umbilicus with high, perpendicular wall. Ornamentation extremely variable with weak,

prorsiradiate constrictions and folds. A few thin, growth lines can be observed. Suture line ceratitic with two broad saddles.

Measurements:
See **Fig. 48**.

Discussion:
The measurements of our specimens are close to *P. aspenensis* (Fig. 48), and the suture line is also similar, but it is not possible to definitely assign them to this species. Indeed, they differ somewhat from *P. aspenensis* by having a wider umbilicus and they are slightly more depressed. They differ in much the same way from *P. hindostanus* (Diener, 1897, pl. 7, figs. 3a-b). Our specimens are also similar to *P. mulleri* (Kummel & Steele 1962), but the latter's coiling is more egressive. *P. ptychoides* (Chao 1959) cannot be separated from *P. aspenensis* as proposed by Kummel & Erben (1968), based only on the small denticulations of the suture line on the umbilical wall.

Paranannites spathi (Frebold, 1930)

Pl. 35, Figs. 10-19

		1930	*Prosphingites spathi* - Frebold, p. 20, pl. 4, figs. 2-3, 3a
		1934	*Prosphingites spathi* - Spath, p. 195, pl. 13, figs. 1a-e, 2
p	?	1959	*Prosphingites kwangsianus* - Chao, p. 296, pl. 28, figs. 17-18
p	?	1959	*Prosphingites sinensis* - Chao, p. 297, pl. 27, figs. 14-17, text-fig. 40a
	?	1982	*Prosphingites spathi* - Korchinskaya, pl. 5, figs. 2a-b
	?	1994	*Paranannites spathi* - Tozer, p. 77, pl. 36, figs. 1-2

Occurrence:
Jin27, 43, 45; Yu1; "*Owenites koeneni* beds".

Description:
Moderately evolute, subglobular shell with a subangular to rounded (as for some juveniles) venter and convex flanks, gradually converging to venter from abruptly rounded umbilical shoulder. Deep, crateriform umbilicus with high, perpendicular wall, wall height increasing proportionally with diameter. Ornamentation similar, but typical of *Paranannites* type species with constrictions of variable strength. Constrictions may possibly correspond to megastriae as indicated by

presence of a marked ventral sinus on one juvenile specimen. Suture line ceratitic, similar to *P. aspenensis,* with two main, broad saddles. Lobes finely indented and an isolated auxiliary saddle is present.

Measurements:
See **Fig. 49**. Whorl height and umbilical diameter exhibit isometric growth.

Discussion:
P. spathi differs from other *Paranannites* species by its subangular venter and deep, crateriform umbilicus. *P. slossi* (Kummel & Steele 1962) exhibits a greater whorl height and narrower width. Some of the specimens described by Chao (1959) as *Prosphingites kwangsianus* and *Prosphingites sinensis* may actually correspond to *P. spathi*. Tozer (1994) provided the most recent description of *P. spathi*. However, these appear to be too rounded and laterally compressed to be assigned to this species. The same observation can be made regarding specimens described by Korchinskaya (1982) from Spitsbergen. However, Korchinskaya's and Tozer's specimens could also be extreme, laterally compressed variants of *P. spathi*.

***Paranannites ovum* n. sp.**

Pl. 34, Figs. 1-6

Diagnosis:
Large-sized *Paranannites* with globular inner whorls having a broadly arched venter and a compressed high-whorled shape at maturity.

Holotype:
PIMUZ 26087, Loc. Yu1, Yuping, "*Owenites koeneni* beds", Smithian.

Etymology:
Named for its ovoid mature shape.

Occurrence:
Jin45; Yu1; T8; "*Owenites koeneni* beds".

Description:

Inner whorls involute and globular with broadly arched venter. Larger specimens less involute, significantly more compressed with rounded venter and gently convergent flanks from umbilical shoulder, becoming more convergent near venter. Umbilicus small, but deep with perpendicular wall and abruptly rounded shoulders. Coiling tends to be egressive at maturity. Ornamentation consists of very fine, forward projected plications that fade on venter, as well as very fine, growth lines visible only on largest specimens. Suture line ceratitic, similar to genus *Owenites*, with four saddles, and well crenulated lobes. Ventral saddle with small indentation on sides.

Measurements:
See **Fig. 50**.

Discussion:
P. ovum n. sp. can be distinguished from other *Paranannites* by its larger adult size and its more compressed shell shape.

***Paranannites globosus* n. sp.**

Pl. 35, Figs. 1-9

p ? 1959 *Paranannites involutus* - Chao, p. 285, pl. 24, figs. 13-14

Diagnosis:
Very involute *Paranannites* with a globular shape and a subangular venter on some specimens.

Holotype:
PIMUZ 26094, Loc. Jin30, Jinya, "*Flemingites rursiradiatus* beds", Smithian.

Etymology:
Named for its globular shape.

Occurrence:
Jin4, 23, 24, 28, 29, 30, 41; FSB1/2; Sha1; T6, T50; "*Flemingites rursiradiatus* beds".

Description:

Small, unusual, very involute *Paranannites* with a globular shape. Venter rounded on most specimens, but a few, more compressed variants may exhibit a subangular venter. Umbilicus deep with perpendicular wall and rounded shoulders. Body chamber length greater than one whorl. No visible ornamentation. Ceratitic suture line with wide saddles, very typical of Paranannitidae.

Measurements:
See **Fig. 51**. Measurements indicate that this species exhibits strong allometric growth, especially for whorl width. A rapid increase in width is readily apparent on medium sized specimens.

Discussion:
This species represents an unusual morphology among the Paranannitidae, as demonstrated by its two extreme variants in venter shape (circular to subangular), but it clearly belongs to this family as evidenced by its suture line. Measurements also indicate a large intraspecific variation. This species is closely linked by its morphology and suture line to the genus *Thermalites*. However, its suture line is apparently more divided.

***Paranannites dubius* n. sp.**

Pl. 33, Figs. 11-14

Diagnosis:
Extremely involute *Paranannites* with conspicuous egressive coiling on mature specimens.

Holotype:
PIMUZ 26084, Loc. Jin4, Jinya, "*Flemingites rursiradiatus* beds", Smithian.

Etymology:
From the Latin, meaning doubtful in the sense of not conforming to a pattern.

Occurrence:
Jin4; "*Flemingites rursiradiatus* beds".

Description:
Small, extremely involute, slightly compressed *Paranannites* with an ovoid whorl section, an arched venter, and convex flanks with maximum curvature near umbilicus, convergent to rounded

venter. Umbilicus deep, but extremely narrow (not always visible), with oblique wall and rounded shoulders. Body chamber exceeds one whorl in length. Mature specimens exhibit obvious egressive coiling. No visible ornamentation. Suture line feebly ceratitic, very simple with only two saddles. Adult shell somewhat reminiscent of *Isculitoides* (Spath 1930) of Late Spathian age.

Measurements:
See **appendix 1**.

Discussion:
Although the morphology of this species is not entirely unlike the Paranannitidae, its suture line is very peculiar and resembles some of the simpler suture lines of the Melagathiceratidae. This new species is attributed to *Paranannites* only on the basis of its morphology, but the validity of this assignment must be confirmed.

Paranannitidae gen. indet.

Pl. 33, Figs.15a-d

Occurrence:
Jin30; "*Flemingites rursiradiatus* beds".

Description:
Moderately involute, slightly compressed shell with a low arched venter, indistinct ventral shoulders, and nearly parallel flanks. Umbilicus moderately deep with perpendicular wall and rounded shoulders. Ornamentation consists only of very small plications. Suture line weakly ceratitic with two saddles.

Measurements:
See **appendix 1**.

Discussion:
This specimen is assigned to the Paranannitidae on the basis of its overall shape. It differs from *P.* aff. *P. aspenensis* by its quadratic whorl section and its more parallel flanks.

Owenites Hyatt & Smith, 1905

Type species: *Owenites koeneni* - Hyatt & Smith, 1905, p. 83, pl. 10, figs. 1-22

Owenites koeneni Hyatt & Smith, 1905

Pl. 36, Figs. 1-8

	1905	*Owenites koeneni* - Hyatt & Smith, p. 83, pl. 10, figs. 1-22
	1915	*Owenites koeneni* - Diener, p. 214
	1922	*Owenites koeneni* - Welter, p. 152
	1932	*Owenites koeneni* - Smith, pl. 10, figs. 1-22
	1932	*Owenites egrediens* - Smith (non Welter), p. 100, pl. 52, figs. 6-8
	1932	*Owenites zitteli* - Smith, p. 101, pl. 52, figs. 1-5
	1934	*Owenites koeneni* - Spath, p. 185, figs. 57a-c
	1947	*Owenites* aff. *O. egrediens* - Kiparisova, p. 139, pl. 32, figs. 1-3
	1955	*Kingites shimizui* - Sakagami, p. 138, pl. 2, figs. 2a-c
	1957	*Owenites koeneni* - Kummel in Arkell *et al.*, pL138, figs. 171-8a-b
v	1959	*Owenites costatus* - Chao, p. 249, pl. 22, figs. 7-18, 22, 23, text-fig. 26c
v	1959	*Owenites pakungensis* - Chao, p. 248, pl. 21, figs. 6-8
v	1959	*Owenites pakungensis* var. *compressus* - Chao, p. 248, pl. 21, figs. 4,5, text-fig. 26a
v	1959	*Pseudowenites oxynotus* - Chao, p. 252, pl. 23, figs. 1-16, text-figs. 27a-d
	1959	*Owenites shimizui* - Kummel, p. 430
	1960	*Owenites shimizui* - Kummel & Sakagami, p. 6, pl. 2, figs. 5,6
	1962	*Owenites koeneni* - Kummel & Steele, p. 674, pl. 101, figs. 3-7
	1962	*Owenites koeneni* - Popov, p. 44, pl. 6, fig. 6
	1965	*Owenites koeneni* - Kuenzi, p. 374, pl. 53, figs. 1-6, text-figs. 3d,6
	1966	*Owenites koeneni* - Hada, p. 112, pl. 4, figs. 2-4
	1968	*Owenites koeneni* - Kummel & Erben, p. 121, fig. 12, pl. 19, figs. 10-15
	1968	*Owenites carinatus* - Shevyrev, p. 189, pl. 16, fig. 1
	1968	*Owenites koeneni* - Zakharov, p. 94, pl. 18, figs. 1-3
	1973	*Owenites koeneni* - Collignon, p. 139, pl. 4, figs. 2, 39a
	1979	*Owenites koeneni* - Nichols & Silberling, pl. 1, figs. 17, 18
	1981	*Owenites koeneni* - Bando, p. 158, pl. 17, fig. 7
	1984	*Owenites carinatus* - Vu Khuc, p. 81, pl. 6, figs. 1-4
	1984	*Pseudowenites oxynotus* - Vu Khuc, p. 82, pl. 7, figs. 3, 4
	1990	*Owenites koeneni* - Shevyrev, p. 118, pl. 1, fig. 5
	1995	*Owenites koeneni* - Shevyrev, p. 51, pl. 5, figs. 1-3

2004 *Owenites pakungensis* - Tong *et al.*, p. 199, pl. 2, figs. 9-10, text-fig. 7

Occurrence:

Jin12, 15, 18, 27, 42, 43, 44, 45, 46, 47, 99; NW1; T5, 8, 11; Yu3; "*Owenites koeneni* beds".

Description:

Slightly involute, somewhat compressed shell with an inflated, lenticular whorl section and a typical, subangular to angular venter that may resemble a keel on mature specimens. Narrow, shallow umbilicus, becoming wider at maturity, with a low, steep wall and narrowly rounded shoulders. Coiling egressive. Surface generally smooth, but may exhibit weak, forward projected constrictions and folds as observed on *Paranannites*. Body chamber about one whorl in length. Suture line ceratitic with several divided umbilical lobes.

Measurements:

See **Fig. 52**. Whorl height and umbilical diameter display significant allometric growth.

Discussion:

On the basis of their similar shell morphology, *O. egrediens* Smith (non Welter) and *O. zitteli* Smith (1932) were synonymized with *O. koeneni* by Kummel & Steele (1962) and Kummel & Erben (1968). *Pseudowenites costatus* was separated from *O. koeneni* by Chao (1959) because of slight variations in the auxiliary series of its suture line, but this can not be justified if its ontogenetic development is considered (Kummel & Erben 1968). Kummel & Erben (1968) placed *O. costatus* Chao (1959) in synonymy with *O. carpenteri* Smith (1932), but measurements indicate that this species cannot be distinguished from *O. koeneni*.

Owenites simplex Welter, 1922

Pl. 35, Figs. 20-22

1922 *Owenites simplex* - Welter, pl. 15, fig. 5

1934 *Parowenites simplex* - Spath, p. 187, fig. 58

1959 *Owenites kwangsiensis* - Chao, p. 250, pl. 22, figs. 1-6, text-fig. 26b

v 1959 *Owenites plicatus* - Chao, p. 251, pl. 22, figs. 19-21, 24, 25, text-fig. 26e

1968 *Owenites simplex* - Kummel & Erben, p. 122, figs. 12k, n, o

Occurrence

Jin45; Yu1; "*Owenites koeneni* beds".

Description:

Slightly involute shell, similar to *O. koeneni*, but more compressed, with a subangular to angular venter, bearing a very weak keel. Narrow, moderately deep umbilicus with a low, perpendicular wall and rounded shoulders. Ornamentation consists of conspicuous, prorsiradiate, sigmoidal ribs, as well as a few, very small, fold-like plications on umbilical shoulder. Suture line first presented as goniatitic (see Kummel & Erben 1968), but it is ceratitic and similar to *O. koeneni*.

Measurements:

See **Fig. 53**.

Discussion:

O. simplex is easily distinguished from *O. koeneni* by its less involute coiling and its more compressed shell (**Fig. 54**).

Owenites carpenteri Smith, 1932

Pl. 43, Figs. 15-16

1932 *Owenites carpenteri* - Smith, p. 100, pl. 54, figs. 31-34
1966 *Owenites carpenteri* - Hada, p. 112, pl. 4, figs. 1a-e
1968 *Owenites carpenteri* - Kummel & Erben, p. 122, fig. 12l
1973 *Owenites carpenteri* - Collignon, p. 139, pl. 4, figs. 5, 5a

Occurrence:

Jin47; T12; "*Owenites koeneni* beds".

Description:

Extremely involute, compressed shell with a slightly inflated, lenticular whorl section, a very narrowly rounded to subangular venter, convex flanks, and an occluded umbilicus. Ornamentation consists of thin, slightly projected growth lines and a few folds. Suture line similar to *O. koeneni*.

Measurements:

See **appendix 1**.

Discussion:

Apparently, our specimens are less ornamented than the American specimens described by Smith (1932). However, the occluded umbilicus and narrowly curved venter of our specimens are diagnostic of this species.

Superfamily Sageceratacеae Hyatt, 1884

Family **Hedenstroemiidae** (Hyatt, 1884)

Pseudosageceras Diener, 1895

Type species: *Pseudosageceras* sp. indet. - Diener, 1895

Pseudosageceras multilobatum Noetling, 1905

Pl. 37, Figs. 1-5

	1905	*Pseudosageceras multilobatum* - Noetling in Frech, pl. 25, figs. 1a, b; pl. 26, figs. 3a, b
	1905	*Pseudosageceras intermontanum* - Hyatt & Smith, p. 99, pl. 4, figs. 1-3; pl. 5, figs. 1-6; pl. 63, figs. 1-2
	1909	*Pseudosageceras multilobatum* - Krafft & Diener, p. 145, pl. 21, fig. 5
	1911	*Pseudosageceras multilobatum* - Wanner, p. 181, pl. 7, fig. 4
	1911	*Pseudosageceras drinense* - Arthaber, p. 201, pl. 17, figs. 6, 7
	1922	*Pseudosageceras multilobatum* - Welter, lief. 11, Abh. 19, p. 94, fig. 3
	1929	*Pseudosageceras intermontanum* - Matthews, p. 3, pl. 1, figs. 18-22
	1932	*Pseudosageceras multilobatum* - Smith, p. 87-89, pl. 4, figs. 1-3; pl. 5, figs. 1-6; pl. 25, figs. 7-16; pl. 60, fig. 32; pl. 63, figs. 1-6
non	1932	A*spenites laevis* - Smith, p. 86, pl. 28, figs. 28-30
	1934	*Pseudosageceras multilobatum* - Collignon, p. 56-58, pl. 11, fig. 2
	1934	*Pseudosageceras multilobatum* - Spath, p. 54, fig. 62
	1947	*Pseudosageceras multilobatum* - Kiparisova, p. 127, pl. 25, figs. 3-4
	1947	*Pseudosageceras multilobatum* var. *giganteum* - Kiparisova, p. 127, pl. 26, figs. 2-5
	1948	*Pseudosageceras* cf. *P. clavisellatum* - Renz & Renz, p. 90, pl. 16, fig. 3
	1948	*Pseudosageceras drinense* - Renz & Renz, p. 92, pl. 16, fig. 6
	1948	*Pseudosageceras intermontanum* - Renz & Renz, p. 90-92, pl. 16, figs. 4, 7
v	1959	*Pseudosageceras multilobatum* - Chao, p. 183, pl. 1, figs. 9, 12
v	1959	*Pseudosageceras curvatum* - Chao, p. 184, pl. 1, figs. 13, 14, text-fig. 5a
v	1959	*Pseudosageceras tsotengense* - Chao, p. 184, pl. 1, figs. 7, 8, text-fig. 5b
?	1959	*Pseudosageceras multilobatum* var. nov. - Jeannet, p. 30, pl. 6, fig. 1
	1961	*Pseudosageceras schamarense* - Kiparisova, p. 31, pl. 7, figs. 3-4
	1961	*Pseudosageceras multilobatum* var. *gigantea* - Popov, p. 13, pl. 2, figs. 1-2

non	1962	*Pseudosageceras multilobatum* - Kummel & Steele, p. 701, pl. 102, figs. 1-2
?	1966	*Pseudosageceras multilobatum* - Hada, p. 112, pl. 4, fig. 6
	1968	*Pseudosageceras multilobatum* - Kummel & Erben, p. 112, pl. 19, fig. 9
	1968	*Pseudosageceras multilobatum* - Shevyrev, p. 791, pl. 1, figs. 1-2
?	1973	*Pseudosageceras multilobatum* - Collignon, p. 5, pl. 1, fig. 1
	1978	*Pseudosageceras multilobatum* - Weitschat & Lehmann, p. 95, pl. 10, figs. 2a-b
	1984	*Pseudosageceras multilobatum* - Vu Khuc, p. 26, pl. 1, fig. 1
	1994	*Pseudosageceras multilobatum* - Tozer, p. 83, pl. 18, figs. 1a-b; p. 384, fig. 17

Occurrence:

Jin4, 11, 13, 28, 29, 30, 51; WFB; FW2, 3, 4, 5; Sha1; "*Flemingites rursiradiatus* beds". Jin27, 44; "*Owenites koeneni* beds".

Description:

Extremely involute, compressed oxycone, with an occluded umbilicus, a very narrow, concave, bicarinate venter, especially on mature specimens, and weakly convex flanks, convergent from umbilicus to venter. Surface smooth without ornamentation. Suture line ceratitic, complex and composed of many adventitious elements with characteristic trifid lateral lobe. Other lobes are bifid.

Measurements:

See **Fig. 55**.

Discussion:

P. multilobatum is one of the most cosmopolitan and long-ranging species of the Early Triassic, and has its acme in the Smithian stage.

Hedenstroemia Waagen, 1895

Type species: *Ceratites hedenstroemi* - Keyserling, 1845, p. 166, pl. 2, figs. 5-7

Hedenstroemia hedenstroemi (Keyserling, 1845)

Pl. 38, Figs. 1-4

	1845	*Ceratites hedenstroemi* - Keyserling, p. 166, pl. 2, figs. 5-7

	1888	*Meekoceras* n. f. ind. ex. aff. *M. hedenstroemi* - Mojsisovics, p. 10, pl. 2, figs. 1a-b; pl. 3, fig. 13
	1897	*Hedenstroemia mojsisovisci* - Diener, p. 63, pl. 8, fig. 3
non	1897	*Hedenstroemia mojsisovisci* - Diener, pl. 20, fig. 1
	1909	*Hedenstroemia mojsisovisci* - Krafft & Diener, p. 152, pl. 9, figs. 3-6; pl. 10, figs. 1-3; pl. 20, fig. 1
	1947	*Hedenstroemia hedenstroemi* - Kiparisova, p. 146, pl. 35, figs. 7a-b
	1961	*Hedenstroemia hedenstroemi* - Popov, p. 15, pl. 8, fig. 3
	1979	*Hedenstroemia hedenstroemi* - Dagys *et al.*, p. 127, pl. 5, fig. 2; pl. 6, fig. 1
	1990	*Hedenstroemia hedenstroemi* - Dagys & Ermakova, p. 70, pl. 31, fig. 1; pl. 33, figs. 1-3; pl. 34**,** fig. 1
	1994	*Hedenstroemia hedenstroemi* - Tozer, p. 84, pl. 25, fig. 3; pl. 27, figs. 2a-b

Occurrence:

Jin62; "*Hedenstroemia hedenstroemi* beds".

Description:

Extremely involute, compressed oxycone with an occluded umbilicus, a subtabulate venter (becoming narrowly rounded on largest specimens), angular ventral shoulders, and nearly flat, but slightly convex and convergent flanks. Ornamentation consists only of thin, sinuous growth lines. Suture line typical of Hedenstroemiidae with complex architecture and wide auxiliary series. Width of auxiliary series may vary and another adventious element may be added during ontogeny and/or with difference in specimen size.

Measurements:

See **Fig. 56**.

Discussion:

This species is extremely important because its stratigraphic position represents the lowermost zone of the Smithian in northwestern Guangxi. With the addition of this new material, the zone is now documented within low paleolatitudes (South China), middle paleolatitudes (British Columbia) and high paleolatitudes (Siberia), thus enabling worldwide correlation. Strata containing this species in northwestern Guangxi are characterized by very low faunal diversity.

***Hedenstroemia augusta* n. sp.**

Pl. 39, Figs. 1-11

Diagnosis:

Hedenstroemiidae with extremely involute coiling, a tabulate venter and flanks with two different angles of slope on juvenile specimens.

Holotype:

PIMUZ 26138, Loc. NW13, Waili, "*Anasibirites multiformis* beds", Smithian.

Etymology:

From the Latin, meaning "noble".

Occurrence:

Jin33, 90, 91, 105, 106; FW7, 12; NW13, 15; Yu5, 6; "*Anasibirites multiformis* beds".

Description:

Extremely involute, compressed oxycone with an occluded umbilicus, a narrow, weakly bicarinate venter (tabulate on internal mold), and flanks on juvenile specimens with weak, but distinct longitudinal line at about mid-flank, marking a very slight change in slope between umbilical and ventral portions of flank. Umbilical portion nearly flat, ventral portion slightly convergent to narrow venter. On larger specimens, this change of slope angle disappears and flanks become slightly convex. Ornamentation consists only of thin, but conspicuous, sinuous growth lines. Concave part of growth line located on ventral half of flank. Suture line typical of Hedenstroemiidae with complex architecture exhibiting numerous saddles and a very long auxiliary series. Lateral lobe displays many indentations, thus differentiating this species from other similarly shaped ammonoids, e.g. *P. multilobatum*.

Measurements:

See **Fig. 57**.

Discussion:

The occurrence of this new species of *Hedenstroemia* at the very end of the Smithian clearly documents that this genus is long-ranging. *H. augusta* n. sp. essentially differs from *H.*

hedenstroemi by the presence of a longitudinal line at about mid-flank on juvenile specimens. The whorl width of *H. augusta* n. sp. is somewhat less than that of *Pseudosageceras* and *Cordillerites* (see **Fig. 59**).

Cordillerites Hyatt & Smith, 1905

Type species: *Cordillerites angulatus* - Hyatt & Smith, 1905, p. 110, pl. 2, figs. 1-8; pl. 68, figs. 1-10; pl. 71, figs. 1-6; pl. 85, figs. 14-20

***Cordillerites antrum* n. sp.**

Pl. 40, Figs. 1-9

Diagnosis:
Hedenstroemid with a distinctive tabulate venter, slightly convex flanks, sinuous plications and suture line similar to *Pseudosageceras*, but with a trifid lateral and a trifid first umbilical lobes.

Holotype:
PIMUZ 26148, Loc. Jin61, Jinya, "*Kashmirites densistriatus* beds", Smithian.

Etymology:
From the Latin, meaning "hollow cave".

Occurrence:
Jin61, 64, 65, 66; "*Kashmirites densistriatus* beds".

Description:
Extremely involute, compressed oxycone with an occluded umbilicus and a concave, bicarinate venter on smaller specimens, becoming subtabulate to slightly rounded on body chamber of largest specimens. Flanks nearly flat and convergent with very slight convex curvature, forming somewhat ovoid whorl section on largest specimens. Ornamentation consists of faint, very thin, sinuous growth lines, not particularly conspicuous on largest specimens. Small plications visible near venter on some specimens. Suture line exhibits two adventitious lobes. The two following lobes are trifid as is lateral lobe of *Pseudosageceras*.

Measurements:

See **Fig. 58**.

Discussion:

This genus clearly belongs to the Hedenstroemiidae based on its morphology, suture line and diagnostic measurements (see **Fig. 59**). *Cordillerites* possesses a combination of several characters exhibited by different genera of Hedenstroemiidae, thus making it very difficult to identify without the aid of its suture line. Although it is similar to that of *Pseudosageceras,* its suture line differs by its less complicated structure and characteristic first umbilical trifid lobe. For juvenile specimens, auxiliary elements are less numerous and complex than *Pseudosageceras*. *Clypites* and *Tellerites* are much different from *Cordillerites* in that their suture lines do not display so many adventious elements.

Cordillerites antrum n. sp. appears to be more compressed than *C. angulatus*, and it also exhibits sinuous plications and striae not present on the type species.

Mesohedenstroemia Chao, 1959

Type species: *Mesohedenstroemia kwangsiana* - Chao, 1959, p. 266, pl. 34, figs. 1-18, text-figs. 33b-d

Mesohedenstroemia kwangsiana Chao, 1959

Pl. 41, Figs. 1-8

v	1959	*Mesohedenstroemia kwangsiana* - Chao, p. 266, pl. 34, figs. 1-18, text-figs. 33b-d
v	1959	*Mesohedenstroemia inflata* - Chao, p. 267, pl. 35, figs. 4-8, text-fig. 33a

Occurrence:

Jin4, 11, 13, 23, 24, 28, 29, 30, 41, 51; FW4/5; Sha1; T6, T50; “*Flemingites rursiradiatus* beds”. Jin10; “*Owenites koeneni* beds”.

Description:

Very involute, compressed, discoidal shell with a broad, distinctive tabulate venter, angular ventral shoulders, and flat or gently convex flanks. Umbilicus generally very small on juvenile specimens, opening somewhat on body chamber, may even be wider on largest specimens. When

open, umbilicus is moderately deep with perpendicular wall and abruptly rounded shoulders. Shell usually smooth, but can be ornamented with growth lines on flanks, curving slightly forward near venter. Suture line exhibits one adventitious lobe, but not with trifid division as seen in some genera of the family.

Measurements:
See **Fig. 60**. Whorl height and umbilical diameter exhibit allometric growth while whorl width displays isometric growth.

Discussion:
Mesohedenstroemia kwangsiana is similar to *Hedenstroemia*, but it is characterized by a wider, distinctive tabulate venter. Kummel & Steele (1962) consider *Mesohedenstroemia* to be a synonym of *Pseudohedenstroemia*, but the latter is actually a synonym of *Hedenstroemia*. *Lingyunites* (Chao, 1950), with its discoidal whorl section, tabulate venter and occluded umbilicus, is closely related to *Mesohedenstroemia*, but its suture line is simpler. It can be difficult to distinguish between these two genera, especially juvenile specimens, without the aid of a well preserved suture line and diagnostic measurements.

Mesohedenstroemia planata Chao, 1959

Pl. 41, Figs. 9a-c

v 1959 Mesohedenstroemia planata - Chao, p. 268, pl. 35, figs. 1-3, text-fig. 33e

Occurrence:
Jin45; "*Owenites koeneni* beds".

Description:
Extremely involute, very compressed, discoidal shell with an occluded umbilicus, a subtabulate venter, abruptly rounded ventral shoulders, and nearly parallel flanks. No visible ornamentation. Suture line simple, ceratitic, similar to *M. kwangsiana*.

Measurements:
See **appendix 1**.

Discussion:

The single specimen illustrated as *M. planata* by Chao (1959) appears to have a somewhat questionable umbilicus that may have been the result of excessive preparation. Other diagnostic characters seem to be similar to those of our only specimen. *M. planata* essentially differs from *M. kwangsiana* by its extreme involute coiling.

Family **Aspenitidae** (Spath, 1934)

Aspenites Hyatt & Smith, 1905

Type species: *Aspenites acutus* - Hyatt & Smith, 1905, p. 96, pl. 2, figs. 9-13; pl. 3, figs. 1-5

Aspenites acutus Hyatt & Smith, 1905

Pl. 42, Figs. 1-9

	1905	*Aspenites acutus* - Hyatt & Smith, p. 96, pl. 2, figs. 9-13; pl. 3, figs. 1-5
?	1909	*Hedenstroemia acuta* - Krafft & Diener, p. 157, pl. 9, figs. 2a-d
	1915	*Aspenites acutus* - Diener, p. 59, fig. 20
	1922	*Aspenites acutus* - Welter, p. 97, fig. 7
	1922	*Aspenites laevis* - Welter, p. 19, pl. 1, figs. 4-5
	1932	*Aspenites acutus* - Smith, p. 86, pl. 2, figs. 9-13; pl. 3, figs. 1-5; pl. 30, figs. 1-26; pl. 60, figs. 4-6
	1932	*Aspenites laevis* - Smith, p. 86, pl. 28, figs. 28-33
	1932	*Aspenites obtusus* - Smith, p. 86, pl. 31, figs. 8-10
	1934	*Aspenites acutus* - Spath, p. 229, fig. 76
?	1934	*Parahedenstroemia acuta* - Spath, p. 221, fig. 70
	1957	*Aspenites acutus* - Kummel in Arkell *et al.*, p. L142, figs. 173-1a-c
v	1959	*Aspenites acutus* - Chao, p. 269, pl. 35, figs. 12-18, 23, text-fig. 34a
v	1959	*Aspenites laevis* - Chao, p. 270, pl. 35, figs. 9-11, 23, text-fig. 34b
	1962	*Aspenites acutus* - Kummel & Steele, p. 692, pl. 99, figs. 16-17
	1962	*Hemiaspenites obtusus* - Kummel & Steele, p. 666, pl. 99, figs. 16-17
	1979	*Aspenites*? cf. *A. acutus* - Nichols & Silberling, pl. 1, figs. 10-11
	1979	*Aspenites acutus* - Nichols & Silberling, pl. 1, figs. 12-14

Occurrence:

Jin4, 23, 28, 29, 30, 41, 51; Sha1; T6, T50; "*Flemingites rursiradiatus* beds". Jin10, 27; "*Owenites koeneni* beds".

Description:

Extremely involute, very compressed oxycone with an acutely keeled venter, an occluded umbilicus and slightly convex flanks with maximum curvature at mid-flank. Umbilical region slightly depressed. Surface generally smooth or ornamented with falcoid growth lines, and radial

folds disappearing near venter. Suture line complex with wide, curved series of small auxiliary saddles.

Measurements:
See **Fig. 61**. Whorl height exhibits isometric growth.

Discussion:
Aspenites acutus is easily distinguishable among the Aspenitidae by its occluded umbilicus and very acute venter. Prior to our study, the genus consisted of only two species: *A. acutus* Hyatt & Smith (1905) and *A. laevis* Welter (1922). Kummel & Steele (1962) differentiated between these two species based only on their assertion that the suture line of *A. laevis* was more complex. However, all comparisons and especially diagnostic measurements, lead us to conclude they should be synonymized within a single species. Undeniably, the suture line of the *A. laevis* type specimen represents the adult stage (see Kummel & Steele [1962] for comparison).
Similarly, the genus *Hemiaspenites* Kummel & Steele (1962) must also be synonymized with *Aspenites*. Indeed, Kummel & Steele stressed that the suture line of *Hemiaspenites* was different, but their illustrations (text-fig. 5f, g) clearly indicate the suture lines, either were excessively ground in preparation, or are poorly preserved, and actually represent a juvenile stage of *A. acutus*.

?*Aspenites* sp. indet.

Pl. 42, Figs. 10-11

Occurrence:
Jin27, 45, 99; NW1; Yu1; "*Owenites koeneni* beds".

Description:
Extremely involute, very compressed oxycone similar to *A. acutus*, but much larger with an acutely keeled venter on largest specimens and flanks slightly more convex than *A. acutus*. Character of umbilicus unknown. Our specimens consist only of adult body chambers. Umbilical area relatively shallow in comparison with large size of our specimens. No visible umbilical shoulders. Only visible ornamentation consists of some sinuous growth lines and folds. Suture line unknown, all specimens are adult body chambers.

Discussion:

Material here referred to as ?*Aspenites* sp. indet. may represent adult body chamber of *A. acutus*. However, given the fragmentary nature of these specimens and the absence of suture line, a more precise identification remains impossible.

Pseudaspenites Spath, 1934

Type species: *Aspenites layeriformis* - Welter, 1922, p. 97, pl. 1, figs. 6-8

Pseudaspenites layeriformis (Welter, 1922)

Pl. 43, Figs. 1-6

p	1922	*Aspenites layeriformis* - Welter, p. 97, pl. 1, figs. 6-7 [fig. 8 = ?*Aspenites acutus*]
	1934	*Pseudaspenites layeriformis* - Spath, p. 230, fig. 77
v	1959	*Inyoites striatus* - Chao, p. 197, pl. 2, figs. 22-26
v	1959	*Inyoites obliplicatus* - Chao, p. 198, pl. 2, figs. 7, 17-21, 27

Occurrence:

Jin4, 13, 23, 28, 29, 30; FW2, 3, 4, 5; Sha1; T6, T50; "*Flemingites rursiradiatus* beds"

Description:

Involute, very compressed oxycone with a relatively broad umbilicus, an acutely keeled venter and generally flat, nearly smooth, convergent flanks. Extremely shallow umbilicus with slightly angular, very short shoulders. Ornamentation on some specimens consists of extremely fine, forward projecting, sigmoidal striation that forms a distinctive keel. On some specimens, these projections form a delicate, crenulated keel. Suture line ceratitic with smaller auxiliary series than *A. acutus*. Lobes also broader and more indented.

Measurements:

See **Fig. 62**.

Discussion:

The formation of a crenulated keel on certain specimens is puzzling when compared to other, similar sized specimens without this unusual ornamentation. One obvious possibility is that

specimens with the crenulated keel represent a different, but very rare species. However, their diagnostic measurements are all consistent with *A. layeriformis*.

The illustration of the suture line of the type species by Welter (1922) strongly resembles that of *Aspenites*. The suture line of *Pseudaspenites layeriformis* has broad, well indented lobes, reduced auxiliary series and lack of adventious elements. These differences suggest the possibility of confusion in Welter's illustration of the suture lines for these two genera.

***Pseudaspenites evolutus* n. sp.**

Pl. 43, Figs. 7-11

Diagnosis:

Pseudaspenites with more evolute coiling than *P. layeriformis* and with a lower keel.

Holotype:

PIMUZ 26186, Loc. Jin30, Jinya, "*Flemingites rursiradiatus* beds", Smithian.

Etymology:

Named for its evolute coiling.

Occurrence:

Jin4, 23, 28, 29, 30; Sha1; *Flemingites rursiradiatus* beds".

Description:

Whorl section nearly identical to *P. layeriformis*, but less involute, with a more acute venter (with a thin keel) and a relatively broad umbilicus. Coiling slightly egressive on largest specimens. Weak folds and growth lines are visible, but do not extend onto the keel as in *P. layeriformis*. Suture line unknown.

Measurements:

See **Fig. 63**.

Discussion:

P. evolutus n. sp. essentially differs from *P. layeriformis* by its more evolute coiling (**Fig. 65**), but this distinction is often tenuous, especially for small-sized specimens.

Pseudaspenites tenuis (Chao, 1959)

Pl. 43, Figs. 12-14

v 1959 *Aspenites tenuis* - Chao, p. 271, pl. 35, figs. 19-22, text-fig. 34c

Occurrence:

Jin4, 10, 23, 30; *Flemingites rursiradiatus* beds" and "*Owenites koeneni* beds".

Description:

Whorl section similar to *P. layeriformis*, but much more compressed. Degree of involution similar to *P. layeriformis* for small specimens. Ornamentation consists only of very weak folds. Suture line typical of *Pseudaspenites* with broad indented lobes and very small auxiliary series.

Measurements:

See **Fig. 64**.

Discussion:

P. tenuis is much more compressed than all other species of *Pseudaspenites* (see **Fig. 65**). It also lacks a keel.

Family **Anderssonoceratidae** Ruzhencev, 1959

Proharpoceras Chao, 1950

Type species: *Proharpoceras carinatitabulatum* - Chao, 1950, p. 8, pl. 1, figs. 8a, b

Proharpoceras carinatitabulatum Chao, 1950

Pl. 38, Figs. 5-9

v	1950	*Proharpoceras carinatitabulatum* - Chao, p. 8, pl. 1, figs. 8a, b
v	1950	*Tuyangites marginalis* - Chao, p. 9, pl. 1, fig. 9
v	1959	*Proharpoceras carinatitabulatum* - Chao, p. 324, pl. 43, figs. 1-7
v	1959	*Tuyangites marginalis* - Chao, p. 327, pl. 43, figs. 17, 18
v	1959	*Prosphingites sinensis* - Chao, p. 297, number 12583
	1968	*Proharpoceras carinatitabulatum* - Zakharov, p. 147, pl. 29, fig. 6

Occurrence:

Jin45; Yu1; "*Owenites koeneni* beds".

Description:

Moderately evolute, thick platycone with a quadratic whorl section, distinctive, "tabulate" to tectiform venter with a raised keel, and parallel, nearly flat or gently convex flanks. On specimens with well preserved outer shell, venter is seen to actually be tricarinate with very small marginal keels rising from ventral shoulders. Umbilicus wide, with moderately high, slightly oblique wall and rounded shoulders. Body chamber ca. one whorl in length. Ornamentation consists of convex growth lines and ridges on flanks, then becoming strongly projected on venter. Projected, ventral growth lines converge at central keel on largest specimens. Suture line composed of narrow ventral lobe and two broad, lateral ceratitic lobes. Saddles asymmetrical. Suture line first described as goniatitic by Chao (1959), and then as ceratitic by Zakharov (1968).

Measurements:

See **Fig. 66**.

Discussion:

The distinctive tricarinate morphology of this species is strongly reminiscent of the Permian Anderssonoceratidae and Araxoceratidae, with the exception of its umbilical shoulders, which are not raised. Its suture line is also similar to the Late Permian Anderssonoceratidae. These characteristics justify its revised systematic placement within this family.

Tuyangites, also described by Chao (1950) exhibits identical morphological characters (especially backward projected ribs on its flanks and marginal ridges), but it differs by having weak nodes on the inner whorls. These inner nodes can be observed not only on the holotype (number 12278) in Chao's collection at Nanjing, but also on some of our *Proharpoceras* specimens. Therefore, the near identical morphology and ornamentation of *Tuyangites* provide ample justification to synonymize these two genera. Chao (1959) also described a second species, *Proharpoceras tricarinatum*, which could not be duplicated here.

INCERTAE SEDIS

***Larenites* n. gen.**

Type species: *Flemingites reticulatus* - Tozer, 1994, p. 71, pl. 20, figs. 5-7

Composition of the genus:
Larenites reticulatus (Tozer, 1994).

Diagnosis:
Very involute with a broad venter, plications and strigation.

Etymology:
Named after the small village of Laren, Guangxi.

Occurrence:
"*Kashmirites densistriatus* beds" and "*Flemingites rursiradiatus* beds".

Discussion:
This species was provisionally assigned to *Flemingites* by Tozer (1994), but it is in fact rather different from the type species of *Flemingites*. Therefore, a new genus is erected and the species name is retained. This genus, with its involute coiling, also resembles *Subflemingites* (Spath, 1934), but the latter is smooth. Assignment of *Larenites reticulatus* to Flemingitidae by Tozer remains uncertain in the absence of illustration of the suture line. Its general shape strongly suggests affinity with Proptychitidae.
Tozer (1994) reported the occurrence of this species from the Late Dienerian Sverdrupi Zone of British Columbia. The new occurrences from Guangxi come from the "*Kashmirites densistriatus* beds" and "*Flemingites rursiradiatus* beds", thus expanding the range of this species across the Dienerian/Smithian boundary.

***Larenites* cf. *L. reticulatus* n. gen.** (Tozer, 1994)

Pl. 24, Figs. 1-2

1994 *Flemingites reticulatus* - Tozer, p. 71, pl. 20, figs. 5-7

Occurrence:
Jin23, 66; "*Kashmirites densistriatus* beds" and "*Flemingites rursiradiatus* beds".

Description:
Involute, thick platycone with a subtabulate venter, rounded ventral shoulders and convex flanks with maximum lateral curvature near mid-flank. Umbilicus with high, slightly overhanging wall and rounded shoulders. Ornamentation consists of conspicuous folds and irregular, sinuous plications as well as obvious strigation on venter and a portion of ventral shoulders. Suture line unknown for our specimens.

***Guodunites* n. gen.**

Type species: *Guodunites phylloceratoides* n. gen., n. sp.

Composition of the genus:
Type species only.

Diagnosis:
Involute, compressed platycone with dense, thickened growth striae, resembling radial lirae of some Phylloceratidae. Suture line ceratitic with a markedly indented ventral saddle.

Etymology:
Named for our colleague Kuang Guodun (Nanning).

Occurrence:
"*Owenites koeneni* beds".

Discussion:
This genus embodies a unique combination of outer shell shape, striation and suture line, which so far, is unknown in the Early Triassic, and consequently, family assignment is not possible.

***Guodunites monneti* n. gen., n. sp.**

Pl. 44, Figs. 1-2

Diagnosis:
As for the genus.

Holotype:
PIMUZ 26193, Loc. Jin99, Jinya, "*Owenites koeneni* beds", Smithian.

Etymology:
Named for C. Monnet (Zurich).

Occurrence:
Jin12, 99; Yu7; "*Owenites koeneni* beds".

Description:
Involute, compressed platycone with a broadly arched to subtabulate venter, becoming more highly arched on larger specimens, and slightly convex flanks with maximum curvature near venter. Umbilicus relatively shallow for juvenile specimens, but umbilical characteristics unknown for largest specimens due to fragmentary nature of material. Ornamentation on large specimens consists of very fine, but conspicuous growth striae. A few plications are visible on smaller specimens. Suture line ceratitic, but incompletely known. It exhibits a high, first lateral saddle, and a large ventral saddle, which is crenulated on its ventral side.

Measurements:
See **appendix 1**.

***Procurvoceratites* n. gen.**

Type species: *Procurvoceratites pygmaeus* n. gen., n. sp.

Composition of the genus:
Three species: *Procurvoceratites pygmaeus* n. gen., n. sp.; *Procurvoceratites ampliatus* n. gen., n. sp.; *Procurvoceratites tabulatus* n. gen., n. sp.

Diagnosis:
Involute, very small platycone with forward projected constrictions.

Etymology:
From the Latin “procurvus”, meaning “bent forward”.

Occurrence:
“*Flemingites rursiradiatus* beds”.

Discussion:
This genus is characterized by its distinctive, forward projected constrictions, which resemble the ornamentation of some Melagathiceratidae (*e.g. Juvenites*). However, its extremely small size, and high projection angle of its constrictions are very unique characteristics. Since its suture line is unknown, it cannot be assigned to a specific family.

***Procurvoceratites pygmaeus* n. gen., n. sp.**

Pl. 44, Figs. 3-5

Diagnosis:
Very small shell with involute coiling and sinuous projections.

Holotype:
PIMUZ 26195, Loc. Jin28, Jinya, “*Flemingites rursiradiatus* beds”, Smithian.

Etymology:
From the Latin “pygmaeus” referring to the extremely small size of its adult stage.

Occurrence:
Jin4, 28, 29, 30; “*Flemingites rursiradiatus* beds”.

Description:
Moderately involute, very small-sized platycone with a circular venter, rounded ventral shoulders, and concave flanks. Umbilicus with short wall and rounded shoulders. Ornamentation consists

only of strongly projected, prorsiradiate constrictions. Maturity is reached at a diameter of about 8 mm. Suture line unknown.

Measurements:
See **Fig. 67**.

***Procurvoceratites ampliatus* n. gen., n. sp.**

Pl. 44, Fig. 6

Diagnosis:
Procurvoceratites with forward projected, concave constrictions and a thick whorl width.

Holotype:
PIMUZ 26198, Loc. Jin30, Jinya, "*Flemingites rursiradiatus* beds", Smithian.

Etymology:
From the Latin "ampliatus" meaning "enlarged".

Occurrence:
Jin30; "*Flemingites rursiradiatus* beds".

Description:
Involute, very small platycone with a circular venter, rounded ventral shoulders and slightly convex flanks. Whorl width slightly thicker than *P. pygmaeus*. Umbilicus with moderately high wall and rounded shoulders. Ornamentation consists only of prorsiradiate and projected concave constrictions.

Measurements:
See **Fig. 67**.

***Procurvoceratites subtabulatus* n. gen., n. sp.**

Pl. 44, Fig. 7

Diagnosis:

Procurvoceratites with forward projected, concave constrictions and a subtabulate venter.

Holotype:

PIMUZ 26199, Loc. Jin30, Jinya, "*Flemingites rursiradiatus* beds", Smithian.

Etymology:

Species name refers to its subtabulate venter.

Occurrence:

Jin30; "*Flemingites rursiradiatus* beds".

Description:

Involute, compressed platycone with a subtabulate venter, abruptly rounded ventral shoulders and nearly parallel flanks. Whorl height greater than *P. pygmaeus*. Umbilical depth moderately shallow with perpendicular wall and rounded shoulders. Ornamentation consists of prorsiradiate, projected, concave constrictions that form small crenulations as they cross the subtabulate venter. Suture line unknown.

Measurements:

See **appendix 1**.

Discussion:

This species is closely linked to *P. pygmaeus* and may represent a laterally compressed variant. However, large enough samples documenting such a large intraspecific variation are not available.

Gen. indet. A

Pl. 45, Fig. 1

Occurrence:

Jin12; "*Owenites koeneni* beds".

Description:

Single specimen consisting only of a portion of the body chamber. Very evolute, serpenticone with a circular venter, rounded ventral and umbilical shoulders and gently convex flanks. Ornamentation consists of deep, distant (5 to 6 on half volution), concave constrictions that form a somewhat corrugated surface on inner mold. Constrictions tend to be less pronounced near aperture. Inner whorls and suture line unknown.

Gen. indet. B

Pl. 45, Fig. 4

Occurrence:

Yu22; "*Anasibirites multiformis* beds".

Description:

Single specimen only represented by a portion of body chamber. Evolute, compressed platycone with a narrowly rounded venter, rounded ventral and umbilical shoulders, and slightly convex flanks. Ornamentation consists of only large folds. Inner whorls and suture line unknown.

Gen. indet. C

Pl. 45, Fig. 2

Occurrence:

Yu22; "*Anasibirites multiformis* beds".

Description:

Small, evolute, compressed platycone with a narrowly rounded venter, rounded ventral and umbilical shoulders, and weakly convex flanks with maximum curvature near venter. Our single specimen is fragmentary, but umbilicus appears relatively shallow with oblique wall. Ornamentation consists of distinctive, straight, radial ribs. Suture line unknown.

Gen. indet. D

Pl. 45, Fig. 3

Occurrence:

Yu22; "*Anasibirites multiformis* beds".

Description:

Genus only represented by part of body chamber. Evolute serpenticone with a low-rounded venter, rounded ventral and umbilical shoulders, and weakly convex flanks. Umbilicus apparently moderately deep with perpendicular wall. Ornamentation consists of weak, distant, and slightly projected plications, more pronounced near venter. Suture line unknown.

Order Phylloceratitida Zittel, 1884

Superfamily Ussuritaceae Hyatt, 1900

Family **Palaeophyllitidae** Popov, 1958

?Palaeophyllitidae gen. indet.

Pl. 8, Figs. 7a-d

Occurrence:
Jin47; Yu7; "*Owenites koeneni* beds".

Description:
Evolute, compressed shell with an ovoid whorl section, a circular venter, rounded ventral shoulders and weakly convex, convergent flanks. Umbilicus moderately deep with perpendicular wall and rounded shoulders. Ornamentation consists of more or less dense, almost straight plications, as well as dense radial lirae, which are easily visible at all developmental stages. Plications appear denser and more regular on inner whorls. Suture line displays phylloid saddles and broad lateral lobe. Lobes are well indented.

Measurements:
See **appendix 1**.

Discussion:
The combination of shell shape and radial lirae displayed by this specimen is somewhat reminiscent of some Spathian Palaeophyllitidae. In addition, the suture line exhibits phylloid saddles and a structural scheme close to those of Spathian Palaeophyllitidae. Upon evaluation of these diagnostic characteristics, we have assigned it, with some reservation, to Palaeophyllitidae, but additional specimens must be collected in order to confirm this assignment. However, this new Chinese specimen does suggest that the origin of Palaeophyllitidae could be older than previously thought (Smithian *contra* Spathian).

Acknowledgements:

Kuang Guodun (Nanning) is gratefully acknowledged for his enthusiasm and invaluable assistance in the field. Thomas Galfetti and Nicolas Goudemand (Zurich) are also thanked for their help in the field. Jim Jenks (Salt Lake City) is thanked for the loan of comparative material and for improving the English text. Claude Monnet (Zurich) is thanked for the use of his statistical analyses software. F. Stiller (Nanjing) kindly opened the doors of Chao's collection. Technical support for photography and preparation was provided by Heinz Lanz, Rosemarie Roth, Markus Hebeisen, Julia Huber and Leonie Pauli (Zurich). This paper is a contribution to the Swiss National Science Foundation project 200020-105090. A.B. has also benefited from a region Rhône-Alpes Eurodoc grant.

References:

Arkell, W.J., Furnish, W.M., Kummel, B., Miller, A.K., Moore, R.C., Schindewolf, O., Sylvester-Bradley, P.C. & Wright, C.W. 1957. Treatise on invertebrate Paleontology, part L., Mollusca 4, Cephalopoda, Ammonoidea. Geological Society of America and University of Kansas Press, 490 pp.

Arthaber, G.v. 1911. Die Trias von Albanien. *Beiträge zur Paläontologie und Geologie 24*, 169-276.

Bando, Y. 1964. The Triassic stratigraphy and ammonite fauna of Japan. *The Science Reports of the Tohoku University, Sendai, Japan - Second Series (Geology) 36*, 1-137.

Bando, Y. 1981. Lower Triassic ammonoids from Guryul Ravine and the Spur three kilometres north of Burus. In: Nakazawa, K. and H.R. Kapoor (Editors), The Upper Permian and Lower Triassic faunas of Kashmir. Palaeontologia Indica, New series, pp. 137-171.

Boulin, J. 1991. Structures in Southwest Asia and evolution of the Eastern Tethys. *Tectonophysics 196*, 211-268.

Brayard, A., Bucher, H., Escarguel, G., Fluteau, F., Bourquin, S. & Galfetti, T. in press. The Early Triassic ammonoid recovery: paleoclimatic significance of diversity gradients. *Palaeogeography Palaeoclimatology Palaeoecology*.

Brayard, A., Héran, M.-A., Costeur, L. & Escarguel, G. 2004. Triassic and Cenozoic palaeobiogeography: two case studies in quantitative modelling using IDL. *Palaeontologia Electronica 7*, 22 pp.

Chao, K. 1950. Some new ammonite genera of Lower Triassic from western Kwangsi. *Palaeontological Novitates 5*, 1-11.

Chao, K. 1959. Lower Triassic ammonoids from Western Kwangsi, China. *Palaeontologia Sinica, New Series B 9*, 355 pp.

Collignon, M. 1933-1934. Paléontologie de Madagascar XX - Les céphalopodes du Trias inférieur. *Annales de Paléontologie 12-13*, 151-162 & 1-43.

Collignon, M. 1973. Ammonites du Trias inférieur et moyen d'Afghanistan. *Annales de Paléontologie 59*, 127-163.

Dagys, A.S., Archipov, Y.V. & Bychkov, Y.M. 1979. Stratigraphy of the Triassic system of northeastern Asia. *USSR Academy of Sciences, Siberian Branch, Transactions of the Institute of Geology and Geophysics 447*, 243 pp (in Russian).

Dagys, A.S., Bucher, H. & Weitschat, W. 1999. Intraspecific variation of *Parasibirites kolymensis* Bychkov (Ammonoidea) from the Lower Triassic (Spathian) of Arctic Asia. *Mitteilungen aus dem Geologischen - Paläontologisches Institut - Universität Hamburg 83*, 163-178.

Dagys, A.S. & Ermakova, S.P. 1988. Boreal Late Olenekian ammonoids. *Transactions of the Academy of Sciences of the USSR 714*, 136 pp. (in Russian).

Dagys, A.S. & Ermakova, S.P. 1990. Early Olenekian ammonoids of Siberia. Nauka, Moskow 112 pp. (in Russian).

Dagys, A.S. & Konstantinov, A.G. 1984. The genus *Dieneroceras* in the Lower Triassic. *Institute of Geology and Geophysics of the Siberian Division of the USSR, Academy of Sciences 600*, 27-40.

Dagys, A.S. & Weitschat, W. 1993. Intraspecific variation in Boreal Triassic ammonoids. *Geobios, M.S. 15*, 107-109.

de Koninck, L. G. 1863. Descriptions of some fossils from India, discovered by Dr. A. Fleming, of Edinburg. *Quaterly Journal of the Geological Society of London 19*, 1-19.

Diener, C. 1895. Triasdische cephalopodenfaunen der Ostsibirischen Küstenprovinz. *Memoires du Comité Géologique 14*, 1-59.

Diener, C. 1897. Part I: the Cephalopoda of the Lower Trias. *Palaeontologia Indica, Ser. 15. Himalayan fossils 2*, 1-181.

Diener, C. 1915. Fossilium Catalogus I, Animalia. Part. 8, Cephalopoda Triadica, 369 pp.

Enkin, R.J., Yang, Z., Chen, Y. & Courtillot, V. 1992. Paleomagnetic constraints on the geodynamic history of the major blocks of China from the Permian to the Present. *Journal of Geophysical Research 97*, 13953-13989.

Ermakova, S.P. 2002. Zonal standard of the Boreal Lower Triassic. Nauka, Moscow 109 pp. (in Russian).

Fan, P.-F. 1978. Outline of the tectonic evolution of Southwestern China. *Tectonophysics 45*, 261-267.

Fraiser, M., Twitchett, R.J. & Bottjer, D.J. 2005. Unique microgastropod biofacies in the Early Triassic: indicator of long-term biotic stress and the pattern of biotic recovery after the end-Permian mass extinction. *C.R. Palevol 4*, 475-484.

Frebold, H. 1930. Die altersstellung des fischhorizontes, des grippianiveaus und des unteren saurierhorizontes in Spitzbergen. *Skrifter om Svalbard og Ishavet 28*, 1-36.

Frech, F. 1902. Lethaea Geognostica, I. Lethaea Palaeozoica, 2, Die Dyas (Schluss), pp. 579-788.

Galfetti, T., Bucher, H., Brayard, A., Hochuli, P.A., Weissert, H., Guodun, K., Atudorei, V. & Guex, J. submitted. Late Early Triassic climate change: insights from carbonate carbon isotopes, sedimentary evolution and ammonoid paleobiogeography. *Palaeogeography, Palaeoclimatology, Palaeoecology*.

Gilder, S.A., Coe, R.S., Wu, H., Guodun, K., Zhao, X. & Wu, Q. 1995. Triassic paleomagnetic data from South China and their bearing on the tectonic evolution of the western circum-Pacific region. *Earth and Planetary Sciences Letters 131*, 269-287.

Guex, J. 1978. Le Trias inférieur des Salt Ranges (Pakistan): problèmes biochronologiques. *Eclogae Geologicae Helvetiae 71*, 105-141.

Hada, S. 1966. Discovery of Early Triassic ammonoids from Gua Musang, Kelantan, Malaya. *Journal of Geosciences, Osaka City University 9*, 111-113.

Hammer, Ø. & Bucher, H. 2005. Buckman's first law of covariation – a case of proportionality. *Lethaia 38*, 67-72.

Hsü, T.-Y. 1940. Some Triassic sections of Kueichow. *Bulletin of the Geological Society of China 20*, 161-172.

Hsü, T.-Y. 1943. The Triassic formations of Kueichou. *Bulletin of the Geological Society of China 23*, 121-128.

Hyatt, A. 1900. Cephalopoda. In: K.A.v. Zittel (Editor), Textbook of paleontology, McMillan, London, pp. 502-604.

Hyatt, A. & Smith, J.P. 1905. The Triassic cephalopod genera of America. *USGS Professional Paper 40*, 1-394.

Jeannet, A. 1959. Ammonites permiennes et faunes triasiques de l'Himalaya central (expédition suisse Arn. Heim et A. Gansser, 1936). *Palaeontologia Indica 34*, 1-189.

Keyserling, A.v. 1845. Beschreibung einiger von Dr. A. Th. v. Middendorff mitgebrachten Ceratiten des arctischen Sibiriens. *Bulletin de l'Académie Impériale des Sciences de St-Pétersbourg 5*, 161-174.

Kiparisova, L.D. 1947. Atlas of the Guide Forms of the fossil faunas of the USSR 7, Triassic. All Union Scientific Geological Research Institute (VSEGEI), Leningrad (in Russian).

Kiparisova, L.D. 1961. Palaeontological fundamentals for the stratigraphy of Triassic deposits of the Primorye region, I, Cephalopod Mollusca. Transactions of the All Union Scientific Geological Research Institute (VSEGEI), new series, 48, Leningrad (in Russian).

Korchinskaya, M.V. 1982. Explanatory note on the biostratigraphic scheme of the Mesozoic (Trias) of Spitsbergen. USSR Ministry of Geology, PGO Sevmorgeologia 99 pp.

Krafft, A.v. & Diener, C. 1909. Lower Triassic cephalopoda from Spiti, Malla Johar, and Byans. *Palaeontologia Indica 6*, 1-186.

Kuenzi, W.D. 1965. Early Triassic (Scythian) ammonoids from Northeastern Washington. *Journal of Paleontology, 39*, 365-378.

Kummel, B. 1952. A classification of the Triassic ammonoids. *Journal of Paleontology 26*, 847-853.

Kummel, B. 1957. See Arkell et al. 1957.

Kummel, B. 1961. The Spitsbergen arctoceratids. *Bulletin of the Museum of Comparative Zoology 123*, 499-532.

Kummel, B. & Erben, H.K. 1968. Lower and Middle Triassic cephalopods from Afghanistan. *Palaeontographica 129*, 95-148.

Kummel, B. & Sakagami, S. 1960. Mid-Scythian ammonites from Iwai formation, Japan. *Breviora, Museum of Comparative Zoology 126*, 1-13.

Kummel, B. & Steele, G. 1962. Ammonites from the Meekoceras gracilitatus zone at Crittenden Spring, Elko County, Nevada. *Journal of Paleontology 36*, 638-703.

Lehrmann, D.J., Payne, J.L., Felix, S.V., Dillett, P.M., Hongmei, W., Youyi, Y. & Jiayong, W. 2003. Permian-Triassic boundary sections from shallow-marine carbonate platforms of the Nanpanjiang basin, South China: implications for oceanic conditions associated with the End-Permian extinction and its aftermath. *Palaios 18*, 138-152.

Lilliefors, H.W. 1967. On the Kolmogorov-Smirnov test for normality with mean and variance unknown. *American Statistical Association Journal 62*, 399-402.

Lindstrom, G. 1865. Om Trias och Juraforsteningar fran Spetsbergen. *Svenska Vetenskap-Akademien Handlingar 6*, 1-20.

Mathews, A.A.L. 1929. The Lower Triassic cephalopod fauna of the Fort Douglas area, Utah. *Walker Museum Memoirs 1*, 1-46.

Mojsisovics, E. 1886. Arktische Triasfaunen. *Mémoires de l'Académie Impériale des Sciences de St-Pétersbourg, VIIe série 33*.

Mojsisovics, E. 1888. Ueber einige arktische Trias-ammoniten des noerdlichen Sibirien. *Mémoires de l'Académie Impériale des Sciences de St-Pétersbourg, VIIe série 36*.

Monnet, C. & Bucher, H. 2005. New Middle and Late Anisian (Middle Triassic) ammonoid faunas from northwestern Nevada (USA): taxonomy and biochronology. *Fossils and Strata 52*, 121 pp.

Nichols, K.M. & Silberling, N.J. 1979. Early Triassic (Smithian) ammonites of Paleoequatorial affinity from the Chulitna terrane, South-central Alaska. *Geological Survey Professional Paper 1121-B*, B1-B5.

Noetling, F. 1905. Die asiatische Trias. In: Frech, F. (Editor), Lethaea geognostica. Verlag der E. Schweizerbart'schen Verlagsbuchhandlung (E. Nägele), Stuttgart, pp. 107-221.

Popov, Y. 1961. Triassic ammonoids of northeastern USSR. *Transactions, Scientific Research Institute for the Geology of the Arctic (NIIGA) 79*, 1-179 (in Russian).

Popov, Y. 1962. Some Early Triassic ammonoids of northern Caucasus. *Transactions of the Academy of Sciences of the USSR 127*, 176-184 (in Russian).

Renz, C. & Renz, O. 1948. Eine untertriadische Ammonitenfauna von der griechischen Insel Chios. *Schweizerische Palaeontologische Abhandlungen 66*, 3-98.

Ruzhencev, V.E. 1959. Classification of the superfamily Otoceratacеae. *Paleontological journal 2*, 56-67.

Sakagami, S. 1955. Lower Triassic ammonites from Iwai, Orguno-Mura, Nishitamagun, Kwanto *massif, Japan. Science Reports Tokyo Kyoiku Diagaku, series C 30*, 131-140.

Shevyrev, A.A. 1968. Triassic ammonoidea from the southern part of the USSR. *Transactions of the Palaeontological Institute, 119*. Nauka, Moscow (in Russian).

Shevyrev, A.A., 1990. Ammonoids and chronostratigraphy of the Triassic. *Trudy Paleontologiceskogo Instituta (Akademija Nauk SSR) 241*, 1-179 (in Russian).

Shevyrev, A.A. 1995. Triassic ammonites of northwestern Caucasus. Nauka, Moscow *264*, 174 pp. (in Russian).

Smith, J.P. 1904. The comparative stratigraphy of the marine Trias of Western America. *Proceedings of the California Academy of Sciences, series 3, 1*, 323-430.

Smith, J.P. 1914. Middle Triassic marine invertebrate faunas of North America. *USGS Professional Paper 83*, 1-254.

Smith, J.P. 1927. Upper Triassic marine invertebrate faunas of North America. *USGS Professional Paper 141*, 1-262.

Smith, J.P. 1932. Lower Triassic ammonoids of North America. *USGS Professional Paper 167*, 1-199.

Spath, L.F. 1930. The Eotriassic invertebrate fauna of east Greenland. *Saertryk af Meddelelser om Gronland 83*, 1-90.

Spath, L.F. 1934. Part 4: the ammonoidea of the Trias, Catalogue of the fossil cephalopoda in the British Museum (Natural History). The Trustees of the British Museum, London, 521 pp.

Tong, J. & Yin, H. 2002. The Lower Triassic of South China. *Journal of Asian Earth Sciences 20*, 803-815.

Tong, J., Yin, H., Zhang, J. & Zhao, L. 2001. Proposed new Lower Triassic stages in South China. *Science in China (series D) 44*, 961-967.

Tong, J., Zakharov, V.A. & Wu, S. 2004. Early Triassic ammonoid succession in Chaohu, Anhui province. *Acta Palaeontologica Sinica 43*, 192-204.

Tozer, E.T. 1967. A standard for Triassic time. *Geologic Survey of Canada Bulletin 156*, 141 pp.

Tozer, E.T. 1981. Triassic ammonoidea: classification, evolution and relationship with Permian and Jurassic forms. In: M.R. House & J.R. Senior (Editors), The ammonoidea. The Systematics association, London, pp. 65-100.

Tozer, E.T. 1994. Canadian Triassic ammonoid faunas. *Geologic Survey of Canada Bulletin 467*, 663 pp.

Twitchett, R.J. & Oji, T. 2005. Early Triassic recovery of echinoderms. *C.R. Palevol 4*, 463-474.

Vu Khuc 1984. Triassic ammonoids in Vietnam. Geoinform and Geodata Institute, Hanoi, 134 pp.

Waagen, W. 1895. Salt-Range fossils. Vol 2: Fossils from the ceratite formation. *Palaeontologia Indica 13*, 1-323.

Wang, Y.-G., Chen, C., He, G.-X. & Chen, J. 1981. An outline of the marine Triassic in China. *International Union of Geological Sciences 7*, 1-22.

Wanner, J. 1911. Triascephalopoden von Timor und Rotti. *Neues Jahrbuch für Mineralogie, Geologie und Palaeontologie 32*, 177-196.

Weitschat, W. & Lehmann, U. 1978. Biostratigraphy of the uppermost part of the Smithian stage (Lower Triassic) at the Botneheia, W-Spitsbergen. *Mitteilungen aus dem Geologischen - Paläontologisches Institut - Universität Hamburg 48*, 85-100.

Welter, O.A.1922. Die ammoniten der Unteren trias von Timor. E. Schweizerbart'sche Verlagsbuchhandlung (Erwin Nägele), Stuttgart, 160 pp.

Westermann, G.E.G. 1966. Covariation and taxonomy of the Jurassic ammonite *Sonninia adicra* (Waagen). *Neues Jahrbuch für Geologie und Paläontologie, Abhandlungen 124*, 289-312.

White, C.A. 1879. Paleontological papers n°9: fossils from the Jura-Trias of south-eastern Idaho. *U.S. Geological and Geographical Survey of the Territories, Bulletin 5*, 105-117.

White, C.A. 1880. Contributions to invertebrate paleontology, n°5: Triassic fossils of south-eastern Idaho. *U.S. Geological Survey of the Territories, 12th Annual Report 1*, 105-118.

Yin, H., Sweet, W.C., Glenister, B.F., Kotlyar, G., Kozur, H.W., Newell, N.D., Sheng, J., Yang, Z. & Zakharov, Y.D. 1996. Recommendation of the Meishan section as Global Stratotype Section and Point for basal boundary of Triassic system. *Newsletter in Stratigraphy 34*, 81-108.

Yin, H., Zhang, K., Tong, J., Yang, Z. & Wu, S. 2001. The global stratotype section and point (GSSP) of the Permian-Triassic boundary. *Episodes 24*, 102-114.

Zakharov, Y.D. 1968. Biostratigraphiya i amonoidei nizhnego triasa Yuzhnogo Primorya (Lower Triassic biostratigraphy and ammonoids of South Primorye). Nauka, Moskva, 175 pp. (in Russian).

Figure captions:

Fig. 1: Location map of sampled sections (Tsoteng, Jinya, Waili, Shanggan, Yuping) in the Guangxi Province.

Fig. 2: Distribution of ammonoid taxa in the Tsoteng section. Open dots indicate occurrences based only on fragmentary or poorly preserved material.

Fig. 3A-C: Distribution of ammonoid taxa in the Jinya composite section. Open dots indicate occurrences based only on fragmentary or poorly preserved material.

Fig. 4: Distribution of ammonoid taxa in the Waili Cave section. Open dots indicate occurrences based only on fragmentary or poorly preserved material.

Fig. 5: Distribution of ammonoid taxa in the Waili Fall section. Open dots indicate occurrences based only on fragmentary or poorly preserved material.

Fig. 6: Distribution of ammonoid taxa in the Waili Laren section. Open dots indicate occurrences based only on fragmentary or poorly preserved material.

Fig. 7: Distribution of ammonoid taxa in the Waili Panorama section. Open dots indicate occurrences based only on fragmentary or poorly preserved material.

Fig. 8: Distribution of ammonoid taxa in the Shanggan section. Open dots indicate occurrences based only on fragmentary or poorly preserved material.

Fig. 9: Distribution of ammonoid taxa in the Yuping section. Open dots indicate occurrences based only on fragmentary or poorly preserved material.

Fig. 10: Synthetic range chart showing the biostratigraphical distribution of Smithian ammonoid genera in northwestern Guangxi.

Fig. 11: Northwestern Guangxi ammonoid zonation for the Smithian and its correlation with high and middle paleolatitude successions or sequences.

Fig. 12: Scatter diagrams of H, W, and U, and of H/D, W/D and U/D for *Kashmirites armatus* (Jinya and Waili, "*Flemingites rursiradiatus* beds").

Fig. 13: Scatter diagrams of H, W, and U, and of H/D, W/D and U/D for *Kashmirites densistriatus* (Waili, "*Kashmirites densistriatus* beds").

Fig. 14: Scatter diagrams of H, W, and U, and of H/D, W/D and U/D against corresponding diameter for *Preflorianites cf. P. radians* (*P. toulai* is given for comparison; data from Kummel & Steele 1962).

Fig. 15: Scatter diagrams of H, W, and D, and of H/D, W/D and U/D against corresponding diameter for *Pseudoceltites angustecostatus* from Guangxi, Oman and Afghanistan (Oman and Afghanistan: data from Kummel & Erben 1968).

Fig. 16: Scatter diagrams of H/D, W/D and U/D against corresponding diameter for the different species of *Hanielites* (Jinya, "*Owenites koeneni* beds").

Fig. 17: Scatter diagrams of H, W, and U, and of H/D, W/D and U/D, and histograms, probability plots of H/D, W/D and U/D, and growth curves for *Xenoceltites variocostatus* n. sp. (Jinya and Yuping, "*Anasibirites multiformis* beds"). "A" indicates allometric growth.

Fig. 18: Scatter diagrams of H, W, and U, and of H/D, W/D and U/D for *Xenolceltites pauciradiatus* n. sp. (Jinya and Yuping, "*Anasibirites multiformis* beds").

Fig. 19: Scatter diagrams of H, W, and U, and of H/D, W/D and U/D for *Sinoceltites admirabilis* n. gen., n. sp. (Waili, "*Kashmirites densistriatus* beds").

Fig. 20: Mean and box plots for different species of Xenoceltitidae found in Guangxi.

Fig. 21: Scatter diagrams of H, W, and U, and of H/D, W/D and U/D, and histograms, probability plots of H/D, W/D and U/D, and growth curves for *Hebeisenites varians* n. gen. (Jinya, "*Flemingites rursiradiatus* beds"). "A" indicates allometric growth. "I" indicates isometric growth.

Fig. 22: Scatter diagrams of H, W, and U, and of H/D, W/D and U/D for *Hebeisenites evolutus* n. gen., n. sp. (Jinya, "*Flemingites rursiradiatus* beds").

Fig. 23: Scatter diagrams of H, W, and U, and of H/D, W/D and U/D for *Hebeisenites compressus* n. gen., n. sp. (Jinya, "*Flemingites rursiradiatus* beds").

Fig. 24: Mean and box plots for different species of *Hebeisenites* found in Guangxi.

Fig. 25: Scatter diagrams of H, W, and U, and of H/D, W/D and U/D, and histograms, probability plots of H/D and U/D, and growth curves for *Jinyaceras bellum* n. gen., n. sp. (Jinya, "*Flemingites rursiradiatus* beds"). "A" indicates allometric growth. "I" indicates isometric growth.

Fig. 26: Scatter diagrams of H, W, and U, and of H/D, W/D and U/D for *Juvenites procurvus* n. gen., n. sp. (Jinya and Yuping, "*Owenites koeneni* beds").

Fig. 27: Scatter diagrams of H, W, and U, and of H/D, W/D and U/D, and histograms, probability plots of H/D and U/D, and growth curves for *Pseudaspidites muthianus* (Jinya, "*Flemingites rursiradiatus* beds"). "A" indicates allometric growth. "I" indicates isometric growth.

Fig. 28: Scatter diagrams of H, W, and U, and of H/D, W/D and U/D for *Xiaoqiaoceras involutus* n. gen., n. sp. (Jinya, "*Flemingites rursiradiatus* beds").

Fig. 29: Scatter diagrams of H, W, and U, and of H/D, W/D and U/D for *Lingyunites discoides* (Jinya, "*Flemingites rursiradiatus* beds").

Fig. 30: Scatter diagrams of H, W, and U, and of H/D, W/D and U/D for *Wailiceras aemulus* n. gen., n. sp. (Waili, "*Kashmirites densistriatus* beds").

Fig. 31: Scatter diagrams of H, W, and U, and of H/D, W/D and U/D for *Gyronites* cf. *G. superior* (Waili, "*Kashmirites densistriatus* beds").

Fig. 32: Scatter diagrams of H, W, and U, and of H/D, W/D and U/D, and histograms, probability plots of H/D and U/D, and growth curves for *Dieneroceras tientungense* (Jinya, "*Flemingites rursiradiatus* beds"). "A" indicates allometric growth. "I" indicates isometric growth.

Fig. 33: Scatter diagrams of H, W, and U, and of H/D, W/D and U/D for *Wyomingites aplanatus* (Jinya, "*Flemingites rursiradiatus* beds").

Fig. 34: Scatter diagrams of H, W, and U, and of H/D, W/D and U/D for *Flemingites flemingianus* (Jinya and Waili, "*Flemingites rursiradiatus* beds").

Fig. 35: Scatter diagrams of H, W, and U, and of H/D, W/D and U/D, and histograms, probability plots of H/D and U/D, and growth curves for *Flemingites rursiradiatus* (Jinya, "*Flemingites rursiradiatus* beds"). "A" indicates allometric growth. "I" indicates isometric growth.

Fig. 36: Scatter diagrams of H, W, and U, and of H/D, W/D and U/D for *Flemingites radiatus* (Jinya, "*Flemingites rursiradiatus* beds").

Fig. 37: Scatter diagrams of H, W, and U, and of H/D, W/D and U/D for *Galfettites simplicitatis* n. gen., n. sp. (Jinya, "*Owenites koeneni* beds").

Fig. 38: Scatter diagrams of H, W, and U, and of H/D, W/D and U/D for *Pseudoflemingites goudemandi* n. sp. (Jinya, "*Owenites koeneni* beds").

Fig. 39: Scatter diagrams of H, W, and U, and of H/D, W/D and U/D for *Anaflemingites hochulii* n. sp. (Jinya, "*Owenites koeneni* beds").

Fig. 40: Scatter diagrams of H, W, and U, and of H/D, W/D and U/D, and histograms, probability plots of H/D and U/D, and growth curves for *Submeekoceras mushbachanum* (Jinya, Waili and Yuping, "*Flemingites rursiradiatus* beds"). "A" indicates allometric growth. "I" indicates isometric growth.

Fig. 41: Scatter diagrams of H, W, and U, and of H/D, W/D and U/D for *Ussuria kwangsiana* and *Metussuria* sp. indet. (Jinya, "*Owenites koeneni* beds").

Fig. 42: Scatter diagrams of H, W, and U, and of H/D, W/D and U/D for *Anasibirites multiformis* (Jinya and Waili, "*Anasibirites multiformis* beds").

Fig. 43: Scatter diagrams of H, W, and U, and of H/D, W/D and U/D for comparison of *Anasibirites evolutus* n. sp. and *A. multiformis* (Jinya and Waili, "*Anasibirites multiformis* beds").

Fig. 44: Scatter diagrams of H, W, and U, and of H/D, W/D and U/D for *Hemiprionites* cf. *H. butleri* (Jinya and Waili, "*Anasibirites multiformis* beds").

Fig. 45: Scatter diagrams of H, W, and U, and of H/D, W/D and U/D for *Hemiprionites klugi* n. sp. (Jinya and Waili, "*Anasibirites multiformis* beds").

Fig. 46: Scatter diagrams of H, W, and U, and of H/D, W/D and U/D for *Inyoites krystyni* n. sp. (Jinya, "*Owenites koeneni* beds").

Fig. 47: Scatter diagrams of H, W, and U, and of H/D, W/D and U/D for *Lanceolites bicarinatus* and *L. compactus*. Solid circles indicate *L. bicarinatus*; open circles indicate *L. compactus*. Area bounded by dotted line represents specimens from Guangxi, Jinya, "*Owenites koeneni* beds". Other data from Vu Khuc 1984 and Shevyrev 1995.

Fig. 48: Scatter diagrams of H, W, and U against corresponding diameter for *Paranannites* aff. *P. aspenensis* (Jinya, "*Flemingites rursiradiatus* beds"; *P. aspenensis* is given for comparison: data from Kummel & Steele 1962).

Fig. 49: Scatter diagrams of H, W, and U, and of H/D, W/D and U/D, and histograms, probability plots of H/D, U/D and growth curves for *Paranannites spathi* (Jinya and Yuping, "*Owenites koeneni* beds"). "A" indicates allometric growth. "I" indicates isometric growth.

Fig. 50: Scatter diagrams of H, W, and U, and of H/D, W/D and U/D for *Paranannites ovum* n. sp. (Tsoteng and Yuping, "*Owenites koeneni* beds").

Fig. 51: Scatter diagrams of H, W, and U, and of H/D, W/D and U/D, and histograms, probability plots of H/D, U/D and growth curves for *Paranannites globosus* n. sp. (Jinya, "*Flemingites rursiradiatus* beds"). "A" indicates allometric growth. "I" indicates isometric growth.

Fig. 52: Scatter diagrams of H, W, and U, and of H/D, W/D and U/D, and histograms, probability plots of H/D, U/D and growth curves for *Owenites koeneni* (Jinya and Waili, "*Owenites koeneni* beds"). "A" indicates allometric growth. "I" indicates isometric growth.

Fig. 53: Scatter diagrams of H, W, and U, and of H/D, W/D and U/D for *Owenites simplex* (Jinya and Waili, "*Owenites koeneni* beds").

Fig. 54: Mean and box plots for the two species of *Owenites* found in Guangxi.

Fig. 55: Scatter diagrams of H, W, and U, and of H/D, W/D and U/D, and histograms, probability plots of H/D, U/D and growth curves for *Pseudosageceras multilobatum* (solid circles indicate specimens from Jinya and Waili, "*Flemingites rursiradiatus* beds"; open circles indicate specimens from other countries).

Fig. 56: Scatter diagrams of H, W, and U, and of H/D, W/D and U/D for *Hedenstroemia hedenstroemi* (solid circles indicate specimens from Waili, "*Hedenstroemia hedenstroemi* beds"; other data from Siberia are given for comparison, by Dagys & Ermakova 1990).

Fig. 57: Scatter diagrams of H, W, and U, and of H/D, W/D and U/D for *Hedenstroemia augusta* n. sp. (Waili, "*Anasibirites multiformis* beds").

Fig. 58: Scatter diagrams of H, W, and U, and of H/D, W/D and U/D for *Cordillerites antrum* n. sp. (Waili, "*Kashmirites densistriatus* beds").

Fig. 59: Mean and box plots for four species of Hedenstroemiidae found in Guangxi.

Fig. 60: Scatter diagrams of H, W, and U, and of H/D, W/D and U/D, and histogram, probability plot of H/D, W/D, U/D, and growth curve for *Mesohedenstroemia kwangsiana* (Jinya, "*Flemingites rursiradiatus* beds"). "A" indicates allometric growth. "I" indicates isometric growth.

Fig. 61: Scatter diagrams of H, W, and U, and of H/D, W/D and U/D, and histogram, probability plot of H/D, and growth curve for *Aspenites acutus* (Jinya and Yuping, "*Flemingites*

rursiradiatus beds"; solid circles indicate specimens from Kummel & Steele 1962 given for comparison). "A" indicates allometric growth. "I" indicates isometric growth.

Fig. 62: Scatter diagrams of H, W, and U, and of H/D, W/D and U/D for *Pseudaspenites layeriformis* (Jinya, "*Flemingites rursiradiatus* beds").

Fig. 63: Scatter diagrams of H, W, and U, and of H/D, W/D and U/D for *Pseudaspenites evolutus* n. sp. (Jinya, "*Flemingites rursiradiatus* beds").

Fig. 64: Scatter diagrams of H, W, and U, and of H/D, W/D and U/D for *Pseudaspenites tenuis* (Jinya, "*Flemingites rursiradiatus* beds").

Fig. 65: Mean and box plots for species of *Pseudaspenites* found in Guangxi.

Fig. 66: Scatter diagrams of H/D, W/D and U/D for *Proharpoceras carinatitabulatum* (Jinya, "*Owenites rursiradiatus* beds").

Fig. 67: Scatter diagrams of H, W, and U, and of H/D, W/D and U/D for *Procurvoceratites pygmaeus* n. gen., n. sp. *P. ampliatus* n. gen., n. sp. represented as a solid circle (Jinya, "*Flemingites rursiradiatus* beds").

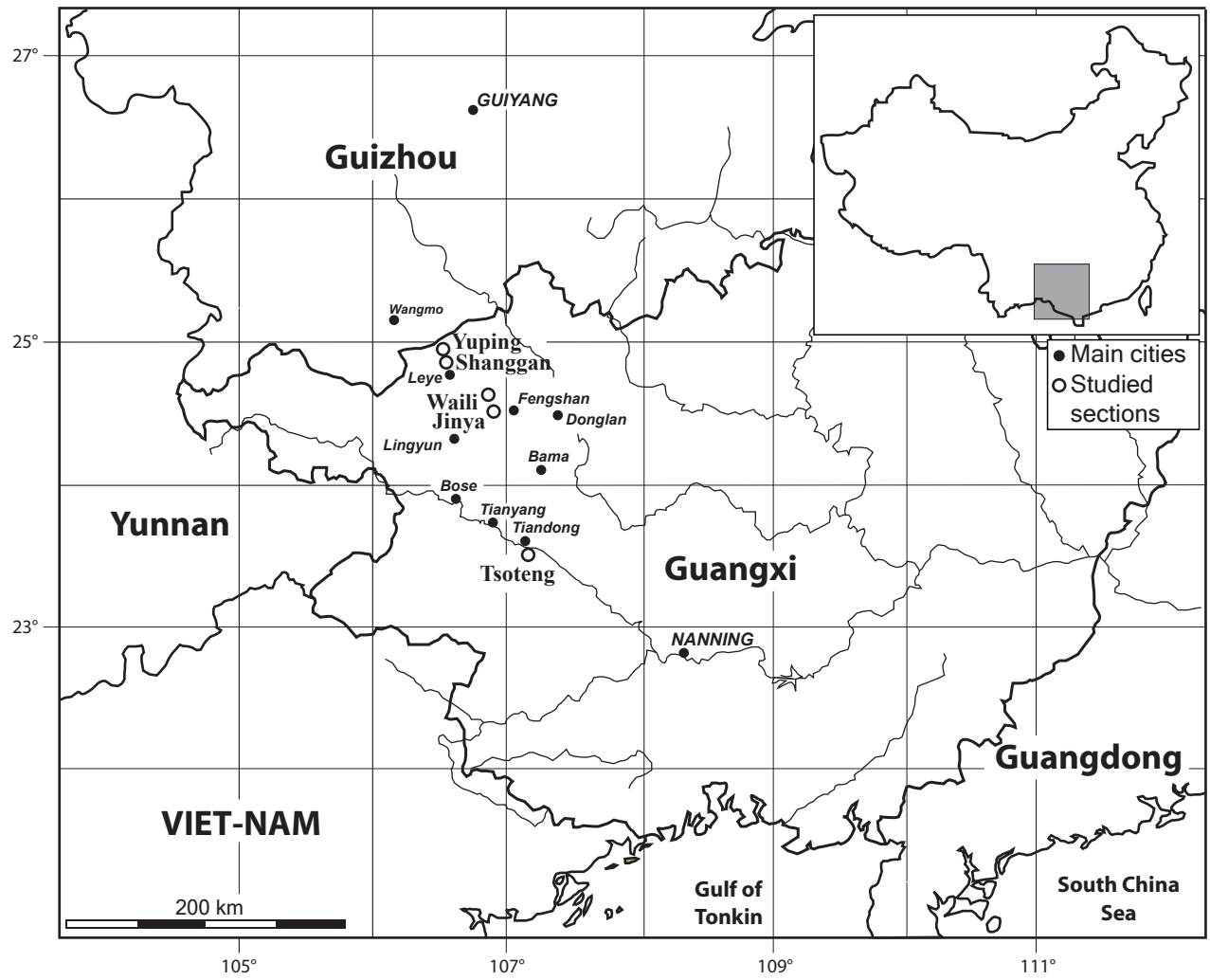

Fig. 1. Brayard & Bucher

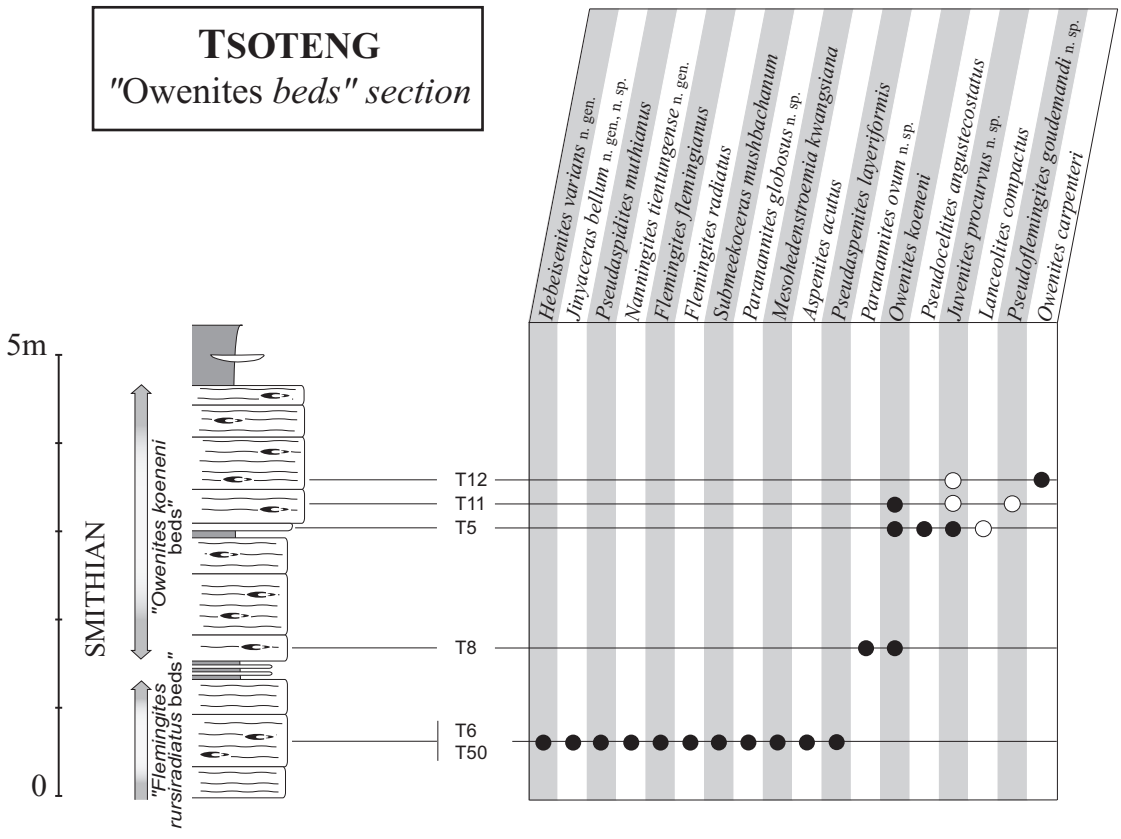

Fig. 2. Brayard & Bucher

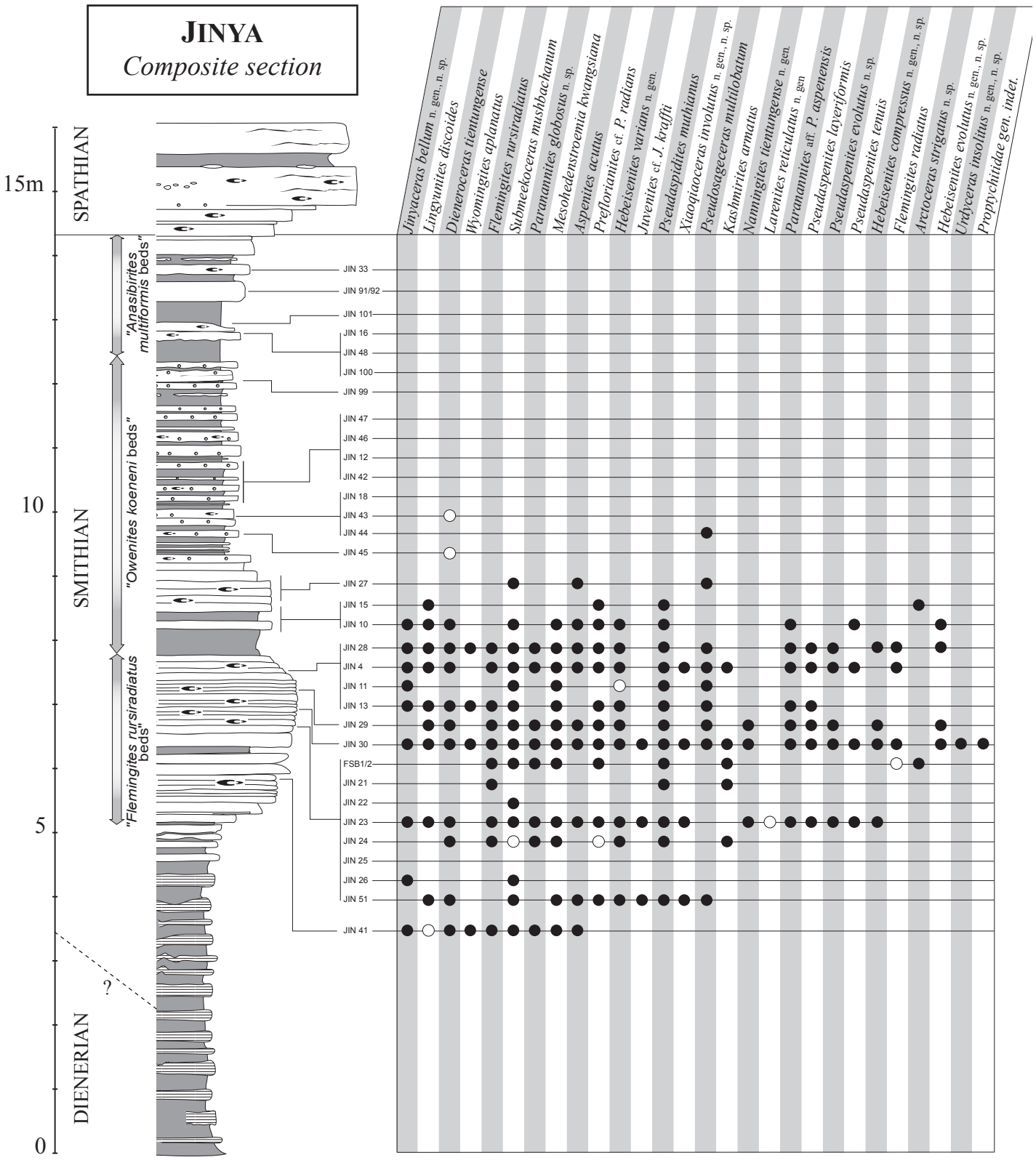

Fig. 3A. Brayard & Bucher

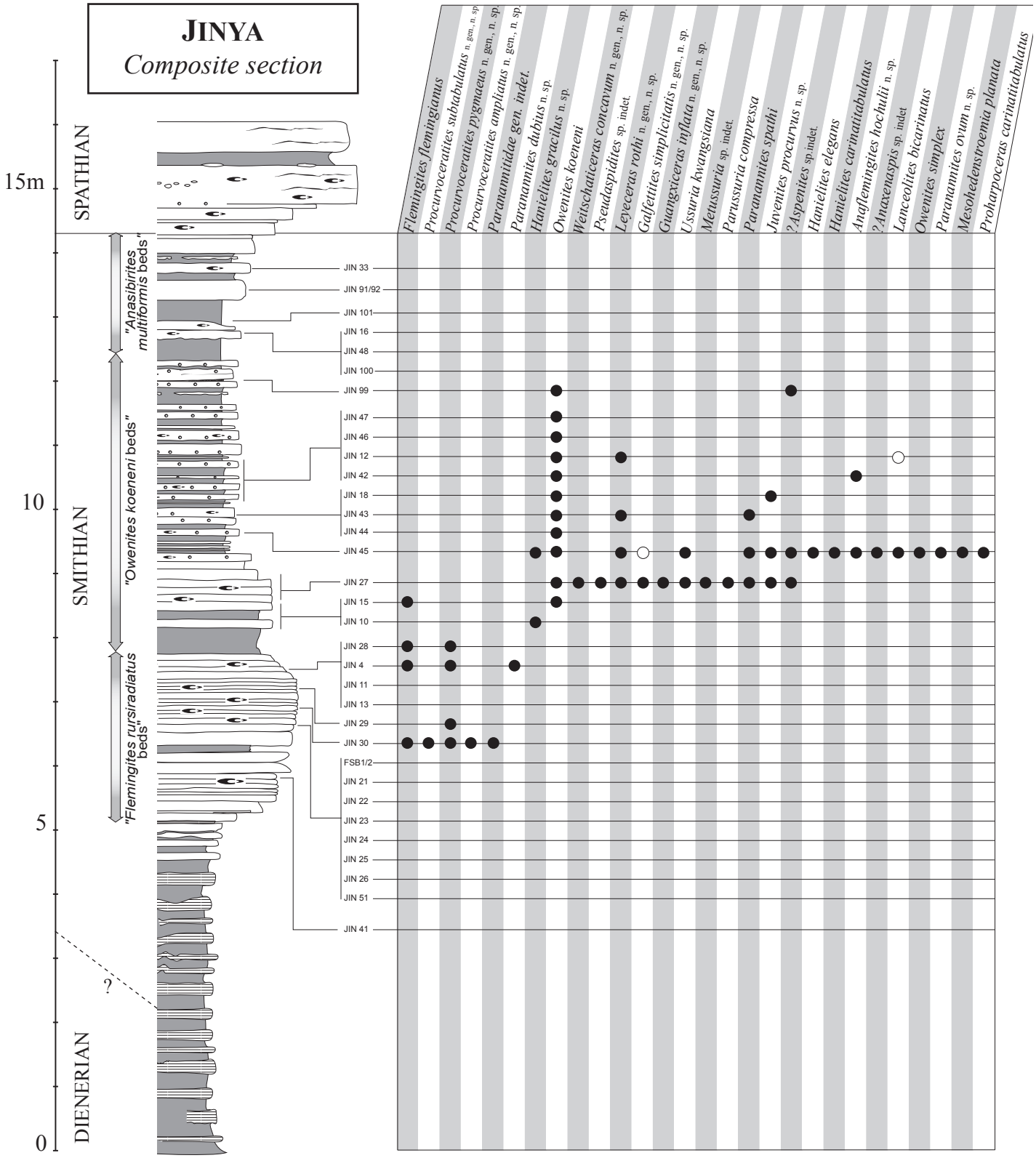

Fig. 3B. Brayard & Bucher

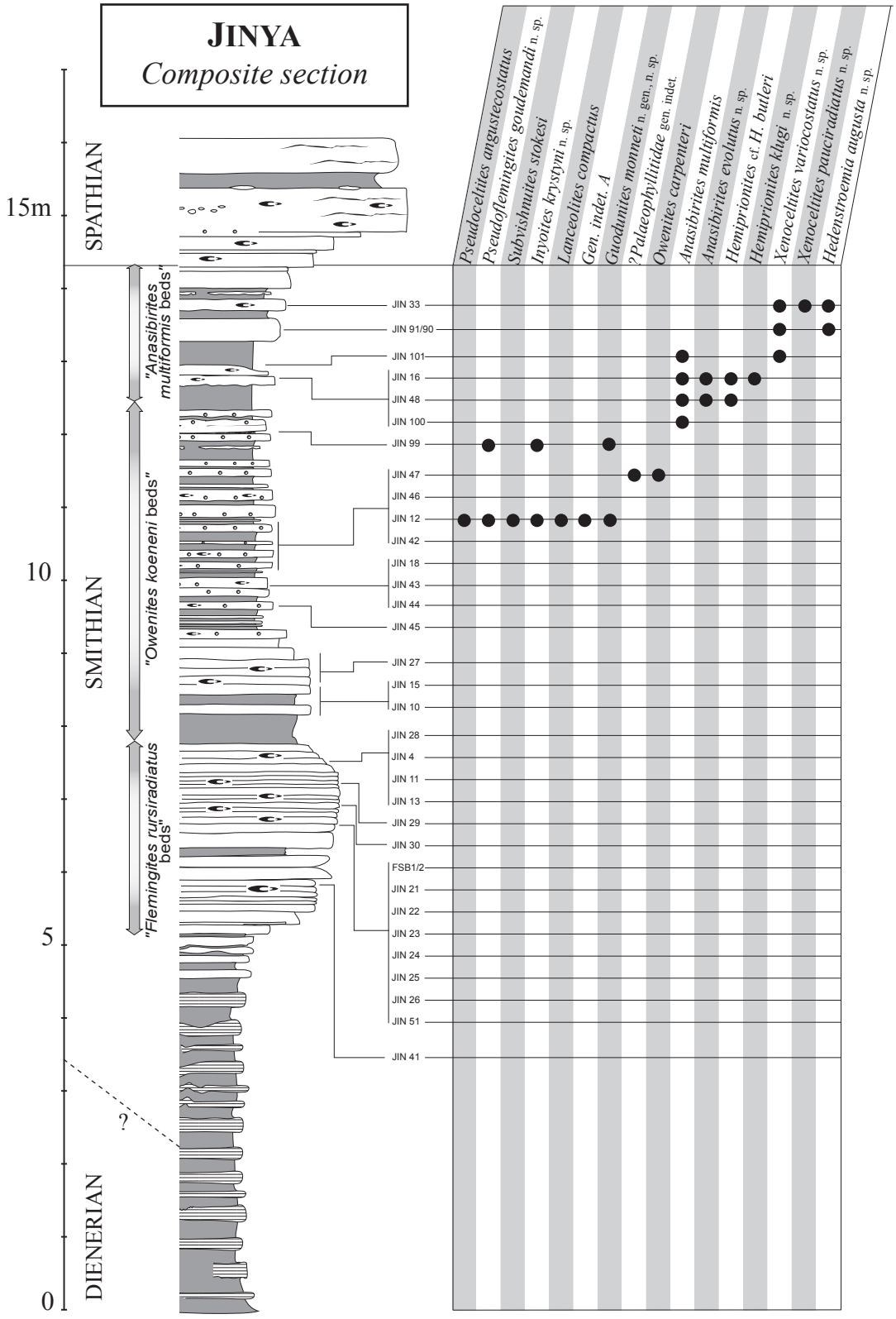

Fig. 3C. Brayard & Bucher

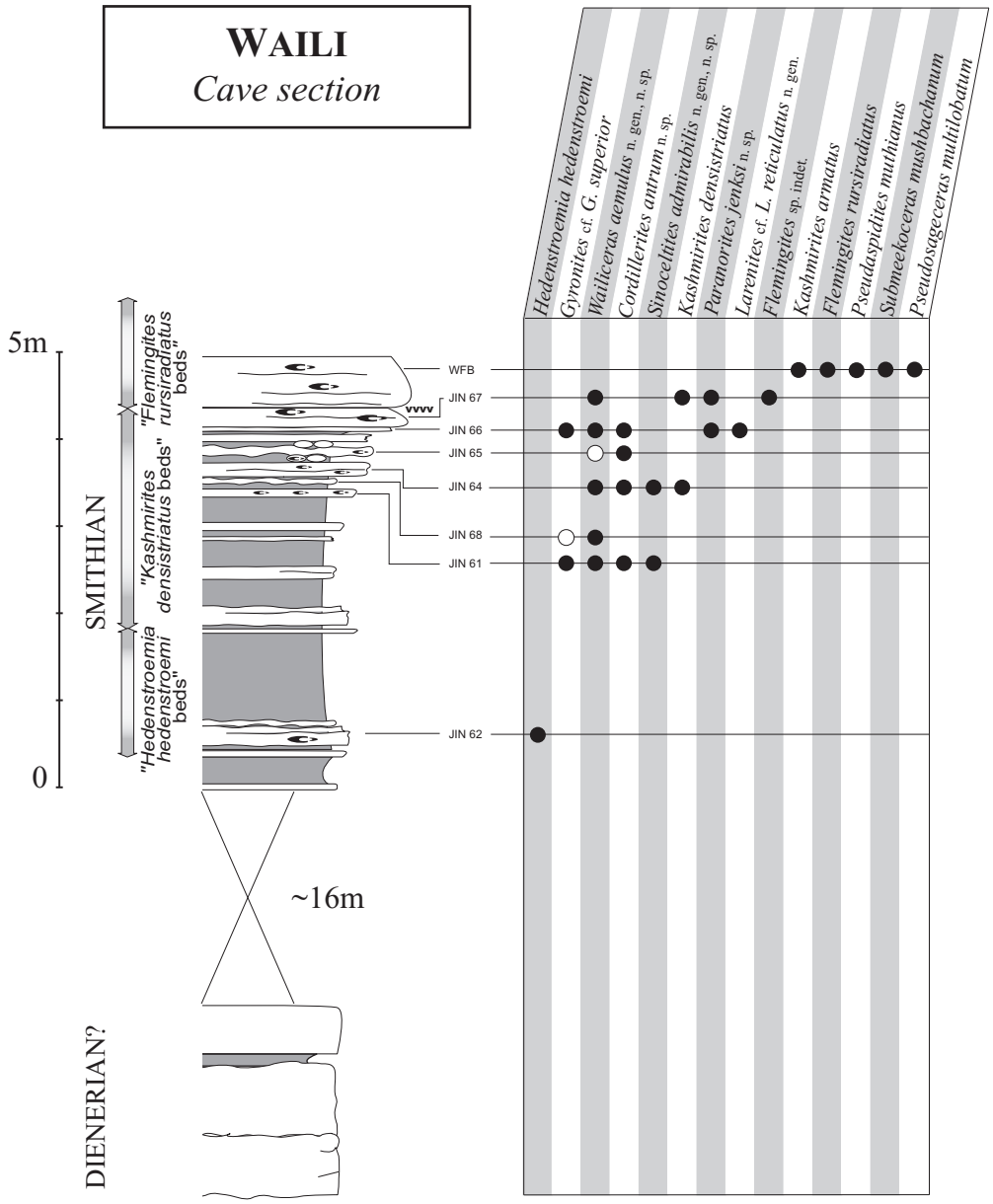

Fig. 4. Brayard & Bucher

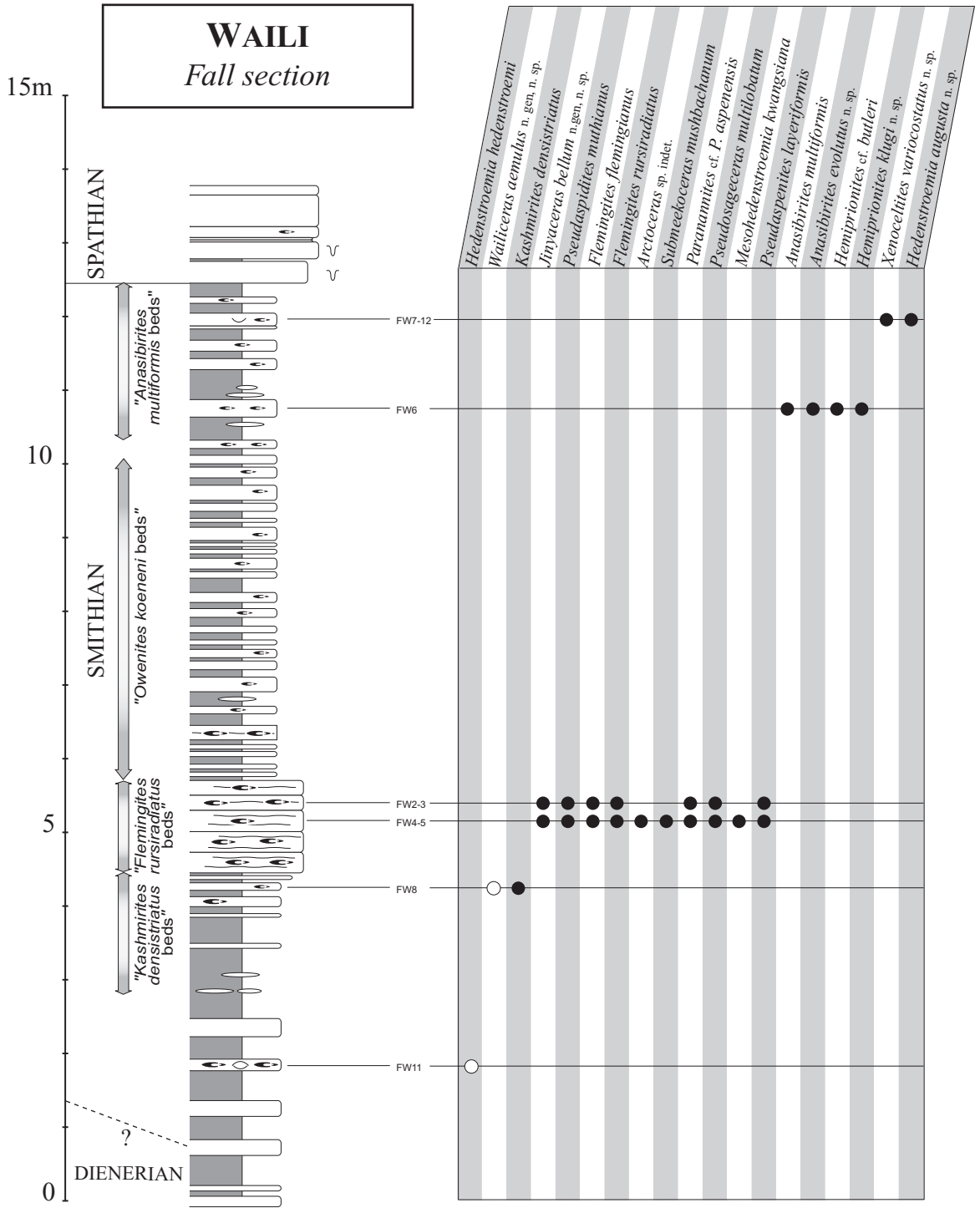

Fig. 5. Brayard & Bucher

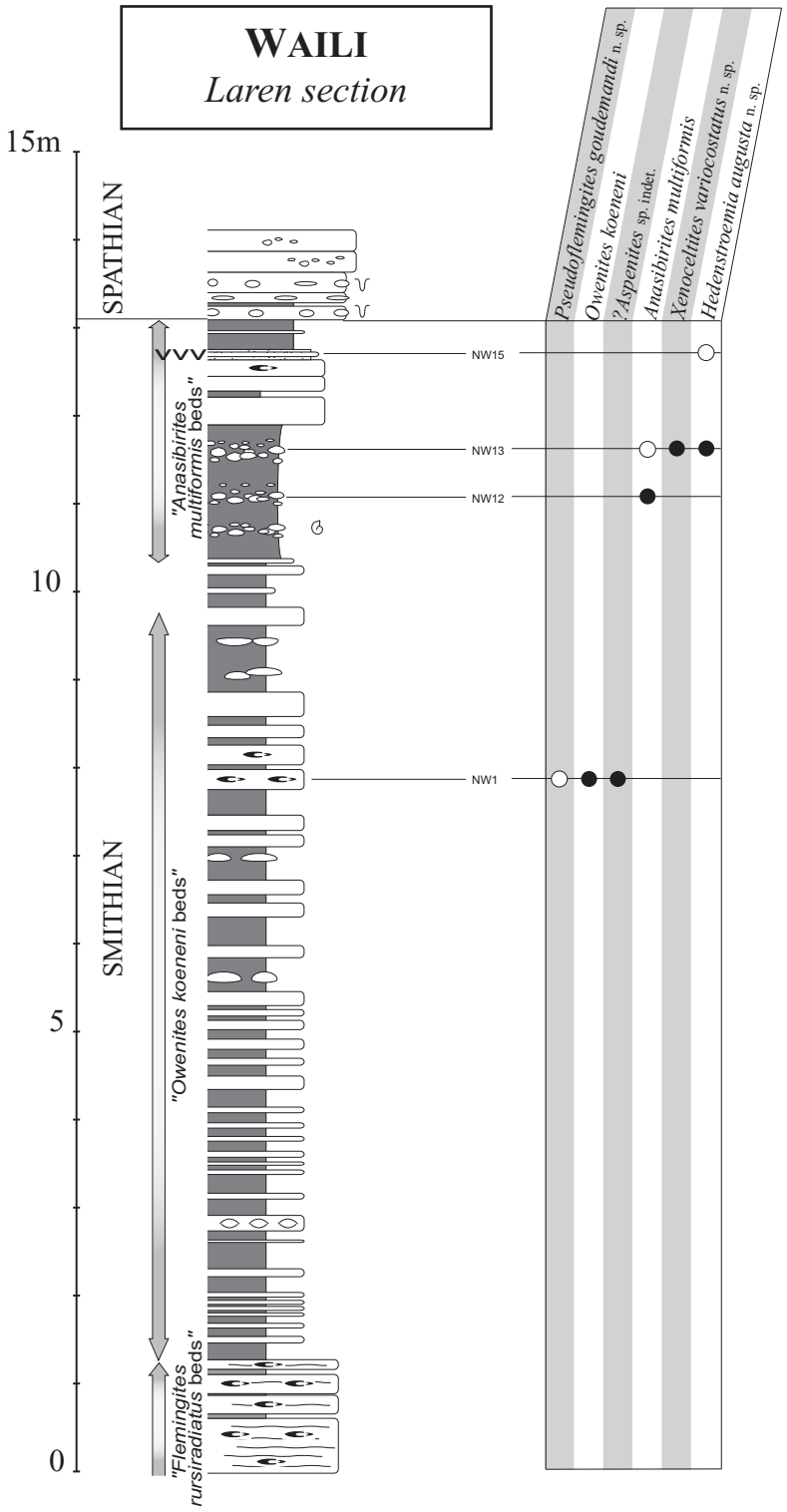

Fig. 6. Brayard & Bucher

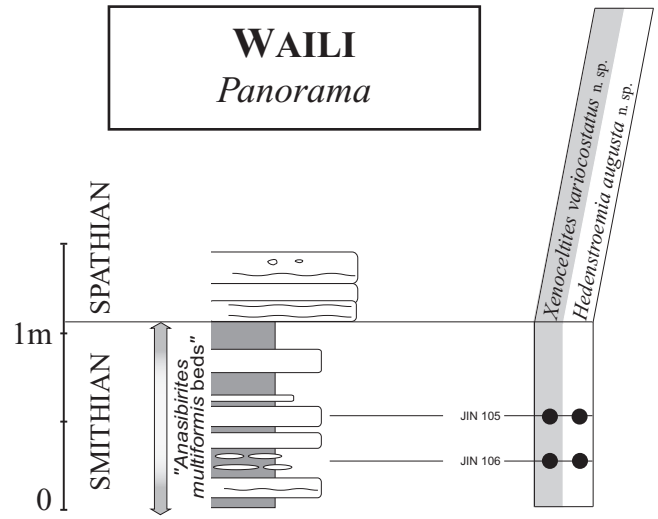

Fig. 7. Brayard & Bucher

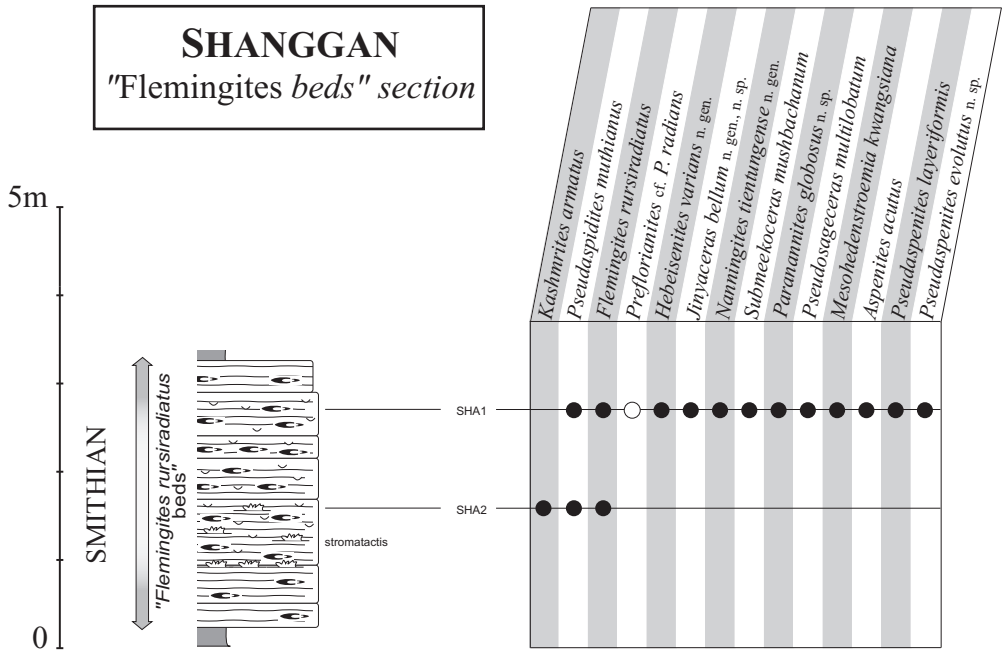

Fig. 8. Brayard & Bucher

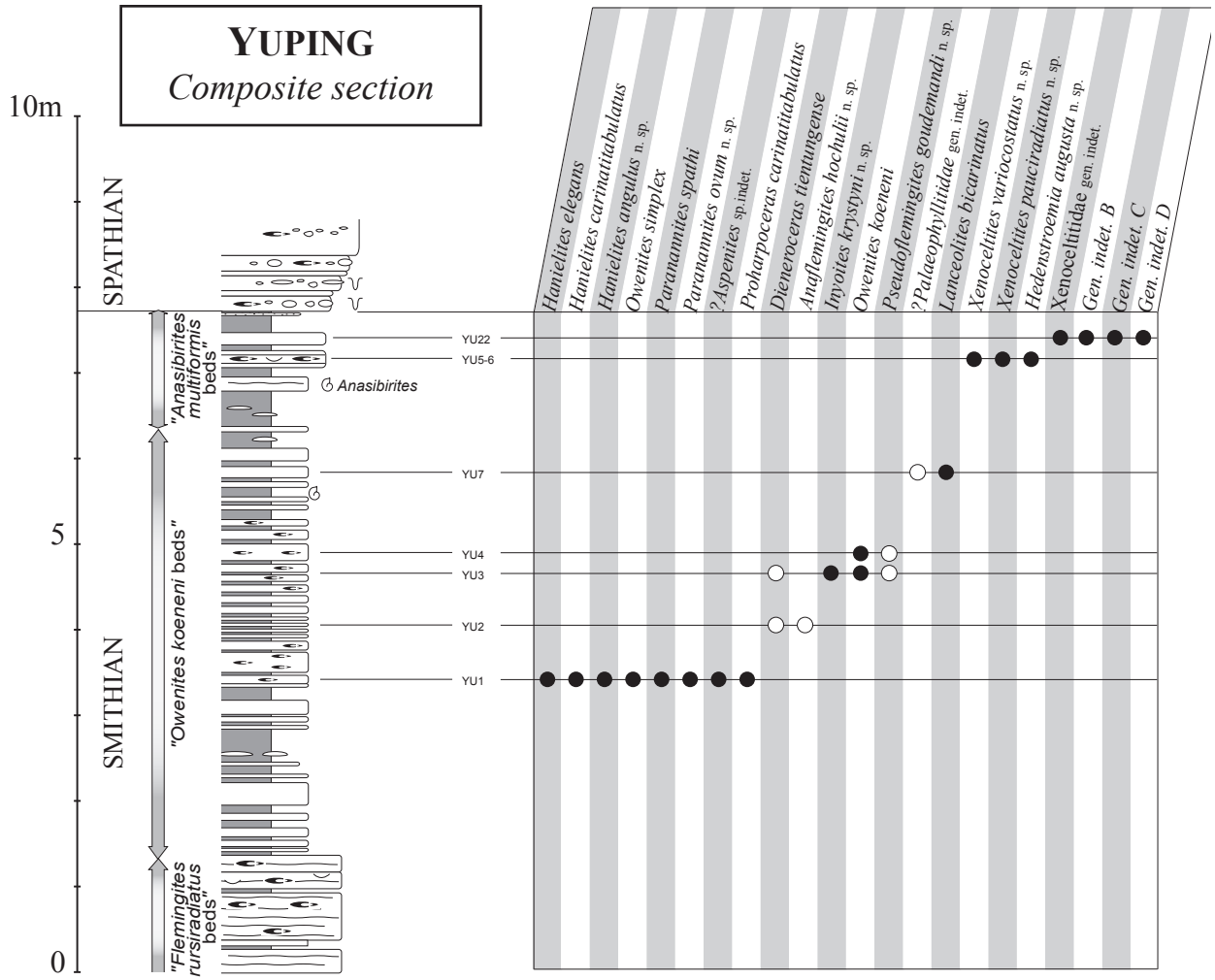

Fig. 9. Brayard & Bucher

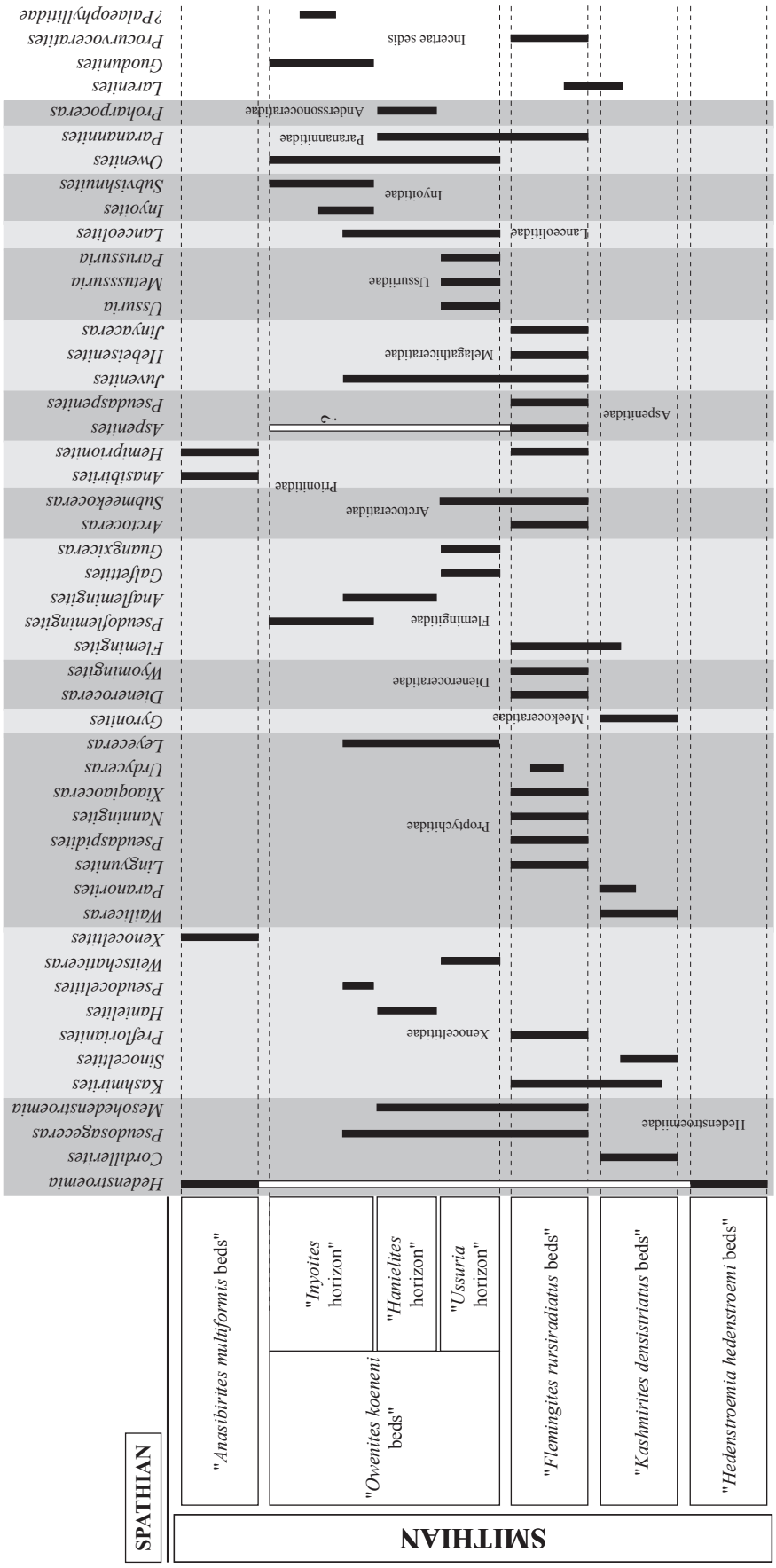

Fig. 10. Brayard & Bucher

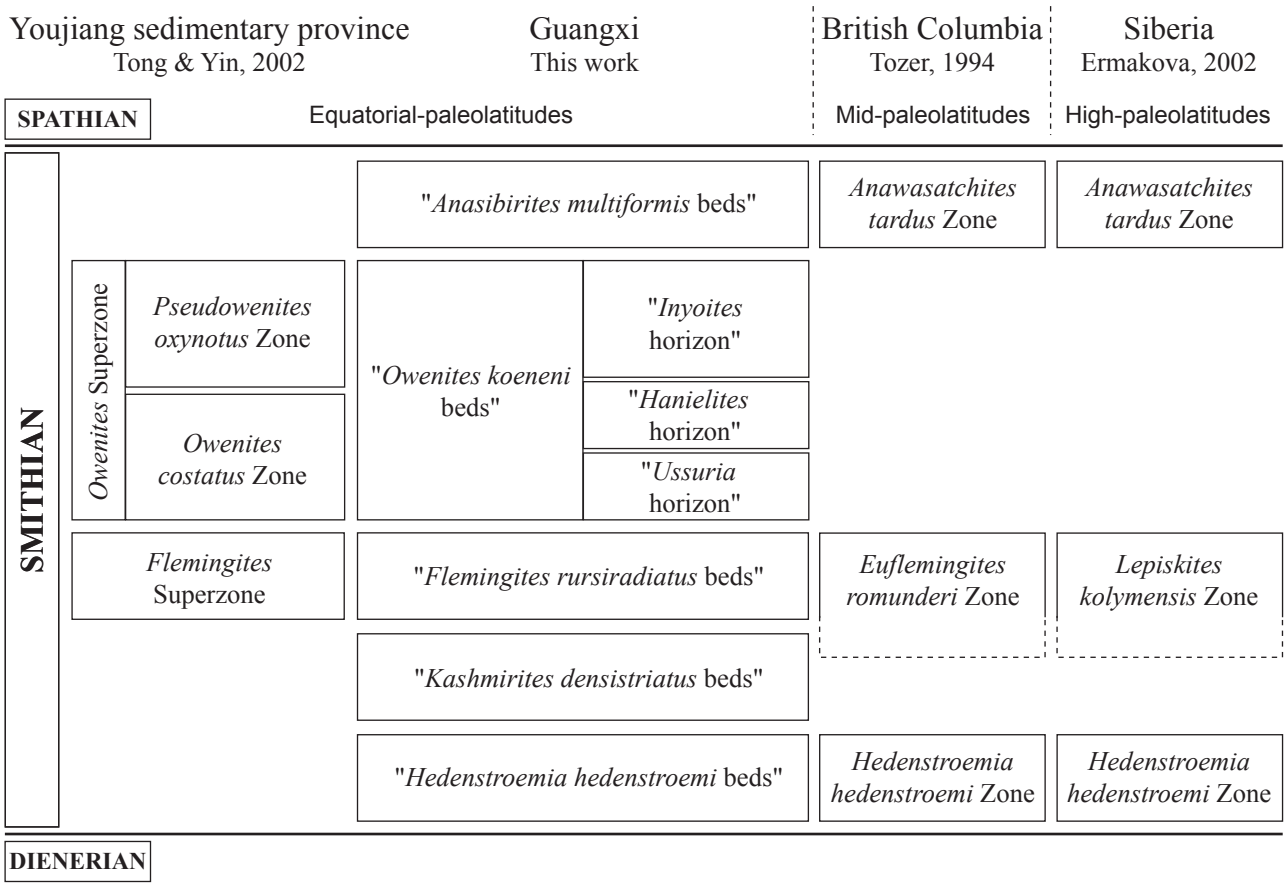

Fig. 11. Brayard & Bucher

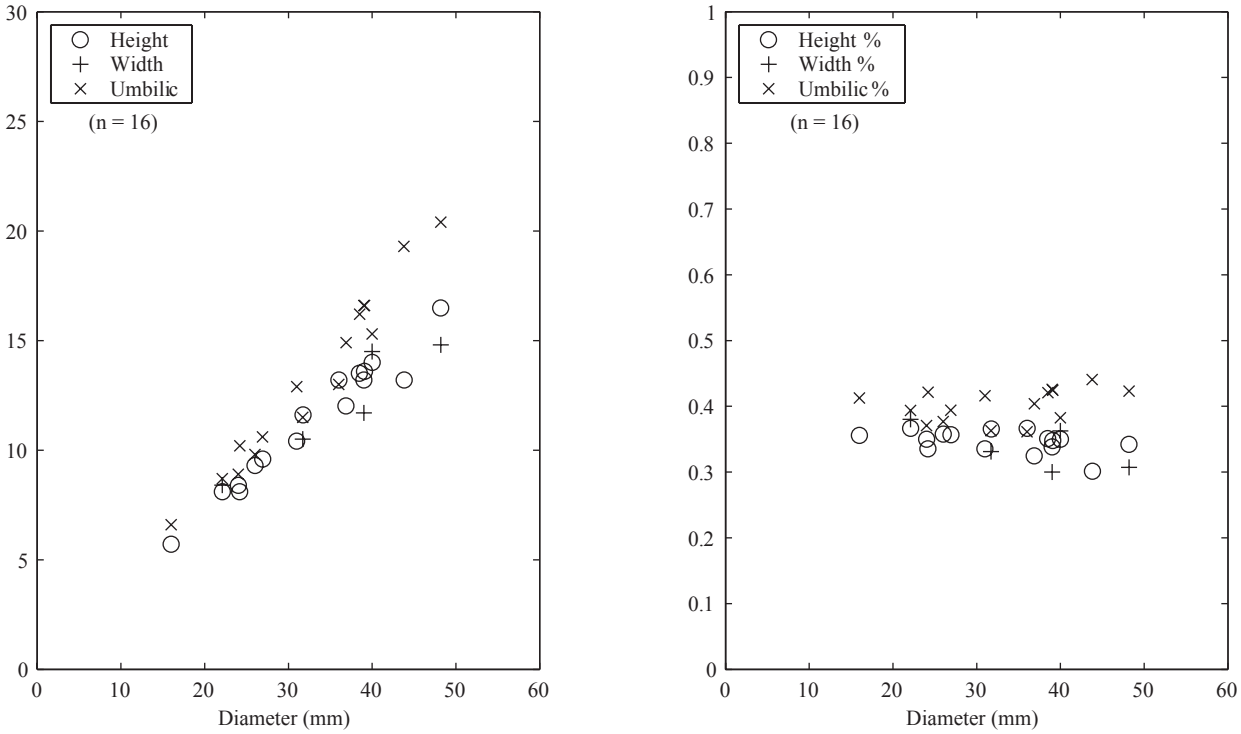

Fig. 12. Brayard & Bucher

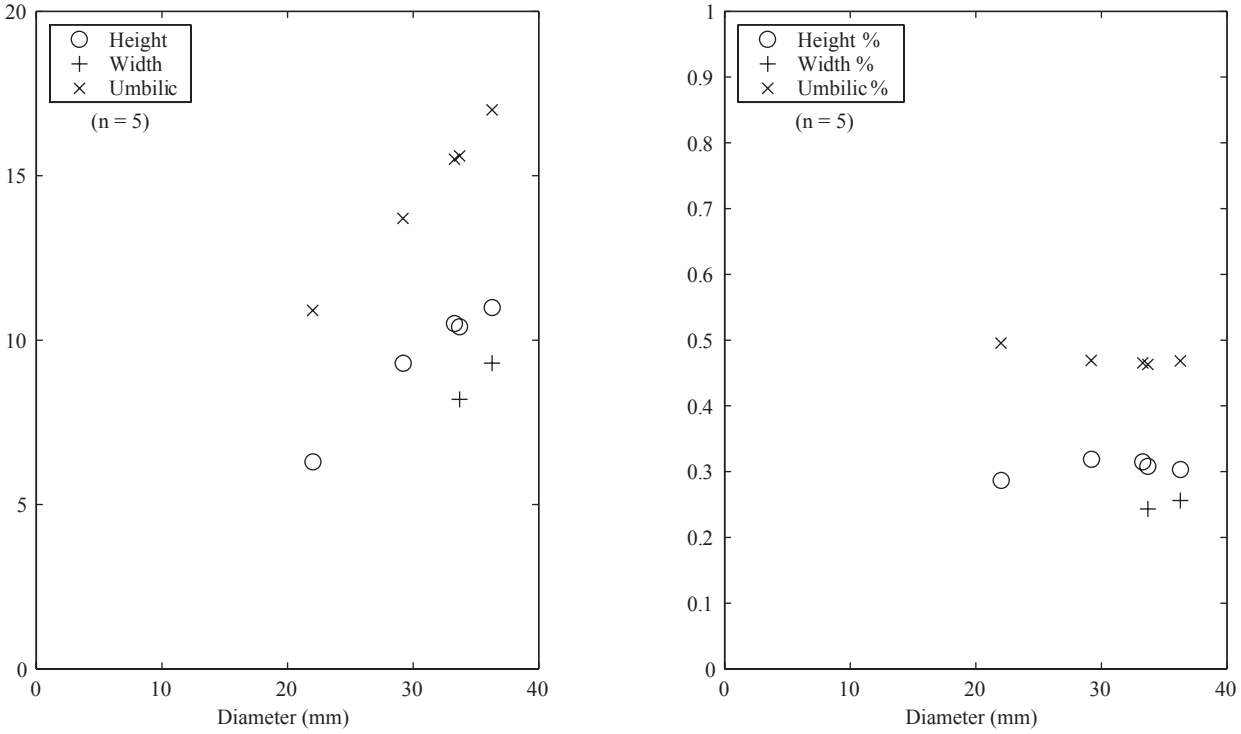

Fig. 13. Brayard & Bucher

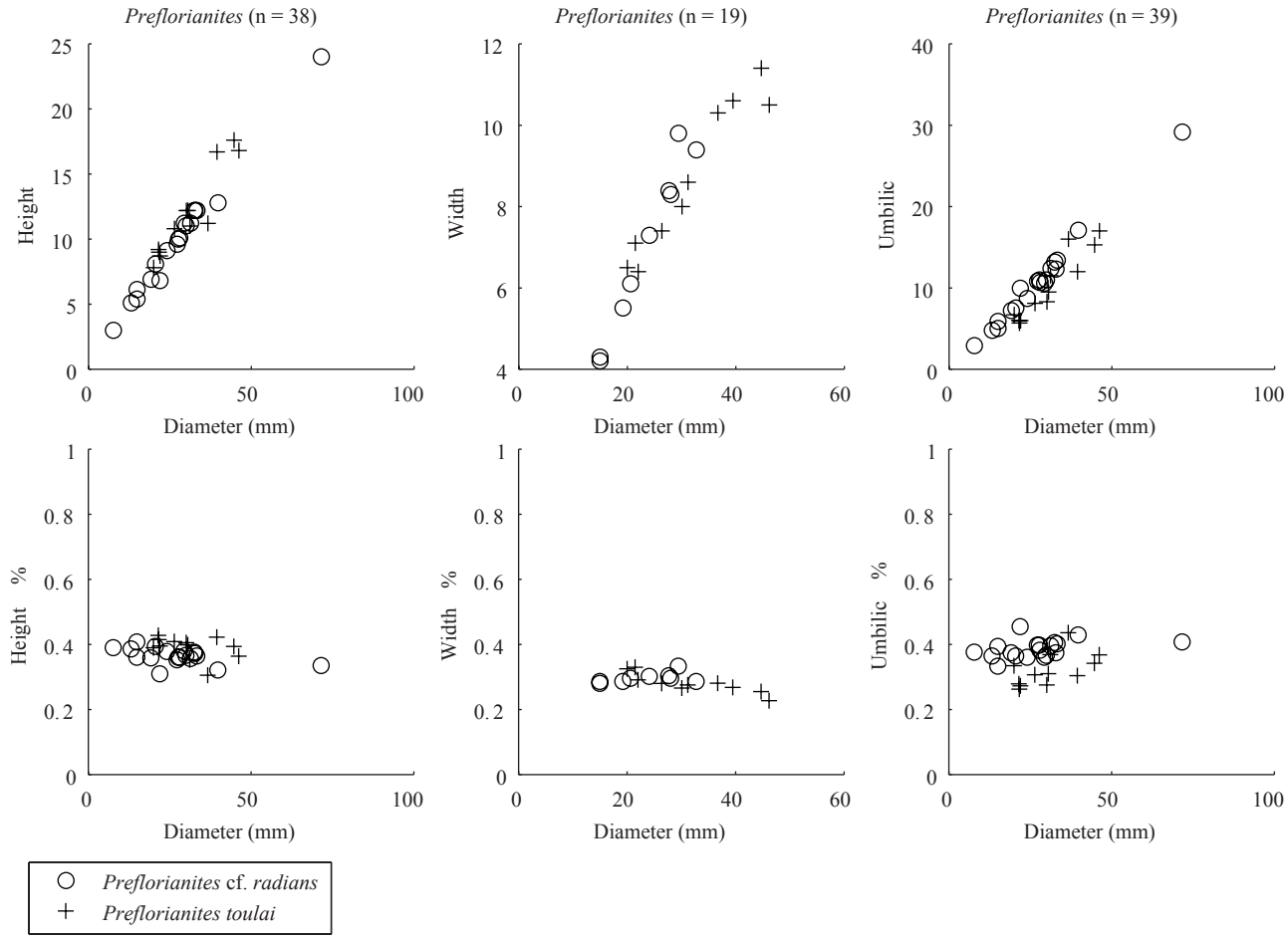

Fig. 14. Brayard & Bucher

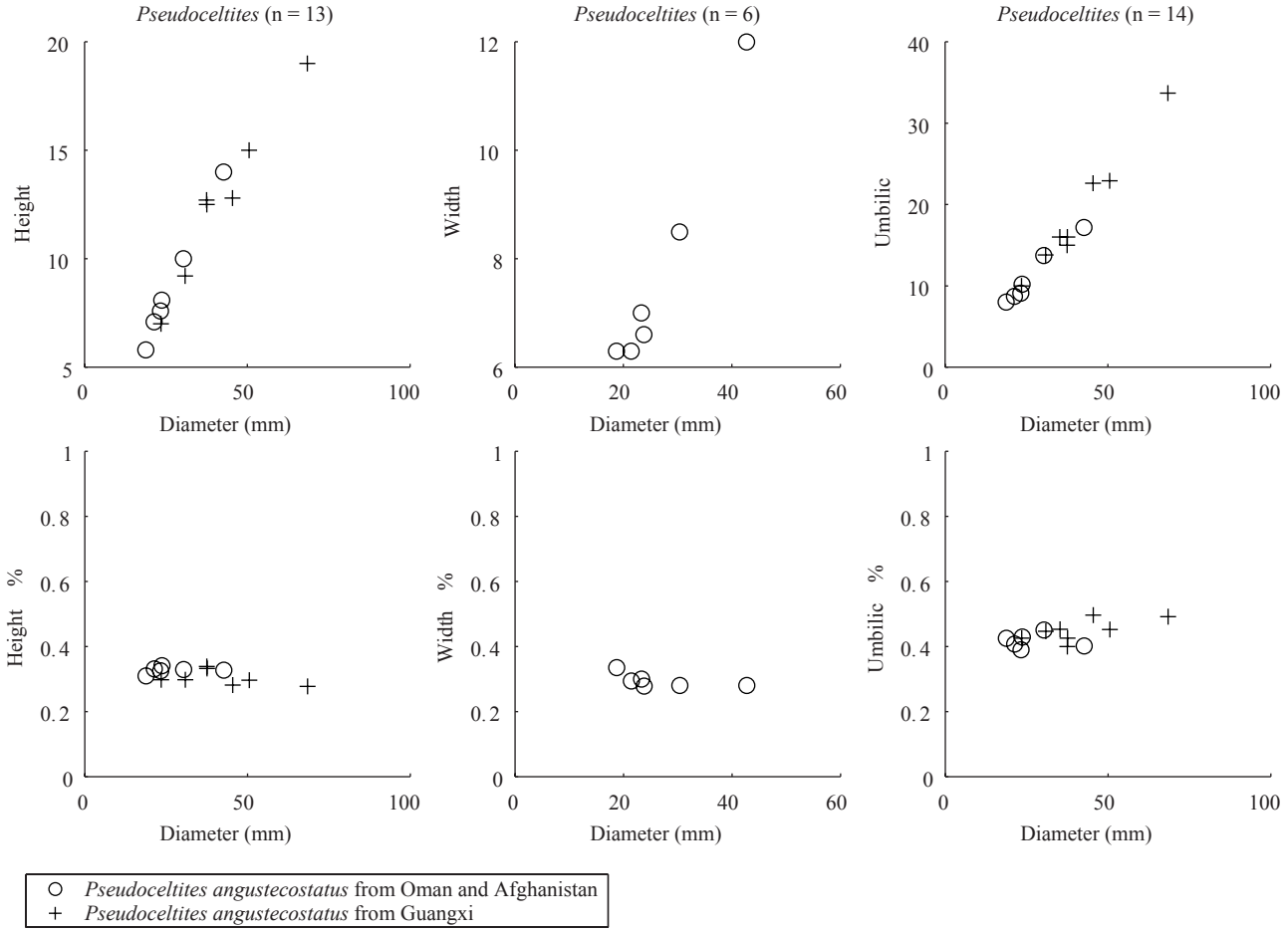

Fig. 15. Brayard & Bucher

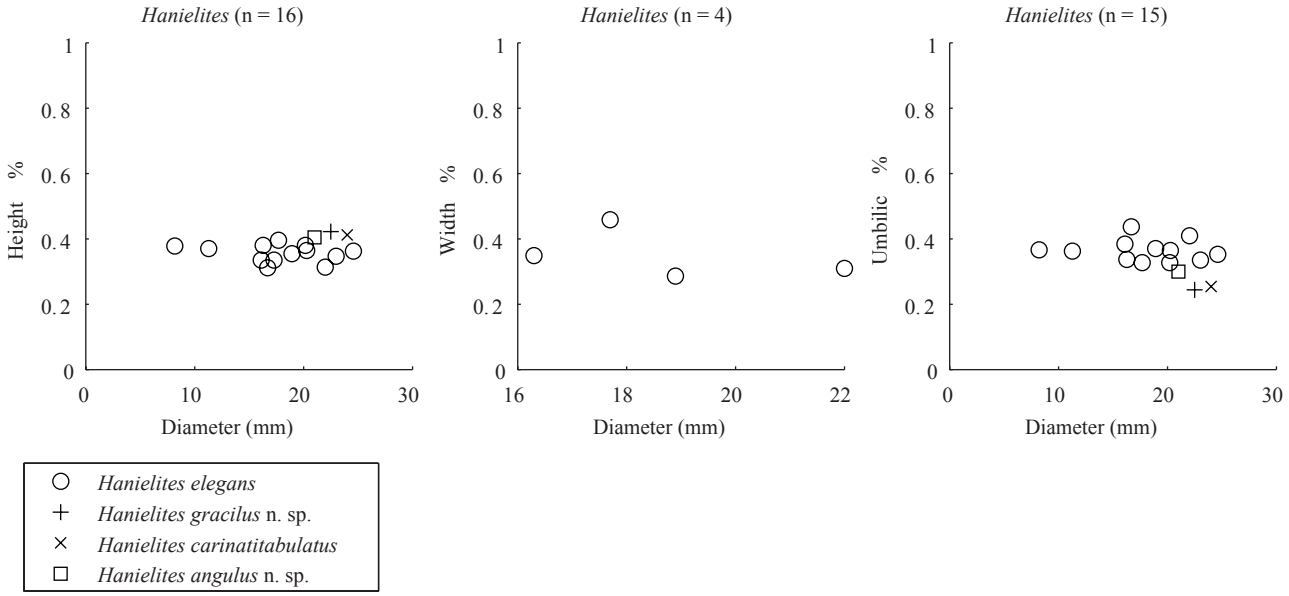

Fig. 16. Brayard & Bucher

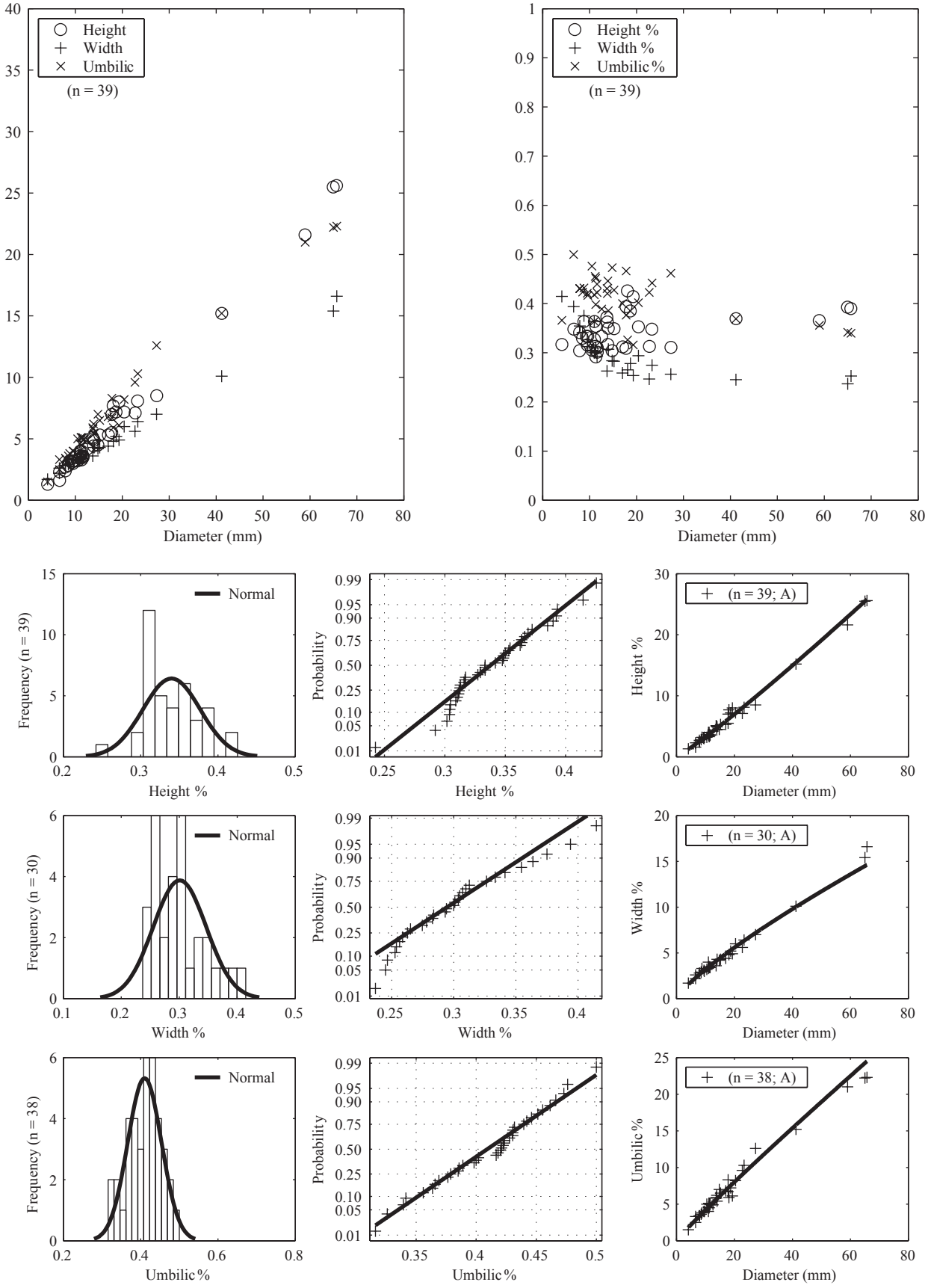

Fig. 17. Brayard & Bucher

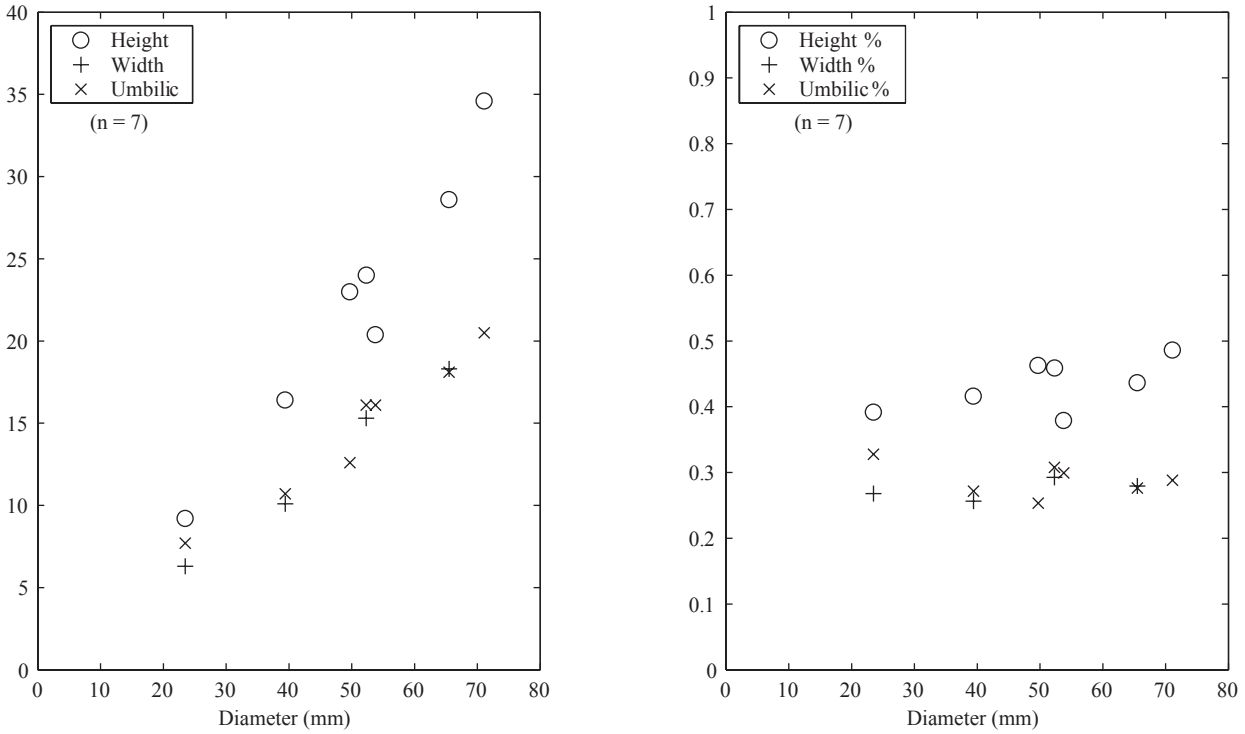

Fig. 18. Brayard & Bucher

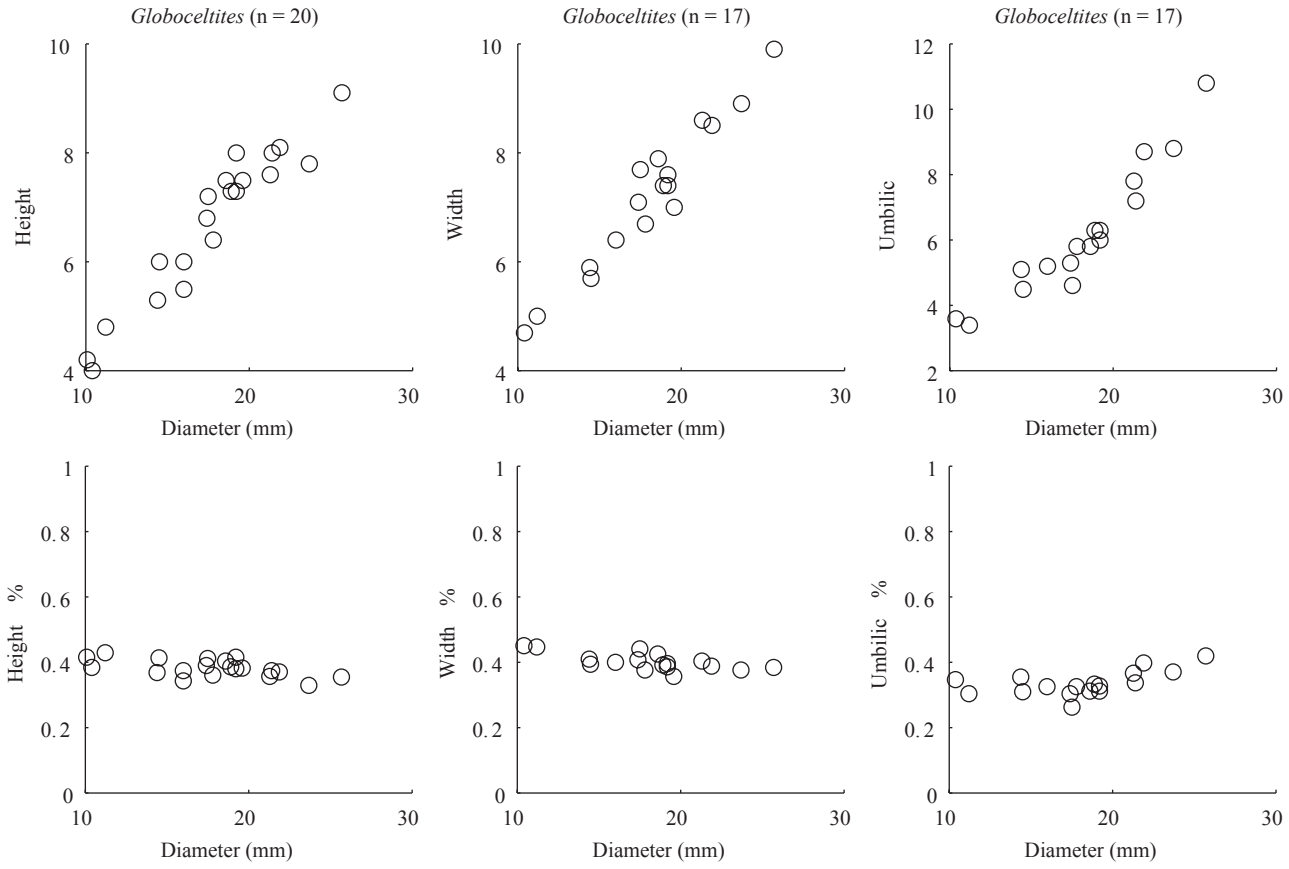

Fig. 19. Brayard & Bucher

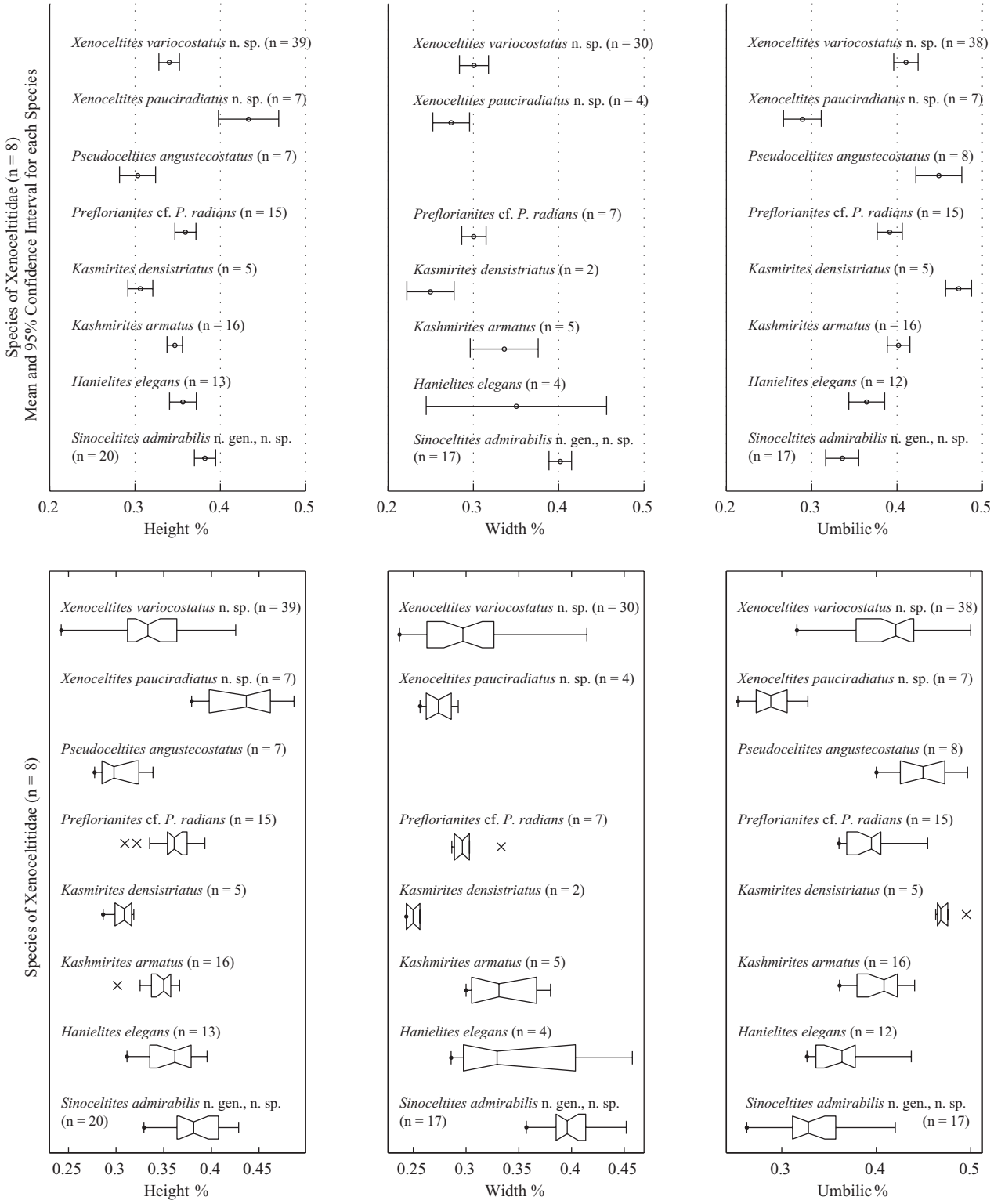

Fig. 20. Brayard & Bucher

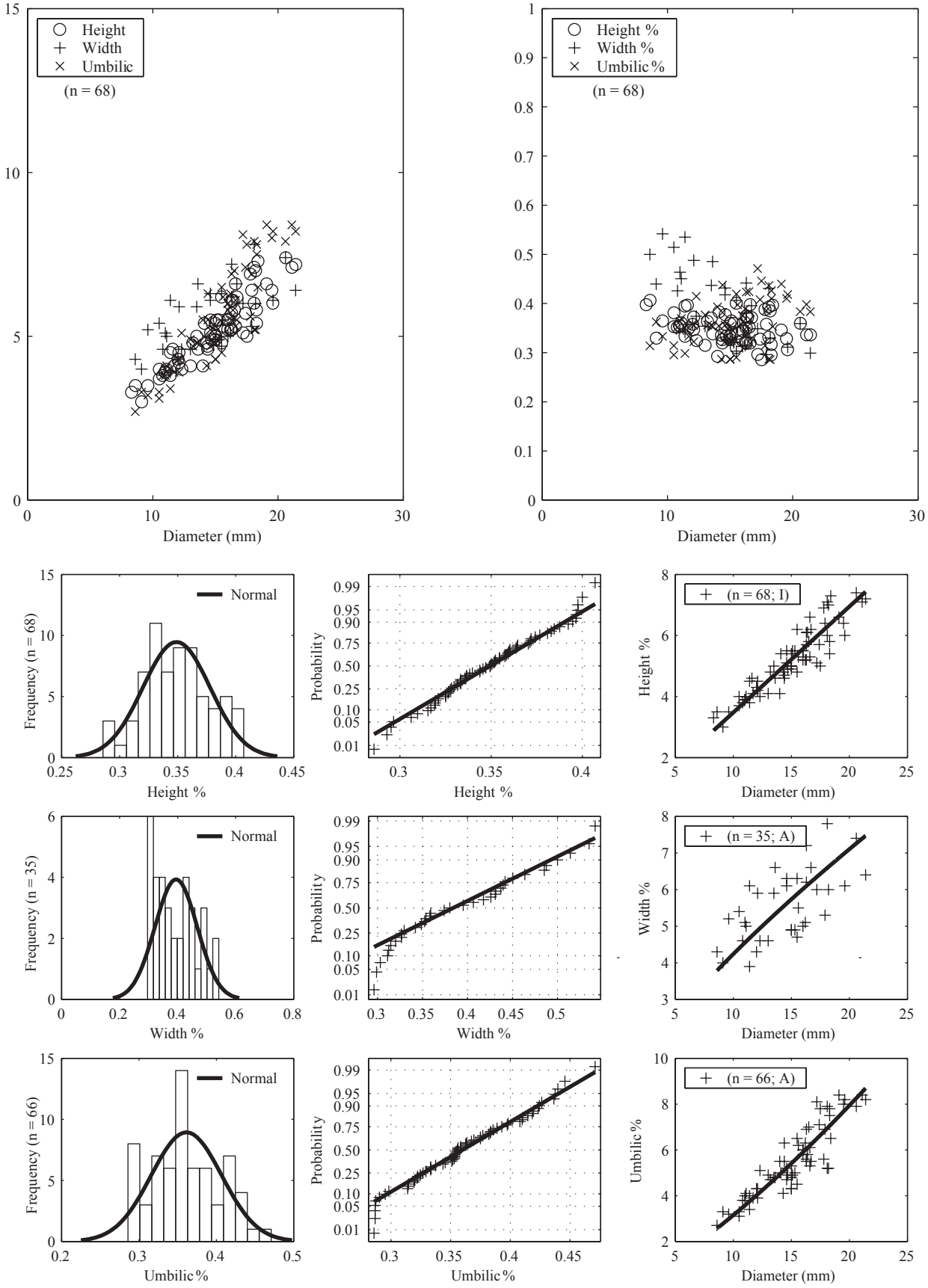

Fig. 21. Brayard & Bucher

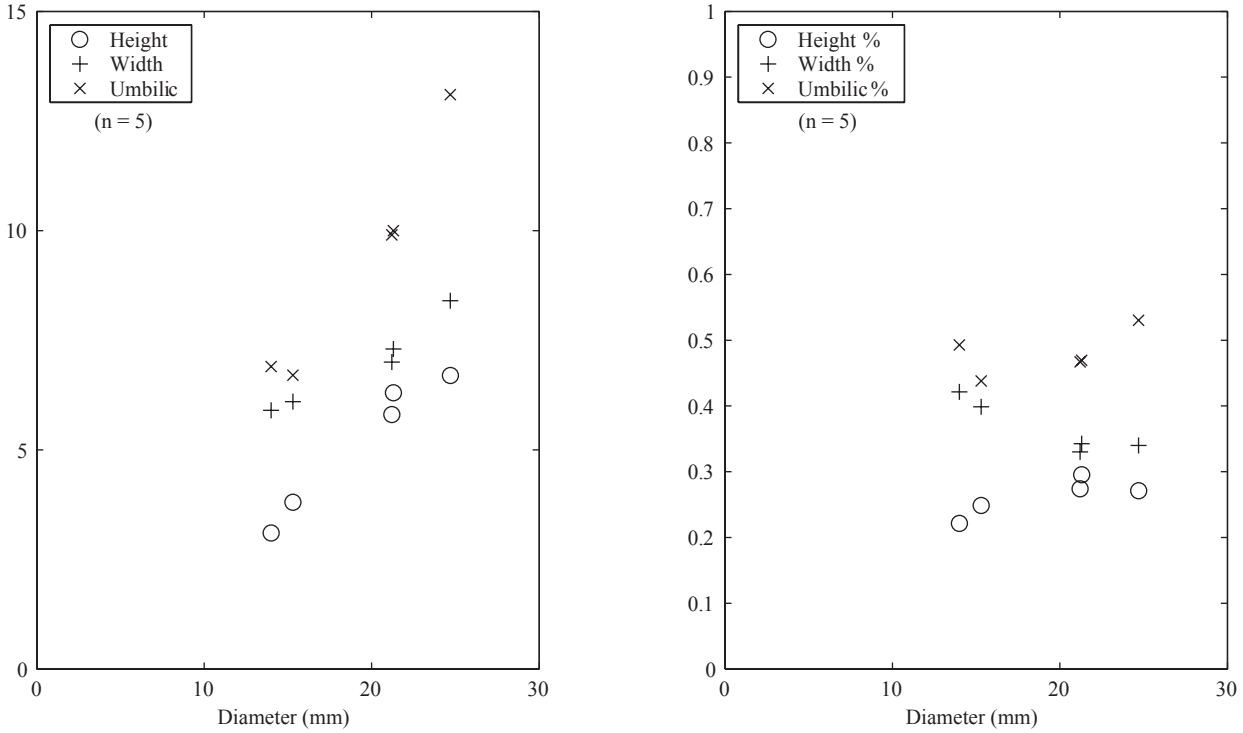

Fig. 22. Brayard & Bucher

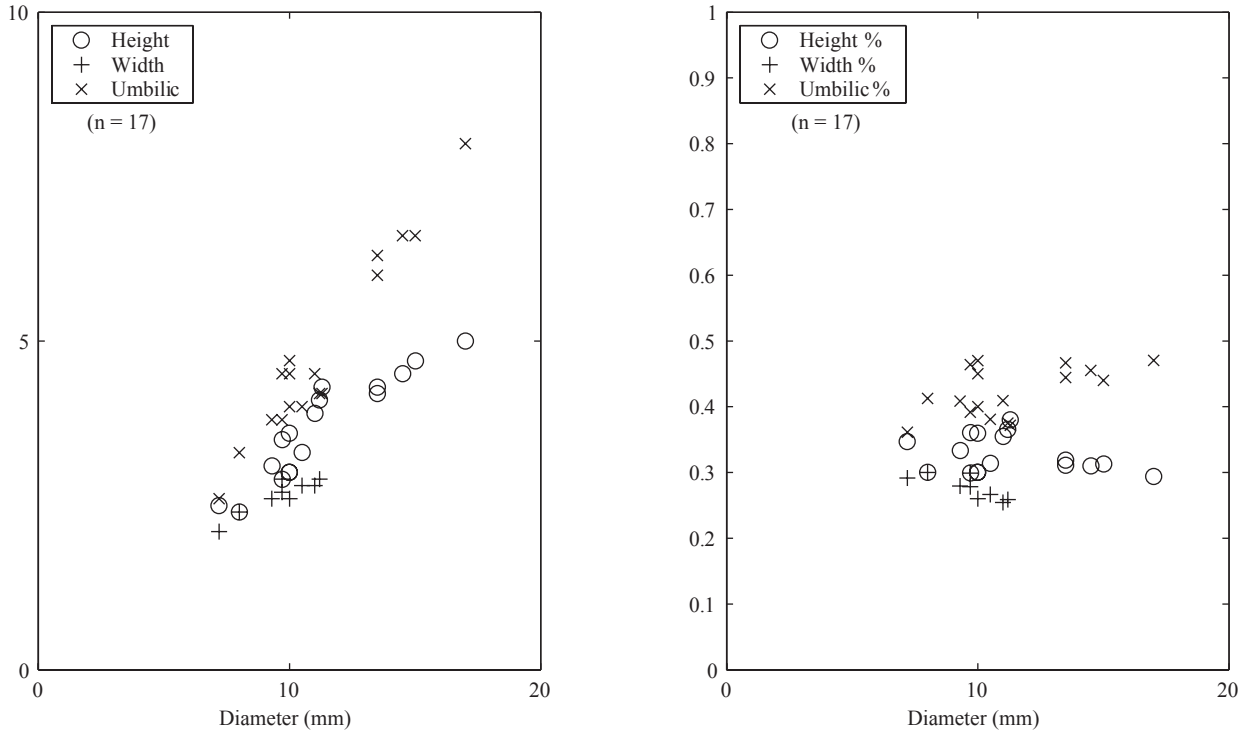

Fig. 23. Brayard & Bucher

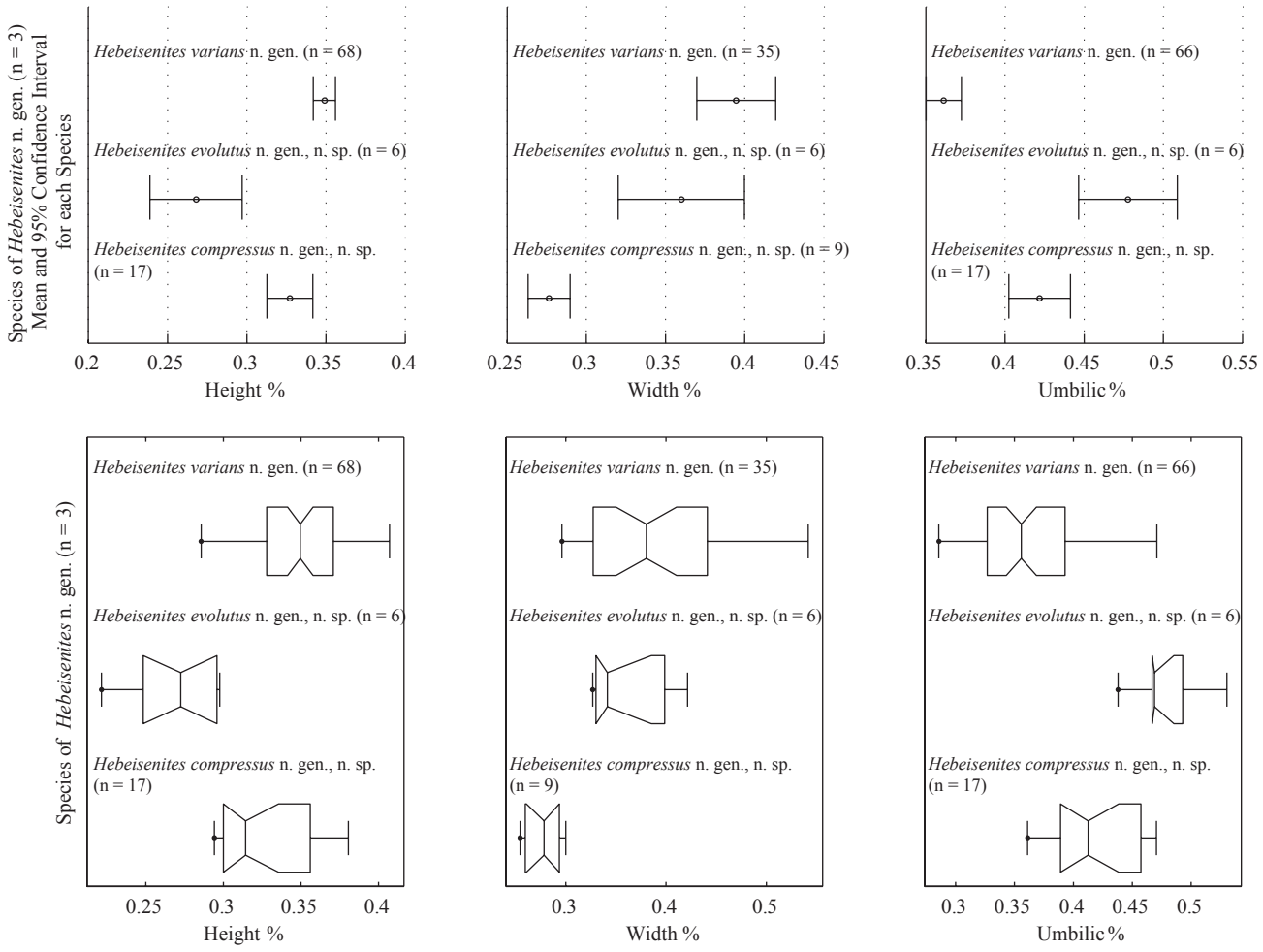

Fig. 24. Brayard & Bucher

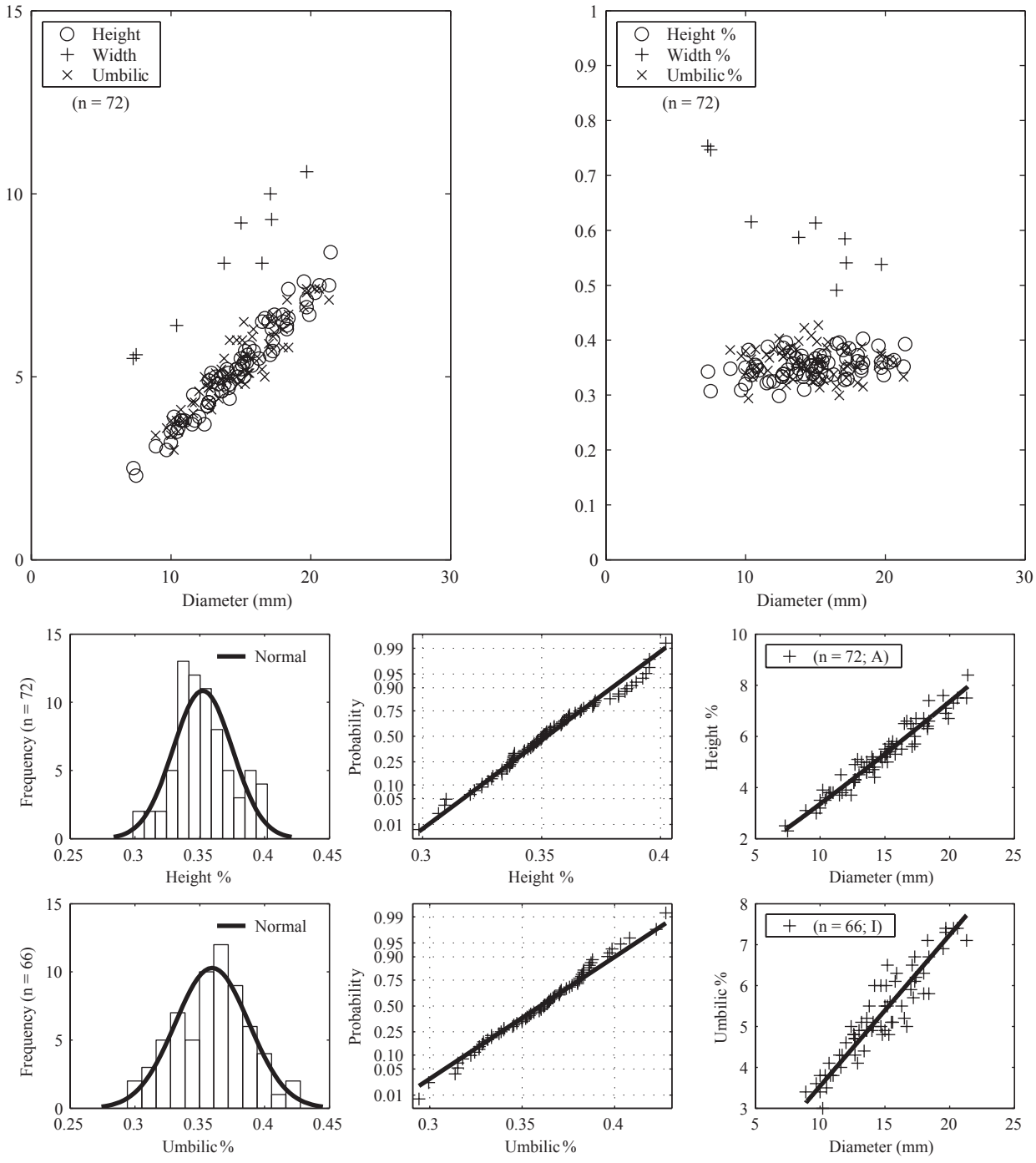

Fig. 25. Brayard & Bucher

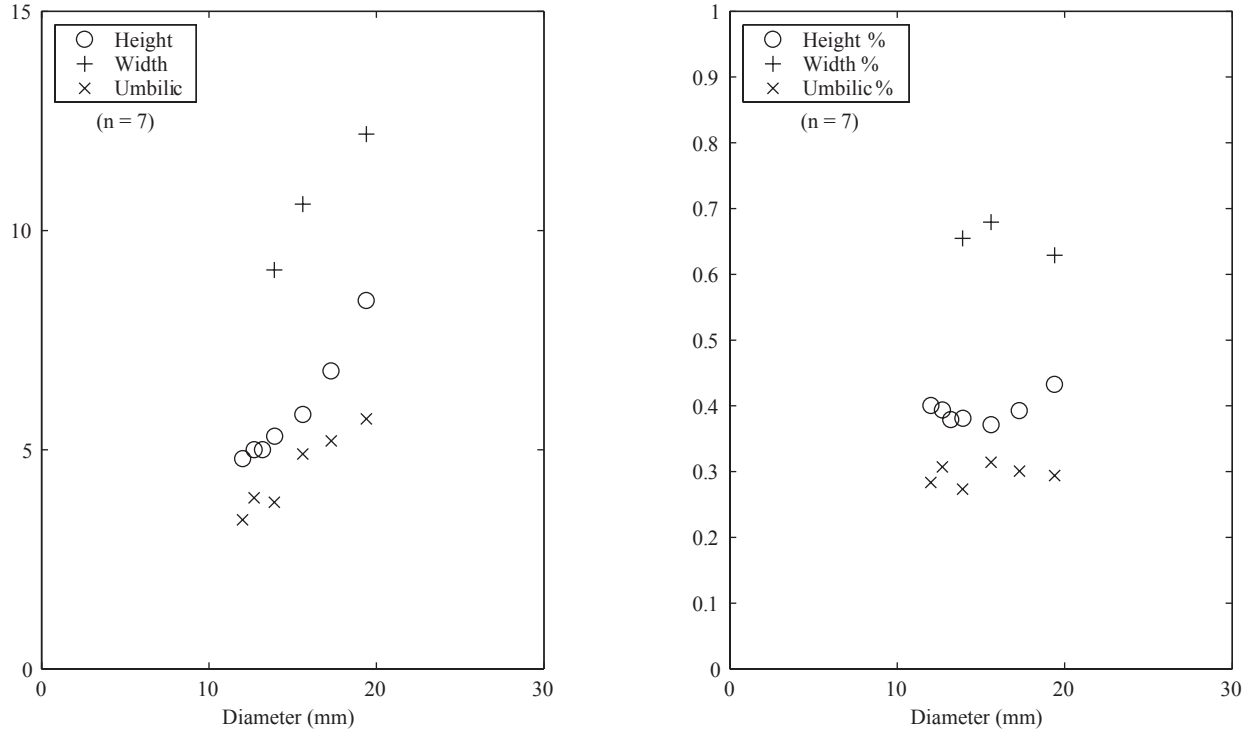

Fig. 26. Brayard & Bucher

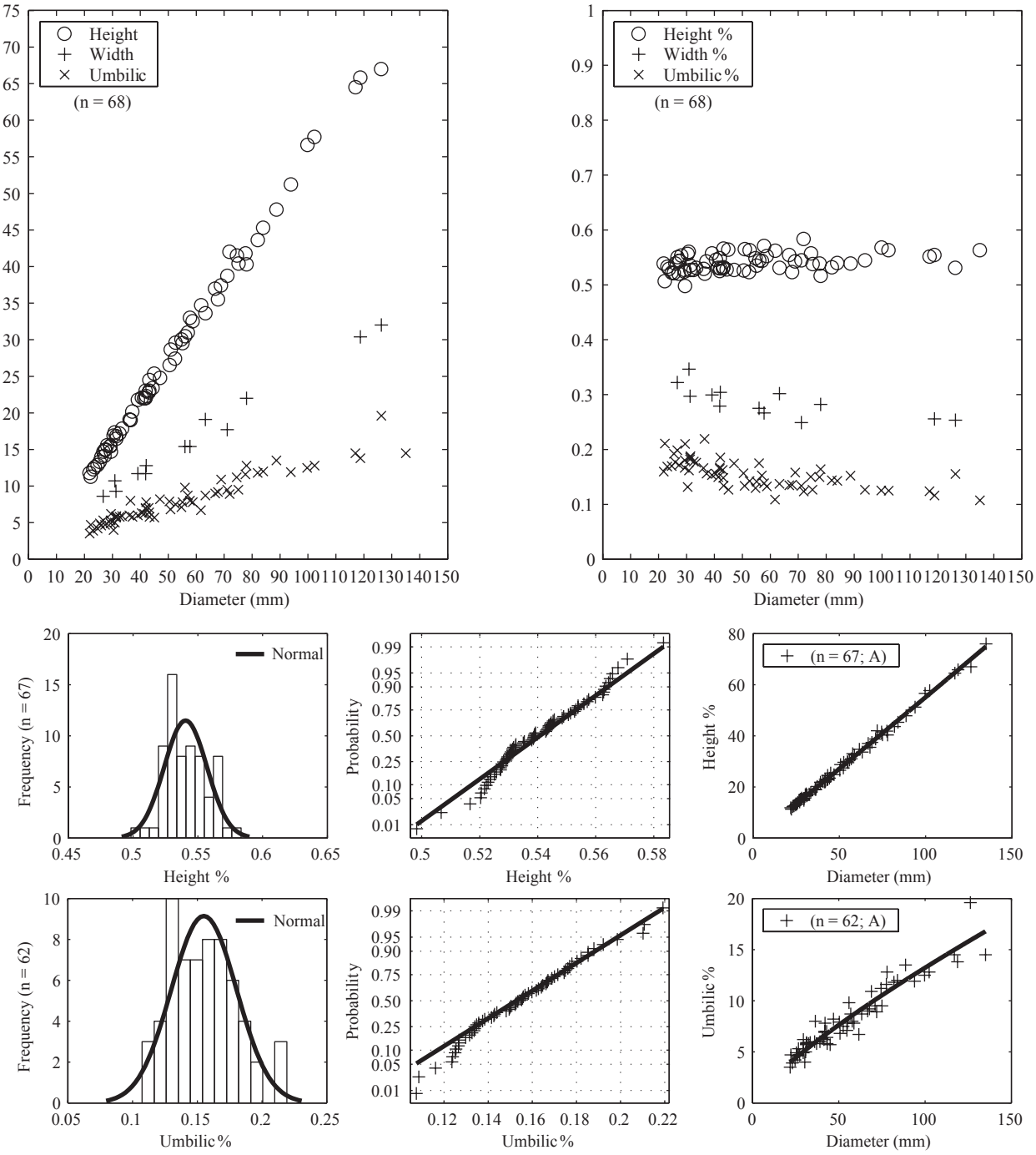

Fig. 27. Brayard & Bucher

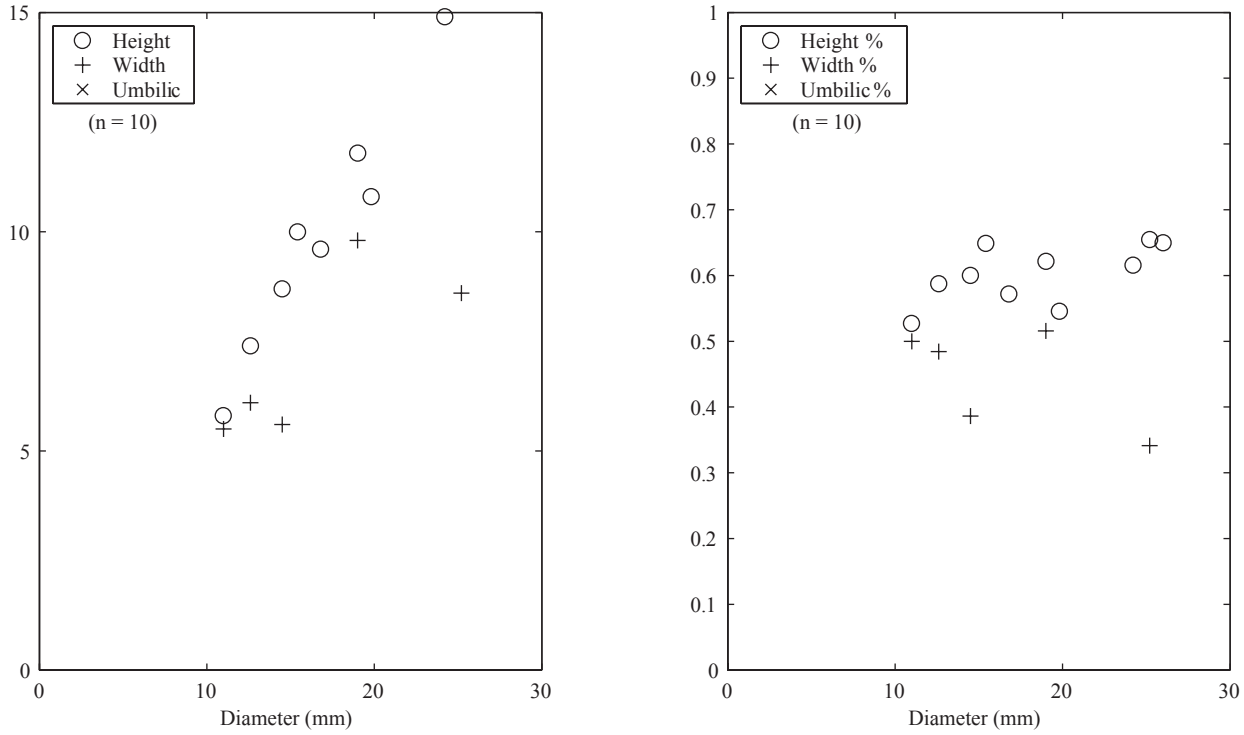

Fig. 28. Brayard & Bucher

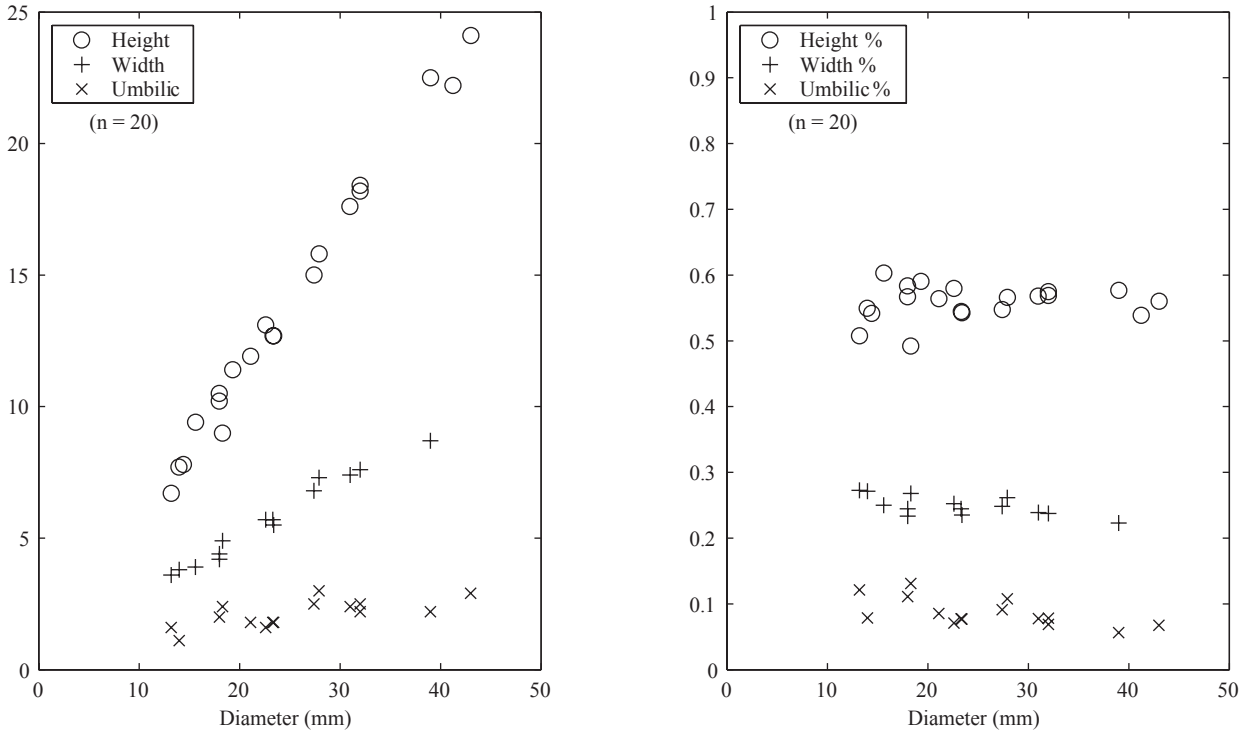

Fig. 29. Brayard & Bucher

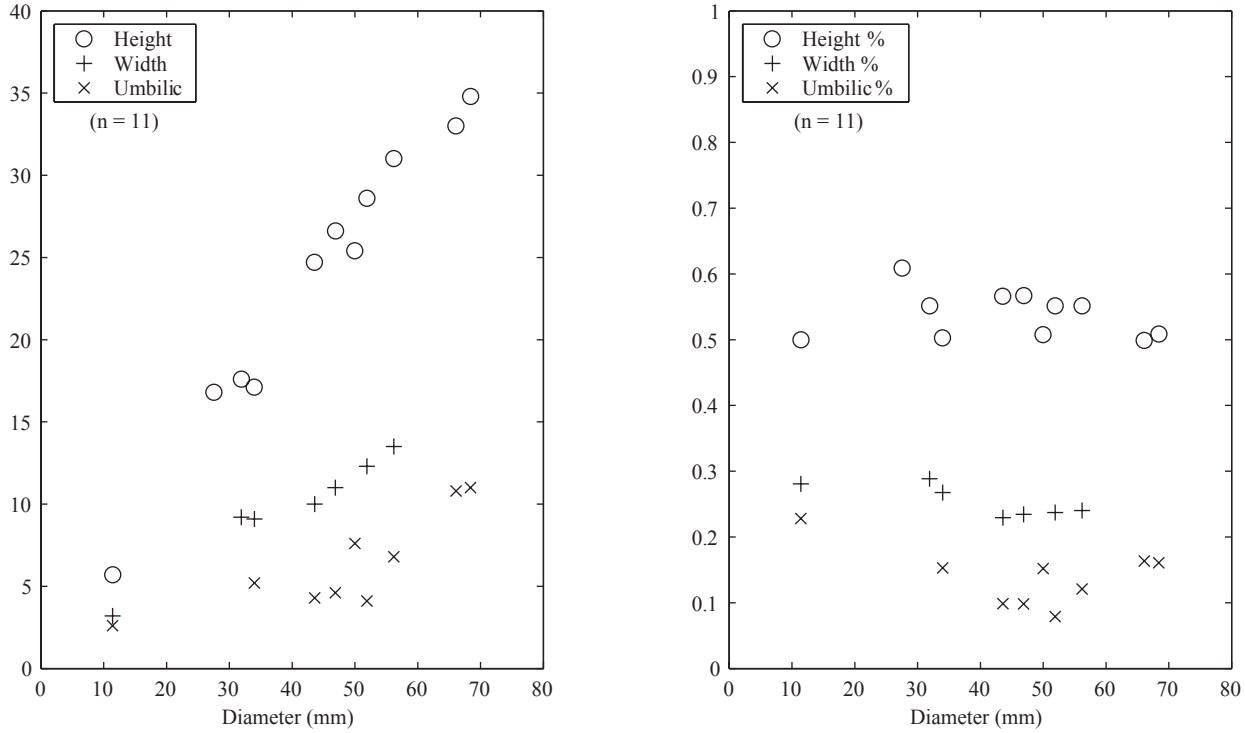

Fig. 30. Brayard & Bucher

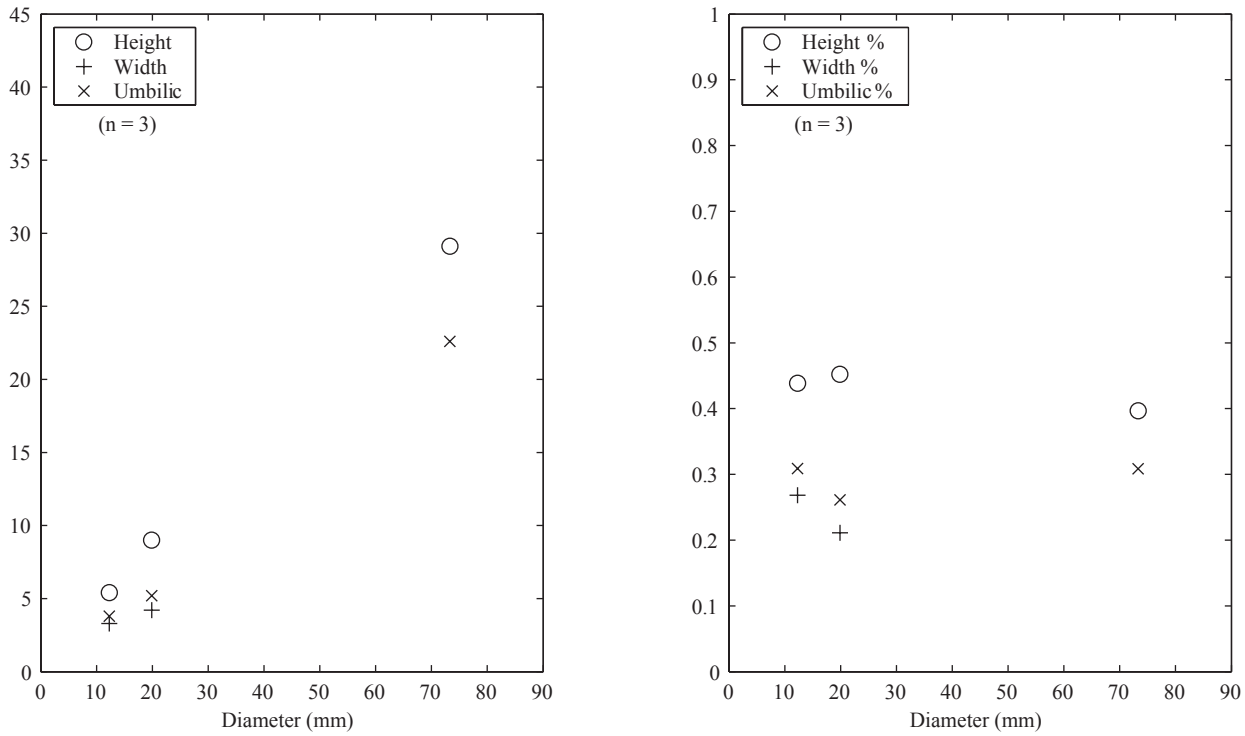

Fig. 31. Brayard & Bucher

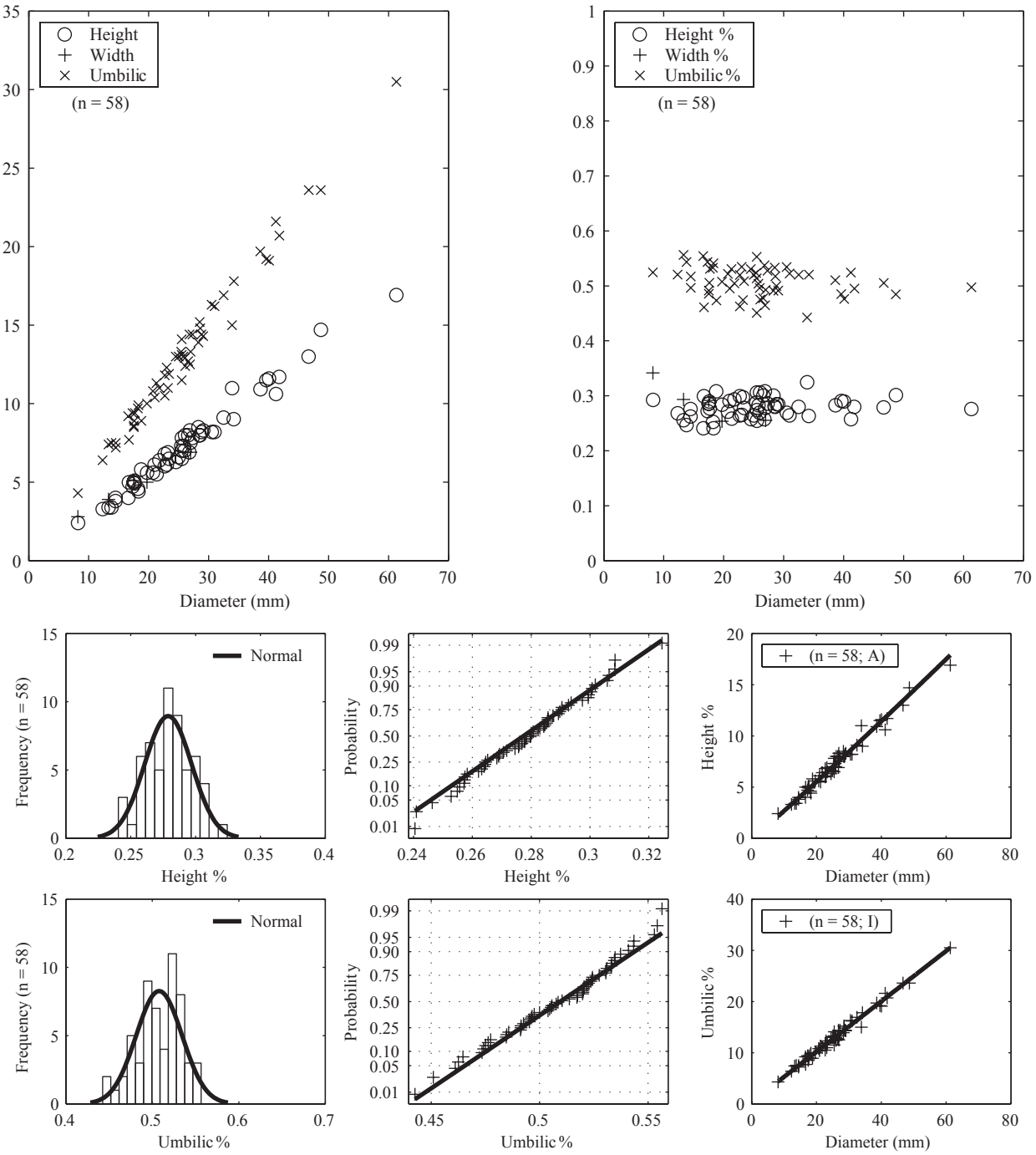

Fig. 32. Brayard & Bucher

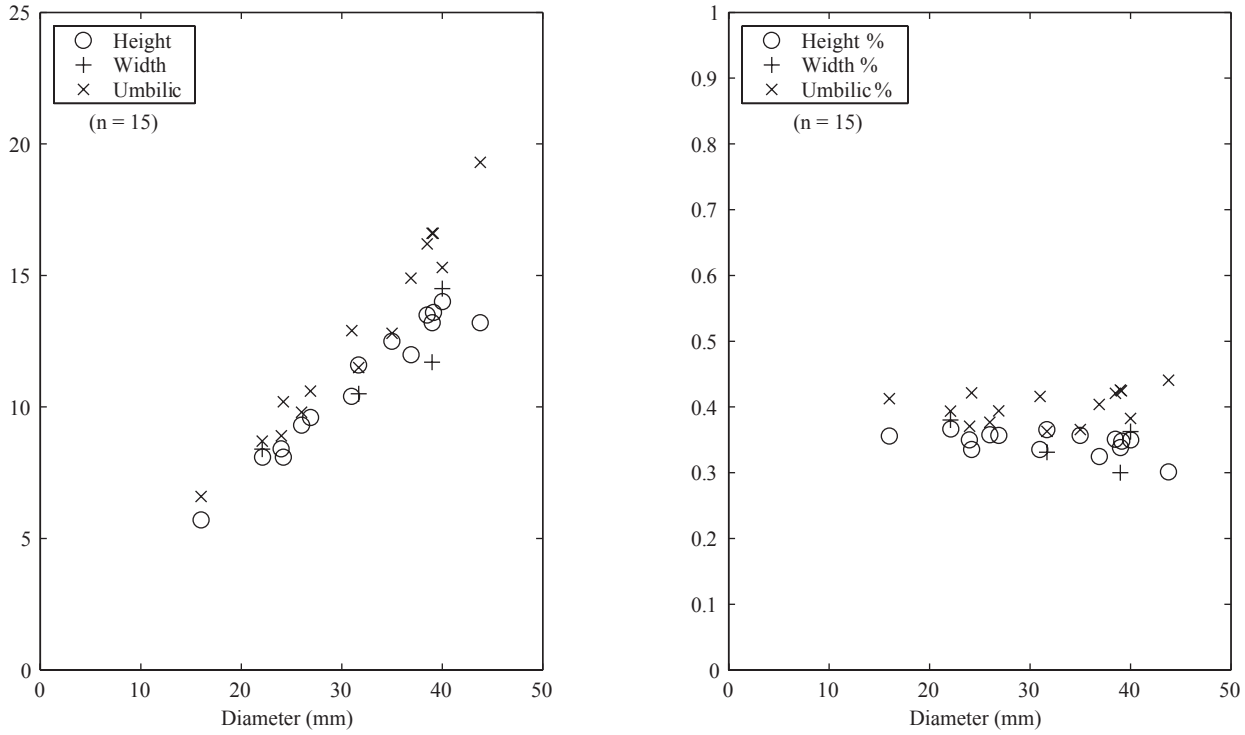

Fig. 33. Brayard & Bucher

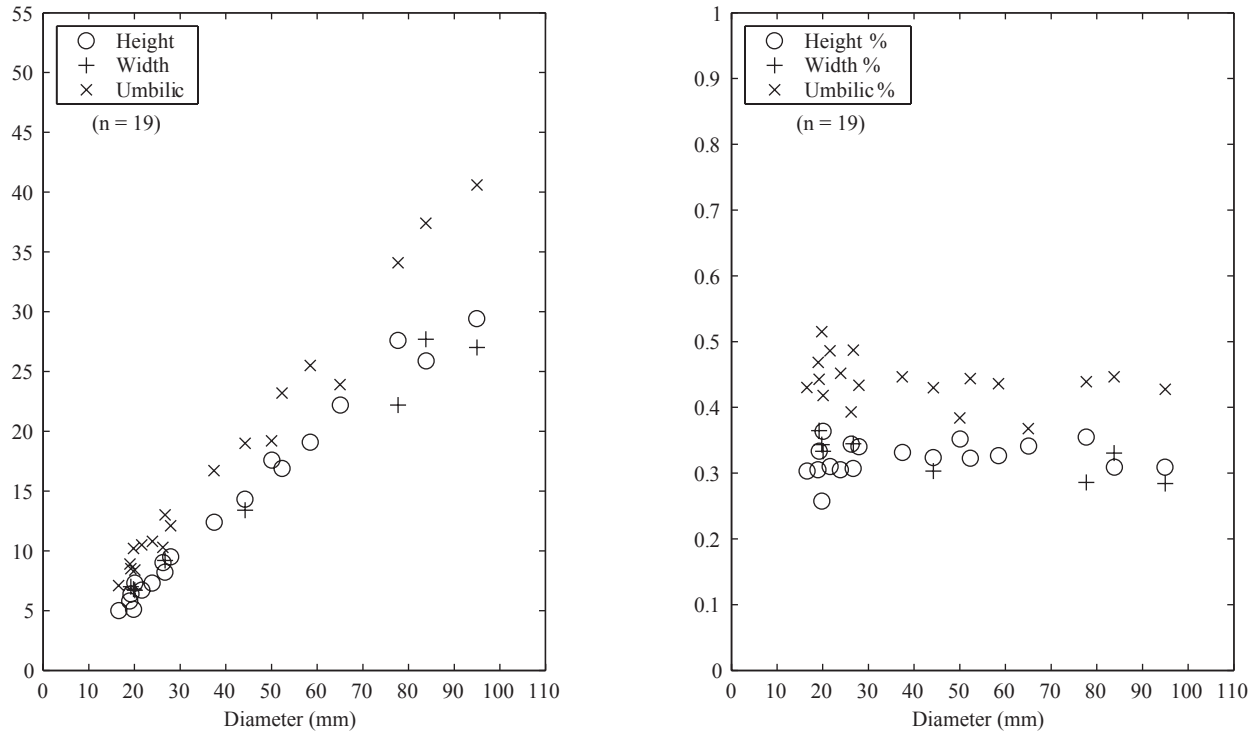

Fig. 34. Brayard & Bucher

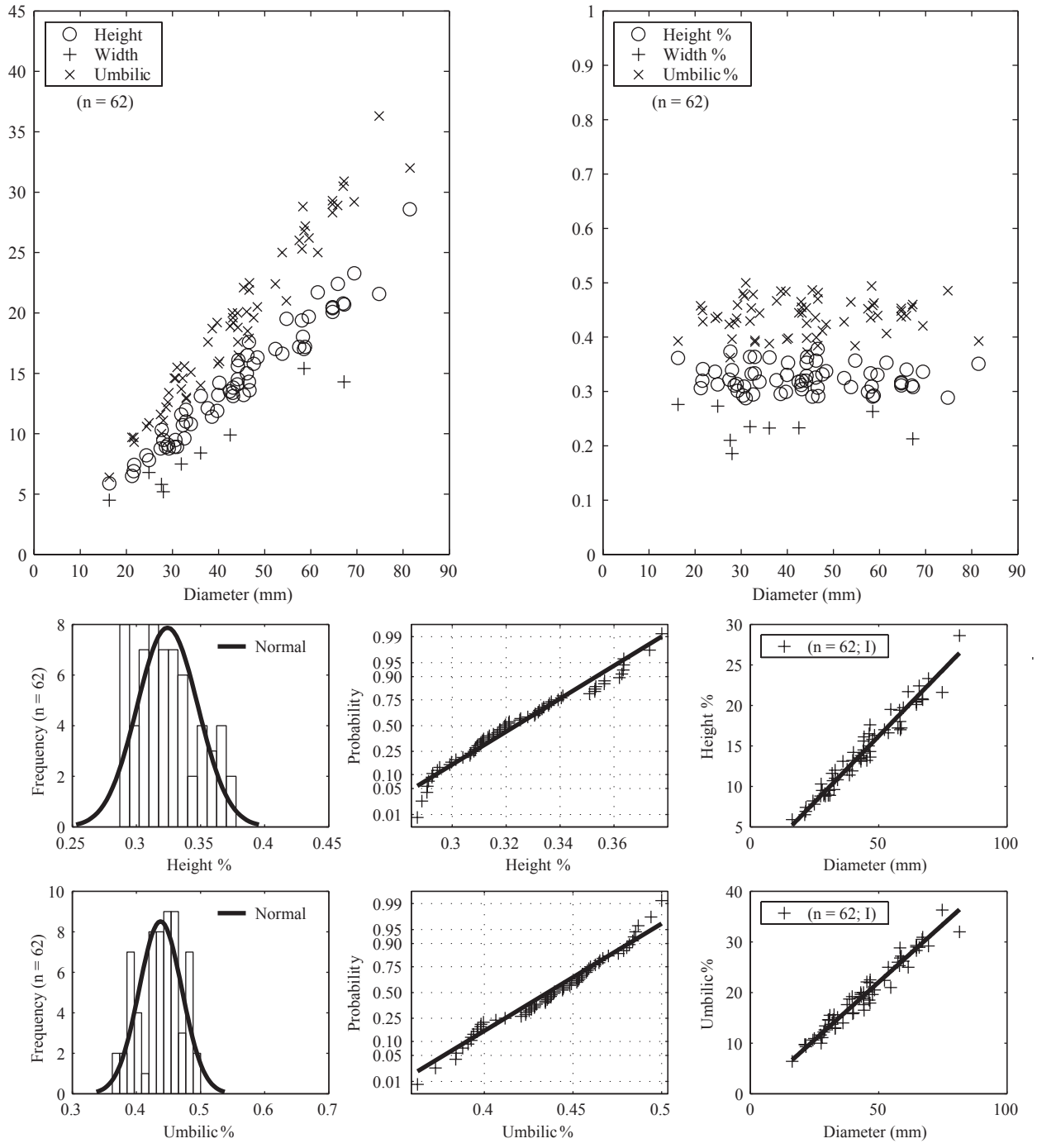

Fig. 35. Brayard & Bucher

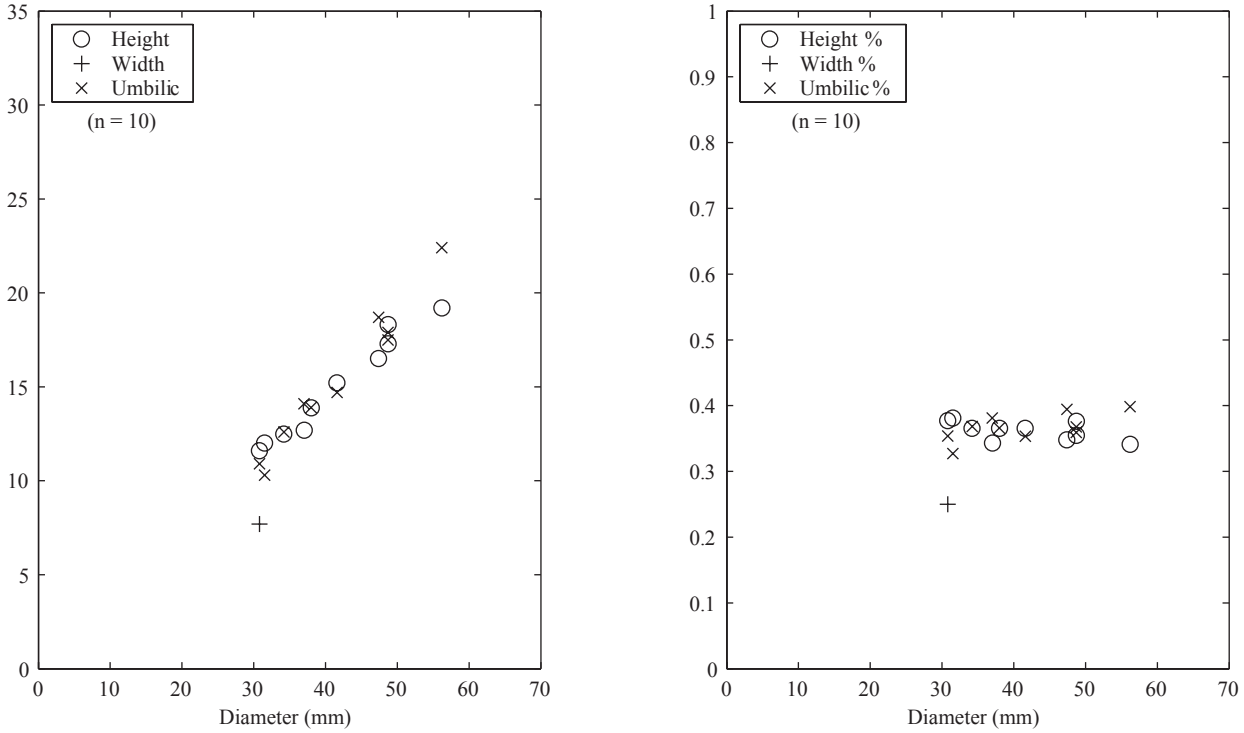

Fig. 36. Brayard & Bucher

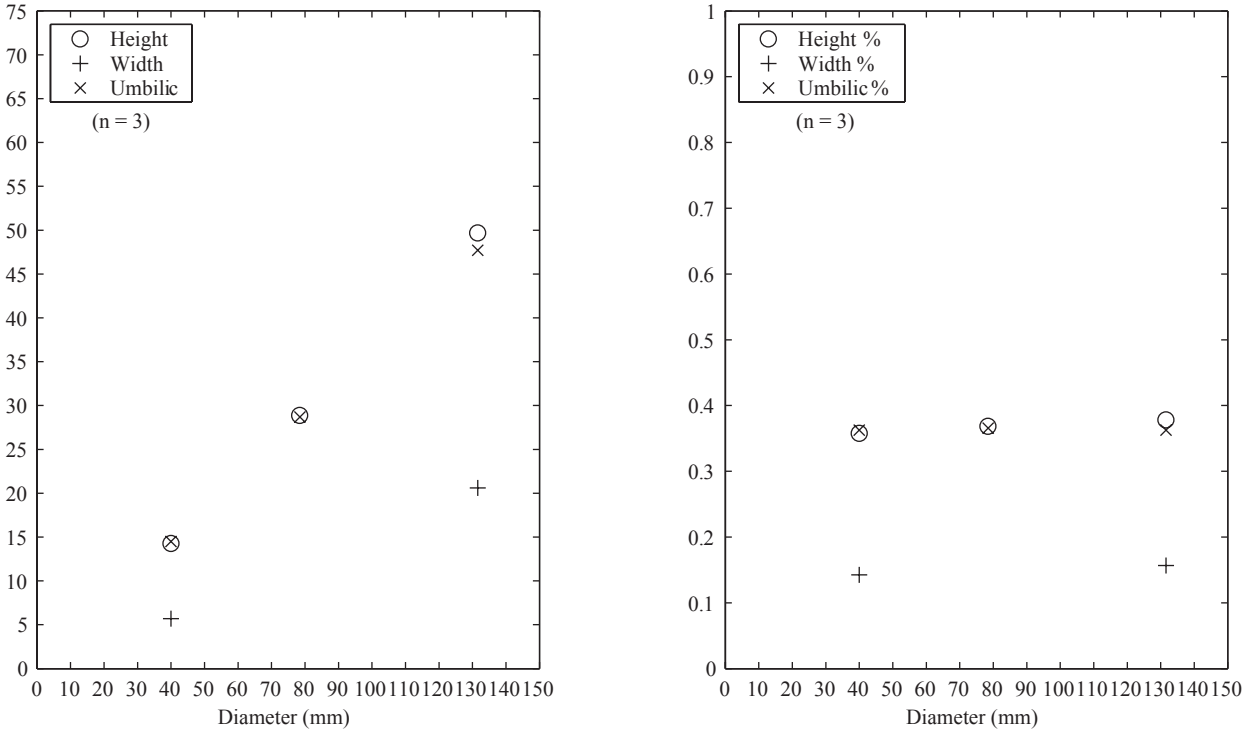

Fig. 37. Brayard & Bucher

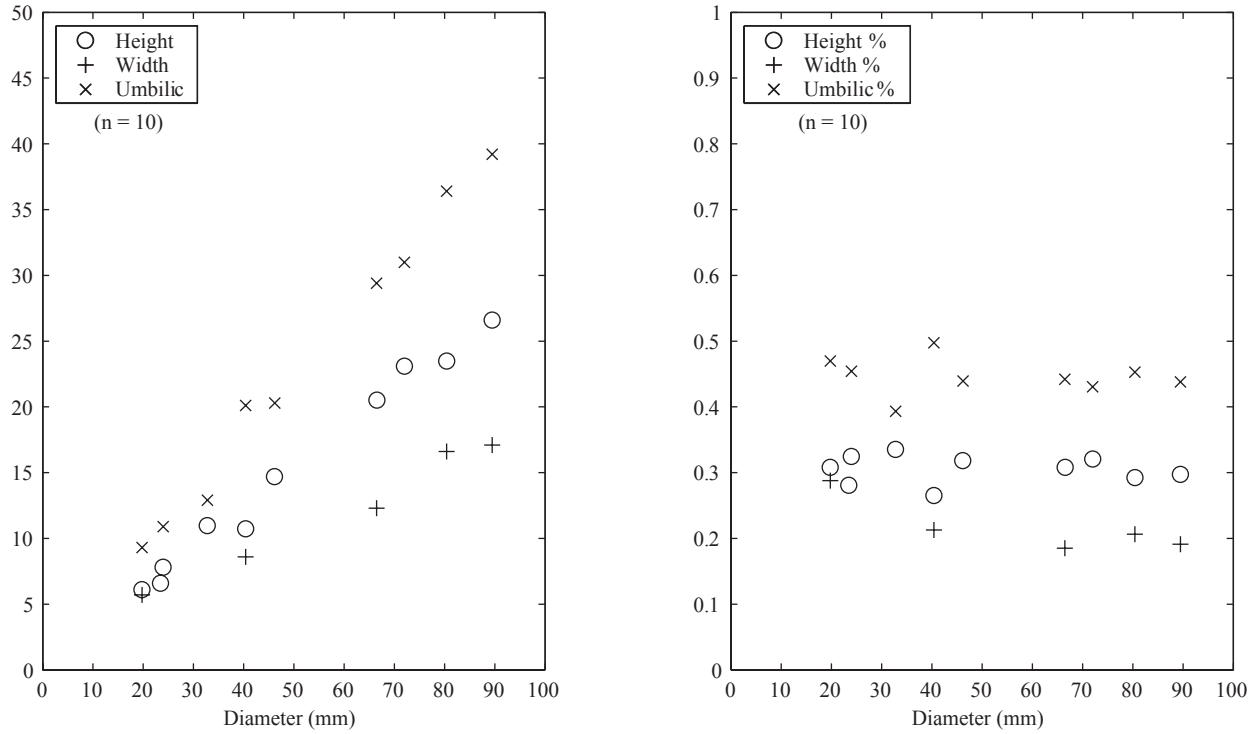

Fig. 38. Brayard & Bucher

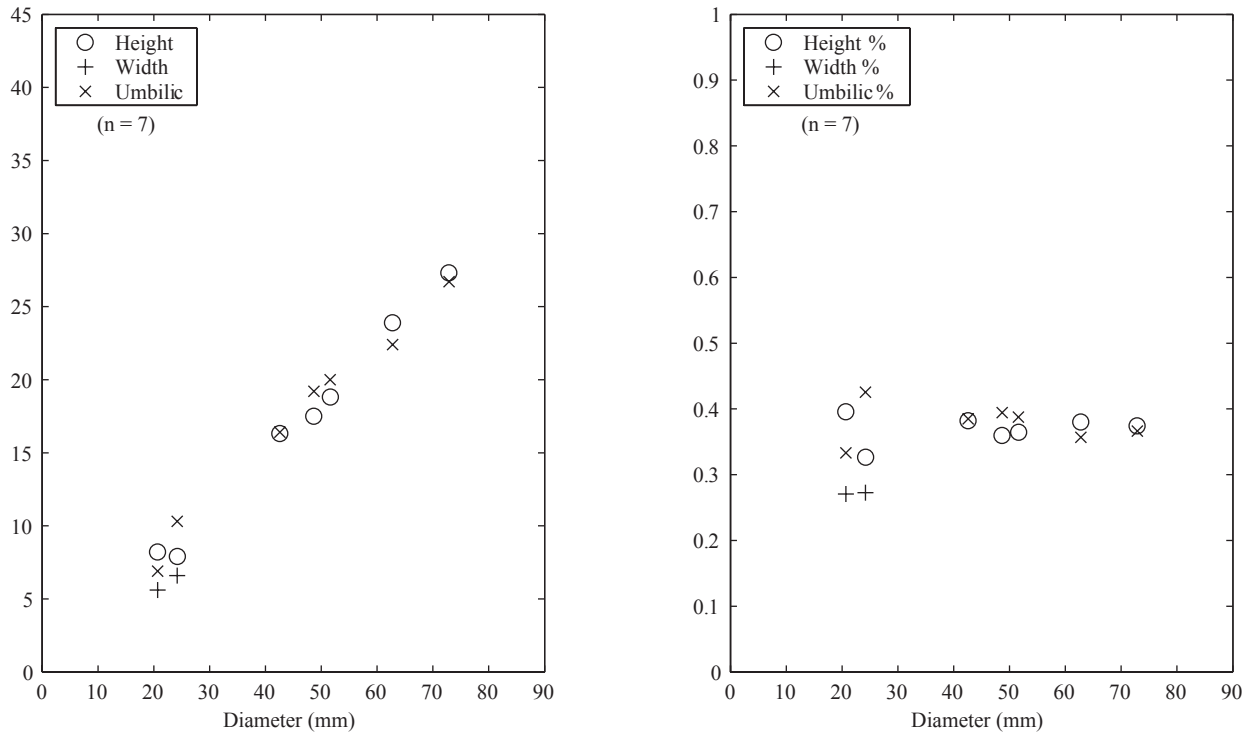

Fig. 39. Brayard & Bucher

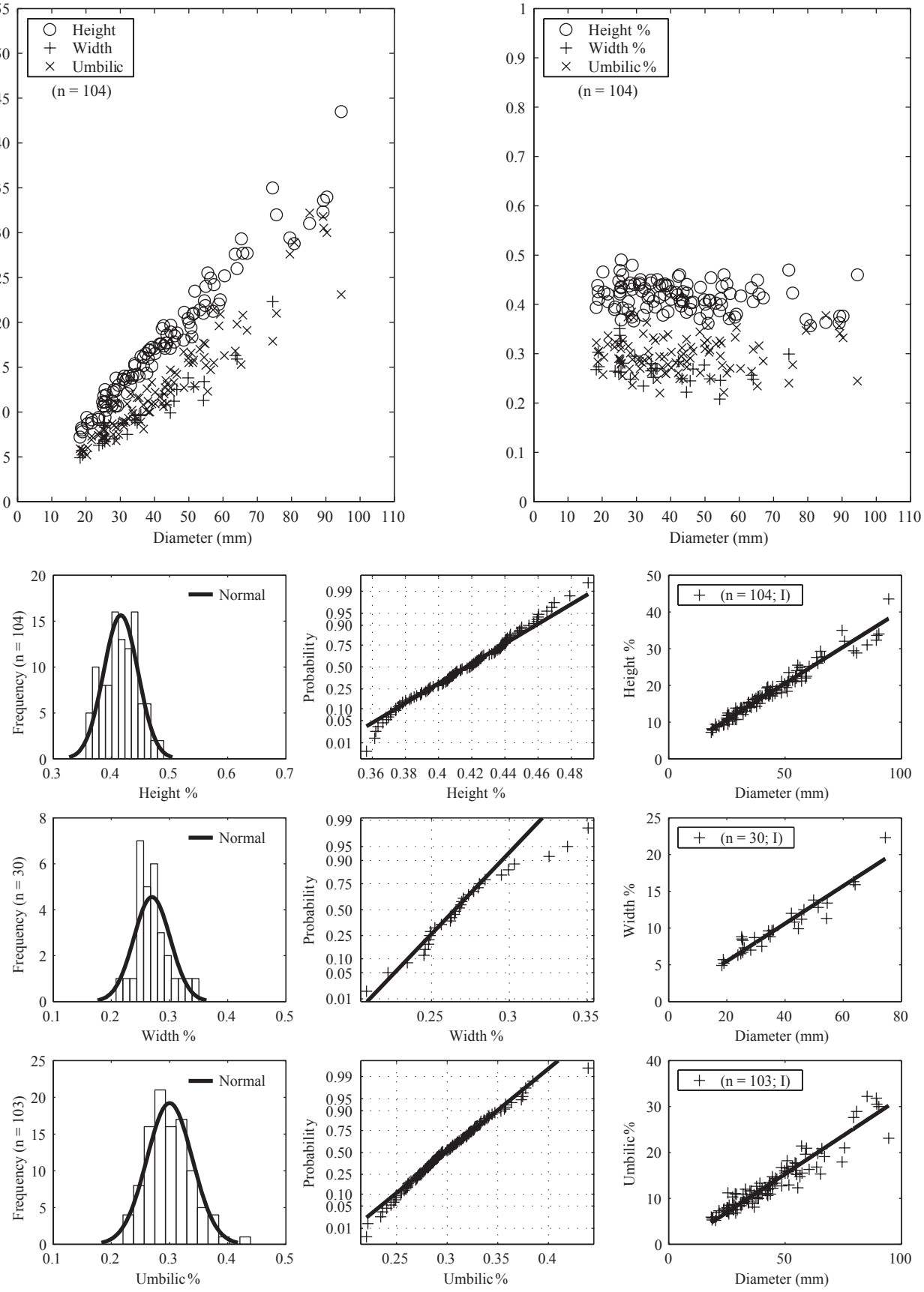

Fig. 40. Brayard & Bucher

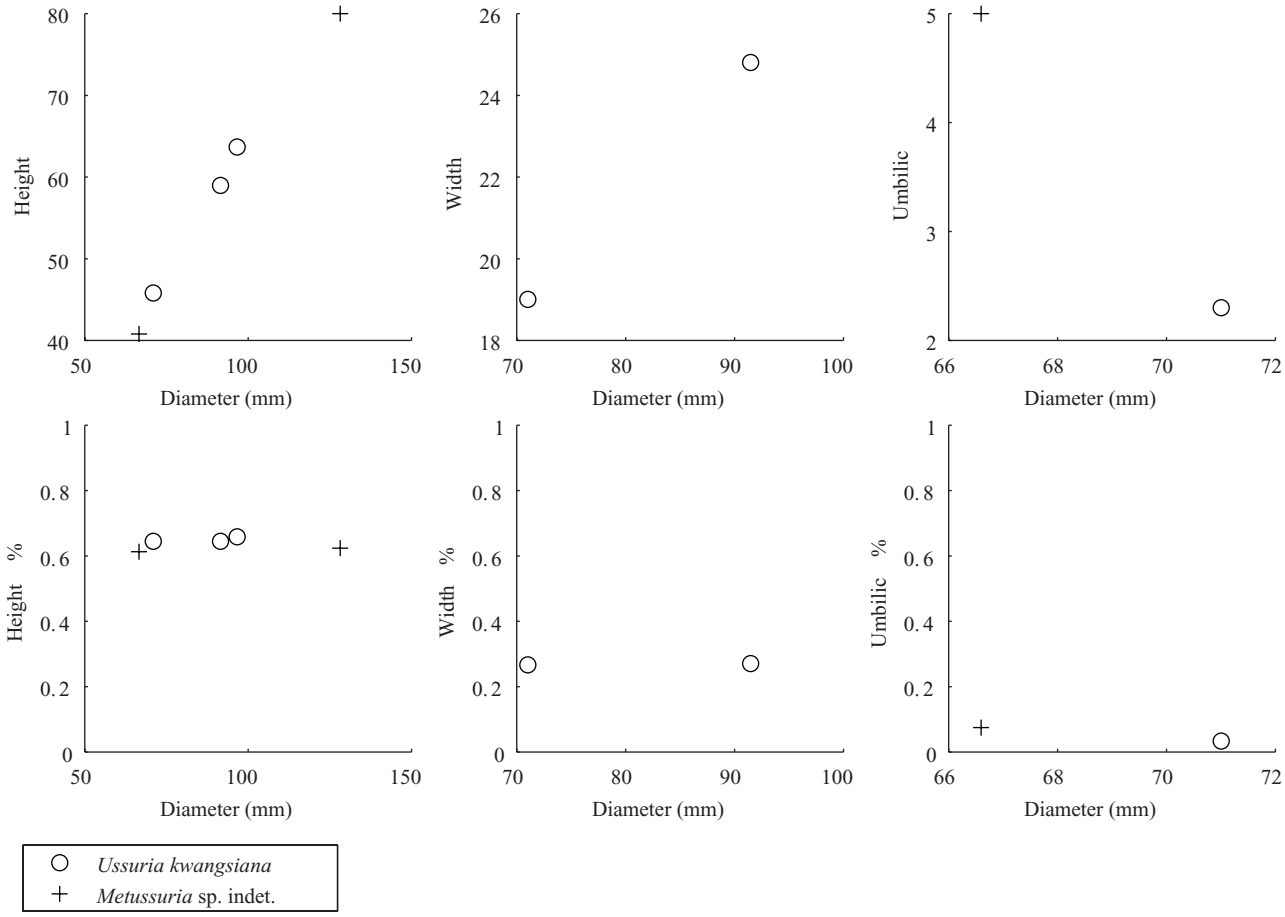

Fig. 41. Brayard & Bucher

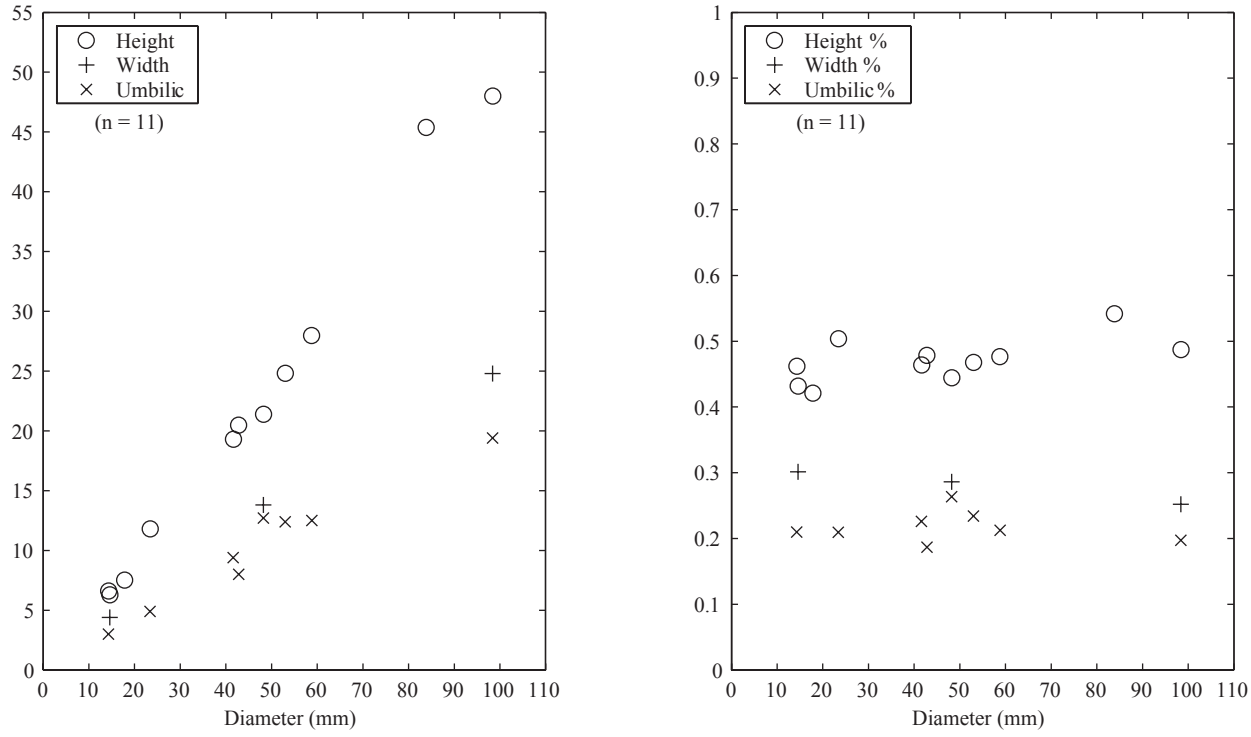

Fig. 42. Brayard & Bucher

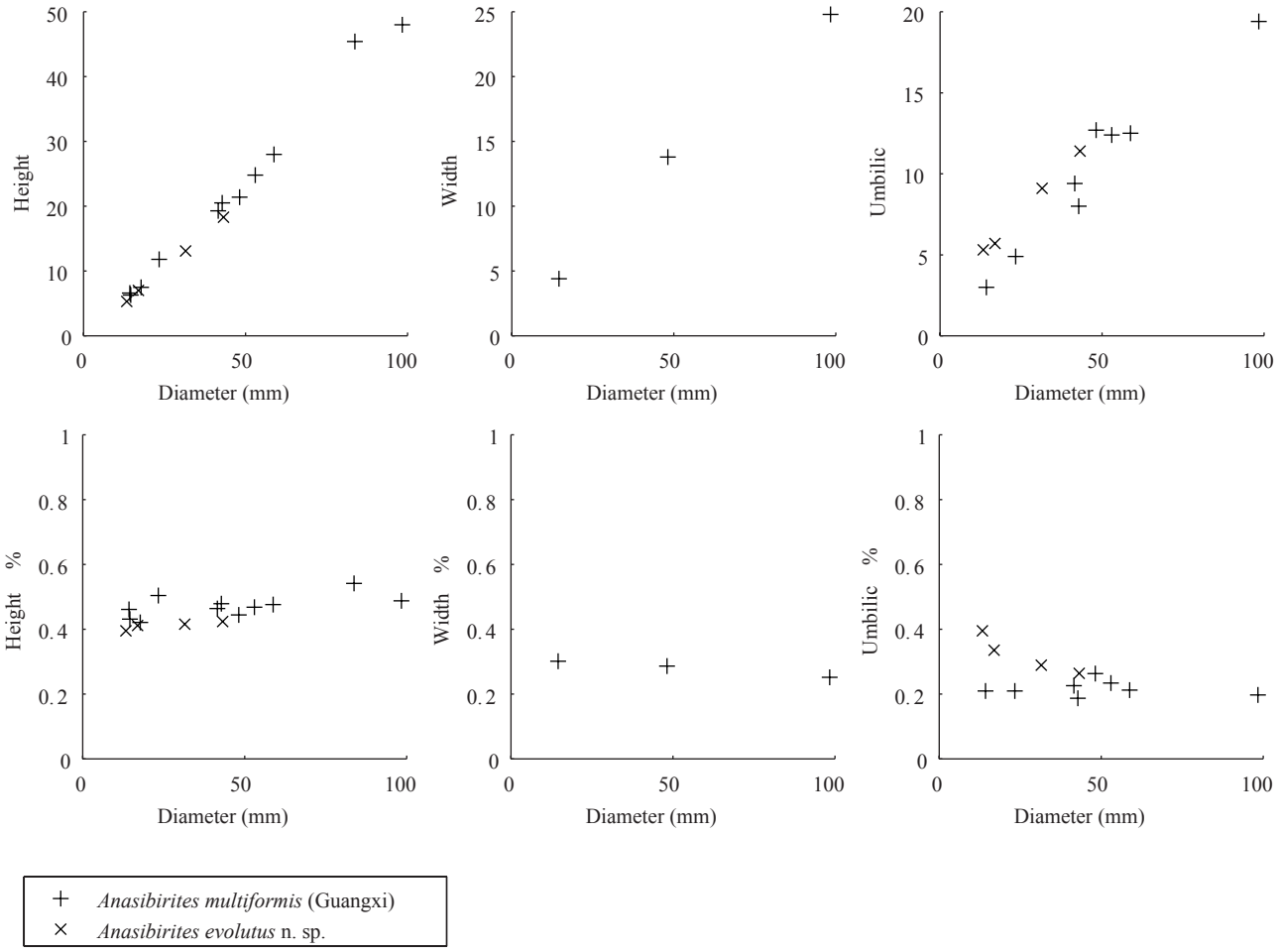

Fig. 43. Brayard & Bucher

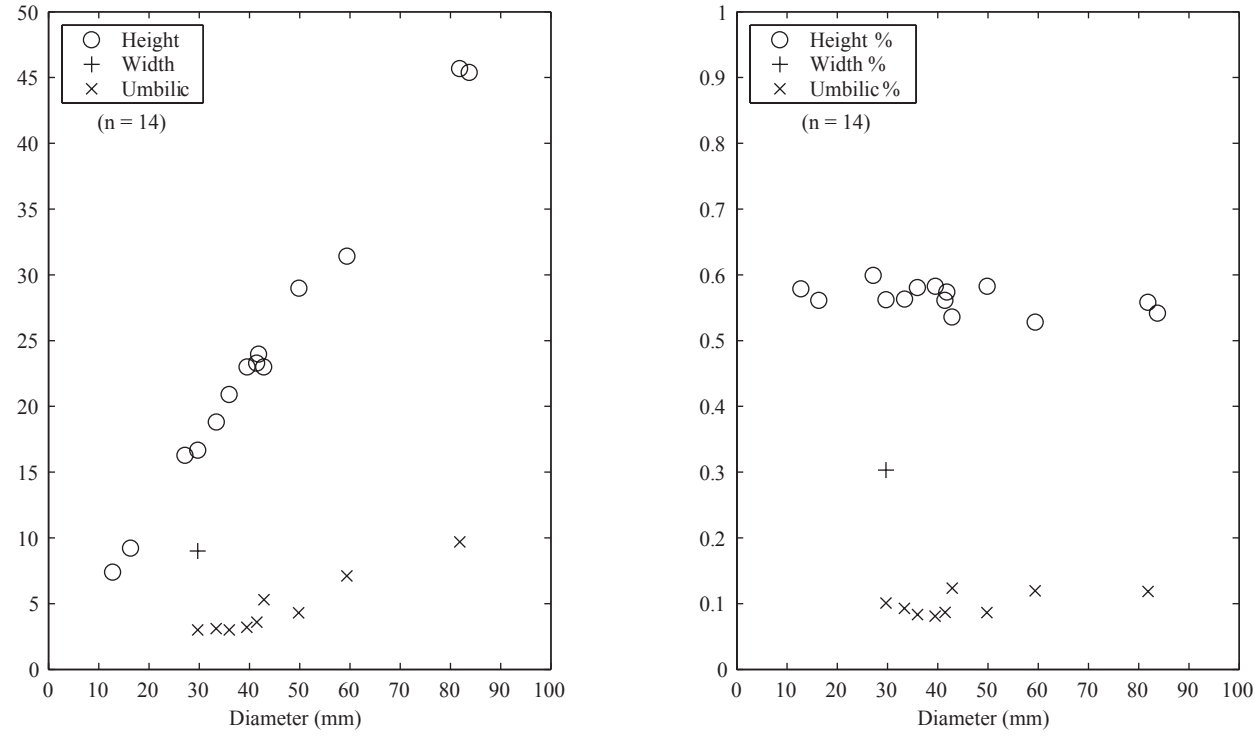

Fig. 44. Brayard & Bucher

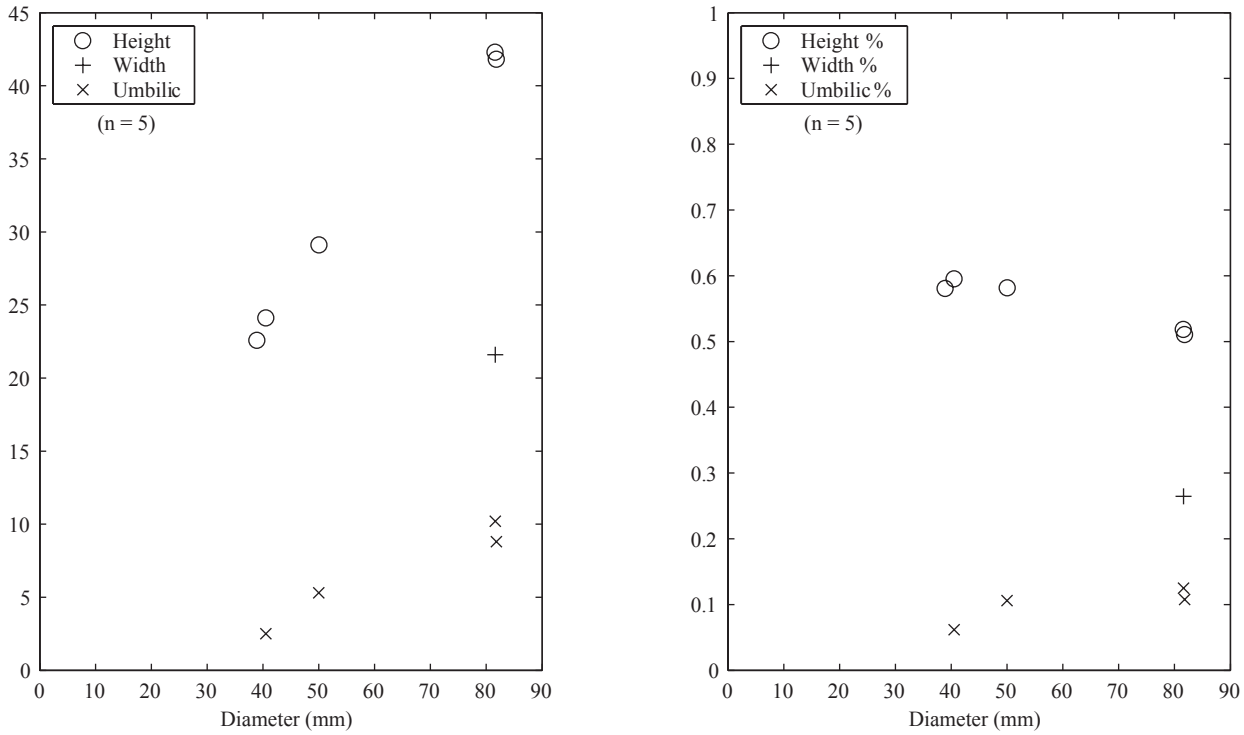

Fig. 45. Brayard & Bucher

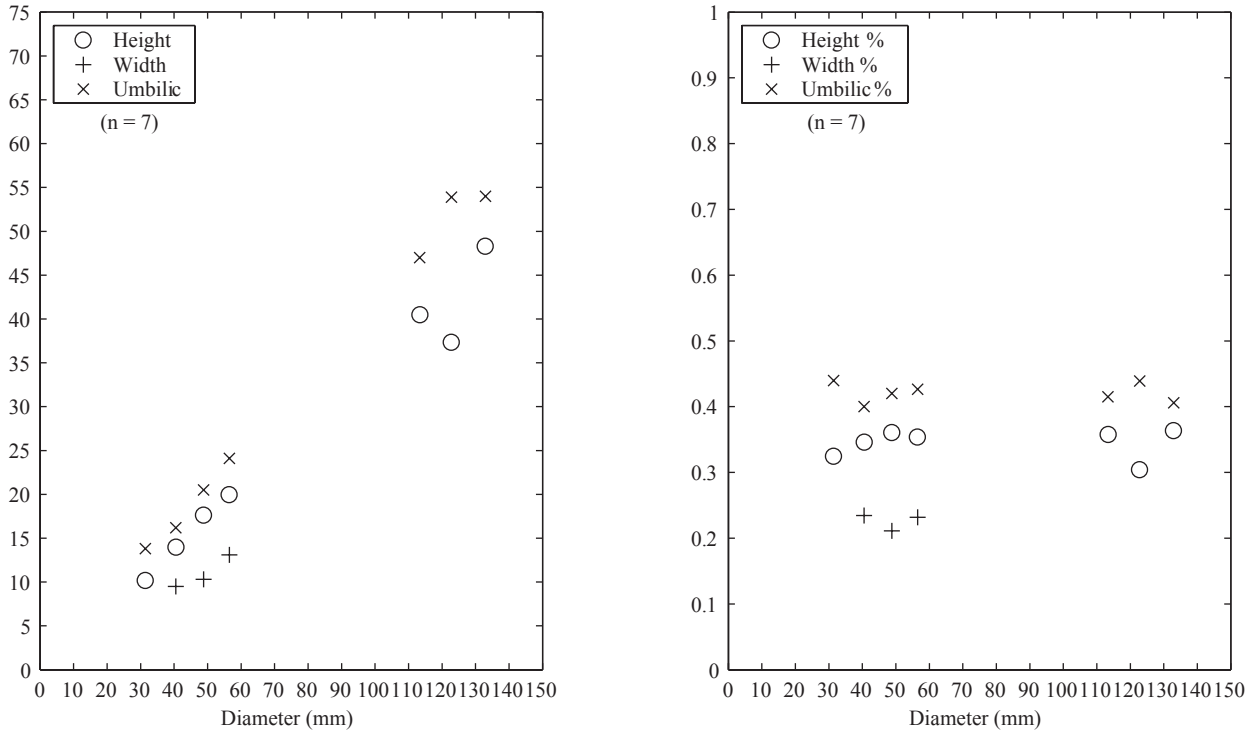

Fig. 46. Brayard & Bucher

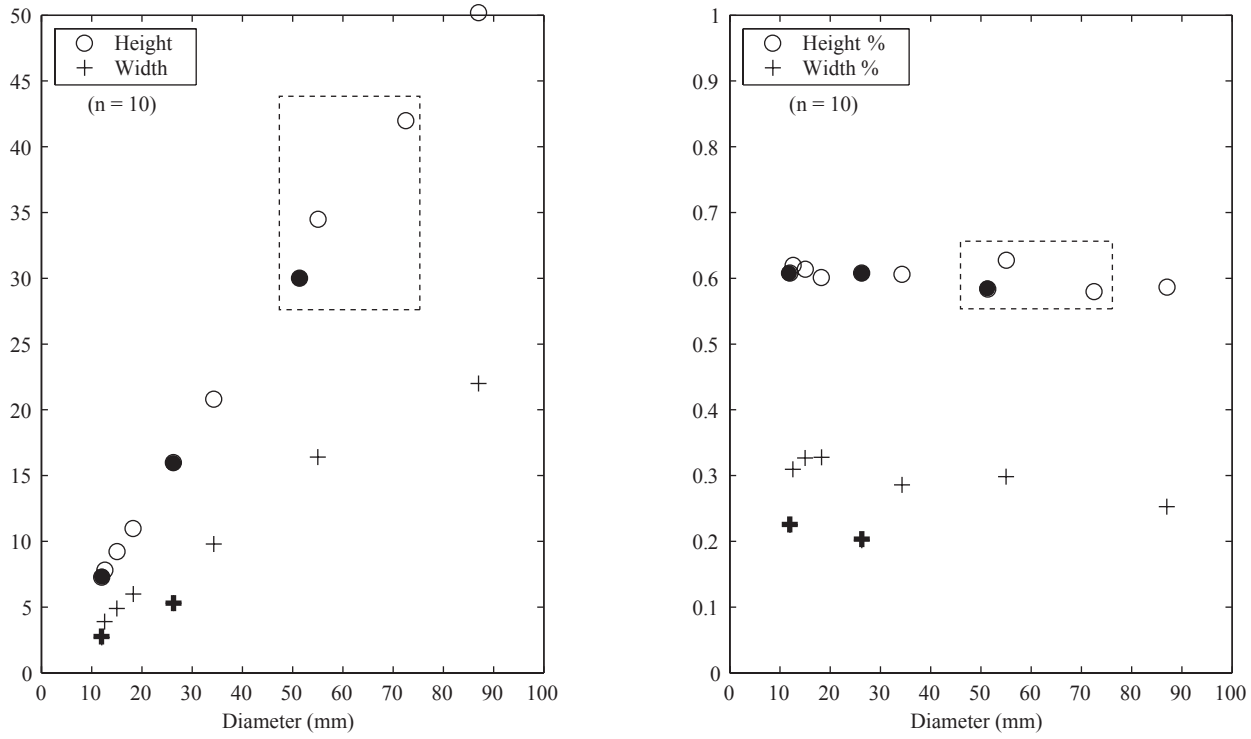

Fig. 47. Brayard & Bucher

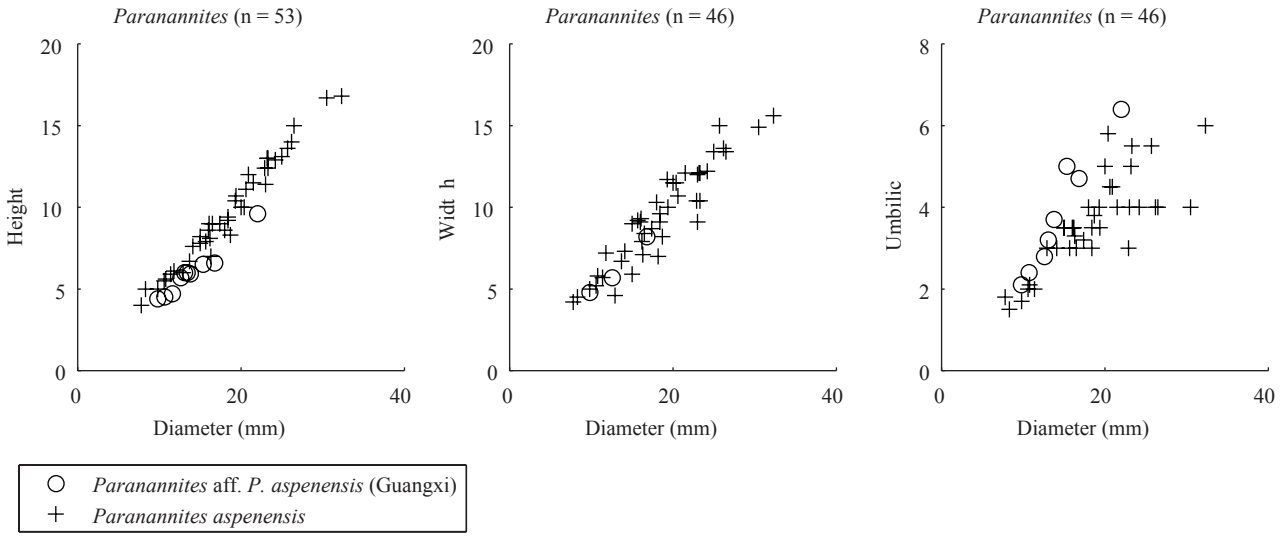

Fig. 48. Brayard & Bucher

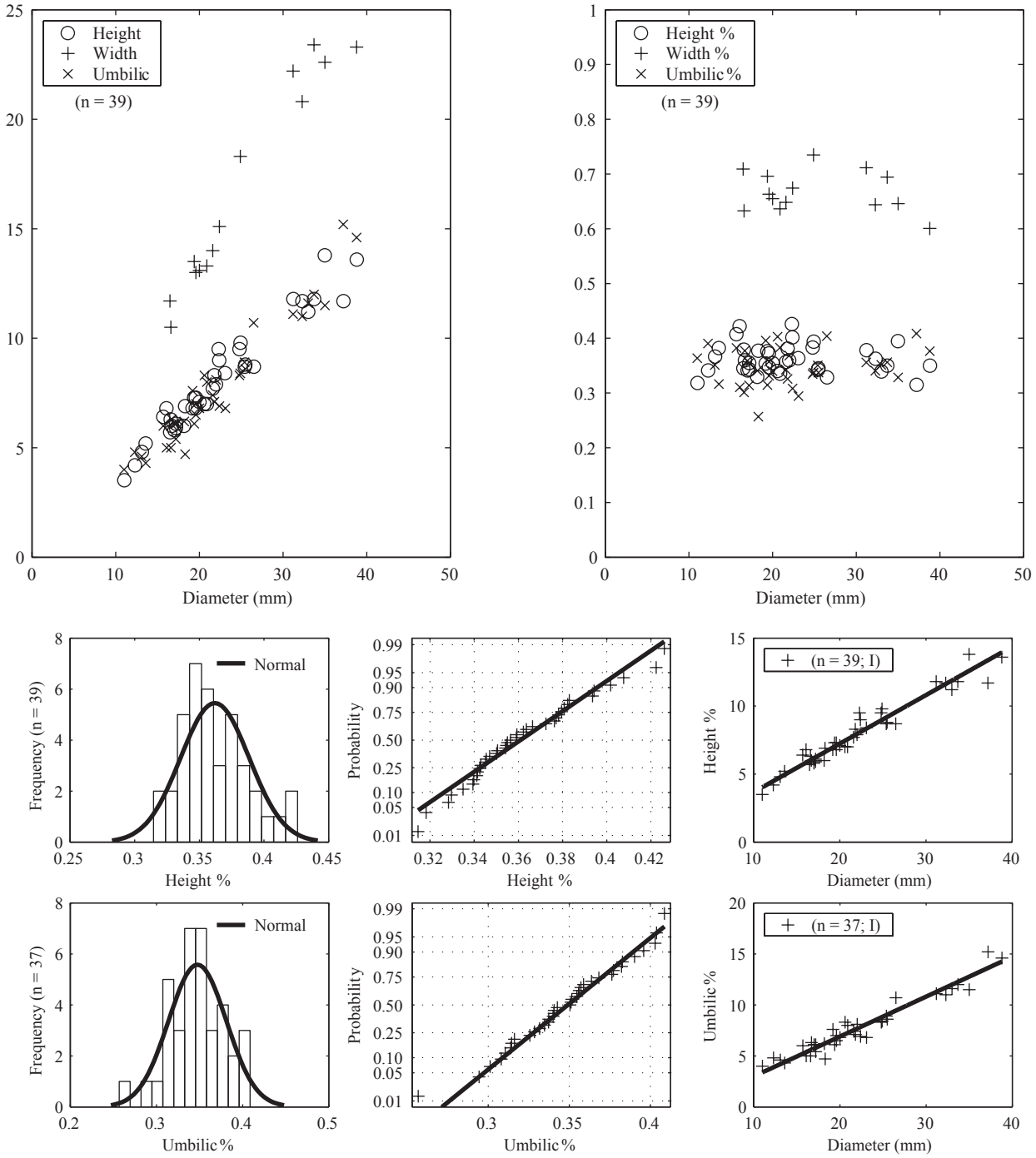

Fig. 49. Brayard & Bucher

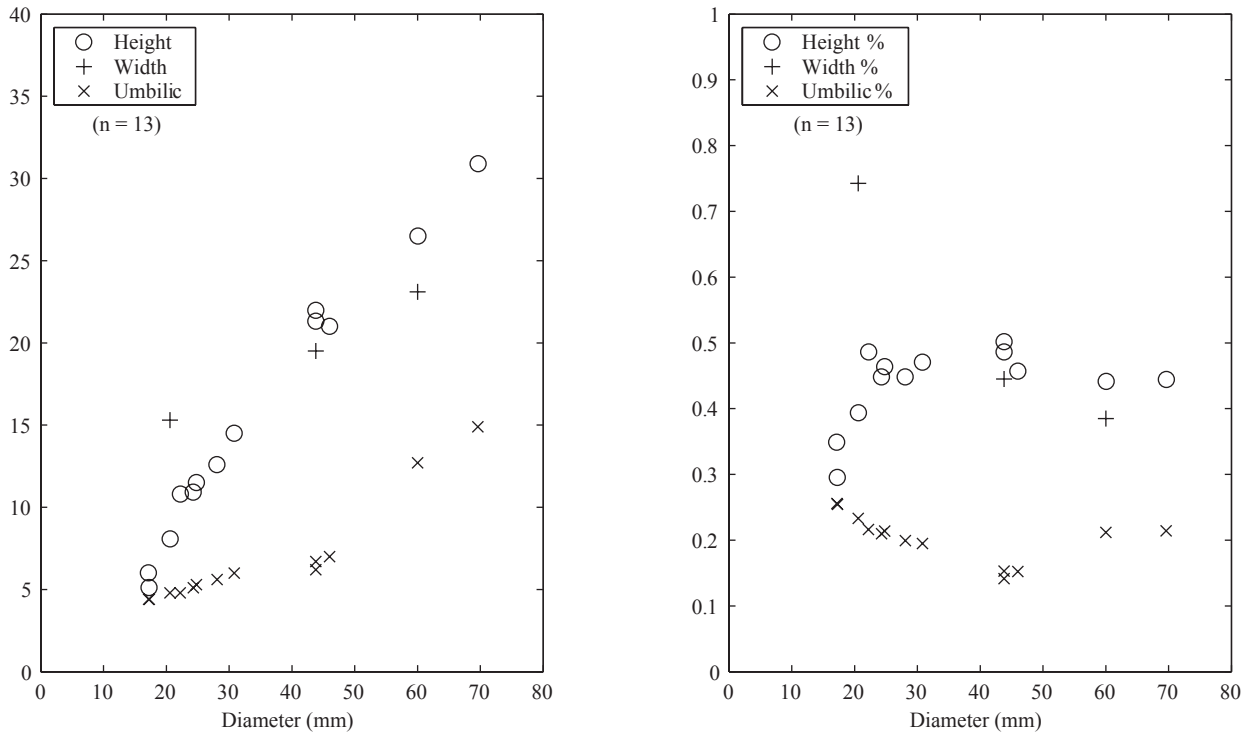

Fig. 50. Brayard & Bucher

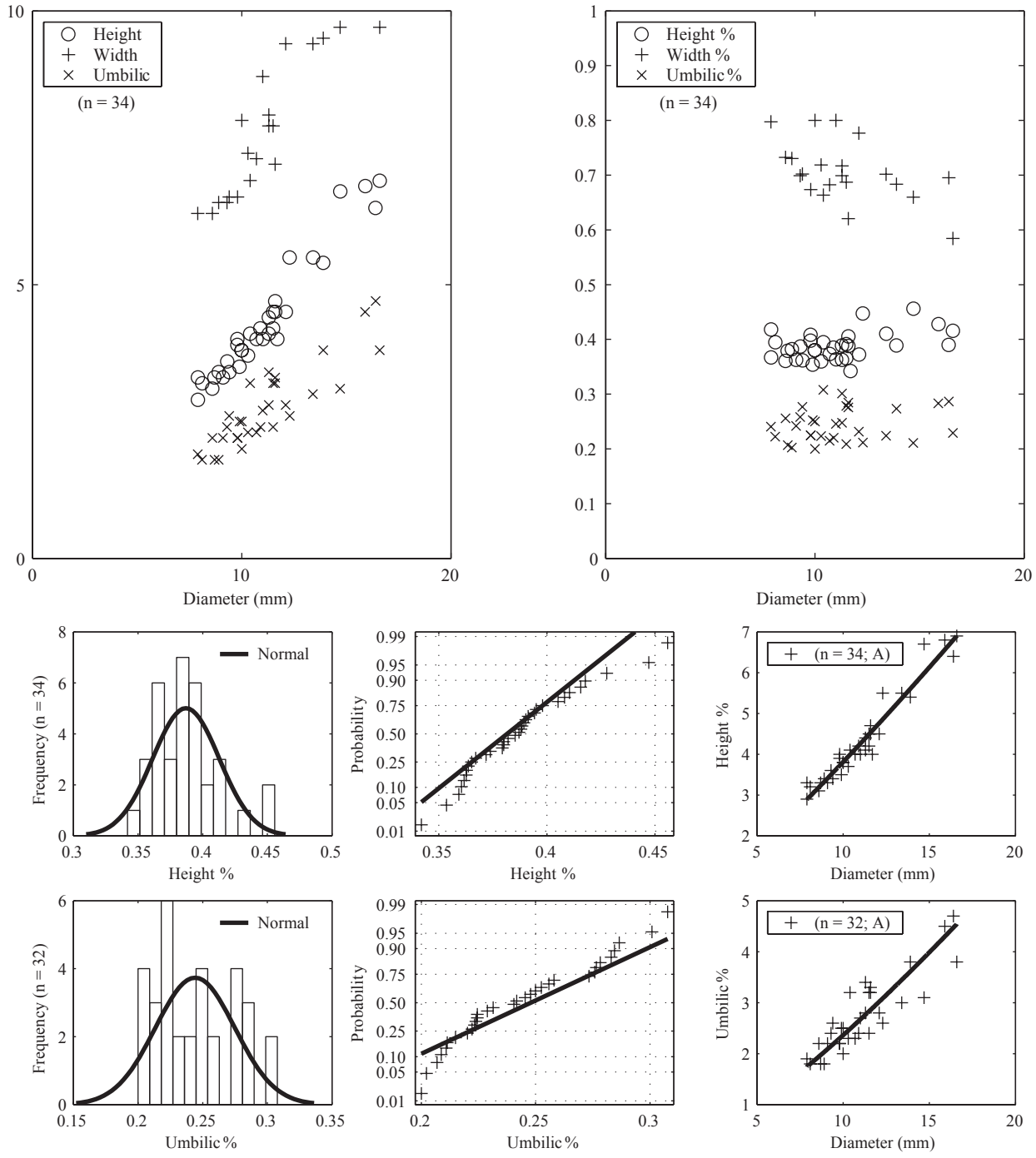

Fig. 51. Brayard & Bucher

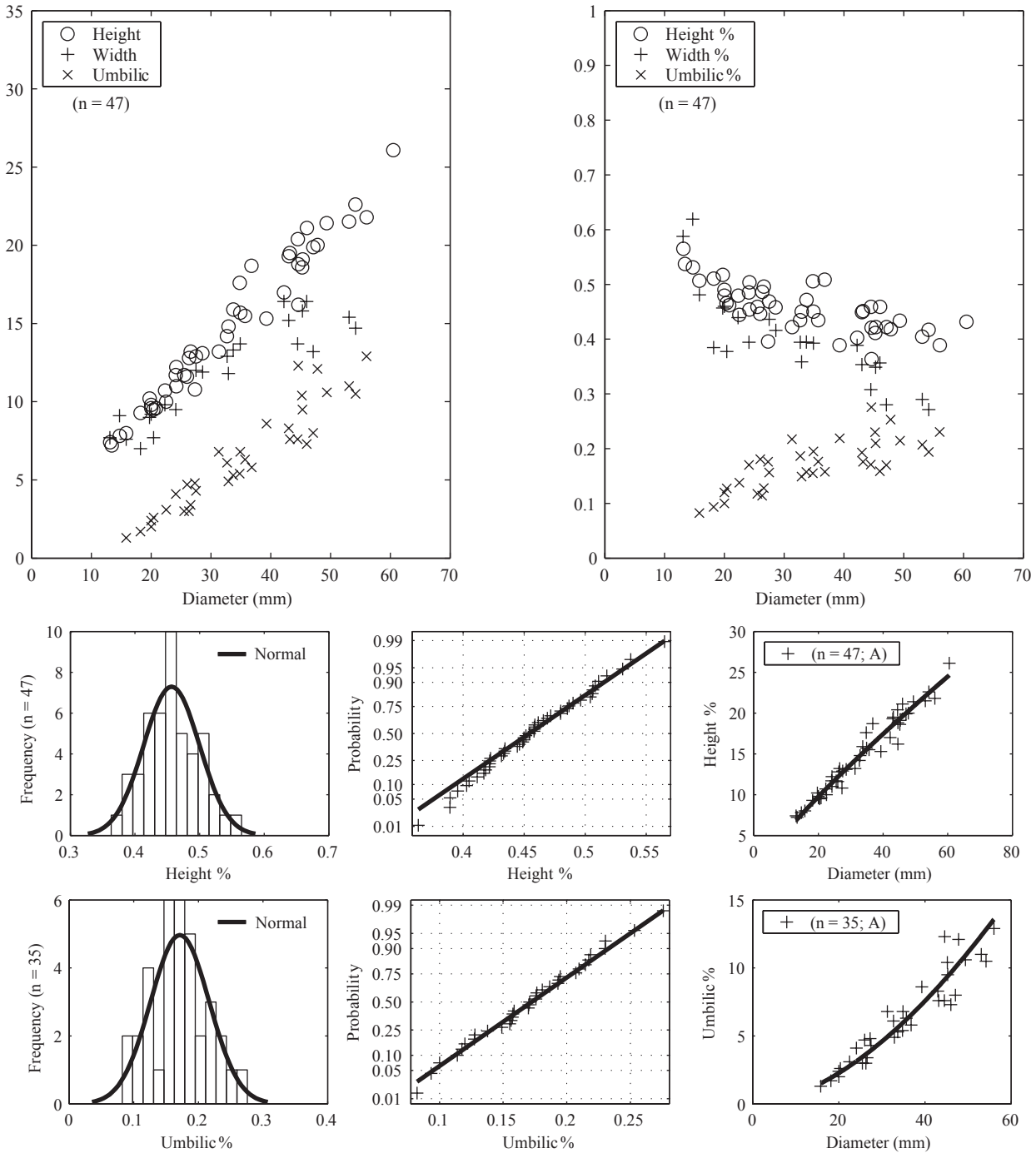

Fig. 52. Brayard & Bucher

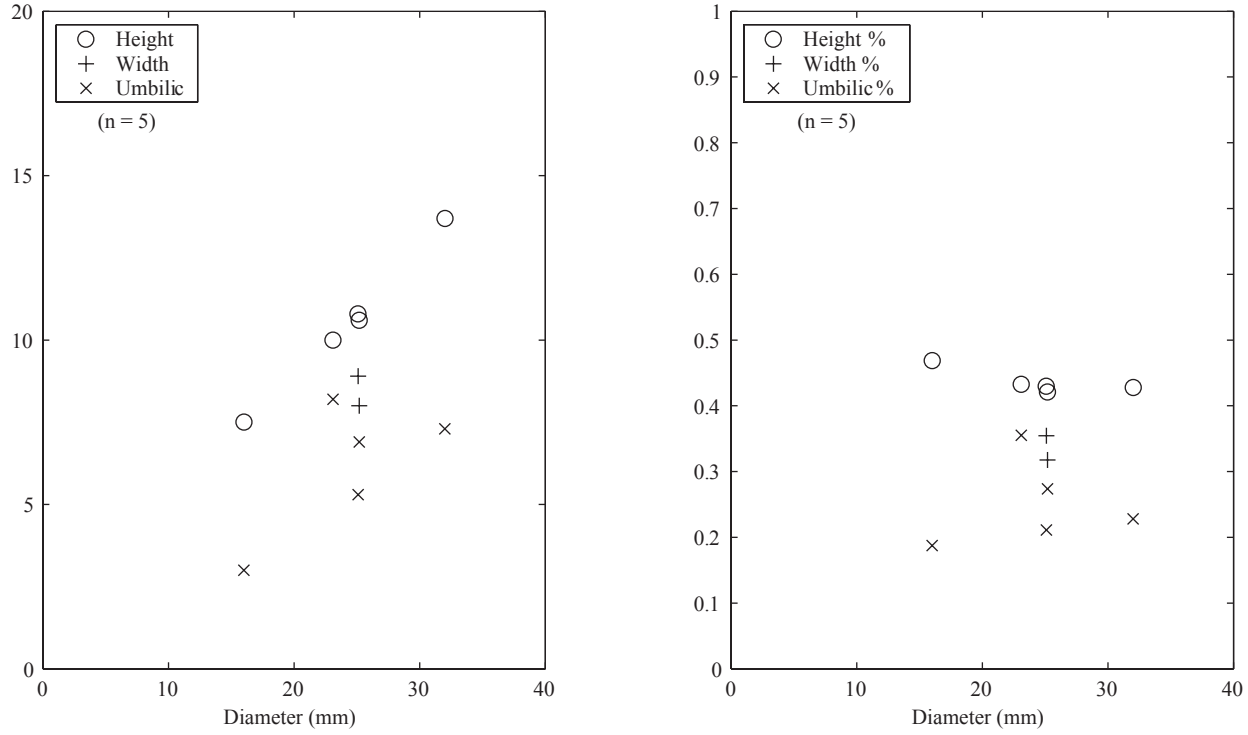

Fig. 53. Brayard & Bucher

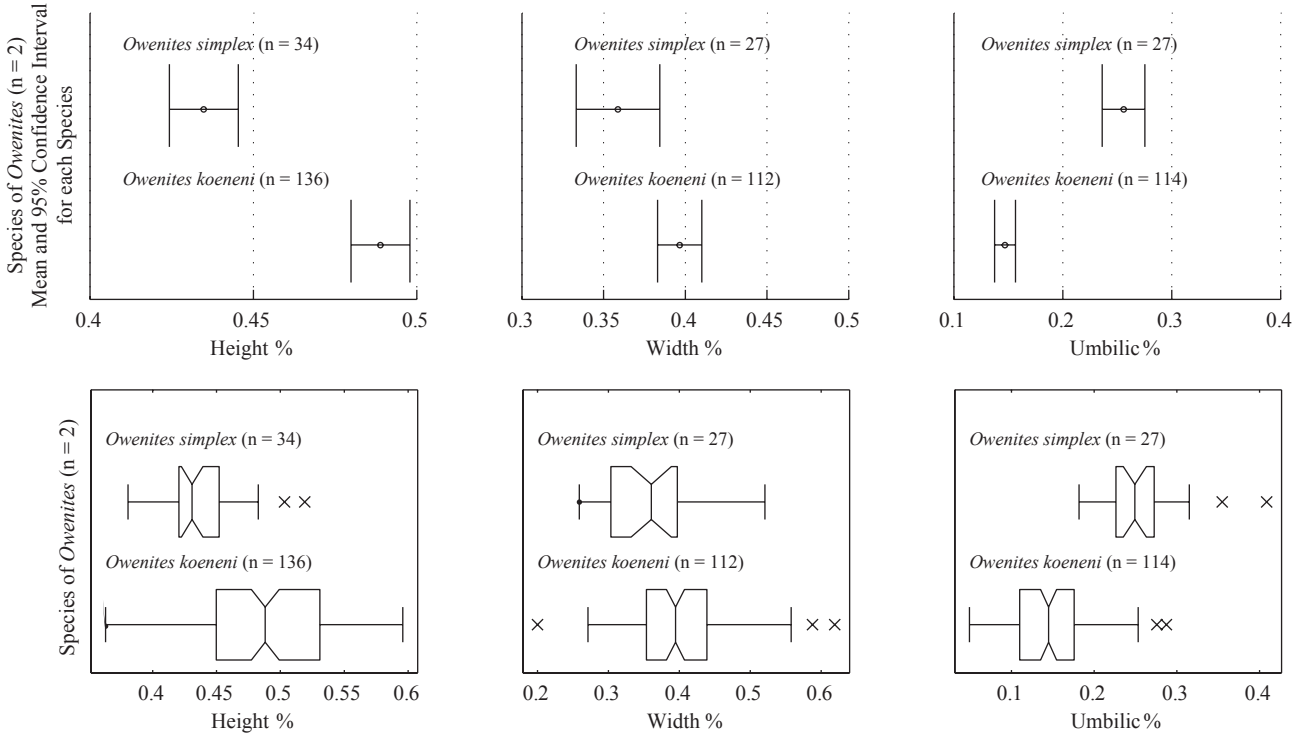

Fig. 54. Brayard & Bucher

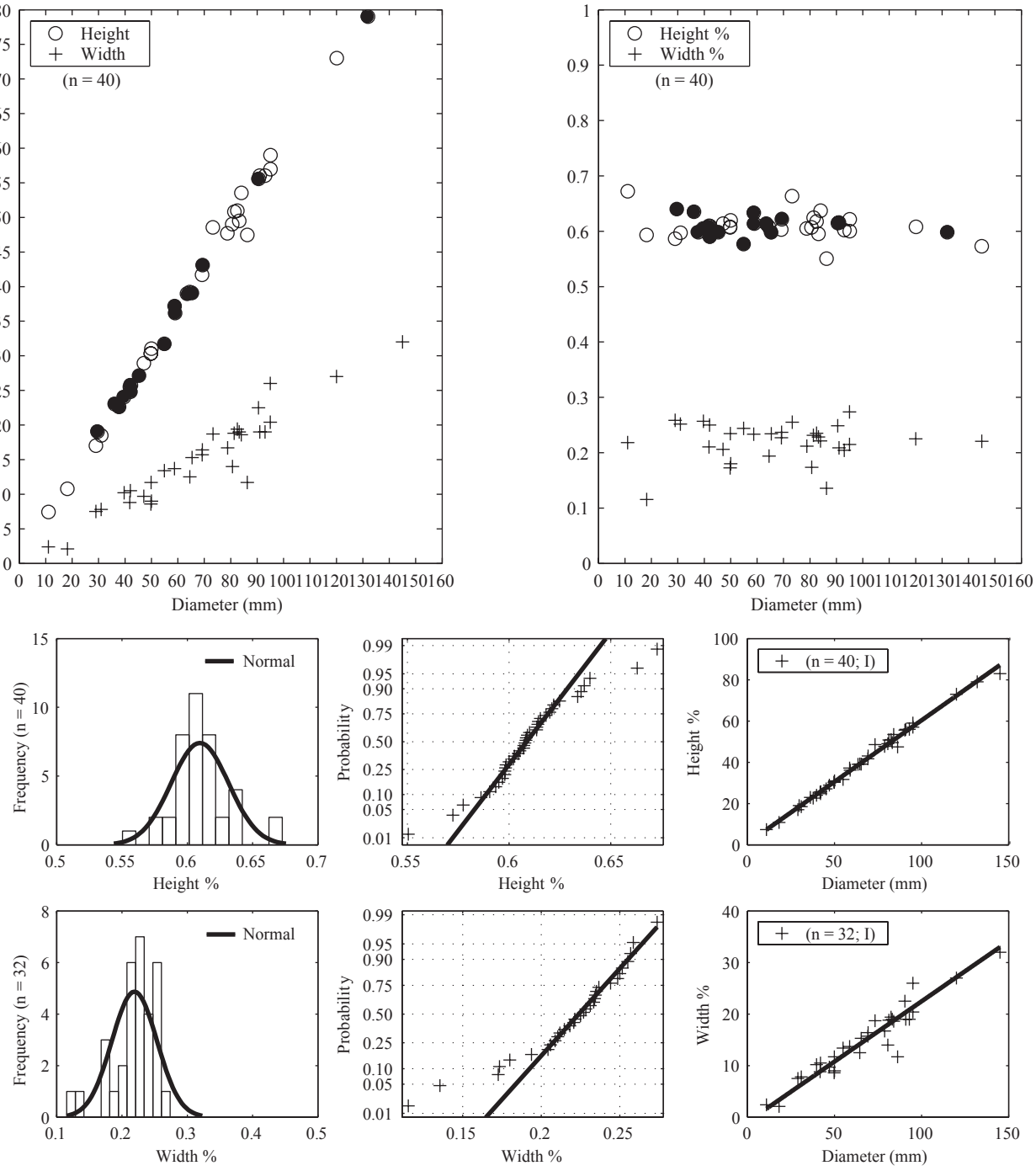

Fig. 55. Brayard & Bucher

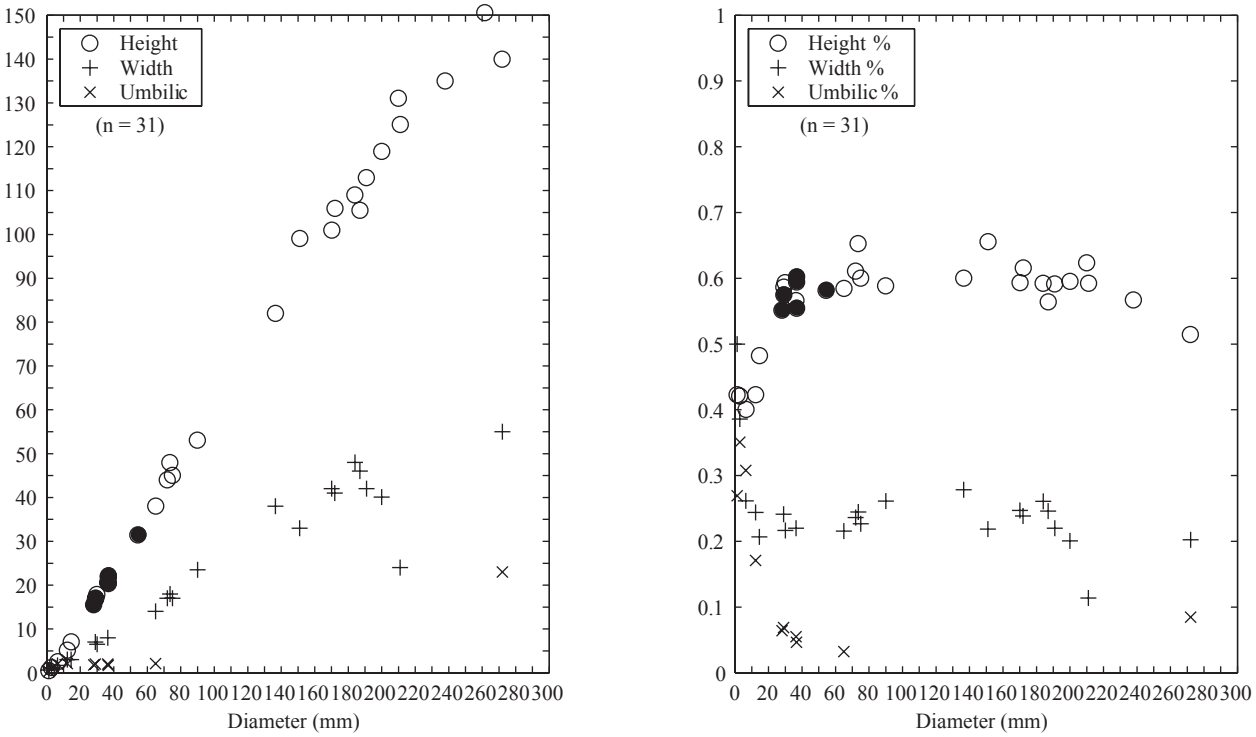

Fig. 56. Brayard & Bucher

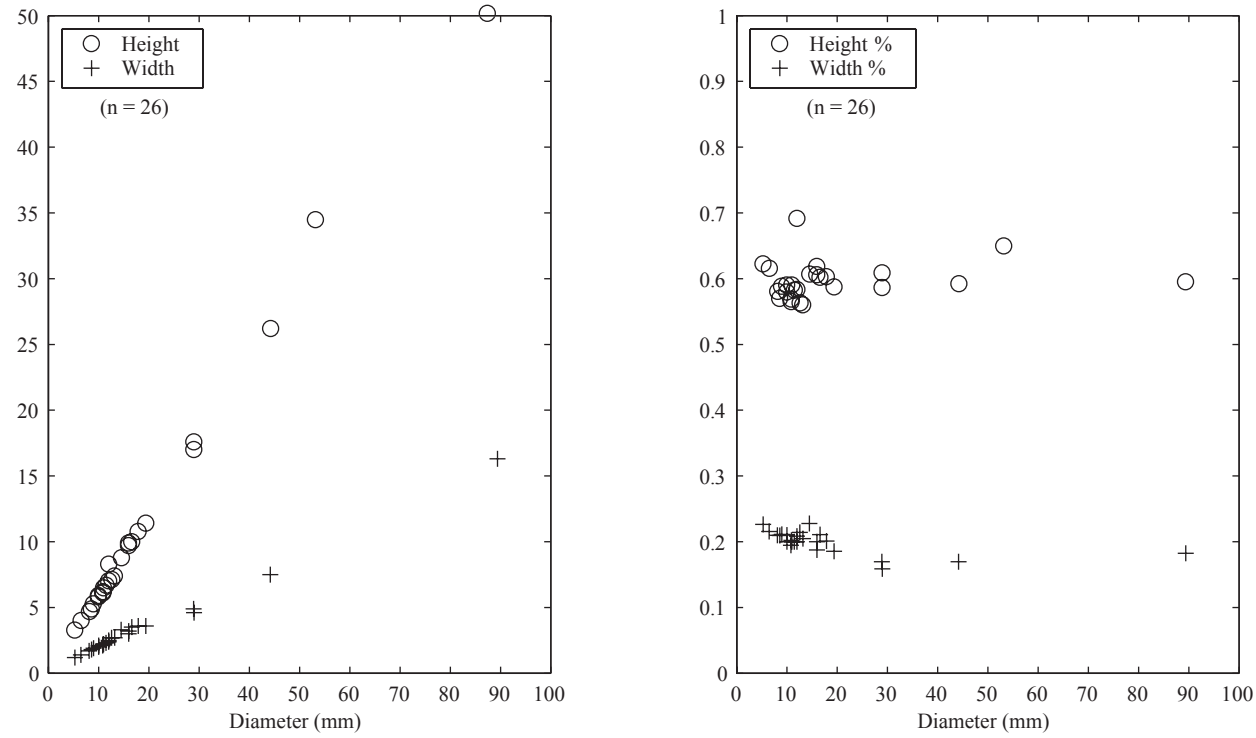

Fig. 57. Brayard & Bucher

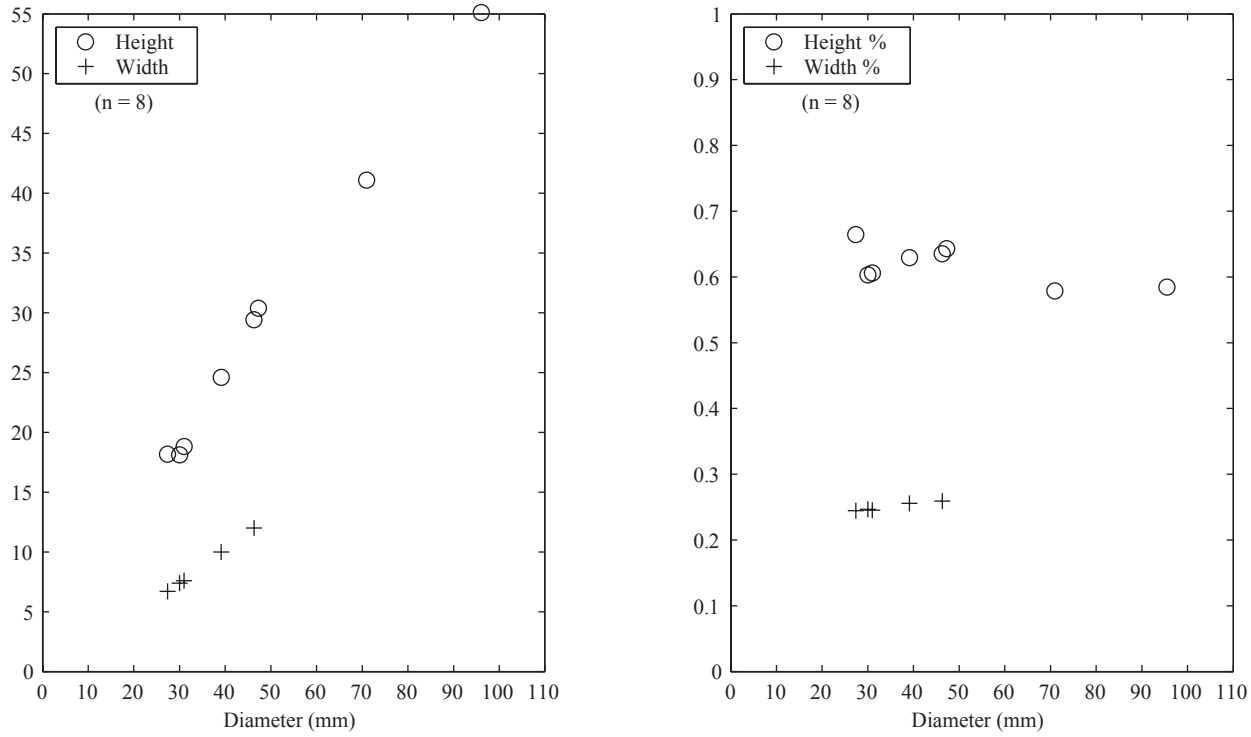

Fig. 58. Brayard & Bucher

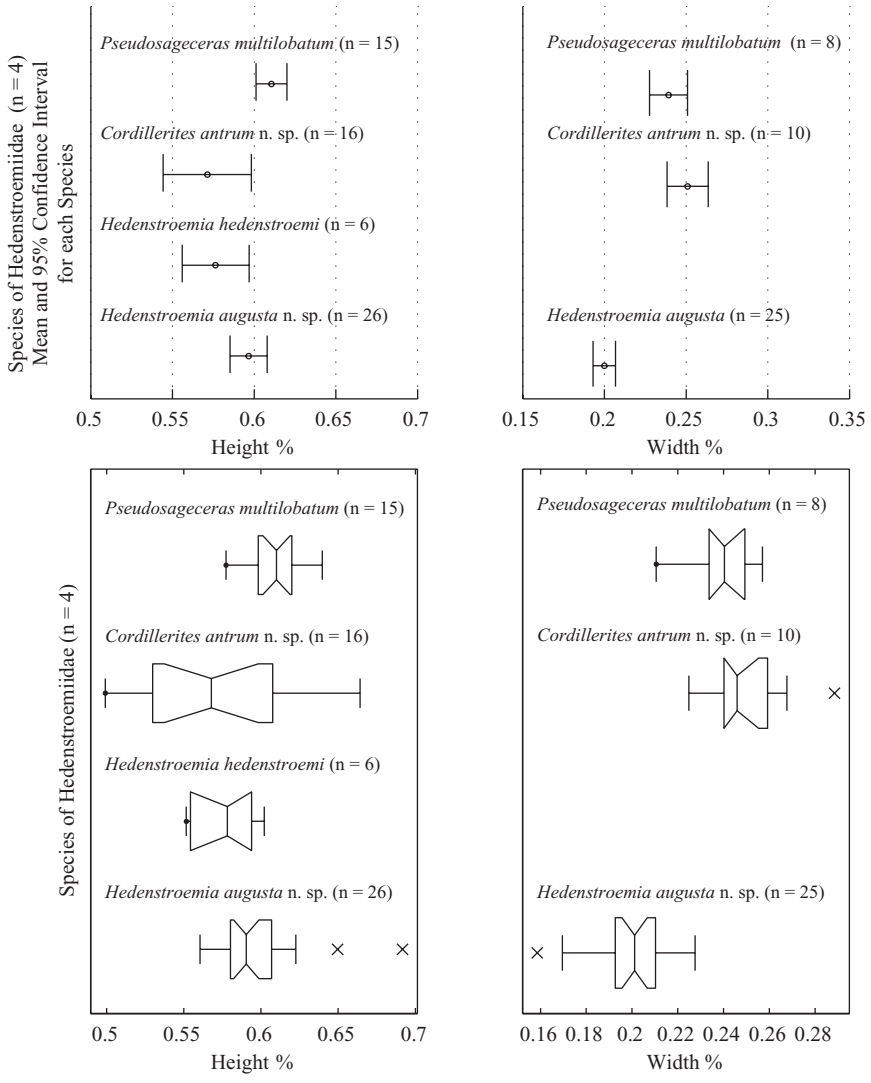

Fig. 59. Brayard & Bucher

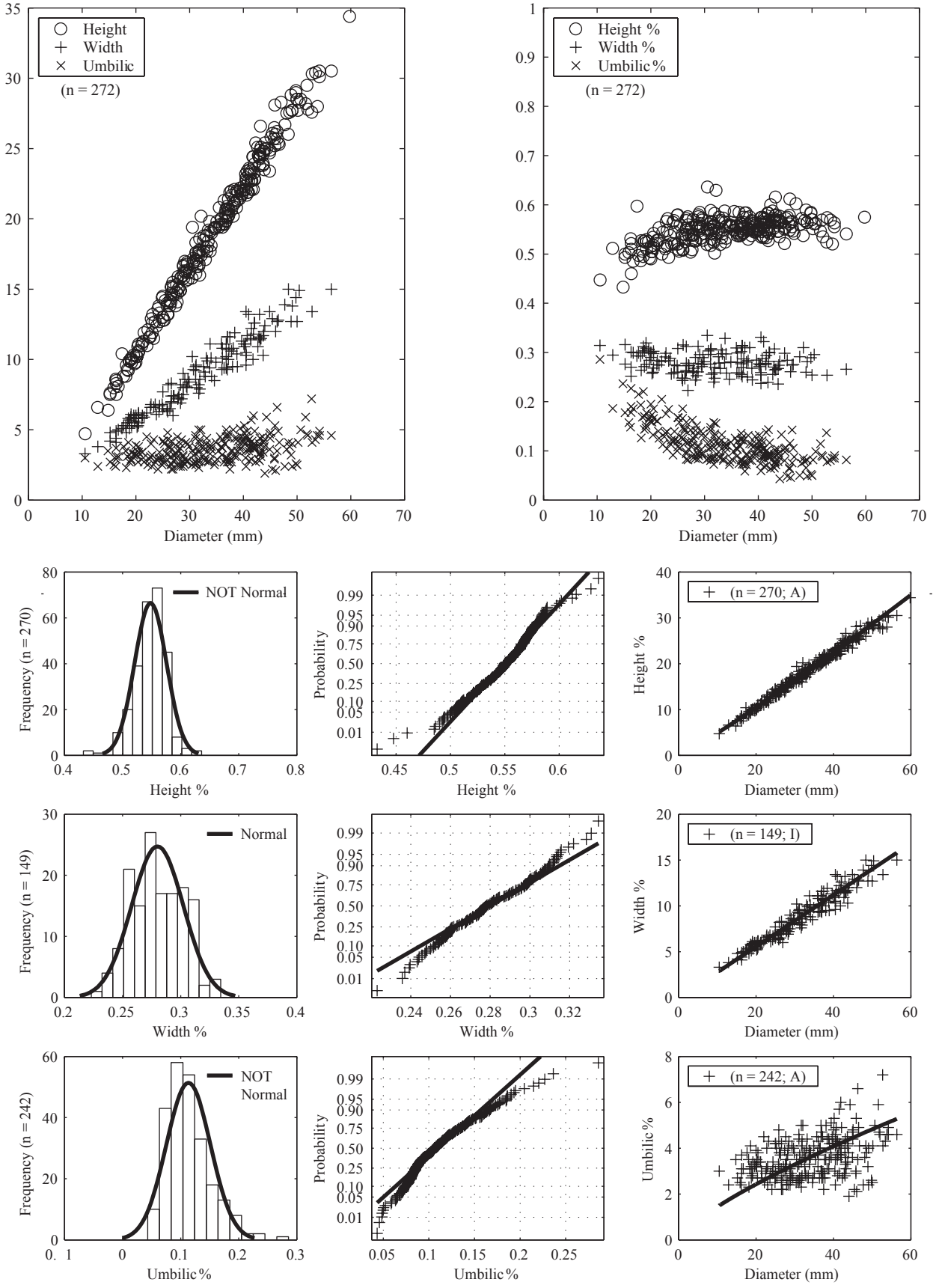

Fig. 60. Brayard & Bucher

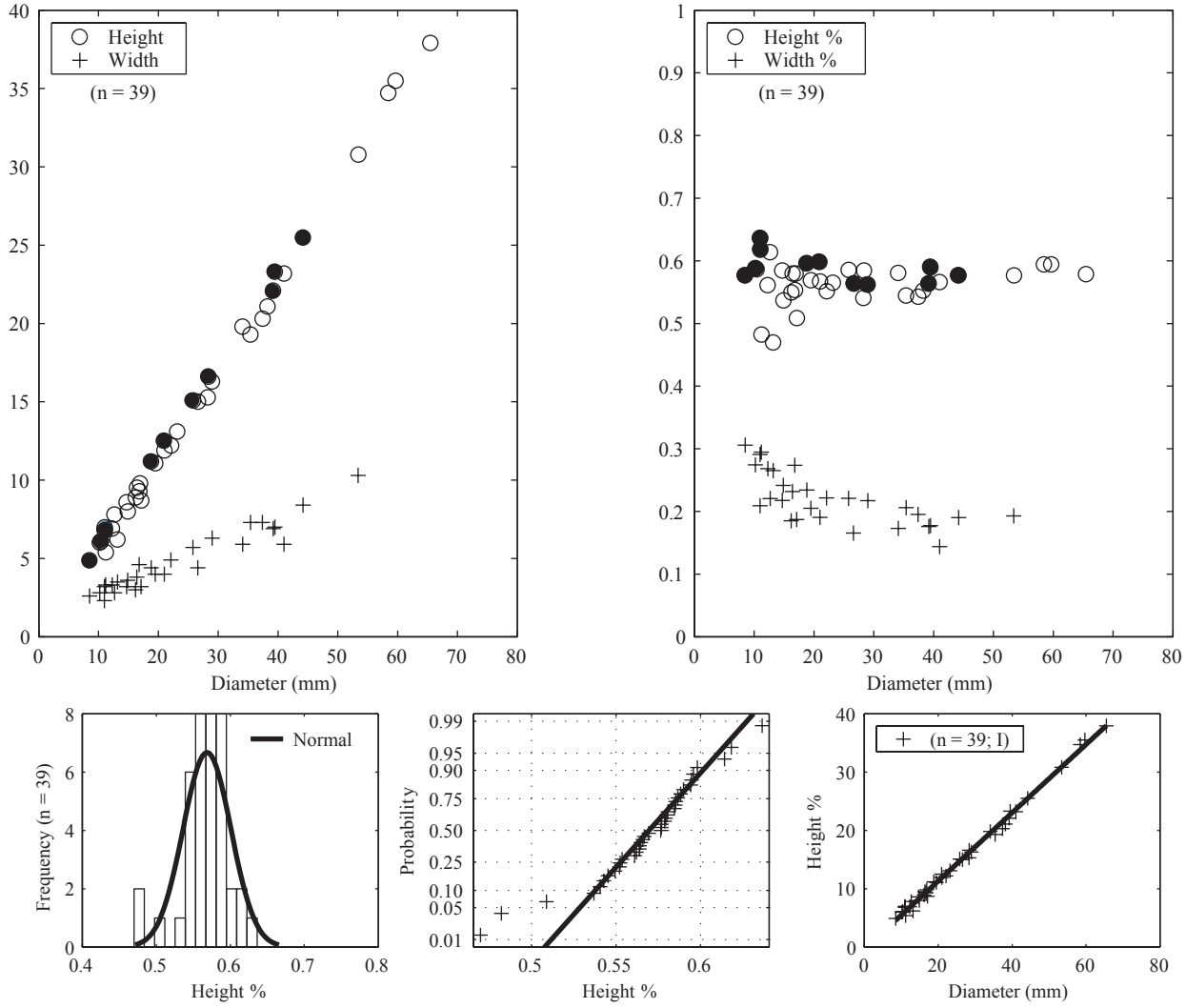

Fig. 61. Brayard & Bucher

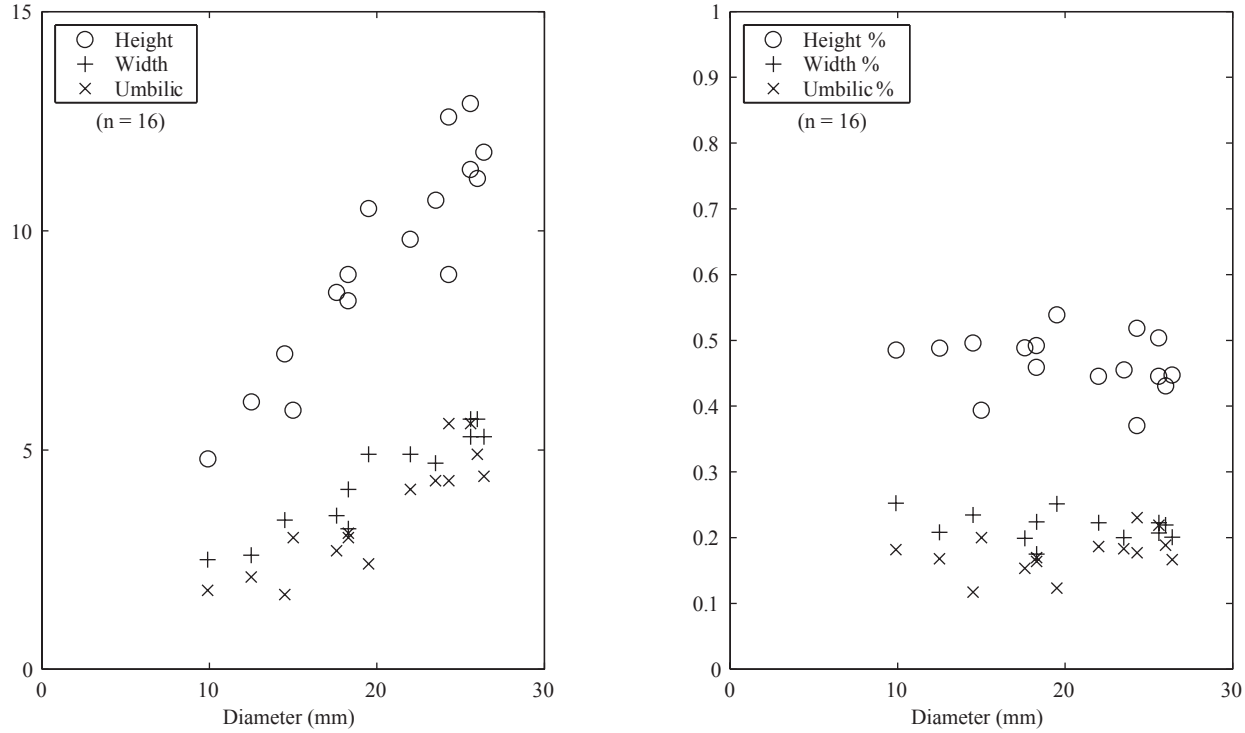

Fig. 62. Brayard & Bucher

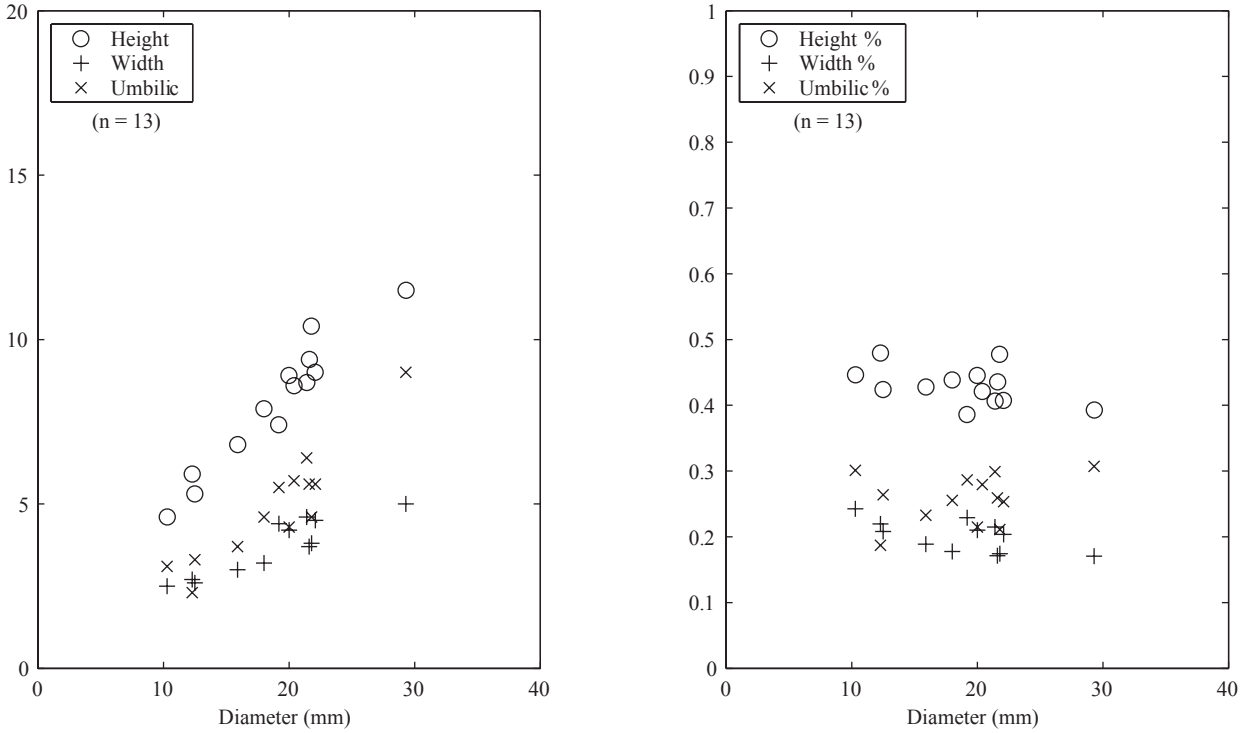

Fig. 63. Brayard & Bucher

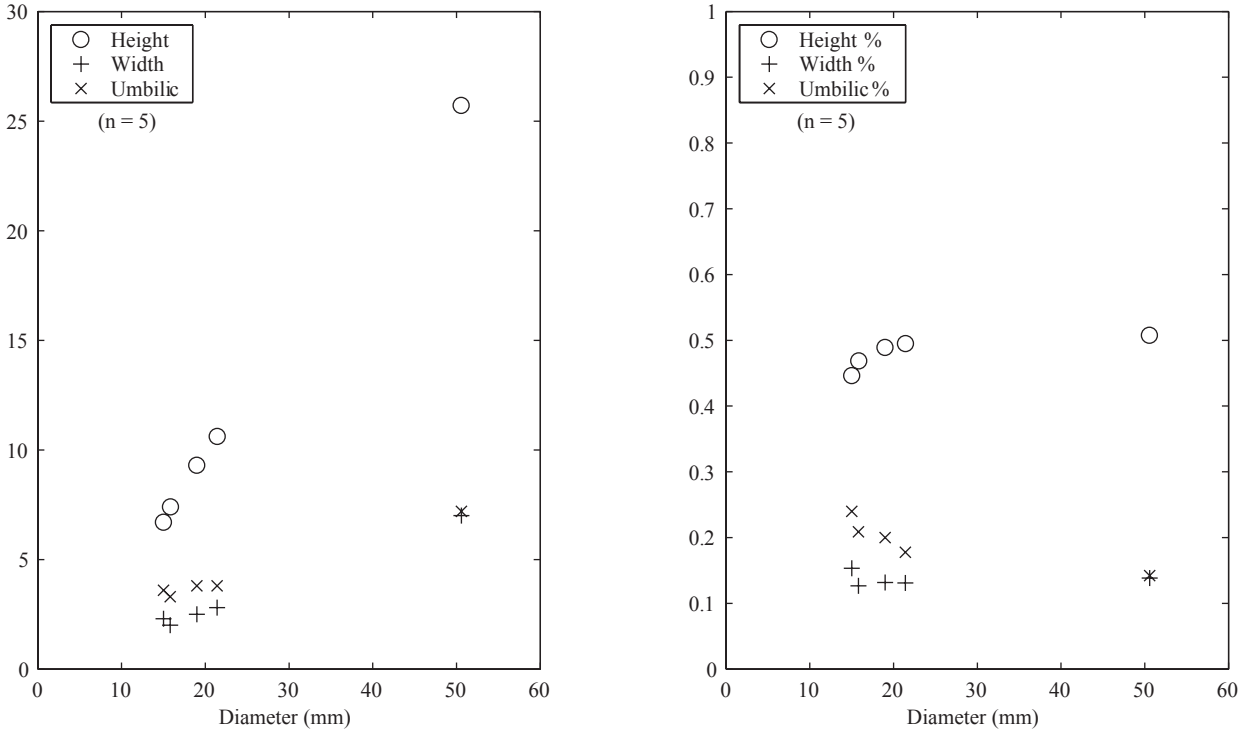

Fig. 64. Brayard & Bucher

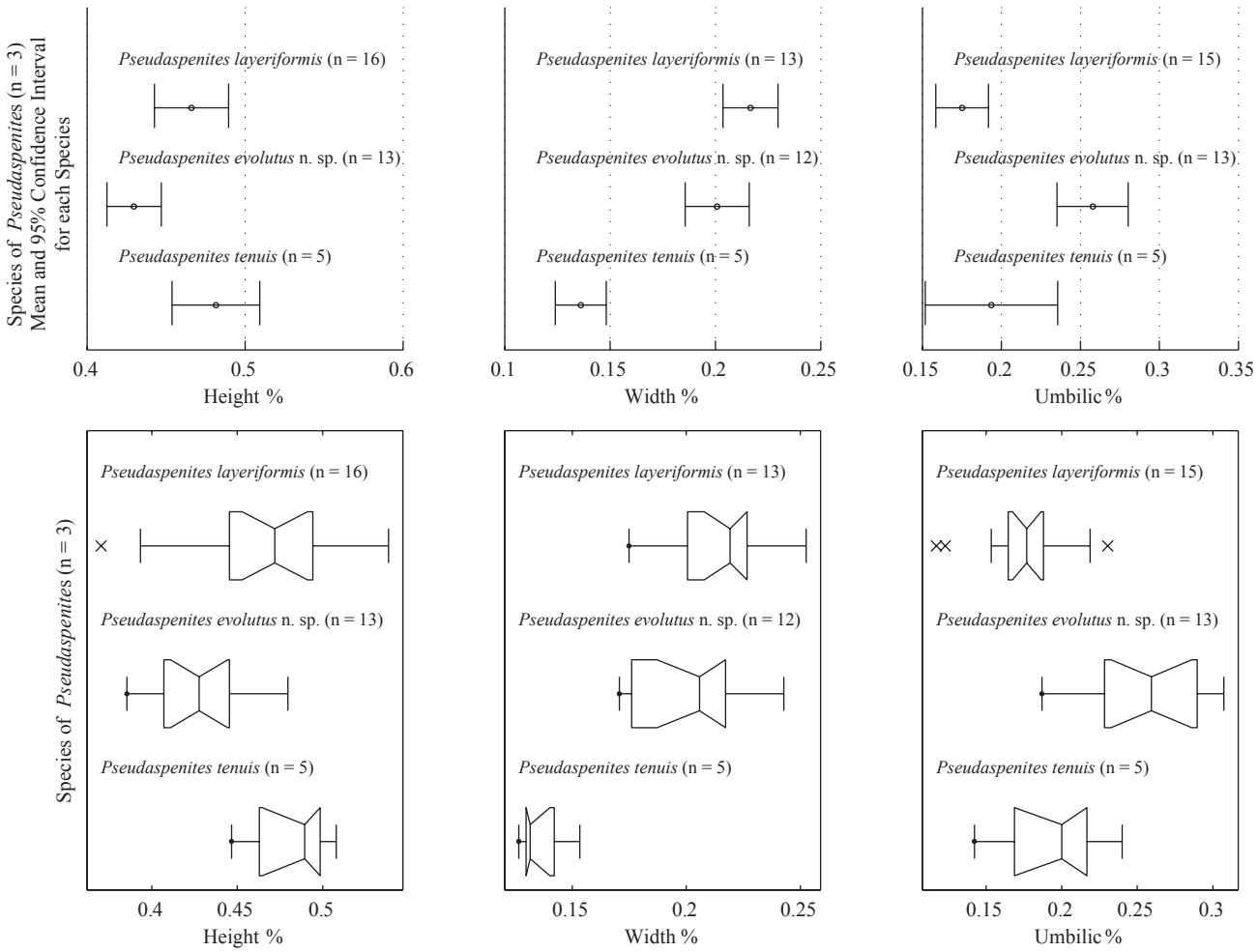

Fig. 65. Brayard & Bucher

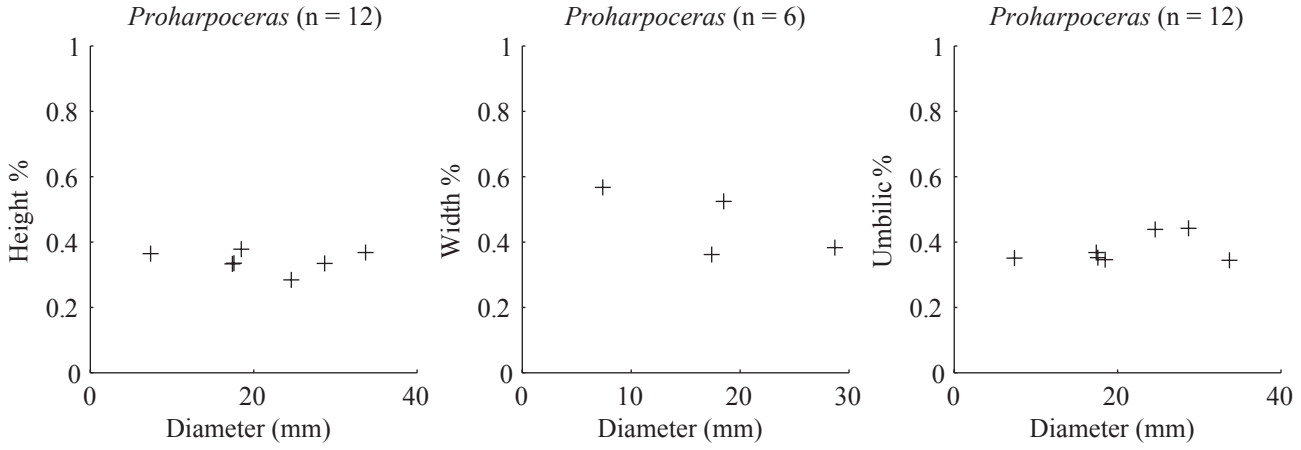

Fig. 66. Brayard & Bucher

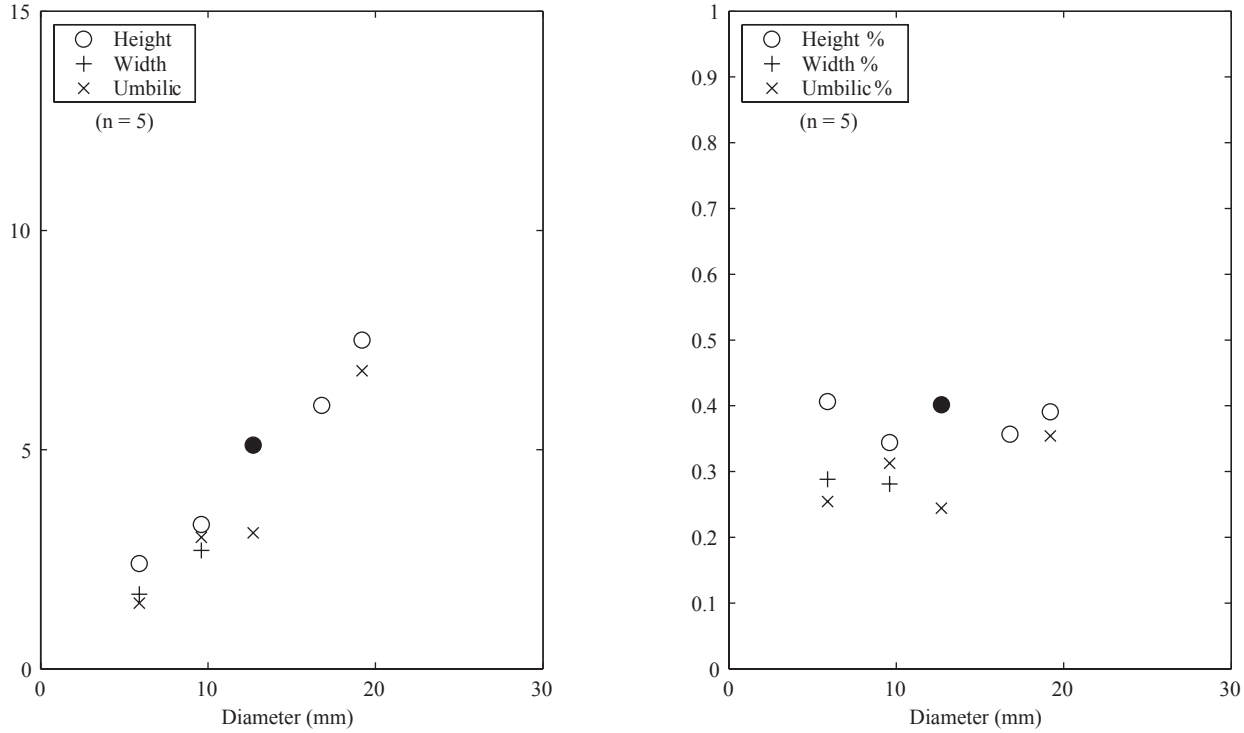

Fig. 67. Brayard & Bucher

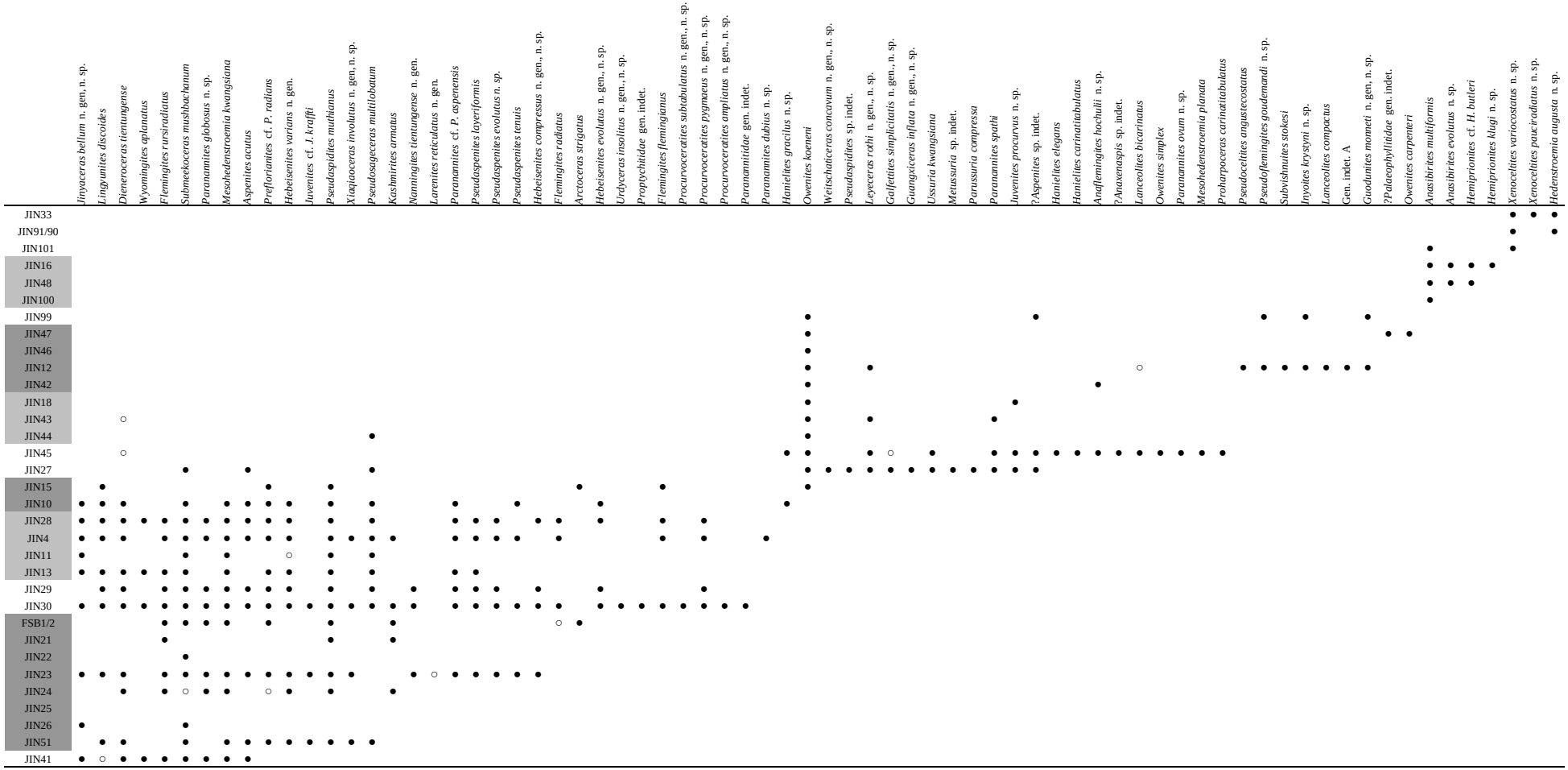

Table 1. Summary of the succession of the Smithian ammonoid genera in the section of Jinya. Localities in grey indicate that they belong to the same group of beds (i.e. without superpositional information).

Genus	species	Specimen number	D	H	W	U
Hanielites	*carinatitabulatus*	PIMUZ 25832	24	9.9	-	6.1
Hanielites	*gracile*	PIMUZ 25834	30.2	12.3	-	6.6
Hanielites	*angulus*	PIMUZ 25836	21	8.5	-	6.3
Weitschaticeras	*concavum*	PIMUZ 25869	40.5	11.8	-	19.7
Juvenites	cf. *J. Kraffti*	PIMUZ 25914	13.6	3.6	8	6.1
Paranorites	*jenksi*	PIMUZ 25917	53	23.8	13.8	13
Paranorites	*jenksi*	PIMUZ 25919	10.6	4.7	3.2	3.3
Pseudaspidites	sp. indet.	PIMUZ 25935	22.3	11.5	-	4.4
Lingyunites	*tientungense*	PIMUZ 25944	23.4	13.4	6	-
Leyeceras	*rothi*	PIMUZ 25963	53.4	24.5	17.1	14.3
Urdyceras	*insolitus*	PIMUZ 25965	44	18.3	-	13.3
Proptychitidae gen. indet.		PIMUZ 25934	57.9	32.2	-	9.6
?*Anaxenaspis*	sp. indet.	PIMUZ 26015	12.3	35	-	40
Guangxiceras	*inflata*	PIMUZ 26016	134.1	50	26.8	52
Arctoceras	*strigatus*	PIMUZ 26024	39.9	19.8	-	7.7
Subvishnuites	*stokesi*	PIMUZ 26060	54.6	17.4	-	26.7
Paranannites	*dubius*	PIMUZ 26084	13.4	5.7	7.2	1.8
Paranannites	*dubius*	PIMUZ 26085	14.8	7	7.5	-
Paranannites	*dubius*	PIMUZ 26082	14	6.4	-	1.9
Paranannitidae gen. indet.		PIMUZ 26086	13	5.5	5.4	3.4
Owenites	*carpenteri*	PIMUZ 26191	23.5	13	-	-
Owenites	*carpenteri*	PIMUZ 26192	18.6	10.6	7.5	-
Mesohedenstroemia	*planata*	PIMUZ 26165	41	26.3	-	-
Guodunites	*monneti*	PIMUZ 26194	70.4	33.7	14.6	12.9
Procurvoceratites	*subtabulatus*	PIMUZ 26199	12.2	5.4	3.1	2.9
?Palaeophyllitidae gen. indet.		PIMUZ 25867	53.5	19.6	19.5	14.4

Appendix 1

PLATE 1

Fig. A: Laren section in Waili. Upper Smithian subdivisions are shown. Note the difference in facies between the Smithian and the Spathian beds. SP.: Spathian; A. m.: "*Anasibirites multiformis* beds"; O. k.: "*Owenites koeneni* beds".

Fig. B: Waili Cave section in Waili. Lower Smithian subdivisions are shown. F. r.: "*Flemingites rursiradiatus* beds"; K. d.: "*Kashmirites densistriatus* beds"; H. h.: "*Hedenstroemia hedenstroemi* beds".
Bed denoted by black rectangle (Jin62) represents the base of the Smithian and the first occurrence of *Hedenstroemia hedenstroemi*. Note the massive nature of the "*Flemingites rursiradiatus* beds" compared to the "*Hedenstroemia hedenstroemi* beds" and "*Kashmirites densistriatus* beds".

Fig. C: Yuping section. "*Flemingites rursiradiatus* beds" and "*Owenites koeneni* beds" are shown. Bed denoted by black rectangle (Yu1) contains *Proharpoceras*.

Fig. D: Waili Cave section in Waili. "*Flemingites rursiradiatus* beds" and "*Kashmirites densistriatus* beds" are shown.

PLATE 1

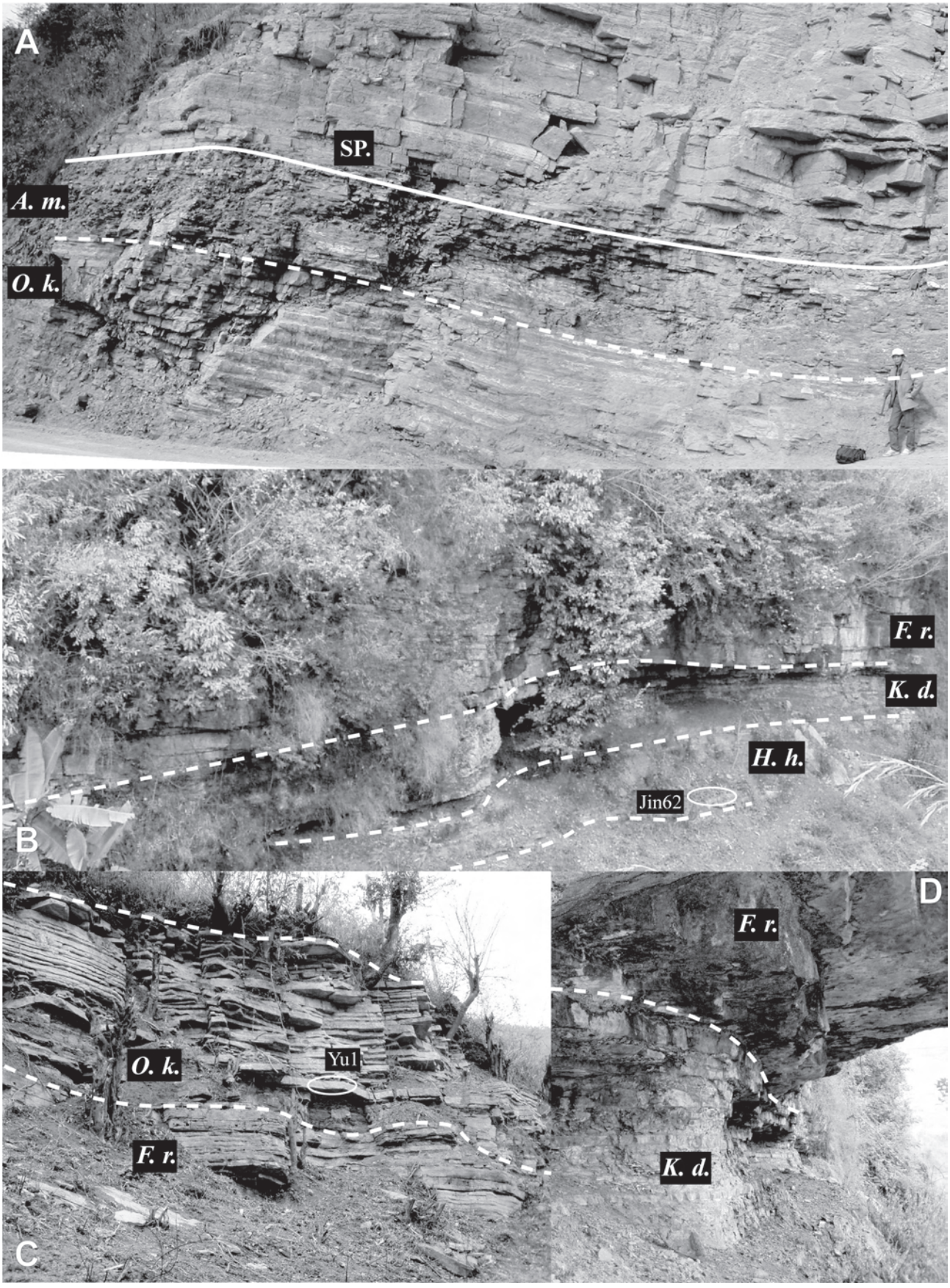

PLATE 2

(All figures natural size)

Figs. 1a-c: ***Kashmirites armatus*** (Waagen, 1895). PIMUZ 25800.
Loc. Jin4, Jinya, "*Flemingites rursiradiatus* beds", Smithian.

Figs. 2a-c: ***Kashmirites armatus*** (Waagen, 1895). PIMUZ 25801.
Loc. Jin4, Jinya, "*Flemingites rursiradiatus* beds", Smithian.

Figs. 3a-b: ***Kashmirites armatus*** (Waagen, 1895). PIMUZ 25802.
Loc. Jin4, Jinya, "*Flemingites rursiradiatus* beds", Smithian.

Figs. 4a-c: ***Kashmirites armatus*** (Waagen, 1895). PIMUZ 25803. Robust variant.
Loc. FSB, Jinya, "*Flemingites rursiradiatus* beds", Smithian.

Figs. 5a-d: ***Kashmirites armatus*** (Waagen, 1895). PIMUZ 25804.
Loc. Jin4, Jinya, "*Flemingites rursiradiatus* beds", Smithian.
a-c) Lateral, ventral and apertural views
d) Suture line. Scale bar = 5 mm; H = 7 mm.

Figs. 6a-c: ***Kashmirites armatus*** (Waagen, 1895). PIMUZ 25805.
Loc. Jin4, Jinya, "*Flemingites rursiradiatus* beds", Smithian.

Figs. 7a-c: ***Kashmirites armatus*** (Waagen, 1895). PIMUZ 25806.
Loc. Jin4, Jinya, "*Flemingites rursiradiatus* beds", Smithian.

Figs. 8a-b: ***Kashmirites armatus*** (Waagen, 1895). PIMUZ 25807.
Loc. Jin30, Jinya, "*Flemingites rursiradiatus* beds", Smithian.

Figs. 9a-d: ***Kashmirites armatus*** (Waagen, 1895). PIMUZ 25808.
Loc. WSB, Waili, "*Flemingites rursiradiatus* beds", Smithian.

Figs. 10a-c: ***Kashmirites armatus*** (Waagen, 1895). PIMUZ 25809.
Loc. WSB, Waili, "*Flemingites rursiradiatus* beds", Smithian.

PLATE 2

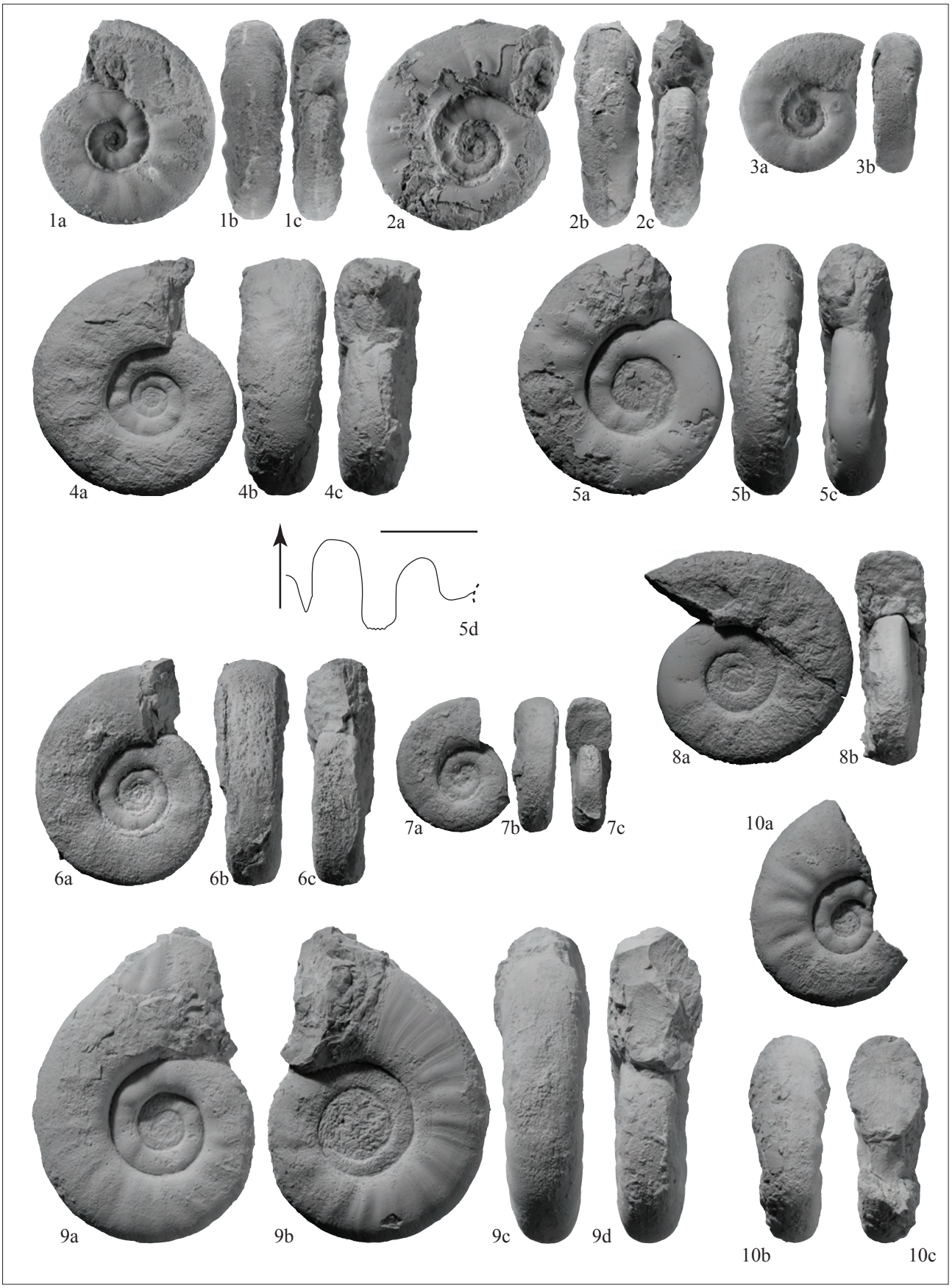
1a
1b
1c
2a
2b
2c
3a
3b
4a
4b
4c
5a
5b
5c
5d
6a
6b
6c
7a
7b
7c
8a
8b
9a
9b
9c
9d
10a
10b
10c

PLATE 3

(All figures natural size)

Figs. 1a-e: ***Kashmirites densistriatus*** Welter, 1922. PIMUZ 25810.
Loc. Jin64, Waili Cave, "*Kashmirites densistriatus* beds", Smithian.
a-d) Lateral, ventral and apertural views.
e) Suture line. Scale bar = 5 mm; H = 8 mm.

Figs. 2a-c: ***Kashmirites densistriatus*** Welter, 1922. PIMUZ 25811.
Loc. Jin67, Waili Cave, "*Kashmirites densistriatus* beds", Smithian.

Figs. 3a-b: ***Kashmirites densistriatus*** Welter, 1922. PIMUZ 25812. Robust variant.
Loc. Jin67, Waili Cave, "*Kashmirites densistriatus* beds", Smithian.

Figs. 4a-b: ***Kashmirites densistriatus*** Welter, 1922. PIMUZ 25813. Robust variant.
Loc. Jin67, Waili Cave, "*Kashmirites densistriatus* beds", Smithian.

Figs. 5a-c: ***Preflorianites* cf. *P. radians*** Chao, 1959. PIMUZ 25814.
Loc. Jin15, Jinya, "*Flemingites rursiradiatus* beds", Smithian.

Figs. 6a-c: ***Preflorianites* cf. *P. radians*** Chao, 1959. PIMUZ 25815.
Loc. 4, Jinya, "*Flemingites rursiradiatus* beds", Smithian.

Figs. 7a-d: ***Preflorianites* cf. *P. radians*** Chao, 1959. PIMUZ 25816.
Loc. Jin30, Jinya, "*Flemingites rursiradiatus* beds", Smithian.

Figs. 8a-d: ***Preflorianites* cf. *P. radians*** Chao, 1959. PIMUZ 25817.
Loc. Jin13, Jinya, "*Flemingites rursiradiatus* beds", Smithian.

Figs. 9a-d: ***Preflorianites* cf. *P. radians*** Chao, 1959. PIMUZ 25818.
Loc. Jin30, Jinya, "*Flemingites rursiradiatus* beds", Smithian.

Figs. 10a-c: ***Preflorianites* cf. *P. radians*** Chao, 1959. PIMUZ 25819.
Loc. FSB, Jinya, "*Flemingites rursiradiatus* beds", Smithian.

Fig. 11: Suture line of ***Preflorianites* cf. *P. radians*** Chao, 1959. PIMUZ 25820.
Loc. Jin30, Jinya, "*Flemingites rursiradiatus* beds", Smithian.
Scale bar = 5 mm; H = 6 mm.

PLATE 3

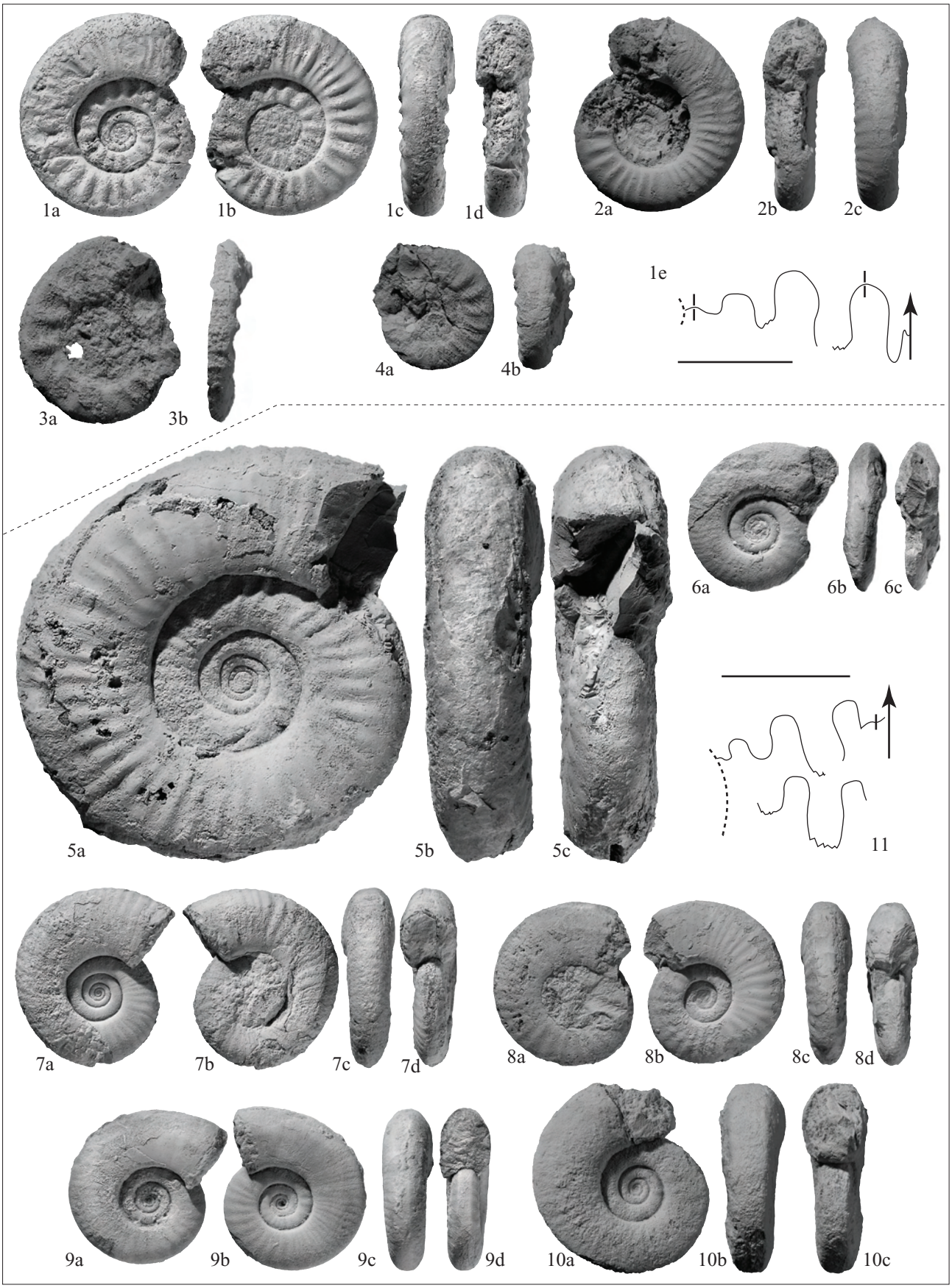
1a
1b
1c
1d
2a
2b
2c
3a
3b
4a
4b
1e
5a
5b
5c
6a
6b
6c
11
7a
7b
7c
7d
8a
8b
8c
8d
9a
9b
9c
9d
10a
10b
10c

PLATE 4

(All figures natural size)

Figs. 1a-d: ***Pseudoceltites angustecostatus*** Welter, 1922. PIMUZ 25821.
Loc. T5, Tsoteng, "*Owenites koeneni* beds", Smithian.

Figs. 2a-c: ***Pseudoceltites angustecostatus*** Welter, 1922. PIMUZ 25822.
Loc. T5, Tsoteng, "*Owenites koeneni* beds", Smithian.

Figs. 3a-c: ***Pseudoceltites angustecostatus*** Welter, 1922. PIMUZ 25823.
Loc. T5, Tsoteng, "*Owenites koeneni* beds", Smithian.

Figs. 4a-c: ***Pseudoceltites angustecostatus*** Welter, 1922. PIMUZ 25824.
Loc. T5, Tsoteng, "*Owenites koeneni* beds", Smithian.

Figs. 5a-c: ***Pseudoceltites angustecostatus*** Welter, 1922. PIMUZ 25825.
Loc. T5, Tsoteng, "*Owenites koeneni* beds", Smithian.

Figs. 6a-d: ***Pseudoceltites angustecostatus*** Welter, 1922. PIMUZ 25826.
Loc. T5, Tsoteng, "*Owenites koeneni* beds", Smithian.
a-c) Lateral, ventral and apertural views.
d) Suture line. Scale bar = 5 mm; H = 5 mm.

Figs. 7a-b: ***Pseudoceltites angustecostatus*** Welter, 1922. PIMUZ 25827.
Loc. T5, Tsoteng, "*Owenites koeneni* beds", Smithian.

PLATE 4

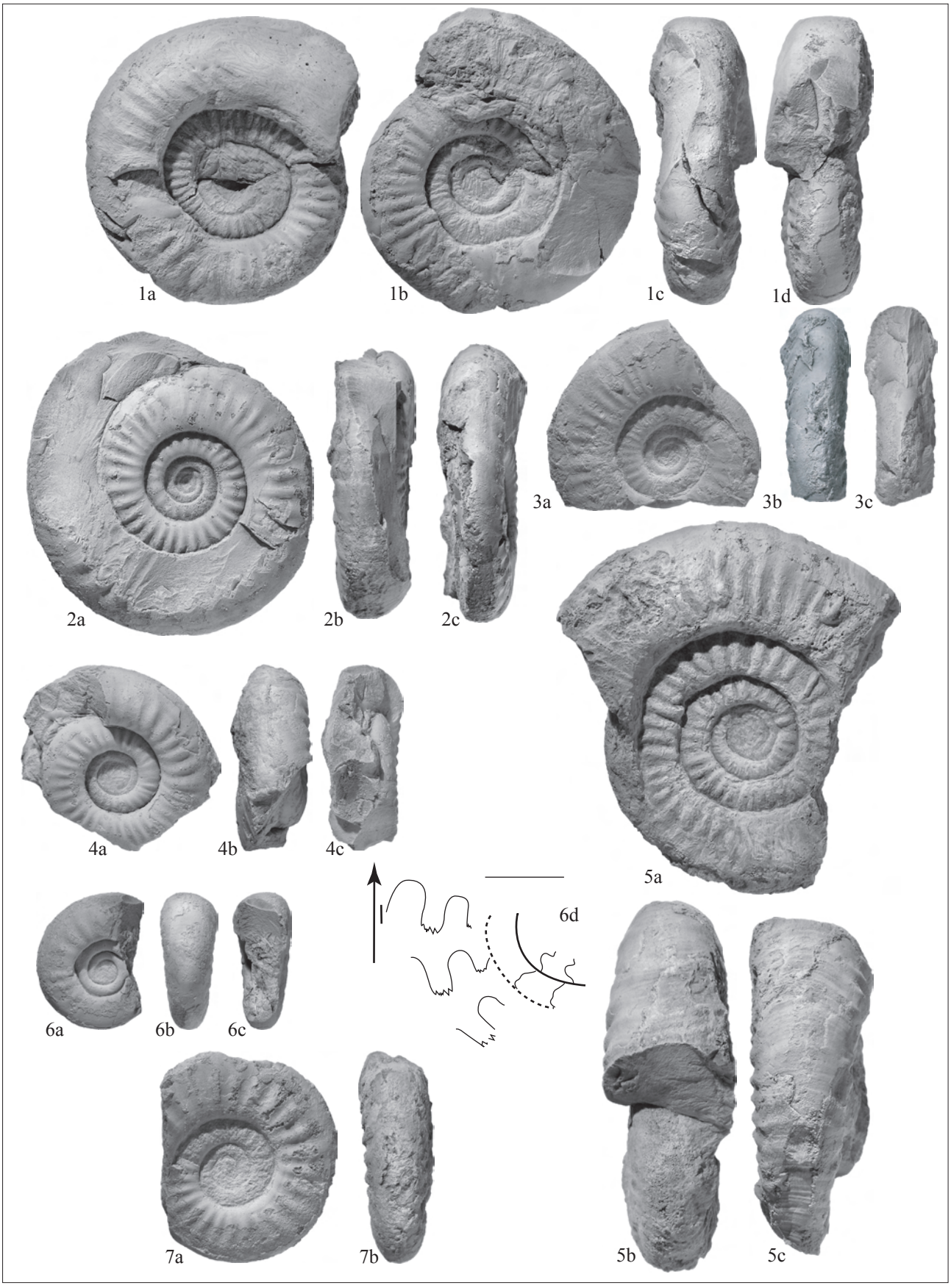

PLATE 5

(All figures natural size unless otherwise indicated)

Figs. 1a-d: ***Hanielites elegans*** Welter, 1922. PIMUZ 25828.
Loc. Jin45, Jinya, "*Owenites koeneni* beds", Smithian.

Figs. 2a-c: ***Hanielites elegans*** Welter, 1922. PIMUZ 25829. Scale ×2.
Loc. Jin45, Jinya, "*Owenites koeneni* beds", Smithian.

Figs. 3a-c: ***Hanielites elegans*** Welter, 1922. PIMUZ 25830. Scale ×2.
Loc. Jin45, Jinya, "*Owenites koeneni* beds", Smithian.

Figs. 4a-d: ***Hanielites elegans*** Welter, 1922. PIMUZ 25831. Scale ×2.
Loc. Jin45, Jinya, "*Owenites koeneni* beds", Smithian.

Fig. 5: Suture line of ***Hanielites elegans*** Welter, 1922. PIMUZ 25837.
Loc. Jin45, Jinya, "*Owenites koeneni* beds", Smithian.
Scale bar = 2.5 mm; H = 5 mm.

Figs. 6a-d: ***Hanielites gracilus*** n. sp. PIMUZ 25833. Paratype.
Loc. Jin45, Jinya, "*Owenites koeneni* beds", Smithian.
Fig. 6d: Scale ×4.

Figs. 7a-d: ***Hanielites gracilus*** n. sp. PIMUZ 25834. Holotype.
Loc. Jin45, Jinya, "*Owenites koeneni* beds", Smithian.
a-c) Lateral, ventral and apertural views.
d) Suture line. Scale bar = 2.5 mm; H = 10 mm.

Figs. 8a-c: ***Hanielites gracilus*** n. sp. PIMUZ 25835.
Loc. Jin10, Jinya, "*Flemingites rursiradiatus* beds", Smithian.

Figs. 9a-c: ***Hanielites carinatitabulatus*** Chao, 1959. PIMUZ 25832. Scale ×2.
Loc. Yu1, Yuping, "*Owenites koeneni* beds", Smithian.
a-b) Lateral and ventral views.
c) Suture line. Scale bar = 2.5 mm; H = 6 mm.

Figs. 10a-d: ***Hanielites angulus*** n. sp. PIMUZ 25836. Holotype.
Loc. Yu1, Yuping, "*Owenites koeneni* beds", Smithian.
Fig. 10d: Scale ×3.

PLATE 5

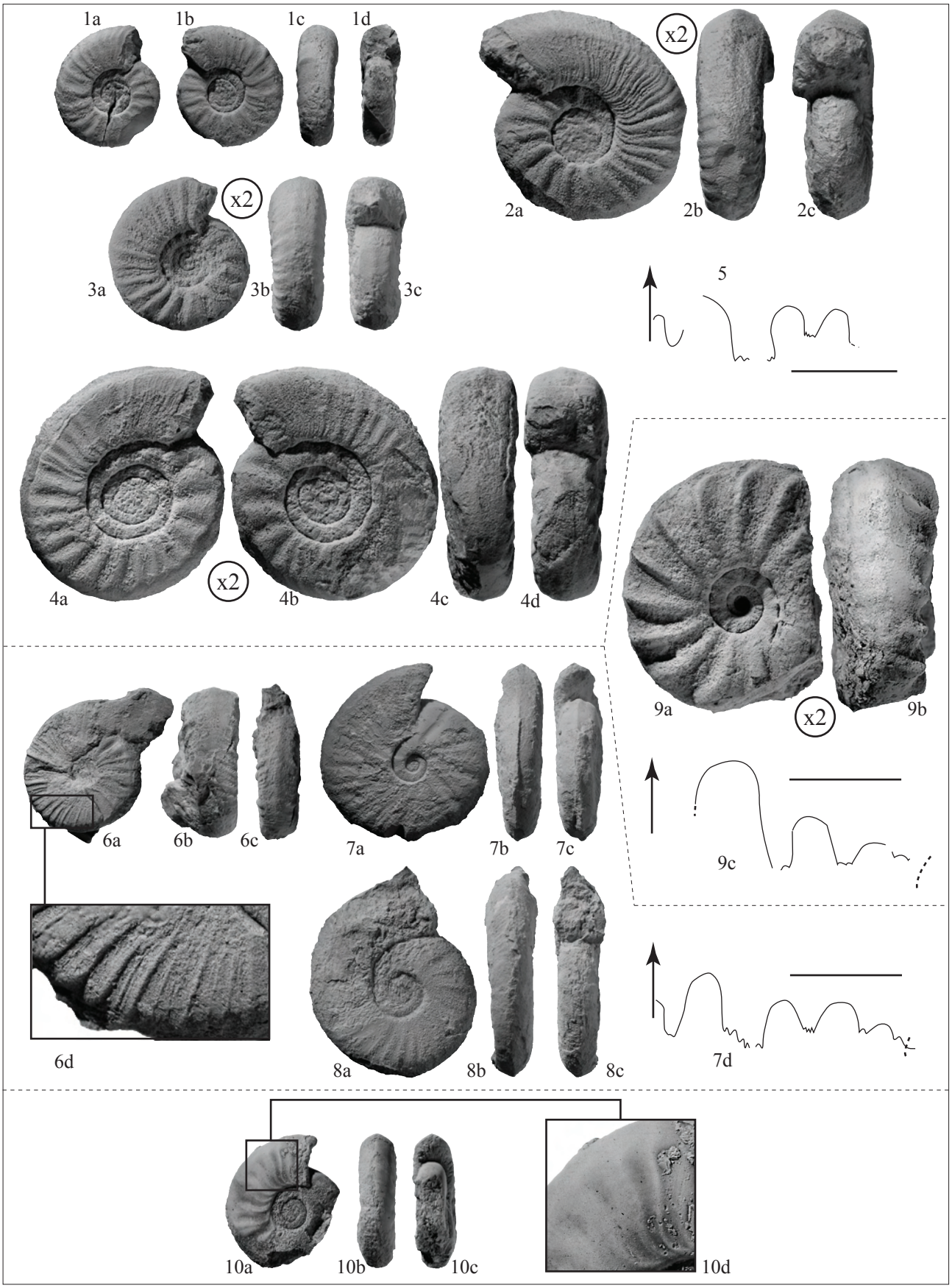
1a
1b
1c
1d
x2
2a
2b
2c
3a
3b
3c
5
4a
x2
4b
4c
4d
9a
x2
9b
6a
6b
6c
7a
7b
7c
9c
6d
8a
8b
8c
7d
10a
10b
10c
10d

PLATE 6

(All figures natural size unless otherwise indicated)

Figs. 1a-d: ***Xenoceltites variocostatus*** n. sp. PIMUZ 25838. Holotype.
Loc. NW13, Waili, "*Anasibirites multiformis* beds", Smithian.

Figs. 2a-c: ***Xenoceltites variocostatus*** n. sp. PIMUZ 25839. Scale ×2. Paratype.
Loc. NW13, Waili, "*Anasibirites multiformis* beds", Smithian.

Figs. 3a-c: ***Xenoceltites variocostatus*** n. sp. PIMUZ 25840. Scale ×2. Paratype.
Loc. NW13, Waili, "*Anasibirites multiformis* beds", Smithian.

Figs. 4a-c: ***Xenoceltites variocostatus*** n. sp. PIMUZ 25841. Paratype.
Loc. NW13, Waili, "*Anasibirites multiformis* beds", Smithian.

Fig. 5: ***Xenoceltites variocostatus*** n. sp. PIMUZ 25842. Paratype.
Loc. NW13, Waili, "*Anasibirites multiformis* beds", Smithian.

Figs. 6a-c: ***Xenoceltites variocostatus*** n. sp. PIMUZ 25843. Paratype.
Loc. NW13, Waili, "*Anasibirites multiformis* beds", Smithian.

Figs. 7a-c: ***Xenoceltites variocostatus*** n. sp. PIMUZ 25844. Paratype.
Loc. NW13, Waili, "*Anasibirites multiformis* beds", Smithian.

Figs. 8a-c: ***Xenoceltites variocostatus*** n. sp. PIMUZ 25845. Scale ×2. Paratype.
Loc. NW13, Waili, "*Anasibirites multiformis* beds", Smithian.

Figs. 9a-c: ***Xenoceltites variocostatus*** n. sp. PIMUZ 25846. Paratype.
Loc. NW13, Waili, "*Anasibirites multiformis* beds", Smithian.

Figs. 10a-d: ***Xenoceltites variocostatus*** n. sp. PIMUZ 25847. Scale ×2. Paratype.
Loc. NW13, Waili, "*Anasibirites multiformis* beds", Smithian.

Figs. 11a-c: ***Xenoceltites variocostatus*** n. sp. PIMUZ 25848. Paratype.
Loc. NW13, Waili, "*Anasibirites multiformis* beds", Smithian.

Figs. 12: ***Xenoceltites variocostatus*** n. sp. PIMUZ 25849. Paratype.
Loc. NW13, Waili, "*Anasibirites multiformis* beds", Smithian.

Figs. 13a-d: ***Xenoceltites variocostatus*** n. sp. PIMUZ 25850. Scale ×2. Paratype.
Loc. NW13, Waili, "*Anasibirites multiformis* beds", Smithian.

Figs. 14a-c: ***Xenoceltites variocostatus*** n. sp. PIMUZ 25851. Paratype.
Loc. NW13, Waili, "*Anasibirites multiformis* beds", Smithian.

PLATE 6


1a
1b
1c
1d
x2
2a
2b
2c
3a
3b
3c
x2
4a
4b
4c
5
6a
6b
6c
7a
7b
7c
8a
8b
8c
x2
9a
9b
9c
10a
10b
10c
10d
x2
11a
11b
11c
12
13a
13b
13c
13d
x2
14a
14b
14c

PLATE 7

(All figures natural size unless otherwise indicated)

Figs. 1a-b: ***Xenoceltites variocostatus*** n. sp. PIMUZ 25852. Scale ×2. Paratype.
Loc. NW13, Waili, "*Anasibirites multiformis* beds", Smithian.

Figs. 2a-c: ***Xenoceltites variocostatus*** n. sp. PIMUZ 25853. Paratype.
Loc. NW13, Waili, "*Anasibirites multiformis* beds", Smithian.

Figs. 3a-c: ***Xenoceltites variocostatus*** n. sp. PIMUZ 25854. Paratype.
Loc. NW13, Waili, "*Anasibirites multiformis* beds", Smithian.

Figs. 4a-c: ***Xenoceltites variocostatus*** n. sp. PIMUZ 25855.
Loc. Jin101, Waili, "*Anasibirites multiformis* beds", Smithian.

Figs. 5a-c: ***Xenoceltites variocostatus*** n. sp. PIMUZ 25856. Paratype.
Loc. NW13, Waili, "*Anasibirites multiformis* beds", Smithian.

Fig. 6: Suture line of ***Xenoceltites variocostatus*** n. sp., PIMUZ 25857. Paratype.
Loc. NW13, Waili, "*Anasibirites multiformis* beds", Smithian.
Scale bar = 5 mm; D = 12 mm.

Figs. 7a-c: ***Xenoceltites pauciradiatus*** n. sp. PIMUZ 25858. Holotype.
Loc. Jin33, Jinya, "*Anasibirites multiformis* beds", Smithian.

Figs. 8a-c: ***Xenoceltites pauciradiatus*** n. sp. PIMUZ 25859. Paratype.
Loc. Jin33, Jinya, "*Anasibirites multiformis* beds", Smithian.

Figs. 9a-c: ***Xenoceltites pauciradiatus*** n. sp. PIMUZ 25860. Paratype.
Loc. Jin33, Jinya, "*Anasibirites multiformis* beds", Smithian.

PLATE 7

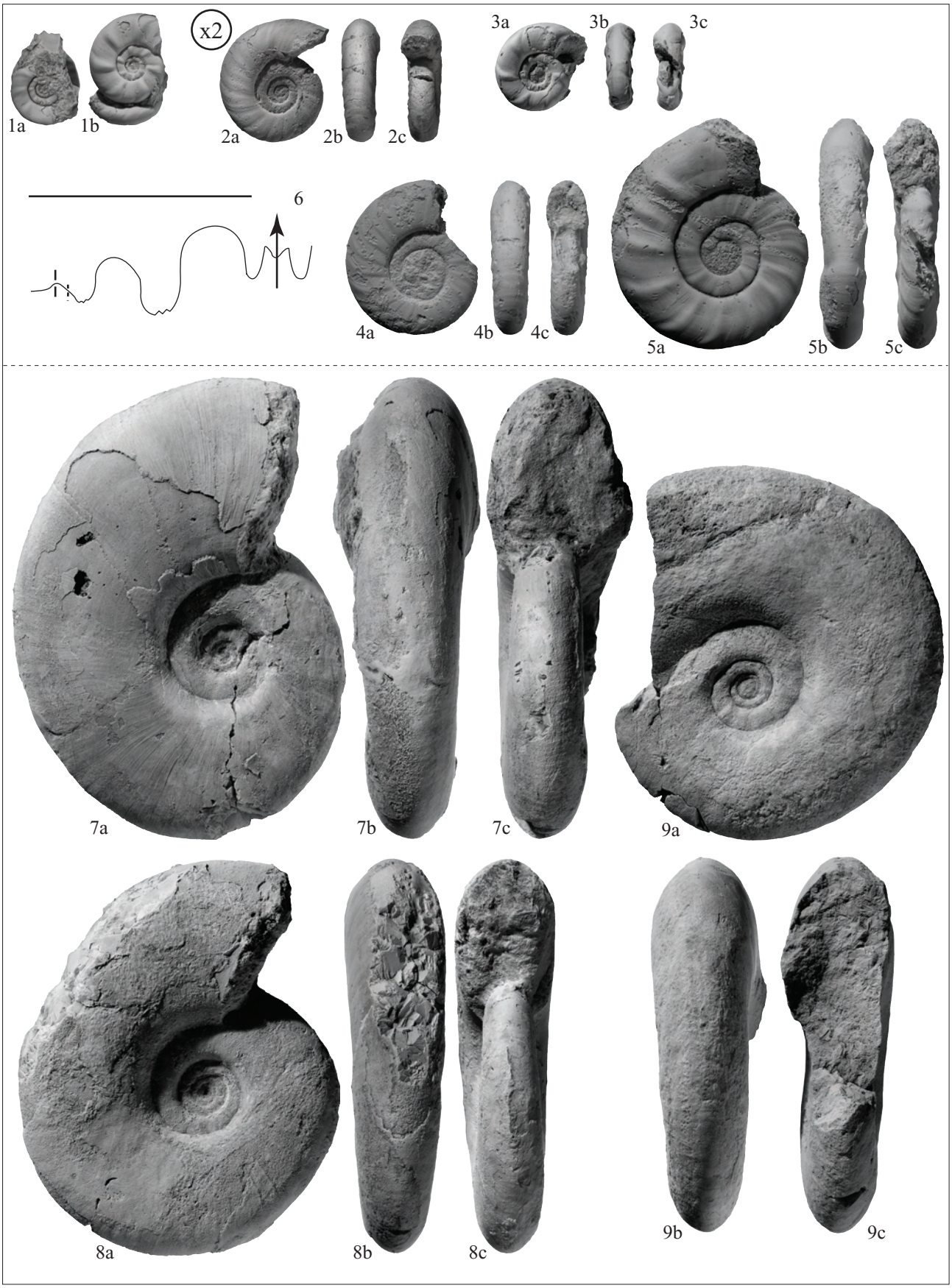

PLATE 8

(All figures natural size unless otherwise indicated)

Figs. 1a-d: ***Sinoceltites admirabilis*** n. gen., n. sp. PIMUZ 25861. Holotype.
Loc. Jin61, Jinya, "*Kashmirites densistriatus* beds", Smithian.

Figs. 2a-c: ***Sinoceltites admirabilis*** n. gen., n. sp. PIMUZ 25862. Paratype.
Loc. Jin61, Jinya, "*Kashmirites densistriatus* beds", Smithian.

Figs. 3a-c: ***Sinoceltites admirabilis*** n. gen., n. sp. PIMUZ 25863. Scale ×1.5. Paratype.
Loc. Jin61, Jinya, "*Kashmirites densistriatus* beds", Smithian.

Figs. 4a-c: ***Sinoceltites admirabilis*** n. gen., n. sp. PIMUZ 25864. Paratype.
Loc. Jin61, Jinya, "*Kashmirites densistriatus* beds", Smithian.

Figs. 5a-c: ***Sinoceltites admirabilis*** n. gen., n. sp. PIMUZ 25865. Paratype.
Loc. Jin61, Jinya, "*Kashmirites densistriatus* beds", Smithian.

Figs. 6a-c: ***Sinoceltites admirabilis*** n. gen., n. sp. PIMUZ 25866.
Loc. Jin64, Jinya, "*Kashmirites densistriatus* beds", Smithian.

Figs. 7a-d: **?Palaeophyllitidae gen. indet.** PIMUZ 25867. Holotype.
Loc. Jin47, Jinya, "*Owenites koeneni* beds", Smithian.
a-c) Lateral, ventral and apertural views. Scale ×1.25
d) Suture line. Scale bar = 5 mm; H = 13 mm.

Figs. 8a-d: **Xenoceltitidae gen. indet.** PIMUZ 25868.
Loc. Yu22, Yuping, "*Kashmirites densistriatus* beds", Smithian.
a-c) Lateral and ventral views. Scale ×0.75.
d) Suture line. Scale bar = 5 mm; H = 16 mm.

Figs. 9a-d: ***Weitschaticeras concavum*** n. gen., n. sp. PIMUZ 25869. Holotype.
Loc. Jin27, Jinya, "*Owenites koeneni* beds", Smithian.
a-c) Lateral, ventral and apertural views.
d) Suture line. Scale bar = 5 mm; H = 9 mm.

PLATE 8


1a
1b
1c
1d
2a
2b
2c
3a
3b
3c
x1.5
4a
4b
4c
5a
5b
5c
6a
6b
6c
7a
7b
7c
x1.25
7d
8a
8b
x3/4
8c
8d
9a
9b
9c
9d

PLATE 9

(All figures natural size unless otherwise indicated)

Figs. 1a-c: ***Hebeisenites varians*** n. gen. PIMUZ 25870.
Loc. Jin29, Jinya, "*Flemingites rursiradiatus* beds", Smithian.
Figs. 2a-c: ***Hebeisenites varians*** n. gen. PIMUZ 25871. Scale ×2.
Loc. Jin29, Jinya, "*Flemingites rursiradiatus* beds", Smithian.
Figs. 3a-c: ***Hebeisenites varians*** n. gen. PIMUZ 25872.
Loc. Jin30, Jinya, "*Flemingites rursiradiatus* beds", Smithian.
Figs. 4a-c: ***Hebeisenites varians*** n. gen. PIMUZ 25873.
Loc. Jin29, Jinya, "*Flemingites rursiradiatus* beds", Smithian.
Figs. 5a-c: ***Hebeisenites varians*** n. gen. PIMUZ 25874.
Loc. Jin4, Jinya, "*Flemingites rursiradiatus* beds", Smithian.
Figs. 6a-b: ***Hebeisenites varians*** n. gen. PIMUZ 25875.
Loc. Jin4, Jinya, "*Flemingites rursiradiatus* beds", Smithian.
Figs. 7a-b: ***Hebeisenites varians*** n. gen. PIMUZ 25876.
Loc. Jin4, Jinya, "*Flemingites rursiradiatus* beds", Smithian.
Figs. 8a-b: ***Hebeisenites varians*** n. gen. PIMUZ 25877.
Loc. Jin4, Jinya, "*Flemingites rursiradiatus* beds", Smithian.
Figs. 9a-b: ***Hebeisenites varians*** n. gen. PIMUZ 25878.
Loc. Jin28, Jinya, "*Flemingites rursiradiatus* beds", Smithian.
Fig. 10: Suture line of ***Hebeisenites varians*** n. gen., PIMUZ 25879.
Loc. Jin23, Jinya, "*Flemingites rursiradiatus* beds", Smithian.
Scale bar = 5 mm; D = 15 mm.
Fig. 11: Suture line of ***Hebeisenites varians*** n. gen., PIMUZ 25880.
Loc. Jin30, Jinya, "*Flemingites rursiradiatus* beds", Smithian.
Scale bar = 5 mm; D = 14 mm.
Figs. 12a-e: ***Hebeisenites evolutus*** n. gen., n. sp. PIMUZ 25881.
Loc. Jin28, Jinya, "*Flemingites rursiradiatus* beds", Smithian.
a-d) Lateral, ventral and apertural views.
e) Suture line. Scale bar = 5 mm; H = 2.5 mm.
Figs. 13a-c: ***Hebeisenites evolutus*** n. gen., n. sp. PIMUZ 25882.
Loc. Jin28, Jinya, "*Flemingites rursiradiatus* beds", Smithian.
Figs. 14a-c: ***Hebeisenites evolutus*** n. gen., n. sp. PIMUZ 25883.
Loc. Jin28, Jinya, "*Flemingites rursiradiatus* beds", Smithian.
Figs. 15a-c: ***Hebeisenites evolutus*** n. gen., n. sp. PIMUZ 25884.
Loc. Jin29, Jinya, "*Flemingites rursiradiatus* beds", Smithian.
Figs. 16a-c: ***Hebeisenites evolutus*** n. gen., n. sp. PIMUZ 25885.
Loc. Jin30, Jinya, "*Flemingites rursiradiatus* beds", Smithian.
Figs. 17a-d: ***Hebeisenites evolutus*** n. gen., n. sp. PIMUZ 25886. Holotype.
Loc. Jin10, Jinya, "*Flemingites rursiradiatus* beds", Smithian.
Figs. 18a-c: ***Hebeisenites compressus*** n. gen., n. sp. PIMUZ 25887. Scale ×2.
Loc. Jin23, Jinya, "*Flemingites rursiradiatus* beds", Smithian.
Figs. 19a-d: ***Hebeisenites compressus*** n. gen., n. sp. PIMUZ 25888. Scale ×2. Holotype.
Loc. Jin30, Jinya, "*Flemingites rursiradiatus* beds", Smithian.
Figs. 20a-b: ***Hebeisenites compressus*** n. gen., n. sp. PIMUZ 25889. Scale ×2. Paratype.
Loc. Jin30, Jinya, "*Flemingites rursiradiatus* beds", Smithian.
Figs. 21a-c: ***Hebeisenites compressus*** n. gen., n. sp. PIMUZ 25890. Scale ×2. Paratype.
Loc. Jin30, Jinya, "*Flemingites rursiradiatus* beds", Smithian.
Figs. 22a-c: ***Hebeisenites compressus*** n. gen., n. sp. PIMUZ 25891. Scale ×2. Paratype.
Loc. Jin30, Jinya, "*Flemingites rursiradiatus* beds", Smithian.
Figs. 23a-d: ***Hebeisenites compressus*** n. gen., n. sp. PIMUZ 25892. Scale ×2. Paratype.
Loc. Jin30, Jinya, "*Flemingites rursiradiatus* beds", Smithian.
Figs. 24a-c: ***Hebeisenites compressus*** n. gen., n. sp. PIMUZ 25893. Scale ×2. Paratype.
Loc. Jin30, Jinya, "*Flemingites rursiradiatus* beds", Smithian.
Fig. 25: Suture line of ***Hebeisenites compressus*** n. gen., n. sp., PIMUZ 26204.
Loc. Jin23, Jinya, "*Flemingites rursiradiatus* beds", Smithian.
Scale bar = 2.5 mm; H = 3 mm.

PLATE 9

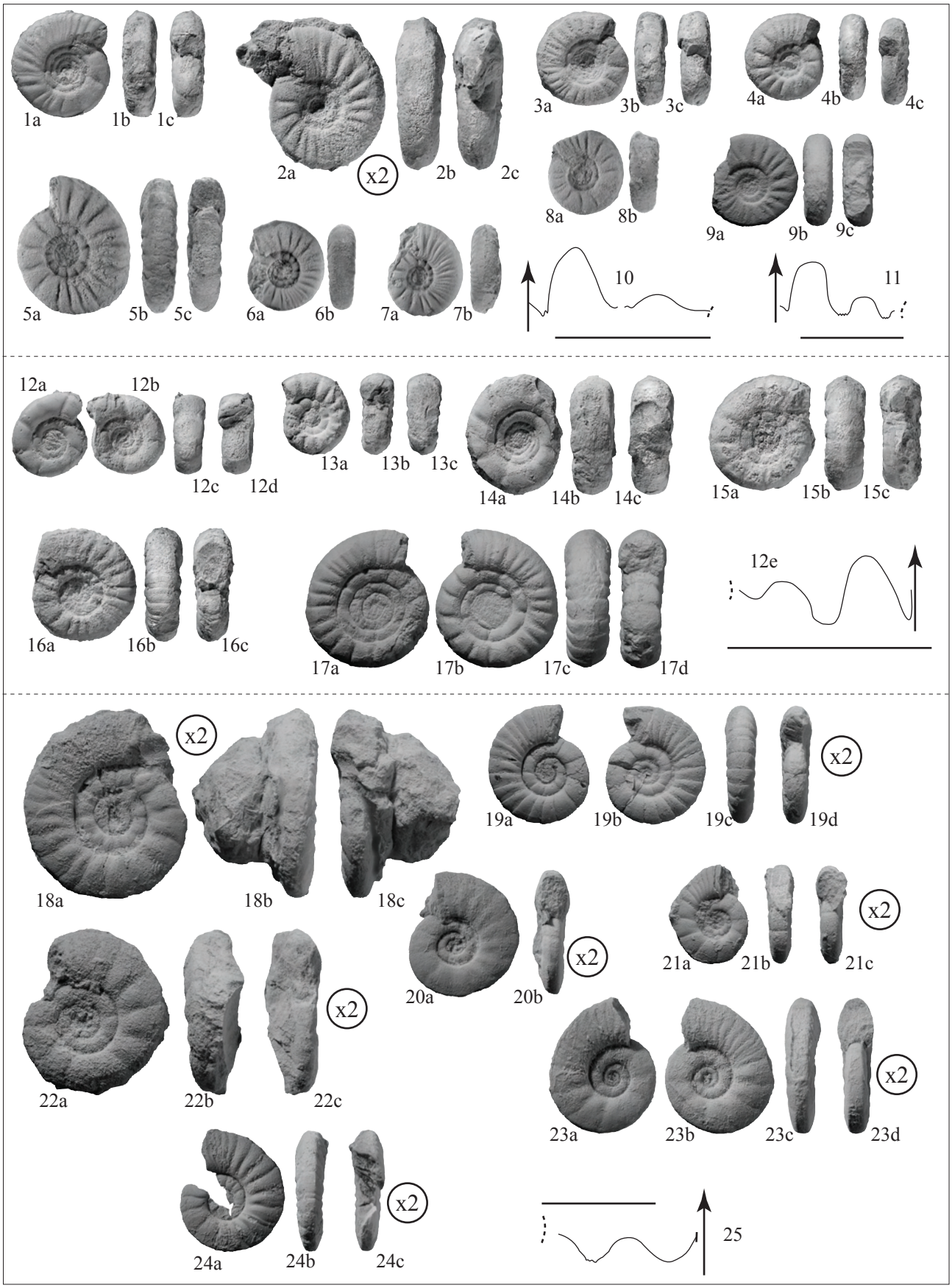
1a
1b
1c
2a
x2
2b
2c
3a
3b
3c
4a
4b
4c
5a
5b
5c
6a
6b
7a
7b
8a
8b
9a
9b
9c
10
11
12a
12b
12c
12d
13a
13b
13c
14a
14b
14c
15a
15b
15c
16a
16b
16c
17a
17b
17c
17d
12e
18a
x2
18b
18c
19a
19b
19c
19d
x2
20a
20b
x2
21a
21b
21c
x2
22a
22b
22c
x2
23a
23b
23c
23d
x2
24a
24b
24c
x2
25

PLATE 10

(All figures natural size)

Figs. 1a-d: ***Jinyaceras bellum*** n. gen., n. sp. PIMUZ 25894. Holotype.
Loc. Jin28, Jinya, "*Flemingites rursiradiatus* beds", Smithian.
Figs. 2a-c: ***Jinyaceras bellum*** n. gen., n. sp. PIMUZ 25895.
Loc. Jin30, Jinya, "*Flemingites rursiradiatus* beds", Smithian.
Figs. 3a-c: ***Jinyaceras bellum*** n. gen., n. sp. PIMUZ 25896.
Loc. Jin4, Jinya, "*Flemingites rursiradiatus* beds", Smithian.
Figs. 4a-c: ***Jinyaceras bellum*** n. gen., n. sp. PIMUZ 25897.
Loc. Jin30, Jinya, "*Flemingites rursiradiatus* beds", Smithian.
Figs. 5a-c: ***Jinyaceras bellum*** n. gen., n. sp. PIMUZ 25898.
Loc. Jin30, Jinya, "*Flemingites rursiradiatus* beds", Smithian.
Figs. 6a-c: ***Jinyaceras bellum*** n. gen., n. sp. PIMUZ 25899.
Loc. Jin30, Jinya, "*Flemingites rursiradiatus* beds", Smithian.
Figs. 7a-c: ***Jinyaceras bellum*** n. gen., n. sp. PIMUZ 25900.
Loc. T50, Tsoteng, "*Flemingites rursiradiatus* beds", Smithian.
Figs. 8a-c: ***Jinyaceras bellum*** n. gen., n. sp. PIMUZ 25901.
Loc. Jin30, Jinya, "*Flemingites rursiradiatus* beds", Smithian.
Figs. 9a-c: ***Jinyaceras bellum*** n. gen., n. sp. PIMUZ 25902.
Loc. Jin30, Jinya, "*Flemingites rursiradiatus* beds", Smithian.
Figs. 10a-c: ***Jinyaceras bellum*** n. gen., n. sp. PIMUZ 25903.
Loc. Jin4, Jinya, "*Flemingites rursiradiatus* beds", Smithian.
Figs. 11a-c: ***Jinyaceras bellum*** n. gen., n. sp. PIMUZ 25904.
Loc. Jin4, Jinya, "*Flemingites rursiradiatus* beds", Smithian.
Figs. 12a-c: ***Jinyaceras bellum*** n. gen., n. sp. PIMUZ 25905. Paratype.
Loc. Jin28, Jinya, "*Flemingites rursiradiatus* beds", Smithian.
Figs. 13a-c: ***Jinyaceras bellum*** n. gen., n. sp. PIMUZ 25906. Paratype.
Loc. Jin28, Jinya, "*Flemingites rursiradiatus* beds", Smithian.
Figs. 14a-c: ***Jinyaceras bellum*** n. gen., n. sp. PIMUZ 25907. Paratype.
Loc. Jin28, Jinya, "*Flemingites rursiradiatus* beds", Smithian.
Figs. 15a-c: ***Jinyaceras bellum*** n. gen., n. sp. PIMUZ 25908.
Loc. Jin30, Jinya, "*Flemingites rursiradiatus* beds", Smithian.
Figs. 16a-c: ***Jinyaceras bellum*** n. gen., n. sp. PIMUZ 25909.
Loc. Jin30, Jinya, "*Flemingites rursiradiatus* beds", Smithian.
Figs. 17a-c: ***Jinyaceras bellum*** n. gen., n. sp. PIMUZ 25910.
Loc. Jin30, Jinya, "*Flemingites rursiradiatus* beds", Smithian.
Figs. 18a-c: ***Jinyaceras bellum*** n. gen., n. sp. PIMUZ 25911.
Loc. Jin30, Jinya, "*Flemingites rursiradiatus* beds", Smithian.
Fig. 19: Suture line of ***Jinyaceras bellum*** n. gen., n. sp., PIMUZ 25912.
Loc. Jin30, Jinya, "*Flemingites rursiradiatus* beds", Smithian.
Scale bar = 5 mm; H = 4 mm.
Figs. 20a-c: ***Juvenites* cf. *J. kraffti***. PIMUZ 25913.
Loc. Jin23, Jinya, "*Flemingites rursiradiatus* beds", Smithian.
Figs. 21a-c: ***Juvenites* cf. *J. kraffti***. PIMUZ 25914.
Loc. Jin30, Jinya, "*Flemingites rursiradiatus* beds", Smithian.
Figs. 22a-c: ***Juvenites* cf. *J. kraffti***. PIMUZ 25915.
Loc. Jin30, Jinya, "*Flemingites rursiradiatus* beds", Smithian.
Figs. 23a-c: ***Juvenites* cf. *J. kraffti***. PIMUZ 25916.
Loc. Jin4, Jinya, "*Flemingites rursiradiatus* beds", Smithian.
Figs. 24a-d: ***Paranorites jenksi*** n. sp. PIMUZ 25917. Holotype.
Loc. Jin67, Waili, "*Kashmirites densistriatus* beds", Smithian.
a-c) Lateral, ventral and apertural views.
d) Suture line. Scale bar = 5 mm; H = 16 mm.
Figs. 25a-d: ***Paranorites jenksi*** n. sp. PIMUZ 25918.
Loc. Jin66, Waili, "*Kashmirites densistriatus* beds", Smithian.
Figs. 26a-d: ***Paranorites jenksi*** n. sp. PIMUZ 25919.
Loc. Jin66, Waili, "*Kashmirites densistriatus* beds", Smithian.

PLATE 10


1a
1b
1c
1d
2a
2b
2c
3a
3b
3c
4a
4b
4c
5a
5b
5c
6a
6b
6c
7a
7b
7c
9a
9b
9c
10a
10b
10c
8a
8b
8c
11a
11b
11c
12a
12b
12c
19
13a
13b
13c
14a
14b
14c
15a
15b
15c
16a
16b
16c
20a
20b
20c
21a
21b
21c
22a
22b
22c
17a
17b
17c
23a
23b
23c
18a
18b
18c
24a
24b
24c
24d
25a
25b
25c
25d
x2
26a
26b
26c
26d

PLATE 11
(All figures natural size)

Figs. 1a-d: ***Pseudaspidites muthianus*** (Krafft & Diener, 1909). PIMUZ 25920.
Loc. Jin28, Jinya, "*Flemingites rursiradiatus* beds", Smithian.
a-c) Lateral, ventral and apertural views.
d) Suture line. Scale bar = 5 mm; H = 15 mm. Slightly smoothed.

Figs. 2a-c: ***Pseudaspidites muthianus*** (Krafft & Diener, 1909). PIMUZ 25921.
Loc. Jin28, Jinya, "*Flemingites rursiradiatus* beds", Smithian.

Figs. 3a-d: ***Pseudaspidites muthianus*** (Krafft & Diener, 1909). PIMUZ 25922.
Loc. Jin28, Jinya, "*Flemingites rursiradiatus* beds", Smithian.

Figs. 4a-c: ***Pseudaspidites muthianus*** (Krafft & Diener, 1909). PIMUZ 25923.
Loc. Jin28, Jinya, "*Flemingites rursiradiatus* beds", Smithian.

Figs. 5a-c: ***Pseudaspidites muthianus*** (Krafft & Diener, 1909). PIMUZ 25924.
Loc. Jin30, Jinya, "*Flemingites rursiradiatus* beds", Smithian.

Figs. 6a-c: ***Pseudaspidites muthianus*** (Krafft & Diener, 1909). PIMUZ 25925.
Loc. Jin30, Jinya, "*Flemingites rursiradiatus* beds", Smithian.

Figs. 7a-e: ***Pseudaspidites muthianus*** (Krafft & Diener, 1909). PIMUZ 25928.
Loc. Jin30, Jinya, "*Flemingites rursiradiatus* beds", Smithian.
a-d) Lateral, ventral and apertural views.
e) Suture line. Scale bar = 5 mm; H = 15 mm. Slightly smoothed.

Fig. 8: Suture line of ***Pseudaspidites muthianus*** (Krafft & Diener, 1909). PIMUZ 25927.
Loc. Jin30, Jinya, "*Flemingites rursiradiatus* beds", Smithian.
Scale bar = 5 mm; D = 35 mm. Slightly smoothed.

Fig. 9: Suture line of ***Pseudaspidites muthianus*** (Krafft & Diener, 1909). PIMUZ 25929.
Loc. Jin30, Jinya, "*Flemingites rursiradiatus* beds", Smithian.
Scale bar = 5 mm; H = 35 mm. Slightly smoothed.

Fig. 10: Suture line of ***Pseudaspidites muthianus*** (Krafft & Diener, 1909), variant with umbilical bullae. PIMUZ 25930.
Loc. Sha1, Shanggan, "*Flemingites rursiradiatus* beds", Smithian.
Scale bar = 5 mm; H = 30 mm.

PLATE 11

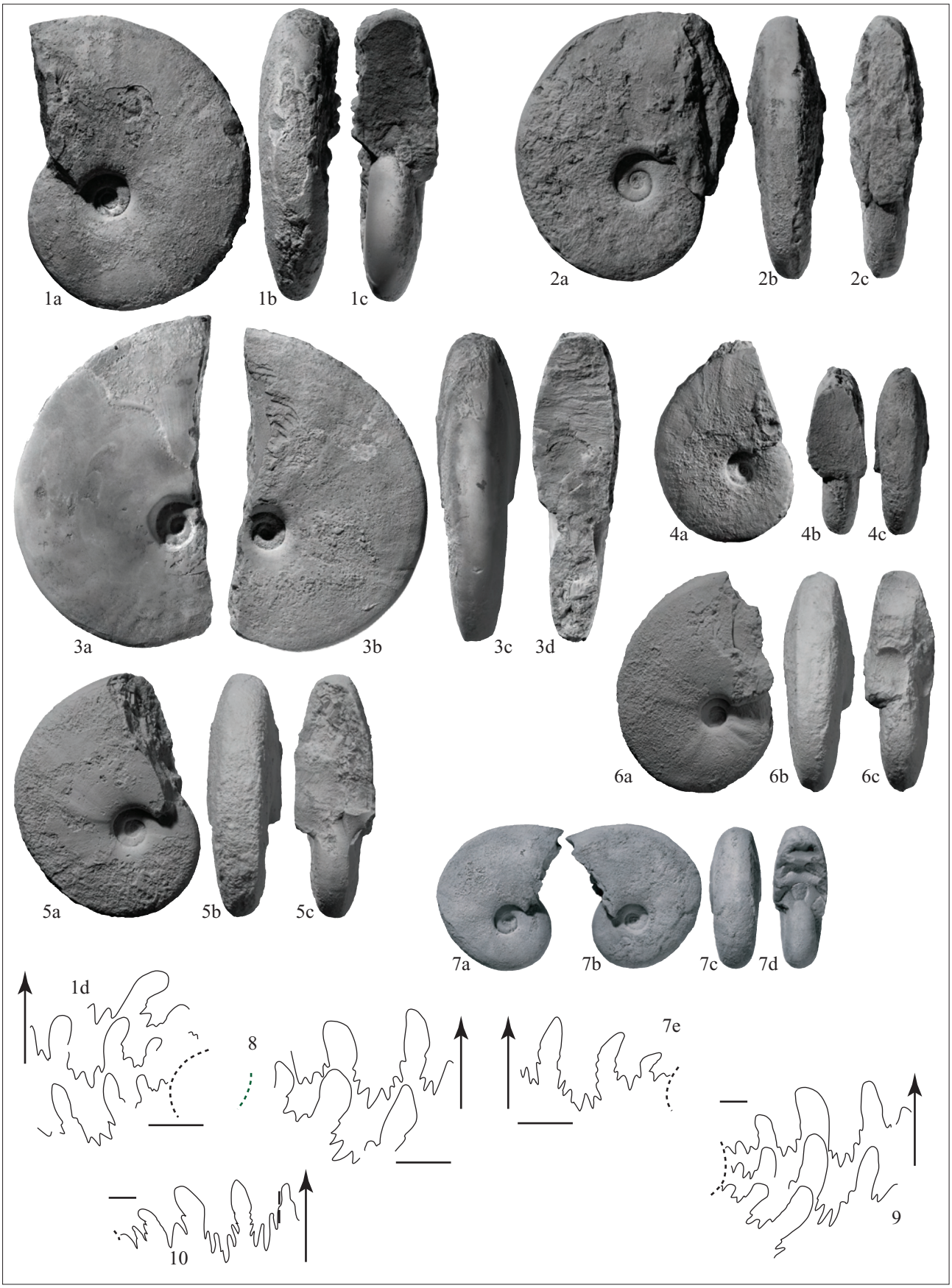
1a
1b
1c
2a
2b
2c
3a
3b
3c
3d
4a
4b
4c
5a
5b
5c
6a
6b
6c
7a
7b
7c
7d
1d
8
7e
9
10

PLATE 12

(All figures natural size unless otherwise indicated)

Figs. 1a-d: ***Pseudaspidites muthianus*** (Krafft & Diener, 1909). PIMUZ 25931. Scale ×0.5.
Loc. Jin4, Jinya, "*Flemingites rursiradiatus* beds", Smithian.

Figs. 2a-d: ***Pseudaspidites muthianus*** (Krafft & Diener, 1909). PIMUZ 25930. Robust variant.
Loc. Sha1, Shanggan, "*Flemingites rursiradiatus* beds", Smithian.

Figs. 3a-c: ***Pseudaspidites muthianus*** (Krafft & Diener, 1909). PIMUZ 25932. Robust variant.
Loc. Jin30, Jinya, "*Flemingites rursiradiatus* beds", Smithian.

Figs. 4a-c: ***Pseudaspidites muthianus*** (Krafft & Diener, 1909). PIMUZ 25933. Robust variant.
Loc. Jin13, Jinya, "*Flemingites rursiradiatus* beds", Smithian.

Figs. 5a-d: **Proptychitidae gen. indet. A**. PIMUZ 25934.
Loc. Jin30, Jinya, "*Flemingites rursiradiatus* beds", Smithian.
a-c) Lateral, ventral and apertural views.
d) Suture line. Scale bar = 5 mm; H = 14 mm.

Figs. 6a-d: ***Pseudaspidites*** **sp. indet.** PIMUZ 25935.
Loc. Jin27, Jinya, "*Owenites koeneni* beds", Smithian.
a-c) Lateral, ventral and apertural views.
d) Suture line. Scale bar = 5 mm; H = 10 mm.

PLATE 12

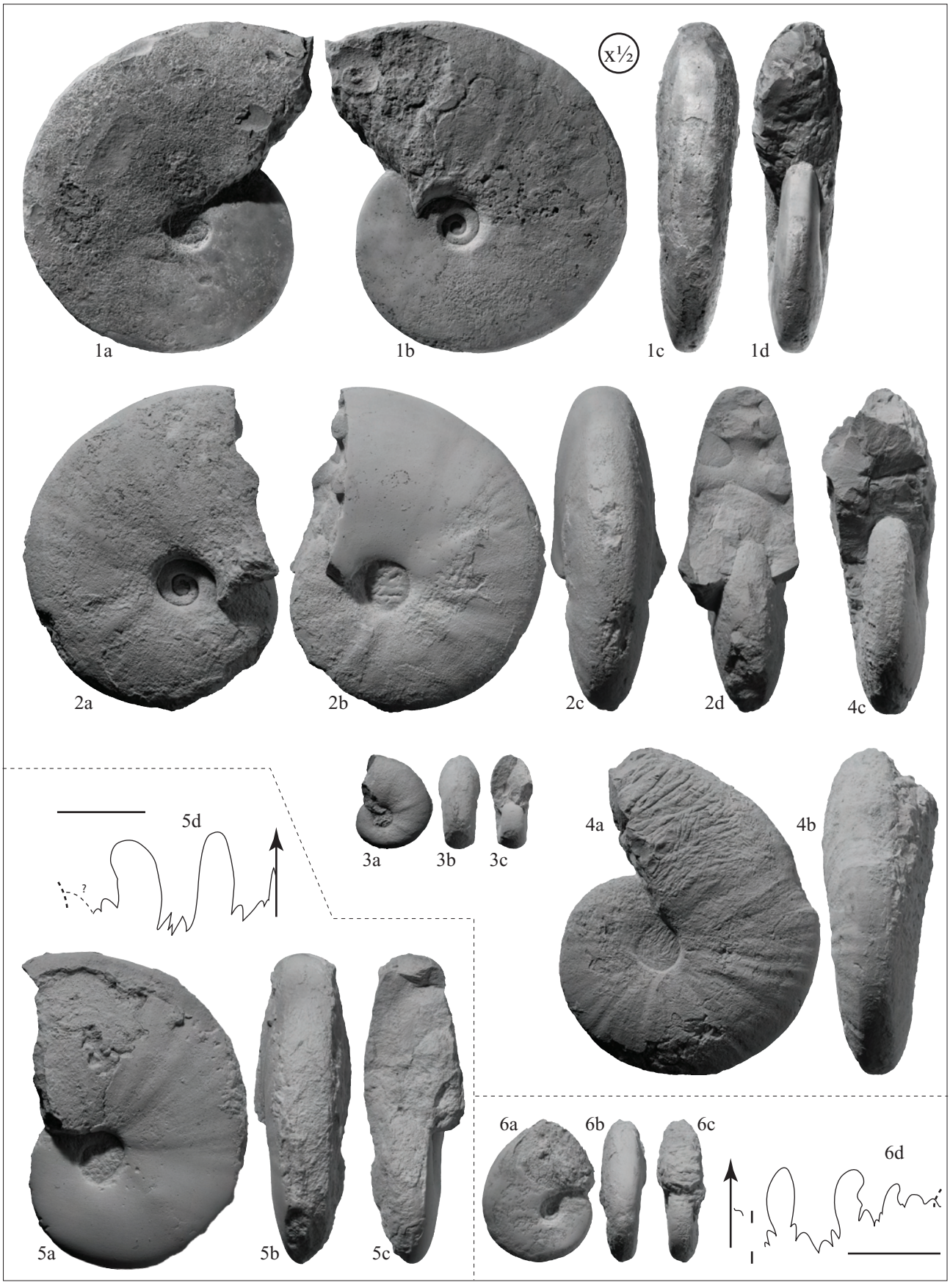

PLATE 13

(All figures natural size)

Figs. 1a-c: ***Lingyunites discoides*** Chao, 1950. PIMUZ 25936.
Loc. Jin30, Jinya, "*Flemingites rursiradiatus* beds", Smithian.

Figs. 2a-c: ***Lingyunites discoides*** Chao, 1950. PIMUZ 25937.
Loc. Jin30, Jinya, "*Flemingites rursiradiatus* beds", Smithian.

Figs. 3a-d: ***Lingyunites discoides*** Chao, 1950. PIMUZ 25938.
Loc. Jin10, Jinya, "*Flemingites rursiradiatus* beds", Smithian.

Figs. 4a-c: ***Lingyunites discoides*** Chao, 1950. PIMUZ 25939.
Loc. Jin30, Jinya, "*Flemingites rursiradiatus* beds", Smithian.

Figs. 5a-c: ***Lingyunites discoides*** Chao, 1950. PIMUZ 25940.
Loc. Jin30, Jinya, "*Flemingites rursiradiatus* beds", Smithian.

Figs. 6a-d: ***Lingyunites discoides*** Chao, 1950. PIMUZ 25941.
Loc. Jin29, Jinya, "*Flemingites rursiradiatus* beds", Smithian.
a-c) Lateral, ventral and apertural views.
d) Suture line. Scale bar = 5 mm; H = 9 mm.

Figs. 7a-c: ***Lingyunites discoides*** Chao, 1950. PIMUZ 25942.
Loc. Jin30, Jinya, "*Flemingites rursiradiatus* beds", Smithian.

Figs. 8a-c: ***Lingyunites discoides*** Chao, 1950. PIMUZ 25943.
Loc. Jin30, Jinya, "*Flemingites rursiradiatus* beds", Smithian.

Figs. 9a-d: ***Nanningites tientungense*** n. gen. PIMUZ 25944.
Loc. Jin29, Jinya, "*Flemingites rursiradiatus* beds", Smithian.
a-c) Lateral, ventral and apertural views.
d) Suture line. Scale bar = 5 mm; D = 21 mm.

Figs. 10a-c: ***Nanningites tientungense*** n. gen. PIMUZ 25945.
Loc. Jin30, Jinya, "*Flemingites rursiradiatus* beds", Smithian.

Figs. 11a-c: ***Nanningites tientungense*** n. gen. PIMUZ 25946.
Loc. Jin30, Jinya, "*Flemingites rursiradiatus* beds", Smithian.

Figs. 12a-c: ***Xiaoqiaoceras involutus*** n. gen., n. sp. PIMUZ 25947. Paratype.
Loc. Jin4, Jinya, "*Flemingites rursiradiatus* beds", Smithian.

Figs. 13a-c: ***Xiaoqiaoceras involutus*** n. gen., n. sp. PIMUZ 25948. Holotype.
Loc. Jin4, Jinya, "*Flemingites rursiradiatus* beds", Smithian.

Figs. 14a-c: ***Xiaoqiaoceras involutus*** n. gen., n. sp. PIMUZ 25949.
Loc. Jin30, Jinya, "*Flemingites rursiradiatus* beds", Smithian.

Figs. 15a-c: ***Xiaoqiaoceras involutus*** n. gen., n. sp. PIMUZ 25950.
Loc. Jin30, Jinya, "*Flemingites rursiradiatus* beds", Smithian.

Fig. 16: Suture line of ***Xiaoqiaoceras involutus*** n. gen., n. sp., PIMUZ 25951.
Loc. Jin30, Jinya, "*Flemingites rursiradiatus* beds", Smithian.
Scale bar = 5 mm; H = 9 mm.

Fig. 17: ***Parussuria compressa*** (Hyatt & Smith, 1905). PIMUZ 25952.
Loc. Jin27, Jinya, "*Owenites koeneni* beds", Smithian.

PLATE 13

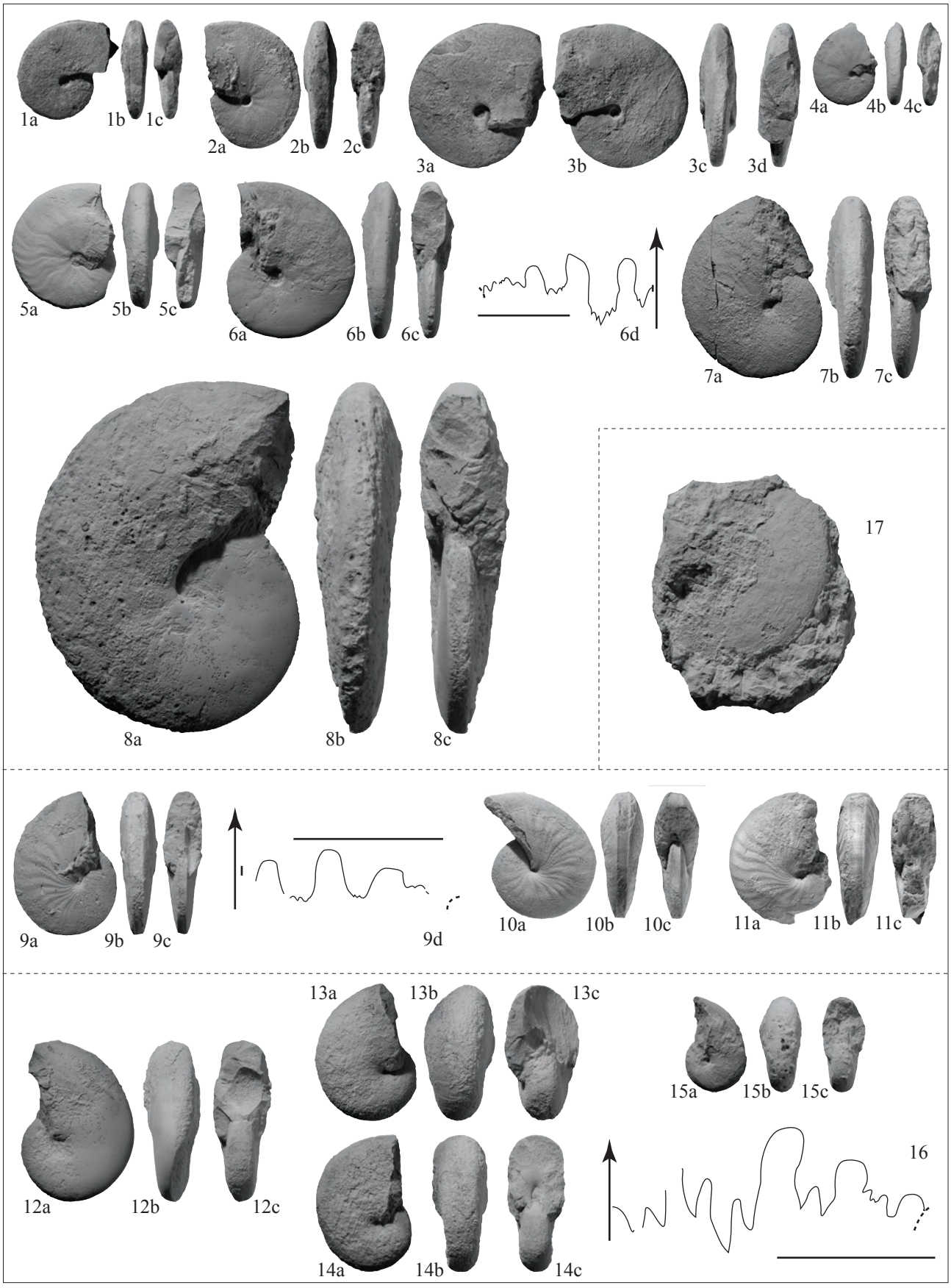
1a
1b
1c
2a
2b
2c
3a
3b
3c
3d
4a
4b
4c
5a
5b
5c
6a
6b
6c
6d
7a
7b
7c
8a
8b
8c
17
9a
9b
9c
9d
10a
10b
10c
11a
11b
11c
12a
12b
12c
13a
13b
13c
14a
14b
14c
15a
15b
15c
16

PLATE 14

(All figures natural size)

Figs. 1a-d: ***Wailiceras aemulus*** n. gen., n. sp. PIMUZ 25953. Holotype.
Loc. Jin61, Waili, "*Kashmirites densistriatus* beds", Smithian.
a-c) Lateral, ventral and apertural views.
d) Suture line. Scale bar = 5 mm; H = 20 mm.

Figs. 2a-c: ***Wailiceras aemulus*** n. gen., n. sp. PIMUZ 25954.
Loc. Jin64, Waili, "*Kashmirites densistriatus* beds", Smithian.

Figs. 3a-c: ***Wailiceras aemulus*** n. gen., n. sp. PIMUZ 25955.
Loc. Jin64, Waili, "*Kashmirites densistriatus* beds", Smithian.

Figs. 4a-b: ***Wailiceras aemulus*** n. gen., n. sp. PIMUZ 25956.
Loc. Jin64, Waili, "*Kashmirites densistriatus* beds", Smithian.

Figs. 5a-c: ***Wailiceras aemulus*** n. gen., n. sp. PIMUZ 25957.
Loc. Jin64, Waili, "*Kashmirites densistriatus* beds", Smithian.

Figs. 6a-c: ***Wailiceras aemulus*** n. gen., n. sp. PIMUZ 25958.
Loc. Jin64, Waili, "*Kashmirites densistriatus* beds", Smithian.

Figs. 7a-e: ***Wailiceras aemulus*** n. gen., n. sp. PIMUZ 25959.
Loc. Jin68, Waili, "*Kashmirites densistriatus* beds", Smithian.
a-d) Lateral, ventral and apertural views.
e) Suture line. Scale bar = 1 mm; H = 2.5 mm. Very small specimen.

Figs. 8a-c: ***Wailiceras aemulus*** n. gen., n. sp. PIMUZ 25960.
Loc. Jin65, Waili, "*Kashmirites densistriatus* beds", Smithian.

Figs. 9a-c: ***Wailiceras aemulus*** n. gen., n. sp. PIMUZ 25961.
Loc. Jin66, Waili, "*Kashmirites densistriatus* beds", Smithian.

PLATE 14


1a
1b
1c
2a
2b
2c
3a
3b
3c
4a
4b
5a
5b
5c
6a
6b
6c
7a
7b
7c
7d
8a
8b
8c
9a
9b
9c
1d
7e

PLATE 15

(All figures natural size)

Figs. 1a-d: ***Leyeceras rothi*** n. gen., n. sp. PIMUZ 25962.
Loc. Jin27, Jinya, "*Owenites koeneni* beds", Smithian.

Figs. 2a-e: ***Leyeceras rothi*** n. gen., n. sp. PIMUZ 25963. Paratype.
Loc. Jin12, Jinya, "*Owenites koeneni* beds", Smithian.
a-d) Lateral, ventral and apertural views.
e) Suture line. Scale bar = 5 mm; H = 18 mm.

Figs. 3a-c: ***Leyeceras rothi*** n. gen., n. sp. PIMUZ 25964. Holotype.
Loc. Jin43, Jinya, "*Owenites koeneni* beds", Smithian.

Figs. 4a-d: ***Urdyceras insolitus*** n. gen., n. sp. PIMUZ 25965. Holotype.
Loc. Jin30, Jinya, "*Flemingites rursiradiatus* beds", Smithian.
a-d) Lateral, ventral and apertural views.
e) Suture line. Scale bar = 5 mm; H = 10 mm.

PLATE 15

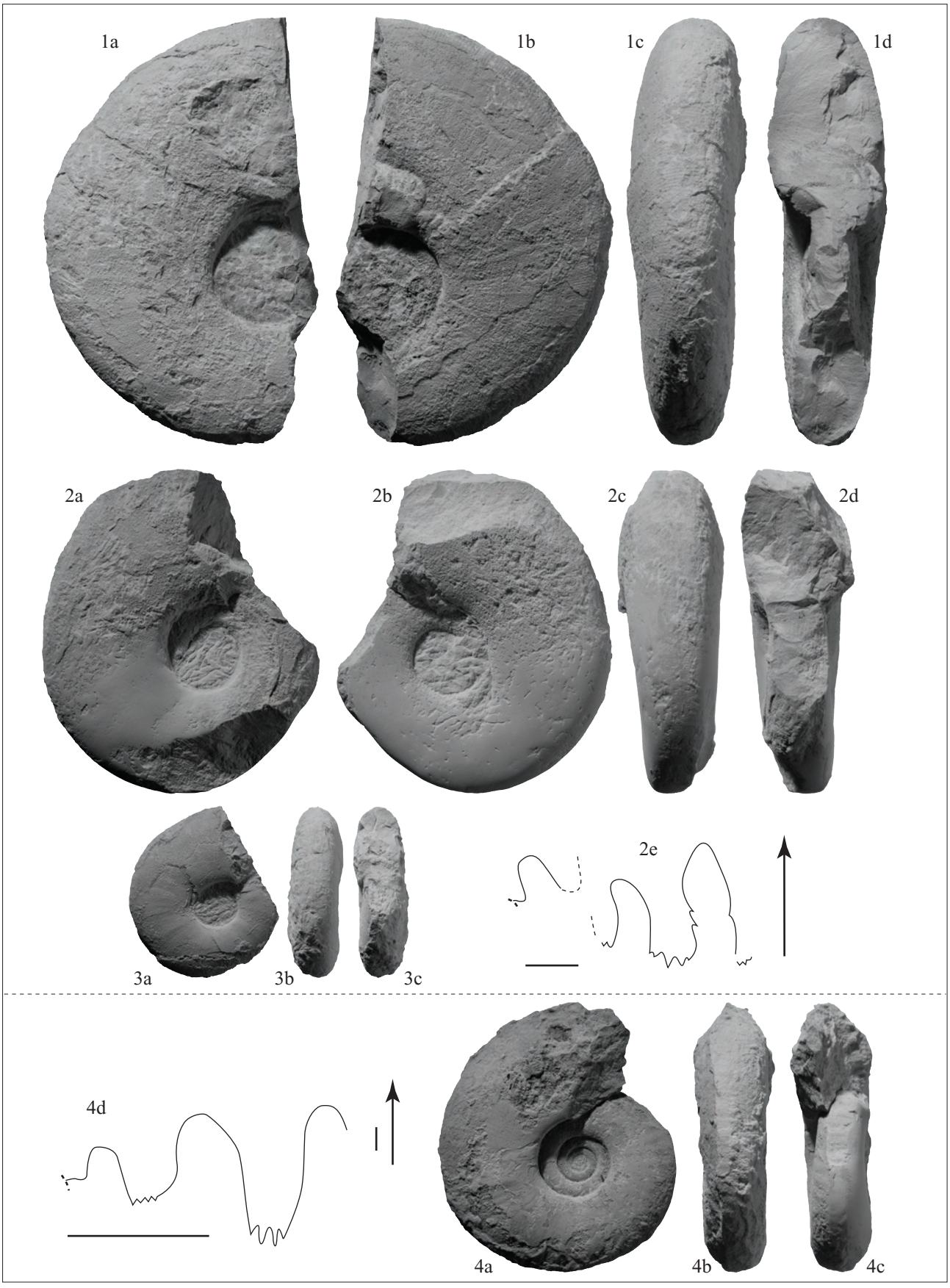

PLATE 16

(All figures natural size)

Figs. 1a-d: ***Gyronites* cf. *G. superior*** Waagen, 1895. PIMUZ 25966.
Loc. Jin61, Waili, "*Kashmirites densistriatus* beds", Smithian.
a-c) Lateral, ventral and apertural views.
d) Suture line. Scale bar = 5 mm; H = 21 mm.

Figs. 2a-d: ***Gyronites* cf. *G. superior*** Waagen, 1895. PIMUZ 25967.
Loc. Jin61, Waili, "*Kashmirites densistriatus* beds", Smithian.

Figs. 3a-c: ***Gyronites* cf. *G. superior*** Waagen, 1895. PIMUZ 25968.
Loc. Jin66, Waili, "*Kashmirites densistriatus* beds", Smithian.

Figs. 4a-c: ***Dieneroceras tientungense*** Chao, 1959. PIMUZ 25969.
Loc. Jin13, Jinya, "*Flemingites rursiradiatus* beds", Smithian.

Figs. 5a-d: ***Dieneroceras tientungense*** Chao, 1959. PIMUZ 25970.
Loc. Jin13, Jinya, "*Flemingites rursiradiatus* beds", Smithian.

Figs. 6a-c: ***Dieneroceras tientungense*** Chao, 1959. PIMUZ 25971.
Loc. Jin13, Jinya, "*Flemingites rursiradiatus* beds", Smithian.

Figs. 7a-c: ***Dieneroceras tientungense*** Chao, 1959. PIMUZ 25972.
Loc. Jin30, Jinya, "*Flemingites rursiradiatus* beds", Smithian.

Figs. 8a-c: ***Dieneroceras tientungense*** Chao, 1959. PIMUZ 25973.
Loc. Jin29, Jinya, "*Flemingites rursiradiatus* beds", Smithian.

Figs. 9a-c: ***Dieneroceras tientungense*** Chao, 1959. PIMUZ 25974.
Loc. Jin30, Jinya, "*Flemingites rursiradiatus* beds", Smithian.

Figs. 10a-b: ***Dieneroceras tientungense*** Chao, 1959. PIMUZ 25975.
Loc. Jin30, Jinya, "*Flemingites rursiradiatus* beds", Smithian.

Fig. 11: Suture line of ***Dieneroceras tientungense*** Chao, 1959. PIMUZ 25976.
Loc. Jin30, Jinya, "*Flemingites rursiradiatus* beds", Smithian.
Scale bar = 5 mm; D = 25 mm.

Fig. 12: Suture line of ***Dieneroceras tientungense*** Chao, 1959. PIMUZ 25977.
Loc. Jin28, Jinya, "*Flemingites rursiradiatus* beds", Smithian.
Scale bar = 5 mm; D = 40 mm.

PLATE 16


1a
1b
1c
2a
2b
2c
2d
3a
3b
3c
1d
4a
4b
4c
5a
5b
5c
5d
6a
6b
6c
7a
7b
7c
8a
8b
8c
9a
9b
9c
10a
10b
11
12

PLATE 17

(All figures natural size)

Figs. 1a-d: ***Wyomingites aplanatus*** (White, 1879). PIMUZ 25978.
Loc. Jin28, Jinya, "*Flemingites rursiradiatus* beds", Smithian.
a-c) Lateral, ventral and apertural views.
d) Suture line. Scale bar = 5 mm; H = 8 mm.

Figs. 2a-c: ***Wyomingites aplanatus*** (White, 1879). PIMUZ 25979.
Loc. Jin30, Jinya, "*Flemingites rursiradiatus* beds", Smithian.

Figs. 3a-c: ***Wyomingites aplanatus*** (White, 1879). PIMUZ 25980.
Loc. Jin30, Jinya, "*Flemingites rursiradiatus* beds", Smithian.

Figs. 4a-c: ***Submeekoceras mushbachanum*** (White, 1879). PIMUZ 25981.
Loc. Jin30, Jinya, "*Flemingites rursiradiatus* beds", Smithian.

PLATE 17

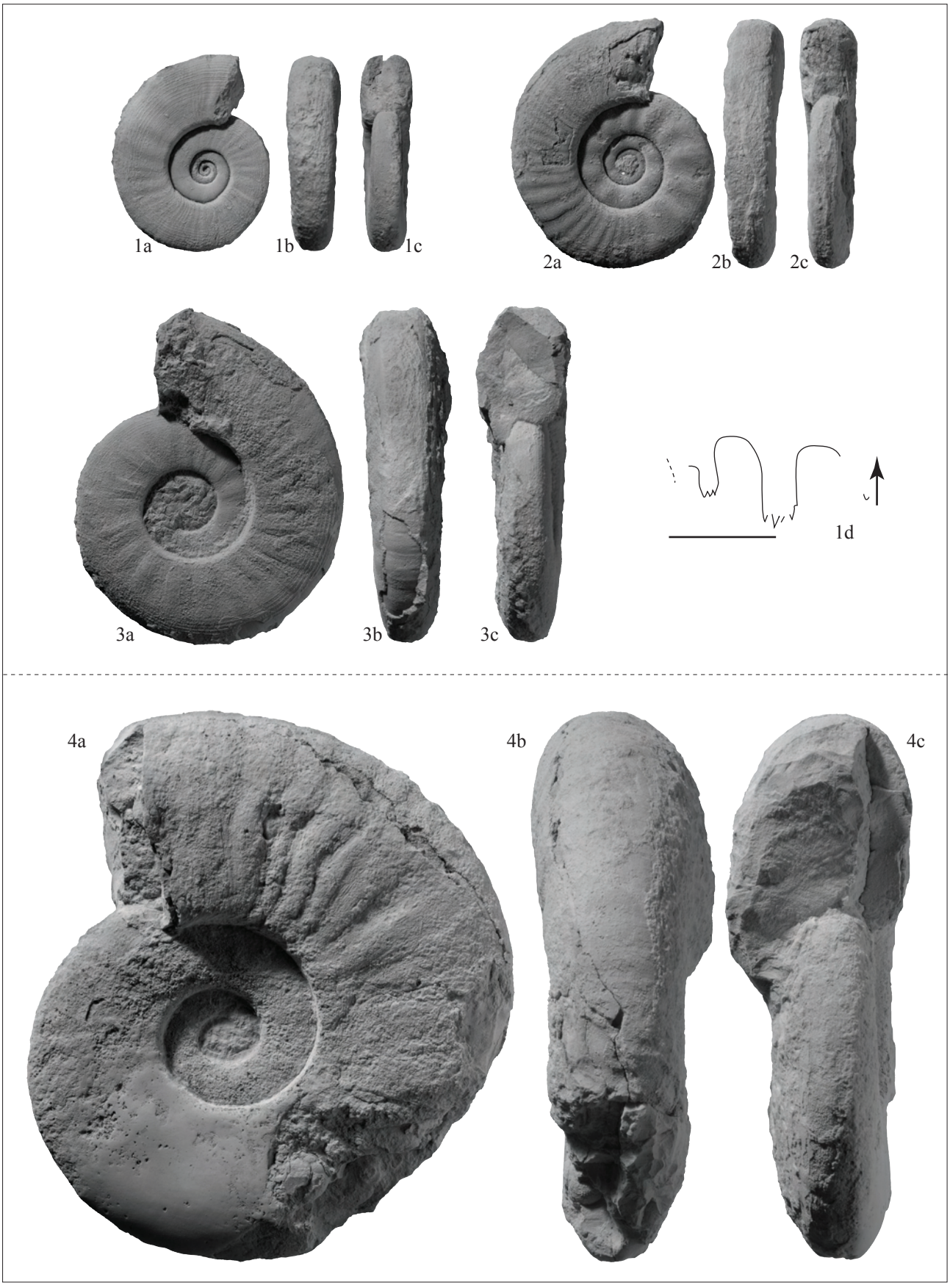

PLATE 18

(All figures natural size unless otherwise indicated)

Figs. 1a-c: ***Flemingites flemingianus*** (de Koninck, 1863). PIMUZ 25982.
Loc. Jin30, Jinya, "*Flemingites rursiradiatus* beds", Smithian.

Figs. 2a-c: ***Flemingites flemingianus*** (de Koninck, 1863). PIMUZ 25983. Scale ×0.5.
Loc. Jin15, Jinya, "*Flemingites rursiradiatus* beds", Smithian.

Figs. 3a-c: ***Flemingites flemingianus*** (de Koninck, 1863). PIMUZ 25984.
Loc. Jin30, Jinya, "*Flemingites rursiradiatus* beds", Smithian.

Figs. 4a-c: ***Flemingites flemingianus*** (de Koninck, 1863). PIMUZ 25985.
Loc. Jin30, Jinya, "*Flemingites rursiradiatus* beds", Smithian.

Figs. 5a-d: ***Flemingites flemingianus*** (de Koninck, 1863). PIMUZ 25986.
Loc. FW5, Waili, "*Flemingites rursiradiatus* beds", Smithian.
a-c) Lateral, ventral and apertural views.
d) Suture line. Scale bar = 5 mm; H = 20 mm.

PLATE 18

PLATE 19

(All figures natural size unless otherwise indicated)

Figs. 1a-c: ***Flemingites rursiradiatus*** Chao, 1959. PIMUZ 25987. Scale ×0.5.
Loc. Jin28, Jinya, "*Flemingites rursiradiatus* beds", Smithian.

Figs. 2a-c: ***Flemingites rursiradiatus*** Chao, 1959. PIMUZ 25988. Scale ×2.
Loc. Jin30, Jinya, "*Flemingites rursiradiatus* beds", Smithian.

Figs. 3a-c: ***Flemingites rursiradiatus*** Chao, 1959. PIMUZ 25989.
Loc. Jin30, Jinya, "*Flemingites rursiradiatus* beds", Smithian.

Figs. 4a-c: ***Flemingites rursiradiatus*** Chao, 1959. PIMUZ 25990.
Loc. Jin29, Jinya, "*Flemingites rursiradiatus* beds", Smithian.

Figs. 5a-c: ***Flemingites rursiradiatus*** Chao, 1959. PIMUZ 25991. Scale ×0.75.
Loc. Jin30, Jinya, "*Flemingites rursiradiatus* beds", Smithian.

Figs. 6a-c: ***Flemingites rursiradiatus*** Chao, 1959. PIMUZ 25992.
Loc. Jin29, Jinya, "*Flemingites rursiradiatus* beds", Smithian.

Fig. 7: Suture line of ***Flemingites rursiradiatus*** Chao, 1959. PIMUZ 25993.
Loc. Jin41, Jinya, "*Flemingites rursiradiatus* beds", Smithian.
Scale bar = 5 mm; H = 21 mm.

PLATE 19

PLATE 20

(All figures natural size)

Figs. 1a-c: ***Flemingites rursiradiatus*** Chao, 1959. PIMUZ 25994. Polygonal variant.
Loc. Jin30, Jinya, "*Flemingites rursiradiatus* beds", Smithian.

Figs. 2a-c: ***Flemingites rursiradiatus*** Chao, 1959. PIMUZ 25995. Polygonal variant.
Loc. Jin28, Jinya, "*Flemingites rursiradiatus* beds", Smithian.

Figs. 3a-d: ***Flemingites rursiradiatus*** Chao, 1959. PIMUZ 25996. Polygonal variant.
Loc. Jin30, Jinya, "*Flemingites rursiradiatus* beds", Smithian.
a-c) Lateral, ventral and apertural views.
d) Suture line. Scale bar = 5 mm; H = 6 mm.

Figs. 4a-c: ***Flemingites radiatus*** Waagen, 1895. PIMUZ 25997.
Loc. Jin28, Jinya, "*Flemingites rursiradiatus* beds", Smithian.

Figs. 5a-c: ***Flemingites radiatus*** Waagen, 1895. PIMUZ 25998.
Loc. Jin28, Jinya, "*Flemingites rursiradiatus* beds", Smithian.

Figs. 6a-c: ***Flemingites radiatus*** Waagen, 1895. PIMUZ 25999.
Loc. Jin28, Jinya, "*Flemingites rursiradiatus* beds", Smithian.

Figs. 7a-c: ***Flemingites*** **sp. indet.** PIMUZ 26000.
Loc. Jin67, Waili, "*Kashmirites densistriatus* beds", Smithian.

PLATE 20

PLATE 21

(All figures natural size)

Figs. 1a-d: ***Galfettites simplicitatis*** n. gen., n. sp. PIMUZ 26001. Paratype.
Loc. Jin27, Jinya, "*Owenites koeneni* beds", Smithian.
a-c) Lateral, ventral and apertural views.
d) Suture line. Scale bar = 5 mm; H = 23 mm.

Figs. 2a-d: ***Galfettites simplicitatis*** n. gen., n. sp. PIMUZ 26002. Holotype.
Loc. Jin27, Jinya, "*Owenites koeneni* beds", Smithian.
a-c) Lateral, ventral and apertural views.
d) Suture line. Scale bar = 5 mm; H = 30 mm.

PLATE 21

PLATE 22

(All figures natural size)

Figs. 1a-b: ***Pseudoflemingites goudemandi*** n. sp. PIMUZ 26003. Paratype.
Loc. Jin99, Jinya, "*Owenites koeneni* beds", Smithian.

Figs. 2a-d: ***Pseudoflemingites goudemandi*** n. sp. PIMUZ 26004. Holotype.
Loc. Jin99, Jinya, "*Owenites koeneni* beds", Smithian.
a-c) Lateral, ventral and apertural views.
d) Suture line. Scale bar = 5 mm; H = 12 mm.

Figs. 3a-c: ***Pseudoflemingites goudemandi*** n. sp. PIMUZ 26005. Paratype.
Loc. Jin99, Jinya, "*Owenites koeneni* beds", Smithian.

Figs. 4a-c: ***Pseudoflemingites goudemandi*** n. sp. PIMUZ 26006. Paratype.
Loc. Jin99, Jinya, "*Owenites koeneni* beds", Smithian.

Figs. 5a-c: ***Pseudoflemingites goudemandi*** n. sp. PIMUZ 26007. Paratype.
Loc. Jin99, Jinya, "*Owenites koeneni* beds", Smithian.

Figs. 6a-d: ***Juvenites procurvus*** n. sp. PIMUZ 26008.
Loc. T5, Tsoteng, "*Owenites koeneni* beds", Smithian.
a-c) Lateral, ventral and apertural views.
d) Suture line. Scale bar = 5 mm; H = 5 mm.

Figs. 7a-c: ***Juvenites procurvus*** n. sp. PIMUZ 26009.
Loc. T5, Tsoteng, "*Owenites koeneni* beds", Smithian.

Figs. 8a-d: ***Juvenites procurvus*** n. sp. PIMUZ 26010. Holotype.
Loc. T11, Tsoteng, "*Owenites koeneni* beds", Smithian.

Figs. 9a-c: ***Juvenites procurvus*** n. sp. PIMUZ 26011.
Loc. Yu3, Yuping, "*Owenites koeneni* beds", Smithian.

Figs. 10a-c: ***Juvenites procurvus*** n. sp. PIMUZ 26012.
Loc. Yu3, Yuping, "*Owenites koeneni* beds", Smithian.

Figs. 11a-c: ***Juvenites procurvus*** n. sp. PIMUZ 26013.
Loc. Jin45, Jinya, "*Owenites koeneni* beds", Smithian.

Figs. 12a-c: ***Juvenites procurvus*** n. sp. PIMUZ 26014.
Loc. Jin45, Jinya, "*Owenites koeneni* beds", Smithian.

PLATE 22


1a
1b
2a
2b
2c
3a
3b
3c
4a
4b
4c
5a
5b
5c
2d
6a
6b
6c
7a
7b
7c
8a
8b
8c
8d
9a
9b
9c
10a
10b
10c
11a
11b
11c
12a
12b
12c
6d

PLATE 23

(All figures natural size unless otherwise indicated)

Figs. 1a-b: **?*Anaxenaspis* sp. indet.** PIMUZ 26015. Scale ×0.75.
Loc. Jin45, Jinya, "*Owenites koeneni* beds", Smithian.

Figs. 2a-e: ***Guangxiceras inflata*** n. gen., n. sp. PIMUZ 26016. Scale ×0.75. Holotype.
Loc. Jin27, Jinya, "*Owenites koeneni* beds", Smithian.
a-d) Lateral, ventral and apertural views.
e) Suture line. Scale bar = 5 mm; H = 25 mm.

PLATE 23

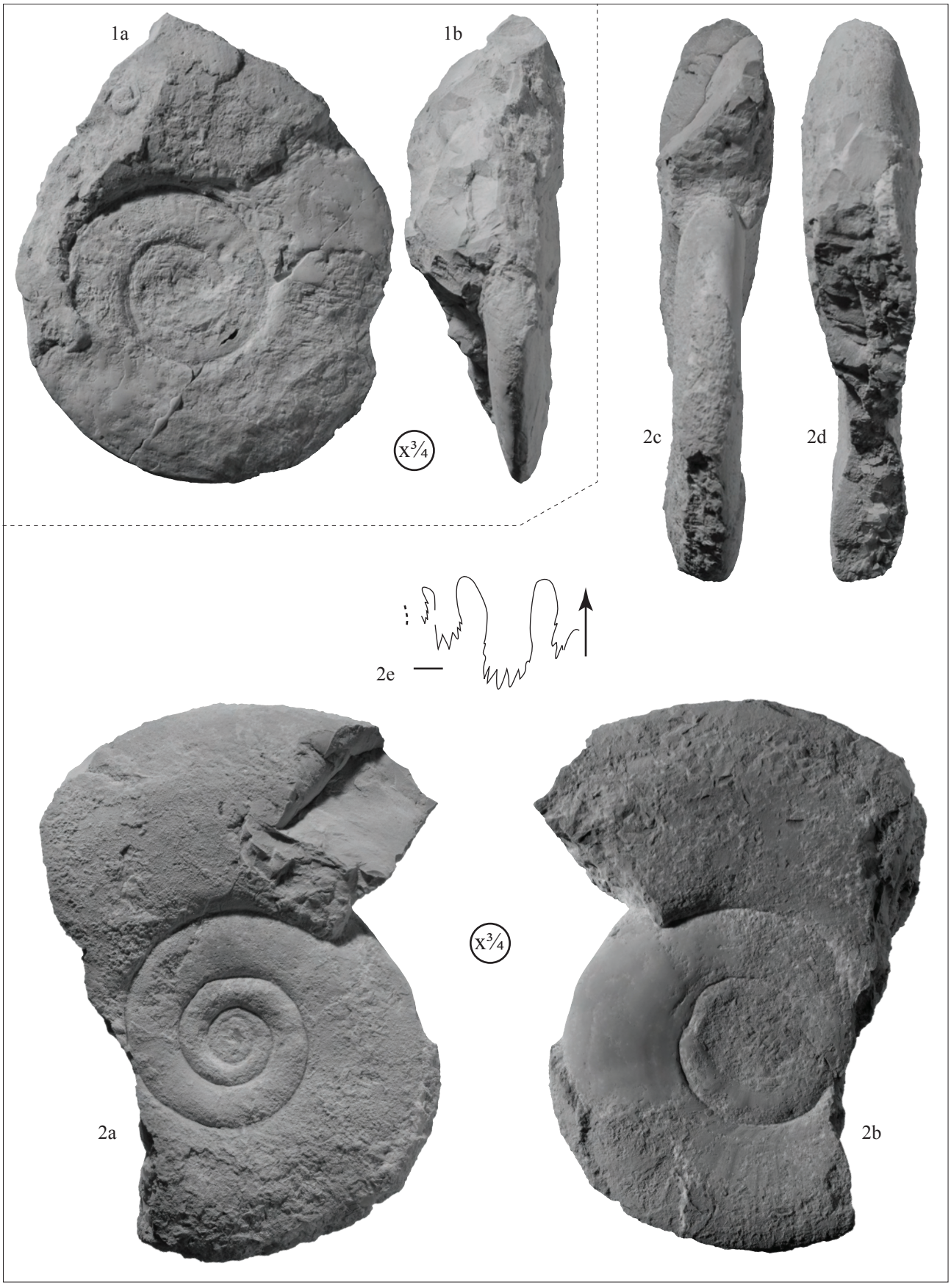

PLATE 24

(All figures natural size unless otherwise indicated)

Figs. 1a-d: ***Larenites* cf. *L. reticulatus*** (Tozer, 1994). PIMUZ 26017.
Loc. Jin66, Waili, "*Flemingites rursiradiatus* beds", Smithian.
Fig. 1d: Scale ×3.

Figs. 2a-c: ***Larenites* cf. *L. reticulatus*** (Tozer, 1994). PIMUZ 26018.
Loc. Jin66, Waili, "*Flemingites rursiradiatus* beds", Smithian.

Figs. 3a-c: ***Anaflemingites hochulii*** n. sp. PIMUZ 26019. Paratype.
Loc. Jin45, Jinya, "*Owenites koeneni* beds", Smithian.

Figs. 4a-d: ***Anaflemingites hochulii*** n. sp. PIMUZ 26020. Paratype.
Loc. Jin45, Jinya, "*Owenites koeneni* beds", Smithian.

Figs. 5a-d: ***Anaflemingites hochulii*** n. sp. PIMUZ 26021. Holotype.
Loc. Jin45, Jinya, "*Owenites koeneni* beds", Smithian.
a-c) Lateral, ventral and apertural views.
d) Suture line. Scale bar = 5 mm; H = 11 mm.

Figs. 6a-c: ***Anaflemingites hochulii*** n. sp. PIMUZ 26022. Paratype.
Loc. Jin45, Jinya, "*Owenites koeneni* beds", Smithian.

PLATE 24

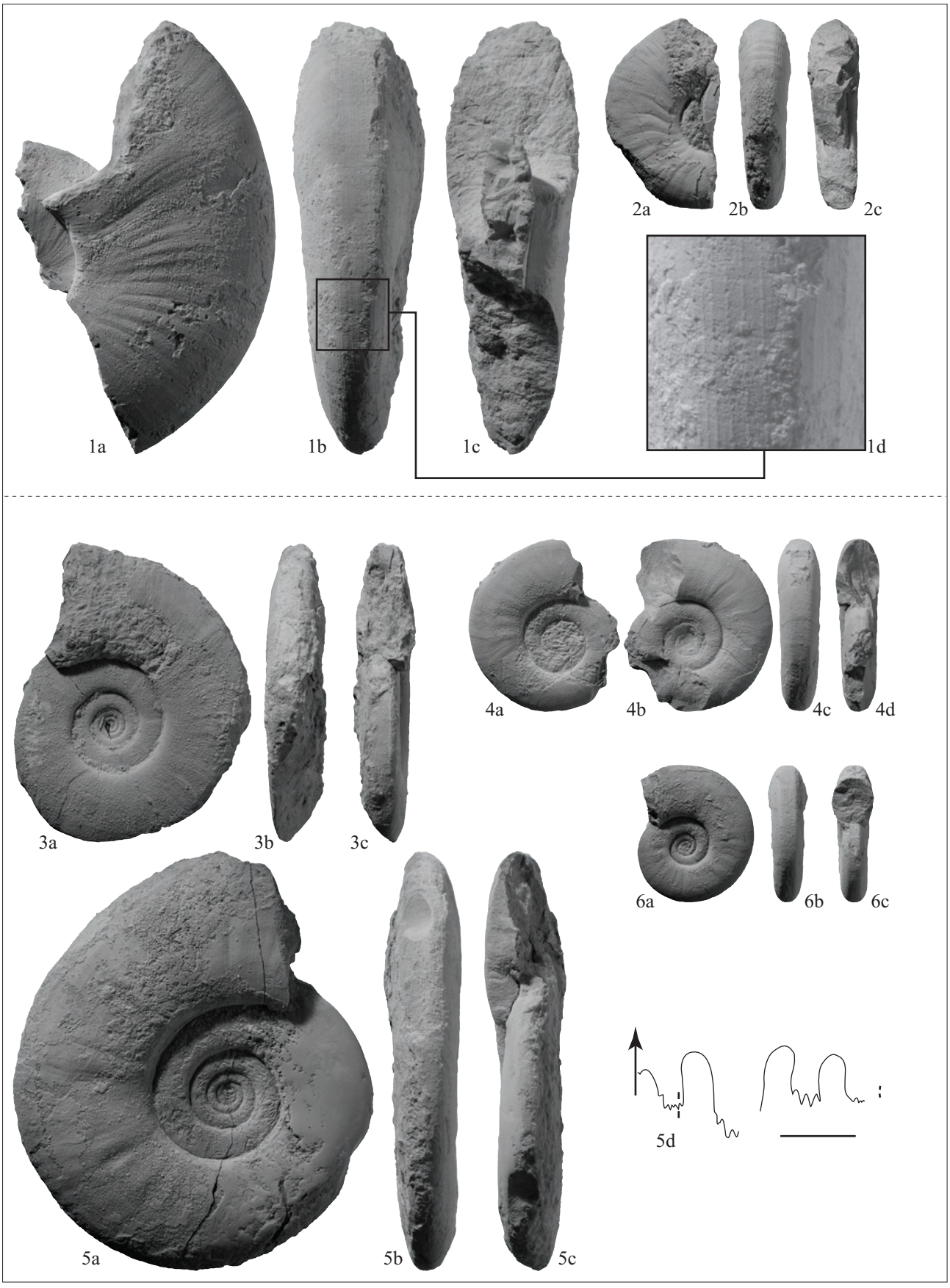

PLATE 25

(All figures natural size)

Figs. 1a-b: ***Arctoceras strigatus*** n. sp. PIMUZ 26023. Holotype.
Loc. Jin15, Jinya, "*Flemingites rursiradiatus* beds", Smithian.

Figs. 2a-d: ***Arctoceras strigatus*** n. sp. PIMUZ 26024.
Loc. FSB1/2, Jinya, "*Flemingites rursiradiatus* beds", Smithian.
a-c) Lateral, ventral and apertural views.
d) Suture line. Scale bar = 5 mm; H = 12 mm.

Figs. 3a-c: ***Metussuria* sp. indet.** PIMUZ 26025. Scale ×0.75.
Loc. Jin27, Jinya, "*Owenites koeneni* beds", Smithian.

Figs. 4a-b: ***Metussuria* sp. indet.** PIMUZ 26026.
Loc. Jin27, Jinya, "*Owenites koeneni* beds", Smithian.

Figs. 5a-b: ***Metussuria* sp. indet.** PIMUZ 26027.
Loc. Jin27, Jinya, "*Owenites koeneni* beds", Smithian.

Figs. 6a-b: ***Metussuria* sp. indet.** PIMUZ 26028.
Loc. Jin27, Jinya, "*Owenites koeneni* beds", Smithian.

Fig. 7: Suture line of ***Metussuria* sp. indet.**, PIMUZ 26029.
Loc. Jin27, Jinya, "*Owenites koeneni* beds", Smithian.
Scale bar = 5 mm; H = 37 mm.

Fig. 8: Suture line of ***Metussuria* sp. indet.**, PIMUZ 26030.
Loc. Jin27, Jinya, "*Owenites koeneni* beds", Smithian.
Scale bar = 5 mm; H = 45 mm.

PLATE 25

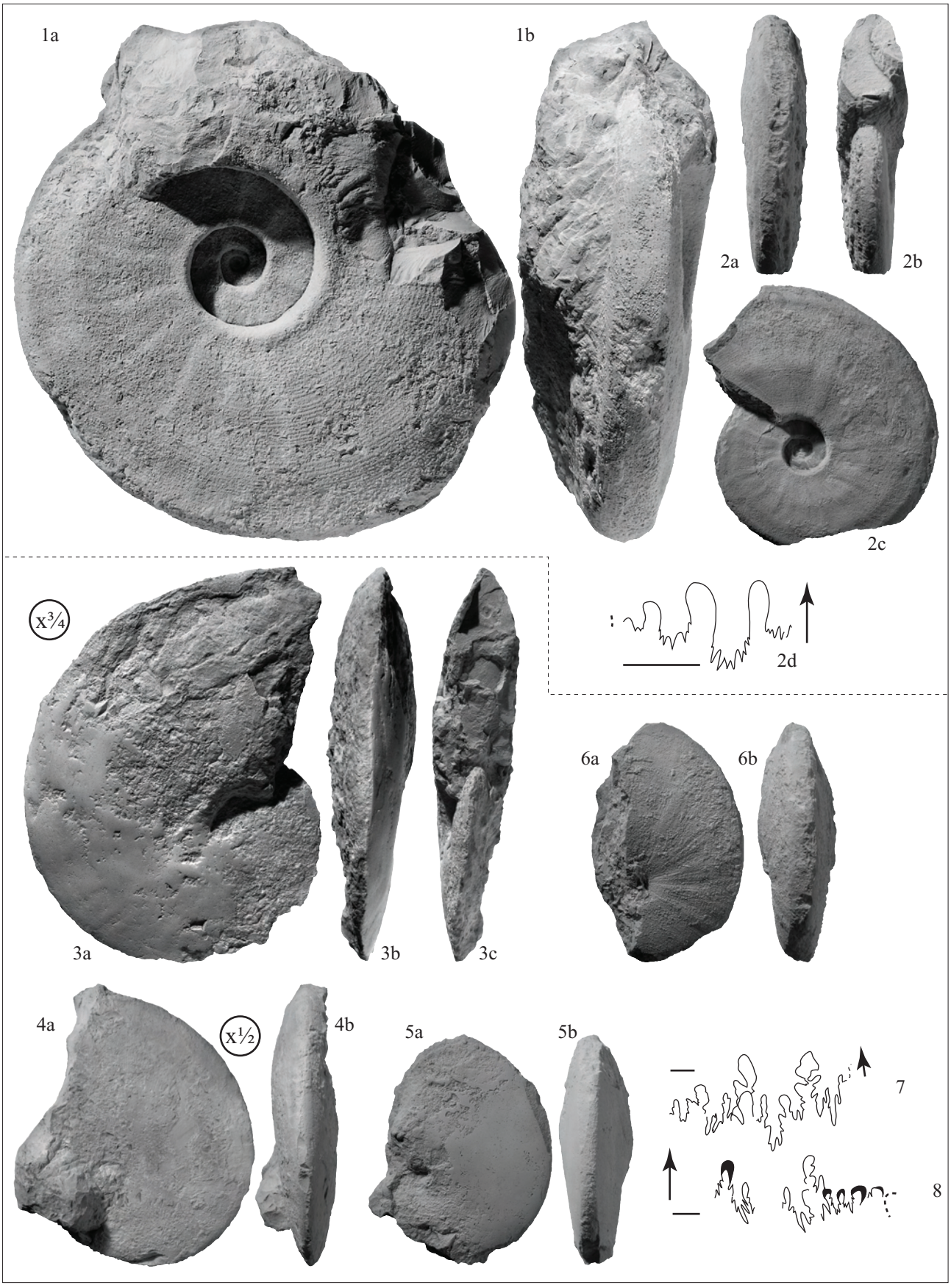

PLATE 26

(All figures natural size unless otherwise indicated)

Figs. 1a-d: ***Submeekoceras mushbachanum*** (White, 1879). PIMUZ 26031.
Loc. Jin28, Jinya, "*Flemingites rursiradiatus* beds", Smithian.

Figs. 2a-c: ***Submeekoceras mushbachanum*** (White, 1879). PIMUZ 26032.
Loc. Jin28, Jinya, "*Flemingites rursiradiatus* beds", Smithian.

Figs. 3a-c: ***Submeekoceras mushbachanum*** (White, 1879). PIMUZ 26033.
Loc. Jin28, Jinya, "*Flemingites rursiradiatus* beds", Smithian.

Figs. 4a-c: ***Submeekoceras mushbachanum*** (White, 1879). PIMUZ 26034.
Loc. Jin28, Jinya, "*Flemingites rursiradiatus* beds", Smithian.

Figs. 5a-d: ***Submeekoceras mushbachanum*** (White, 1879). PIMUZ 26035.
Loc. Jin28, Jinya, "*Flemingites rursiradiatus* beds", Smithian.
a-c) Lateral, ventral and apertural views.
d) Suture line. Scale bar = 5 mm; H = 10 mm.

Figs. 6a-c: ***Submeekoceras mushbachanum*** (White, 1879). PIMUZ 26036.
Loc. Jin28, Jinya, "*Flemingites rursiradiatus* beds", Smithian.

Figs. 7a-b: ***Submeekoceras mushbachanum*** (White, 1879). PIMUZ 26037. Scale ×0.75.
Loc. Jin13, Jinya, "*Flemingites rursiradiatus* beds", Smithian.

Figs. 8a-c: ***Submeekoceras mushbachanum*** (White, 1879). PIMUZ 26038.
Loc. Sha1, Shanggan, "*Flemingites rursiradiatus* beds", Smithian.

Fig. 9: Suture line of ***Submeekoceras mushbachanum*** (White, 1879). PIMUZ 26039.
Loc. Jin28, Jinya, "*Flemingites rursiradiatus* beds", Smithian.
Scale bar = 5 mm; H = 25 mm.

PLATE 26


1a
1b
1c
1d
2a
2b
2c
3a
3b
3c
4a
4b
4c
5a
5b
5c
6a
6b
6c
7a
7b
X3/4
8a
8b
8c
5d
9

PLATE 27

(All figures natural size unless otherwise indicated)

Figs. 1a-d: ***Ussuria kwangsiana*** Chao, 1959. PIMUZ 26040.
Loc. Jin45, Jinya, "*Owenites koeneni* beds", Smithian.
a-c) Lateral, ventral and apertural views. Scale ×0.75.
d) Suture line. Scale bar = 5 mm; H = 30 mm.

Figs. 2a-c: ***Ussuria kwangsiana*** Chao, 1959. PIMUZ 26041. Scale ×0.75.
Loc. Jin45, Jinya, "*Owenites koeneni* beds", Smithian.

Figs. 3a-c: ***Ussuria kwangsiana*** Chao, 1959. PIMUZ 26042. Scale ×0.75.
Loc. Jin45, Jinya, "*Owenites koeneni* beds", Smithian.

Figs. 4a-c: ***Arctoceras* sp. indet.**. PIMUZ 26043. Scale ×0.5.
Loc. FW5, Waili, "*Flemingites rursiradiatus* beds", Smithian.

PLATE 27

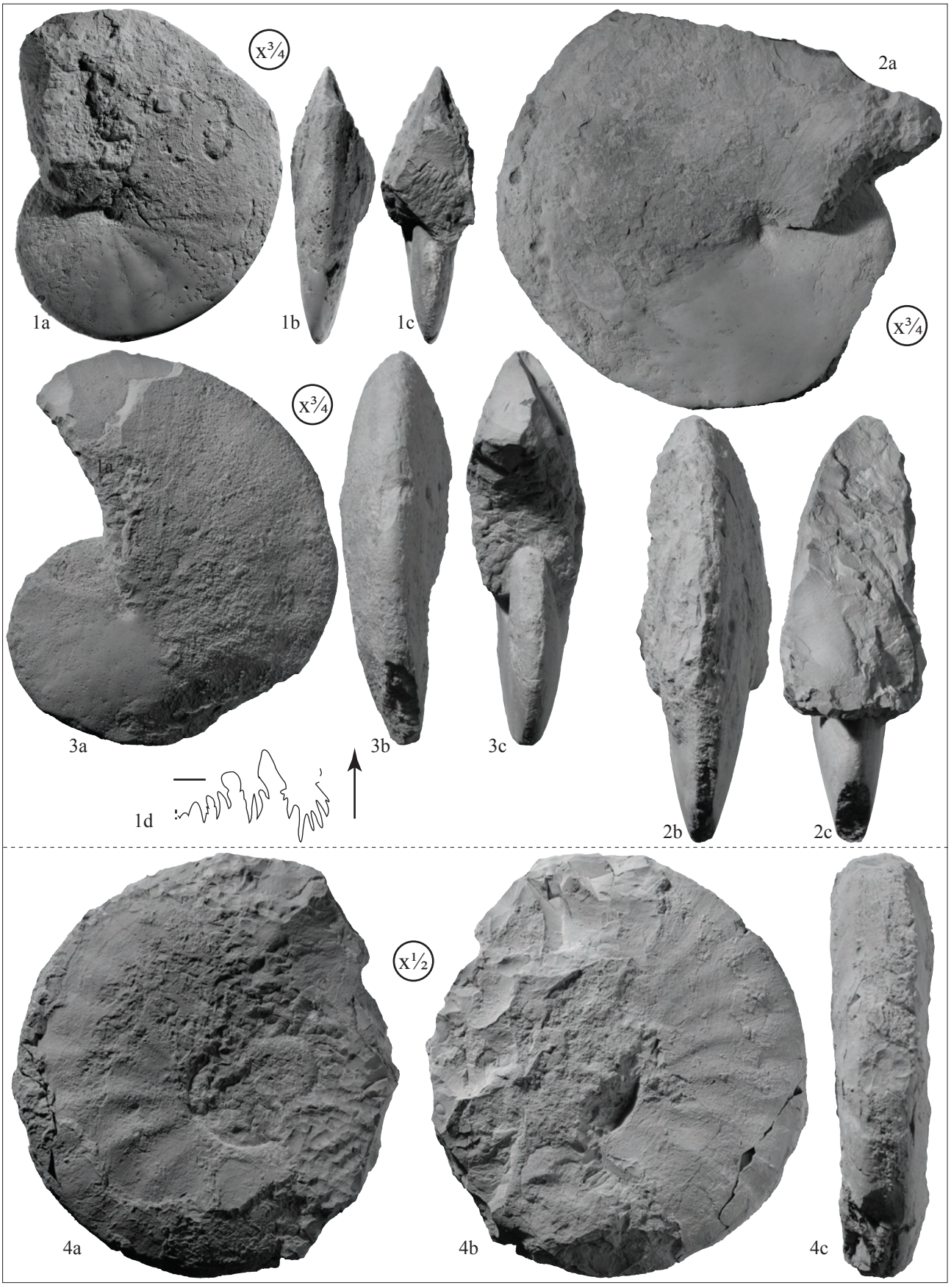

PLATE 28

(All figures natural size unless otherwise indicated)

Figs. 1a-b: ***Anasibirites multiformis*** Welter, 1922. PIMUZ 26044. Scale ×0.75.
Loc. Jin48, Jinya, "*Anasibirites multiformis* beds", Smithian.

Figs. 2a-c: ***Anasibirites multiformis*** Welter, 1922. PIMUZ 26045.
Loc. Jin48, Jinya, "*Anasibirites multiformis* beds", Smithian.

Figs. 3a-b: ***Anasibirites multiformis*** Welter, 1922. PIMUZ 26046.
Loc. Jin101, Jinya, "*Anasibirites multiformis* beds", Smithian.

Figs. 4a-c: ***Anasibirites multiformis*** Welter, 1922. PIMUZ 26047.
Loc. Jin101, Jinya, "*Anasibirites multiformis* beds", Smithian.

Figs. 5a-b: ***Anasibirites multiformis*** Welter, 1922. PIMUZ 26048.
Loc. FW6, Waili, "*Anasibirites multiformis* beds", Smithian.

Fig. 6: Suture line of ***Anasibirites multiformis*** Welter, 1922. PIMUZ 26049.
Loc. FW6, Waili, "*Anasibirites multiformis* beds", Smithian.
Scale bar = 5 mm; H = 13 mm.

Figs. 7a-c: ***Anasibirites evolutus*** n. sp. PIMUZ 26050.
Loc. Jin16, Jinya, "*Anasibirites multiformis* beds", Smithian.

Figs. 8a-d: ***Anasibirites evolutus*** n. sp. PIMUZ 26051. Holotype.
Loc. FW6, Waili, "*Anasibirites multiformis* beds", Smithian.

Figs. 9a-c: ***Anasibirites evolutus*** n. sp. PIMUZ 26052. Paratype.
Loc. FW6, Waili, "*Anasibirites multiformis* beds", Smithian.

PLATE 28

PLATE 29
(All figures natural size)

Figs. 1a-c: ***Hemiprionites* cf. *H. butleri*** (Mathews, 1929). PIMUZ 26053.
Loc. Jin48, Jinya, "*Anasibirites multiformis* beds", Smithian.

Figs. 2a-e: ***Hemiprionites* cf. *H. butleri*** (Mathews, 1929). PIMUZ 26054.
Loc. Jin48, Jinya, "*Anasibirites multiformis* beds", Smithian.
a-d) Lateral, ventral and apertural views.
e) Suture line. Scale bar = 5 mm; H = 12 mm.

Figs. 3a-c: ***Hemiprionites* cf. *H. butleri*** (Mathews, 1929). PIMUZ 26055.
Loc. Jin48, Jinya, "*Anasibirites multiformis* beds", Smithian.

Figs. 4a-c: ***Hemiprionites* cf. *H. butleri*** (Mathews, 1929). PIMUZ 26056.
Loc. Jin48, Jinya, "*Anasibirites multiformis* beds", Smithian.

Figs. 5a-c: ***Hemiprionites* cf. *H. butleri*** (Mathews, 1929). PIMUZ 26057.
Loc. Jin48, Jinya, "*Anasibirites multiformis* beds", Smithian.

Figs. 6a-c: ***Hemiprionites* cf. *H. butleri*** (Mathews, 1929). PIMUZ 26058.
Loc. Jin16, Jinya, "*Anasibirites multiformis* beds", Smithian.

Figs. 7: ***Hemiprionites* cf. *H. butleri*** (Mathews, 1929). PIMUZ 26059.
Loc. Jin48, Jinya, "*Anasibirites multiformis* beds", Smithian.

Figs. 8a-d: ***Subvishnuites stokesi*** (Kummel & Steele, 1962). PIMUZ 26060.
Loc. Jin12, Jinya, "*Owenites koeneni* beds", Smithian.
a-c) Lateral, ventral and apertural views.
d) Suture line. Scale bar = 5 mm; H = 13 mm.

PLATE 29

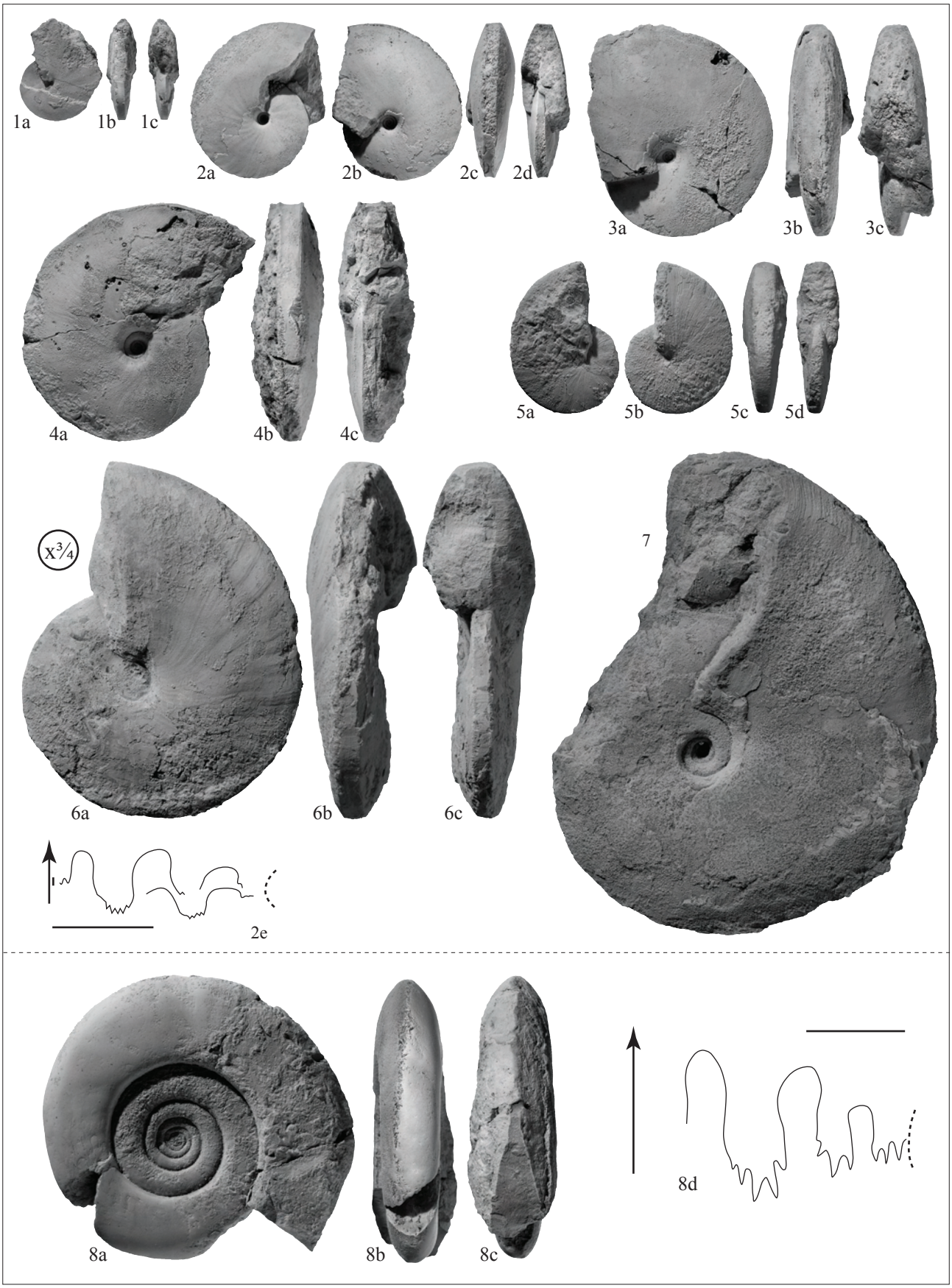
1a
1b
1c
2a
2b
2c
2d
3a
3b
3c
4a
4b
4c
5a
5b
5c
5d
x3/4
6a
6b
6c
7
2e
8a
8b
8c
8d

PLATE 30

(All figures natural size)

Figs. 1a-c: ***Hemiprionites klugi*** n. sp. PIMUZ 26061. Paratype.
Loc. Jin16, Waili, "*Anasibirites multiformis* beds", Smithian.

Figs. 2a-c: ***Hemiprionites klugi*** n. sp. PIMUZ 26062. Holotype.
Loc. FW6, Waili, "*Anasibirites multiformis* beds", Smithian.

Figs. 3a-c: ***Hemiprionites klugi*** n. sp. PIMUZ 26063.
Loc. FW6, Jinya, "*Anasibirites multiformis* beds", Smithian.

Fig. 4: Suture line of ***Hemiprionites klugi*** n. sp., PIMUZ 26064.
Loc. FW6, Waili, "*Anasibirites multiformis* beds", Smithian.
Scale bar = 5 mm; H = 15 mm.

Figs. 5a-c: ***Lanceolites compactus*** Hyatt & Smith, 1905. PIMUZ 26065.
Loc. Jin12, Jinya, "*Owenites koeneni* beds", Smithian.

Figs. 6a-d: ***Lanceolites bicarinatus*** Smith, 1932. PIMUZ 26066.
Loc. Yu7, Yuping, "*Owenites koeneni* beds", Smithian.
a-c) Lateral, ventral and apertural views.
d) Suture line. Scale bar = 5 mm; H = 17 mm.

PLATE 30

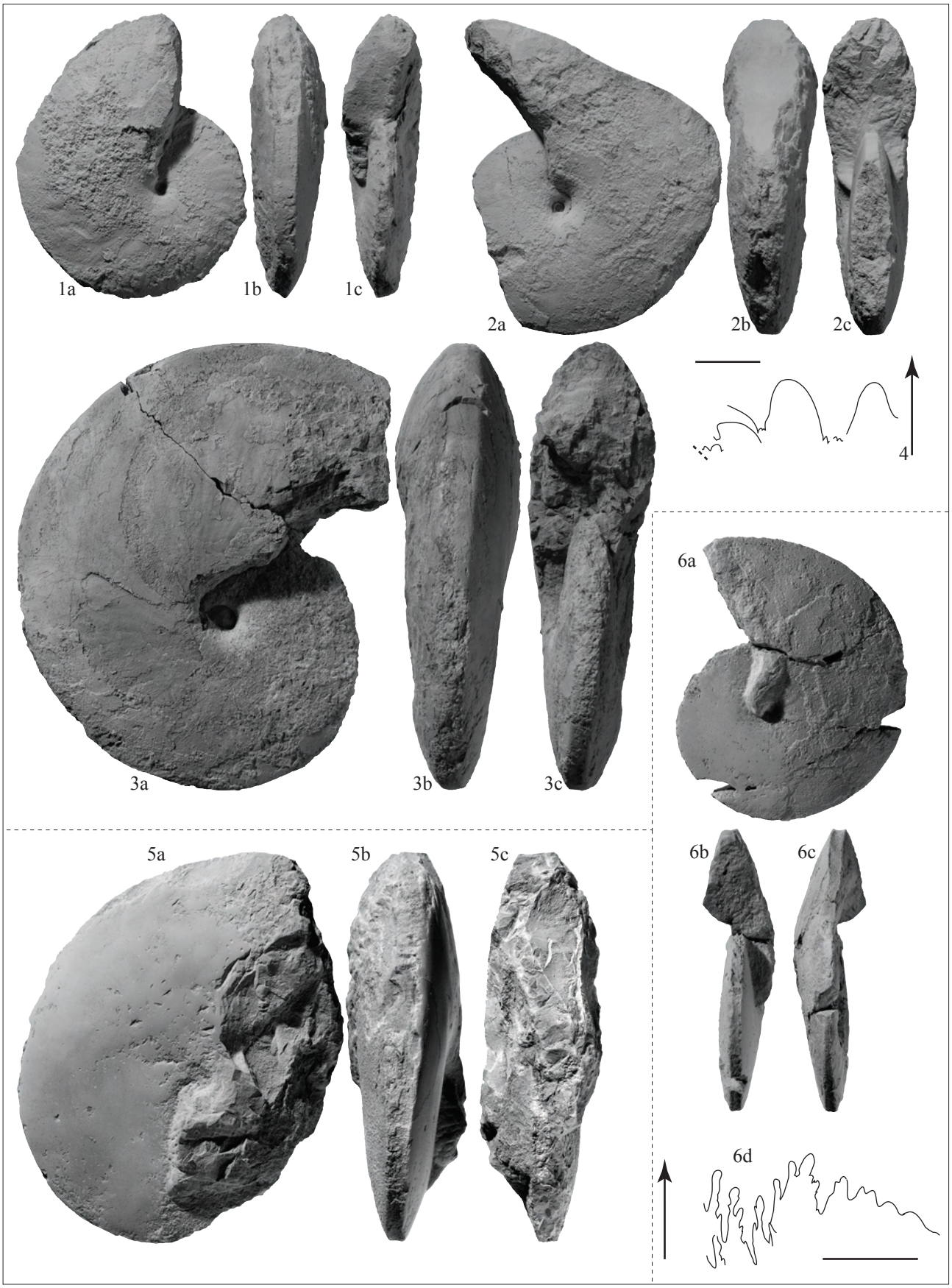

PLATE 31

(All figures natural size)

Figs. 1a-c: ***Inyoites krystyni*** n. sp. PIMUZ 26067. Holotype.
Loc. Yu3, Yuping, "*Owenites koeneni* beds", Smithian.

Figs. 2a-d: ***Inyoites krystyni*** n. sp. PIMUZ 26068. Paratype.
Loc. Yu3, Yuping, "*Owenites koeneni* beds", Smithian.

Figs. 3a-c: ***Inyoites krystyni*** n. sp. PIMUZ 26069.
Loc. Jin12, Jinya, "*Owenites koeneni* beds", Smithian.

Fig. 4: Suture line of ***Inyoites krystyni*** n. sp., PIMUZ 26070.
Loc. Jin99, Jinya, "*Owenites koeneni* beds", Smithian.
Scale bar = 5 mm; H = 27 mm.

PLATE 31

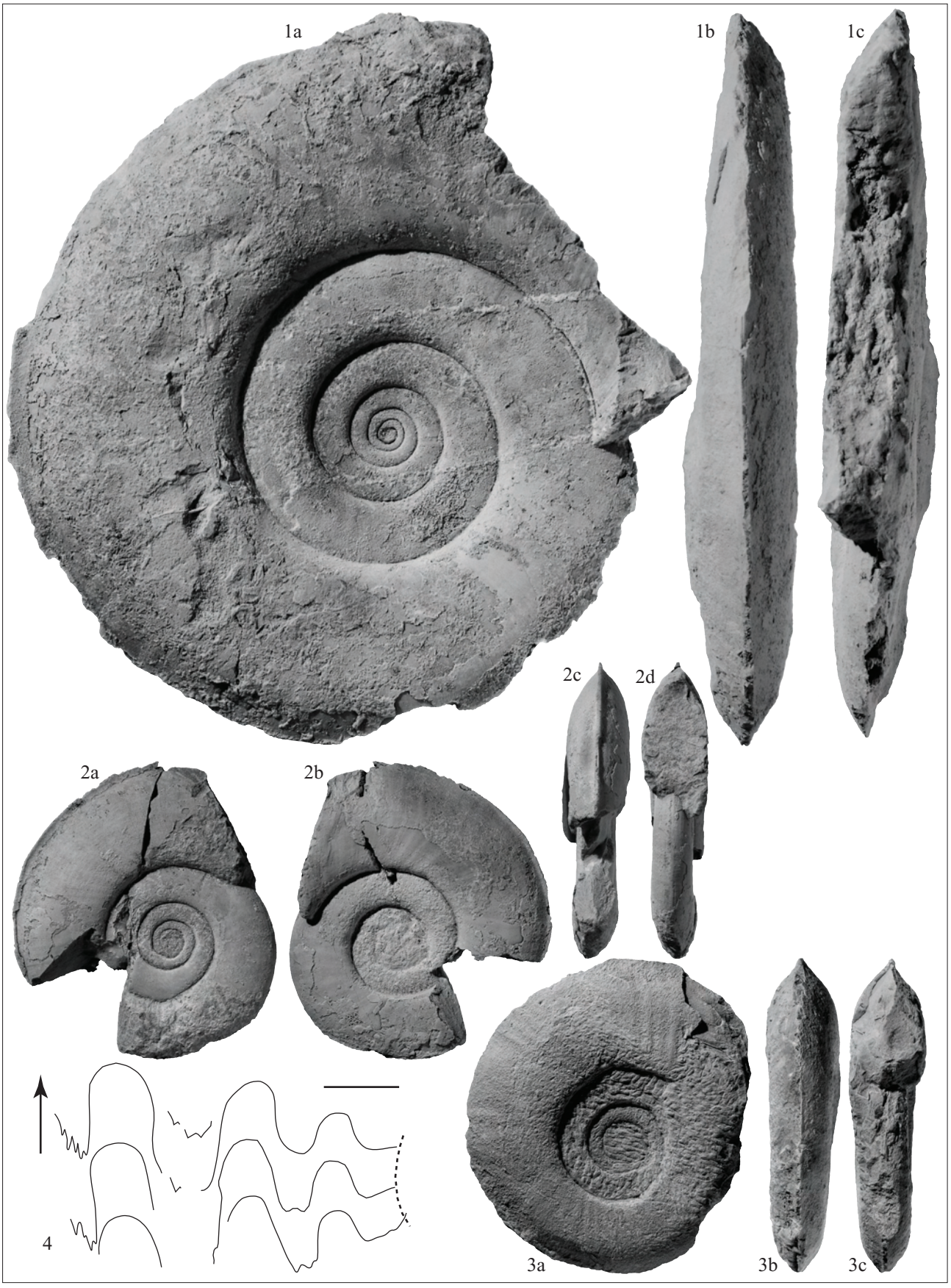

PLATE 32

(All figures natural size unless otherwise indicated)

Figs. 1a-c: ***Inyoites krystyni*** n. sp. PIMUZ 26070. Scale ×0.75.
Loc. Jin99, Jinya, "*Owenites koeneni* beds", Smithian.

Figs. 2a-c: ***Inyoites krystyni*** n. sp. PIMUZ 26071. Scale ×0.75.
Loc. Jin99, Jinya, "*Owenites koeneni* beds", Smithian.

PLATE 32

PLATE 33

(All figures natural size unless otherwise indicated)

Figs. 1a-c: ***Paranannites* aff. *P. aspenensis*** Hyatt & Smith, 1905. PIMUZ 26072.
Loc. Jin4, Jinya, "*Flemingites rursiradiatus* beds", Smithian.

Figs. 2a-c: ***Paranannites* aff. *P. aspenensis*** Hyatt & Smith, 1905. PIMUZ 26073.
Loc. FW5, Waili, "*Flemingites rursiradiatus* beds", Smithian.

Figs. 3a-c: ***Paranannites* aff. *P. aspenensis*** Hyatt & Smith, 1905. PIMUZ 26074.
Loc. Jin23, Jinya, "*Flemingites rursiradiatus* beds", Smithian.

Figs. 4a-c: ***Paranannites* aff. *P. aspenensis*** Hyatt & Smith, 1905. PIMUZ 26075.
Loc. Jin4, Jinya, "*Flemingites rursiradiatus* beds", Smithian.

Figs. 5a-c: ***Paranannites* aff. *P. aspenensis*** Hyatt & Smith, 1905. PIMUZ 26076.
Loc. FW5, Waili, "*Flemingites rursiradiatus* beds", Smithian.

Figs. 6a-c: ***Paranannites* aff. *P. aspenensis*** Hyatt & Smith, 1905. PIMUZ 26077.
Loc. Jin4, Jinya, "*Flemingites rursiradiatus* beds", Smithian.

Figs. 7a-d: ***Paranannites* aff. *P. aspenensis*** Hyatt & Smith, 1905. PIMUZ 26078.
Loc. Jin4, Jinya, "*Flemingites rursiradiatus* beds", Smithian.
a-c) Lateral, ventral and apertural views.
d) Suture line. Scale bar = 5 mm; H = 3 mm.

Figs. 8a-c: ***Paranannites* aff. *P. aspenensis*** Hyatt & Smith, 1905. PIMUZ 26079.
Loc. Jin30, Jinya, "*Flemingites rursiradiatus* beds", Smithian.

Figs. 9a-c: ***Paranannites* aff. *P. aspenensis*** Hyatt & Smith, 1905. PIMUZ 26080.
Loc. Jin28, Jinya, "*Flemingites rursiradiatus* beds", Smithian.

Figs. 10a-c: ***Paranannites* aff. *P. aspenensis*** Hyatt & Smith, 1905. PIMUZ 26081.
Loc. Jin4, Jinya, "*Flemingites rursiradiatus* beds", Smithian.

Figs. 11a-d: ***Paranannites dubius*** n. sp. PIMUZ 26082. Scale ×2. Paratype.
Loc. Jin4, Jinya, "*Flemingites rursiradiatus* beds", Smithian.

Figs. 12a-d: ***Paranannites dubius*** n. sp. PIMUZ 26083. Scale ×2. Paratype.
Loc. Jin4, Jinya, "*Flemingites rursiradiatus* beds", Smithian.
a-c) Lateral, ventral and apertural views.
d) Suture line. Scale bar = 5 mm; H = 12 mm.

Figs. 13a-c: ***Paranannites dubius*** n. sp. PIMUZ 26084. Scale ×2. Holotype.
Loc. Jin4, Jinya, "*Flemingites rursiradiatus* beds", Smithian.

Figs. 14a-c: ***Paranannites dubius*** n. sp. PIMUZ 26085. Scale ×2. Paratype.
Loc. Jin4, Jinya, "*Flemingites rursiradiatus* beds", Smithian.

Figs. 15a-d: **Paranannitidae gen. indet.** PIMUZ 26086.
Loc. Jin30, Jinya, "*Flemingites rursiradiatus* beds", Smithian.
a-c) Lateral, ventral and apertural views.
d) Suture line. Scale bar = 5 mm; H = 3 mm.

PLATE 33

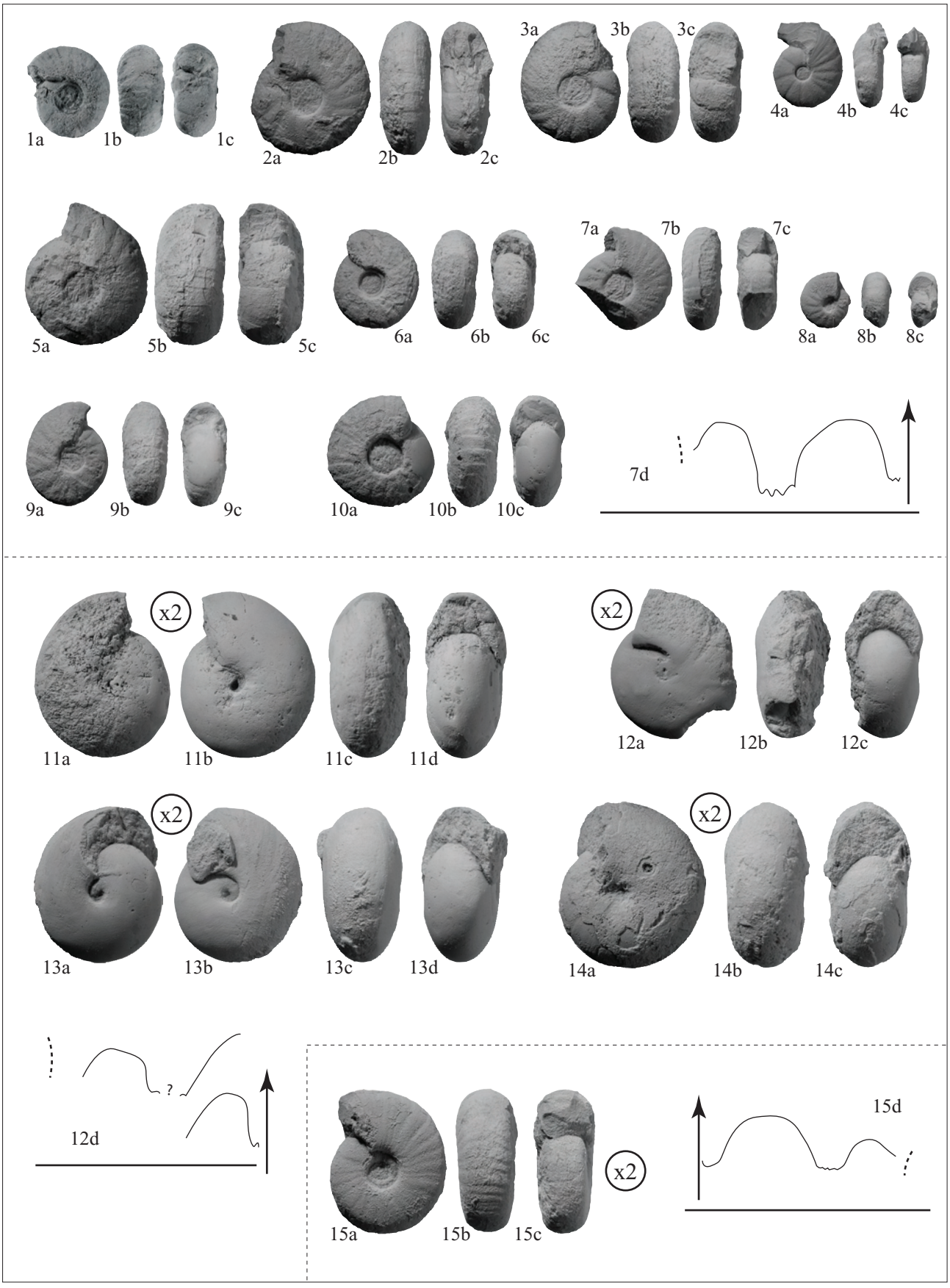
1a
1b
1c
2a
2b
2c
3a
3b
3c
4a
4b
4c
5a
5b
5c
6a
6b
6c
7a
7b
7c
8a
8b
8c
9a
9b
9c
10a
10b
10c
7d
x2
11a
11b
11c
11d
x2
12a
12b
12c
x2
13a
13b
13c
13d
x2
14a
14b
14c
12d
?
15a
15b
15c
x2
15d

PLATE 34

(All figures natural size)

Figs. 1a-d: ***Paranannites ovum*** n. sp. PIMUZ 26087. Paratype.
Loc. Yu1, Yuping, "*Owenites koeneni* beds", Smithian.

Figs. 2a-d: ***Paranannites ovum*** n. sp. PIMUZ 26088. Paratype.
Loc. Yu1, Yuping, "*Owenites koeneni* beds", Smithian.

Figs. 3a-c: ***Paranannites ovum*** n. sp. PIMUZ 26089. Holotype.
Loc. Yu1, Yuping, "*Owenites koeneni* beds", Smithian.

Figs. 4a-b: ***Paranannites ovum*** n. sp. PIMUZ 26090.
Loc. T8, Tsoteng, "*Owenites koeneni* beds", Smithian.

Figs. 5a-c: ***Paranannites ovum*** n. sp. PIMUZ 26091.
Loc. T8, Tsoteng, "*Owenites koeneni* beds", Smithian.

Fig. 6: Suture line of ***Paranannites ovum*** n. sp., PIMUZ 26092.
Loc. T8, Tsoteng, "*Owenites koeneni* beds", Smithian.
Scale bar = 5 mm; H = 11 mm.

PLATE 34

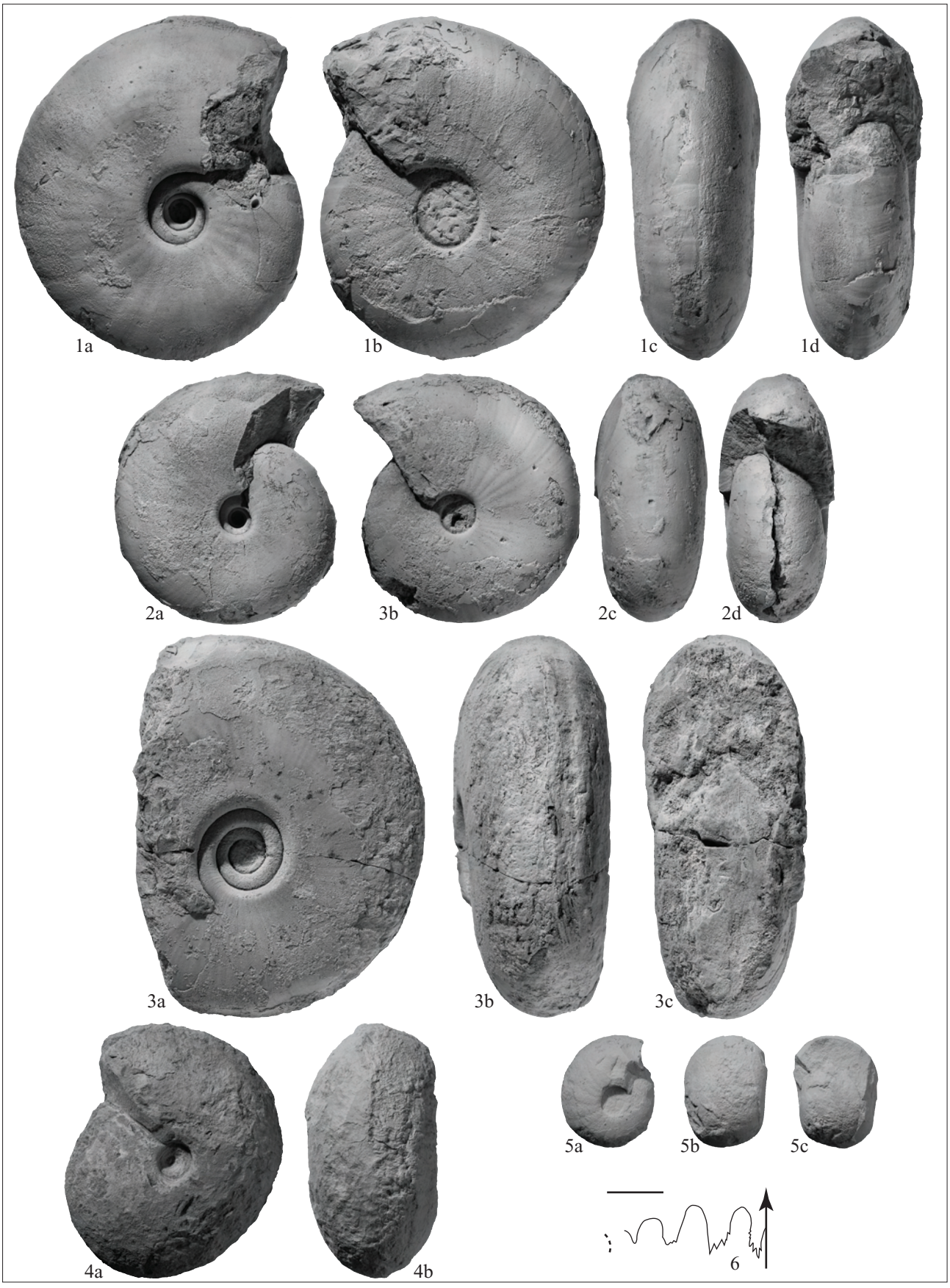

PLATE 35

(All figures natural size)

Figs. 1a-c: ***Paranannites globosus*** n. sp. PIMUZ 26093.
Loc. Jin29, Jinya, "*Flemingites rursiradiatus* beds", Smithian.
Figs. 2a-d: ***Paranannites globosus*** n. sp. PIMUZ 26094. Holotype.
Loc. Jin30, Jinya, "*Flemingites rursiradiatus* beds", Smithian.
a-c) Lateral, ventral and apertural views.
d) Suture line. Scale bar = 5 mm; H = 13 mm.
Figs. 3a-c: ***Paranannites globosus*** n. sp. PIMUZ 26095. Paratype.
Loc. Jin30, Jinya, "*Flemingites rursiradiatus* beds", Smithian.
Figs. 4a-c: ***Paranannites globosus*** n. sp. PIMUZ 26096.
Loc. Jin29, Jinya, "*Flemingites rursiradiatus* beds", Smithian.
Figs. 5a-c: ***Paranannites globosus*** n. sp. PIMUZ 26097.
Loc. Jin4, Jinya, "*Flemingites rursiradiatus* beds", Smithian.
Figs. 6a-c: ***Paranannites globosus*** n. sp. PIMUZ 26098. Paratype.
Loc. Jin30, Jinya, "*Flemingites rursiradiatus* beds", Smithian.
Figs. 7a-c: ***Paranannites globosus*** n. sp. PIMUZ 26099. Paratype.
Loc. Jin30, Jinya, "*Flemingites rursiradiatus* beds", Smithian.
Figs. 8a-c: ***Paranannites globosus*** n. sp. PIMUZ 26100. Paratype.
Loc. Jin30, Jinya, "*Flemingites rursiradiatus* beds", Smithian.
Fig. 9: Suture line of ***Paranannites globosus*** n. sp., PIMUZ 26101.
Loc. Jin23, Jinya, "*Flemingites rursiradiatus* beds", Smithian.
Scale bar = 5 mm; H = 4 mm.
Figs. 10a-c: ***Paranannites spathi*** (Frebold, 1930). PIMUZ 26102.
Loc. Jin45, Jinya, "*Owenites koeneni* beds", Smithian.
Figs. 11a-c: ***Paranannites spathi*** (Frebold, 1930). PIMUZ 26103.
Loc. Jin45, Jinya, "*Owenites koeneni* beds", Smithian.
Figs. 12a-c: ***Paranannites spathi*** (Frebold, 1930). PIMUZ 26104.
Loc. Jin45, Jinya, "*Owenites koeneni* beds", Smithian.
Figs. 13a-c: ***Paranannites spathi*** (Frebold, 1930). PIMUZ 26105.
Loc. Yu1, Yuping, "*Owenites koeneni* beds", Smithian.
Figs. 14a-c: ***Paranannites spathi*** (Frebold, 1930). PIMUZ 26106.
Loc. Yu1, Yuping, "*Owenites koeneni* beds", Smithian.
Figs. 15a-c: ***Paranannites spathi*** (Frebold, 1930). PIMUZ 26107.
Loc. Yu1, Yuping, "*Owenites koeneni* beds", Smithian.
Figs. 16a-c: ***Paranannites spathi*** (Frebold, 1930). PIMUZ 26108.
Loc. Jin45, Jinya, "*Owenites koeneni* beds", Smithian.
Figs. 17a-c: ***Paranannites spathi*** (Frebold, 1930). PIMUZ 26109.
Loc. Yu1, Yuping, "*Owenites koeneni* beds", Smithian.
Figs. 18a-c: ***Paranannites spathi*** (Frebold, 1930). PIMUZ 26110.
Loc. Yu1, Yuping, "*Owenites koeneni* beds", Smithian.
Figs. 19: Suture line of ***Paranannites spathi*** (Frebold, 1930). PIMUZ 26111.
Loc. Jin45, Jinya, "*Owenites koeneni* beds", Smithian.
Scale bar = 5 mm; H = 5 mm.
Figs. 20a-c: ***Owenites simplex*** Welter, 1922. PIMUZ 26112.
Loc. Jin45, Jinya, "*Owenites koeneni* beds", Smithian.
Figs. 21a-c: ***Owenites simplex*** Welter, 1922. PIMUZ 26113.
Loc. Jin45, Jinya, "*Owenites koeneni* beds", Smithian.
Figs. 22a-d: ***Owenites simplex*** Welter, 1922. PIMUZ 26114.
Loc. Jin45, Jinya, "*Owenites koeneni* beds", Smithian.

PLATE 35

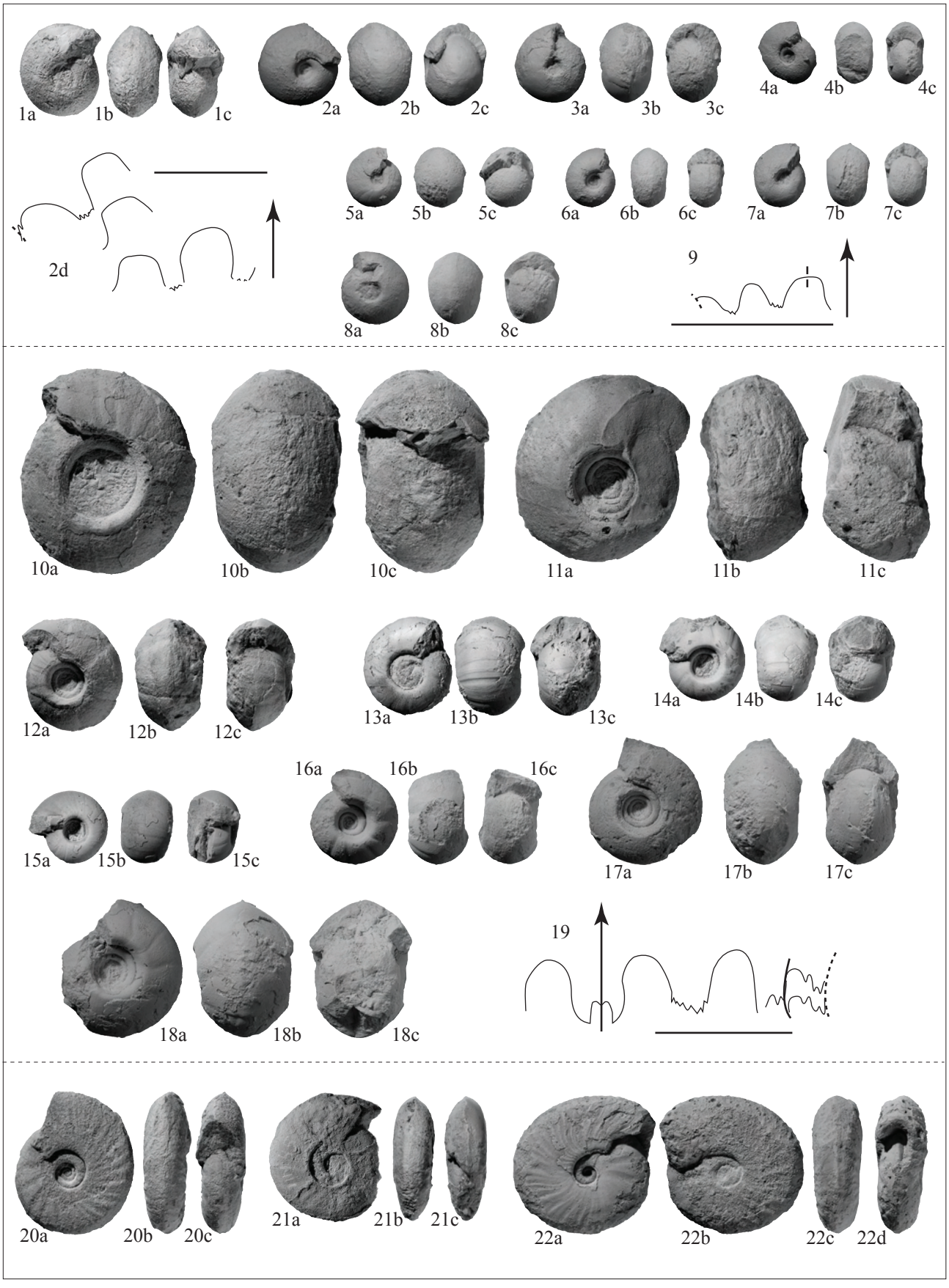
1a
1b
1c
2a
2b
2c
3a
3b
3c
4a
4b
4c
2d
5a
5b
5c
6a
6b
6c
7a
7b
7c
8a
8b
8c
9
10a
10b
10c
11a
11b
11c
12a
12b
12c
13a
13b
13c
14a
14b
14c
15a
15b
15c
16a
16b
16c
17a
17b
17c
18a
18b
18c
19
20a
20b
20c
21a
21b
21c
22a
22b
22c
22d

PLATE 36

(All figures natural size)

Figs. 1a-d: ***Owenites koeneni*** Hyatt & Smith, 1905. PIMUZ 26115.
Loc. T5, Tsoteng, "*Owenites koeneni* beds", Smithian.

Figs. 2a-c: ***Owenites koeneni*** Hyatt & Smith, 1905. PIMUZ 26116.
Loc. Jin27, Jinya, "*Owenites koeneni* beds", Smithian.

Figs. 3a-d: ***Owenites koeneni*** Hyatt & Smith, 1905. PIMUZ 26117.
Loc. T5, Tsoteng, "*Owenites koeneni* beds", Smithian.

Figs. 4a-d: ***Owenites koeneni*** Hyatt & Smith, 1905. PIMUZ 26118.
Loc. T5, Tsoteng, "*Owenites koeneni* beds", Smithian.

Figs. 5a-c: ***Owenites koeneni*** Hyatt & Smith, 1905. PIMUZ 26119.
Loc. Jin27, Jinya, "*Owenites koeneni* beds", Smithian.

Figs. 6a-d: ***Owenites koeneni*** Hyatt & Smith, 1905. PIMUZ 26120.
Loc. Jin99, Jinya, "*Owenites koeneni* beds", Smithian.
a-c) Lateral, ventral and apertural views.
d) Suture line. Scale bar = 5 mm; D = 60 mm. Slightly smoothed.

Fig. 7: Suture line of ***Owenites koeneni*** Hyatt & Smith, 1905. PIMUZ 26121.
Loc. T5, Tsoteng, "*Owenites koeneni* beds", Smithian.
Scale bar = 5 mm; H = 12 mm.

Fig. 8: Suture line of ***Owenites koeneni*** Hyatt & Smith, 1905. PIMUZ 26122.
Loc. Jin44, Jinya, "*Owenites koeneni* beds", Smithian.
Scale bar = 5 mm; H = 25 mm. Slightly smoothed.

PLATE 36

PLATE 37

(All figures natural size unless otherwise indicated)

Figs. 1a-d: ***Pseudosageceras multilobatum*** Noetling, 1905. PIMUZ 26123.
Loc. Jin30, Jinya, "*Flemingites rursiradiatus* beds", Smithian.
a-c) Lateral, ventral and apertural views.
d) Suture line. Scale bar = 5 mm; H = 25 mm.

Figs. 2a-c: ***Pseudosageceras multilobatum*** Noetling, 1905. PIMUZ 26124.
Loc. Jin30, Jinya, "*Flemingites rursiradiatus* beds", Smithian.

Figs. 3a-c: ***Pseudosageceras multilobatum*** Noetling, 1905. PIMUZ 26125.
Loc. Jin4, Jinya, "*Flemingites rursiradiatus* beds", Smithian.

Figs. 4a-c: ***Pseudosageceras multilobatum*** Noetling, 1905. PIMUZ 26126.
Loc. Jin30, Jinya, "*Flemingites rursiradiatus* beds", Smithian.

Figs. 5a-c: ***Pseudosageceras multilobatum*** Noetling, 1905. PIMUZ 26127. Scale ×0.75.
Loc. Jin4, Jinya, "*Flemingites rursiradiatus* beds", Smithian.

PLATE 37

PLATE 38

(All figures natural size unless otherwise indicated)

Figs. 1a-c: ***Hedenstroemia hedenstroemi*** (Keyserling, 1845). PIMUZ 26128.
Loc. Jin62, Waili, "*Hedenstroemia hedenstroemi* beds", Smithian.

Figs. 2a-d: ***Hedenstroemia hedenstroemi*** (Keyserling, 1845). PIMUZ 26129.
Loc. Jin62, Waili, "*Hedenstroemia hedenstroemi* beds", Smithian.
a-c) Lateral, ventral and apertural views.
d) Suture line. Scale bar = 5 mm; H = 11 mm

Figs. 3a-c: ***Hedenstroemia hedenstroemi*** (Keyserling, 1845). PIMUZ 26130.
Loc. Jin62, Waili, "*Hedenstroemia hedenstroemi* beds", Smithian.

Figs. 4a-c: ***Hedenstroemia hedenstroemi*** (Keyserling, 1845). PIMUZ 26131.
Loc. Jin62, Waili, "*Hedenstroemia hedenstroemi* beds", Smithian.

Figs. 5a-d: ***Proharpoceras carinatitabulatus*** Chao, 1950. PIMUZ 26132.
Loc. Jin45, Jinya, "*Owenites koeneni* beds", Smithian.

Figs. 6a-d: ***Proharpoceras carinatitabulatus*** Chao, 1950. PIMUZ 26133.
Loc. Jin45, Jinya, "*Owenites koeneni* beds", Smithian.

Figs. 7: ***Proharpoceras carinatitabulatus*** Chao, 1950. PIMUZ 26134.
Loc. Jin45, Jinya, "*Owenites koeneni* beds", Smithian.

Figs. 8a-c: ***Proharpoceras carinatitabulatus*** Chao, 1950. PIMUZ 26135. Scale ×2.
Loc. Jin45, Jinya, "*Owenites koeneni* beds", Smithian.

Figs. 9a-d: ***Proharpoceras carinatitabulatus*** Chao, 1950. PIMUZ 26136.
Loc. Yu1, Yuping, "*Owenites koeneni* beds", Smithian.
a-c) Lateral, ventral and apertural views.
d) Suture line. Scale bar = 5 mm; H = 6 mm.

PLATE 38

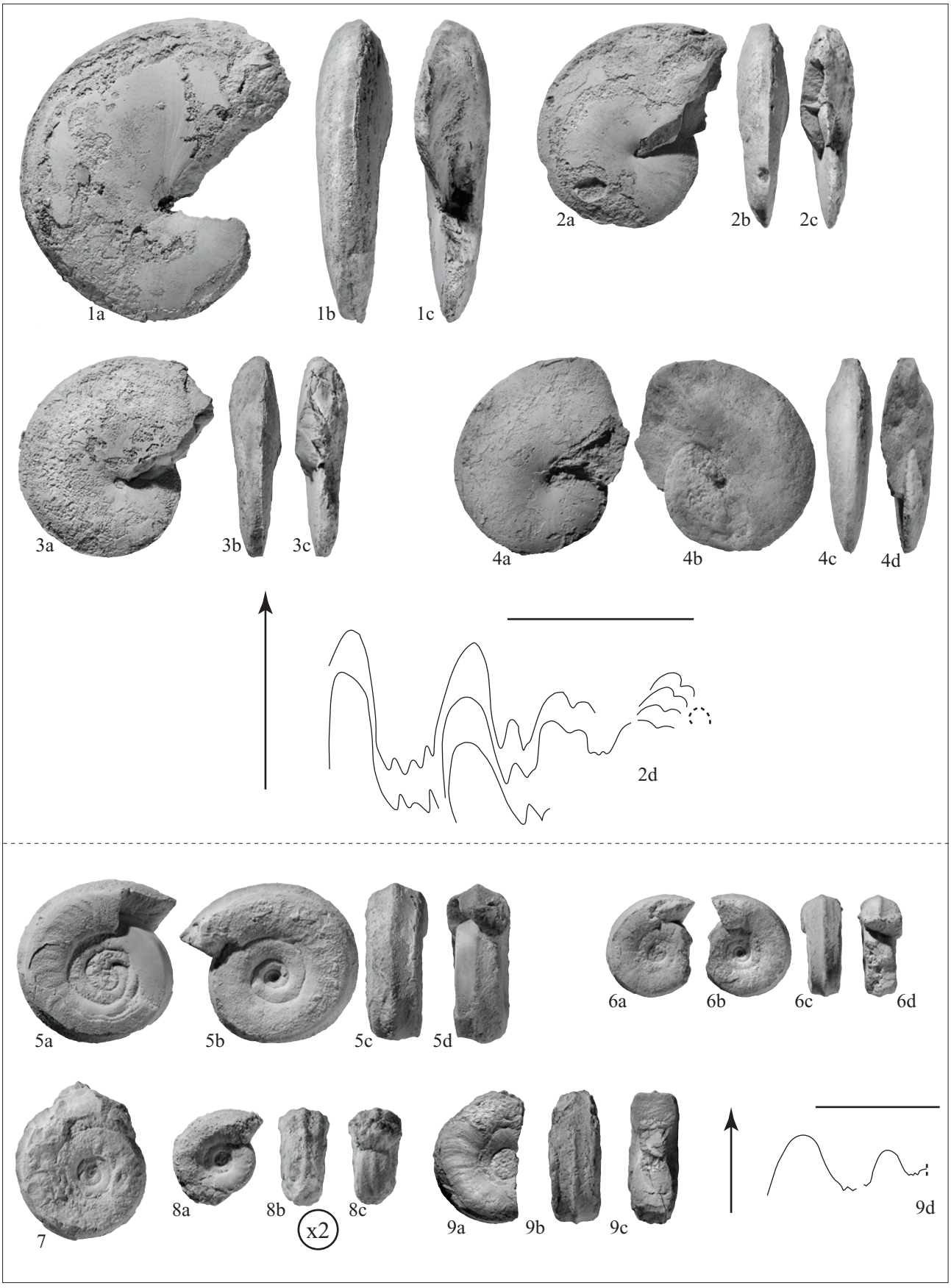
1a
1b
1c
2a
2b
2c
3a
3b
3c
4a
4b
4c
4d
2d
5a
5b
5c
5d
6a
6b
6c
6d
7
8a
8b
x2
8c
9a
9b
9c
9d

PLATE 39

(All figures natural size unless otherwise indicated)

Figs. 1a-b: ***Hedenstroemia augusta*** n. sp. PIMUZ 26137. Paratype.
Loc. NW13, Waili, "*Anasibirites multiformis* beds", Smithian.

Figs. 2a-c: ***Hedenstroemia augusta*** n. sp. PIMUZ 26138. Holotype.
Loc. NW13, Waili, "*Anasibirites multiformis* beds", Smithian.

Figs. 3a-c: ***Hedenstroemia augusta*** n. sp. PIMUZ 26139. Paratype.
Loc. NW13, Waili, "*Anasibirites multiformis* beds", Smithian.

Figs. 4a-c: ***Hedenstroemia augusta*** n. sp. PIMUZ 26140. Paratype. Scale ×2.
Loc. NW13, Waili, "*Anasibirites multiformis* beds", Smithian.

Figs. 5a-d: ***Hedenstroemia augusta*** n. sp. PIMUZ 26141. Paratype. Scale ×2.
Loc. NW13, Waili, "*Anasibirites multiformis* beds", Smithian.

Figs. 6a-d: ***Hedenstroemia augusta*** n. sp. PIMUZ 26142. Paratype. Scale ×2.
Loc. NW13, Waili, "*Anasibirites multiformis* beds", Smithian.

Figs. 7a-d: ***Hedenstroemia augusta*** n. sp. PIMUZ 26143. Paratype.
Loc. NW13, Waili, "*Anasibirites multiformis* beds", Smithian.

Figs. 8a-c: ***Hedenstroemia augusta*** n. sp. PIMUZ 26144. Paratype. Scale ×2.
Loc. NW13, Waili, "*Anasibirites multiformis* beds", Smithian.

Figs. 9a-d: ***Hedenstroemia augusta*** n. sp. PIMUZ 26145. Paratype. Scale ×2.
Loc. NW13, Waili, "*Anasibirites multiformis* beds", Smithian.

Figs. 10a-c: ***Hedenstroemia augusta*** n. sp. PIMUZ 26146.
Loc. Jin33, Jinya, "*Anasibirites multiformis* beds", Smithian.

Fig. 11: Suture line of ***Hedenstroemia augusta*** n. sp., PIMUZ 26147.
Loc. NW13, Waili, "*Anasibirites multiformis* beds", Smithian.
Scale bar = 5 mm; H = 20 mm.

PLATE 39

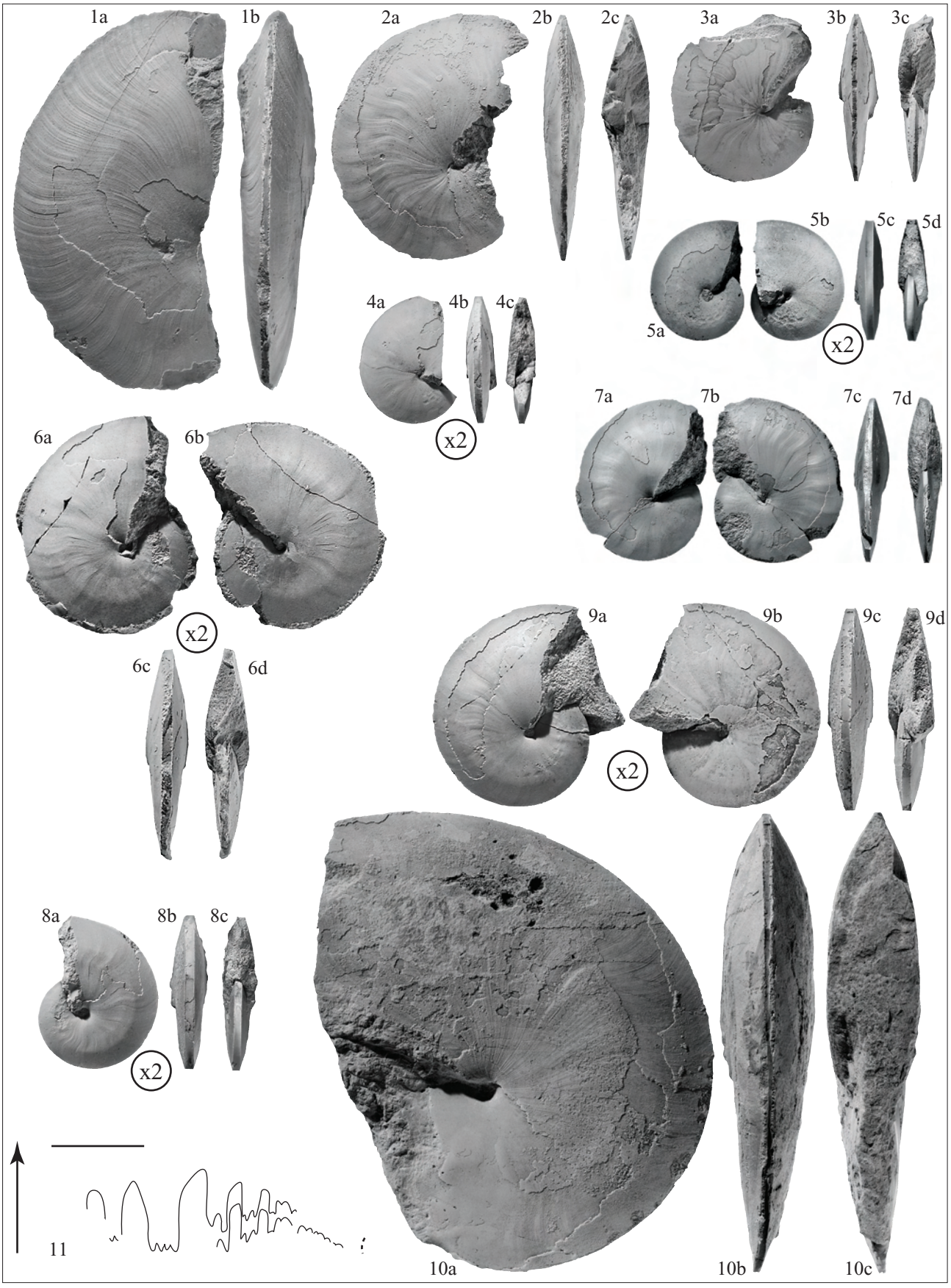
1a
1b
2a
2b
2c
3a
3b
3c
4a
4b
4c
x2
5a
5b
5c
5d
x2
6a
6b
x2
6c
6d
7a
7b
7c
7d
8a
8b
8c
x2
9a
9b
x2
9c
9d
10a
10b
10c
11

PLATE 40

(All figures natural size unless otherwise indicated)

Figs. 1a-e: ***Cordillerites antrum*** n. sp. PIMUZ 26148. Holotype.
Loc. Jin61, Waili, "*Kashmirites densistriatus* beds", Smithian.
a-d) Lateral, ventral and apertural views.
e) Suture line. Scale bar = 5 mm; H = 13 mm.

Figs. 2a-c: ***Cordillerites antrum*** n. sp. PIMUZ 26149. Paratype.
Loc. Jin61, Waili, "*Kashmirites densistriatus* beds", Smithian.

Figs. 3a-d: ***Cordillerites antrum*** n. sp. PIMUZ 26150.
Loc. Jin64, Waili, "*Kashmirites densistriatus* beds", Smithian.

Figs. 4a-c: ***Cordillerites antrum*** n. sp. PIMUZ 26151.
Loc. Jin64, Waili, "*Kashmirites densistriatus* beds", Smithian.

Figs. 5a-b: ***Cordillerites antrum*** n. sp. PIMUZ 26152. Paratype.
Loc. Jin61, Waili, "*Kashmirites densistriatus* beds", Smithian.

Fig. 6a-b: ***Cordillerites antrum*** n. sp. PIMUZ 26153. Paratype.
Loc. Jin61, Waili, "*Kashmirites densistriatus* beds", Smithian.

Figs. 7a-d: ***Cordillerites antrum*** n. sp. PIMUZ 26154.
Loc. Jin64, Waili, "*Kashmirites densistriatus* beds", Smithian.
a-c) Lateral, ventral and apertural views. Scale ×0.75.
d) Suture line. Scale bar = 5 mm; H = 30 mm.

Fig. 8: ***Cordillerites antrum*** n. sp. PIMUZ 26155. Paratype.
Loc. Jin61, Waili, "*Kashmirites densistriatus* beds", Smithian.

Figs. 9a-d: ***Cordillerites antrum*** n. sp. PIMUZ 26156.
Loc. Jin66, Waili, "*Kashmirites densistriatus* beds", Smithian.

PLATE 40

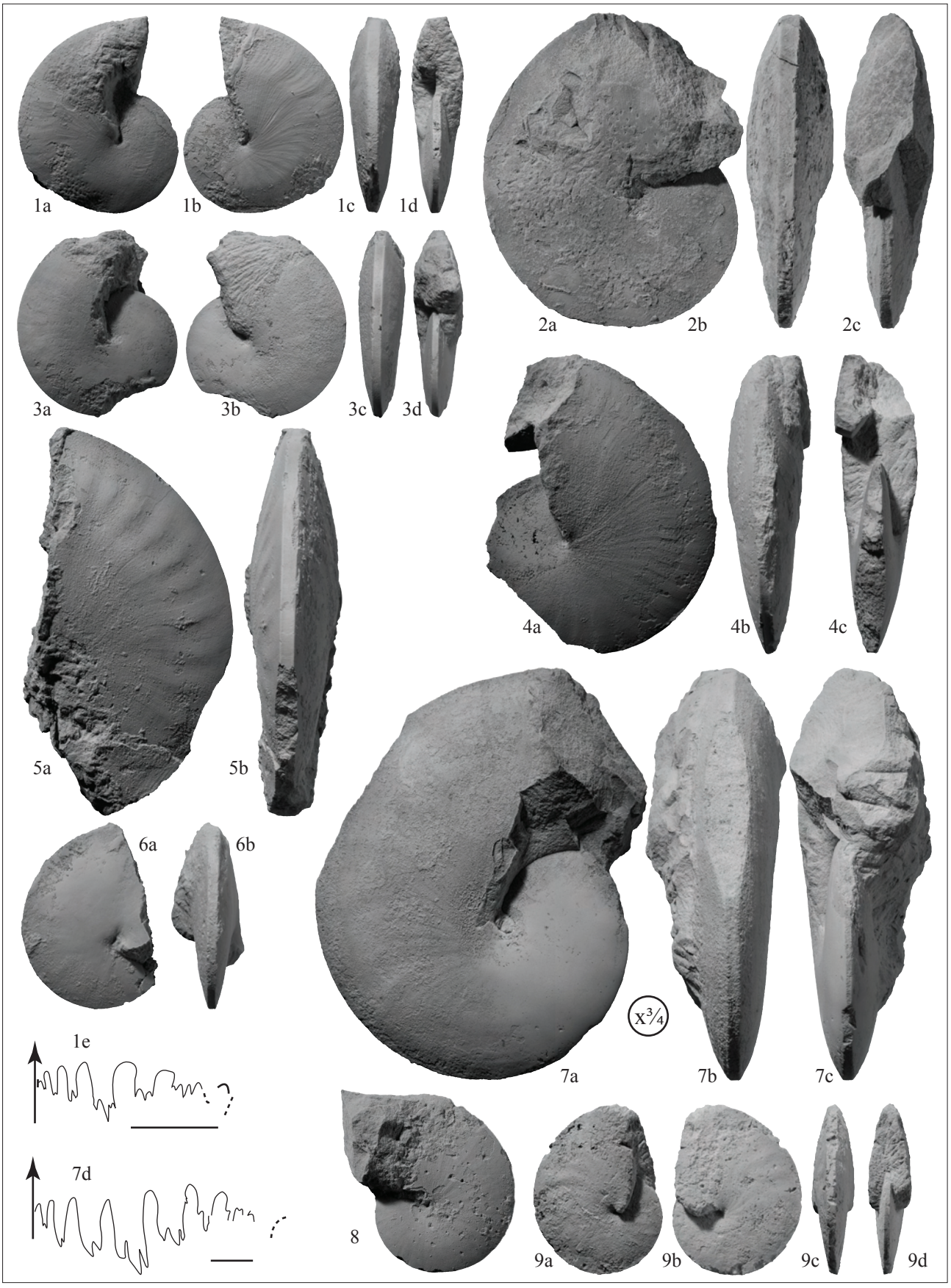
1a
1b
1c
1d
2a
2b
2c
3a
3b
3c
3d
4a
4b
4c
5a
5b
6a
6b
7a
7b
7c
x¾
1e
7d
8
9a
9b
9c
9d

PLATE 41

(All figures natural size)

Figs. 1a-b: ***Mesohedenstroemia kwangsiana*** Chao, 1959. PIMUZ 26157.
Loc. Jin4, Jinya, "*Flemingites rursiradiatus* beds", Smithian.

Figs. 2a-c: ***Mesohedenstroemia kwangsiana*** Chao, 1959. PIMUZ 26158.
Loc. Jin4, Jinya, "*Flemingites rursiradiatus* beds", Smithian.

Figs. 3a-c: ***Mesohedenstroemia kwangsiana*** Chao, 1959. PIMUZ 26159.
Loc. Jin4, Jinya, "*Flemingites rursiradiatus* beds", Smithian.

Figs. 4a-c: ***Mesohedenstroemia kwangsiana*** Chao, 1959. PIMUZ 26160.
Loc. Jin4, Jinya, "*Flemingites rursiradiatus* beds", Smithian.

Figs. 5a-c: ***Mesohedenstroemia kwangsiana*** Chao, 1959. PIMUZ 26161.
Loc. Jin4, Jinya, "*Flemingites rursiradiatus* beds", Smithian.

Figs. 6a-c: ***Mesohedenstroemia kwangsiana*** Chao, 1959. PIMUZ 26162.
Loc. Jin29, Jinya, "*Flemingites rursiradiatus* beds", Smithian.

Figs. 7a-c: ***Mesohedenstroemia kwangsiana*** Chao, 1959. PIMUZ 26163.
Loc. Jin10, Jinya, "*Flemingites rursiradiatus* beds", Smithian.

Fig. 8: Suture line of ***Mesohedenstroemia kwangsiana*** Chao, 1959. PIMUZ 26164.
Loc. Jin28, Jinya, "*Flemingites rursiradiatus* beds", Smithian.
Scale bar = 5 mm; H = 13 mm.

Figs. 9a-c: ***Mesohedenstroemia planata*** Chao, 1959. PIMUZ 26165.
Loc. Jin45, Jinya, "*Owenites koeneni* beds", Smithian.
a-b) lateral and ventral views.
c) Suture line. Scale bar = 5 mm; H = 15 mm.

PLATE 41

PLATE 42

(All figures natural size)

Figs. 1a-b: ***Aspenites acutus*** Hyatt & Smith, 1905. PIMUZ 26166.
Loc. Jin4, Jinya, "*Flemingites rursiradiatus* beds", Smithian.

Figs. 2a-c: ***Aspenites acutus*** Hyatt & Smith, 1905. PIMUZ 26167.
Loc. Jin4, Jinya, "*Flemingites rursiradiatus* beds", Smithian.

Figs. 3a-b: ***Aspenites acutus*** Hyatt & Smith, 1905. PIMUZ 26168.
Loc. Jin4, Jinya, "*Flemingites rursiradiatus* beds", Smithian.

Figs. 4a-c: ***Aspenites acutus*** Hyatt & Smith, 1905. PIMUZ 26169.
Loc. Jin28, Jinya, "*Flemingites rursiradiatus* beds", Smithian.

Figs. 5a-c: ***Aspenites acutus*** Hyatt & Smith, 1905. PIMUZ 26170.
Loc. Jin28, Jinya, "*Flemingites rursiradiatus* beds", Smithian.

Figs. 6a-c: ***Aspenites acutus*** Hyatt & Smith, 1905. PIMUZ 26171.
Loc. Jin28, Jinya, "*Flemingites rursiradiatus* beds", Smithian.

Figs. 7a-c: ***Aspenites acutus*** Hyatt & Smith, 1905. PIMUZ 26172.
Loc. Jin28, Jinya, "*Flemingites rursiradiatus* beds", Smithian.

Fig. 8: Suture line of ***Aspenites acutus*** Hyatt & Smith, 1905. PIMUZ 26173.
Loc. Jin27, Jinya, "*Owenites koeneni* beds", Smithian.
Scale bar = 5 mm; H = 24 mm.

Fig. 9: Suture line of ***Aspenites acutus*** Hyatt & Smith, 1905. PIMUZ 26174.
Loc. Jin27, Jinya, "*Owenites koeneni* beds", Smithian.
Scale bar = 5 mm; H = 25 mm.

Figs. 10a-b: ***?Aspenites*** **sp. indet.** PIMUZ 26175.
Loc. Yu1, Yuping, "*Owenites koeneni* beds", Smithian.

Figs. 11a-b: ***?Aspenites*** **sp. indet.** PIMUZ 26176.
Loc. NW1, Waili, "*Owenites koeneni* beds", Smithian.

PLATE 42

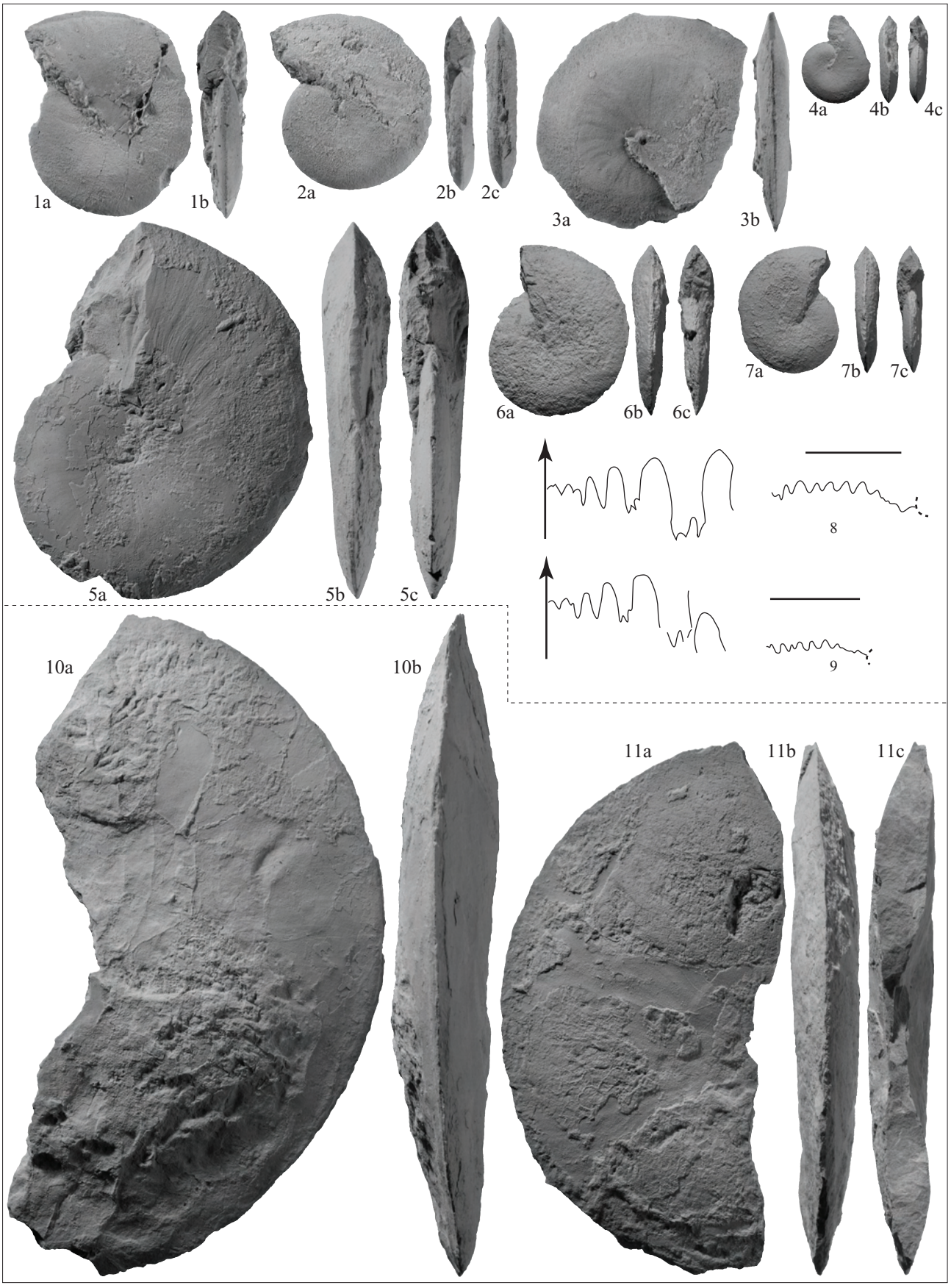
1a
1b
2a
2b
2c
3a
3b
4a
4b
4c
5a
5b
5c
6a
6b
6c
7a
7b
7c
8
9
10a
10b
11a
11b
11c

PLATE 43

(All figures natural size)

Figs. 1a-d: ***Pseudaspenites layeriformis*** (Welter, 1922). PIMUZ 26177.
Loc. Jin30, Jinya, "*Flemingites rursiradiatus* beds", Smithian.

Figs. 2a-c: ***Pseudaspenites layeriformis*** (Welter, 1922). PIMUZ 26178.
Loc. Jin30, Jinya, "*Flemingites rursiradiatus* beds", Smithian.

Figs. 3a-b: ***Pseudaspenites layeriformis*** (Welter, 1922). PIMUZ 26179.
Loc. Jin30, Jinya, "*Flemingites rursiradiatus* beds", Smithian.

Figs. 4a-d: ***Pseudaspenites layeriformis*** (Welter, 1922). PIMUZ 26180.
Loc. T50, Tsoteng, "*Flemingites rursiradiatus* beds", Smithian.
a-c) Lateral, ventral and apertural views.
d) Suture line. Scale bar = 5 mm; H = 8 mm.

Figs. 5a-c: ***Pseudaspenites layeriformis*** (Welter, 1922). PIMUZ 26181.
Loc. Jin29, Jinya, "*Flemingites rursiradiatus* beds", Smithian.

Figs. 6a-c: ***Pseudaspenites layeriformis*** (Welter, 1922). PIMUZ 26182.
Loc. Jin28, Jinya, "*Flemingites rursiradiatus* beds", Smithian.

Figs. 7a-c: ***Pseudaspenites evolutus*** n. sp. PIMUZ 26183.
Loc. Jin4, Jinya, "*Flemingites rursiradiatus* beds", Smithian.

Figs. 8a-c: ***Pseudaspenites evolutus*** n. sp. PIMUZ 26184.
Loc. Jin4, Jinya, "*Flemingites rursiradiatus* beds", Smithian.

Figs. 9a-c: ***Pseudaspenites evolutus*** n. sp. PIMUZ 26185.
Loc. Jin29, Jinya, "*Flemingites rursiradiatus* beds", Smithian.

Figs. 10a-d: ***Pseudaspenites evolutus*** n. sp. PIMUZ 26186. Paratype.
Loc. Jin30, Jinya, "*Flemingites rursiradiatus* beds", Smithian.

Figs. 11a-d: ***Pseudaspenites evolutus*** n. sp. PIMUZ 26187. Holotype.
Loc. Jin30, Jinya, "*Flemingites rursiradiatus* beds", Smithian.

Figs. 12a-e: ***Pseudaspenites tenuis*** (Chao, 1959). PIMUZ 26188.
Loc. Jin10, Jinya, "*Flemingites rursiradiatus* beds", Smithian.
a-d) Lateral, ventral and apertural views.
e) Suture line. Scale bar = 5 mm; H = 15 mm.

Figs. 13a-d: ***Pseudaspenites tenuis*** (Chao, 1959). PIMUZ 26189.
Loc. Jin30, Jinya, "*Flemingites rursiradiatus* beds", Smithian.

Figs. 14a-d: ***Pseudaspenites tenuis*** (Chao, 1959). PIMUZ 26190.
Loc. Jin30, Jinya, "*Flemingites rursiradiatus* beds", Smithian.

Figs. 15a-c: ***Owenites carpenteri*** Smith, 1932. PIMUZ 26191.
Loc. Jin47, Jinya, "*Owenites koeneni* beds", Smithian.

Figs. 16a-c: ***Owenites carpenteri*** Smith, 1932. PIMUZ 26192.
Loc. T12, Tsoteng, "*Owenites koeneni* beds", Smithian.

PLATE 43

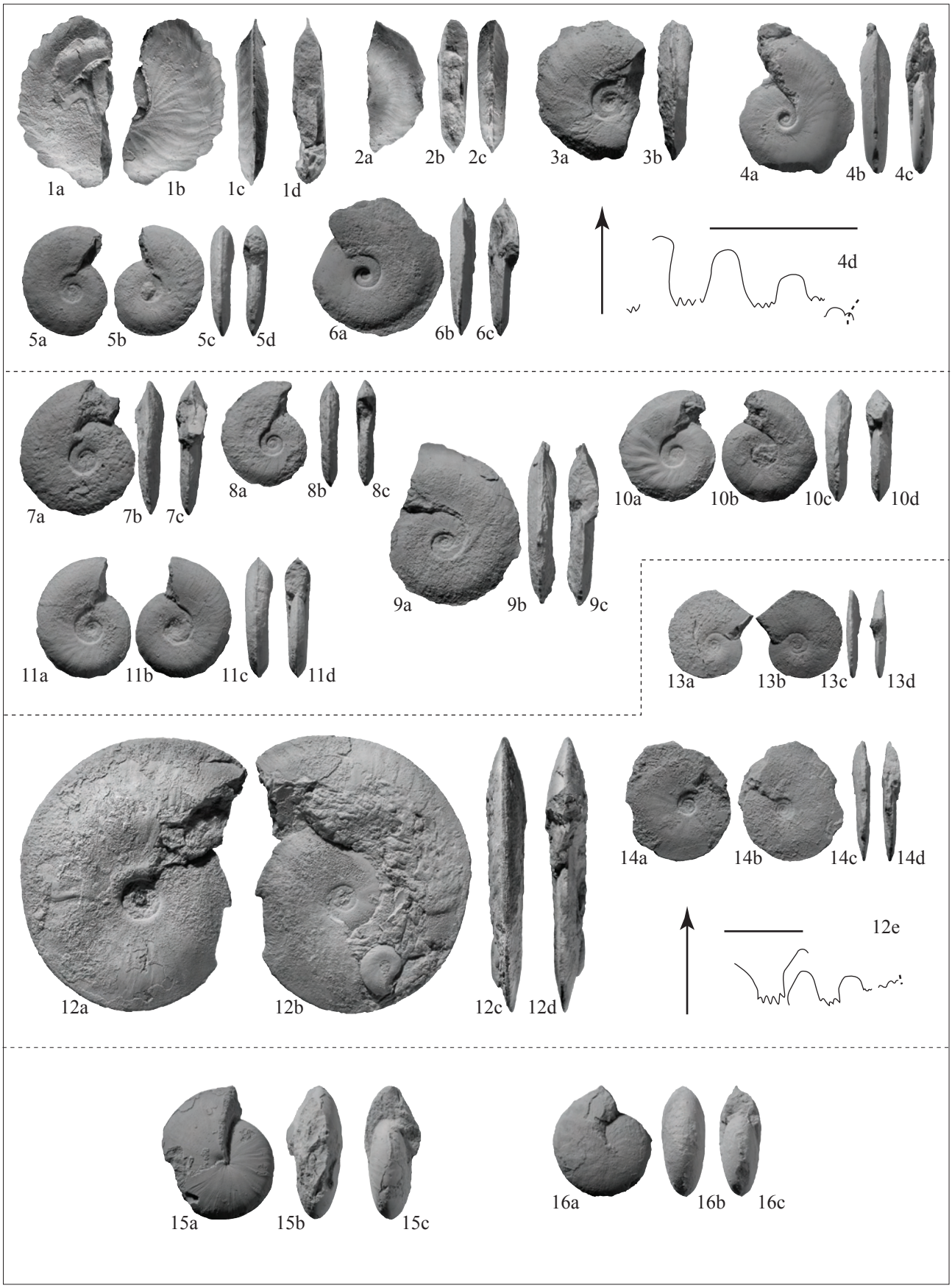
1a
1b
1c
1d
2a
2b
2c
3a
3b
4a
4b
4c
4d
5a
5b
5c
5d
6a
6b
6c
7a
7b
7c
8a
8b
8c
9a
9b
9c
10a
10b
10c
10d
11a
11b
11c
11d
12a
12b
12c
12d
12e
13a
13b
13c
13d
14a
14b
14c
14d
15a
15b
15c
16a
16b
16c

PLATE 44

(All figures natural size unless otherwise indicated)

Figs. 1a-d: ***Guodunites monneti*** n. gen., n. sp. PIMUZ 26193. Holotype.
Loc. Jin99, Jinya, "*Owenites koeneni* beds", Smithian.
a-c) Lateral, ventral and apertural views. Scale ×0.5.
d) Suture line. Scale bar = 5 mm; H = 32 mm.

Figs. 2a-d: ***Guodunites monneti*** n. gen., n. sp. PIMUZ 26194.
Loc. Jin12, Jinya, "*Owenites koeneni* beds", Smithian.
a-c) Lateral, ventral and apertural views. Scale ×0.75.
d) Suture line. Scale bar = 5 mm; H = 35 mm.

Figs. 3a-d: ***Procurvoceratites pygmaeus*** n. gen., n. sp. PIMUZ 26195. Holotype. Scale ×2.
Loc. Jin28, Jinya, "*Flemingites rursiradiatus* beds", Smithian.

Figs. 4a-b: ***Procurvoceratites pygmaeus*** n. gen., n. sp. PIMUZ 26196. Scale ×2.
Loc. Jin4, Jinya, "*Flemingites rursiradiatus* beds", Smithian.

Figs. 5a-b: ***Procurvoceratites pygmaeus*** n. gen., n. sp. PIMUZ 26197. Scale ×2.
Loc. Jin4, Jinya, "*Flemingites rursiradiatus* beds", Smithian.

Figs. 6a-c: ***Procurvoceratites ampliatus*** n. gen., n. sp. PIMUZ 26198. Holotype. Scale ×2.
Loc. Jin30, Jinya, "*Flemingites rursiradiatus* beds", Smithian.

Figs. 7a-c: ***Procurvoceratites tabulatus*** n. gen., n. sp. PIMUZ 26199. Holotype. Scale ×2.
Loc. Jin30, Jinya, "*Flemingites rursiradiatus* beds", Smithian.

PLATE 44

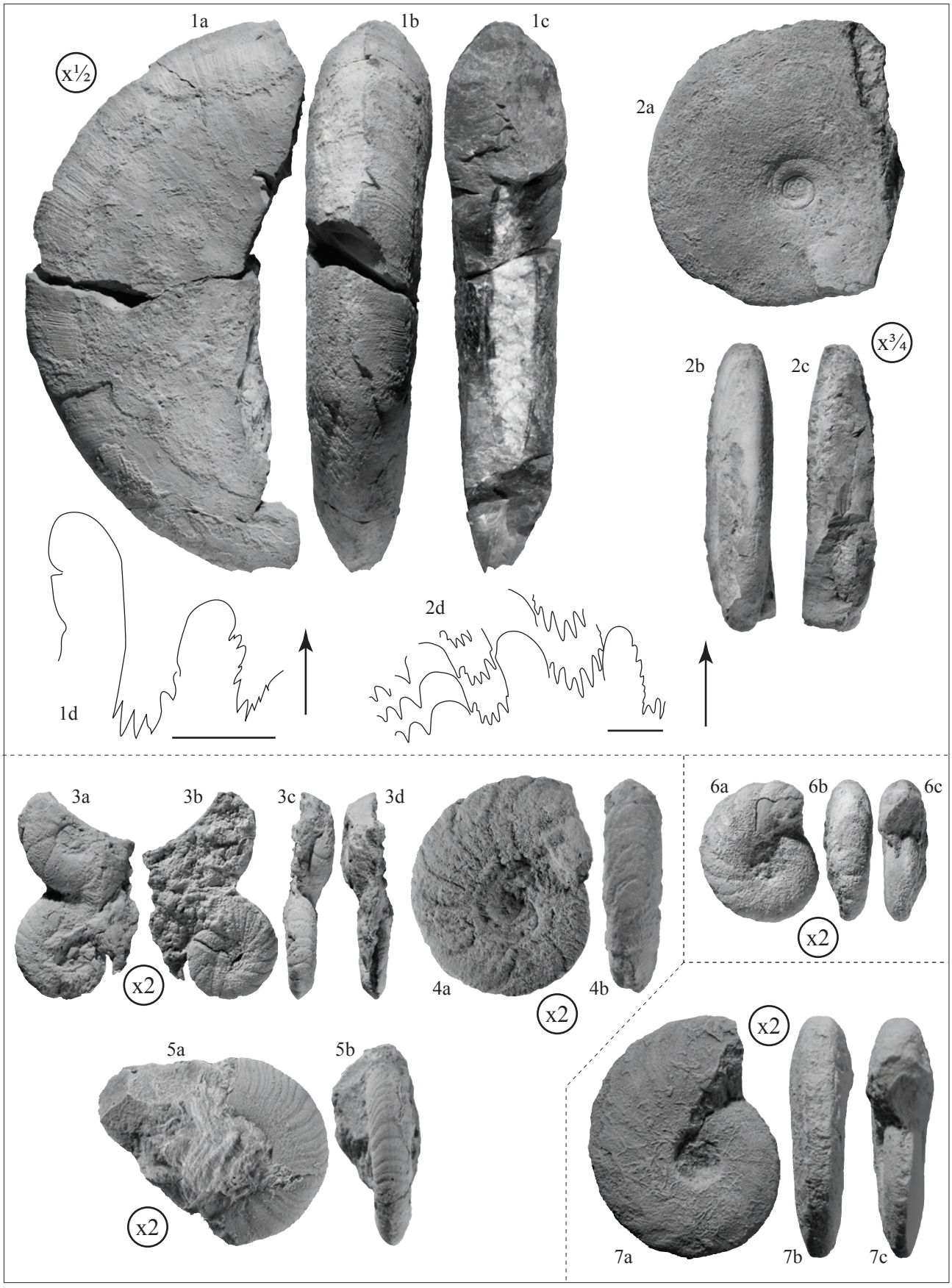
1a
1b
1c
x½
2a
x¾
2b
2c
1d
2d
3a
3b
3c
3d
x2
4a
4b
x2
6a
6b
6c
x2
5a
5b
x2
x2
7a
7b
7c

PLATE 45

(All figures natural size)

Figs. 1a-b: **Gen. indet. A**. PIMUZ 26200.
Loc. Jin12, Jinya, "*Owenites koeneni* beds", Smithian.

Figs. 2a-b: **Gen. indet. C.** PIMUZ 26201.
Loc. Yu22, Yuping, "*Anasibirites multiformis* beds", Smithian.

Figs. 3a-c: **Gen. indet. D**. PIMUZ 26202.
Loc. Yu22, Yuping, "*Anasibirites multiformis* beds", Smithian.

Figs. 4a-c: **Gen. indet. B**. PIMUZ 26203.
Loc. Yu22, Yuping, "*Anasibirites multiformis* beds", Smithian.

PLATE 45

CONCLUSIONS TO CHAPTERS 3, 4 AND 5
(Questions 2, 3 and 4)

The standardised incidence (presence/absence) data set presented in this dissertation allows the investigation of global temporal and spatial patterns of distribution of the Early Triassic ammonoids. It also allows the qualitative and quantitative studies of diversity and endemicity patterns at an ecologically meaningful and objective level of spatial resolution, i.e. at the basin level, thus differing from previous published studies where these patterns are assessed at the less interpretative level of the biogeographical realm. The recovery of ammonoids and changes in diversity and endemicity patterns (Brayard et al. in press) can be summarized as follows:

- based on the available fossil record, ammonoids clearly appear as recovering much faster than other marine organisms after the end-Permian mass extinction (less than ca. 2 myr);
- the recovery consists of a global increasing trend in diversity, more precisely illustrated by a series of ups and downs;
- the increasing trend in diversity was accompanied by a progressive shift from cosmopolitan to latitudinally-restricted distributions;
- two major drops in diversity, corresponding to two brief episodes of ammonoid cosmopolitanism, most likely due to short time intervals of very weak SST gradients, drastically affected ammonoids at the Smithian/Spathian and Spathian/Anisian boundaries. Causes that triggered these possible climatic events remain to be clearly established (Galfetti et al. submitted; Hochuli et al. submitted);
- a clear latitudinal diversity gradient emerge during most of the Smithian and Spathian stages;
- the edification of this latitudinal diversity gradient is most probably the consequence of the increased steepeness of the Sea Surface Temperature gradient during the Early Triassic as modelled by Brayard et al. (2004, 2005);
- the analysis of endemicity by Occurrence Ratio Profiles indicates a rapid biogeographical maturing and structuring of faunas concomitant with the edification of the latitudinal diversity gradient.

The quantitative comparisons of faunal assemblages in time and space by three complementary numerical approaches including a new, non-hierarchical clustering strategy (Brayard et al., submitted) allows the more precise definition of Early Triassic biogeographical structures:

- the identified inter-localities relationships indicate that the very beginning of the Early Triassic (Griesbachian) corresponds to a very simple biogeographical context representing a time of great cosmopolitanism for ammonoids;
- the recovery parallels a marked increase of the overall biogeographical heterogeneity and corresponds to the edification and steepening of the latitudinal gradient of taxonomic richness. Thus, the initially homogeneous biogeographical context shifts rapidly to a more complex configuration associated to a more endemic and latitudinally-restricted distribution of the ammonoids during the second part of the Early Triassic (Smithian and Spathian), as previously evidenced by diversity and endemicity studies.

The important field data from northwestern Guangxi, presented in the chapter 5 (Brayard & Bucher to be submitted), indicate that South China was a center of marked endemism and high taxonomic richness during the Smithian. It was also the case during the Spathian (Bucher, in progress). Some outstanding points have to be emphasized because they confirm the results obtained from data at a global scale:

- The high values of taxonomic richness found in South China is fully compatible with the existence of a marked latitudinal gradient of diversity during the Smithian;
- Equatorial faunas from South China and eastern Panthalassa (California, Nevada, Idaho) are partly congeneric and conspecific (e.g. *Aspenites acutus*, *Pseudaspenites layeriformis*, *Wyomingites aplanatus*, etc.), demonstrating the importance of faunal exchanges by the Panthalassic oceanic circulation. Many genera are also common to South China and some Tethyan localities, indicating that Guangxi was really at the interface between the Tethyan and the Panthalassic biogeographical domains;
- "Cosmopolitanism" events, at the very beginning and end of the Smithian, are easily identified in South China sections ("*Hedenstroemia hedenstroemi* beds" and "*Anasibirites multiformis* beds", respectively).
- The high diversity found very early in the Smithian, coupled with new radiometric ages (Ovtcharova et al. 2006), clearly show that the ammonoid recovery after the Permo-Triassic mass extinction was much more rapid than previously though, representing less than 2 myr.

References:

Brayard, A. and Bucher, H., to be submitted. Smithian (Early Triassic) ammonoid faunas from Northwestern Guangxi (South China): taxonomy and biochronology. *Fossils and Strata*.

Brayard, A., Bucher, H., Escarguel, G., Fluteau, F., Bourquin, S. and Galfetti, T., in press. The Early Triassic ammonoid recovery: paleoclimatic significance of diversity gradients. *Palaeogeography, Palaeoclimatology, Palaeoecology*.

Brayard, A., Escarguel, G. and Bucher, H., 2005. Latitudinal gradient of taxonomic richness: combined outcome of temperature and geographic mid-domains effects? *Journal of Zoological Systematics and Evolutionary Research*, **43**: 178-188.

Brayard, A., Escarguel, G. and Bucher, H., submitted. The biogeography of Early Triassic ammonoid faunas: clusters, gradients, and networks. *Journal of Biogeography*.

Brayard, A., Héran, M.-A., Costeur, L. and Escarguel, G., 2004. Triassic and Cenozoic palaeobiogeography: two case studies in quantitative modelling using IDL. *Palaeontologia Electronica*, **7**: 22 pp.

Galfetti, T., Bucher, H., Brayard, A., Hochuli, P.A., Weissert, H., Guodun, K., Atudorei, V. and Guex, J., submitted. Late Early Triassic climate change: insights from carbonate carbon isotopes, sedimentary evolution and ammonoid paleobiogeography. *Palaeogeography, Palaeoclimatology, Palaeoecology*.

Hochuli, P., Galfetti, T., Brayard A., Bucher, H., Weissert, H. and Vigran, J.O., submitted: Stepwise biotic recovery from the Permian/Triassic boundary event related to climatic forcing. Evidence from palynology, ammonoids and stable isotopes. *Geology*.

Ovtcharova, M., Bucher, H., Schaltegger, U., Galfetti., T., Brayard, A. and Guex, J. 2006. New Early to Middle Triassic U-Pb ages from South China: calibration with ammonoid biochronozones and implications for the timing of the Triassic biotic recovery. *Earth and Planetary Science Letters*, **243**: 463-475.

CONCLUSIONS & PERSPECTIVES

1. Paleontological and paleobiological perspectives from this dissertation

1.1. The Early Triassic recovery dynamics in its paleoenvironmental framework

New data from Guangxi emphasize that the phylogenetic scheme of the Early Triassic ammonoids is still far from clear, especially at the family level. Moreover, the divergence of many Smithian families may be sought in the Dienerian, which is still poorly documented. Biostratigraphic constraints may help in sorting alternative phylogenetic hypotheses and are therefore of prime importance. Rare occurrences are also likely to influence our views on faunal turnovers. In this respect, *Proharpoceras*, which is probably a representative of the Permian Anderssonoceratidae, suggests that this family went extinct not at the Permian/Triassic boundary but during the Smithian (Brayard et al. in prep).

First radiometric ages from Guangxi (Ovtcharova et al. 2006) clearly indicate that the ammonoid recovery was much more rapid (less than 2 myr) than previously thought. Their precocious recovery also brings many questions about the real "simplicity" of the Early Triassic environments and trophic webs. Indeed, a clade of this importance, by its distribution and evolutionary rates, could only rediversify if sufficient resources (i.e. phyto- and zooplankton) were available in the Oceans. Consequently, the Guangxi data strongly suggest that the classical view of unusually delayed recovery for all marine organisms, as well as very impoverished marine faunas and simple structure of the marine environments during the Early Triassic (e.g. Payne et al. 2004, 2006) has probably to be reassessed.

In this context, the Guangxi area also provides data for different types of marine organisms (e.g. ostracods (Crasquin-Soleau et al. in press), conodonts (Goudemand in progress), bivalves, nautiloids), thus allowing the study of the Early Triassic recovery phases at a temporal and spatial resolution not yet available. We wager that future works at a regional scale on this topic, combined with data from various areas, will bring many new insights on the post-crisis evolutionary dynamics of diversity.

The standardised data set studied in the chapter 3 and 4 of this dissertation indicates that some basins (e.g. Oman, Madagascar) need to be resampled to supplement and test some diversity patterns. This is currently being done for Oman (Brühwiler, in progress) and preliminary results indicate that its taxonomic richness was underestimated. Yet, it is likely that new additions to the data set will confirm and reinforce the latitudinal diversity patterns described in this work. A much less well documented pattern is the longitudinal gradient within the Tethys during the Smithian (Brayard et al. in press). Now, only the discovery of new Smithian occurrences in the western Tethys would make possible to confirm or discard the existence of this longitudinal gradient.

A part of the data set was not analysed in this dissertation and pertains to some terranes from the Tethys and Panthalassa (e.g. Vietnam, South Kitakami massif from Japan, South Primorye from eastern Russia, Chulitna from Alaska, etc.). The integration of these new ammonoid data, combined with methods used in the chapter 4, and especially the "*Bootstrapped Spanning Network*", could provide insights on the Early Triassic position of these terranes and/or on the Panthalassic paleoceanographic circulation (Brayard et al., in progress).

Finally, this dissertation demonstrates that the Early Triassic is far away to have revealed all its secrets. Yet, progresses are within reach.

1.2. Other large-scale patterns

In this work, we only considered the "taxonomic richness" aspect of "diversity". Yet, "diversity" involves many other aspects such as the phylogenetic (genetical) diversity, the ecological (functional) diversity or the morphological disparity. The phylogenetic and ecological diversities are impossible or difficult to assess in paleontological studies, especially when the considered organisms do not have close extent relatives. Nevertheless, morphological disparity can easily be analysed in paleontological studies. Indeed, spatial and temporal morphological gradients (ornamentation, size, etc.) are observed in studies of well sampled present-day or Cenozoic organisms (e.g. bivalves and gastropods, see Jablonski 1997; Roy et al. 1998, 2000, 2002; Roy & Martien 2001). Nevertheless, few of these trends are concerned by large-scale geographical and temporal analyses. The stable and relatively simple Early Triassic paleogeography, appears as an appropriate context to search for any gradient in morphological disparity (e.g. of ammonoid body size or coiling) at a large geographical and temporal scale. The main expected result is the confirmation (or not) of the existence of morphological gradients (of size, shape, ornamentation, etc.) coinciding with the latitudinal gradient of taxonomic richness of the Smithian or Spathian.

1.3. The “geophyletic” model

Except the direct perspectives concerning the present-day context and the technical improvements of the “geophyletic” model (see Brayard et al. 2005), the latter can easily be applied to other paleontological data. For instance, the mid-Cretaceous context, and notably the Western Interior Basin at the Late Cenomanian/Early Turonian boundary, could provide a well appropriate paleogeographical framework. Indeed, the geographical extent of this Cretaceous seaway is perfectly latitudinally delimited. Thus, the geographical frame is perfectly adapted to run the “geophyletic” model. Paleontological data from this area are also abundant (e.g. ammonoids; Monnet 2004). Moreover, foraminiferal data indicate that the Cenomanian/Early Turonian boundary is concomitant with an important weakening of the SST gradient (Bice & Norris 2002). The “geophyletic” model could thus be used to further test the influence of changing SST gradients.

2. Insertion of this work in the present-day macroecological debate

As illustrated by the diversity of the scientific journals where the articles presented in this dissertation have been submitted and published, this thesis work is at the interface between many disciplines (paleontology, [paleo]ecology, [paleo]biogeography, numerical modelling and simulations, geology, etc…) and tries to integrate paleobiological data into a macroecological perspective.

The observation of the Early Triassic ammonoid recovery provides many insights on the mechanisms governing the distribution of taxa. For instance, the maximum of taxonomic richness is concomitant with the intensification of the SST gradient. A change to an opposite configuration (i.e. a weak SST gradient) generates a diversity drop. A major conclusion of this dissertation is that past and present-day diversity patterns can realistically be modelled under similar constraints, among which SST gradients are likely to play a first-order role, at least for marine organisms. Thus, our results illustrate the outstanding importance of environmental gradients (e.g. temperature, productivity, chemistry, etc.) in structuring real communities, a role which has been strongly underestimated by community ecologists in recent years. *"Much of recent community ecology ignore the fact that real communities [i.e. a set of species co-occurring at a given time and place] occur on gradients of temperature, moisture and soil chemistry. [… A] major goal of community ecology is to explain why communities change in a systematic fashion across space. For example, predicting the ecological impact of global warming requires an understanding of how communities are affected by the environment, which is most easily understood by investigating variations along gradients"* (McGill et al. 2006).

Indeed, when applied to the neontological context, our conclusions cast a new eye over the present-day biodiversity crisis. This one is considered to be much more severe than the Permo-Triassic mass extinction with unexpected and terrible effects (Wilson 1992, Leakey & Lewin 1995, Eldredge

1998). Isolating the multiple direct anthropogenic effects on living organisms (e.g. hunting, pollution, etc.), the present-day crisis is also partly the result of the intense climate warming and instability. Consequences on taxa distributions are already well visible by, e.g. ranges quickly shifting toward higher latitudes (e.g. Thomas & Lennon 1999; Parmesan et al. 1999; Davies & Shaw 2001; Walther et al. 2002; Parmesan & Yohe 2003; Thomas et al. 2004). In this way, the Early Triassic ammonoid recovery and its modelling allow some predictions (at least for marine organisms) on the present-day crisis and its associated post-events:

- If the present global climate warming ultimately leads to an equal climate, low levels of diversity with generalist and opportunist surviving taxa are to be expected. These taxa should have cosmopolitan distributions corresponding to a weak diversity gradient controlled by a weakened temperature gradient;
- the post-crisis return to contrasted climatic conditions should generate more latitudinally restricted distributions of taxa and thus, a steeper diversity gradient;
- at a deep-time scale, the recovery could be extremely rapid depending on the studied clade (see Lu et al. 2006 and Brayard et al. submitted).

Diachronic deep-time analyses are still rare within macroecological studies and modelling. Within the intense present-day macroecological debate, paleontologists can provide many insights to the knowledge and understanding of extent diversity patterns and their evolutionary dynamics. They can also suggest and/or refine the calibration of the parameters controlling numerical models, including evolutionary rates or long-terms environmental changes, which are impossible to fully apprehend on the sole basis of neontological studies. Thus, combining these parameters with data from present-day patterns can generate more realistic modelling and provide more robust explanations to past and present-day macroecological patterns (e.g. Leighton 2005).

From this point of view, this thesis dissertation may directly contribute to the anticipation of future problems implicated by the present-day warming and biodiversity crisis. Ammonoids appear as a well informative past example of how taxa respond to global events and climate change (e.g. cosmopolitan and low diversity events of the very beginning and end of the Smithian). This example also allows several suggestions, notably concerning the relative contribution of extrinsic (e.g. SST gradient, currents, etc.) and intrinsic (e.g. evolutionary rates) parameters on the distribution of marine organisms.

Macroecology seeks to find general rules for the field of community ecology (e.g. Lawton 1999). When concerned by diversity distributions and gradients, ecologists traditionally focus on a few, spatially variable environmental parameters and rarely take into account their historical dynamics, i.e. their time variability. Indeed, time and space dimensions of the environmental parameterisation are both crucial if we are to construct realistic short and long terms projections for the magnitude of the

present-day and future taxa loss. The validity of numerical models developed in order to understand how the present global warming does and will affect the biosphere, is intimately linked to these invaluable inputs. Not taking them into account is likely to yield under-estimates of the overall intensity of the present-day diversity crisis. In a time of global environmental changes and biodiversity conservation strategies involving worldwide decisions and policies, deep-time and gradient-based analyses as done in this dissertation could provide fundamental insights on the possible ways to protect what remains to be saved.

References:

Bice, K.L. and Norris, R.D., 2002. Possible atmospheric CO_2 extremes of the Middle Cretaceous (Late Albian-Turonian). *Paleoceanography*, **17**: 1070.

Brayard, A., Bucher, H., Escarguel, G., Fluteau, F., Bourquin, S. and Galfetti, T., in press. The Early Triassic ammonoid recovery: paleoclimatic significance of diversity gradients. *Palaeogeography, Palaeoclimatology, Palaeoecology*.

Brayard, A., Bucher, H., Galfetti, T., Brühwiler, T., Jenks, J., Guodun, K. and Escarguel, G., in prep. The last Permian ammonoid survivor: *Proharpoceras* Chao.

Brayard, A., Escarguel, G. and Bucher, H., 2005. Latitudinal gradient of taxonomic richness: combined outcome of temperature and geographic mid-domains effects? *Journal of Zoological Systematics and Evolutionary Research*, **43**: 178-188.

Brayard, A., Escarguel, G. and Bucher, H., submitted. The biogeography of Early Triassic ammonoid faunas: clusters, gradients, and networks. *Journal of Biogeography*.

Crasquin-Soleau, S., Galfetti, T., Bucher, H. and Brayard, A., in press: Early Triassic ostracods from northwestern Guangxi Province, South China. *Rivista Italiana di Paleontologia e Stratigrafia*, **112**.

Davies, M.B. and Shaw, R.G., 2001. Range shifts and adaptive responses to quaternary climate change. *Science*, **292**: 673-679.

Eldredge, N., 1998. *Life in the balance: humanity and the biodiversity crisis.* Princeton University Press, 224pp.

Jablonski, D., 1997. Body-size evolution in Cretaceous molluscs and the status of Cope's rule. *Nature*, **385**: 250-252.

Lawton, J.H., 1999. Are there general laws in ecology? *Oikos*, **84**: 177-192.

Leakey, R.E. and Lewin, R., 1995. *The sixth extinction: patterns of life and the future of the humankind*. Anchor, 271pp.

Leighton, L.R., 2005. The latitudinal diversity gradient through deep time: testing the "Age of Tropics" hypothesis using Carboniferous productidine brachiopods. Evolutionary *Ecology*, **19**: 563-581.

Lu, P.J., Yogo, M. and Marshall, C.R., 2006. Phanerozoic marine biodiversity dynamics in light of the incompleteness of the fossil record. *Proceedings of the National Academy of Sciences of the United States of America*, **103**: 2736-2739.

McGill, B.J., Enquist, B.J., Weiher, E. and Westoby, M., 2006. Rebuilding community ecology from functional traits. *Trends in Ecology and Evolution*, **21**: 178-185.

Monnet, C., 2004. *Anisian (Middle Triassic) and Cenomanian (mid-Cretaceous) ammonoids: biochronology, biodiversity, and evolutionary trends*. Unpublished PhD thesis, University of Zurich.

Ovtcharova, M., Bucher, H., Schaltegger, U., Galfetti, T., Brayard, A. and Guex, J., 2006. New Early to Middle Triassic U-Pb ages from South China: calibration with ammonoid biochronozones and implications for the timing of the Triassic biotic recovery. *Earth and Planetary Sciences Letters*, **243**: 463-475.

Parmesan, C., Ryrholm, N., Stephanescu, C., Hill, J.K., Thomas, C.D., Descimon, H., Huntley, B., Kaila, L., Kullberg, J., Tammaru, T., Tennent, W.J., Thomas, J.A. and Warren, M., 1999. Poleward shifts in geographical ranges of butterfly species associated with regional warming. *Nature*, **399**: 579-583.

Parmesan, C. and Yohe, G., 2003. A globally coherent fingerprint of climate change impacts across natural systems. *Nature*, **421**: 37-42.

Payne, J.L., Lehrmann, D.J., Wei, J., Orchard, M.J., Schrag, D.P. and Knoll, A.H., 2004. Large perturbations of the carbon cycle during recovery from the end-Permian mass extinction. *Science*, **305**: 506-509.

Payne, J.L., Lehrmann, D.J., Wei, J. and Knoll, A.H., 2006. The pattern and timing of biotic recovery from the end-Permian extinction on the Great Bank of Guizhou, Guizhou province, China. *Palaios*, **21**: 63-85.

Roy, K., Jablonski, D. and Martien, K.K., 2000. Invariant size-frequency distributions along a latitudinal gradient in marine bivalves. *Proceedings of the National Academy of Sciences of the United States of America*, **97**: 13150-13155.

Roy, K., Jablonski, D. and Valentine, J.W., 2001. Climate change, species range limits and body size in marine bivalves. *Ecology Letters*, **4**: 366-370.

Roy, K., Jablonski, D. and Valentine, J.W., 2002. Body size and invasion success in marine bivalves. *Ecology Letters*, **5**: 163-167.

Roy, K., Jablonski, D., Valentine, J.W. and Rosenberg, G., 1998. Marine latitudinal diversity gradients: test of causal hypotheses. *Proceedings of the National Academy of Sciences of the United States of America*, **95**: 3699-3702.

Thomas, C.D. and Lennon, J.J., 1999. Birds extend their ranges northwards. *Nature*, **399**: 213.

Walther, G.-R., Post, E., Convey, P., Menzel, A., Parmesan, C., Beebee, T.J.C., Fromentin, J.-M., Hoegh-Guldberg, O. and Bairlein, F., 2002. Ecological responses to recent climate change. *Nature*, **416**: 389-395.

Wilson, E.O., 1992. *The diversity of Life*. Harvard University Press, 424pp.

APPENDICES

Co-authored references linked to this dissertation (published and submitted):

1. Ovtcharova, M., Bucher, H., Schaltegger, U., Galfetti., T., Brayard, A. and Guex, J. 2006. New Early to Middle Triassic U-Pb ages from South China: calibration with ammonoid biochronozones and implications for the timing of the Triassic biotic recovery. *Earth and Planetary Science Letters*, **243**: 463-475.
2. Galfetti, T., Bucher, H., Brayard, A., Hochuli, P.A., Weissert, H., Guodun, K., Atudorei, V. and Guex, J., submitted. Late Early Triassic climate change: insights from carbonate carbon isotopes, sedimentary evolution and ammonoid paleobiogeography. *Palaeogeography, Palaeoclimatology, Palaeoecology*.
3. Hochuli, P., Galfetti, T., Brayard A., Bucher, H., Weissert, H. and Vigran, J.O., submitted: Stepwise biotic recovery from the Permian/Triassic boundary event related to climatic forcing. Evidence from palynology, ammonoids and stable isotopes. *Geology*.

Available online at www.sciencedirect.com
SCIENCE DIRECT®
Earth and Planetary Science Letters 243 (2006) 463–475
EPSL
www.elsevier.com/locate/epsl

New Early to Middle Triassic U–Pb ages from South China: Calibration with ammonoid biochronozones and implications for the timing of the Triassic biotic recovery

Maria Ovtcharova [a], Hugo Bucher [b,*], Urs Schaltegger [a], Thomas Galfetti [b], Arnaud Brayard [b], Jean Guex [c]

[a] *Department of Mineralogy, University of Geneva, rue des Maraîchers 13, CH-1205 Geneva, Switzerland*
[b] *Institute and Museum of Paleontology, University of Zürich, Karl Schmid-Strasse 4, CH-8006 Zürich, Switzerland*
[c] *Institute of Geology, University of Lausanne, BFSH2, CH-1015 Lausanne, Switzerland*

Received 24 September 2005; received in revised form 11 January 2006; accepted 23 January 2006
Available online 3 March 2006
Editor: V. Courtillot

Abstract

New zircon U–Pb ages are proposed for late Early and Middle Triassic volcanic ash layers from the Luolou and Baifeng formations (northwestern Guangxi, South China). These ages are based on analyses of single, thermally annealed and chemically abraded zircons. Calibration with ammonoid ages indicate a 250.6±0.5 Ma age for the early Spathian *Tirolites*/*Columbites* beds, a 248.1±0.4 Ma age for the late Spathian *Neopopanoceras haugi* Zone, a 246.9±0.4 Ma age for the early middle Anisian *Acrochordiceras hyatti* Zone, and a 244.6±0.5 Ma age for the late middle Anisian *Balatonites shoshonensis* Zone. The new dates and previously published U–Pb ages indicate a duration of ca. 3 my for the Spathian, and minimal durations of 4.5±0.6 my for the Early Triassic and of 6.6+0.7/−0.9 my for the Anisian. The new Spathian dates are in a better agreement with a 252.6±0.2 Ma age than with a 251.4±0.3 Ma age for the Permian–Triassic boundary. These dates also highlight the extremely uneven duration of the four Early Triassic substages (Griesbachian, Dienerian, Smithian, and Spathian), of which the Spathian exceeds half of the duration of the entire Early Triassic. The simplistic assumption of equal duration of the four Early Triassic subdivisions is no longer tenable for the reconstruction of recovery patterns following the end Permian mass extinction.

Keywords: U–Pb ages; zircon; Early Triassic; ammonoids; biotic recovery

1. Introduction

Following the biggest mass extinction of the Phanerozoic, the Early Triassic biotic recovery is generally assumed to have had a longer duration than that of other major mass extinctions. Understanding the mode and tempo of the recovery requires calibration of high-resolution biochronozones based

* Corresponding author. Fax: +41 44 634 49 23.
E-mail addresses: maria.ovtcharova@terre.unige.ch (M. Ovtcharova), Hugo.FR.Bucher@pim.unizh.ch (H. Bucher), urs.schaltegger@terre.unige.ch (U. Schaltegger), jean.guex@unil.ch (J. Guex).

0012-821X/$ - see front matter © 2006 Elsevier B.V. All rights reserved.
doi:10.1016/j.epsl.2006.01.042

on the maximal association principle [1] with high-resolution radio-isotopic ages. Mass extinctions are usually followed by a survival phase and a recovery phase before ecosystems become fully re-organized, i.e. until diversity reaches a new equilibrium phase. For the Early Triassic, proposed estimates for the duration of the survival and recovery phases are so far not constrained by primary (i.e. non-interpolated) radio-isotopic ages (see compilation by [2]). Moreover, as indicated by the Early Triassic ammonoid recovery, the leading taxonomic group for correlation of Mesozoic marine rocks, the return to a new equilibrium phase was not a smooth, gradual process. The recovery underwent several fluctuations and was severely set back during end Smithian time [3]. Calibrating such diversity fluctuations by means of U–Pb ages is critical for a better understanding of the various abiotic and biotic factors that shaped the recovery, and for the improvement of the geological time scale, as well.

Based on the unrivaled North American ammonoid record, Tozer [4] and Silberling and Tozer [5] introduced four Early Triassic stages: Griesbachian, Dienerian, Smithian, and Spathian, in ascending order. In 1992, a decision of the Subcommission of Triassic Stratigraphy downgraded these four stages to substages to adopt the Russian two-stage subdivisions scheme, i.e. the Induan and Olenekian stages as originally defined by [6]. However, the global correlation of the boundary between these two stages still poses problems because these are defined within two different realms, the Induan within the Tethyan Realm, and the Olenekian within the Boreal Realm. The Induan stage correlates approximately with the Griesbachian and the Dienerian, whereas the Olenekian stage correlates approximately with the Smithian and the Spathian. Here, we deliberately use the scheme of Tozer which by far best reflects global ammonoid faunal changes during the Early Triassic. Whether Tozer's subdivisions should be ranked at the stage or substage level remains a minor, essentially formalistic point. Essential is the construction of a high resolution faunal succession permitting objective correlation of distant basins.

Only a few calibrations between isotopic and paleontological ages are available for the Early and Middle Triassic. U–Pb ages ranging from 253 [7] to ca. 251 Ma [8] have been proposed for the Permian–Triassic boundary. The U–Pb age for the Anisian–Ladinian boundary is of ca. 241 Ma [9,10]. Preliminary U–Pb ages of 247.8 Ma are available for the base of the early Anisian, and of 246.5 Ma for the early middle Anisian [11,12]. This leaves a 10 to 12 my interval for the Early Triassic (Griesbachian, Dienerian, Smithian, and Spathian) and the Anisian stage, whose respective boundaries are primarily defined by changes in ammonoid faunas. Due to the lack of absolute age constraints, extrapolation or interpolation of the respective durations of the Early Triassic stages or substages and of the Anisian are usually based on the flawed assumption of equal duration of zones or subzones (e.g., [13], p. 284). Recent simulations have demonstrated that this assumption is even more unrealistic for extinction and recovery phases [14], which stresses again the need for radio-isotopic age calibrations during such biological crises. With increasing knowledge of Early Triassic and Anisian ammonoid faunas, the number of zones reflecting newly documented faunas intercalated between those previously known is rapidly growing ([15] for the synthesis of the Anisian from North America; [16] and ongoing work by Bucher and Guex for the Spathian). Because the number of zones or subzones reflects the combined effects of the completeness of the record, of sampling efforts, as well as the variable evolutionary rates in time and space, it cannot be used to interpolate the duration of zones or stages comprised between two calibration points, regardless what the distance of these points in time may be. Here, we report on four new U–Pb ages calibrated with the ammonoid-rich series of the Early Triassic and Anisian marine record of northwestern Guangxi (Fig. 1A) and their correlation with the North American ammonoid biochronozones.

2. Geological setting and ammonoid age control

The investigated volcanic ash layers were sampled from the Luolou Formation of Early Triassic age and from the overlying Baifeng Formation of Anisian age [17]. These formations belong to the Nanpanjiang Basin (see [18] for a synthesis) of the South China Block, which occupied an equatorial position during Early and Middle Triassic times as indicated by paleomagnetic data [19]. At its type locality, and in the Jinya, Leye and Wangmo areas, the Luolou Formation is composed of mixed carbonate-siliciclastic, ammonoid- and conodont-rich rocks deposited in an outer platform setting. As evidenced by ammonoid age control, most of the vertical facies changes within the 70 to 100 m thick Luolou Fm. (Fig. 1B) are synchronous within a 100 km long, NW–SE oriented belt extending from Wangmo (southern Guizhou) to Leye and Fengshan (northwestern Guangxi, see Fig. 1A).

Two coarse-grained volcanic ash layers (CHIN-10 and CHIN-23, see Fig. 1B) consistently occur within the upper, carbonate unit of Spathian age of the Luolou Fm.

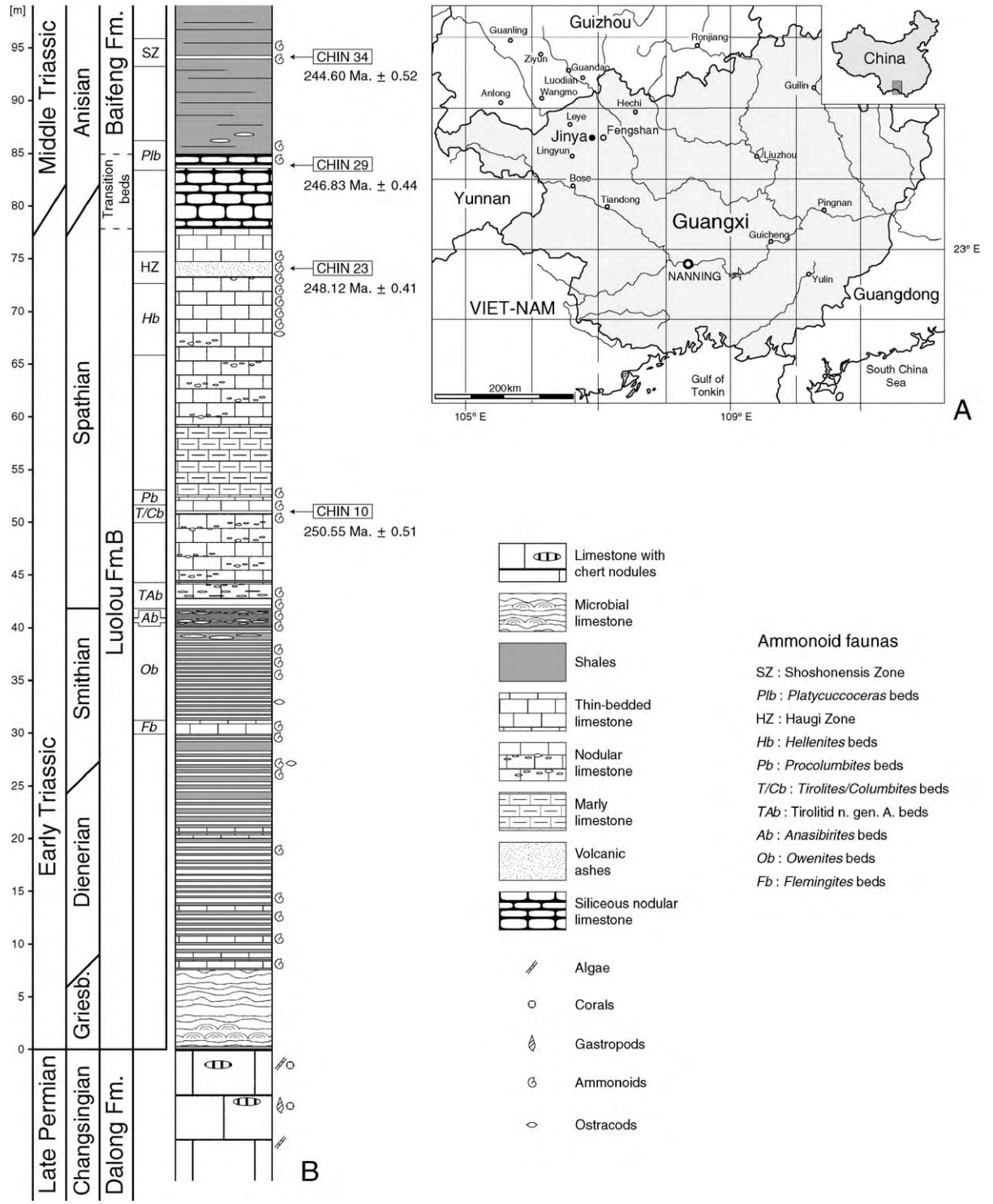

Fig. 1. (A) Location map of the various localities mentioned in the text. (B) Jinya section showing the stratigraphic position of the analyzed ash beds, and sample numbers with U–Pb ages obtained in this work. GPS coordinates of samples: CHIN-10 (N24°36′26.2″; E106°52′39.6″), CHIN-23 (N24°36′48.9″; E106°52′34.0″), CHIN-29 (N24°35′25.8″; E106°52′09.7″), CHIN-34 (N24°35′22.0″; E106°53′13.6″).

The lower, 15 to 25 cm thick ash layer (CHIN-10) shows a remarkable lateral continuity between the Jinya and Wangmo areas, over a distance of ~100 km. The upper, 60 to 260 cm thick ash layer (CHIN-23) can be traced laterally from Jinya to Leye (~60 km). The *Tirolites*/*Columbites* ammonoid assemblage associated with CHIN-10 indicates an early Spathian age (see Fig. 2). This fauna has a global, low-paleolatitudinal distribution. It is known from numerous Tethyan localities, as well as from the plate-bound Union Wash Formation (California) and the Thaynes Formation (Idaho). The low-paleolatitudinal *Neopopanoceras haugi* Zone fauna, associated with CHIN-23, is diagnostic of a late Spathian age (Fig. 2) and correlates with the high-paleolatitudinal *Keyserlingites subrobustus* Zone [20]. The *N. haugi* Zone is well documented in the Union Wash Formation (eastern California) and the Prida Formation (northwestern Nevada). It is here first reported from South China.

Transition from the Luolou Fm. to the overlying Baifeng Fm. is marked by a conspicuous, approximately 10 m thick unit composed of nodular siliceous limestones (i.e. "Transition beds" in Fig. 1B), which occurs in the Leye, Jinya, and Tiandong areas (see Fig. 1A), The "Transition beds" indicate a generalized drowning of the basin and contain abundant volcanic ash layers. Among these, a unique 25 cm thick, four-event ash layer (CHIN-29, see Fig. 1A) is intercalated within the uppermost part of the unit. It has been recognized in Jinya as well as in the vicinity of Tiandong, more than 200 km to the South. In the Jinya area, the poorly preserved, *Platycuccoceras*-dominated ammonoid assemblage (*Platycuccoceras* sp. indet., *Acrochordiceras* cf. *A. hyatti*, *Pseudodanubites* sp. indet.) associated with CHIN-29 indicates an early middle Anisian age (*A. hyatti* Zone, [21]).

The Baifeng Formation consists of a siliciclastic, thickening and coarsening upward turbiditic succession whose minimal thickness exceeds 1000 m. The predominantly shaly base of the formation contains rare, thin (mm to cm) medium-grained ash layers. One of these (CHIN-34, see Fig. 1B) is bracketed by layers containing a late middle Anisian ammonoid assemblage diagnostic of the low-paleolatitudinal *Balatonites shoshonensis* Zone [22]. So far, no clear high-paleolatitudinal correlative of this zone has been recognized [15].

The drastic change of the sedimentary regime between the Luolou and Baifeng formations suggests a concomitant modification in directions or rates of the convergence between the South and North China blocks [19]. It is worth noting that the higher abundance of volcanic ash layers observed in the "Transition beds" coincides with this profound change in the sedimentary regime. A reduced sedimentation rate within the "Transition beds" could also lead to this apparent concentration of volcanic ash layers.

3. Isotopic ages of the Early Triassic and the Anisian

The Permian–Triassic boundary was first radioisotopically dated by [23] at Meishan (stratotype of the Permian/Triassic boundary, South China) by SHRIMP ion microprobe techniques. Zircons from the so-called "boundary clay" (a 5 cm thick bentonite layer, bed 25 in [24] in Meishan yielded an age of 251.2±3.4 Ma. The same bentonite contains sanidine which has been dated by $^{40}Ar/^{39}Ar$ analysis to 249.9±0.2 Ma [25] (all further cited U–Pb and Ar–Ar ages do not include uncertainties on decay constants, tracer calibrations, natural standards and flux monitors). Subsequently, Bowring et al. [8] dated a succession of ash beds closely bracketing the Permian–Triassic boundary in three South Chinese sections (Meishan, Heshan, and Laibin) by multiple and single zircon grain U–Pb analyses. These authors placed the boundary at 251.4±0.3 Ma, excluding a concordant cluster consisting of 5 multi-grain analyses at an age of 252.7±0.4 Ma from their calculation (assuming inheritance of slightly older grains, perhaps incorporated during eruption). Mundil et al. [7] emphasized biases generated by the averaging effect resulting from multiple crystal analyses in [8] and proposed an age of 253 Ma for the boundary exclusively based on new and previous single grain analyses from the Meishan ash beds. Recently, Mundil et al. [26] proposed a revised age of 252.6±0.2 Ma for the Permian–Triassic boundary. Here, we emphasize the fact that for a comparison between ages derived from different isotopic systems, systematic errors have to be taken into a account. Recent studies [27,28] indicate that $^{40}Ar/^{39}Ar$ ages are generally younger (by ca. 1%) than U–Pb ages.

Only preliminary U–Pb ages exist for the early Anisian and the base of the middle Anisian [11,12]. However, an assessment of these data is impossible since details have not been published. Accordingly, these authors [11] emphasized that their dates "should not be cited as certain boundary ages". These two preliminary dates are from ash layers intercalated within slope series of Early and Middle Triassic age (Guandao sections in southern Guizhou) regarded as an equivalent of the Luolou Fm. by [11]. Paleontological age constraints are provided by conodonts (Orchard, in [11], Fig. 17). The older age of 247.8 Ma is associated

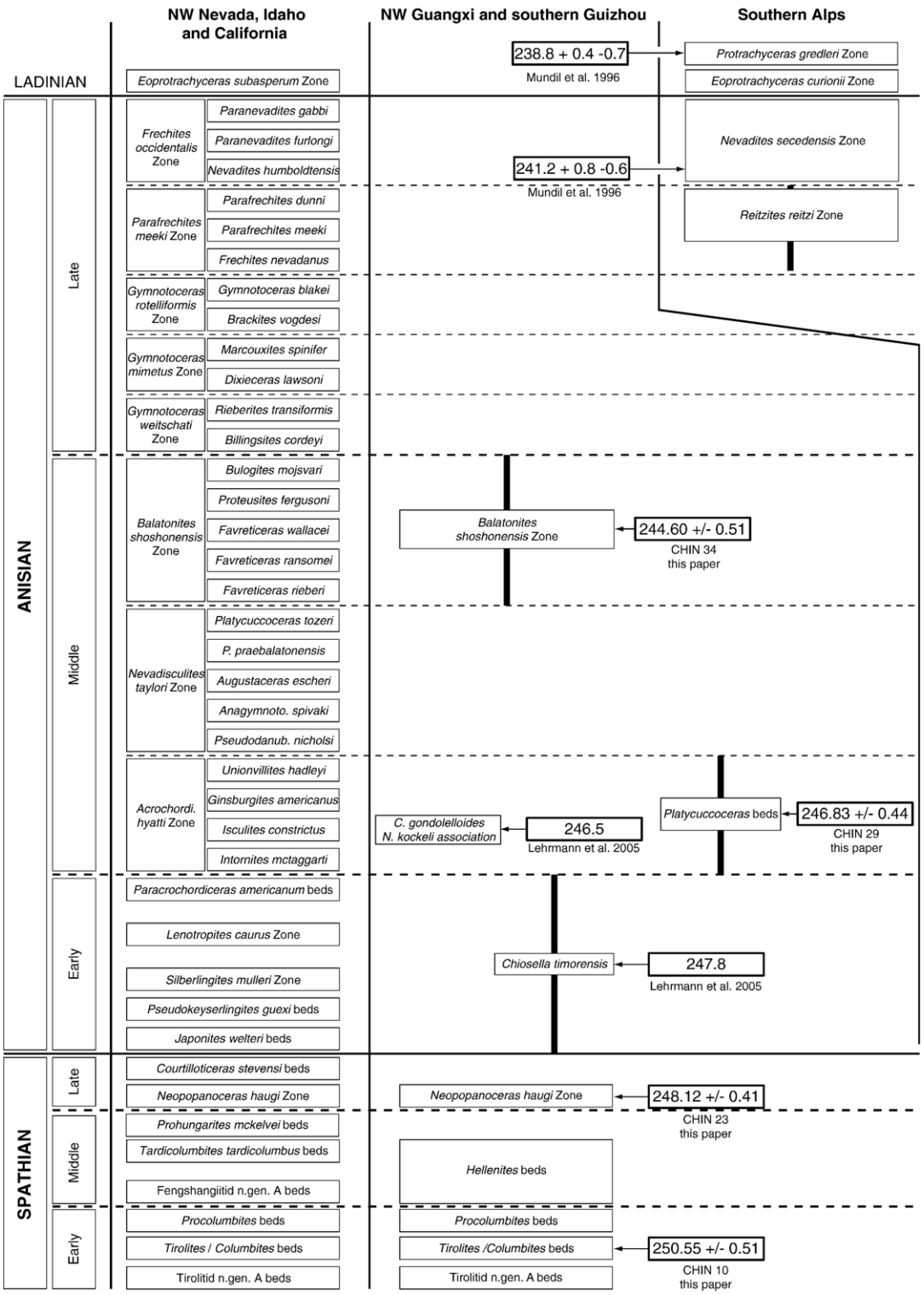

Fig. 2. Calibration of all new and published Early and Middle Triassic U–Pb ages from northwestern Guangxi, southern Guizhou, and the southern Alps with local ammonoid or conodont ages. Uncertainties in the biochronological correlations between the high-resolution North American ammonoid zonation and the Chinese and Alpine paleontological ages calibrated with U–Pb ages are indicated by the vertical black bars. See text for further explanation.

with *Chiosella timorensis*, whose range is restricted to the early Anisian in Nevada and elsewhere (Orchard, personal communication 2005). In the Guandao sequence, the two other associated conodonts, *Chiosella gondolelloides* and *Neogondolella regalis*, range higher into the early middle Anisian (Orchard, personal communication 2005) and are thus of less value in trying to narrow down the paleontological age. Hence, this first age falls within the early Anisian, but cannot be precisely tied to any of the refined ammonoid zones or beds as revised by Monnet and Bucher [15]. So far, this age is the only one that provides an upper limit for the Early–Middle Triassic boundary. The younger age of 246.5 Ma is associated with *C. gondolelloides*, *Nicoraella germanicus*, and *Nicoraella kockeli.* In the Nevadan ammonoid sequence, the overlap of *N. germanicus* with *N. kockeli* is only seen in the *Isculites constrictus* Subzone of the *A. hyatti* Zone (Orchard, personal communication 2005), which is early middle Anisian in age.

The next younger available radio-isotopic ages in the Triassic time scale are around the Anisian–Ladinian boundary in the Southern Alps, where tuff layers are bracketed by ammonoid faunas [9,29]. Based on U–Pb analyses of single zircon crystals, Mundil et al. [30] and Brack et al. [31] dated the base of the *Nevadites secedensis* Zone (late Anisian) to 241.2±0.8 Ma and the *Protrachyceras gredleri* Zone (Ladinian) to 238.8+0.5/−0.2 Ma. By interpolation, they proposed an age of 240.7 Ma for the base of the *Eoprotrachyceras curionii* Zone, which is the oldest Ladinian Zone [29]. Palfy et al. [10] used the U–Pb method on multiple zircon grain fractions to date tuff layers intercalated with faunas they considered to be near the Anisian–Ladinian boundary in the Balaton Highlands (Hungary). As a result, they proposed an age of 240.5±0.5 Ma for the base of *Reitzites reitzi* Zone in Hungary. However, as shown by [7], multigrain analyses are prone to yield inaccurate, generally younger ages, as a result of unrecognized Pb loss. Based on the above results, Ogg ([13], Fig. 17.1) extrapolated an age of 237±2 Ma for the Anisian–Ladinian boundary, which conflicts with the 238.8+0.5/−0.2 Ma age obtained for the Ladinian *P. gredleri* Zone.

4. U–Pb geochronological method and results

The most accurate available isotopic system for dating ash layers is the decay of ^{238}U and ^{235}U to radiogenic lead isotopes ^{206}Pb and ^{207}Pb in zircon. In undamaged zircon, the diffusion coefficients for Pb and U are negligible [32]. The analytical techniques of low-blank isotope-dilution thermal ionization mass spectrometry (ID-TIMS) applied to a number of single crystals from a zircon population of the same sample offer the possibility to date the crystallization of this population with permil uncertainty. Precise and accurate zircon ages can mainly be biased by three effects: (1) post-crystallization lead loss resulting from open system behaviour of crystal domains, which then yield apparently younger age; (2) incorporation of old cores acting as nuclei during crystallization,–or more generally–of foreign lead with a radiogenic composition indicative for a pre-ash depositional age, leading to too old apparent ages; (3) incorporation of xenocrysts (or "antecrysts") from a previous magmatic cycle, often slightly older than the original magmatic population and particularly common during multiple volcanic events.

Our U–Pb data indicate that the tuffs contain entirely magmatic grains yielding concordant results, as well as zircons with an important inherited component of Late Proterozoic age. The cathodoluminescence (CL) imaging revealed that there are grains with undisturbed oscillatory zoning patterns (OZPs), which are considered to be representative of magmatic growth (Fig. 3a). Some grains from the same sample, however, display a conspicuous discordant core, which may account for the presence of older inherited lead components (Fig. 3b). CL images may also show a distinct fainting of the OZP, indicating a replacement of the magmatic zoning by structureless high-luminescent zones (Fig. 3c). These processes are well-known to cause U–Pb interelement fractionation and lead loss (see, e.g., [33,34]).

4.1. Analytical technique

Zircons were prepared by standard mineral separation and purification methods (crushing and milling, concentration via Wilfley Table or hand washing, magnetic separation, and heavy liquids). For each sample, least-magnetic zircon crystals were selected and mounted in epoxy resin and imaged by cathodoluminescence to assess whether the population contains inherited cores.

In order to minimize the effects of secondary lead loss two techniques were employed: (1) conventional air-abrasion [35] and (2) "CA (chemical abrasion)-TIMS" technique involving high-temperature annealing followed by a HF leaching step [36]. The latter has been shown to be more effective in removing strongly radiation damaged zircon domains, which underwent lead-loss during post crystallization fluid processes [26,36]. Air-abraded zircons were washed first in diluted HNO_3, followed by distilled water and acetone in an ultrasonic bath prior to weighing. For the zircons

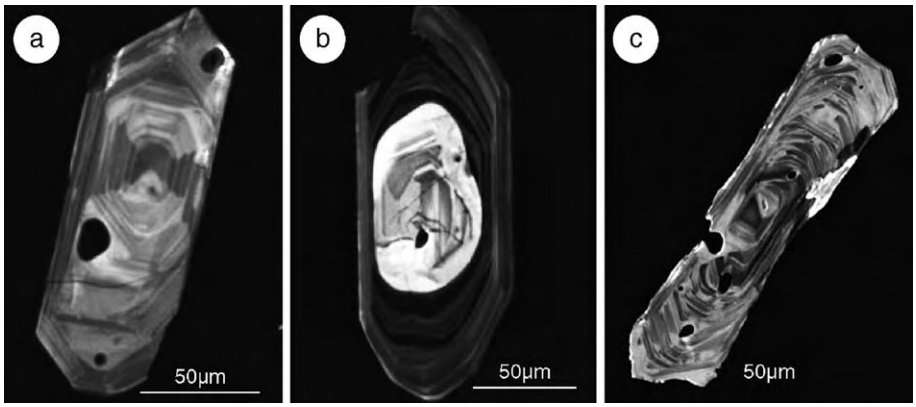

Fig. 3. Representative cathodoluminescence (CL) pictures of zircon: (a) undisturbed oscillatory zoning pattern (sample CHIN-29); (b) crystal with a core indicating the presence of an inherited lead component (sample CHIN-23); (c) oscillatory zoning with diffuse zone boundaries, indicating a disturbed lattice and therefore possible lead loss (sample CHIN-23).

subjected to chemical abrasion techniques, annealing was performed by loading 20–40 zircon grains of each sample in quartz crucibles and placing them into a furnace at 900 °C for approximately 60 h. Subsequently, for the leaching (chemical abrasion) step, zircons from each sample were transferred in 3 ml screw-top Savillex vials with ca. 120 μl concentrated HF. Loosely capped Savillex vials were arranged into a Teflon Parr™ vessel with 1 ml concentrated HF, and placed in an oven at 180 °C for 12–15 h. After the partial dissolution step, the leachate was completely pipetted out and the remaining zircons were fluxed for several hours in 6 N HCl (on a hotplate at a temperature of ca. 80 °C), rinsed in ultrapure H_2O and then placed back on the hot plate for an additional 30 min in 4 N HNO_3 for a "clean-up" step. The acid solution was removed and the fractions were again rinsed several times in ultra-pure water and acetone in an ultrasonic bath. Single zircons were selected, weighed and loaded for dissolution into pre-cleaned miniaturized Teflon vessels. After adding a mixed ^{205}Pb–^{235}U spike zircons were dissolved in 63 μl concentrated HF with a trace of 7 N HNO_3 at 180 °C for 5 days, evaporated and re-dissolved overnight in 36 μl 3 N HCl at 180 °C. Pb and U were separated by anion exchange chromatography in 40 μl micro-columns, using minimal amounts of ultra-pure HCl, and finally dried down with 3 μl 0.2 N or 0.06 N H_3PO_4.

Isotopic analysis was performed in ETH-Zurich on a MAT262 mass spectrometer equipped with an ETP electron multiplier backed by a digital ion counting system. The latter was calibrated by repeated analyses of the NBS 982 standard using the $^{208}Pb/^{206}Pb$ ratio of 1.00016 for mass bias correction [37] and the U500 standard, in order to correct for the 0.3% multiplier-inherent logarithmic rate effect [38]. Mass fractionation effects were corrected for 0.09±0.05 per a.m.u. Both lead and uranium were loaded with 1 μl of silica gel-phosphoric acid mixture [39] on outgassed single Re-filaments, and Pb as well as U (as UO_2) isotopes were measured sequentially on the electron multiplier. Total procedural common Pb concentrations were measured at values between 0.4 and 3.5 pg and were attributed solely to laboratory contamination. They were corrected with the following isotopic composition: $^{206}Pb/^{204}Pb$: 18.5 ±0.6% (1σ), $^{207}Pb/^{204}Pb$: 15.5±0.5% (1σ), $^{208}Pb/^{204}Pb$: 37.9±0.5% (1σ), representing the average values for 13 blank determinations in the Geneva laboratory 2004–2005. The uncertainties of the spike and blank lead isotopic composition, mass fractionation correction, and tracer calibration were taken into account and propagated to the final uncertainties of isotopic ratios and ages. The ROMAGE program was used for age calculation and error propagation (Davis, unpublished). The international R33 standard zircon [40] has been dated at an age of 420.7±0.7 Ma during the same analytical period (n=6). Calculation of concordant ages and averages was done with the Isoplot/Ex v.3 program of Ludwig [41]. Ellipses of concordia diagrams represent 2 sigma uncertainties.

4.2. Results

4.2.1. Sample CHIN-10

Zircons from sample CHIN-10 are short to long prismatic (up to 150 μm in their longest dimensions), often cracked, rich in apatite and fluid inclusions. CL zircon imaging revealed that there are grains with undisturbed oscillatory zoning, predominantly long

Table 1
U–Pb isotopic data of analyzed zircons

Sample no.	Weight (mg)	Concentration			Th/U[a]	Atomic ratios							Correlation coefficient	Ages		
		U (ppm)	Pb (ppm)	Pb com. (pg)		$^{206}Pb/^{204}Pb$[b]	$^{207}Pb/^{206}Pb$[c,d]	Error 2σ (%)	$^{207}Pb/^{235}U$[c]	Error 2σ (%)	$^{206}Pb/^{238}U$[c,d]	Error 2σ (%)		$^{206}Pb/^{238}U$	$^{207}Pb/^{235}U$	$^{207}Pb/^{206}Pb$
Chin-10																
1[e]	0.0024	378	16.28	2.62	0.45	888	0.051460	0.74	0.2812	0.94	0.03962	0.64	0.62	250.50	251.59	261.68
2[e]	0.0024	244	10.74	2.97	0.37	513	0.051330	0.78	0.2808	0.90	0.03968	0.44	0.50	250.83	251.29	255.58
3	0.0032	348	14.77	3.31	0.49	1027	0.051210	0.68	0.2791	1.34	0.03953	0.78	0.73	249.94	249.97	250.29
4	0.0010	194	10.22	2.45	0.56	226	0.053080	1.80	0.3030	2.06	0.04141	0.72	0.51	261.54	268.74	332.01
5	0.0032	345	14.83	0.60	0.63	4612	0.051320	0.24	0.2810	0.46	0.03971	0.36	0.86	251.03	251.43	255.15
6	0.0028	258	9.61	0.95	0.49	1712	0.051140	0.38	0.2481	0.52	0.03518	0.38	0.68	222.89	224.99	247.98
7	0.0031	78	3.33	0.49	0.61	1250	0.051210	0.62	0.2789	0.88	0.03950	0.58	0.71	249.74	249.78	250.17
8	0.0020	225	9.00	0.98	0.34	1159	0.051310	0.66	0.2799	0.86	0.03956	0.52	0.64	250.10	250.55	254.81
Chin-23																
9[e]	0.0039	438	17.73	0.88	0.46	4818	0.051190	0.46	0.2757	0.59	0.03907	0.44	0.64	247.05	247.26	249.25
10[e]	0.0045	241	9.89	1.94	0.43	1404	0.050950	0.48	0.2746	0.62	0.03910	0.46	0.64	247.22	246.40	238.53
11	0.0030	377	15.79	0.69	0.32	4335	0.051330	0.44	0.2960	0.94	0.04183	0.94	0.85	264.14	263.27	255.53
12	0.1010	260	10.02	2.04	0.24	3219	0.051120	0.22	0.2767	0.42	0.03925	0.38	0.85	248.20	248.00	246.15
13	0.0095	272	10.87	1.13	0.38	5707	0.051220	0.20	0.2771	0.40	0.03923	0.36	0.87	248.08	248.34	250.78
14	0.0055	410	16.48	1.51	0.40	3733	0.051200	0.22	0.2771	0.42	0.03925	0.36	0.85	248.18	248.32	249.73
15	0.0075	347	13.48	2.08	0.27	3132	0.051080	0.20	0.2761	0.62	0.03919	0.58	0.95	247.88	247.55	244.37
16	0.0051	188	7.36	0.98	0.31	2432	0.051160	0.48	0.2764	0.56	0.03918	0.48	0.58	247.78	247.79	247.91
17	0.0108	240	9.17	0.99	0.24	6545	0.051200	0.16	0.2772	0.42	0.03927	0.36	0.93	248.29	248.43	249.74
18	0.0180	95	21.49	0.68	0.13	34422	0.149840	0.10	4.4198	0.38	0.21393	0.33	0.97	1249.70	1716.00	2344.10
Chin-29																
19[e]	0.0013	172	24.67	1.48	0.63	957	0.069730	1.72	1.2208	1.86	0.12697	0.64	0.38	770.55	810.14	920.53
20[e]	0.0010	338	15.88	3.03	0.48	293	0.051320	1.56	0.2757	1.68	0.03896	0.54	0.38	246.36	247.21	255.25
21	0.0012	857	36.54	0.73	0.66	3484	0.051300	0.42	0.2758	0.50	0.03900	0.52	0.66	246.61	247.34	254.23
22	0.0033	264	10.85	0.88	0.52	2466	0.051190	0.34	0.2757	0.54	0.03906	0.44	0.78	246.99	247.22	249.41
23	0.0090	149	6.41	3.29	0.54	1023	0.051420	0.42	0.2766	0.60	0.03902	0.36	0.73	246.74	247.96	259.54
24	0.0010	279	11.67	0.62	0.58	1136	0.051130	0.68	0.2756	0.82	0.03907	0.42	0.56	247.19	247.15	246.78
25	0.0058	33	1.37	0.69	0.56	692	0.051170	0.98	0.2754	1.18	0.03904	0.48	0.58	246.88	247.03	248.46
Chin-34																
26[e]	0.0100	268	11.07	0.83	0.50	1044	0.051070	1.66	0.2707	1.78	0.03845	0.66	0.36	243.21	243.29	244.02
27[e]	0.0017	282	11.40	0.63	0.46	1441	0.051160	1.20	0.2719	1.39	0.03854	0.92	0.52	243.79	244.18	247.92
28	0.0020	338	13.81	1.81	0.51	1121	0.051100	0.70	0.2728	1.12	0.03872	0.60	0.84	244.87	244.91	245.39
29	0.0010	236	10.47	1.62	0.55	375	0.051050	1.26	0.2722	1.40	0.03867	0.44	0.46	244.58	244.42	242.88
30	0.0026	285	12.12	2.10	0.55	882	0.051110	0.50	0.2724	0.64	0.03865	0.34	0.63	244.45	244.57	245.73
31	0.0007	581	25.05	1.67	0.51	617	0.051030	0.68	0.2723	0.80	0.03870	0.46	0.53	244.75	244.51	242.16
32	0.0004	1114	59.83	3.57	0.66	168	0.051870	2.20	0.2700	2.38	0.03775	0.68	0.40	238.88	242.70	279.76

[a] Calculated on the basis of radiogenic $^{208}Pb/^{206}Pb$ ratios, assuming concordancy.

[b] Corrected for fractionation and spike.

[c] Corrected for fractionation, spike and blank.

[d] Corrected for initial Th disequilibrium, using an estimated Th/U ratio of 4 for the melt.

[e] Air-abraded zircons.

prismatic, needle-like crystals. Some short prismatic and sub-equant zircons contain inherited cores. Eight single long prismatic crystals (assuming undisturbed oscillatory zoning) were analyzed from this sample following the laboratory procedure outlined above (analytical data are given in Table 1). There is no difference in age obtained by zircons pre-treated by air-abrasion or chemical-abrasion. Two of the chemically abraded zircons yielded variably discordant dates—one is significantly older (analysis 4) and thus indicates the presence of inherited component; and the one (analysis 6) shows lead loss (Fig. 4a). The remaining data are concordant within analytical error and define a weighted mean $^{206}Pb/^{238}Pb$ age of 250.55±0.51 Ma (MSWD=0.7; Fig. 4a), which we consider to be the best estimate for the age of this ash bed associated with the *Tirolites*/*Columbites* beds (early Spathian).

4.2.2. Sample CHIN-23

Zircons from this sample are similar in size and morphology to those described above. The CL zircon images display a clear oscillatory zoning pattern which often shows diffuse contacts between neighboring zones ("fainting"), grading into a replacement of the magmatic zoning by structureless high-luminescent zones. The CL images also revealed the presence of a core and an oscillatory rim in some of the short prismatic crystals. Therefore, only single long-prismatic, to acicular crystals were selected for analysis. Nevertheless, two of the chemically abraded zircons (analyses 11 and 18) are older in age and assumed to represent xenocrysts or contain inherited components. Two air-abraded zircons (analyses 9 and 10) are slightly younger than the chemically abraded zircons (Fig. 4b). This is interpreted as a result of the more efficient chemical abrasion technique which allows complete removal of more internal zones that underwent diffusive lead loss. The remaining six chemically abraded zircons are perfectly concordant and define a weighted mean $^{206}Pb/^{238}Pb$ age of 248.12±0.41 Ma (MSWD=0.13; Fig. 4b). We consider this to be the best estimate for the age of these zircons and hence, of the ash bed intercalated within the *N. haugi* Zone (late Spathian).

4.2.3. Sample CHIN-29

Zircons from this sample vary from short to long prismatic (up to 150 μm in their longest dimensions).

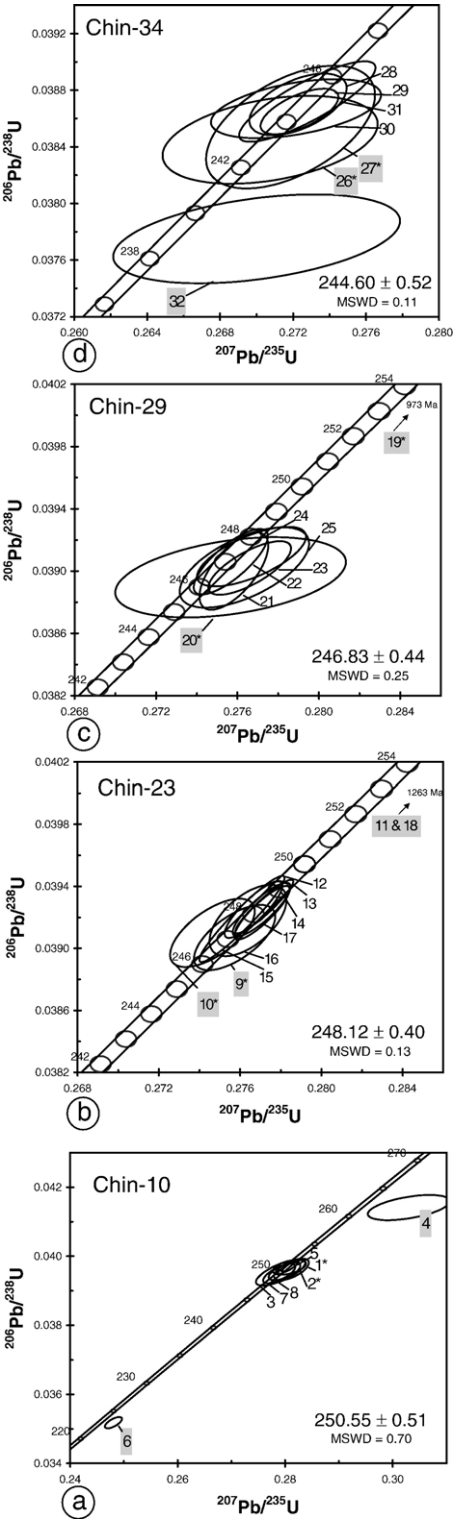

Fig. 4. Concordia plots showing the results of single-zircon analyses from volcanic ash bed samples, from the Jinya section (see Fig. 1B); (a) CHIN-10; (b) CHIN-23; (c) CHIN-29; (d) CHIN-34. Individual analyses are shown as 2σ error ellipses (grey numbers—analyses not included in weighted mean calculation; *—air-abraded zircons; the numbers correspond to the zircon numbers in Table 1). Given ages are weighted mean $^{206}Pb/^{238}U$ ages at 95% confidence level.

The CL imaging revealed that the large long prismatic or equant grains usually contain cores, whereas the needle-like crystals have usually magmatic oscillatory zoning. Air-abrasion of the latter is more difficult because they used to crack and disintegrate. Seven single long prismatic crystals (which would assumingly show undisturbed oscillatory zoning) were analyzed. There is no difference in age obtained by zircons pre-treated by air-abrasion or chemical-abrasion (Fig. 4c), except one of the air-abraded zircons (analysis 19), which is significantly older and thus indicates the presence of inherited component. The remaining data are concordant within analytical error and define a weighted mean $^{206}Pb/^{238}Pb$ age of 246.83±0.44 Ma (MSWD=0.25; Fig. 4c), which is interpreted to be the best estimate for the age of these zircons and inferentially the age of this ash bed associated with the *A. hyatti* Zone (early middle Anisian).

4.2.4. Sample CHIN-34

Zircons from this sample are larger than those in the previously described samples and range in size from 200×30 μm to short prismatic and rarely equant 50×50 μm grains. CL zircon imaging displays a clear oscillatory zoning pattern, which is often fainted, indicating some replacement or recrystallization process in the magmatic zones. CL also revealed the presence of cores and oscillatory rims in some of the short prismatic crystals, thus only single long prismatic, "needle-like" crystals were selected for analysis. Seven single grains were analyzed, all of which define a linear array on a concordia diagram and are anchored by four concordant analyses of chemically abraded zircons (Fig. 4d). Two air-abraded grains (analyses 26 and 27) are concordant within analytical error but slightly younger in age than the chemically abraded zircons and thus excluded from the calculation of the weighted mean $^{206}Pb/^{238}Pb$ age. Another of the chemically abraded zircons is also excluded from the mean, because it clearly shows effects of Pb loss (analysis 32). If only the most concordant four analyses are considered (analyses 28–31) a weighted mean $^{206}Pb/^{238}Pb$ age of 244.60±0.52 Ma (MSWD=0.11; Fig. 4d) is obtained. We consider this to be the age of the zircons and inferentially the age of the ash layer intercalated within the *B. shoshonensis* Zone (late middle Anisian).

5. Calibration of U–Pb ages and ammonoid zones

All new and previous dates are summarized in Fig. 2. All available U–Pb ages show a remarkable coherence, including the preliminary ages of [11]. The low-paleolatitudinal North American record provides the most comprehensive ammonoid succession for the Spathian and the Anisian, against which calibrated ages from South China and from the Southern Alps are correlated. The Anisian part of the North American zonation is derived from the recent synthesis of [15]. The Spathian part of the zonation is still in a preliminary stage ([16] and ongoing work by Bucher and Guex), but it correlates well with the faunal succession from the Luolou Fm. The poorer Anisian ammonoid record from the Baifeng Fm. can also be correlated, although with the obvious uncertainties as indicated by the black vertical bars (see Fig. 2).

The Early/Middle Triassic boundary is here now bracketed between 248.1±0.4 Ma and 247.8 Ma. With a *N. secedensis* Zone age of 241.2+0.8/−0.6 Ma [9], a minimal duration of 6.6+0.7/−0.9 my can be inferred for the Anisian. Considering a 252.6±0.2 Ma age for Permian/Triassic boundary [26] and a *N. haugi* Zone age of 248.1±0.4 Ma, the minimal duration of the Early Triassic amounts to 4.5±0.6 my. Alternatively, a Permian/Triassic boundary age of 251.4±0.3 Ma [8] would reduce the duration of the Early Triassic to 3.3 ±0.7 my. In this study, a minimum duration of 2.4 ±0.9 my is established for the Spathian. However, because the lowermost and uppermost Spathian ammonoid zones are not comprised within the interval bounded by our two U–Pb ages (see Fig. 2), a duration of ca. 3 my appears as a more realistic estimate. Regardless what the cumulative error on the Spathian duration may be, our results clearly highlight that the four Early Triassic substages are of extremely uneven duration. Consequently, the respective durations of the Induan and Olenekian stages are even more disparate. When taking all uncertainties of available U–Pb ages into account, a Permian–Triassic boundary of 251.4 ±0.3 Ma [8] implies that the minimal duration of the Spathian would represent 52% to unrealistic values in excess of 100% (!) of the entire Early Triassic. More realistically, a Permian–Triassic boundary of 252.6±0.2 Ma [26] implies that the minimal duration of the Spathian represents 41% to 95% of the entire Early Triassic.

6. Implications for the Early Triassic biotic recovery

Our calibration of new U–Pb ages with ammonoid zones implies that the use of stages or substages of supposedly equal duration irremediably leads to an exaggerated delayed recovery during the Early Triassic. The obvious consequence of the new calibrations is that

the survival and recovery phases of well-documented clades such as ammonoids [3], conodonts [42,43], or even brachiopods [44] must be significantly shorter than previous estimates.

As far as ammonoids are concerned [3], they return to a full diversity equilibrium in the Spathian, i.e. 1 to 3 my after the Permian–Triassic boundary, depending on which of the two available ages is considered for the latter. This equilibrium phase is characterized by a very steep, bimodal latitudinal gradient of taxonomic richness. Numerical simulations strongly support the fundamental causal link between the latitudinal gradient of sea-surface temperatures (SST) and the shape of the latitudinal gradient of taxonomic richness for marine organisms having at least one planktonic or pseudoplanktonic stage in their life-cycles [45]. Simply stated, a flat SST latitudinal gradient generates a low global diversity and a flat latitudinal diversity gradient, whereas a steep SST gradient generates a high global diversity and a steep, bimodal diversity gradient, similar to that of the Spathian ammonoids and to that of the present-day, Atlantic planktonic foraminifera used to calibrate the model in the simulations [45].

The transition leading from the Griesbachian low global diversity and flat latitudinal diversity gradient to the Spathian high global diversity and steep, bimodal diversity gradient was not a single, smooth and gradual rebound for the ammonoids [3]. It was interrupted during the end Smithian (the *Anasibirites pluriformis* Zone and its high paleolatitude correlative, the *Wasatchites tardus* Zone) by a sudden diversity collapse coupled with a drastic increase of cosmopolitan distributions, thus suggesting the resurgence of a flat SST gradient. The end Smithian ammonoid extinction also correlates with a global perturbation of the carbon cycle ([46,47]). It also coincides with the ultimate peak of anoxia in several Tethyan outer platforms ([46]). A warm and equal climate triggered by high concentrations of greenhouse gases appears as a likely explanation for such a flat SST gradient. Depending on the two alternative ages available for the Permian–Triassic boundary, the global end Smithian diversity drop of ammonoids can be inferred to have occurred no later than 0.5 my to 2.5 my after the beginning of the Triassic. However, a 0.5 my duration is evidently too short to accommodate all the ammonoid zones included into the Griesbachian, Dienerian, and Smithian substages.

More speculatively, it is tempting to relate these end Smithian events to a late volcanic pulse which would have occurred after the main eruption of the Siberian traps. $^{40}Ar/^{39}Ar$ ages of the huge basaltic flows from the Siberian Craton, the West Siberian Basin, Taimyr, and even possibly Kazakstan indicate that the main eruptive phase lasted no longer than 1 or 2 my [48–51]. Yet, genetically related, less intensive igneous activity at the southern fringe of the Siberian Craton apparently continued at least some 6 my after the main volcanic pulse [52]. A late eruptive activity in the Western Siberian Basin was also suggested by magnetostratigraphic constraints [53]. We also note that relevant information on the age of the youngest volcanic flows is extremely sparse, mainly because the upper boundary of the traps is either erosional and/or capped by terrestrial, poorly dated Triassic sediments. An upper age limit for the cessation of the main flood-volcanic event is nevertheless provided by a U–Pb baddeleyite age of 250.2±0.3 Ma from a carbonatite intruding the Guli volcanic-intrusive complex in the Maymecha-Kotuy area [54]. In the eastern Taimyr Peninsula (Chernokhrebetnaya River), Sobolev (personal communication 2005) documented that the oldest Early Triassic ammonoids within the Vostochnyi-Taymir Formation are of early Smithian age and occur 120 m above the uppermost basaltic flows of the Tsvekovomys Formation. This ammonoid age constraint apparently supports a short duration (1 to 2 my) for the main eruptive phase and the hypothesis that the end Smithian events must have been triggered by a distinct, later episode.

7. Conclusions

Our new Early Triassic dates indicate that the duration of the Spathian (ca. 3 my) amounts to at least half of the duration of the Early Triassic. The four Early Triassic substages are therefore of extremely uneven duration, not to mention the case of the Induan and the Olenekian stages. A minimal duration of $6.6+0.7/-0.9$ my is also proposed for the Anisian stage.

Our results confirm that U–Pb ages obtained from thermally annealed/chemically abraded zircons show improved concordancy, thus corroborating the results of [26,36]. This indicates that the chemical abrasion technique is obviously more efficient in removing Pb loss zones than air abrasion. This is more important in zircon populations consisting of acicular and skeletal grains, which are not well suited for thorough air-abrasion. However, zircon grains with undisturbed oscillatory zoning pattern represent a stable crystalline state and yielded comparable age results for both preparation techniques.

Our new U–Pb ages provide reliable tie points for the timing of the Triassic recovery. However, additional calibration points are needed for the Griesbachian,

Dienerian and Smithian substages. The new Spathian U–Pb ages also narrow the time interval between the end Smithian global diversity drop of ammonoids and the coeval carbon cycle perturbation on one hand, and the end of the main eruptive phase of the Siberian traps on the other. However, the timing of the ammonoid recovery and the age constraint from eastern Taimyr suggest that the end Smithian events were triggered by a later–yet unknown–volcanic pulse distinct from the main eruptive phase.

Acknowledgements

P. Brack, P.A. Hochuli and N. Goudemand are thanked for their thorough comments on an earlier version of the manuscript. Constructive reviews by the three EPSL referees R. Mundil, S. Kamo and N. Silberling were deeply appreciated. Kuang Guodun provided invaluable assistance in the field. M. Orchard shared useful information on the calibration between Anisian conodonts and ammonoids. E. Sobolev and V. Pavlov helped with the Russian literature on the Siberian traps. E. Sobolev also shared information on the Triassic stratigraphy of eastern Taimyr. A. von Quadt and M.-O. Diserens are thanked for helping with mass spectrometry and electron microscopy. U–Pb analyses were supported by the Swiss NSF project 200021-103335 (to U.S.). Fieldwork and paleontological work was supported by the Swiss NSF project 200020-105090/1 (to H.B) and a Rhône-Alpes-Eurodoc grant (to A.B). The Association Franco-chinoise pour la Recherche Scientifique et Technique (PRA T99-01) supported an initial field survey in Guangxi.

References

[1] J. Guex, Biochronologic Correlations, Springer-Verlag, 1991, p. 252.
[2] D.H. Erwin, S.A. Bowring, Y. Yin, End-Permian mass extinctions: a review, Spec. Pap.-Geol. Soc. Am. 356 (2002) 363–383.
[3] A. Brayard, H. Bucher, G. Escarguel, Diversity gradients of Early Triassic ammonoids and their paleoclimatic significance, Sixth International Symposium Cephalopods—Present and Past, Fayetteville, Arkansas, 2004.
[4] E.T. Tozer, A standard for Triassic Time, Bull.-Geol. Surv. Can. 156 (1967) 1–103.
[5] N.J. Silberling, E.T. Tozer, Biostratigraphic classification of the marine Triassic in North America, Spec. Pap.-Geol. Soc. Am. 110 (1968) 1–63.
[6] L.D. Kiparisova, Y.D. Popov, Subdivision of the lower series of the Triassic System into stages, Trans. Acad. Sci. USSR, Nauka 109 (1956) 842–845.
[7] R. Mundil, I. Metcalfe, K.R. Ludwig, P.R. Renne, F. Oberli, R. S. Nicoll, Timing of the Permian–Triassic biotic crisis: implications from new zircon U/Pb age data (and their limitations), Earth Planet. Sci. Lett. 187 (2001) 131–145.
[8] S.A. Bowring, D.H. Erwin, Y.G. Jin, M.W. Martin, K. Davidek, W. Wang, U/Pb zircon geochronology and tempo of the End-Permian mass extinction, Science 280 (1998) 1039–1045.
[9] P. Brack, H. Rieber, A. Nicora, The Global Boundary Stratotype Section and Point (GSSP) for the base of the Ladinian Stage (Middle Triassic). A proposal for the GSSP at the base of the Curionii Zone in the Bagolino section (Southern Alps, Northern Italy), Albertiana 28 (2003) 13–25.
[10] J. Palfy, R.R. Parrish, K. David, A. Vöros, Mid-Triassic integrated U–Pb geochronology and ammonoid biochronology from the Balaton Highland (Hungary), J. Geol. Soc. 160 (2003) 271–284.
[11] D.J. Lehrmann, J.L. Payne, P. Enos, P. Montgomery, J. Wei, Y. Yu, J. Xiao, M.J. Orchard, Field excursion 2: Permian–Triassic boundary and a Lower–Middle Triassic boundary sequence on the Great Bank of Guizhou, Nanpanjiang basin, southern Guizhou Province, Albertiana 33 (2005) 169–186.
[12] M.V. Martin, D.J. Lehrmann, S.A. Bowring, P. Enos, J. Ramenazi, J. Wei, J. Zhang, Anonymous, Timing of Lower Triassic carbonate bank buildup and biotic recovery following the end-Permian extinction across the Nanpanjiang Basin, South China, Abstr. Programs-Geol. Soc. Am. 33 (2001) 201.
[13] J.G. Ogg, The Triassic period, in: F.M. Gradstein, J.G. Ogg, A.G. Smith (Eds.), A Geological Time Scale, Cambridge Univ. Press, 2004, pp. 271–306.
[14] G. Escarguel, H. Bucher, Counting taxonomic richness from discrete biochronozones of unknown duration: a simulation, Palaeogeogr. Palaeoclimatol. Palaeoecol. 202 (2004) 181–208.
[15] C. Monnet, H. Bucher, Anisian (Middle Triassic) ammonoids from North America: quantitative biochronology and biodiversity, Stratigraphy 2 (2005) 281–296.
[16] J. Guex, A. Hungerbühler, J. Jenks, D. Taylor, H. Bucher, Dix-huit nouveaux genres d'ammonites du Spathien (Trias inférieur) de l'Ouest américan (Idaho, Nevada, Californie), Note préliminaire, Bull. Géol. Lausanne 362 (2005) 1–31.
[17] GXBGMR, (Guangxi, Bureau of Geology and Mineral Resources), Regional Geology of Guangxi Zhuang Autonomous Region, Geol. Mem. ser. 1 n. 3, Geol. Publ. House, Beijing, 1985, p. 853.
[18] D.J. Lehrmann, P. Enos, J.L. Payne, P. Montgomery, J. Wei, Y. Yu, J. Xiao, M.J. Orchard, Permian and Triassic depositional history of the Yangtze platform and Great Bank of Guizhou in the Nanpanjiang basin of Guizhou and Guangxi, south China, Albertiana 33 (2005) 149–168.
[19] S.A. Gilder, R.S. Coe, H.R. Wu, G.D. Kunag, X.X. Zhao, Q. Wu, Triassic paleomagnetic data from South China and their bearing on the tectonic evolution of the western Circum-Pacific Region, Earth Planet. Sci. Lett. 131 (1995) 269–287.
[20] H. Bucher, Lower Anisian ammonoids from the Northern Humboldt Range (Northwestern Nevada, USA) and their bearing upon the Lower–Middle Triassic boundary, Eclogae Geol. Helv. 82 (1989) 945–1002.
[21] H. Bucher, Ammonoids of the Hyatti Zone and the Anisian transgression in the Triassic Star Peak Group, Northwestern Nevada, USA, Palaeontogr. Abt. A 223 (1992) 137–166.
[22] H. Bucher, Ammonoids of the Shoshonensis Zone (Middle Anisian, Middle Triassic) from northwestern Nevada (USA), Jahrb. Geol. Bundesanst., Wien 135 (1992) 425–465.

[23] J.C. Claoué-Long, Z. Zhang, M. Guogan, D. Shaohua, The age of the Permian–Triassic boundary, Earth Planet. Sci. Lett. 105 (1991) 182–190.
[24] H.F. Yin, K.X. Zhang, J.N. Tong, Z.Y. Yang, S.B. Wu, The Global Stratotype Section and Point (GSSP) of the Permian–Triassic Boundary, Episodes 24 (2001) 102–114.
[25] P.R. Renne, Z.C. Zhang, M.A. Richards, M.T. Black, A.R. Basu, Synchrony and causal relations between Permian–Triassic Boundary crises and Siberian flood volcanism, Science 269 (1995) 1413–1416.
[26] R. Mundil, K.R. Ludwig, I. Metcalfe, P.R. Renne, Age and timing of the Permian mass extinctions: U/Pb dating of closed-system zircons, Science 305 (2004) 1760–1763.
[27] K. Min, R. Mundil, P.R. Renne, K.R. Ludwig, A test for systematic errors in 40Ar/39Ar geochronology through comparison with U/Pb analysis of a 1.1-Ga rhyolite, Geochim. Cosmochim. Acta 64 (2000) 73–98.
[28] P.R. Renne, R. Mundil, K. Min, K.R. Ludwig, Intercalibration of the U–Pb and Ar-40/Ar-39 geochronometers: status, prognosis, and proscription, Geochim. Cosmochim. Acta 69 (2005) A321.
[29] P. Brack, H. Rieber, R. Mundil, A. Nicora, The Global Boundary Stratotype Section and Point (GSSP) of the Ladinian Stage (Middle Triassic) at Bagolino (Southern Alps, Northern Italy) and its implications for the Triassic time scale, Episodes 28 (2005) 233–244.
[30] R. Mundil, P. Brack, M. Meier, H. Rieber, F. Oberli, High resolution U–Pb dating of Middle Triassic volcaniclastics: time-scale calibration and verification of tuning parameters for carbonate sedimentation, Earth Planet. Sci. Lett. 141 (1996) 137–151.
[31] P. Brack, R. Mundil, F. Oberli, M. Meier, H. Rieber, Biostratigraphic and radiometric age data question the Milankovitch characteristics of the Latemar cycles (southern Alps, Italy), Geology 24 (1996) 371–375.
[32] D.J. Cherniak, E.B. Watson, Pb diffusion in zircon, Chem. Geol. 172 (2001) 5–24.
[33] U. Schaltegger, C.M. Fanning, D. Gunther, J.C. Maurin, K. Schulmann, D. Gebauer, Growth, annealing and recrystallization of zircon and preservation of monazite in high-grade metamorphism: conventional and in-situ U–Pb isotope, cathodoluminescence and microchemical evidence, Contrib. Mineral. Petrol. 134 (1999) 186–201.
[34] P.W.O. Hoskin, U. Schaltegger, The composition of zircon and igneous and metamorphic petrogenesis, Zircon, Rev. Mineral. Geochem., Min. Soc. Am. 53 (2003) 27–62.
[35] T.E. Krogh, Improved accuracy of U–Pb zircon dating by selection of more concordant fractions using a high-gradient magnetic separation technique, Geochim. Cosmochim. Acta 46 (1982) 631–635.
[36] J.M. Mattinson, Zircon U–Pb chemical abrasion ("CA-TIMS") method: combined annealing and multi-step partial dissolution analysis for improved precision and accuracy of zircon ages, Chem. Geol. 220 (2005) 47–66.
[37] W. Todt, R.A. Cliff, A. Hanser, A.W. Hofmann, Evaluation of a 202Pb–205Pb double spike for high-precision lead isotope analysis, in: A. Basu, S. Hart (Eds.), Earth Processes: Reading the Isotopic Code, Am. Geophys. Union Monograph, vol. 95, 1996, pp. 429–437.
[38] S. Richter, S.A. Goldberg, P.B. Mason, A.J. Traina, J.B. Schwieters, Linearity tests for secondary electron multipliers used in isotope ratio mass spectrometry, Int. J. Mass Spectrom. 206 (2001) 105–127.
[39] H. Gerstenberger, G. Haase, A highly effective emitter substance for mass spectrometric Pb isotope ratio determinations, Chem. Geol. 136 (1997) 309–312.
[40] L.P. Black, S.L. Kamo, C.M. Allen, D.W. Davis, J.N. Aleinikoff, J.W. Valley, R. Mundil, I.H. Campbell, R.J. Korsch, I.S. Williams, C. Foudoulis, Improved Pb-206/U-238 microprobe geochronology by the monitoring of a trace-element-related matrix effect; SHRIMP, ID-TIMS, ELA-ICP-MS and oxygen isotope documentation for a series of zircon standards, Chem. Geol. 205 (2004) 115–140.
[41] K. Ludwig, Isoplot/Ex. V. 3., USGS Open-File Rep (2005).
[42] M.J. Orchard, Multielement conodont apparatuses of Triassic Gondolelloidea, Spec. Pap. Palaeontol. 73 (2005) 1–29.
[43] M.J. Orchard, On the explosive ratiation of Lower Triassic conodonts: a new multielement perspective, Albertiana 33 (2005) 65.
[44] Z.Q. Chen, K. Kaiho, A.D. George, Early Triassic recovery of the brachiopod faunas from the end-Permian mass extinction: a global review, Palaeogeogr. Palaeoclimatol. Palaeoecol. 224 (2005) 270–290.
[45] A. Brayard, G. Escarguel, H. Bucher, Latitudinal gradient of taxonomic richness: combined outcome of temperature and geographic mid-domains effects? J. Zoolog. Syst. Evol. Res. 43 (2005) 178–188.
[46] T. Galfetti, H. Bucher, A. Brayard, K. Guodun, V. Atudorei, P.A. Hochuli, H. Weissert, J. Guex, Biotic recovery and paleoclimate in Early Triassic times as reflected in carbonate carbon isotopes, sedimentary evolution and ammonoid fauna: records from South China and North India, in: F. Buzek, M. Novák (Eds.), 6th Int. Symp. Appl. Isotope. Geochem. Czech Geol. Surv., Prague, 2005, p. 268.
[47] J.L. Payne, D.J. Lehrmann, J.Y. Wei, M.J. Orchard, D.P. Schrag, A.H. Knoll, Large perturbations of the carbon cycle during recovery from the end-Permian extinction, Science 305 (2004) 506–509.
[48] V.E. Courtillot, P.R. Renne, On the ages of flood basalt events, C. R. Géosci. 335 (2003) 113–140.
[49] A.D. Saunders, R.W. England, M.K. Relchow, R.V. White, A mantle plume origin for the Siberian traps: uplift and extension in the West Siberian Basin, Russia, Lithos 79 (2005) 407–424.
[50] M.K. Reichow, A.D. Saunders, R.V. White, M.S. Pringle, A.I. Al'Mukhamedov, A.I. Medvedev, N.P. Kirda, Ar-40/Ar-39 dates from the West Siberian Basin: Siberian flood basalt province doubled, Science 296 (2002) 1846–1849.
[51] J.J. Lyons, R.S. Coe, X.X. Zhao, P.R. Renne, A.Y. Kazansky, A. E. Izokh, L.V. Kungurtsev, D.V. Mitrokhin, Paleomagnetism of the early Triassic Semeitau igneous series, eastern Kazakstan, J. Geophys. Res., [Solid Earth] 107 (B7) (2002) 1–15.
[52] A.V. Ivanov, S.V. Rasskazov, G.D. Feoktistov, H.Y. He, A. Boven, Ar-40/Ar-39 dating of Usol'skii sill in the south-eastern Siberian Traps Large Igneous Province: evidence for long-lived magmatism, Terra Nova 17 (2005) 203–208.
[53] M. Westphal, E.L. Gurevitch, B.V. Samsonov, H. Feinberg, J.P. Pozzi, Magnetostratigraphy of the lower Triassic volcanics from deep drill SG6 in western Siberia: evidence for long-lasting Permo-Triassic volcanic activity, Geophys. J. Int. 134 (1998) 254–266.
[54] S.L. Kamo, G.K. Czamanske, Y. Amelin, V.A. Fedorenko, D.W. Davis, V.R. Trofimov, Rapid eruption of Siberian flood-volcanic rocks and evidence for coincidence with the Permian–Triassic boundary and mass extinction at 251 Ma, Earth Planet. Sci. Lett. 214 (2003) 75–91.

Late Early Triassic climate change: insights from carbonate carbon isotopes, sedimentary evolution and ammonoid paleobiogeography

GALFETTI Thomas[a,*], BUCHER Hugo[a], BRAYARD Arnaud[a,b], HOCHULI Peter A.[a], WEISSERT Helmut[c], GUODUN Kuang[d], ATUDOREI Viorel[e] and GUEX Jean[f]

[a]*Paläontologisches Institut der Universität Zürich, Karl Schmid-Strasse 4, 8006 Zürich, Switzerland*
[b]*UMR-CNRS 5125, Université Claude Bernard Lyon I, 69622 Villeurbanne Cedex, France*
[c]*Department of Earth Science, ETH, Sonneggstrasse 5, 8006 Zürich, Switzerland*
[d]*Guangxi Bureau of Geology and Mineral Resources, Jiangzheng Road 1, 530023 Nanning, China*
[e]*Department of Earth and Planetary Sciences, University of New Mexico, USA*
[f]*Department of Geology, University of Lausanne, 1015 Lausanne, Switzerland*

*Corresponding author: Paläontologisches Institut und Museum der Universität Zürich, Karl-Schmid Strasse 4, CH-8006 Zürich, Switzerland.
Tel.: +41 (0) 44 634 23 47
Fax : +41 (0) 44 634 49 23
E-mail address: galfetti@pim.unizh.ch

Submitted to *Palaeogeography, Palaeoclimatology, Palaeoecology*

Manuscript information: Number of text pages: 24

Number of figures: 7

Number of tables: 1

Total number of characters: ~61100

Total number of words: ~9000

Abbreviations: NIM: Northern Indian Margin
SCB: Southern China Block
SST : Sea Surface Temperature
LGGR : Latitudinal Gradient of Generic Richness

Abstract

The late Early Triassic sedimentary-facies evolution and carbonate carbon-isotope marine record ($\delta^{13}C_{carb}$) of ammonoid-rich, outer platform settings show striking similarities between the Southern China Block (SCB) and the widely distant Northern Indian Margin (NIM). The studied sections are located within the Triassic Tethys Himalayan belt (Losar section, Himachal Pradesh, India) and the Nanpanjiang Basin in the South China Block (Jinya section, Guangxi Province), respectively. Carbon isotopes from the studied sections confirm the previously observed carbon cycle perturbations at a time of major paleoceanographic rearrangements in the wake of the end-Permian biotic crisis. This study documents the coincidence between a sharp increase in the carbon isotope composition and the worldwide ammonoid evolutionary turnover (extinction followed by a radiation) occurring around the Smithian-Spathian boundary.

Based on recent modeling studies on ammonoid paleobiogeography and taxonomic diversity, we demonstrate that the late Early Triassic (Smithian and Spathian) was a time of a major climate change. More precisely, the end Smithian climate can be characterized by a warm and equable climate underlined by a flat, pole-to-equator, Sea Surface Temperature (SST) gradient, while the steep Spathian SST gradient suggests latitudinally-differentiated climatic conditions. Moreover, sedimentary evidence suggests a transition from a humid and hot climate during the Smithian to a dryer climate from the Spathian onwards. By analogy with comparable carbon isotope perturbations in the Late Devonian, Jurassic and Cretaceous we propose that high CO_2 levels could have been responsible for the observed carbon cycle disturbance at the Smithian-Spathian boundary. We suggest that the end Smithian ammonoid extinction has been caused by a warm and equable climate related to an increased CO_2 flux. This CO_2 pulse could have also led to a lowered carbonate seawater supersaturation and consequently to a biocalcification crisis which in turn could have engendered the ammonoid extinction.

Keywords: Early Triassic; Carbon isotopes; Ammonoid paleobiogeography; Climate; South China Block; Northern Indian Margin.

1. Introduction

During the past two decades, several research programs have focused on mass extinctions and their aftermaths. The end-Permian mass extinction is considered to be the largest biotic and ecological crisis ever recorded in the Earth's history (see Erwin, 2006). Although Berner (2002) questioned the significance of certain geochemical signatures observed at the Permo-Triassic boundary, namely if they represent causes or effects of the extinction. Numerous scenarios for the end-Permian biotic crisis have been proposed: sea–level regression (Holser et al., 1989), voluminous volcanism (Renne and Basu, 1991; Renne et al., 1995), global marine anoxia (Hallam and Wignall, 1997; Isozaki, 1997), hypercapnia (Knoll et al., 1996) and temporary pH decrease in the atmosphere-ocean system (Gruszczynski et al., 2003), methane release (Krull et al., 2000), and extraterrestrial impacts (Becker et al., 2004). However, increasing evidence suggests that the extinction was most probably triggered by a combination of factors rather than by a single cause (for a review see Berner, 2002).

In order to define the pattern and the duration of the Early Mesozoic biotic recovery, taxonomic and diversity dynamics are currently receiving increased attention (e.g. Fraiser et al., 2005; Fraiser and Bottjer, 2005; Nützel, 2005; Payne, 2005; Pruss and Bottjer, 2005; Twitchett and Oji, 2005). It has been argued that a series of short- and long-term changes in ecosystems were responsible for the delayed biotic recovery, which is assumed to have occurred in conjunction with the reestablishment of metazoan reefs during the Middle Triassic (Pruss and Bottjer, 2005). Yet, ammonoids are one of the faunal groups, which quickly recovered after the Permo-Triassic event. The study of their evolutionary dynamics and distribution in space (biogeography) and time (diversity) provide proxies for paleoclimatic and/or paleoceanographic changes (see section 7 below, and Brayard et al., 2005 and in press).

In another way, marine carbonates are considered to be sensitive indicators of ancient oceanic and atmospheric chemistry. For this reason carbon isotopes are commonly employed as paleoceanographic and paleoclimatic proxies. The few well-dated carbon isotope profiles from the Tethys show that the Early Triassic $\delta^{13}C$ record did not return to Permian values, but indicate that the carbon isotope budget underwent synchronous, large and short-lived fluctuations before reaching a more stable state from the early Middle Triassic onwards (Baud et al., 1996; Atudorei and Baud, 1997; Atudorei, 1999; Payne et al., 2004; Richoz, 2004; Corsetti et al., 2005; Galfetti et al., 2005, Horacek et al., 2005). The surprising coincidence of the carbon cycle instability with the delayed Early Triassic biotic recovery, suggests a direct link between carbon cycling and biological rediversification following the P/T mass extinction (Payne et al., 2004).

In this study we present a late Early Triassic high resolution carbonate carbon isotope record, calibrated with ammonoid and conodont ages for the Tethyan marine outer platform sections from the Northern Indian margin (NIM) and from the South China Block (SCB). In order to check whether the carbon cycle could be linked to the biotic evolution, the late Early Triassic C-isotope fluctuations are compared with variations in the distribution of ammonoids in space and time. By analogy with comparable carbon cycle perturbations and biotic crises documented through the Earth history, we focus on the possible impact of the carbon cycle perturbation on climate at a time of a major ammonoid extinction event occurring near the Smithian-Spathian boundary.

2. Early Triassic paleogeography and paleoclimate

At the end of the Paleozoic the Earth's surface (Fig. 1) was characterized by a relatively simple landmass configuration with three main continents (Gondwana, Laurussia and Angara) coalescing to form the Pangean supercontinent (Ziegler et al., 1983). The oceanic domain was defined in its major part by Panthalassa and partially by the Tethys. No major geographic rearrangement of continents and oceans has been documented for the Permian - Triassic transition and for the Early Triassic, except for the northward translation motion of entire Pangea (Stampfli and Borel, 2002). Geological evidence (e.g. Parrish, 1993) and modeling studies (e.g. Wilson et al., 1994) suggest that the Late Permian to Early Triassic was a time of global climate change. Climate simulations inferred from paleoclimatic indicators (e.g. palynofloras, coal and evaporites distribution) predict a warm and temperate climate for the Late Permian – Middle Triassic interval (e.g. Crowley et al., 1989; Rees et al., 1999; Fluteau et al., 2001; Kidder and Worsley, 2004; Kiehl and Shields, 2005). In addition, the Pangean paleogeographic configuration is thought to have caused extreme continentality, and consequently large scale summer and winter monsoon circulation over the Tethys (Crowley et al., 1989; Kutzbach and Gallimore, 1989; Parrish, 1993). However, in a more recent climate simulation, Péron et al. (2005) discarded this scenario and suggested that the monsoonal system ended at the P/T boundary.

Geochemical data and climate modeling studies suggest that climate fluctuations are strongly linked to natural variations in the atmospheric CO_2 (e.g. Barron and Washington, 1985). Among the multiple scenarios involving a drastic climate change, the Siberian Traps, long recognized as the largest igneous province on Earth, are seen as one of the main contributors of high-levels of greenhouse gases (mainly CO_2) at the end of the Permian. Therefore it has been argued that this massive volcanism caused not only a climate change but was also responsible for the mass extinction (Renne et al., 1995; Wignall, 2001; Courtillot and Renne, 2003).

3. Regional paleogeography and location of the NIM and the SCB

The studied late Early Triassic series belong to two distinct tectono-sedimentary domains, the Northern Indian Margin (NIM) (Losar section – Himachal Pradesh – India) and the South China Block (SCB) (Jinya section – Guangxi Province – China), which were widely separated (> 5000 km) during Early Triassic times (Fig. 1).

Paleomagnetic reconstructions indicate that Early Triassic sediments in Losar were deposited between 30°S and 40°S on the peri-Gondwanan margin (e.g. Baud et al., 1993, Marcoux et al., 1993, Smith et al., 1994, Golonka and Ford, 2000). The Losar section exemplifies the main characteristics of the Early Triassic sedimentary evolution of the Northern Indian Margin (NIM). This succession, mainly composed of siliciclastic rocks interrupted by carbonate episodes, shows a large lateral extent without significant changes between Ladahk and Nepal (Garzanti and Pagni Frette, 1991).

Southern China is composed of several blocks that were distributed throughout the Tethyan ocean (Fig. 1) during the Paleozoic and Mesozoic transition (Yin et al., 1999). The main blocks were situated at low latitudes, at the boundary between the Tethyan and Paleopacific domains (Chen et al., 1994). As indicated by paleomagnetic data, the South China Block occupied an equatorial position during the Early and Middle Triassic (Gilder et al., 1995). With the northward drift of the eastern Tethyan blocks and

the subsequent collision with the northern continents, the Indosinian movement resulted in the uplift of most parts of South China as well as in a change from marine to continental depositional environments during Middle Triassic (Tong and Yin, 2002). The investigated Early Triassic Luolou Formation belongs to the Nanpanjiang Basin (see Lehrmann et al., 1998). At its type locality and in the studied section this formation is mainly composed of mixed siliciclastic-carbonate, ammonoid-rich rocks deposited in an outer platform setting.

4. Lithostratigraphy and age control

4.1 *Losar – Spiti Valley – NIM*

Earlier descriptions of the Early Triassic in Losar were given by Hayden (1904), Diener (1907), Garzanti et al. (1995) and Atudorei (1999). Formational names used here are from Bhargava et al. (2004) and Krystyn et al. (2004).

The Early Triassic transgressive deposits (Fig. 2 and Fig. 3a) of the Mikin Fm. unconformably overlie the Late Permian Gungri shales of the Kuling Formation (Bucher et al., 1997). The first lithological unit of the Mikin Formation is represented by the 50 cm thick "*Otoceras* bed". Age control, provided by ammonoids and conodonts, indicates a Griesbachian age for its lower part and a lower Dienerian age for its upper part (Orchard and Krystyn, 1998). The overlying "*Flemingites* beds" consist of thin-bedded, nodular, silty limestone. They are overlain by the "*Parahedenstroemia* beds", a ~25m thick sequence composed of black mudrocks interbedded with grey, thin to medium-bedded, thickening-upward bioclastic limestones of Smithian age (Garzanti et al., 1995) (cf. Fig. 3a and Fig. 4c). According to the distribution of conodonts and ammonoids, the Smithian-Spathian boundary is situated in the uppermost part of the "*Parahedenstroemia* beds", at the *Pseudomonotis himaica* horizon (Hayden, 1904; Diener, 1912; Garzanti et al., 1995). The transition from the Smithian to the Spathian series coincides with an abrupt lithological change, from siliciclastic-dominated depositional environments during the Smithian to carbonate-dominated deposits during the Spathian. The Spathian succession, known as the "Niti Limestone" (Noetling, *in* Diener, 1912) is a very prominent, ~15 m thick, medium-bedded, light-grey, bioturbated, nodular limestones (Fig. 3a and Fig. 4a). In its middle part it includes a thin (~2 m) distinctly marlier and thinner bedded interval. In the "Niti limestone" ammonoids are very rare, thus age control is provided by conodonts (Garzanti et al., 1995). A single tirolitid ammonoid, indicating an early Spathian age, is known from the very base of the Niti Limestone in Losar (Bucher, unpublished data).

The 6 m thick ammonoid-rich condensed sequence overlying the "Niti Limestone", known as the Himalayan Muschelkalk (Diener, 1907) is of Anisian age. It is represented by a strongly condensed interval of dark-grey, phosphate and iron-rich, coarse nodular limestones and marls (Garzanti et al., 1995). A remarkable concentration of brachiopods (*Spiriferina stracheyi*) is observed in its lower part, which contains conodonts of early Anisian age (Balini and Krystyn, 1997). In a recent revision of the Early Triassic substage boundaries of Spiti, Krystyn et al. (2004) positioned the Spathian-Anisian boundary one meter below the base of the Himalayan Muschelkalk.

As described by Garzanti et al. (1995), the overlying *Daonella* Shales of the Kaga Formation consists of grey marls with minor dark-grey, marly mudstones. Ammonoids and conodonts indicate an early Ladinian age.

4.2 Jinya - Guangxi Province – SCB

The Early Triassic sedimentary succession in Jinya (Fig. 2 and Fig. 3b) belongs to the Luolou Formation, whose ammonoid faunas were first described by Chao (1959).

Largely because of small-scale, post-depositional faulting no complete Early Triassic exposures are available. However, thanks to contrasting lithologies, and the occurrence of marker beds (e.g. volcanic ash layers) it was possible to construct a composite profile spanning from the early Smithian to the early Anisian interval (Fig. 2). The early Smithian succession consists of dark shales alternating with thin-bedded, laminated, pyrite-rich, micritic limestones devoid of bioturbation. These recessive rocks are usually only partly exposed. Since ammonoids are relatively rare in these rocks, the exact position of the Dienerian-Smithian boundary remains to be precisely established. A prominent, ~3 m-thick, thin-bedded, ammonoid-rich, grey limestone (*"Flemingites* beds*"*, Fig. 4h) with minor silt content is intercalated in the lowermost part of the shale-dominated, early Smithian series. Highly diversified flemingitids are restricted to this unit. Large-sized arctoceratids and proptychitids occur frequently in the lower half of these beds, whereas *Juvenites*, *Aspenites* and *Pseudaspenites* are restricted to their uppermost part. The late Smithian is represented by ammonoid-rich, dark, laminated, thickening-upward, micritic limestones intercalated with dark shales (*"Owenites* beds*"*), which in turn are overlain by dark reddish-weathering carbonate silts (*"Anasibirites* beds*"*). The uppermost few meters of these beds are composed of black shales containing small-sized, diagenetic limestone nodules. This nodule horizon yielded rare plant remains and a distinct *Xenoceltites* fauna of latest Smithian age (*Anasibirites pluriformis* Zone) (Fig. 3b and Fig. 4d). With the exception of the "*Flemingites* beds", the dark, thin laminated micrites of this Smithian series frequently display stratiform, fine-grained pyrite aggregates.

The Smithian-Spathian transition coincides with an abrupt lithologic change from siliciclastic-dominated depositional environment during the Smithian to carbonate dominated deposition during the Spathian. (Fig. 3b and Fig. 4d). The overlying 40 m rocks of Spathian age are composed of prominent, medium-bedded, light-grey, fine-grained, nodular limestones (Fig. 3b and Fig. 4b). Its middle part stands out by the intercalation of ~15m thick, greenish, marly limestones. The entire sequence is intensively bioturbated, probably by *Planolites* (ichnofabric index of 3-4; Droser and Bottjer, 1986). Traces are oriented parallel to the bedding plane and show subcylindrical sections with a diameter up to 10 mm (Fig. 4g).

The Spathian nodular limestone has a high bioclastic content mainly represented by abundant ostracods, microbrachiopods and microgastropods as well as rare benthic bivalves (Fig. 4e and Fig. 4f). Thin-section analyses and field observations indicate that the appearance of this comparatively more diversified fauna coincides with the drastic facies change observed around the Smithian-Spathian boundary. From the base to top the nodular limestone contains an ammonoid sequence comprising: (i) a Tirolitid n. gen. A fauna, (ii) a *Tirolites*/*Columbites* fauna, (iii) a *Procolumbites* fauna, (iv) a *Hellenites* fauna, and (v) a *Haugi* Zone fauna (see Fig. 2).

In addition, the unit includes two thinning-upward, green/grey, laterally continuous ash layers, which have been dated recently (see Ovtcharova et al., 2006). The 10 to 25 cm thick lower ash bed occurs about 7-8 m above the base of the nodular limestone and is associated with the *Tirolites*/*Columbites* ammonoid assemblage, while the northward-thickening upper ash bed, varying from 30 cm to up to 250 cm, occurs four meters below its top and is located within the late Spathian *Neopopanoceras haugi* Zone.

The transition from the carbonate-dominated rocks (Luolou Formation) to the siliciclastic deposits of Anisian age (Baifeng Formation) corresponds to a distinct 6 to 10 m thick, red-brownish weathering unit composed of highly siliceous shales interbedded with limestone nodules and numerous ash layers ("Transition beds"). These beds, which are reminiscent of the Alpine Buchenstein facies of Ladinian age, suggest a generalized drowning of the platform. The poorly preserved *Platycuccoceras*-dominated ammonoid assemblage found in the upper part of these beds including *Platycuccoceras* sp. indet., *Acrochordiceras* cf. *A. hyatti*, *Pseudodanubites* sp. indet. suggests an early middle Anisian age without further precision. The Baifeng Formation corresponds to a very thick (>1000m), thickening- and coarsening-upward series of siliciclastic turbidites. Generally ammonoids are rare within this formation, except for the common occurrence of a late middle Anisian *Balatonites* fauna about 15 m above the base of the formation. Daonellas of late Anisian age occur within the hemipelagic fraction of the turbidites about 100 m above the base of the Baifeng Formation.

5. Carbon Isotope Profiles

5.1 Samples and Methods

In order to obtain a complete record of the bulk carbonate carbon isotope fluctuations through the sedimentary series of the Losar and Jinya areas, samples were collected with an average stratigraphic separation of less than 50 cm. Heterogeneous samples, containing weathered parts, calcite veins or voids were cautiously cleaned, cut in thin slabs and selectively drilled with a diamond-tipped drill to produce a fine powder from the most homogenous regions. The drilled samples were treated with 100% phosphoric acid at 90°C on an automated carbonate device connected to a VG-PRISM mass spectrometer calibrated with NBS 19, NBS 18 and NBS 20 standards. Reproducibility of replicate analyses was better than ±0.1‰ for standards and ±0.15‰ for sediment samples for both carbon and oxygen. All isotope results are reported using the conventional δ notation, defined as per mil (‰) deviation vs. VPDB. The results are displayed in Table 1, the $\delta^{13}C_{carb}$ values and the $\delta^{13}C_{carb}$ versus $\delta^{18}O_{carb}$ crossplots are plotted in Fig. 2 and Fig. 5, respectively.

5.2 $\delta^{13}C_{carb}$ – Losar (NIM)

The carbon isotope composition of Losar samples (Fig. 2) varies over a wide range between -3‰ ("*Parahedenstroemia* beds") and +3‰ (Himalayan Muschelkalk). The curve illustrates three, well-defined $\delta^{13}C_{carb}$ excursions through the late Early Triassic sedimentary succession. The first C-isotope shift occurs just across the Smithian/Spathian boundary. It begins in the upper part of the "*Parahedenstroemia* beds" (around ~ -2‰) and peaks within the first meter of the Spathian nodular limestone reaching values of +2.5‰. The second excursion is positioned in the middle part of the "Niti Limestone" where the sediments record a gradual decrease of the $\delta^{13}C_{carb}$ to about -1‰. The latter is then followed by a third excursion where the carbon isotopic composition increases gradually, reaching values of +3‰ within the lower part of the Himalayan Muschelkalk.

5.3 $\delta^{13}C_{carb}$ - Jinya (SCB)

The $\delta^{13}C_{carb}$ values vary between -0.3‰ (lower part of the "*Hellenites* beds") and +3.1‰ ("Transition beds"). Similarly to Losar, the Jinya section displays the following three distinct $\delta^{13}C_{carb}$ isotope excursions: (i) a sharp, positive shift from -0.2‰ to +2.4‰ across the Smithian-Spathian boundary, (ii) a negative excursion, reaching values around -0.3‰ within the marly interval in the middle part of the Spathian nodular limestone, and (iii) a significant $\delta^{13}C_{carb}$ positive shift from +1‰ to +3‰ located between the *Haugi* Zone (late Spathian) and the transition to the Anisian.
The C-isotope composition recorded within the lower part of the "Transition beds" displays no significant variations; the signal remains essentially constant around +3‰. The transition from the nodular siliceous facies to the Baifeng Formation is again marked by a progressive decrease of the $\delta^{13}C_{carb}$ from +3‰ to 0‰. However, the scarcity of Anisian carbonate sediments does not permit obtaining a better resolved trend of the $\delta^{13}C_{carb}$ signal for the uppermost part of the section.

5.4 Diagenetic alteration of the isotope record

Since Losar and Jinya samples generally display very low $\delta^{18}O_{carb}$ values (cf. Table 1 and Fig. 5), one may question whether the primary marine signature is preserved or if the measured values represent diagenetic features. In Losar the $\delta^{18}O_{carb}$ values vary between -4.5‰ and -15.7‰ (mostly between -8‰ and -14‰) and at Jinya they vary between -10.8‰ and -1.1‰., however, in both cases the $\delta^{13}C_{carb}$ / $\delta^{18}O_{carb}$ cross-plots show no covariance (Fig. 5).
An outstanding characteristic of the C-isotope profile in Losar is that the lowest $\delta^{13}C$ values are restricted to the "*Parahedenstroemia* beds". Keeping in mind that the Losar area experienced a low regional metamorphism (Steck, pers. comm., 2006), we interpret these very low $\delta^{13}C$ - $\delta^{18}O$ values (Fig. 5a) as the result of decarbonation reactions in the presence of siliciclastic components (e.g. Kaufman and Knoll, 1995). Another possibility could be precipitation of ^{13}C-depleted cements through diagenetic processes related to the degradation of organic matter.
On the other hand, because of the very thick (>1000m) Middle Triassic siliciclastic sequence (Baifeng Fm.) overlying the Early Triassic section in the Jinya area, we suspect an overprint of the isotope signal by deep burial diagenesis, shifting the isotope record toward more negative values.
In summary, the carbonate carbon isotope profiles for Jinya and Losar section seem to record both primary and diagenetic signatures. However, if we consider that the shape of the Losar and Jinya carbon isotope curves correlate perfectly with other age-constrained Tethyan carbon isotope profiles (e.g. Nammal Gorge section - Pakistan, Atudorei, 1999; Chaohu section - South China, Tong et al., 2003; Great Bank of Guizhou – South China, Payne et al., 2004; see hereafter section 8 and Fig. 6), it can be assumed that the measured carbon isotope signals reflect relative variations of the carbon reservoir's composition.

6. Lithostratigraphic and Carbon Isotope Correlations

The comparison of the ammonoid age-constrained, late Early Triassic, outer platform sedimentary successions of Losar (NIM) and Jinya (SCB) reveals a remarkable resemblance in both lithostratigraphic and chemostratigraphic ($\delta^{13}C_{carb}$) trends (Fig. 2).

In ascending order, these similarities include: (i) a first conspicuous carbonate episode of early Smithian age (i.e. "*Flemingites* beds") consisting of a prominent, ammonoid-rich silty limestone; (ii) the predominance of an alternation of dark/black, pyrite-rich shales alternating with dark, micritic limestones devoid of bioturbation (i.e "*Parahedenstroemia /Owenites* beds"), which display the lowest $\delta^{13}C_{carb}$ values of the studied stratigraphic interval; (iii) a sharp positive $\delta^{13}C_{carb}$ excursion of up to ~ +3‰ across the Smithian-Spathian boundary; (iv) an almost exclusive carbonate deposition during the Spathian consisting of a prominent, medium-bedded, highly bioturbated, grey, nodular limestone; (v) a marly interval located in the middle part of the Spathian nodular limestone, where the carbon isotope signals show a synchronous gradual decline followed by (vi) a positive $\delta^{13}C_{carb}$ shift at the Spathian-Anisian boundary.

The depositional history of the two series appears to diverge from the Early-Middle Triassic boundary onward. In Losar, as indicated by the ammonoid record, the entire Anisian is condensed, consisting of only 6 m thick, coarse, nodular limestones pervaded with several gaps (Balini and Krystyn, 1997). In contrast, the Anisian in Jinya consists of a +1000m thick series of siliciclastic turbidites. The end of carbonate sedimentation and the beginning of turbidite accumulation is most likely related to the regional subsidence and/or to the collision between the North and South China blocks (Yin and Nie, 1993, 1996; Wang et al., 2003).

7. Paleobiogeography and diversity patterns of ammonoids: a climate link?

As first noticed by Tozer (1982) a major, global ammonoid turnover (i.e. extinction followed by rediversification) occurred around the Smithian/Spathian boundary. This event was marked by a nearly total extinction followed by a major radiation of this group. A marked decrease in diversity characterizes the latest Smithian ammonoid assemblages, which were dominated world-wide by prionitids (e.g. *Anasibirites*, *Wasatchites*, etc.). Among the few Smithian lineages that crossed the Smithian/Spathian boundary, such as the protychitids, sageceratids and xenoceltitids, the latter group includes the potential ancestor for the vast majority of new taxa evolving during the Spathian radiation.

As described in a recent modeling study, changes in global taxonomic diversity and biogeographic patterns of ammonoids provide evidence for changing gradients of sea-surface temperatures during Early Triassic times (see Brayard et al., 2005 and in press). These authors highlighted a fundamental link between the latitudinal diversity cline and climatic belts (i.e. thermal domains defined by the Sea Surface Temperature = SST).

In their simulation, validated on extant planktic Foraminifera, the SST gradient appears as the main physical parameter controlling the emergence and shape of the Latitudinal Gradient of Generic Richness (LGGR), which is expressed for ammonoids by a decreasing number of taxa (species or genera) from low to high latitudes. Simply stated a flat SST gradient induces a flat LGGR and hence low global diversity, whereas a steep SST gradient produces a steep LGGR and therefore a high global diversity. Consequently, assuming ammonoids as temperature-sensitive organisms, like most of modern cephalopods, changes in their global taxonomic diversity and biogeographic distribution provide a proxy for changing SST gradients, and thus for climatic conditions through geological time.

The LGGR, compiled from twenty Tethyan and Panthalassic basins yielding Early Triassic faunas, indicate

that biogeographic distribution and taxonomic diversity underwent consistent modifications during the period of recovery after the P/T event (Fig. 7). The gradual increase of the LGGR, beginning with a flat trend in the Griesbachian, followed by a minor differentiation of the gradients during the Dienerian and developing steep gradients for the major part of the Smithian, suggests increasing latitudinally contrasted climatic conditions. A gradual decline of ammonoid diversity within the "*Owenites* beds" is accompanied by an abrupt and severe diversity drop at the very end of the Smithian ("*Anasibirites* beds"). The *Anasibirites pluriformis* Zone is known as a time span of remarkable cosmopolitanality of ammonoid and pelagic bivalve faunas (Tozer, 1982) which, according to Brayard et al. (in press), underlines an homogenous climate (i.e. a flat SST gradient). The poorly diversified faunas of the latest Smithian are followed by an extreme diversification during the Spathian. This major change in the evolutionary history of Triassic ammonoids is accompanied by a drastic reorganization of their spatial distribution, switching from an essentially cosmopolitan to a latitudinally-restricted pattern with a steep LGGR. Although much less severe, a second decrease in ammonoid diversity occurred at the Spathian-Anisian boundary (Bucher, 1989 and unpublished data).

8. Discussion

The extraordinary synchronism of the lithostratigraphic and chemostratigraphic events recorded in the distant NIM/SCB marine sedimentary basins, together with the global ammonoid diversification pattern allows proposing a new Smithian-Spathian paleoceanographic scenario. From our data the following trends can be inferred: (i) an increased carbonate production and/or a reduction of the clastic input during the Spathian; (ii) a transition from suboxic conditions during the Smithian toward a well-oxygenated environment from the Spathian onwards; (iii) an ammonoid diversity collapse followed by an extreme rediversification near the Smithian/Spathian boundary; (iv) a significant increase in the abundance and diversity of microfauna (mainly ostracods) from the Spathian onwards and (v) a rapid rise in the $\delta^{13}C_{carb}$ values across the Smithian-Spathian boundary.

The carbonate carbon isotope studies carried out on the Jinya and Losar profiles reveal that the composition of the Early Triassic marine carbon reservoir experienced several severe fluctuations (Fig. 2). Similar changes have been previously reported from other Tethyan basins by Baud et al. (1996), Atudorei (1999), Corsetti et al. (2005), Horacek et al. (2005) and Tong et al. (2003) and from inner platform sections of the Nanpanjiang Basin (Payne et al., 2004). Such large fluctuations undoubtedly reflect unstable environmental conditions and profound changes in marine ecosystems in the Early Triassic (see also Wignall and Hallam, 1996; Knoll et al., 1996; Baud et al., 1999). With our comparison of several other well dated Tethyan carbon isotope profiles we demonstrate the synchronicity of the carbon isotope signal within the Tethys (see Fig. 6).

The most prominent Early Triassic carbon isotope excursion occurring at the Smithian-Spathian boundary coincides with profound changes in sedimentary facies and with a global faunal turnover. A positive excursion in the $\delta^{13}C$ composition is best explained by an increase in the burial of isotopically light organic carbon (Scholle and Arthur, 1980; Holser, 1997). This increased burial may be caused by anoxia or by an increase in primary production (e.g. Menegatti et al., 1998). The coincidence of the *Anasibirites pluriformis* Zone black shales deposition with the time of most rapidly changing C-isotope

values suggests that increased burial rates of organic carbon in marine environments might be responsible for the observed carbon isotope anomaly. By analogy with comparable carbon isotope perturbations in the Late Devonian (Chen et al., 2005), Jurassic (e.g. Jenkyns and Clayton, 1986) and Cretaceous (e.g. Arthur et al., 1985; Weissert and Erba, 2004) we propose that high CO_2 levels were responsible for the observed global carbon cycle disturbance. The ammonoid collapse, observed worldwide within the *Anasibirites pluriformis* Zone (latest Smithian), could thus be explained by a warm and equable climate related to an increased CO_2 flux, which is compatible with flat LGGRs gradients and/or by a lowered carbonate seawater supersaturation, which in turn could have induced a biocalcification crisis (see Wissler et al., 2003; Hautmann, 2004; Galli et al., 2005). Elevated pCO_2 values may have led to changes in the biological carbon pump, which consequently would have contributed to a drawdown of atmospheric CO_2. Thus, a significant decrease of atmospheric CO_2, coupled with enhanced burial of organic matter in the ocean at the time of increasing C-isotope values could have stimulated a (polar) cooling (see Knoll et al., 1996) from the Smithian-Spathian boundary onward. This hypothesis is also in agreement with steep Spathian LGGRs gradients. Similar to other C-isotope anomalies in the Mesozoic, peak values in the C-isotope record correspond to the reestablishment of carbonate facies (e.g. Weissert and Erba, 2004). The recovery of the carbonate system at the time where C-isotope values peaked (~2.5‰), as measured in the first meter of the Spathian limestone seems to record more favorable climatic and chemical oceanographic conditions for carbonate-producing organisms, including ammonoids.

The hypothesis of a major late Early Triassic climate shift is corroborated by the drastic lithostratigraphic changes recorded near the Smithian-Spathian boundary. For the Dienerian/Late Smithian interval it is conceivable that the predominating clastic sedimentation may be due to increased hinterland weathering, resulting from an uniform, humid and hot climate (e.g. Cecil, 1990). Subsequently, a possible attenuation of the monsoonal regime over the Tethys may have provoked a short term transition from a humid to a dryer climate, thus leading to a reduction and/or interruption of clastic input during the Spathian. This modification of the depositional setting is also compatible with coeval shifts in the distribution patterns of boreal spore-pollen assemblages indicating a major shift from humid to dryer conditions at the Smithian-Spathian boundary (Hochuli et al., in prep.).

As a response to a major perturbation of the global carbon cycle, the impact of factors like ocean circulation patterns and nutrient cycling should be considered. In a recent study, Crasquin-Soleau et al. (Crasquin-Soleau et al., 2006) outlined a significant rise in ostracod abundance and diversity with the onset of the Spathian carbonate sequence in South China. These changes coincide with the global ammonoid turnover, with the end of the radiolarite gap within the Tethys (Kakuwa, 1996; Kozur, 1998) and are also contemporaneous with the C-isotope rise. As previously described in section 4.2, the Smithian rocks, with the exception of the "*Flemingites* beds", are mainly composed of dark suboxic shales intercalated by dark-grey, pyritic, laminated micrites devoid of bioturbation. Except for the "*Flemingites* beds" no ostracods were found before the onset of the Spathian carbonate sedimentation. The discontinuous distribution of ostracods is probably caused by the temporary installation of poorly-oxygenated bottom waters. In contrast with the hypothesis that marine anoxia persisted throughout the Early Triassic e.g. Hallam and Wignall, 1997; Isozaki, 1997), our current investigations on the Early Triassic series of Jinya demonstrate that anoxic conditions occur intermittently (see also Crasquin-Soleau et al., 2006). The return to more stable, oxic conditions possibly took place at the beginning of the Spathian. This hypothesis in agreement with the view of Twitchett and Wignall (1996), who

first evoked the relationship between environmental conditions and diversity changes in the faunas of the Werfen Formation (Dolomites, northern Italy) and the possibility of a climate change across the Smithian-Spathian boundary.

We finally propose that latitudinally contrasted climatic conditions, inferred from steep Spathian ammonoid LGGRs and from changes in boreal palynological assemblages, may explain the return to more favorable shelf environments and the subsequent recovery of marine biota from the Spathian onwards.

9. Conclusions

The marine Early Triassic sedimentary facies evolution and carbon-isotope record of ammonoid-rich, outer platform settings show striking similarities between the Northern Indian Margin and the Southern China Block. Our data undoubtedly exclude that such resemblance in lithostratigraphic and chemostratigraphic patterns could originate from common tectonically controlled forces acting on depositional settings. Therefore, we propose that changes in the sedimentary/carbon isotope record of the two widely-separated basins are most probably generated by large scale factors.

Paleontological investigations, carbon isotope studies and sedimentological data obtained from the studied Tethyan sections reveal the existence of an at least Tethys-wide, or even global paleoceanographic signal controlling the biotic/abiotic system during the late Early Triassic (i.e. Smithian and Spathian). The most prominent carbon isotope event at the Smithian-Spathian boundary (i) coincides with black shales deposition during the *Anasibirites pluriformis* Zone and thus records a major modification of global organic burial rates and (ii) is coeval with the ammonoid evolutionary turnover.

Extensive volcanic activity, related to the formation of large igneous provinces (LIP) has been widely recognized as the most plausible trigger for major biotic crises (e.g. Courtillot and Renne, 2003; Isozaki et al., 2004; Galli et al., 2005;) and global climate changes (e.g. Weissert and Erba, 2004). Depending on the age accepted for the Permo-Triassic boundary, the calibration with ammonoid biostratigraphy of new U/Pb ages suggests that the latest Smithian ammonoid turnover could have occurred within 0.5 Myr to 2.5 Myr after the beginning of the Triassic (see Ovtcharova et al., 2006). Therefore, this interval could conceivably fall within the time range of a late eruptive phase of the Siberian igneous province. Westphal et al. (1998) and Ivanov et al. (2005) provide evidence suggesting that the Siberian trap magmatism may have persisted for several million years after the main eruptive phase. This opens the possibility for a massive injection of CO_2 of volcanic origin into the atmosphere, which in turn could have contributed to the observed large perturbation of the global carbon cycle and to the latest Smithian ammonoid extinction. In addition, patterns of ammonoid LGGRs, palynological and sedimentological data suggest a major climate change, most probably related to high CO_2 values at the Smithian-Spathian boundary. Nevertheless, the validity of this hypothesis can only be ultimately established by further investigations and dating of the youngest possible flows of the Siberian traps, or of any other, yet unknown, volcanic activity of compatible age.

Regardless of the implications relating to the biotic recovery from the end-Permian mass extinction, the Smithian-Spathian as well as the Spathian-Anisian carbon isotope event (Atudorei, 1999) represent useful and reliable stratigraphical markers, which may help in the correlation of marine Triassic carbonate deposits.

Acknowledgements

Stefano Bernasconi is thanked for his advices on isotope systematics and for providing access to the stable isotope laboratory of the Geology Department of the ETH Zürich. Jim Jenks and Christian Klug improved the English version of this work. Sylvain Richoz and Sylvie Crasquin-Soleau are also gratefully acknowledged for stimulating discussions about Tethyan Early Triassic carbon isotope profiles and Early Triassic ostracods. This work is a contribution to the Swiss NSF project 200020-105090/1 (to H.B.).

10. References

Arthur M. A., Dean W. E., Schlanger S. O., 1985. Variation in the global carbon cycle during the Cretaceous related to climate, volcanism and changes in atmospheric CO2: natural variations Archean to present. In: E. Sundquist and Broecker W. S. (Eds.). The Carbon Cycle and Atmospheric CO2. American Geophysical Union. pp. 504-529.

Atudorei V., 1999. Constraints on the Upper Permian to Upper Triassic marine carbon isotope curve. Case studies from the Tethys. Ph.D. Thesis, University of Lausanne, Switzerland, 161 p.

Atudorei V., Baud A., 1997. Carbon isotope events during the Triassic. Albertiana 20, 45-49.

Balini M., Krystyn L., 1997. Middle Triassic ammonoids from Spiti Himalayas - A chance for major improvements in Tethyan Anisian subdivisions?, Albertiana 19, 37-40.

Barron E. J., Washington W. M., 1985. Warm Cretaceous climates, high atmospheric CO2 as a pausible mechanism. In: E. T. Sundquist and Broecker W. S. (Eds.). The Carbon Cycle and Atmospheric CO2: Natural Variations Archean to Present. American Geophysical Union. Washington, DC, pp. 546-553.

Baud A., Atudorei V., Marcoux J. (1999), The Permian-Triassic boundary interval (PTBI) in Oman: Carbon isotope and facies changes, paper presented at International Conference on Pangea and the Paleozoic-Mesozoic Transition, China University of Geosciences Press. Wuhan, China, Wuhan.

Baud A., Atudorei V., Sharp Z., 1996. Late Permian and Early Triassic evolution of the Northern Indian margin : Carbon isotope and sequence stratigraphy. Geodinamica Acta 9, 57-77.

Baud A., Magaritz M., Holser W. T., 1989. Permian-Triassic of the Tethys: carbon isotope studies. Geologische Rundschau 78, 649-677.

Baud A., Marcoux J., Guiraud R., Ricou L. E., Gaetani M., 1993. Late Murgabian (266 to 264 Ma). In: J. Dercourt , Ricou L. E. and Vrielynck B. (Eds.). Atlas Tethys Palaeoenvironmental Maps. Explanatory notes. Gauthier-Villars. Paris, pp. 307.

Becker L., Poreda R. J., Basu A. R., Pope K. O., Harrison T. M., Nicholson C., Iasky R., 2004. Bedout: A Possible End-Permian Impact Crater Offshore of Northwestern Australia. Science 304, 1469-

1476.

Berner R. A., 2002. Examination of hypothesis for the Permo-Triassic boundary extinction by carbon cycle modeling. Proceedings of the National Academy of Sciences of the United States of America 99, 4172-4177.

Bhargava O. N., Krystyn L., Balini M., Lein R., Nicora A., 2004. Revised Litho- and Sequence Stratigraphy of the Spiti Triassic. Albertiana 30, 21-39.

Brayard A., Bucher H., Escarguel G., Fluteau F., Bourquin S., Galfetti T., in press. The Early Triassic ammonoid recovery: Paleoclimatic significance of diversity gradients. Palaeogeography Palaeoclimatology Palaeoecology.

Brayard A., Escarguel G., Bucher H., 2005. Latitudinal gradient of taxonomic richness: combined outcome of temperature and geographic mid-domains effects?, Journal of Zoological Systematics and Evolutionary Research 43, 178-188.

Bucher H., 1989. Lower Anisian ammonoids from the northern Humboldt Range (northwestern Nevada, USA) and their bearing upon the Lower-Middle Triassic boundary. Eclogae geol. Helv. 82, 943-1002.

Bucher H., Nassichuck W. W., Spinosa C., 1997. A new occurrence of the Permian Ammonoid *Stacheoceras trimurti* from the Himalayas; Himachal Pradesh, India. Eclogae geol. Helv. 90, 599-604.

Cecil C. B., 1990. Paleoclimate controls on stratigraphic repetition of chemical and siliciclastic rocks. Geology 18, 533-536.

Chao K., 1959. Lower Triassic ammonoids from Western Kwangsi, China., 355 pp., Science Press, Peking.

Chen D., Qing H., Li R., 2005. The Late Devonian Frasnian-Famennian (F/F) biotic crisis: Insights from [delta]13Ccarb, [delta]13Corg and 87Sr / 86Sr isotopic systematics. Earth and Planetary Science Letters 235, 151-166.

Chen H., Sun S., Li J., 1994. Paleomagnetic constraints on Early Triassic tectonics of South China. Scientia Geologica Sinica 29, 1-9.

Corsetti F. A., Baud A., Marenco P. J., Richoz S., 2005. Summary of Early Triassic carbon isotope records. Comptes Rendus Palevol 4, 405-418.

Courtillot V. E., Renne P. R., 2003. On the ages of flood basalt events. Comptes Rendus Geoscience 335, 113-140.

Crasquin-Soleau S., Galfetti T., Bucher H., Brayard A., 2006. Palaeoecological changes after the end-permian mass extinction: Early Triassic ostracods from northwestern Guangxi Province, South China. Rivista Italiana di Paleontologia e Stratigrafia 112, 55-75.

Crowley T. H., Hyde W. T., Short D. A., 1989. Seasonal cycle variations on the supercontinent of Pangea: implications for Early Permian vertebrate extinction. Geology 34, 457-460.

Diener C., 1907. The fauna of the Himalayan Muschelkalk., Mem. Geol. Surv, India, Palaeontol. Indica 15, 1-140.

Diener C., 1912. The Trias of Himalayas. Mem. Geol. Surv. India 36, 1-176.

Droser M. L., Bottjer D. J., 1986. A semiquantitative field classification of ichnofabric. Journal of Sedimentary Petrology 56, 558-559.

Erwin D. L., 2006. Extinction. How life on Earth nearly ended 250 Million years ago, 296 pp., Princeton

University Press.

Fluteau F., Besse J., Broutin J., Berthelin M., 2001. Extension of Cathaysian flora during the Permian: Climatic and paleogeographic constraints. Earth and Planetary Science Letters 193, 603-616.

Fraiser M. L., Bottjer D. J., 2005. Restructuring in benthic level-bottom shallow marine communities due to prolonged environmental stress following the end-Permian mass extinction. Comptes Rendus Palevol 4, 515-523.

Fraiser M. L., Twitchett R. J., Bottjer D. J., 2005. Unique microgastropod biofacies in the Early Triassic: Indicator of long-term biotic stress and the pattern of biotic recovery after the end-Permian mass extinction. Comptes Rendus Palevol 4, 475-484.

Galfetti T., Bucher H., Brayard A., Guodun K., Atudorei V., Hochuli P. A., Weissert H., Guex J., 2005. Biotic recovery and paleoclimate in Early Triassic times as reflected in carbonate carbon isotopes, sedimentary evolution and ammonoid fauna: records from South China and North India. In: F. Buzek and Novák M. (Eds.). 6th International Symposium on Applied Isotope Geochemistry, Abstracts. Czech Geological Survey. Prague, Czech Republic, pp. 83.

Galli M. T., Jadoul F., Bernasconi S. M., Weissert H., 2005. Anomalies in global carbon cycling and extinction at the Triassic/Jurassic boundary: evidence from a marine C-isotope record. Palaeogeography, Palaeoclimatology, Palaeoecology 216, 203-214.

Garzanti E., Jadoul F., Nicora A., Berra F., 1995. Triassic of Spiti (Tethys Himalaya, N India). Rivista Italiana di Paleontologia e Stratigrafia 101, 267-300.

Garzanti E., Pagni Frette M., 1991. The stratigraphic succession of Thakkhola region (central Nepal). Comparison with the northwestern Tethys Himalaya., Rivista Italiana di Paleontologia e Stratigrafia 97, 3-26.

Gilder S. A., Coe R. S., Wu H. R., Kunag G. D., Zhao X. X., Wu Q., 1995. Triassic Paleomagnetic Data from South China and Their Bearing on the Tectonic Evolution of the Western Circum-Pacific Region. Earth and Planetary Science Letters 131, 269-287.

Golonka J., Ford D., 2000. Pangean (Late Carboniferous-Middle Jurassic) paleoenvironment and lithofacies. Palaeogeography, Palaeoclimatology, Palaeoecology 161, 1-34.

Gruszczynski M., Malkowski K., Szaniawski H., Cheng-Yuan W., 2003. The carbon biogeochemical cycle across the Permian - Triassic boundary strata and its implications: isotope record from the Changhsingian Stage at Meishan, south China. . Acta Geologica Polonica 53, 167-169.

Guex J., 1978. Le Trias inférieur des Salt Ranges (Pakistan): problèmes biochronologiques. Eclogae geol. Helv. 71, 105-141.

Hallam A., Wignall P. B., 1997. Mass extinctions and their aftermath, 320 pp., Oxford University Press, New York, NY, United States.

Hayden H. H., 1904. The geology of Spiti, with parts of Bashar and Rupshu. Mem. Geol. Surv. India 36, 1-129.

Holser W. T., 1997. Geochemical events documented in inorganic carbon isotopes. Palaeogeography Palaeoclimatology Palaeoecology 132, 173-182.

Holser W. T., Schönlaub H.-P., Attrep M., Boeckelmann K., Klein P., Magaritz M., Orth C. J., Fenninger A., Jenny C., Kralik M., Mauritsch H., Pak E., Schramm J.-M., Stattegger K., Schmöller R., 1989. A unique geochemical record at the Permian/Triassic boundary. Nature 337, 39-44.

Horacek M., Richoz S., Brandner R., Krystyn L., Spotl C., 2005. $\delta^{13}C$ curve of Lower Triassic marine

sediments in Iran. Albertiana 33, 40-40.

Isozaki Y., 1997. Permo-triassic boundary superanoxia and stratified superocean: Records from lost deep sea. Science 276, 235-238.

Isozaki Y., Yao J., Matsuda T., Sakai H., Ji Z., Shimizu N., Kobayashi N., Kawahata H., Nishi H., Takano M., Kubo T., 2004. Stratigraphy of the Middle-Upper Permian and Lowermost Triassic at Chaotian, Sichuan, China. Record of Late Permian double mass extinction event. Proceeding of the Japan Acadademy 80, 10-16.

Ivanov A. V., Rasskazov S. V., Feoktistov G. D., He H., Boven A., 2005. 40Ar/39Ar dating of Usol'skii sill in the south-eastern Siberian Traps Large Igneous Province: evidence for long-lived magmatism. Terra Nova 17, 203-208.

Jenkyns H. C., Clayton C. J., 1986. Black Shales and Carbon Isotopes in Pelagic Sediments from the Tethyan Lower Jurassic. Sedimentology 33, 87-106.

Kakuwa Y., 1996. Permian-Triassic mass extinction event recorded in bedded chert sequence in southwest Japan. Palaeogeography, Palaeoclimatology, Palaeoecology 121, 35-51.

Kaufman A. J., Knoll A. H., 1995. Neoproterozoic variations in the C-isotopic composition of seawater: stratigraphic and biogeochemical implications. Precambrian Research 73, 27-49.

Kidder D. L., Worsley T. R., 2004. Causes and consequences of extreme Permo-Triassic warming to globally equable climate and relation to the Permo-Triassic extinction and recovery. Palaeogeography, Palaeoclimatology, Palaeoecology 203, 207-237.

Kiehl J. T., Shields C. A., 2005. Climate simulation of the latest Permian: Implications for mass extinction. Geology 33, 757-760.

Knoll A. H., Bambach R. K., Canfield D. E., Grotzinger J. P., 1996. Comparative Earth History and Late Permian Mass Extinction. Science 273, 452-457.

Kozur H. W., 1998. Some aspects of the Permian-Triassic boundary (PTB) and of the possible causes for the biotic crisis around this boundary. Palaeogeography Palaeoclimatology Palaeoecology 143, 227-272.

Krull E. S., Retallack G. J., Campbell H. J., Lyon G. L., 2000. delta C-13(org) chemostratigraphy of the Permian-Triassic boundary in the Maitai Group, New Zealand: evidence for high-latitudinal methane release. New Zealand Journal of Geology and Geophysics 43, 21-32.

Krystyn L., Balini M., Nicora A., 2004. Lower and Middle Triassic stage and substage boundaries in Spiti. Albertiana 30, 40-53.

Kutzbach J. E., Gallimore R. G., 1989. Pangaean Climates: Megamonsoons of the Megacontinent. Journal of Geophysical Research 94, 3341-3357.

Lehrmann D. J., Wei J. Y., Enos P., 1998. Controls on facies architecture of a large Triassic carbonate platform: The Great Bank of Guizhou, Nanpanjiang Basin, South China. Journal of Sedimentary Research 68, 311-326.

Marcoux J., Baud A., Ricou L. E., Gaetani M., Krystyn L., Bellion Y., Guiraud R., Moreau C., Besse J., Gallet Y., Jaillard E., Theveniaul H., 1993. Late Anisian (237-234 Ma). In: J. Dercourt, Ricou L. E. and Vrielynck B. (Eds.). Atlas Tethys, Palaeonvironmental maps, explanatory notes. Gauthier-Villars. Paris, pp. 21-34.

Menegatti A. P., Weissert H., Brown R. S., Tyson R. V., Farrimond P., Strasser A., Caron M., 1998. High-resolution delta C-13 stratigraphy through the early Aptian "Livello Selli" of the Alpine Tethys.

Paleoceanography 13, 530-545.

Nützel A., 2005. Recovery of gastropods in the Early Triassic. Comptes Rendus Palevol 4, 433-447.

Orchard M. J., Krystyn L., 1998. Conodonts of the lowermost Triassic of Spiti, and new zonation based on *Neogondolella* successions. Rivista Italiana di Paleontologia e Stratigrafia 104, 341-368.

Ovtcharova M., Bucher H., Schaltegger U., Galfetti T., Brayard A., Guex J., 2006. New Early to Middle Triassic U-Pb ages from South China: Calibration with ammonoid biochronozones and implications for the timing of the Triassic biotic recovery. Earth and Planetary Science Letters 243, 463-475.

Pakistani-Japanese Research Group, 1985. Permian and Triassic systems in the Salt Range and Surghar Range, Pakistan. In: K. Nakazawa and Dickins J. M. (Eds.). The Tethys: Her Paleogeography and Paleobiogeography from Paleozoic to Mesozoic. Tokai University Press. Tokyo, Japan, pp. 221-312.

Parrish J. T., 1993. Climate of the Supercontinent Pangea. Journal of Geology 101, 215-233.

Payne J. L., 2005. Evolutionary dynamics of gastropod size across the end-Permian extinction and through the Triassic recovery interval. Paleobiology 31, 269-290.

Payne J. L., Lehrmann D. J., Wei J., Orchard M. J., Schrag D. P., Knoll A. H., 2004. Large Perturbations of the Carbon Cycle During Recovery from the End-Permian Extinction. Science 305, 506-509.

Péron S., Bourquin S., Fluteau F., Guillocheau F., 2005. Paleoenvironment reconstructions and climate simulations of the Early Triassic: impact of the sediment supply on the preservation of fluvial systems. Geodinamica Acta.

Pruss S. B., Bottjer D. J., 2005. The reorganization of reef communities following the end-Permian mass extinction. Comptes Rendus Palevol 4, 485-500.

Rees P. M., Gibbs M. T., Ziegler A. M., Kutzbach J. E., Behling P. J., 1999. Permian climates: Evaluating model predictions using global paleobotanical data. Geology 27, 891-894.

Renne P. R., Basu A. R., 1991. Rapid Eruption of the Siberian Flood Basalts at the Permo-Triassic Boundary. Science 253, 176-179.

Renne P. R., Zhang Z., Richardson M. A., Black M. T., Basu A. R., 1995. Synchrony and causal relations between Permo-Triassic boundary crises and Siberian flood volcanism. Science 269, 1413-1416.

Richoz S., 2004. Stratigraphie et variations isotopiques du carbone dans le Permien supérieur et le Trias inférieur de la Néotéthys (Turquie, Oman et Iran). PhD Thesis, University of Lausanne, Switzerland, 281 p.

Scholle P. A., Arthur M. A., 1980. Carbon Isotope Fluctuations in Cretaceous Pelagic Limestones - Potential Stratigraphic and Petroleum-Exploration Tool. American Association of Petroleum Geologists Bulletin 64, 67-87.

Smith A. G., Smith D. G., Funnell B. M., 1994. Atlas of Mesozoic and Cenozoic coastlines, 109 pp., Cambridge University Press, Cambridge.

Stampfli G. M., Borel G. D., 2002. A plate tectonic model for the Paleozoic and Mesozoic constrained by dynamic plate boundaries and restored synthetic oceanic isochrons. Earth and Planetary Science Letters 196, 17-33.

Tong J., Yin H., 2002. The Lower Triassic of South China. Journal of Asian Earth Sciences 20, 803-

815.

Tong J., Zakharov Y. D., Orchard M. J., Hongfu Y., Hansen H. J., 2003. A candidate of the Induan-Olenekian boundary stratotype in the Tethyan region. Science in China Series D 46, 1182-1200.

Tozer E. T., 1982. Marine Triassic Faunas of North America: Their Significance for Assessing Pate and Terrane Movements. Geologische Rundschau 71, 1077-1104.

Twitchett R. J., Oji T., 2005. Early Triassic recovery of echinoderms. Comptes Rendus Palevol 4, 463-474.

Twitchett R. J., Wignall P. B., 1996. Trace fossils and the aftermath of the Permo-Triassic mass extinction: evidence from northern Italy. Palaeogeography, Palaeoclimatology, Palaeoecology 124, 137-151.

Wang E., Meng Q., Burchfiel B. C., Zhang G., 2003. Mesozoic large-scale lateral extrusion, rotation, and uplift of the Tongbai-Dabie Shan belt in east China. Geology 31, 307-310.

Weissert H., Erba E., 2004. Volcanism, CO2 and palaeoclimate: a Late Jurassic-Early Cretaceous carbon and oxygen isotope record. Journal of the Geological Society 161, 695-702.

Westphal M., Gurevitch E. L., Samsonov B. V., Feinberg H., Pozzi J. P., 1998. Magnetostratigraphy of the lower Triassic volcanics from deep drill SG6 in western Siberia: evidence for long-lasting Permo-Triassic volcanic activity. Geophys J Int 134, 254-266.

Wignall P. B., 2001. Large igneous provinces and mass extinctions. Earth-Science Reviews 53, 1-33.

Wignall P. B., Hallam A., 1996. Facies change and the end-Permian mass extinction in S.E. Sichuan, China. Palaios 11, 587-596.

Wilson K. M., Pollard D., Hay W. W., Thompson S. L., Wold C. N., 1994. General circulation simulations of Triassic climates: Preliminary results. In: G. D. Klein (Ed.) Pangea, Paleoclimate, Tectonics, and Sedimentation During Accretion, Zenith and Breakup of a Supercontinent. Geological Society of America Special Paper 288. pp. 91-116.

Wissler L., Funk H., Weissert H., 2003. Response of Early Cretaceous carbonate platforms to changes in atmospheric carbon dioxide levels. Palaeogeography Palaeoclimatology Palaeoecology 200, 187-205.

Yin A., Nie S., 1993. An indentation model for the North and South China collision and the development of the Tan-Lu and Honam fault systems, Eastern Asia. Tectonics 12, 801-813.

Yin A., Nie S., 1996. A Phanerozoic palinspastic reconstruction of China and its neighboring regions. In: A. Yin and M. H. T. (Eds.). The Tectonic Evolution of Asia. Cambridge University Press. Los Angeles, pp. 442-485.

Yin H., Wu S., Du. Y., Peng Y., 1999. South China defined as part of Tethyan archipelagic ocean system. Earth Science - Journal of China University of Geosciences 24, 1-12.

Ziegler A. M., Scotese C. R., Barrett S. F., 1983. Mesozoic And Cenozoic paleogeographic maps. In: P. Broesche and Sündermann J. (Eds.). Tidal Friction and the Earth's Rotation II. Springer-Verlag. Berlin, pp. 240-252.

Figure captions :

Fig. 1. (a) Early Triassic paleogeography (modified after Smith et al., 1994 and Golonka and Ford, 2000) and position of the Northern Indian Margin (NIM) and of the South China Block (SCB). (b) Present day location of the studied sections: (1) Losar – Himachal Pradesh – India; (2) Jinya - Guangxi Province - South China.

Fig. 2. Lithology and carbonate carbon isotopes correlations between Losar section (Himachal Pradesh - India - NIM) and Jinya section (Guangxi Province - South China - SCB). Abbreviations: T = volcanic ash layers; G = Griesbachian; D = Dienerian; *Otb* = "*Otoceras* beds"; *Fb* = "*Flemingites* beds"; *Ob* = "*Owenites* beds"; *Ab* = "*Anasibirites* beds"; *TAb* = "Tirolitid n. gen. A. beds"; *T*/*Cb* = "*Tirolites*/*Columbites* beds"; *Pb* = "*Procolumbites* beds"; *Hb* = "*Hellenites* beds"; HZ = *Haugi* Zone; *Plb* = "*Platycuccoceras* beds"; SZ = *Shoshonensis* Zone. The three main isotope excursions are numbered from 1 to 3. See text for further details.

Fig. 3. Photographs of lithological successions of (a) Losar section (Himachal Pradesh - India); (b) Jinya section (Guangxi Province - South China). Note the major change from a siliciclastic-dominated regime to a carbonate-dominated regime at the Smithian-Spathian boundary. See text for further details and Fig. 2 for abbreviations.

Fig. 4. Details of outcrops and specimens: (a) Niti nodular Limestone, Spathian. Losar; (b) Nodular limestone of Spathian age. Jinya; (c) "*Parahedenstroemia* beds". Losar; (d) "*Anasibirites* beds" of latest Smithian age composed of black shales and small-sized, diagenetic nodules. Jinya; (e) Thin-section photograph showing the microfacies of the "*Tirolites* beds", Jinya. Note the abundance of thin-shelled bivalves and ostracods. (f) Specimen of an ostracod and microbrachiopod-rich limestone, late Spathian. Jinya. (g) Bioturbated bedding plane (*Planolites*), earliest Spathian; Jinya. (h) Detailed view of an outcrop of the Smithian "*Flemingites* beds". Note abundant ammonoid cross-sections. Jinya. See text for further details.

Fig. 5. $\delta^{13}C_{carb}$ versus $\delta^{18}O_{carb}$ crossplots of the Losar section (a) and of the Jinya section (b). The symbols are used to distinguish specific beds: 1 - "*Otoceras* beds" and Dienerian samples (Losar only); 2 - "*Flemingites* beds"; 3 - "*Parahedenstroemia* beds"(Losar) & "*Owenites* beds"(Jinya); 4 - Spathian nodular limestone; 5 - Himalayan Muschelkalk (Losar) and "Transition beds" & Anisian turbidites (Jinya).

Fig. 6. Comparison and correlations between four Tethyan Early Triassic carbonate carbon isotope profiles: (a) Great Bank of Guizhou (SCB, Guizhou Province, South China), modified after Payne et al. (2004). (b) Losar Section (NIM, Himachal Pradesh, India), modified after Atudorei (1999). (c) Jinya section (SCB, Guangxi Province, South China), this study. (d) Chaohu section (SCB, Anhui Province, South China), modified after Tong et al. (2003). (e) Nammal Gorge Section (NIM, Pakistan), modified after Baud et al. (1989) and Atudorei (1999). Ammonoid age constraints in Nammal Gorge

are provided by Guex (1978, Pl. 9). However, the ammonoid content of bed 21, situated 2 m below the boundary between the Upper Ceratite Limestones (UCL) and the *Niveaux Intermédiares* (NI) is restricted to "*Nordophiceras*" *planorbe*, which appears to be an equivocal identification. The occurrence of *Neospathodus triangularis* in the same horizon (Pakistani-Japanese Research Group, 1985) indicates a Spathian age. Hence, the Smithian/Spathian boundary is bracketed by beds 20 and 21 of Guex (1978) corresponding to a three meter-thick interval placed well below the UCL/NI boundary. This interval yields the most positive values of the Smithian/Spathian carbon isotope excursion recorded in the other Tethyan profiles.

Fig. 7. Summary chart showing the global Early Triassic trends in ammonoid endemism and latitudinal distribution (modified after Brayard et al., in press) with simplified lithology, carbonate carbon isotopes and anoxic trends from Jinya (SCB) and Losar (NIM). Darker shading denotes greater intensity of anoxia. See Fig. 2 for the abbreviations.

Table 1. Carbonate carbon / oxygen isotope data (relative to VPDB) from Losar- Spiti Valley - India (data from Atudorei, 1999) and from Jinya - Guangxi Province - South China (this study).

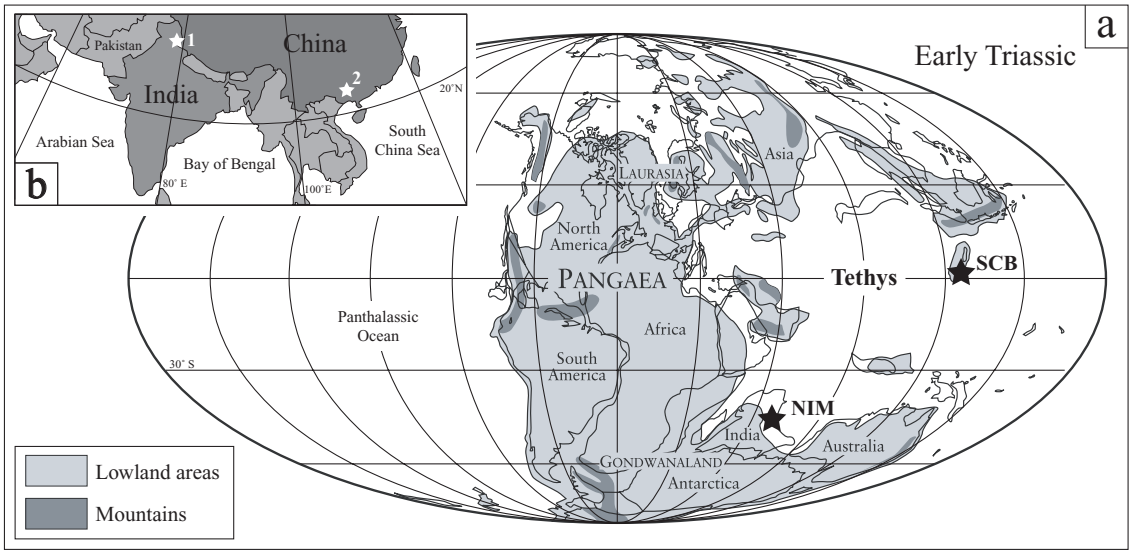

Fig. 1. Galfetti et al.

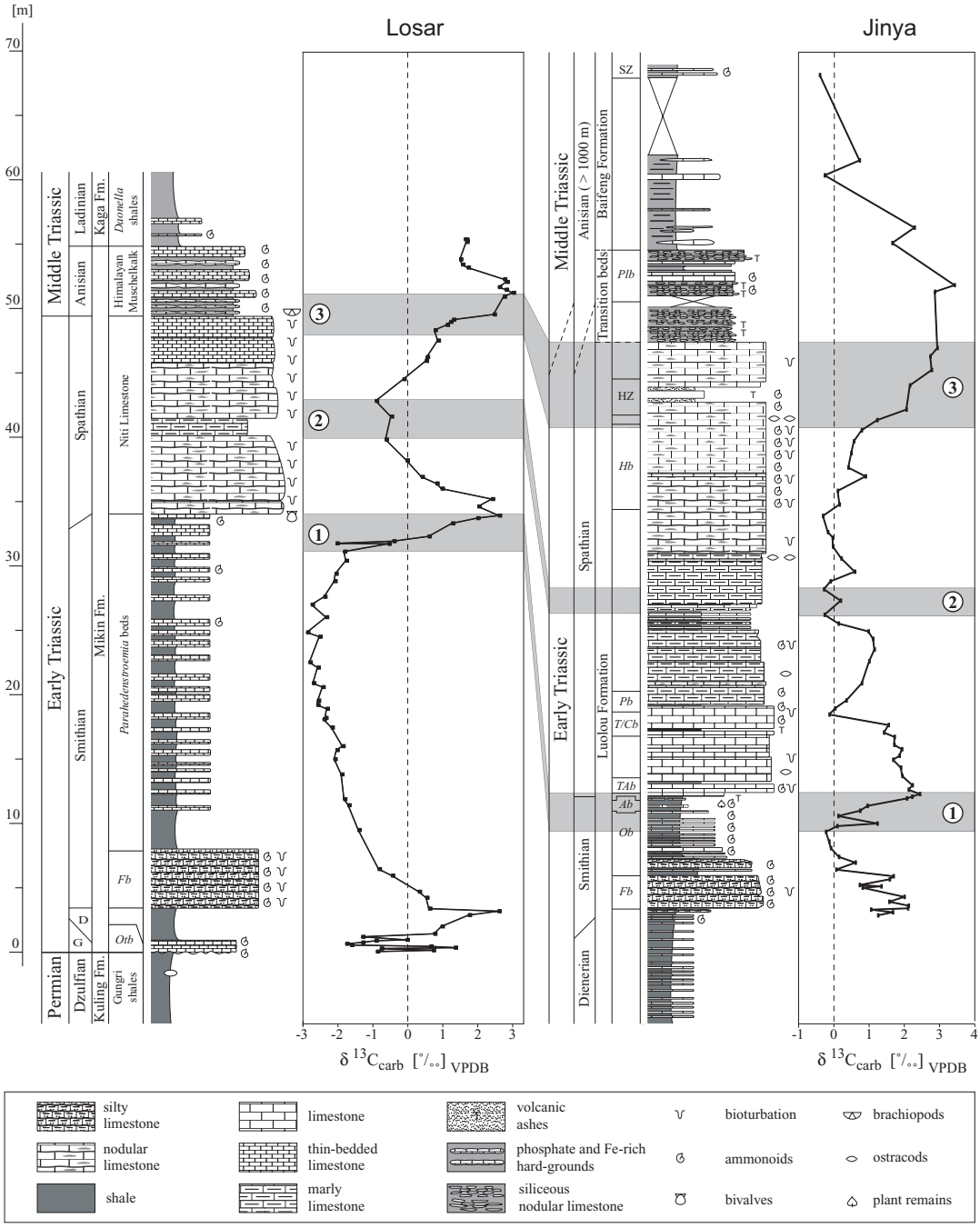

Fig. 2. Galfetti et al.

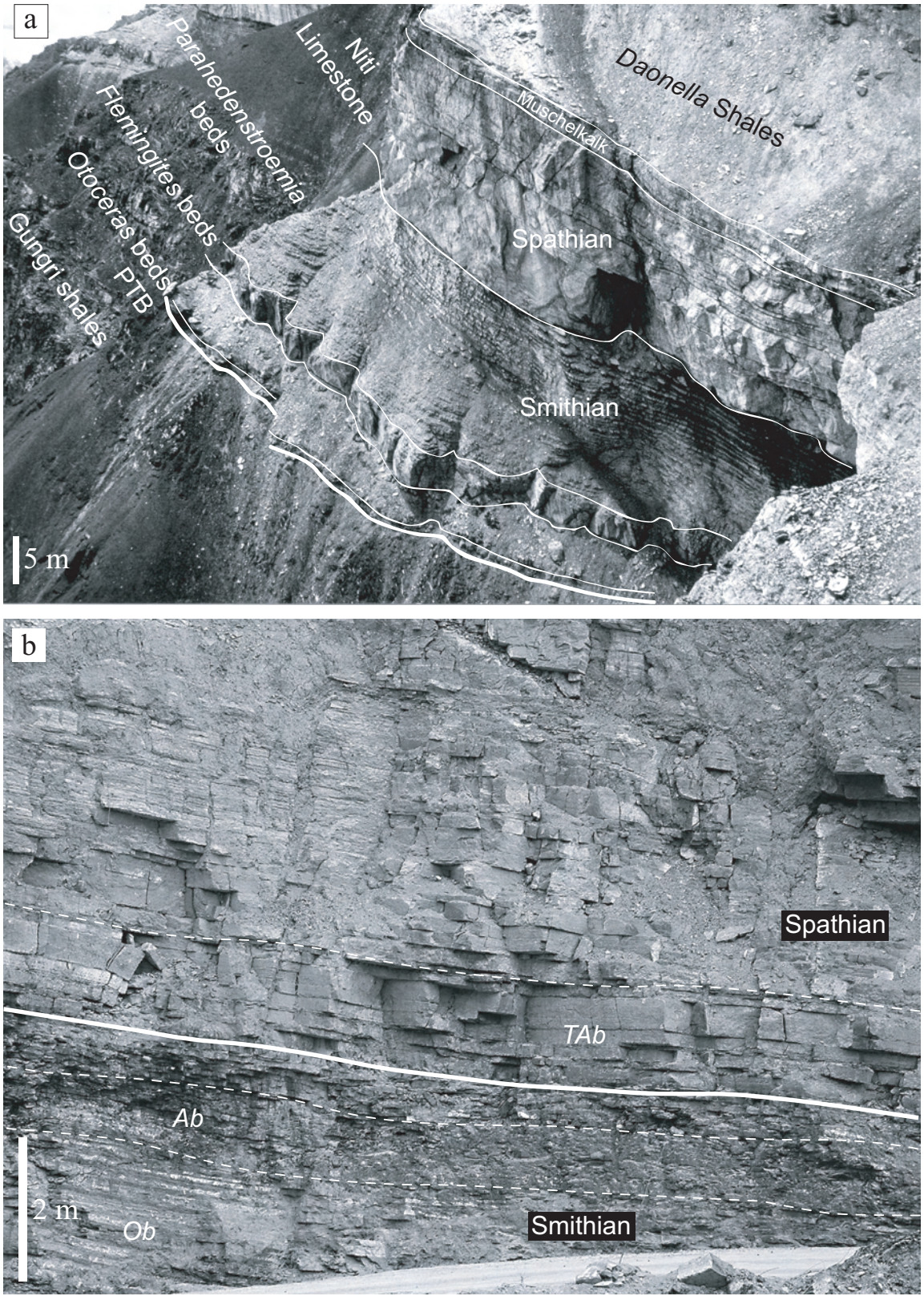

Fig. 3. Galfetti et al.

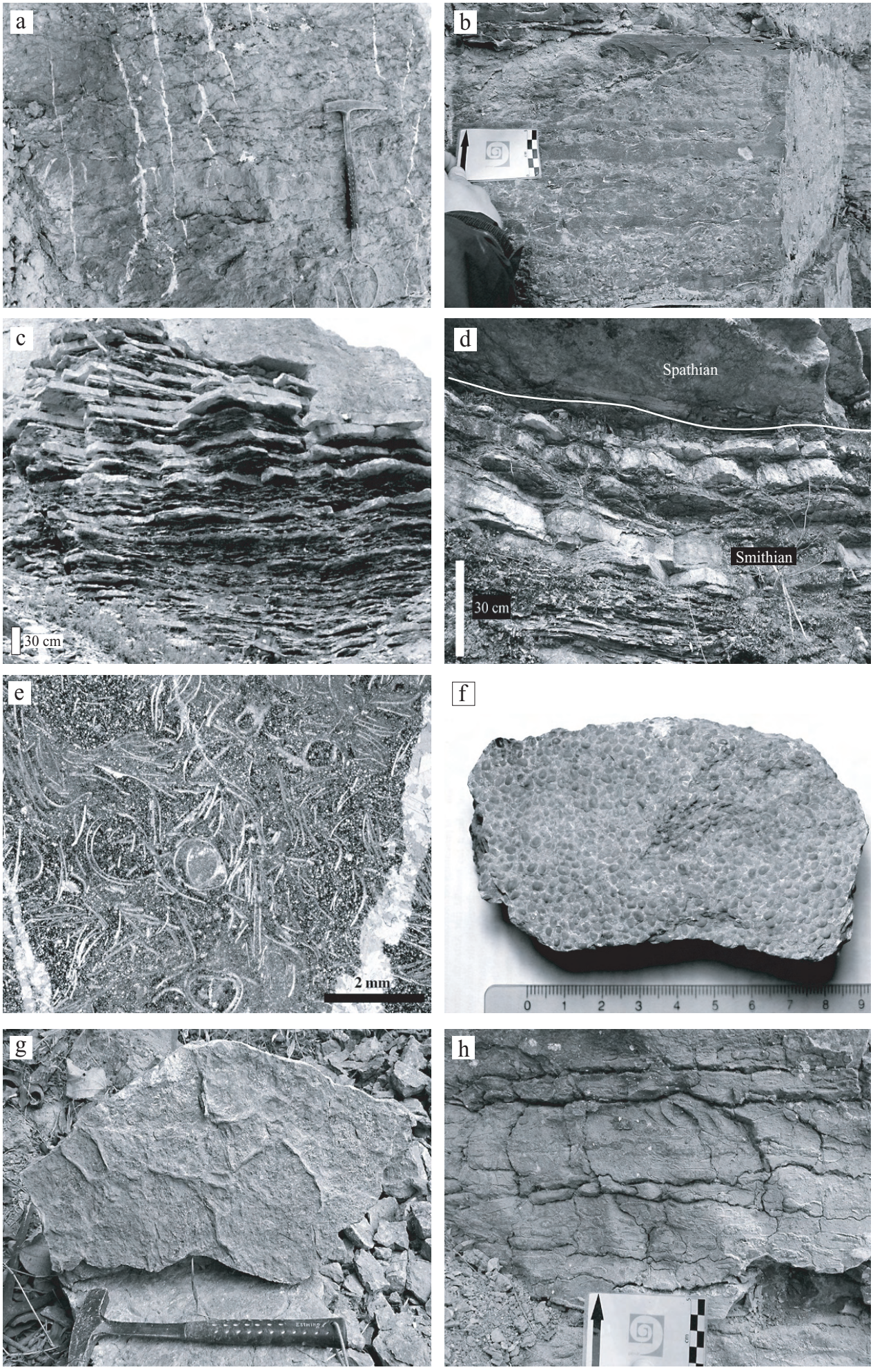

Fig. 4. Galfetti et al.

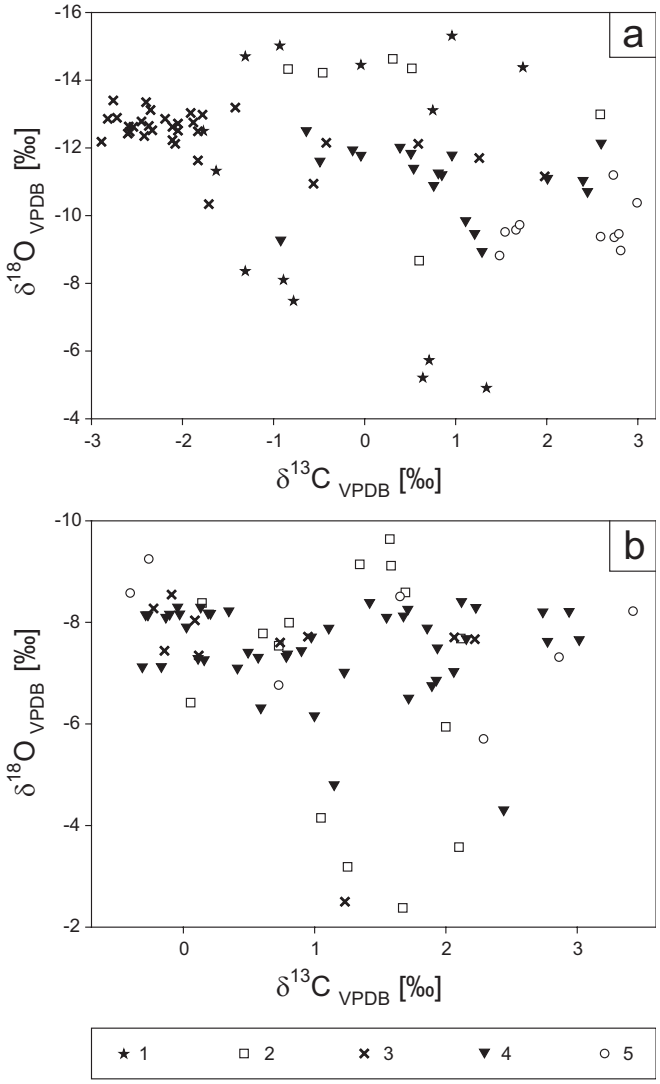

Fig. 5. Galfetti et al.

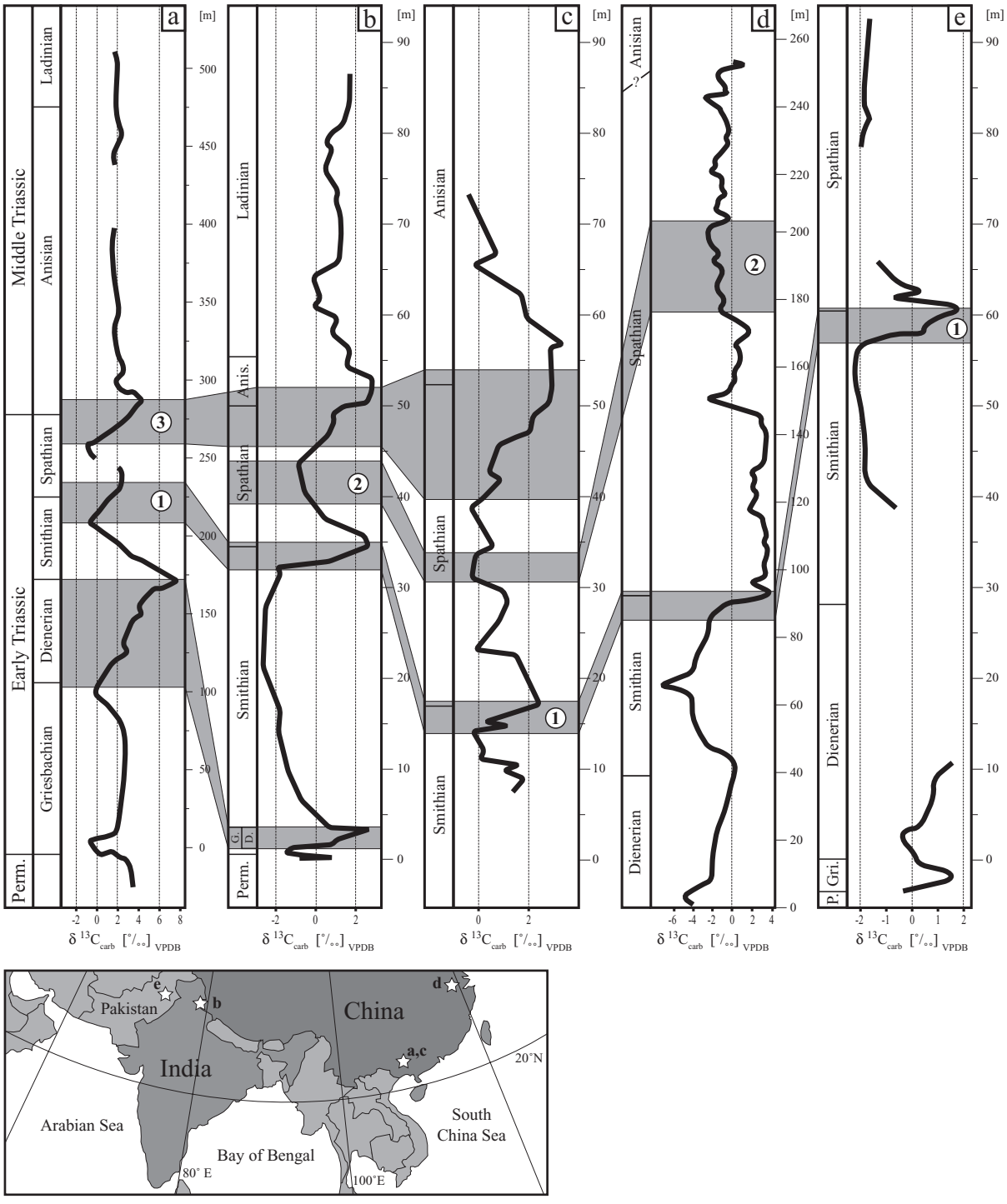

Fig. 6. Galfetti et al.

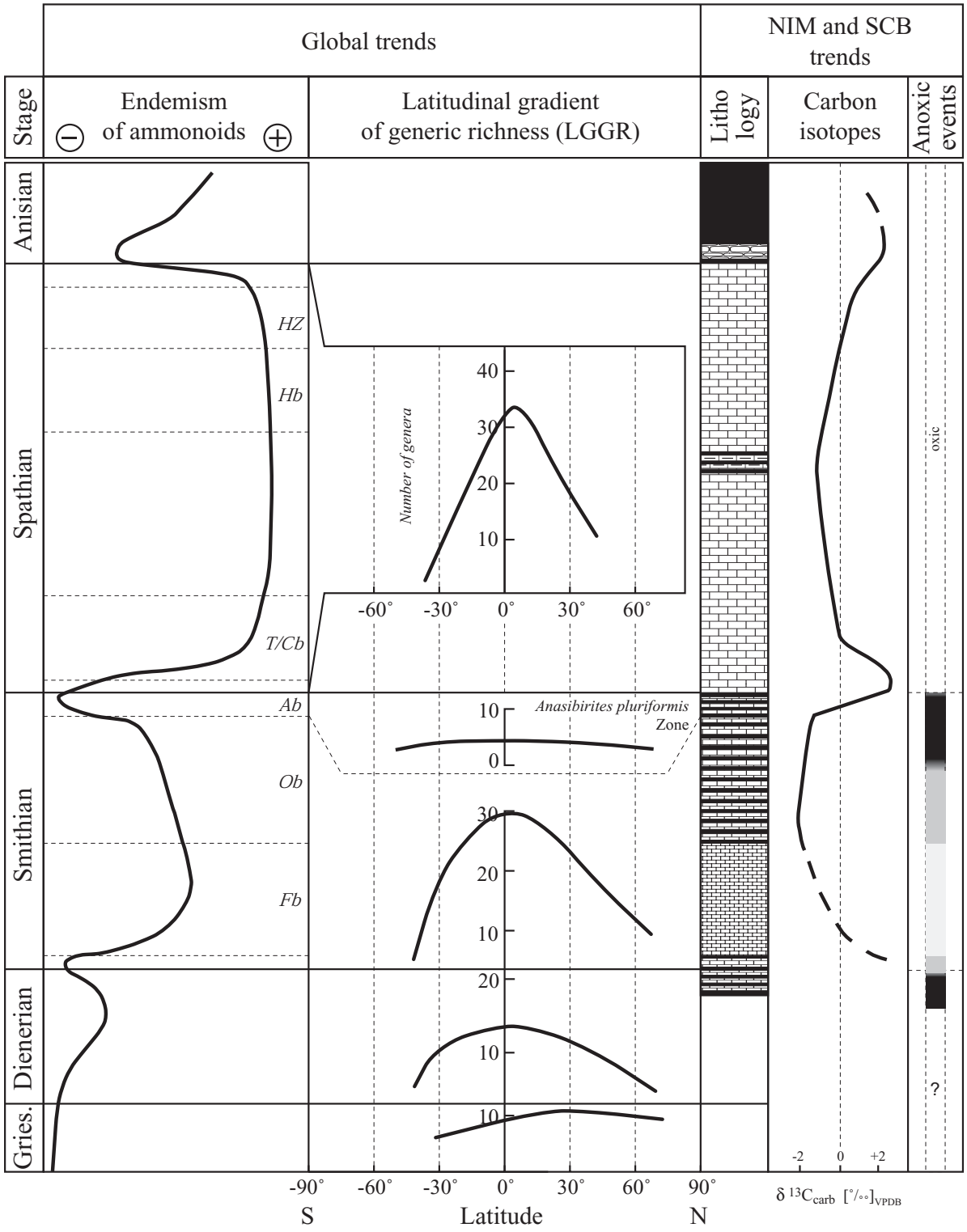

Fig. 7. Galfetti et al.

LOSAR - NIM			
sample	stage	$\delta^{13}C$ °/₀₀	$\delta^{18}O$ °/₀₀
1328		1.67	-9.56
1288	Anisian	1.49	-8.8
1286		1.55	-9.5
1285		1.71	-9.71
1282		2.75	-9.34
1281		2.82	-8.95
1278		2.6	-9.36
1277		2.8	-9.44
1214		3	-10.36
1213		2.74	-11.18
1210	Spathian	2.45	-10.71
1305		1.29	-8.94
1304		1.21	-9.47
1209		1.11	-9.85
1208		0.76	-10.89
1206		0.85	-11.21
1204		0.54	-11.4
1203		0.51	-11.84
1201		-0.13	-11.94
1199		-0.92	-9.28
1197		-0.49	-11.61
1195		-0.64	-12.51
1194		-0.04	-11.78
1193		0.39	-12.02
1192		0.81	-11.26
1191		0.96	-11.79
1190		2.4	-11.04
1189		2.01	-11.1
1188		2.6	-12.14
1187	Smithian	1.98	-11.16
1186		1.26	-11.7
1184		0.59	-12.12
1183		-0.42	-12.15
1182		-2.05	-12.51
1181		-0.56	-10.94
1179		-1.83	-11.63
1177		-1.78	-12.98
1175		-2.08	-12.12
1173		-2.11	-12.23
1171		-2.4	-13.35
1170		-2.76	-13.4
1168		-2.35	-13.12
1164		-2.89	-12.18
1163		-2.54	-12.62
1159		-2.82	-12.86
1158		-2.59	-12.63
1155		-2.72	-12.89
1154		-2.45	-12.78
1152		-2.58	-12.48
1151		-2.6	-12.42
1150		-2.331	-12.52
1148		-2.37	-12.65
1147		-2.42	-12.35
1146		-2.19	-12.86
1143		-1.88	-12.75
1141		-2.05	-12.72
1139		-2.11	-12.62
1136		-1.91	-13.03
1134		-1.83	-12.49
1133		-1.71	-10.34
1130		-1.42	-13.19
1122		-0.84	-14.33
1121		-0.46	-14.22
1118		0.31	-14.63
1117		0.52	-14.35
1115		0.6	-8.67
1114		2.59	-12.99
1113	Dienerian	1.74	-14.38
1111		0.96	-15.31
1215		0.75	-13.11
1110		-1.31	-8.36
1109		-0.04	-14.45
1108	Griesbachian	-0.93	-15.02
1107		-1.31	-14.7
1106		-1.77	-12.5
1105		-1.63	-11.32
1104		0.64	-5.21
1103		1.34	-4.91
1102		-0.78	-7.48
1101		0.71	-5.73
1100		-0.89	-8.1

JINYA - SCB			
sample	stage	$\delta^{13}C$ °/₀₀	$\delta^{18}O$ °/₀₀
122	Anisian	-0.40	-8.56
98		0.73	-6.75
97		-0.26	-9.24
99		2.29	-5.69
100		1.66	-8.50
101		3.43	-8.21
102		2.87	-7.30
103	Spathian	2.94	-8.21
104		2.74	-8.21
105		2.78	-7.63
106		2.16	-7.68
107		2.06	-7.03
109		1.23	-7.02
108		0.79	-7.38
110		0.57	-7.31
111		0.50	-7.41
112		0.41	-7.10
113		0.90	-7.44
114		0.11	-7.29
115		0.16	-7.26
116		-0.31	-7.13
118		-0.17	-7.13
119		3.02	-7.66
93		-0.04	-8.30
94		-0.03	-8.17
90		0.21	-8.18
88		0.59	-6.32
89.1		-0.10	-8.16
87		-0.29	-8.15
86		0.19	-8.18
85		-0.27	-8.15
84		0.13	-8.30
83		0.98	-7.71
81		1.11	-7.89
80		1.15	-4.80
79		1.00	-6.16
78		0.79	-7.33
96		0.35	-8.23
74		0.03	-7.91
95		-0.13	-8.10
76		1.55	-8.10
53		1.42	-8.39
52		1.72	-6.51
51		1.71	-8.26
50		1.93	-6.86
49		1.86	-7.89
61		1.68	-8.13
41		1.90	-6.75
40		1.94	-7.50
39		2.23	-8.29
38		2.12	-8.41
37		2.44	-4.31
35	Smithian	2.22	-7.67
36		2.07	-7.70
46		0.95	-7.72
73		0.74	-7.60
45		0.12	-7.35
26		1.23	-2.50
27		0.09	-8.04
28		-0.23	-8.27
29		-0.14	-7.44
33		-0.09	-8.55
42		0.14	-8.38
31		0.61	-7.78
34		0.06	-6.42
22		1.69	-8.59
23		1.58	-9.12
10		0.73	-7.54
9		1.35	-9.14
5		0.81	-7.99
6		2.00	-5.94
8		1.57	-9.64
7		2.12	-7.68
12		2.10	-3.57
14		1.05	-4.15
15		1.67	-2.38
16		1.25	-3.19

Table 1. Galfetti et al.

The Smithian/Spathian boundary event: a major climatic turnover following the end-Permian biotic crisis. Evidence from palynology, ammonoids and stable isotopes

Peter A. Hochuli, Thomas Galfetti, Arnaud Brayard, Hugo Bucher,
Paleontological Institute and Museum, University Zürich, Karl Schmid-Strasse 4, CH-8006 Zürich, Switzerland
UMR 5125 CNRS Université Claude Bernard Lyon I, F-69622 Villeurbanne, France
Helmut Weissert,
Department of Earth Science, ETH - Zentrum, CH-8092 Zürich, Switzerland
Jorunn Os Vigran
Mellomila 2, N-7034Trondheim, Norway

E-mail corresponding author: Peter.Hochuli@erdw.ethz.ch

Submitted to Geology

Abstract

Using palynological data, global ammonoid distribution patterns and stable isotope data we show that the marine and terrestrial ecosystems underwent a major change at the Smithian/Spathian boundary. This change occurred during the recovery phase from the major biotic crisis at the Permian/Triassic boundary. This event might represent one of the causes responsible for the stepwise and delayed recovery of the marine, and probably to a minor degree, of the terrestrial ecosystems during the Early Triassic. A major disturbance of the global carbon cycle, which is expressed by a prominent shift in the marine $\delta_{13}C_{carb}$ isotopes, is consistent with a radical climatic change during late Early Triassic times. The observed reestablishment of highly diverse plant ecosystems, including the raise of woody gymnosperms and decline of the formerly dominating lycopods, occurring in the Boreal realm during this time is interpreted as a direct consequence of the climatic turnover.

Keywords: Early Triassic, Climate, Palynology, Ammonoids, Carbon Isotopes

Introduction

The Permian-Triassic boundary event, known as one of the most severe extinction events in Earth history, led to profound changes in terrestrial and marine ecosystems. Duration, mechanism and evolutionary significance of the subsequent recovery of the marine and terrestrial ecosystems are still a matter of ongoing debates. The fossil record for terrestrial ecosystems of the Early Triassic is very fragmentary. Palynological and paleobotanical records of this epoch are sporadic and very heterogeneous, especially for low paleolatitudes. Due to the difficulty to date terrestrial successions they are also poorly calibrated. These poor records led some authors to speculate about extremely decimated Early Triassic floras (Looy et al. 1999), whereas others, ignoring macrofossil evidence and in situ pollen and spores, considered essential parts of the Early Triassic palynological assemblages as being reworked (Utting et al. 2004). The latter interpretation is based on the fact that numerous spore-pollen groups dominating these assemblages originate in the Paleozoic and on many common features of Late Permian and Early Triassic floras. Recently, reviewing the global paleobotanical record of the Early Triassic, Grauvogel-Stamm and Ash (2005) demonstrated the relatively slow recovery of the terrestrial floras and stressed the essential role of climate in this process. Most Early Triassic plant remains are preserved in terrestrial red beds (cf. Grauvogel-Stamm and Ash 2005 and references therein); hence, the paleobotanical record is fragmentary and difficult to correlate with marine sections or to link with marine biotas. Boreal areas, with continuous and rapid sedimentation in marine environments, yield the best preserved archives documenting the recovery of terrestrial floras during this interval. Considering the relatively high diversity of boreal palynomorph assemblages these areas might be regarded as the most likely refuges of plants and sites of early recovery after the P/T boundary event. The wide distribution of palynomorphs being present in marine and unoxidized continental rocks allows bridging the gap between the terrestrial and the marine realms. In this paper we discuss the palynological record of the Early Triassic ammonoid dated sections from the Barents Sea (Vigran et al. 1998), which has been presented and discussed so far exclusively from the biostratigraphic point of view. Grouped into paleoecologically relevant categories we discuss it here within the context of ammonoid distribution patterns and with Tethyan carbon isotope records. The observed coeval changes in the terrestrial spore-pollen record, the global turnover in the ammonoid distribution patterns and the Tethyan $\delta_{13}C_{carb}$ isotope data are interpreted to reflect a major global event at the Smithian/Spathian boundary, affecting likewise marine and terrestrial ecosystems. During the Early Triassic the Barents Sea sites were located approx. 50°N (cf. Mørk et al. 1982) with a palynological record reflecting the vegetation of a warm, relatively humid climatic zone. The ammonoid distribution patterns include records from all climatic belts, whereas $\delta_{13}C_{carb}$ isotope records comprise several Tethyan sections, covering essentially low latitudinal sites. Thus our 77 proxies are not only of completely different nature but also cover different climatic zones; and the coeval changes necessarily reflect global signals.

Palynological record from the Boreal realm

Marine Early Triassic sediments of the Barents Sea area yield well preserved palynological successions, which based on the co-occurrence of ammonoids, are directly tied to the chronostratigraphic framework (Hochuli et al. 1989, Mørk et al. 1993, Vigran et al. 1998). Cored sections of Early Triassic rocks, subcropping on the Svalis dome area (Barents Sea, N-Norway) provide the so far most continuous and best dated palynological successions (Vigran et al. 1998). For the purpose of this paper the data, originally represented in a semi quantitative manner, have been transferred into a quantitative scheme by attributing figures to the semi-quantitative classifications. Listed taxa have been assigned to 10 major spore pollen groups of paleoecological significance. Considering the high number of samples and species, we assume that with this approach over- and under- representation of individual taxa are balanced out. The resulting quantitative distribution of these major groups (Fig. 1) shows consistent and homogeneous patterns within specific intervals. Following the scheme of Visscher and van der Zwan (1981) who inferred paleoclimatic trends from Late Triassic spore-pollen assemblages by comparing ratios of major spore-pollen groups, classified as hygro- or xerophytic elements, we consider variations in the distribution of these groups as paleoclimatic proxies, reflecting essentially availability of humidity for terrestrial ecosystems. Figure 1 includes ratios of hygro- and xerophytic elements calculated for 62 assemblages from the late Smithian to the early Anisian interval.

Similar to the scheme of Visscher and van der Zwan (1981) the following groups are regarded as hygrophytic elements (cf. fig. 1): i) cavate trilete spores (herbaceous and arboreal lycopods, e.g. Isoetales), ii) *Aratrisporites* (herbaceous lycopods, e.g. Isoetales), iii) smooth trilete and monolete spores (mostly Filicales), iv) ornamented trilete spores (mostly Filicales), vi) *Cycadopites* group (gymnosperms; Bennettitales, Cycadales, Ginkgoales and Caytoniales).

On the other hand we treat as xerophytic elements: i) taeniate bisaccate pollen (Coniferales), ii) monolete and trilete bisaccate pollen (Coniferales, Voltziales), iii) *Ephedripites* (Peltaspermales and Gnetales), iv) *Vitreisporites* group (Caytoniales and Peltaspermales).

Alete bisaccate pollen, attributable to Coniferopsida and Gingkoopsida, very heterogeneous in origin and ecological requirements, are regarded as a separate group. To illustrate the marked changes in the composition of plant assemblages diversity trends of two dominating groups - cavate trilete spores and taeniate bisaccate pollen - are plotted together with the overall diversity of spore-pollen (fig. 1).

From the distribution of the hygrophytic and xerophytic elements the following trends can be inferred: late Smithian assemblages show stable composition considering abundance and diversity of the major groups. They are strongly dominated by spores, especially by those of herbaceous and arboreal lycopods. Other pteridophyte spores (essentially Filicales) are also very common. Xerophytic elements, mostly taeniate pollen (Coniferales) and representatives of the *Ephedripites* group are relatively rare and poorly diversified.

A distinct turnover in spore-pollen assemblages occurs at the late Smithian/early Spathian

boundary with substantial increases in the abundance of xerophytic elements and of alete bisaccate pollen. Due to increased diversity of conifer pollen and unchanged diversity of lycopods the overall diversity increases also considerably.

Assemblages from the lower part of the late Spathian section are again dominated by spores, resulting in another peak of hygrophytic elements, accompanied by significantly reduced abundance of gymnosperm pollen. This apparently short-lived peak of hygrophytes is followed by their gradual decrease and a corresponding increase of xerophytes. The strong xerophytic trend in the assemblages of the middle part of the Spathian is emphasized by consistent to common occurrence of the *Ephedripites* group and high numbers of taeniate bisaccate pollen. Around the late Spathian/early Anisian boundary, preserved in core 04, this trend is broken by another peak of hygrophytes, mainly ornamented trilete spores. The temporary reduction of the *Ephedripites* group is supporting evidence for this relatively humid phase, which is followed by a gradual increase in the abundance of conifers (taeniate and monolete/trilete bisaccate pollen). Pteridophytes are well represented except for the lycopods. The significant turnover in Spathian assemblages is also expressed in changes of diversity; after culminating in the lower part of the Spathian section it drops, essentially due to decreased diversity of lycopods, in its middle part and remains low during most of the late Spathian. A renewed diversity increase, starting in the uppermost Spathian, subsequently leads to the highly diverse Middle Triassic floras.

Global distribution patterns of ammonoids and climatic implications

Several distinct turnovers in ammonoid faunas mark the recovery phase of the Early Triassic after their near-extinction by the P/T boundary event. A marked decrease in diversity characterizes the latest Smithian ammonoid faunas. As first noticed by Tozer (1982) a major, global ammonoid turnover occurred around the Smithian/Spathian boundary, which is marked by another nearly total extinction and followed by a major radiation. Recent modeling studies of Brayard et al. (2005) demonstrated the close relationship between generic richness and climatic gradients showing that sea surface temperatures (SST) gradients are crucial physical parameters controlling the latitudinal gradient of generic richness (LGGR), expressed for the ammonoids by a decreasing number of taxa from low to high latitudes. Accepting ammonoids as temperature-sensitive organisms, changes in their global taxonomic diversity and paleobiogeographic patterns provide a proxy for changing SST gradients. LGGRs compiled from twenty Tethyan and Panthalassic basins yielding Early Triassic faunas indicate that biogeographic distribution and taxonomic diversity changed considerably during the period of recovery from the P/T boundary event (cf. Fig. 2). After an initial phase of low LGGR characterizing the Griesbachian period, the LGGR increase during the Dienerian and up to the Smithian. The trend from flat LGGR in the Griesbachian, to a minor differentiation during the Dienerian and to steep gradients for the major part of the Smithian can be associated with latitudinally more contrasted climatic gradients. An abrupt decline of faunal diversity at the end of the Smithian led to poorly diversified faunas during the *Anasibirites pluriformis* zone just below the Smithian-Spathian boundary. This zone

is characterized by remarkable cosmopolitanism of ammonoids (Tozer, 1982) indicating low SST gradients. This profound change is followed by an extreme diversification of ammonoids during the Spathian. Although much less severe, a second decrease in ammonoid diversity occurred around the Spathian-Anisian boundary. Thus, the major changes in the evolutionary history of Early Triassic ammonoids are accompanied by drastic reorganization of their spatial distribution, switching from essentially cosmopolitan to latitudinally restricted patterns reflected by steep LGGRs.

Tethyan $\delta_{13}C_{carb}$ isotope C13 records

Our new Early Triassic $\delta_{13}C_{carb}$ data from South China (Galfetti et al. 2005) together with the records from South and South-east China (Payne et al. 2004, Tong et al. 2003), North India and Pakistan (Atudorei 1999) show that during the Early Triassic the carbon cycle underwent synchronous, long and short scale fluctuations before reaching a more stable state in the early Middle Triassic. In particular, the C-isotope curve illustrates a rapid, strong positive excursion of up to 4‰ across the Smithian/Spathian boundary (Fig. 2). The transition to most positive carbon isotope values, occurring within a single biozone at the very end of the Smithian, coincides with the *Anasibirites pluriformis Zone* organic-rich shale deposition and with the abovementioned diversity collapse in ammonoid faunas. Peak values in the C-isotope record occur together with the reestablishment of the carbonate system during the early Spathian (Atudorei 1999, Galfetti et al. 2005) and are accompanied by the major worldwide ammonoid diversification and by the reorganization of their paleobiogeographic distribution. Similar to the Smithian-Spathian boundary a synchronous, although less important evolutionary step in the ammonoid diversity is accompanied by another positive carbon isotope excursion, reaching up to 3‰ at the Spathian- Anisian boundary (Atudorei 1999, Galfetti et al. 2005).

Discussion and conclusions

During the Early Triassic interval lycopod – mostly herbaceous plant dominated associations were replaced by assemblages dominated by conifers and ferns, resulting in one of the major floral turnovers of the Mesozoic. In this paper we interpret the distinct turnover in the distribution of major floral elements at the Smithian/Spathian boundary as severe modification in the terrestrial ecosystem related to the climatic evolution. Using ratios between hygrophytic and xerophytic elements the following climatic trends can be inferred.

Spore dominated late Smithian assemblages reflect relatively stable humid conditions. The prominent change with a marked decrease of the hygrophytic elements at the Smithian/Spathian boundary indicates a rapid change to considerably dryer conditions, favoring the reestablishment of conifer dominated ecosystems. In the lower part of the late Spathian this phase is followed by another abundance peak of pteridophytes, interpreted as a more humid phase of relatively short duration. In this interval several typical taxa of the lower Early Triassic disappear, resulting in reduced overall diversities. The gradual increase of xerophytic elements towards

the upper part of the late Spathian implies again dryer conditions. This trend is interrupted by increased abundance of hygrophytes across Spathian/Anisian boundary suggesting another relatively short-lived humid phase. It is marked by the onset of a distinct diversity increase, which continues in the early Anisian. Gradual increase of xerophytic elements, suggesting dryer conditions characterizes the early Anisian assemblages.

The importance of considering biogeographic differences to assess the recovery of the terrestrial ecosystems has been expressed by several authors (Grauvogel and Ash 2005, and references therein). Our data show that the reestablishment of diverse conifer and fern dominated assemblages occurred in the Boreal realm in the Early Spathian compared to the Early Anisian in southern latitudes (cf. Looy et al. 1999).

One of the possible causes for global climate changes is the extensive volcanic activity related to the formation of large igneous provinces. The Siberian traps, recognized as the largest continental flood volcanism event on Earth is interpreted as one of the most probable mechanism triggering the mass-extinction at the P/T boundary (Renne et al. 1995). According to some authors (e.g. Westphal et al. 1998; Ivanov et al. 2005, and references therein) the Siberian traps are not the product of a single volcanic pulse at the P/T boundary but of persistent activity lasting at least 3 m.y.

Therefore, the sustained release of greenhouse gases might be responsible for continuous disturbances of marine and terrestrial ecosystems during the Early Triassic, including the observed ammonoid and spore-pollen assemblage turnover at the Smithian/Spathian boundary. A massive injection of CO_2 of volcanic origin would have stimulated humid and warm conditions at the end of the Smithian. Elevated pCO_2 levels may have led to changes in the ocean chemistry and triggered a biocalcification crisis (Berner, 2005. Wissler et al. 2003). Consequently, this warming pulse and sudden change in ocean chemistry may have induced the observed collapse of the ammonoid fauna and led to the dominance of hygrophytic plant assemblages in the Boreal realm. During the late Smithian to early Anisian interval, considered crucial for the global biotic recovery from the P/T boundary event, changes in the composition of spore-pollen assemblages, in the global distribution patterns of ammonoid and stable isotopes reflect major disturbances in terrestrial and marine ecosystems. In sections from South China and Northern India these events also coincide with a sudden change from suboxic, clastic-dominated sedimentation during late Smithian to an oxic, carbonate-dominated regime in the Spathian (Atudorei 1999, Galfetti et al. 2005). The C-isotope peak values of the earliest Spathian mark the end of CO_2 drawdown and accelerated organic carbon burial. The climatic change to dryer and possibly cooler conditions, the stabilization of ocean chemistry favored renewed carbonate sedimentation and an accelerated diversification of ammonoids.

Acknowledgements

We acknowledge financial support from the SNF (AB, HB) and the *Région Rhône-Alpes* (AB). The authors would like to thank Atle Mørk (IKU) for valuable comments to this paper.

References

Atudorei, V., 1999, Constraints on the Upper Permian to Upper Triassic marine carbon isotope curve. Case studies from the Tethys. [Ph.D. thesis], Lausanne, University of Lausanne, Switzerland, 161 p.

Berner, R.A., 2005, The carbon and sulfur cycles and atmospheric oxygen from middle Permian to middle Triassic. Geochimica et Cosmochimica Acta, v. 69, p. 3211-3217.

Brayard, A., Escarguel, G., Bucher, H., 2005, Latitudinal gradient of taxonomic richness: combined outcome of temperature and geographic mid-domains effects? Journal of Zoological Systematic and Evolutionary Research, v. 43, p. 178-188.

Galfetti, T., Bucher, H., Brayard, A., Guodun, K., Atudorei, V., Hochuli, P. A., Weissert, H., Guex, J., 2005, Biotic recovery and paleoclimate in Early Triassic times as reflected in carbonate carbon isotopes, sedimentary evolution and ammonoid fauna: records from South China and North India. 6th International Symposium on Applied Isotope Geochemistry. Czech Geological Survey, Prague, Czech Republic, Abstracts, p. 83.

Grauvogel-Stamm, L. and Ash, S.R., 2005, Recovery of the Triassic land flora from the end-Permian life crisis. Comptes Rendus Palevol, v. 4, p. 593-608.

Hochuli, P.A., Colin, J.P. and Vigran, J.O., 1989, Triassic biostratigraphy of the Barents Sea area, *in* Collinson, J.D. (Ed.), Correlation in Hydrocarbon Exploration. Graham and Trotman, London, p. 131–153.

Ivanov, A.V., Rasskazov, S.V. Feoktistov, G.D., He, H. and Boven, A., 2005, $^{40}Ar/^{39}Ar$ dating of Usol'skii sill in the south-eastern Siberian Traps Igneous Province: evidence for long-lived magmatism. Terra Nova, v. 17, p. 203-208.

Looy, C.V., Brugman, W.A., Dilcher, D.L., Visscher H., 1999, The delayed resurgence of equatorial forests after the Permian–Triassic ecologic crisis. National Academy of Sciences Proceedings, v. 96, p.13857–13862.

Mørk, A., Vigran, J.O., Korchinskaya, M.V., Pchelina, T.M., Fefilova, L.A., Vavilov, M.N., and Weitschat, W., 1993, Triassic rocks in Svalbard, the Arctic Soviet islands and the Barents Sea: bearing on their correlations, *in* Vorren, T.O. et al. (Eds.), Arctic Geology and Petroleum potential, Norwegian Petroleum Society, Special Publication 2, p. 457-479.

Mørk, A., Knarud, A., Worsley, D., 1982, Depositional and diagenetic environments of the Triassic and Lower Jurassic succession of Svalbard, *in* Mørk, A., Knarud, A., Worsley, D. (Eds.). Arctic geology and geophysics: proceedings of the 3rd International symposium on arctic geology. Canadian Society of Petroleum Geologists. Calgary, Canada, p. 371-398.

Payne, J. L., Lehrmann, D. J., Wei, J., Orchard, M. J., Schrag, D. P., Knoll, A. H., 2004, Large perturbations of the carbon cycle during recovery from the end-Permian extinction. Science, v. 305, p. 506-509.

Renne, P. R., Zhang, Z., Richardson, M. A., Black, M. T., Basu, A. R., 1995, Synchrony and causal relations between Permo-Triassic boundary crises and Siberian flood volcanism. Science, v. 269, p. 1413-1416.

Tong, J., Zakharov, Y. D., Orchard, M. J., Hongfu, Y., Hansen, H. J., 2003, A candidate of the Induan-Olenekian boundary stratotype in the Tethyan region. Science in China Series D 46, p. 1182-1200.

Tozer, E. T., 1982, Marine Triassic faunas of North America: Their significance for assessing plate and terrane movements. Geologische Rundschau v. 71, p. 1077-1104.

Utting, J., Spina, A., Jansonius, J., McGregor, D.C. and Marshall, J.E.A., 2004, Reworked miospores in the upper Paleozoic and lower Triassic of the northern circum-polar area and selected localities. Palynology, v. 28, p. 75-119.

Vigran, J.O., Mangerud, G., Mørk, A., Bugge, T. and Weitschat, W., 1998, Biostratigraphy and sequence stratigraphy of the Lower and Middle Triassic deposits from the Svalis Dome, Central Barents Sea, Norway. Palynology*, v.*22, p. 89–141.

Visscher, H. and Van Der Zwan, W.A., 1981, Palynology of the circum-Mediterranean Triassic: phytogeographical and palaeoclimatological implications. Geologische Rundschau, v. 70, p. 625-636.

Westphal, M, Gurewitch, E.L., Samsonov, B.V., Feinberg, H. and Pozzi, J.P., 1998, Magnetostratigraphy of the lower Triassic volcanics from deep drill SG6 in western Siberia: evidence for long-lasting Permo-Triassic volcanic activity. Geophysical Journal International, v. 134, p. 254-266.

Wissler, L., Funk, H. and Weissert, H., 2003, Response of Early Cretaceous carbonate platforms to changes in atmospheric carbon dioxide levels. Palaeogeography Palaeoclimatology Palaeoecology, v. 200, p. 187-2005.

Figure captions

Fig.1. Distribution of major floral elements in the Smithian to middle Anisian interval of the Svalis dome area (Barents Sea, N-Norway) classified as hygro and xerophytes (for details and references see Vigran et al. 1998).

Fig. 2. Summary of Early Triassic, (1) global trends in ammonoid paleobiogeography (LGGR), (2) $\delta 13C_{carb}$ isotope record from Northern India (Atudorei 1999), (3) boreal humidity trend inferred from palynological data from the Barents Sea (cf. Fig.1).

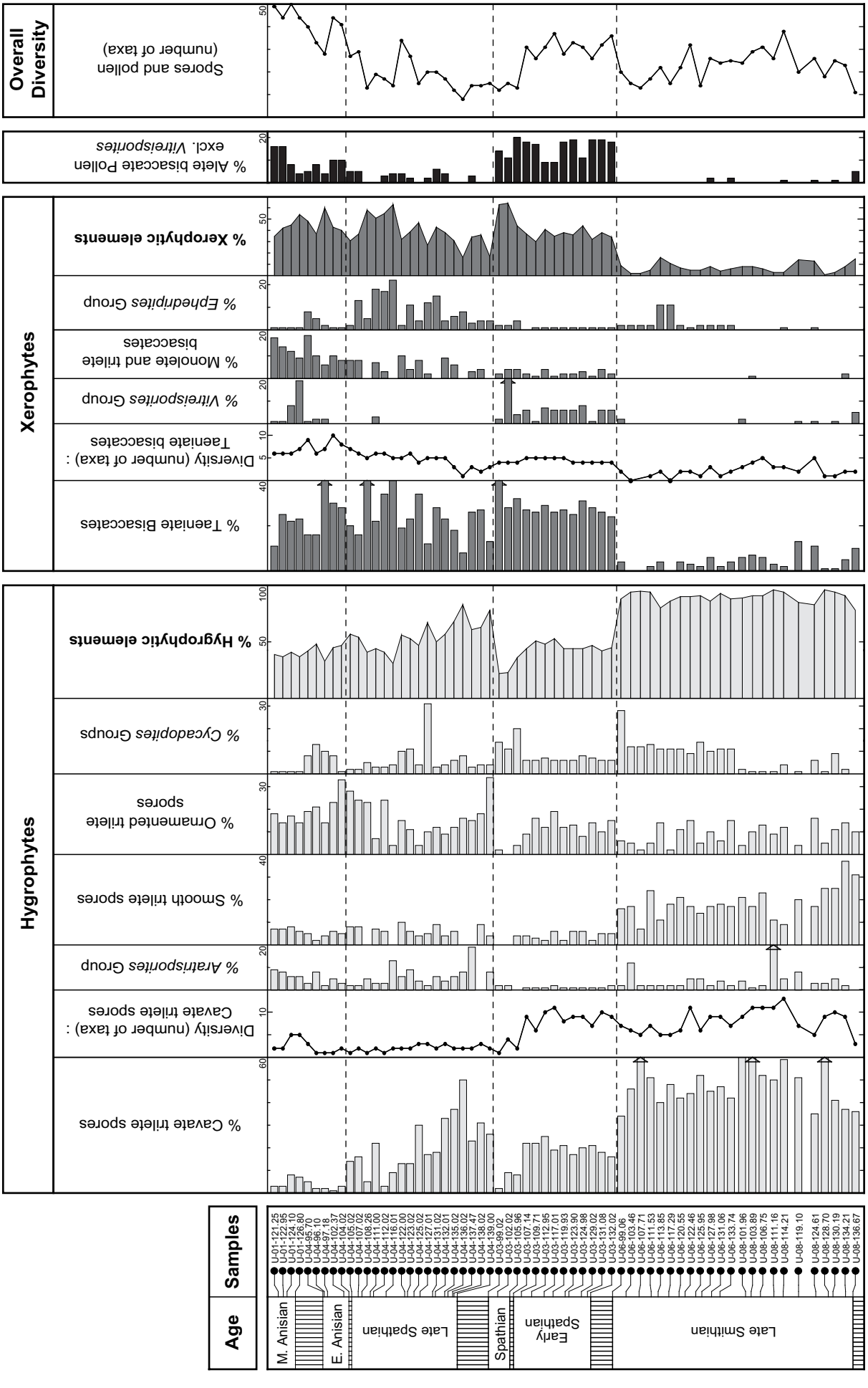

Fig. 1. Hochuli et al.

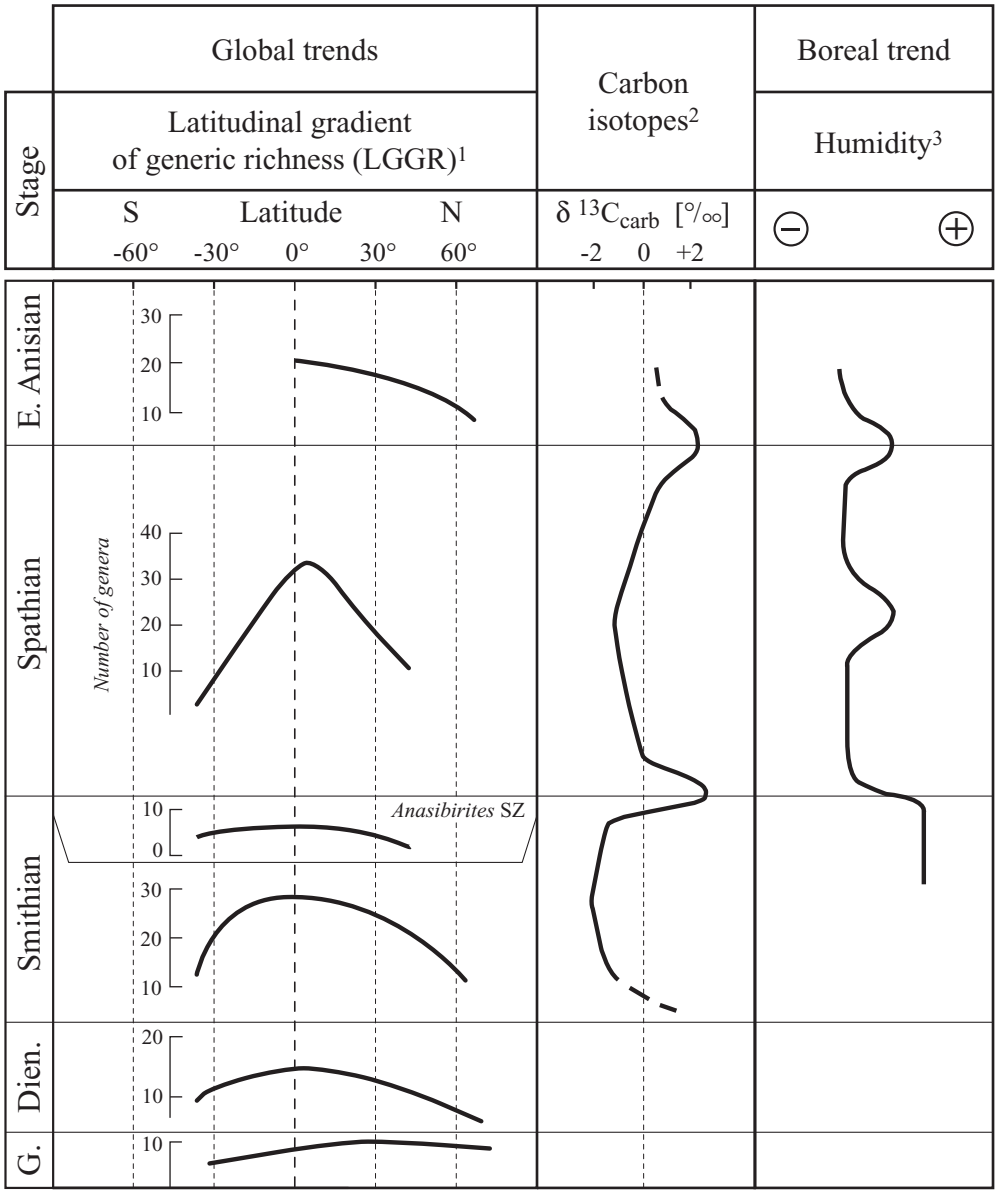

Fig. 2. Hochuli et al.